

**ATTENUATION OF RADIO COMMUNICATION SIGNALS BY RAIN AT  
MILLIMETER WAVE BAND AT SOME LOCATIONS IN NIGERIA**

**BY**

**OSITA IBE**

**B.Sc. (Nsukka), M.Sc. (Ibadan)**

**Matric. No.: 102112**

**A thesis in the Department of Physics**

**Submitted to the Faculty of Science in partial fulfilment of the requirements for  
the Degree of**

**DOCTOR OF PHILOSOPHY**

**of the**

**UNIVERSITY OF IBADAN**

**April 2021**

## **CERTIFICATION**

I certify that this work was carried out by Mr. Osita Ibe in the Department of Physics,  
University of Ibadan, Nigeria

---

Supervisor

Dr E. F. Nymphas

B.Sc. (Maiduguri), M.Sc., PhD (Ibadan)

Department of Physics,

University of Ibadan, Nigeria

## **DEDICATION**

This thesis is dedicated to the Almighty God, my very present help.

## ACKNOWLEDGEMENTS

I am deeply grateful to God almighty, the Father of our Lord Jesus Christ who has been my very present help.

I wish to convey my profound appreciation to Dr Nymphas E. F., my supervisor, for guiding me painstakingly through this research work and for the fatherly care and concern he extended to me during the arduous tasks of the research.

The progress in this research would have been hampered but for the timely intervention of Prof. P. N. Okeke who graciously linked me up to the major source of the research data used. Dr. Lorenzo Luini of the Dipartimento di Elettronica e Informazione (DEI) – Politecnico di Milano Piazza Leonardo da Vinci 32, Milano (Italy) is worthy of mention for his swift interventions in providing me with relevant journals and online academic guidance. Dr. Ojo of the Federal University of Technology Akure (FUTA) is greatly appreciated for provision of some of the data used and for technical guidance on the analysis and application of the results. I heartily appreciate Prof. Adimula of the University of Ilorin, Prof. Ajewole of FUTA, Dr. Durodola of the University of Jos, Prof. J.A. Adegoke of the Department of Physics, University of Ibadan. To the Atmospheric physics members, Department of Physics, University of Ibadan – Prof. Oladiran, Drs Adeniyi, Nymphas, Otunla and Ogunsola, I owe a debt of gratitude for their invaluable contributions to the research work. The concern and support of my friends, Mr. Oyewole of Bowen University, Dr. Aremu of the Polytechnic Ibadan, Mr. Adeleke of the University of Ibadan, and Mr. Oyedotun Gbenga of the Cocoa Research Institute of Nigeria (CRIN), is greatly appreciated. My Head of Department at CRIN, Mr. Fagbami O. is appreciated for his permission and well wishes.

I am also grateful to the Head of Geography Department, University of Ibadan, Professor C.O. Ikporukpo, for graciously providing me data from their meteorological station free of charge. Mr. Alabi of the International Institute of Tropical Agriculture (IITA), Ibadan and Mr. Najib of the Centre for Atmospheric Research, Ayingba are greatly appreciated for providing me with data.

I hereby acknowledge the magnanimity of the Tropospheric Data Acquisition Network (TRODAN) for making available to me free of charge 5-minutes integration time data on most of the stations used in this research work.

The members of the Deeper Life Bible Church Oluyole region are greatly appreciated; the fellowship availed me with the spiritual atmosphere that strengthened my spirit to pull through the prevailing pressures of the research.

I owe a debt of gratitude to the entire management of the Cocoa Research Institute of Nigeria (CRIN), Ibadan for graciously granting me permission to embark on this work.

To all my siblings Mrs. Chinwe Chijioke, Emmanuel, Christopher, Benjamin Ibe and their families; my uncle and aunty, Louis and Ify Alagbogu, I am indeed grateful for their prayers and support. To my in-laws Mrs. Funke Akinyemi and Dr & Mrs Komolafe, your support has been invaluable.

This work may not have seen the limelight but for the cooperation, prayers and support of my dear wife, Dr (Mrs) Bolatito Ibe, my son, Chidiebere, my daughters, Tochukwu and late Amarachukwu. To them, I remain eternally grateful.

## ABSTRACT

Millimeter Wave (MMW) radio systems operating at 30 to 300GHz band provides higher bandwidth, frequency reuse and communications security but suffers greatly from attenuation by rain. The design of radio communication equipment has been based on predicted rain rate and attenuation from the International Telecommunication Union-Radio (ITU-R) model. However, such equipment fails in the tropics because rainfall in this region is more intense with larger drop sizes than those in the temperate regions on which the ITU-R model was based. Thus, Rain Rates (RR) and attenuation information from the tropics are needed for the design of radio communication equipment for the region. This study was therefore aimed at estimating rain induced attenuation of radio communication signals at some locations across Nigeria.

The RR data was obtained from 14 automatic weather stations across eco-climatic zones of Nigeria. The equipment measures rainfall at 1- min (2 locations) and 5-min (12 locations) integration time. Lavergnat and Gole model was used to convert the 5-min to 1-min RR, while logarithmic scale was used to convert the RR to exceedance time percentages (0.001 to 1%). These RR were compared with those predicted by the ITU-R model using the MatLab RR statistics. The specific rain attenuation ( $\gamma_R$ ) for Horizontal ( $\gamma_R H_p$ ) and Vertical ( $\gamma_R V_p$ ) Polarisation at MW Frequencies (MWFs) were estimated at 0.01% RR ( $R_{0.01}$ ) using the power law ( $\gamma_R = kR_{0.01}^\alpha$ ) relationship where k and  $\alpha$  are regression coefficients. These estimated values were then compared with the ITU-R predicted values. The Path Attenuation (PA) at 20 km (at 0.01%,  $A_{0.01}$ ) Path Length (PL) was computed using  $A_{0.01} = \gamma_R d_{eff} dB$  to determine the Clear Signal Bands (CSBs) at MWFs ( $d_{eff}$  is the effective path length).

The mean annual 1-minute RR (mm/hr) ranged from 22.78 in Mid Altitude Savanna (MAS) to 116.67 mm/hr in Southern Guinea Savanna (SGS). Throughout the country, the ITU-R predicted RR ranged from 87.10 mm/hr in the MAS to 91.60 mm/hr in the SGS. The highest value of  $\gamma_R$  for all 14 locations occurred at 120 and 150 GHz MWFs and  $\gamma_R H_p > \gamma_R V_p$ . The estimated maximum  $\gamma_R H_p$  vs ITU-R values at 120 GHz were: 35.05, 29.85; 26.96, 17.90; 30.94, 18.01; 11.85, 28.86; 29.78, 30.56; and 35.91, 33.52 dB/km at SGS, Sudan Savanna (SS), Northern Guinea Savanna (NGS), MAS, Derived Savanna (DS) and Humid Forest (HF), respectively. The corresponding  $\gamma_R V_p$  vs ITU-R values were: 34.64, 29.52; 26.68, 17.74; 30.60, 17.85; 11.77, 28.55; 29.46, 20.00; and 35.48, 33.14 dB/km, respectively at the 0.01%. At 150 GHz, maximum  $\gamma_R H_p$  vs ITU-R were: 34.81, 29.74; 26.93, 18.03; 30.81, 18.14; 12.05, 28.78; 29.68, 30.43 and 35.63, 33.32 dB/km, respectively. The corresponding maximum  $\gamma_R V_p$  vs ITU-R were: 34.50, 29.50; 26.72, 17.93; 30.55, 18.04; 12.00, 28.56; 29.44, 30.18 and 35.32, 33.03 dB/km, respectively. The CSBs at 20 km PL were estimated to be 40 and 45 GHz across the zones, while the predicted value by ITU-R included 150 GHz and overlaps with 45 GHz band. The estimated PA at 40 and 45 GHz ranged from 64.65-206.85 dB and 71.40-219.45 dB, respectively; the ITU-R predicted range of PA at 40, 45 and 150 GHz were 90.01-192.18 dB, 107.79-204.43 dB and 135-150 dB, respectively.

The rain rates across the eco-climatic zones have been determined. The estimated specific, path attenuation and clear signal bands varies from the International Telecommunication Union-Radio predictions for Nigeria.

**Keywords:** Rain rates, Rain attenuation, Path attenuation, Propagation frequency, ITU-R

**Word count:** 497

## TABLE OF CONTENTS

	Pages
Title Page	i
Certification	ii
Dedication	iii
Acknowledgements	iv
Abstract	vi
Table of Contents	viii
List of Tables	xii
List of Figures	xiv
Appendices	xx
Acronyms and Abbreviations	xxi
<b>CHAPTER ONE: INTRODUCTION</b>	
1.1 Research background	1
1.2 Problem Statement	5
1.3 Justification of the study	6
1.4 Study aim and objectives	8
<b>CHAPTER TWO: REVIEW OF LITERATURES</b>	
2.1 Tropical rainfall pattern	9
2.2 The Nigerian climate	14
2.3 Rainfall measurements at a point	15
2.3.1 Rain gauge measurements error sources	16
2.3.2 Wind-induced errors	18
2.4 Rain Rate Measurements	18
2.4.1 Segal Method (1986)	19
2.4.2 Falvin (1981)	20
2.4.3 Burgueno <i>et al.</i> Method (1988)	20
2.4.4 Chebil and Rahman (1999)	20
2.4.5 Joo <i>et al.</i> method (2002)	20
2.4.6 Ajayi (1996)	21
2.4.7 Semire et al. (2012)	21
2.4.8 Ojo <i>et al.</i> (2016)	24
2.5 Radio wave propagation on terrestrial paths	25



2.6	Millimeter wave propagation characteristics	27
2.7	Millimeter wave transmission loss factors	30
2.7.1	Fog attenuation	31
2.7.2	Attenuation by snow	32
2.7.3	Free space loss	32
2.7.4	Losses by atmospheric gases	32
2.7.5	Attenuation by water vapor	33
2.7.6	Foliage losses	33
2.7.7	Attenuation by rain	34
<b>CHAPTER THREE - METHODOLOGY</b>		
3.1	Data collection	39
3.2	Data analysis	46
3.2.1	Conversion from rainfall to rain rate	46
3.3	Rain rate prediction models	48
3.3.1	Moupfouma model	48
3.3.2	Rice and Holmberg model	49
3.3.3	Ito & Hosoya model	50
3.3.4	ITU-R (837-5) model	51
3.3.5	Prediction models testing	51
3.4	Rainfall rate characterization for worst month	52
3.5	Determination of rain attenuation statistics	54
3.5.1	ITU-R p. 530-17 (2015) Recommendations	54
3.5.2	Moupfouma model	55
3.5.3	The Global Model by Crane	57
3.5.4	Prediction of rain attenuation at 33.4 GHz and 31.8 GHz in Nigeria	58
3.5.5	Contour mapping of rain attenuation distribution in Nigeria	58
<b>CHAPTER FOUR – RAINFALL CHARACTERIZATION</b>		
4.1	Rainfall Characterisation at the Study Locations	60
4.1.1	Accumulated rainfall distribution	62
4.1.1.1	Derived savanna zone	62
4.1.1.2	Humid forest zone	69
4.1.1.3	Northern guinea savanna zone	72

4.1.1.4 Mid altitude savanna zone	72
4.1.1.5 Southern guinea savanna zone	75
4.1.1.6. Sudan Savanna Zone	79
4.1.2 Cumulative distribution function (CDF) of rain rates based on different integration times	81
4.1.2.1 Annual rainfall rates cumulative distribution	83
4.1.2.2 Comparison with other tropical and sub-tropical locations	85
4.1.3 Diurnal variation of rain	87
4.1.4 Time series of rainfall events	89
4.1.5 Dependence of annual average rainfall intensity on hour of the day	92
4.1.6 Comparison of measured rain rate and rain rate derived from ITU-R model	101
4.1.7 Worst month rain rate characterization	109
4.1.7.1 Deduction of worst months	109
4.1.7.2 Relationship between Annual and Worst Month rainfall rate	117
4.1.7.3 Evaluation of conversion factor parameters $\beta$ and $Q_1$	119
4.1.8 Modelling of Rainfall Rate Cumulative Distribution	136
4.1.9 Rainfall rate prediction modeling and model validation	139
4.1.10 Validation of the Models	142
4.2 Statistics of Rain Attenuation	144
4.2.1 Computation of specific attenuation	144
4.2.2 Estimating Path Attenuation Using Different Existing Models for Terrestrial Paths	162
4.2.3 Path Attenuations at the 40GHz and 45GHz frequency bands	193
4.2.4 Contour Mapping of Rainfall Attenuation Distribution at 40 GHz and 45 GHz Frequency Bands in Nigeria	199
4.2.5 Path Attenuations on the 31.8 GHz to 33.4 GHz NCC frequency bands	212
4.2.6 Contour mapping of rainfall attenuation distribution at 31.8GHz and 33.4GHz frequency bands	228

<b>CHAPTER FIVE: CONCLUSION AND RECOMMENDATION</b>	
5.1 Conclusion	239
5.2 Recommendations	240
5.3 Suggestions for further research	240
<b>REFERENCES</b>	242
<b>APPENDICES</b>	259

## LIST OF TABLES

<b>Table</b>	<b>Title</b>	<b>Pages</b>
2.1	Integration time coefficients	23
2.2	Percentage availability/outages of radio waves	36
3.1	Features of the study sites	42
4.1	Characteristics of the stations used in this study	61
4.2	Summary of the worst hour and the corresponding rainfall rates in all the locations	100
4.3	ITU percentage of exceedance at different rainfall rates CD in the derived savanna zone	102
4.4	ITU percentage of exceedance at different rainfall rates CD in the humid forest zone	104
4.5	ITU percentage of exceedance at different rainfall rates CD in the Northern Guinea Savanna zone	105
4.6	ITU percentage of exceedance at different rainfall rates CD in the mid altitude savanna location	106
4.7	ITU percentage of exceedance at different rainfall rates CD in the Southern Guinea Savanna locations	107
4.8	ITU percentage of exceedance at different rainfall rates CD for Sudan savanna locations	108
4.9	Model Parameters for worst months in Nigeria, other tropical countries and ITU	135
4.10	The conversion factor parameters	138
4.11	Prediction models validation	143
4.12	Rain rate statistics at 0.01% exceedance	145
4.13	Specific attenuation values at 120GHz and 150GHz	161
4.14	Estimated path attenuation for 40GHz and 45GHz frequency bands at 0.01%	198
4.15	Path attenuation for different values of system availability at 40 GHz	200
4.16	Path attenuation for different values of system availability at 45 GHz	201
4.17	Path attenuation at 0.001% to 1% rain rate exceedance for 40 GHz frequency band using Inverse Distance Weighing Interpolation	202

4.18	Path attenuation at 0.001% to 1% rain rate exceedance for 45 GHz frequency band using Inverse Distance Weighing Interpolation	203
4.20	Path attenuation for different values of system availability at 33.4 GHz	227
4.21	Path Attenuation at 0.001% to 1% rain rate exceedance for 31.8 GHz frequency band using Inverse Distance Weighing Interpolation	229
4.22	Path Attenuation at 0.001% to 1% rain rate exceedance for 33.4 GHz Frequency band Using Inverse Distance Weighing Interpolation	230

## LIST OF FIGURES

Figures	Title	Pages
1.1	Electromagnetic spectrum and applications	3
2.1	Typical area depth rainfall curve	11
2.2	Influence of rain cell size on rain rate	13
2.3	Classification of rain gauge measurement errors	17
2.4	vertical profiles of the atmosphere	26
2.5	Millimeter wave Vs Microwave beam	29
2.6	Attenuation of millimeter wave	35
2.7	Interference of Signals by Rain Drop	37
3.1	Map showing the stations covered by the study	41
3.2a	A typical Setup of TRODAN Equipment	43
3.2b	The electronic weather station of Davis Vantage Vue door console units and the outdoor ISS	44
3.2c	HOBO rain Gauge Equipment	45
4.1	Cumulative monthly rainfall distribution (mm) in (a) Nsukka, (b) Eburumiri, (c) Anyigba (d) Makurdi, (e) Iwo and (f) Mowe	68
4.2	Cumulative monthly rainfall distribution (mm) in (a) Akure, (b) Port Harcourt	71
4.3	Cumulative monthly rainfall distribution (mm) at Bauchi	73
4.4	Cumulative monthly rainfall distribution (mm) at Jos	74
4.5	Cumulative monthly rainfall distribution (mm) in (a) Minna, (b) Yola, (c) Ogbomosho	78
4.6	Cumulative monthly rainfall distribution (mm) at Kano	80
4.7	Cumulative distribution function of rain rates	82
4.8	Annual cumulative distribution of rainfall rates	84
4.9	Comparison of cumulative distribution of rainfall rates with other tropical/sub-tropical locations	86
4.10	Diurnal variation of rainfall for each eco-climatic zone	88
4.11	Time series of rainfall rates during rain events	91
4.12	Diurnal variation of annual average rainfall rate events over the derived Savanna Zone	93

4.13	Diurnal variation of annual average rainfall rate events over the humid forest zone	94
4.14	Diurnal variation of annual average rainfall rate events over the Northern Guinea Savanna zone	95
4.15	Diurnal variation of annual average rainfall rate events over the mid altitude Savanna zone	96
4.16	Diurnal variation of annual average rainfall rate events over the southern Guinea Savanna Zone	97
4.17	Diurnal Variability of annual average rainfall rate events over the Sudan Savanna zone	98
4.18	Monthly variation of rainfall rate distribution	110
4.19	Cumulative distribution of rainfall rates in an average year and the worst months over (a) Derived Savanna Zone (b) Humid Forest Zone (c) Mid Altitude Savanna Zone (d)Northern Guinea Savanna Zone (e) Sudan Savanna Zone and (f) southern guinea savanna Zone	116
4.20	Relationship between average annual and worst month rainfall rate	118
4.21	Determination of conversion factors $\beta$ and $Q_1$ for Nsukka (Derived Savanna Zone)	121
4.22	Determination of conversion factors $\beta$ and $Q_1$ for Eburumiri (Derived Savanna Zone)	122
4.23	Determination of conversion factors $\beta$ and $Q_1$ for Anyigba (Derived Savanna Zone)	123
4.24	Determination of conversion factors $\beta$ and $Q_1$ for Anyigba (Derived Savanna Zone)	124
4.25	Determination of conversion factors $\beta$ and $Q_1$ for Iwo (Derived Savanna Zone)	125
4.26	Determination of conversion factors $\beta$ and $Q_1$ for Ogun (Derived Savanna Zone)	126
4.27	Determination of conversion factors $\beta$ and $Q_1$ for Akure (Humid Forest Zone)	127
4.28	Determination of conversion factors $\beta$ and $Q_1$ for Port Harcourt (Humid Forest Zone)	128

4.29	Determination of conversion factors $\beta$ and $Q_1$ for Bauchi (Northern Guinea Savanna Zone)	129
4.30	Determination of conversion factors $\beta$ and $Q_1$ for Jos (Mid Altitude Savanna Zone)	130
4.31	Determination of conversion factors $\beta$ and $Q_1$ for Ogbomosho (Southern Guinea Savanna Zone)	131
4.32	Determination of conversion factors $\beta$ and $Q_1$ for Minna (Southern Guinea Savanna Zone)	132
4.33	Determination of conversion factors $\beta$ and $Q_1$ for Yola (Southern Guinea Savanna Zone)	133
4.34	Determination of conversion factors $\beta$ and $Q_1$ for the Kano (Sudan Savanna Zones)	134
4.35	Power law relationship between rainfall rates	137
4.36	1- minute rainfall rate prediction models comparison for Akure	140
4.37	1- minute rainfall rate prediction models comparison for Kano	141
4.38	Specific rain attenuation versus frequency for horizontal polarisation over the derived savanna zone	147
4.39	Specific rain attenuation versus frequency for vertical polarisation over the derived savanna zone	148
4.40	Specific rain attenuation versus frequency for horizontal polarisation over the humid forest zone	149
4.41	Specific rain attenuation versus frequency for vertical polarisation over the humid forest zone	150
4.42	Specific rain attenuation versus frequency for horizontal polarisation over the the northern guinea savanna zone	151
4.43	Specific rain attenuation versus frequency for vertical polarisation over the northern guinea savanna zone	152
4.44	Specific rain attenuation versus frequency for horizontal polarisation over the mid altitude savanna zone	153
4.45	Specific rain attenuation versus frequency for vertical polarisation over the mid altitude savanna zone	154
4.46	Specific rain attenuation versus frequency for horizontal polarisation over the southern guinea savanna zone	155



4.47	Specific rain attenuation versus frequency for vertical polarisation over the southern guinea savanna zone	156
4.48	Specific rain attenuation versus frequency for horizontal polarisation over the Sudan savanna zone	157
4.49	Specific rain attenuation versus frequency for vertical polarisation over the Sudan savanna zone	158
4.50	Specific rain attenuation at vertical and horizontal polarisation at 0.01% exceedance rainfall rate	160
4.51	Path attenuation at 0.01% rain rate exceedance	163
4.52a	Path attenuation at 0.01% measured rain rate exceedance at Nsukka	165
4.52b	Path attenuation at 0.01% ITU-R rain rate prediction at Nsukka	166
4.53a	Path attenuation at 0.01% measured rain rate exceedance at Eburumiri	167
4.53b	Path attenuation at 0.01% ITU R rain rate prediction at Eburumiri	168
4.54a	Path attenuation at 0.01% measured rain rate exceedance at Anyiba	169
4.54b	Path attenuation at 0.01% ITU R rain rate prediction at Anyigba	170
4.55a	Path attenuation at 0.01% measured rain rate exceedance at Makurdi	171
4.55b	Path attenuation at 0.01% ITU R rain rate prediction at Makurdi	172
4.56a	Path attenuation at 0.01% measured rain rate exceedance at Iwo	173
4.56b	Path attenuation at 0.01% ITU R rain rate prediction at Iwo	174
4.57a	Path attenuation at 0.01% measured rain rate exceedance at Ogun	175
4.57b	Path attenuation at 0.01% ITU R rain rate prediction at Ogun	176
4.58a	Path attenuation at 0.01% measured rain rate exceedance at Akure	177
4.58b	Path attenuation at 0.01% ITU R rain rate prediction at Akure	178
4.59a	Path attenuation at 0.01% measured rain rate exceedance at Port Harcourt	179
4.59b	Path attenuation at 0.01% ITU R rain rate prediction at Port Harcourt	180
4.60a	Path attenuation at 0.01% measured rain rate exceedance at Bauchi	181
4.60b	Path attenuation at 0.01% ITU R rain rate prediction at Bauchi	182
4.61a	Path attenuation at 0.01% measured rain rate exceedance at Jos	183
4.61b	Path attenuation at 0.01% ITU R rain rate prediction at Jos	184
4.62a	Path attenuation at 0.01% measured rain rate exceedance at Minna	185
4.62b	Path attenuation at 0.01% ITU R rain rate prediction at Minna	186
4.63a	Path attenuation at 0.01% measured rain rate exceedance at Yola	187
4.63b	Path attenuation at 0.01% ITU R rain rate prediction at Yola	188

4.64a	Path attenuation at 0.01% measured rain rate exceedance at Ogbomosh	189
4.64b	Path attenuation at 0.01% ITU R rain rate prediction at Ogbomosh	190
4.65a	Path attenuation at 0.01% measured rain rate exceedance at Kano	191
4.65b	Path attenuation at 0.01% ITU R rain rate prediction at Ogbomosh	192
4.66	Derived path attenuation for 40 GHz frequency bands at 0.01%	194
4.67	Derived path attenuation for 45 GHz frequency bands at 0.01%	195
4.68	ITU predicted path attenuation for 40 GHz frequency bands at 0.01%	196
4.69	ITU predicted path attenuation for 45 GHz frequency bands at 0.01%	197
4.70	Contour Mapping of Path Attenuation at 0.001% rain rate Exceedance for 40GHz Frequency band in Nigeria	204
4.71	Contour Mapping of Path Attenuation at 0.01% rain rate Exceedance for 40GHz Frequency band in Nigeria	205
4.72	Contour Mapping of Path Attenuation at 0.1% rain rate Exceedance for 40GHz Frequency band in Nigeria	206
4.73	Contour Mapping of Path Attenuation at 1% rain rate Exceedance for 40GHz Frequency band in Nigeria	207
4.74	Contour Mapping of Path Attenuation at 0.001% rain rate Exceedance for 45GHz Frequency band in Nigeria	208
4.75	Contour Mapping of Path Attenuation at 0.01% rain rate Exceedance for 45GHz Frequency band in Nigeria	209
4.76	Contour Mapping of Path Attenuation at 0.1% rain rate Exceedance for 45GHz Frequency band in Nigeria	210
4.77	Contour Mapping of Path Attenuation at 1% rain rate Exceedance for 45GHz Frequency band in Nigeria	211
4.78	Path attenuation for horizontal polarisation at 31.8 GHz and 20 km path length in Derived Savanna zone	213
4.79.	Path attenuation at horizontal polarisation at 31.8 GHz and 20 km path length in humid forest zone	214
4.80	Path attenuation at horizontal polarisation at 31.8 GHz and 20 km path length in Northern Guinea Savanna	215
4.81	Path attenuation at horizontal polarisation at 31.8 GHz and 20 km path length in the mid altitude savanna zone	216
4.82	Path attenuation at horizontal polarisation at 31.8 GHz and	

	20 km path length in the Southern Guinea Savanna zone	217
4.83	Path attenuation at horizontal polarisation at 31.8 GHz and 20 km path length in the Sudan Savanna zone	218
4.84	Path attenuation at horizontal polarisation at 33.4 GHz and 20 km path length in the Humid Forest zone	219
4.85	Path attenuation at horizontal polarisation at 33.4 GHz and 20 km path length in humid forest zone	220
4.86.	Path attenuation at horizontal polarisation at 33.4 GHz and 20 km path length in northern guinea Savanna	221
4.87	Path attenuation at horizontal polarisation at 33.4 GHz and 20 km path length in the mid altitude savanna zone	222
4.88	Path attenuation at horizontal polarisation at 33.4 GHz and 20 km path length in the Southern Guinea Savanna zone	223
4.89	Path attenuation at horizontal polarisation at 33.4 GHz and 20 km path length in the Sudan Savanna zone	224
4.90	Contour Mapping of Path Attenuation at 0.001% rain rate exceedance for 31.8 GHz Frequency band in Nigeria	231
4.91	Contour Mapping of Path Attenuation at 0.01% rain rate exceedance for 31.8 GHz Frequency band in Nigeria	232
4.92	Contour Mapping of Path Attenuation at 0.1% rain rate exceedance for 31.8 GHz Frequency band in Nigeria	233
4.93	Contour Mapping of Path Attenuation at 1% rain rate exceedance for 31.8 GHz Frequency band in Nigeria	234
4.94	Contour Mapping of Path Attenuation at 0.001% rain rate exceedance for 33.4 GHz Frequency band in Nigeria	235
4.95	Contour Mapping of Path Attenuation at 0.01% rain rate exceedance for 33.4 GHz Frequency band in Nigeria	236
4.96	Contour Mapping of Path Attenuation at 0.1% rain rate exceedance for 33.4 GHz Frequency band in Nigeria	237
4.97	Contour Mapping of Path Attenuation at 1% rain rate exceedance for 33.4 GHz Frequency band in Nigeria	238

## APPENDICES

Appendix		Pages
1	Annual Accumulated Rainfall at the Sites	259
2	Cumulative distribution function (CDF) of rain rates based on different integration times	261
3	Annual cumulative distribution rainfall rates over study locations	263
4	Time Series of rainfall rate during rain events	266
5	Scatter Plots of rainfall Events	271
6	Cumulative rainfall rates Vs ITU-R estimate	274
7	Deduction of worst months	276
8	Relationship between Annual and Worst Month Rainfall Rate	278
9	Power law relationship between rainfall rates across all the stations	280
10	Specific attenuation by rain at 0.01% of time	282
11	Prediction models path attenuation exceedance at 0.01%	288
12	Rain Rate Prediction Models	290
13	Frequency allocation Tables by ITU to the Nigerian Communications Commission and the usage	297
14	Computations of Path Attenuation at 150GHz Frequency Threshold	300

## **ACRONYMS AND ABBREVIATIONS**

DSD – Drop Sizes Distribution  
LG – Lavergnat and Gole  
NCC – Nigerian Communications Commission  
CAR – Centre for Atmospheric Research  
RN – Radio Navigation  
TB – Tipping Bucket  
FS – Fixed Service  
ITCZ – Inter tropical Convergence Zone  
RA – Radio Astronomy  
FCC – Federal Communications Commission  
EESS – Earth Exploration Satellite Services  
SR – Space Research  
IITA – International Institute of Tropical Agriculture  
ISS – Inter Satellite Service  
ESA – European Space Agency  
COST – Cooperation on Scientific and Technical Resresearch  
NIMET – Nigerian Meteorological Agency  
TRMM – Tropical Rain Measuring Mission  
GPCP – Global Precipitation Climatology Project  
WCRP – World Climate Research Program  
TRODAN – Tropospheric Data Acquisition Network  
AWH – Average Worst Hour  
AWM – Average Worst Month

## CHAPTER ONE

### INTRODUCTION

#### 1.1 Research background

The pressing need for developing diversities of communication systems in order to satisfy the yearnings of telecommunication companies pushed scientists and engineers to explore for the potential use of the higher frequency bands (microwave and millimeter wave) of the electromagnetic spectrum (Karmakar *et al.*, 2010). The preference for these bands is premised on the availability of large bandwidth, higher channel capacities, high speed data transmission, miniaturized device size (antenna with other equipment) and expanse in the availability of spectrum (Owolawi *et al.*, 2009, 2012; Ramakrishna and Punyaseshudu, 2014). Millimeter wave also called mm wave or Extremely High Frequency (EHF) is the highest radio frequency band in practical use (Figure 1.1), it is the next band above microwave or Super High Frequency (SHF) and lies between 30-300 GHz of the electromagnetic spectrum. It corresponds to wavelengths of 1 to 10 millimeters and is characterized by narrow beamwidth, wide bandwidth spectrum and high frequency re-use potential (Shafi *et al.*, 2018; He and Huang, 2019; Chittimoju and Yalavarthi, 2021). When compared to microwaves (cm), mm Waves have considerably broader bandwidths, small component/subsystem sizes, light weight, reduced multipath effects, reduced vulnerability to jamming, better sea clutter operability and selective atmospheric attenuation (Rao, 2010; Al-Samman *et al.*, 2020). With the increase in spectrum occupancy and higher bandwidth demand to accommodate complex radio access network evolution, the need to explore the merits of millimetric wave band has become imperative.

Millimeter wave is an ideal candidate for certain applications such as provision of higher data rates in supporting applications such as Internet calls (Voice-Over-IP),

local network remote access, inter- active audio-visual conferencing, wireless internet access of high speed, multimedia information broadcasting and file transfer (Qamar et al., 2021; Karipidis, 2021). The mm wave communication links that are densely packed hence provides communication transmissions increased security and efficiency in spectrum utilization (Chittimoju and Yalavarthi, 2021). The utilization of millimeter wave frequency bands will also permit telecommunication operators to increase traffic and ultimately reduce telecommunication costs.

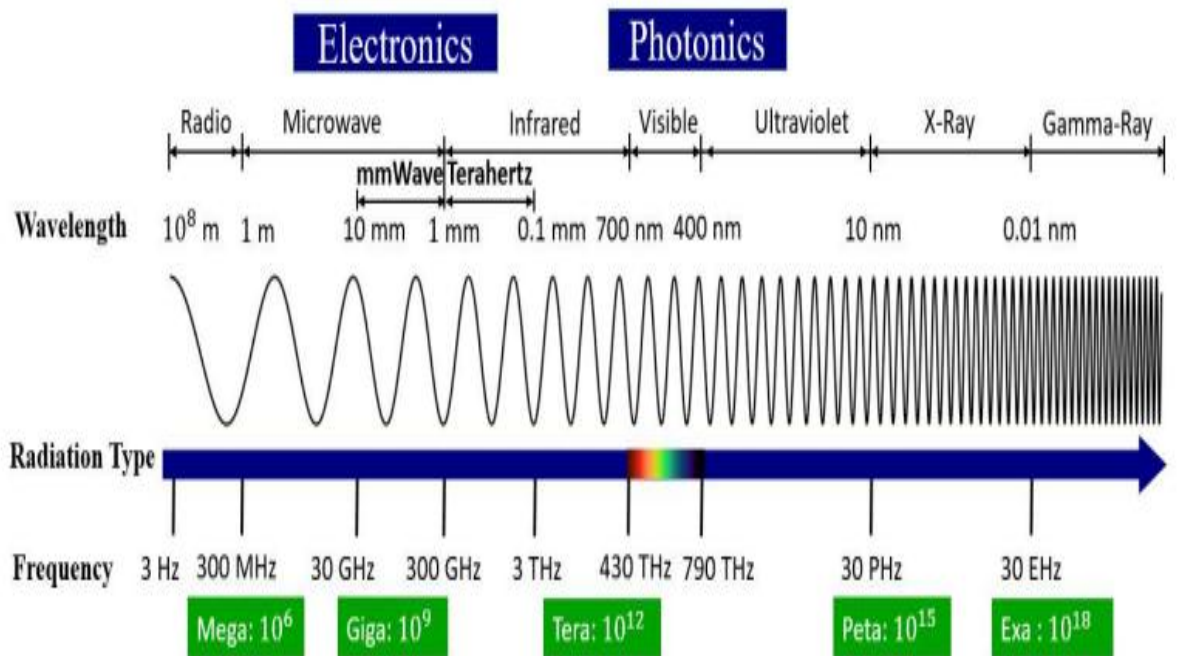


**Figure 1.1.** Electromagnetic spectrum and applications  
(Source: Rappaport, 2019)



With the available wide bandwidth, millimeter wave equipment is capable of achieving 10 Gbps full duplex capacities. This bandwidth is far beyond the capability of lower radio frequencies wireless technologies. The availability of this extraordinary amount of bandwidth enables the capability of radio propagation engineers to scale millimeter wave wireless links up to 10 Gbps as demanded by market needs. As the demand increases for higher capacity links, Millimeter wave technology is designed to meet the increasing demand for higher capacity links by using more efficient modulation schemes (Prasanna, 2008).

Millimeter wave (mm) wireless communication systems that operate on terrestrial paths constitute a crucial telecommunication infrastructure. This is due to the congestion at the lower frequency bands occasioned by the escalating number of competing telecommunication services (Fashuyi, 2006; Vclav *et al.*, 2010). With the large bandwidth availability, mm wave offer higher data transmission capacity when compared to other systems that operates in the lower frequency bands. Therefore radio communication systems designed to operate at frequencies greater than 30 GHz will be of more frequent use in the future (Juneja *et al.*, 2021).

In general, the performance of all radio systems is related to the propagation of electromagnetic waves from transmitters to receivers.

Weather conditions influence the transmission of millimetre waves through the lower troposphere. At the millimetre wave frequency bands, attenuation by rain is considered the most crucial limiting factors that impairs the performance of fixed terrestrial wireless systems (Lam *et al.*, 2017; Rappaport *et al.*, 2017; Shrestha and Choi, 2017; Shayea *et al.*, 2018; Singh *et al.*, 2018; Abayomi *et al.*, 2019).

Rain induced attenuation is the main constraint in the atmosphere on the distance coverage of communication systems (Ippolito, 1986; Pratt *et al.*, 2003). The severity of rainfall impairments is more predominant in the equatorial and tropical climates which are characterized by rainfall events that are intense with larger raindrop sizes (Ajayi *et al.*, 1996; Nandi and Maitra, 2019). According to Prasanna (2008), the rainfall characteristic of the location of millimeter wave link deployment determines its percentage availability. The wide variation between the nature of precipitation in the temperate regions and that of the tropics, and the lack of reliable rain study at the tropics is the major reason why the models from rain studies in temperate climates have been inappropriate in the design of systems for the tropical regions (Bryant *et al.*,

1998; Ajayi *et al.*, 1996). The study of the rain attenuation phenomenon in Nigeria is therefore imperative for millimetre wave terrestrial wireless communication systems efficient planning and utilization (Vclav and Martin, 2010).

## 1.2 Problem Statment

Rain hampers radio signals propagated at millimeter wavelength adversely through scattering and absorption (Kestwal *et al.*, 2014). This attenuating effect determine how much of the transmitted signal actually makes it to a receiver and how much of it gets lost in the atmosphere. This development, as opined by Shrestha and Choi (2017) severely limits the coverage distance of radio systems deployed on line-of-sight in the millimetric spectrum region. Snow, Rain, humidity, hail, fog, oxygen as well as other gases present in the atmosphere (also called hydrometeors) absorb and scatter radio waves at millimetric frequency band (Hogg *et al.*, 1975; Doble, 1996). According to Ramakrishna and Punyaseshudu (2014), rain is the most serious form of hydrometers which produces large displacement current because of its high dielectric constant. Lin and Chen (2001) submitted further that in consideration of the adverse atmospheric effects on radio wave propagation, attenuation rain is the primary cause.

Rain causes loss of propagating signal through its absorption, scattering and depolarisation of radio waves (Adimula, 2003; Omotosho *et al.*, 2009). The adverse effect of rain on the quality of radio links makes it a critical factor for consideratrion during satellite and terrestrial links system deployment. Communication links reliability, availability and performance is adversely affected by the absorption and scattering of radio signals by rain which causes a decrease in the amplitude of the propagated signal (Sarkar, 1998; Ojo *et al.*, 2008, Shrestha *et al.*, 2019). Rain induced attenuation decreases the path length over which reliable radio communication systems can be established (Semire *et al.*, 2011). Moreover rain causes differential attenuation, differential phase shift of the signal leading to cross talk (Okamura and Oguchi, 2010).

The major challenge confronting engineers working on higher frequency bands is the attenuating effects of rain on radio waves and bandwidth availabilities (Rafiqul *et al.*, 2012). Most of the millimetric system designs are done in temperate climates by the use of data that are based on ice crystal precipitation. According to Bryant *et al.* (1998), the nature of precipitation in the temperate regions varies widely from that of the tropics. Furthermore, rain drop size distribution is usually larger in the tropics

hence  $^{\circ}\text{C}$  isotherm heights at the tropics is greater than that at the temperate regions. Hence, systems designed in the temperate regions are unsuitable for the tropics.

Rainfall of integration time of 1-minute or less is scarce. In the tropical regions such as Nigeria, this development restrains the study of communication systems rain induced impairments (Olurotimi and Ojo, 2014). The lack of reliable telecommunication rain study at the tropics and the sole dependence on the deductions from the temperate climate underscores the imminent failures of millimetric systems in the tropics. This limits the implementation of reliable millimetric systems in commercial scales in the tropics and will ultimately hamper the deployment of the 5G network in Nigeria (NCC, 2018)

### **1.3 Justification of the study**

Many organizations have been deeply concerned by the paucity of reliable data on rain measurement from the tropics for verification and modelling of propagation impairment on communication systems and these includes among others: European Cooperation in Scientific and Technical (COST), the European Space Agency (ESA) and the International Telecommunication Union (ITU). This has been necessitated by the peculiarity of the prevailing rainfall events in the tropical regions which as opined by Ajayi *et al.* (1996) that rain in the tropics are more intense, more frequent and are of larger drops as against what obtains in temperate climates. Though a methodological approach has been developed by the ITU-R (Radio Communication Sector of the ITU) which is useful for radio signal attenuation prediction due to rain on any terrestrial paths, however, in the tropical climate, the ITU-R model does not perform well because of its dependence on temperate climates based data (Mello *et al.*, 2007).

The works of Moupfouma and Martin (1995) have shown that ITU-R method is not appropriate for the tropical climate. The Global Precipitation Climatology Project (GPCP) and Tropical Rain Measurement Mission (TRMM) is another significant exertion towards harnessing more information to improve dependable rainfall attenuation in the tropics. As averred by Ojo *et al.* (2008) apart from the fact that these platforms are satellite based, the data available from these projects are unemployable directly in the design of systems, due to their long integration time. In Nigeria, the Nigerian Meteorological Agency (NIMET) harbours the largest database of rainfall data in the country. The long integration time of their data, makes it unsuitable for rain attenuation modelling.

Furthermore, several authors such as Uzunoglu *et al.* (1977); Crane, (1980), (1996); Lin and Chen, (2002); Adimula, (2003); Adimula, (2005); Ojo, (2008), (2014); Omotoso *et al.* (2009); Semire, (2011); Oluwadare *et al.*, (2012); Agber and Johnson, (2013) and ITU-R 530-17, (2017) have proposed several methods (which range from empirical to theoretical) for rain attenuation prediction peculiar to the tropics. While the vast majority of these authors concentrated on impairments of radio wave signals by rainfall on microwave frequencies and earth-space path, others used theoretical modelling due to paucity of data. Yussuff and Nor (2014) carried out study on model for rain attenuation prediction of mm wave on earth-satellite path for Lagos.

This research differs from the scope of previous studies as it addresses rain attenuation of radio links on terrestrial paths across all the eco-climatic zones of Nigeria (savanna, rain forest and mid altitude Savannas) at millimeter wave bands. To achieve this aim, 5-minute integration time rainfall data from the Centre for Atmospheric Research in Nigeria (CAR) database – tagged Tropospheric Data Acquisition Network (TRODAN) which was established in 2007 was employed. TRODAN was designed to monitor the lower atmosphere from the surface of the Earth to a height of 11km above sea level. Other 5 minute integration time data that was used were obtained from the rainfall database of Bowen University Iwo, Osun State Nigeria. The International Institute of Tropical Agriculture (IITA) and Federal University of Technology Akure (FUTA) Nigeria provided one minute integration time rainfall data. This was used for the validation of existing rainfall rate prediction models; hence appropriate model for Nigeria was deduced.

The present research uses 1-minute rainfall rate cumulative distribution with respect to the average worst month and year. It was however extended to cover the mean of the worst hour cumulative distribution of the rainfall rate. Olurotimi and Ojo (2014) seems to be the only researcher that considered the concept of the average worst hour, howbeit only in two stations (Lagos and Akure) in South Western Nigeria. Furthermore, as against the common use of Moupfouma (1985) method, Moupfouma and Martins (1995) method as well as Chebil and Rahman (1999) power law by most scientists with bias on radio propagation studies, in this research, we have employed the Lavergnat and Gole - LG (1998) model for the determination of rainfall rate distribution. As averred by Ito and Hosoya, (2006), almost every other model are derived through experiments, hence the need to exercise caution during their

application to different locations with varied intergration times. The LG model has reliable theoretical background and the major overriding merit of this model is its accommodation of arbitrary integration time conversions (Ito and Hosoya, 2006).

#### **1.4 Study aim and objectives**

The aim of this study is to estimate and model rain induced attenuation at millimeter wave frequency bands on terrestrial paths over some selected locations in Nigeria.

The specific objectives of this study are to:

1. characterise rainfall patterns in terms of diurnal and seasonal variation over the period under review;
2. deduce power law regression coefficients for each of the locations under study;
3. make comparison with existing rain conversion models and propose a suitable model that will be applicable to each of the location under study; and
4. estimate rain induced attenuation at different percentages of occurrence on terrestrial paths over the study locations.

## CHAPTER TWO

### REVIEW OF LITERATURES

#### 2.1 Tropical rainfall pattern

Rainfall pattern is non homogeneous both in terms of time and location. The non homogeneity varies diurnally, seasonally and yearly (Ajayi, 1996). The movement of the Inter Tropical Discontinuity (ITD) determines the rainfall structure of any location and the seasonal weather patterns in the tropics (Ojo *et al.*, 2014). The Inter Tropical Convergence Zone (ITCZ) variations determine the position of the ITD.

Some researchers (Simpson, 1949 and Chalmers, 1967) have classified rain events as either showers (if the duration is less than one hour) or continuous (if the duration is in excess of one hour). Each type of rain was further classified as either thundery or quiet depending on whether or not the effect was accompanied by lightening discharges (Oladiran, 1976). Owolawi *et al.* (2009) further classified rainfall into three kinds namely stratiform rain, convective rain, and all the rain, such as monsoon, that is not included in the above categories. According to Moupfouma, (1987), rain is broadly classified into two major categories, convective and stratiform rain, although smaller sub divisions are found in literatures such as thunderstorm, shower, widespread and drizzle which constitutes tropical rainfall types (Adimula, 2003). Other researchers in the tropics and sub-tropics such as Mandeep *et al.* (2007) classified rain into four categories: these are stratiform rain, convective rainfall, the Monsoon precipitation rainfall and the tropical storm.

Convective rain is brought about by zero degree Celsius isothermal cloud formation. The effect of the tropospheric pressure leads to strong movement of the air masses. Water droplets are formed at the course of the movement of the air masses; these drops increases in size until gravity precipitates them and this results in convective heavy rain. Convective rain is characterized as shor

duration rainfall covering a small area with high rain rate. This fact is expressed by the so-called area-depth curves (Weible *et al.*, 1967) as shown in Figure 2.1. Stratiform rain is low rain rate that covers widespread regions of several kilometres and exceeds one hour (Mandeep and Allnut, 2007). Monsoon rainfall constitutes a sequence of admixture of convective precipitation and stratiform precipitation intervals. Tropical storm precipitation coverage exceeds 100 km with the possibility of intense convection regions. As reported by Joss *et al.* (1968) and Adimula, thunderstorm and shower are classified as convective rain types whereas widespread and drizzle are classified as stratiform. Drizzle distribution constitutes rainfall of about 5.0 mm/h maximum intensity and drop order of 1.0 mm while widespread distribution refers to rainfall of 50 mm/h maximum intensity and raindrops of 1.0 mm and 3.5 mm diameter range. Shower rainfall is of maximum intensity of 150 mm/hr; it lasts for a short time and is made up of extremely few rain drops with a diameter of about 2.0 mm. Thunderstorm distribution deals with rainfall of about 210 mm/h intensity with large number of raindrops that are greater than 3.0 mm.

However, according to Oladiran (1976), radius of rain drops does not vary much for different types of rain. As averred by Oladiran (1976), Ette *et al.*, (1980), mean drop radius of continuous rain events is in the order of 0.61 m while 0.60 m is the mean radius of all other types of rain. According to Oladiran (1976), the estimate of minimum value of drop radius from measurements in a tropical region was 0.152 m while computation based on Best (1950a) equation put the drop radius at 0.60 m. According to Obiyemi *et al.* (2014), rainfall distributions are classified as follows: Drizzle rainfall ( $0 < R \leq 5$ ) mm/hr, widespread rainfall ( $5 < R \leq 10$ ) mm/hr, showers rainfall ranges from 10 mm/hr to 40 mm/hr while thunderstorm rain constitutes rainfall rate greater than 40 mm/hr.

According to Adimula (2003), rain in the tropics in most cases occur as a complex mixture of convective and stratiform rain in the form of cell; however, most of the rain is convective in nature and this accounts for about 70% of the total rain in the tropics (Adimula, 2003). Stressing further, convective type of rain, often encountered in the tropical region, is a much localized time and space phenomenon, contrary to the stratiform rain which is normally dominating in the temperate regions. Das *et al.* (2013) stressed further that the pattern of rainfall that takes place in the tropics varies diurnally and it depends on the variations of atmospheric aerosol and

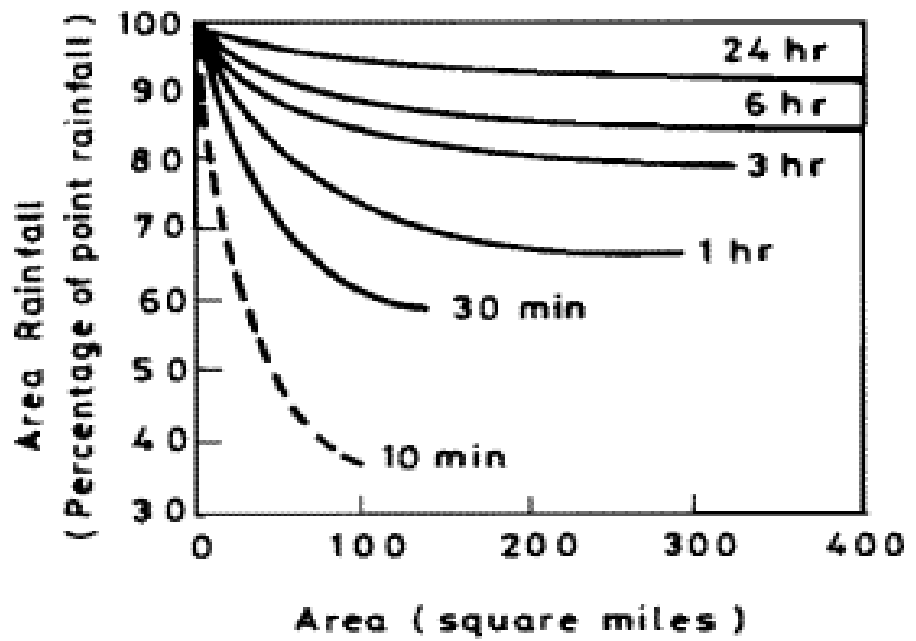


**Figure 2.1.** Typical area depth rainfall curve (Source: Hassan *et al.*, 1985)



temperature in this region. Furthermore, Moron *et al.* (2020) stressed the predominant convective nature of tropical rainfall and the challenging seasonal-to-seasonal prediction. As deduced from the works of Ibe *et al.* (2010), there is a positive correlation (0.199) between rainfall and temperature throughout the country, also the coastal areas experiences annual rainfall variation as high as 4.0407 mm per annum which proposes that the nation is at the very edge of global warming and the coastal regions are the most vulnerable.

Irrespective of the type of precipitation, the existence of cells of variable structure that depends on space and time, characterizes rainfall and the cells move on a level plane with speed contingent upon the winds of the troposphere and the clouds heights (Joss *et al.*, 1968). Rain cell can be defined as a region of locally intensified precipitation. Some investigators defined them as small regions of increased reflectivity (3 dB down the peak contour). Others defined it as the areas of reflectivity enclosed within fixed contours (Segal *et al.* 1978). As shown in Figure 2.2, the cell diameter/size generally decreases with increasing rain rates (Freeman, 1981). Rain cells possibly cover from about one kilometre to several kilometres of the path during the rainfall period. According to Yussuff and Nor (2012), the structure of rain cells can assume various shapes. For instance, for small, medium and large size rain cells it is admitted to be spherical, oblate spheroidal or oblate distorted respectively.

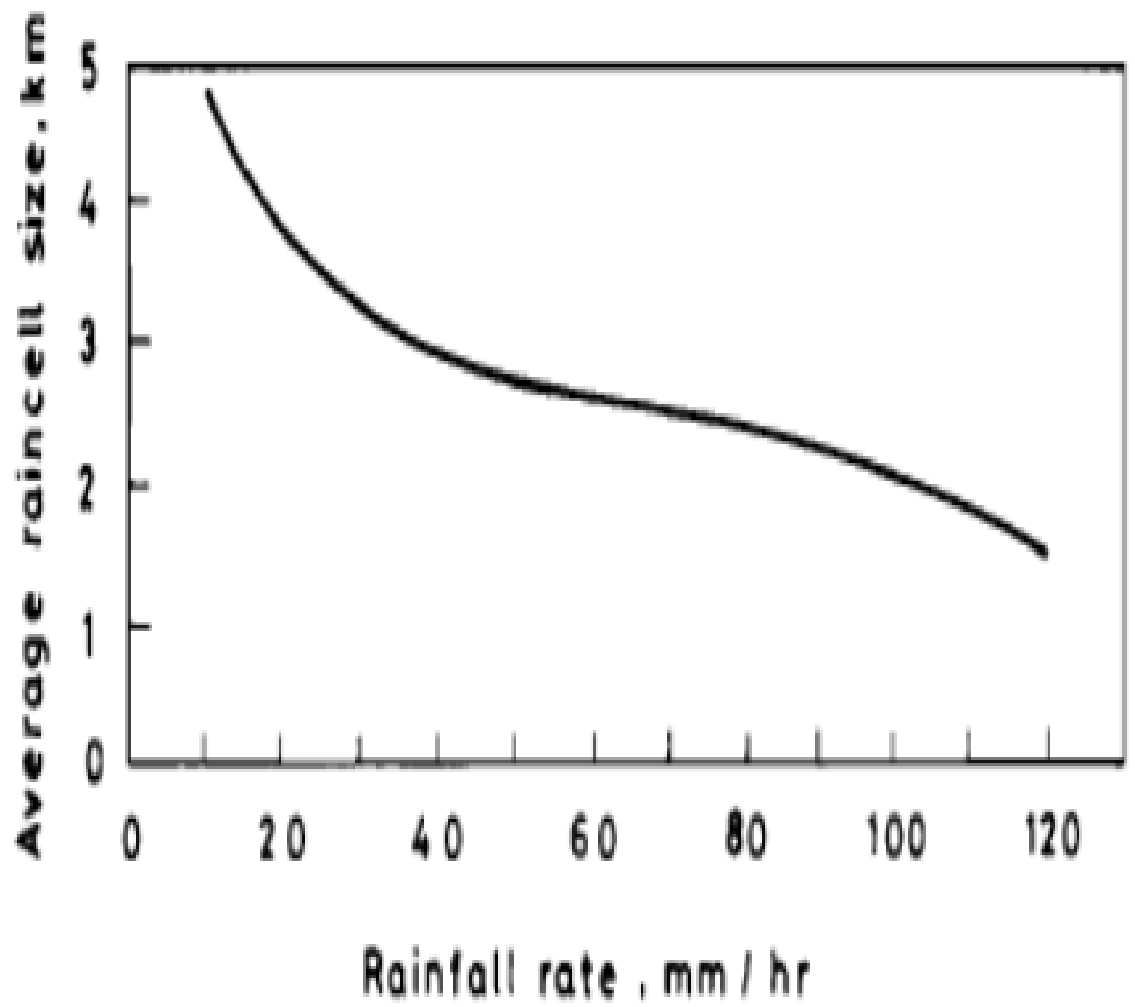


Figure 2.2. Influence of rain cell size on rain rate (Source: Hassan *et al.*, 1985)

## 2.2 The Nigerian climate

Nigeria lies within the tropical zone and enjoys a tropical humid-climate, which is dominated by West African monsoon system. Nigeria experiences two seasons: in the south, the wet season is between March and October, while the dry season starts from November to February of the following year. In the northern part of the country, the wet season starts in May and ends in early November, while the end of November heralds the onset of dry season which terminates in May. In Nigeria, during the wet season there is usually heavy rainfall and the Inter-Tropical Convergence Zone (ITCZ) moves across the country during this period (Ojo and Falodun, 2012). The rainfall is known to be dominated by the convective type and it occurs in short time spell over shorter distances.

In the wet season, moisture-laden south westerly wind from the Atlantic brings cloudy and rainy weather. In the dry season, the dry north easterly winds from the Sahara (harmattan) bring dusty and cold weather. The prevalence of these alternating winds over the country influences the movement of the ITCZ north and south of the equator (UNDP, 2006).

However, in various regions of Nigeria, there are wide variations in climate and these are determined by topographic relief. During the rainy season, seasonal mean temperatures are consistently lower throughout Nigeria than in the dry season, and there is little variation from the coast to inland areas. The wettest month in Nigeria is June in the Southern part and the wettest area is the east coast, parts of which receive over 4000 mm rainfall annually. Regions along the coast in western part receive about 1800 mm rainfall annually. This amount decreases to between about 500-1000 mm in central and northern Nigeria (UNDP, 2006).

The Southern part of Nigeria experiences extended period of rain which commences in March and continues till July ending; the rain peaks in June in this zone. In August there is a short break in rainfall (dry season) and this lasts for about 2-3 weeks (Adeyemi *et al.*, 2004). A brief wet season which commences in September to middle of October succeeds the August break but the wet season peaks at the end of September. Long dry season sets in during late October to early march and this season peaks in early December till late February; this is referred to as harmattan condition (Adeyemi *et al.*, 2004).

In the northern part of Nigeria, the seasons witnessed is limited to two, that is, wet season which lasts for a short duration from the month of May to early November and this is succeeded by an extended period of dry season which stretches from November to May (Emmanuel *et al.*, 2013).

### **2.3 Rainfall measurements at a point**

The instrument designed to capture the rainfall amount reaching the surface of the ground during a storm is referred to as rain gauge. Rainfall measurements are usually provided in units of water depth (inches or millimeters). There are different types of rain gauges that can be classified into two main categories: non-recording gauges, and recording gauges (AMS Glossary, 2000). The non-recording gauges- are basic storage devices that measure the cumulative amount of rain. The major source of error with this gauge is evaporation and wetting losses, the magnitude of which depends on temperature, humidity and time between rain and collection of measurement. Unlike non-recording gauges, a recording gauge is designed to automatically record the amount of rainfall reaching the surface of the raingauge which is as a function of time during the lifespan of a storm. The most common types of recording gauges are the tipping bucket, weighing and optical rain gauge (AMS Glossary, 2000). Calibration error and possible electrical and mechanical breakdown are some of the sources of error.

Rainfall changes rapidly at a point, hence the integration (sampling) time of raingauge used determines the observed cumulative rainfall intensity distribution at any given time (Mandeep *et al.*, 2006). The most popular type of the rainfall measuring instrument that is used by both the research and operational applications is the Tipping Bucket (TB) rain gauge; this gauge type can provide fairly accurate measurements at a relatively low cost (Habib *et al.*, 2010).A typical tipping bucket gauge is composed of a funnel that drains the water into a pair of joined buckets that are balanced in unstable equilibrium on a horizontal axis. When a pre-specified amount of rain has accumulated in the upper bucket, the buckets become unstable and tip over so that the other bucket starts filling. The movement of both buckets as they tip over excites an electronic switch to record the timing of each tip. The rain rate and accumulation can be determined from the timing and the number of the recorded tips (Habib *et al.*, 2010). However, at high rain rates a tipping-bucket gauge may suffer from underestimation problems due to the fact that the tipping buckets cannot keep up with

heavy rain during a severe thunderstorm. This gauges under-estimates rainfall at high intensities (>50 mm/h) (AMS Glossary, 2000). This may be curtailed by proper calibration and increase in raingauge networks at the location.

### **2.3.1 Rain gauge measurements error sources**

Like most meteorological sensors, rain gauge measurements are fraught with error sources. These rain gauge measurement errors are defined as the deviations of a measurement from the corresponding true value of rainfall that one attempts to determine, falling on the rain gauge collection area. A schematic classification of these errors is presented in Figure 2.3.

The wide use of data from TB gauges indicates the importance of understanding their measurement errors and their ability to capture the complex structure of the rainfall process. Several studies showed that TB gauge data are corrupted by errors, both random and systematic (Sevruk and Lapin 1993). The systematic error is the most significant source of error and includes losses due to wind, wetting, evaporation, and splashing. The wind-induced error, which is the largest component, has been extensively investigated using different methodologies ranging from field intercomparisons e.g. Sevruk and Hamon (1984) to the use of numerical simulation of the airflow around the gauge body e.g. (Nes̆por and Sevruk 1999).

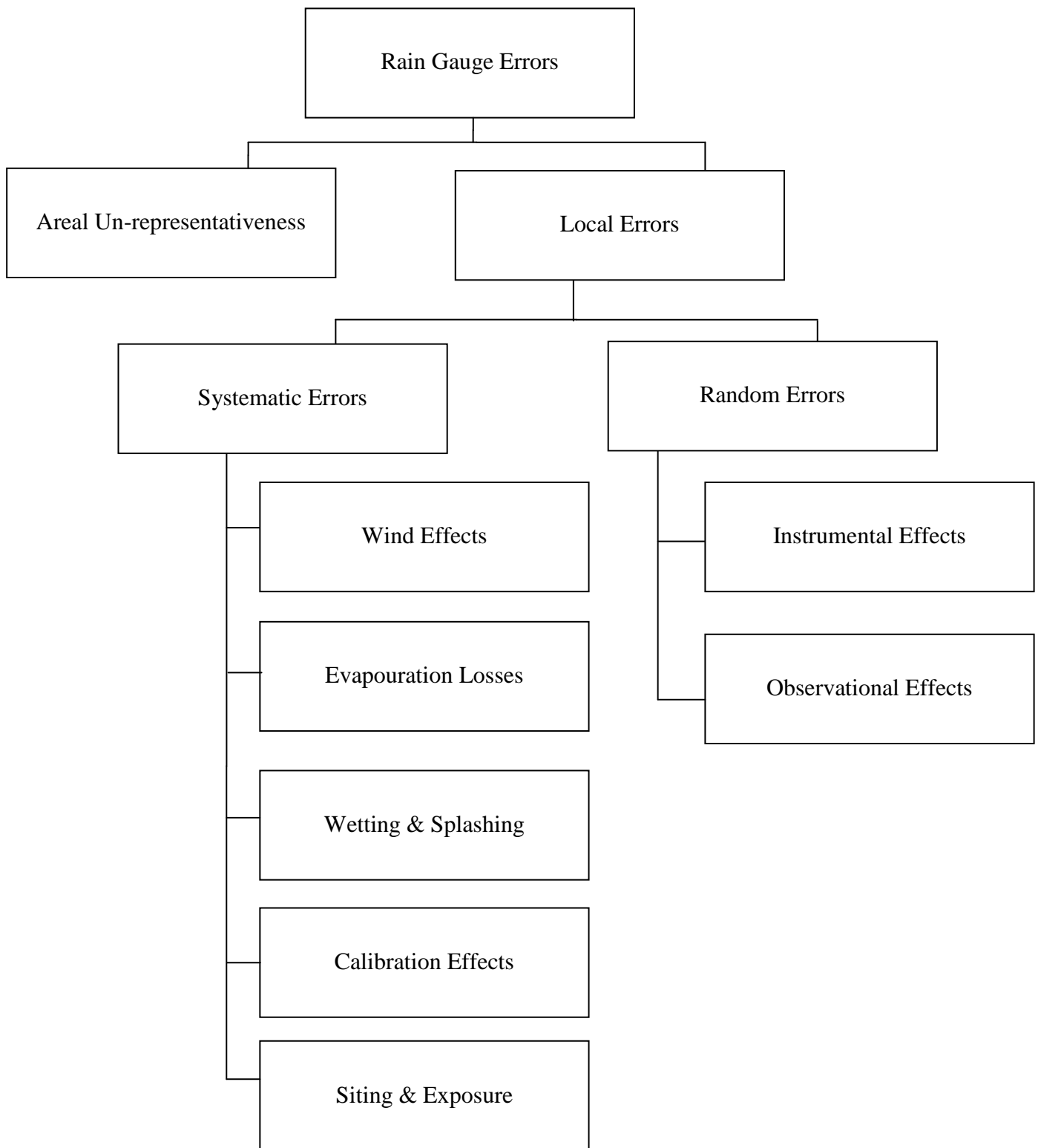


**Figure 2.3.** Classification of rain gauge measurement errors  
(Source: Habib *et al.*, 2010)

### **2.3.2 Wind-induced errors**

The elevation of most rain gauges above the ground causes the formation of wind eddies around the gauge orifice. These wind eddies reduce the capture of small rain drops and this problem is referred to as wind-induced gauge under-catch. This problem is considered as a serious and most common source of rainfall measurement errors. The most dominant factor in the environment that leads to precipitation undercatch is wind speed. Wind field deformation results from the measurement instrument, which provokes a blocking of air stream leading to higher wind speeds and a higher intensity of turbulences. The aerodynamic blockage of the gauge body causes the trajectories of precipitation particles to become distorted in a wind through the displacement and acceleration of wind flow over the top of the gauge. The lighter particles are carried beyond the gauge opening, which results in a reduced catch. The extent of the under catch depends on the wind speed, the falling velocity of the particles, and the aerodynamic properties of the individual type of gauge (Wagner, 2009).

The amount of loss due to wind field deformation varies with wind speed, form and size of precipitation and aerodynamic characteristics of the gauge (Sevruk 2004). The installation of wind shield around rain gauges can minimize wind effects.

## **2.4 Rain Rate Measurements**

High intense rainfall apart from being variable inter-annually, is hard to record. In any case, in system design, the highest rainfall rate is of great interest (Isikwue, 2003). During the analysis of rainfall attenuation, the prediction of rain rate is the main step (Tamosiunas, 2007). Rainfall is measured in millimeters (mm), and rain intensity (or rainfall rate) in millimeters per hour (mm/hr). Although the rainfall rate is presented in mm/hr, an important parameter is the integration time, i. e. the time between readings of the rainfall (Ivanov *et al.*, 2006). Sampling interval of rain gauged determines the rain rate distribution at a point. The peak of rainfall for a short period of time will be missed by rain gauge of high sampling interval. This will cause the rain gauge to underestimate the rain rate measured (Chun, 2013). Measurement of rainfall with high resolution rain gauge ranging from 1-2 minutes integration, as opposed to longer integration times measurements which fails to capture the peak values of rain rates, resolves rain cells which though small but are significant.

Rainfall meteorological data of 1-minute integration time from a locality is the requirement by most methods for attenuation prediction. One minute accumulation or averaging time removes the irregularities occasioned by the processes of rain gauge measurement but maintains the crucial geophysical differences (Crane, 1996). Due to limited availability of one-minute rainfall data in many cases, the methods of conversion of rainfall rate distribution over a long integration time such as one-hour, five-minutes and ten-minutes into the distribution for one-minute rate have been developed by Segal (1986), Burgueno *et al.* (1988), Chebil and Rahman (1999) and Emiliani *et al.* (2008) among others. These conversion methods were developed with the ITU-R 530-17 recommendations as well as the revised Moupfouma method for the deduction of terrestrial and satellite rain induced attenuation. In Nigeria, Ajayi *et al.* (1996), Semire *et al.* (2012) and Ojo *et al.* (2016) have made similar efforts at developing rainfall conversion methods. These methods of conversion of long integration time rainfall rate distribution are discussed thus:

#### 2.4.1 Segal Method (1986)

Segal method was developed from the rain data measured from Canada. The parameter  $P_{\tau}(P)$  was the converting factor useful for converting raingauge data with a higher integrating time  $\tau$  minutes to the 1-minute equivalence (Segal, 1986).

Traditionally in Segal (1986), one uses a conversion factor that depends on the probability of exceedance considered and on the integration time of raingauge:

$$\rho_{\tau(p)} = R_1(p) / R_{\tau}(p) \quad (2.1)$$

The equiprobable rainfall rate exceedances  $P$  for 1 and  $\tau$  integration times are represented by  $R_1$  and  $R_{\tau}$  are. Equation (2.1) is the power law representing  $\rho_{\tau}(p)$ :

$$p_{\tau}(p) = a \cdot p^b \quad (2.2)$$

where  $a$  and  $b$  are rain rate coefficients for different integration times over the range  $0.001\% \leq p \leq 0.03\%$ .

$\rho_{\tau}(p)$  is a conversion factor used for obtaining the equivalent 1- minute rainfall rate of a rain gauge having a cycle (integration) time of  $\tau$  minutes.



### 2.4.2 Falvin (1981)

Falvin (1981) examined the cumulative distribution of effective 6 and 1-minute rainfall rate across locations in Canada, United States, Europe and Australia respectively and these are the relation:

$$R_1 = 0.990R_6^{1.054} \quad (2.3)$$

where  $R_1$  is 1-minute rainfall rate,  $R_6$  is 6 minutes equiprobable rain rate.

### 2.4.3 Burgueno *et al.* Method (1988)

Burgueno *et al.*, (1988) used a Jardi raingauge for the rain data collection in Barcelona, Spain. The direct power law between rain rates of  $T$ -min to 1-min was the conversion principle that was used and it is stated as:

$$R_1(p) = aR_T^b(p) \quad (2.4)$$

where  $R_T(P)$  and  $R_1(P)$  are the  $T$ - and 1-min rainfall rates integration times with  $P$  as the occurrence probability at regression coefficients  $a$  and  $b$ .

### 2.4.4 Chebil and Rahman (1999)

Chebil and Rahman method used rainfall measurement in Malaysia to modify Segal method. The conversion factor in equation (2.5) was used to represent the relationship as shown (Chebi, 1999):

$$\rho_{60}(p) = R_1(p)/R_{60}(p) \quad (2.5)$$

where  $\rho_{60}(P)$  implies the combined exponential -power Law expression

$$\rho_{60}(p) = ap^b + ce^{(dp)} \quad (2.6)$$

Equation (2.6) is the expression for the combined exponential power law. Here,  $p$ ,  $R_1(P)$  and  $R_{60}$  are the probability of occurrence for rain rate of 1-min and 60-min rain rate respectively while the constants  $(a, b, c, d)$  stands for the regression coefficients.

### 2.4.5 Joo *et al.* method (2002)

Rain data of Korea are measured by optical rain gauge and is used by Joo to develop the conversion method as follow (Joo, 2002):

$$p_1 = ap_{\tau}10^{[bexp(-t/24.28)]} \quad (2.7)$$

The Parameters  $P_{\tau}$  and  $P_1$  = probability of rainfall rate occurrence at  $\tau$ .minute and 1-minute respectively, while the integration time (min) is represented by  $t$  and the regression coefficients are  $a$  and  $b$ .

This model as well as almost all others are derived experimentally, hence the need to exercise caution towards applying these methods to other locations and integration times that were not used to derive them (Ito *et al.*, 2006).

#### 2.4.6 Ajayi (1996)

According to this model, the relationship between two equi-probable rainfall rates (power law relationship) is stated as:

$$R_{\tau} = aR_T^b \quad (2.8)$$

where the rain rate is denoted by R and the required rain rate cycle/integration time and available rainfall rate cycle time is denoted by the symbols  $\tau$  and  $T$  respectively. The result obtained between 1 and 5 minutes rain rates cycle time applied to Ile-Ife. The relationship is given as:

$$R_1 = 0.99R_5^{1.098} \quad (2.9)$$

where  $R_1$  and  $R_5$  are the 1- and 5- min. equiprobable rain rates

#### 2.4.7 Semire *et al.* (2012)

Regression coefficients that were based on cumulative distribution function analysis of 2 years rainfall measurement at Ogbomosho, Oyo state, Nigeria by Semire *et al.* (2012), yielded power law as well as conversion factors. The work relied heavily on the conversion of  $\tau$  – minute integration time to  $T$ - minutes as described by Segal (1986).

$$p_{\tau}(p) = R_T / R_{\tau} \quad (2.10)$$

and

$$\rho_{\tau}(p) = a \cdot p^b \quad (2.11)$$

As well as the works of Ajayi *et al.* (1996) in which the conversion factor for 1-minute rainfall rate to n- minute rainfall rate is given as

$$R_{\tau} = a \cdot R_T^b \quad (2.12)$$

and this eventually yielded this power law relation for converting from 5 minutes to 1- minutes integration time:

$$R_1 = 0.99R_5^{1.098} \quad (2.13)$$

Semire *et al.* (2012) through her measurement at Ogbomosho for equiprobable rain

rates for 1, 5, 10, 15, 20, 30, 60 minutes integration times and by the transformation of (2.11) to logarithmic relationship:

$$\ln R_{\tau} = \ln a + b \ln R_T \quad (2.14)$$

The regression equation in terms of a and b was obtained by fitting the 1-minute data against all other integration times. The values of a and b was derived by plotting  $\log R_T$  against  $\log a$ . Table 2.1 shows the coefficients obtained:

**Table 2.1.** Integration time coefficients (Semire *et al.*, 2012)

Model	T (min)	a	b
Ajayi et al., (1996)	5	0.991	1.098
	15	-	-
	20	4.311	0.853
Semire et al (2012)	5	0.7972	1.195
	15	0.302	1.497
	20	0.1825	2.842

The slight difference in the regression coefficient between Ogbomosho and Ile Ife which are expected to have similar rainfall pattern was attributed to the drastic changes in climate (Semire *et al.*, 2012).

#### 2.4.8 Ojo *et al.* (2016)

Ojo *et al.* (2016) presented a dynamic and empirical model for the derivation of rainfall of higher integration to 1-minute integration time for a tropical location – Akure, Nigeria. An integration time of 10 seconds was averaged over intervals of 1, 5, 10, 30 and 60 minutes and comparison was effected with measured 1-minute rainfall rate at the site. These models were employed in the work:

Power Law (PL) model:

$$R_1(p) = aR_\tau^b(p) \text{mm/hr} \quad (2.15)$$

$R_1(p)$  and  $R_\tau(p)$  = Required and available 1-min and  $\tau$  – min rainfall rate respectively,  $p$  = rain rate percentage exceedance at regression coefficients  $a$  and  $b$  (Ajayi *et al.*, 1996).

Exponential model:

$$R_1(p) = c \exp^{dR_\tau(p)} \quad (2.16)$$

where  $c$  and  $d$  are the regression coefficients

Logarithmic model:

$$R_\tau(p) = e \ln(R_\tau) + f \quad (2.17)$$

where  $e$  and  $f$  are the regression coefficients.

Polynomial Model:

$$R_1(p) = gR_\tau^2(p) + hR_\tau(p) + i \quad (2.18)$$

where  $g$ ,  $h$  and  $i$  are the regression coefficients.

The function,  $P$ , the percentage of time of rain rate exceedance, was used to model the conversion factor by using power law of Segal (1986).

$$\rho_\tau(p) = R_1(p) / R_\tau(p) \quad (2.19)$$

where

$$\rho_\tau(p) = ap^b \quad (2.20)$$

Combining equation (2.18) and (2.19) gives the model

$$R_1(p) = ap^b R_\tau(p) \quad \text{mm/hr} \quad (2.21)$$

Where  $R_1(p)$  and  $R_\tau(p)$  are required 1- minute and available  $\tau$  – minute rainfall rate,  $P$  is the percentage of exceedance.  $\rho_\tau(p)$  is the conversion factor at  $\tau$  – minute while regression yielded the regression coefficients  $a$  and  $b$ . This method is analogous to the Segal model (Ojo *et al.*, 2016). In the performance analysis of the different models compared, Lavergnat and Gole model which is semi-empirical/ physical stochastic performs best over all integration times and climate regions (Ojo *et al.*, 2016). Hence, it was used for the conversion from the measured 5 to 1-minutes integration time.

## **2.5 Radio wave propagation on terrestrial paths**

The atmosphere is divided into different layers by the changes in temperature with heights above sea level. These layers are the troposphere, stratosphere, mesosphere and thermosphere. Upon examination, the atmosphere is found to be a complex system not a simple chemical nor even a compound, but a relatively stable mixture of a number of gases (Blair, 1957). The altitudinal changes in the layers of the atmosphere are as shown in Figure 2.4.

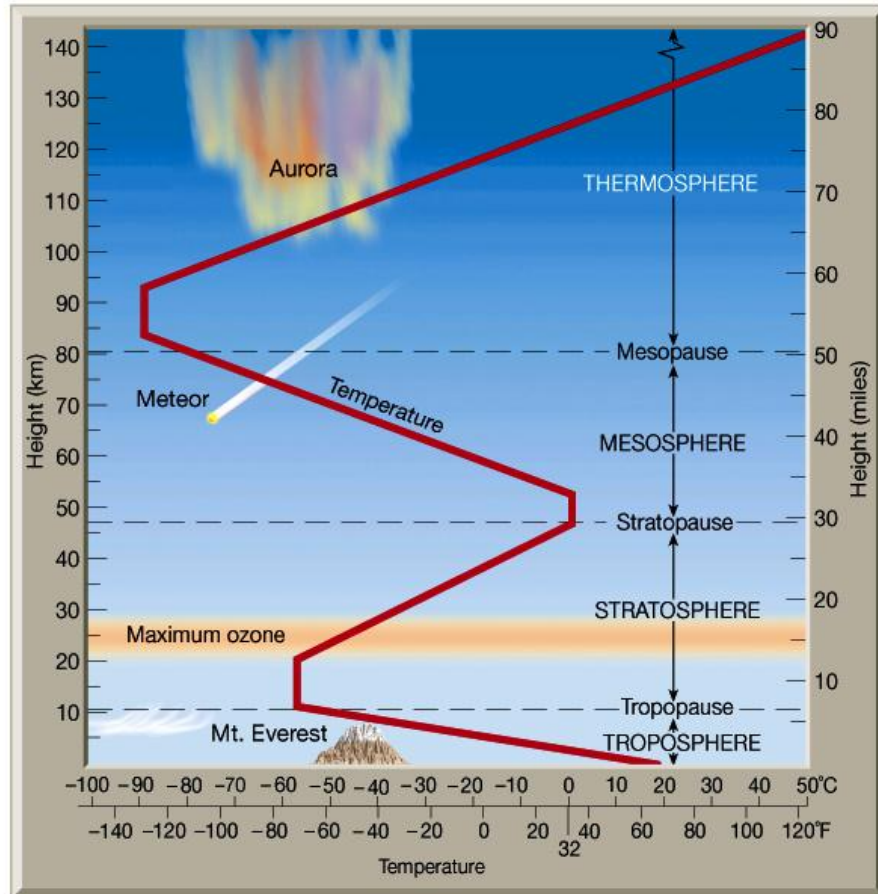


**Figure 2.4.** vertical profiles of the atmosphere  
(Lutgens and Tarbuck, *The Atmosphere*, 8th edition, 2013)

The lowest part of the earth's atmosphere is the troposphere. The average altitude from the surface of the earth 11 km and this can range as high as 16 km in the tropics to less than 9 km over the poles. This range is due to the temperature differences between the tropics and poles (Barry and Chorly, 1987; Hall *et al.*, 1996). The weather system of the earth which is confined in the troposphere experiences conditions of continual motion (Burrows, 1968) and the changes in conditions of the atmosphere such as temperature, pressure and humidity cause point to point variations on the refractive index of the air in this layer. The physical properties of this complex gaseous region are known to have considerable influence on a high-frequency wave propagation; the extent of the influence does not, however, appear to be clearly understood (Aloaba *et al.*, 2000). It is in this context that the troposphere assumes a vital role in the propagation of radiowaves. The meteorological conditions therefore influence the manner in which radiowave propagation occurs on spatial and temporal scale in the troposphere.

The presence of the troposphere in the link model for any Line-of-sight links will introduce five main effects (Panter, 1972). These are: Excess attenuation, depending on link length and slope, due to atmospheric gases (mainly oxygen and water vapour) and hydrometeors (rain, fog, hail, snow); Modification in the ray path shape which ceases to be a straight line and becomes curved, in response to the changes in the refraction index along the path; Creation of privileged directions for wave propagation (ducts) which enable signals to reach distances much larger away than would be possible without the atmosphere; Considerable variations in the maximum displacements of the received signal due to the existence of various signal paths, each with its own time delay, which interfere with each other and finally scattering due to irregularities in the higher layers of the troposphere which enable signals to reach very large distances (a few kilometers) and may be used to provide troposcatter links (Fashuyi, 2006). Hence, the troposphere has a crucial role to play in signal propagation on terrestrial and earth-space paths.

## **2.6 Millimeter wave propagation characteristics**

The propagation of millimeter wave through the atmosphere is a function of atmospheric constituents such as oxygen, humidity, fog and rain (Prasanna, 2008). The short wavelength of mmWave predisposes it to challenges that are technical in nature such as signal loss along the transmission path, vulnerability to obstacles and



directivity (Uwaechia *et al.*, 2020). There is growing interest in the use of mmWave for wireless communications over a short range; this mainly due to its large bandwidth which makes it ideal for cellular or fifth generation communications (Ahmed *et al.*, 2020; Etinger *et al.*, 2020).

Millimeter wave links contrasts from microwave links in the beam widths (Figure 2.5). While microwave links cast very wide beam widths which reduces the reusability of spectrum within a given eco-climatic area, the beam width of millimeter wave is very narrow and this enhances the implementation of multiple independent links in close proximity (Prasanna, 2008).

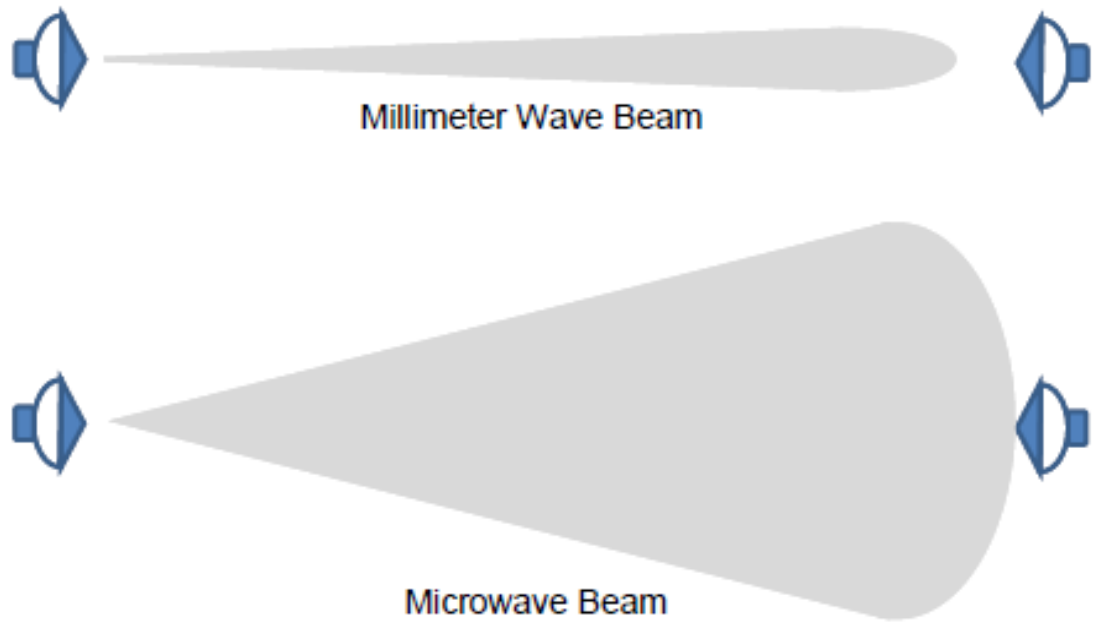


**Figure 2.5.** Millimeter wave Vs Microwave beam  
(Source: Prasanna, 2008)

A key usefulness of the millimeter wave links is the scalability of their deployments (Prasanna, 2008). The propagation characteristics of radio signals at the millimeter wave spectrum must be taken into account when planning for its use. As averred by Perlman (1995), the maximum propagation distance of millimeter wave is 20 km as against the propagation characteristics of signals at lower frequency bands which covers greater distance and can even penetrate walls. As corroborated by FCC (1997), the advantage of millimeter wave lies in its capacity to accommodate densely packed communication links and permission of frequency reuse as well as secure communication. Millimeter wave is also useful for systems that utilize high data rate with low intercept probability; it is particularly applicable for local area networks of short range point-to-point systems (Perlman, 1995).

Millimeter wave interaction with atmospheric constituents'vis-à-vis it's large bandwidth and short wavelengths, is both merits and demerits. According to Skolnik (1970) and Bhartia and Bahl (1984) and some of the disadvantages of millimeter waves are the smaller component size as a result of the smaller wavelength; this increases the cost of manufacturing as a result of the greater precision required. Others disadvantages are limited communication between the ranges of 10-20 km due to atmospheric attenuation. However, as averred by Prasanna (2008), the large amount of available bandwidth is one of the key benefits of millimeter wave communication technology. Wireless links that are millimeter wave technology dependent can achieve capacities as high as 10 Gbpsfull duplex and this is not likely to be matched by any Radio Frequency (RF) wireless technologies operating at lower frequency (Prasanna, 2008).The availability of this extraordinary amount of bandwidth also enables the scalability of millimeter wave wireless links as demanded by market needs. (Prasanna, 2008).According to Skolnik (1970) and Richard (1976), other advantages of millimeter wave technologies are: large bandwidth, narrow beam width, average power requirement, smaller wavelength, high gain and lower peak antenna as well as high immunity to jamming.

## **2.7 Millimeter wave transmission loss factors**

The principal factors that led to loss in transmission of the microwave systems, is the free space loss which is also referred to as clear sky attenuation (FCC, 1997). When considering signal transmission in the millimeter wave bands, foliage blockage,

snow, fog, losses due to scattering/diffraction, gaseous losses and rain are some additional loss factors encountered. According to Al-Saman et al. (2020), these should be considered in link budgeting. The effects of these factors on mm wave propagation loss are discussed as follows:

### 2.7.1 Fog attenuation

Fog is composed of suspended spherical water droplets with radii small enough to keep them suspended in air by micro turbulence (Liebe et. al., 1989). Attenuation by fog is comparatively smaller at millimeter wavelength; it however has some disruptive effects on millimeter wave signals propagation (Etinger *et al.*, 2020). It is caused mostly by absorption and scattering which in turn relies on the extent of the fog density and its index of refraction. According to Gibbins (1988), the fog density  $M$  is given in terms of visibility  $V$  (km) by

$$M = \left(\frac{0.024}{V}\right)^{1.54} \text{ gm}^3 \quad (2.22)$$

Comparing the size of the suspended water droplets (fog) and the wavelength in the millimeter wave band, the Rayleigh approximation may be adopted for defining the fogrefractivity model. Using the Rayleighabsorption approximation (Van de Hulst, 1957), refractivity  $N$  is written as

$$N = M \left(\frac{3}{2m_w}\right) \left(\frac{\epsilon-1}{\epsilon+1}\right) \text{ ppm} \quad (2.23)$$

where,  $m_w$ = specific weight for water = 1.0 and  $M$  is defined by equation (2.22) and is the complex permittivity. According to Liebe *et al.* (1989) we define the power loss  $\alpha$  of the radio wave while propagating through fog as

$$\alpha = 0.812fN''(f) \text{ dB/km}$$

where  $N''(f)$  is complex refractivity.

The derivation of millimeter wave attenuation prediction theoretically by fog is similar to that of rain; however, fog differs from rain in that it constitutes suspended mist of small diameter water drops (Collins, 1985). While the structure of raindrops can assume various shapes; rain drop shape has been found to be spherical for small size cells, while it is considered oblate spheroidal or oblate distorted for medium and large size rain (Yussuff and Nor, 2014). Attenuation of radio wave by fog as opposed

to rain attenuation is less significant hence radio equipment that are suited for rain induced attenuation will invariably overcome fog induced attenuation.

### 2.7.2 Attenuation by snow

Snow constitutes air, water and ice crystals in complex mixture. The shape of snow varies and this makes estimate of snow induced radio wave attenuation more demanding than rain induced attenuation. It has been established that communication equipment that operate wirelessly with the aid of millimeter wave suffers attenuation due to snow (Nakamura *et al.*, 2020). However, the consistency of snow determines its effect on millimeter wave propagation (Collins, 1985). It has been established that at 20 GHz, rain induced radio wave attenuation is greater than that of dry snow. However, Investigations has shown that the attenuation that occurs in wet snow is in excess of that of rain.

### 2.7.3 Free space loss

Two antennas of isotropic type operating at frequencies ( $f$ ) and separated by distance ( $R$ ) suffers losses which are expressed in absolute numbers by the following equation:

$$L_{FSR} = \left(\frac{4\pi R}{\lambda}\right)^2 \quad (2.24)$$

$L_{FSL}$ : Free Space Loss where  $R$  is the transmit, and receive antenna separation;  $\lambda$  is the operating wavelength. After converting to units of frequency and putting in dB form, the equation becomes:

$$L_{FSL}(dB) = 92.4 + 2\log f + 20\log R \quad (2.25)$$

The parameters  $R$  and  $f$  stands for the line of sight range between antennas in km and frequency (GHz) respectively. For every octave change in range, the differential attenuation changes by 6 dB. For example, in going from a 2-kilometer to a 4-kilometer range, the increase in loss is 6 dB. Owing to the high prevalence of free space loss in millimeter wave spectrum, only communication links of short distance coverage is supported (FCC, 1997; Al-Saman *et al.*, 2021).

### 2.7.4 Losses by atmospheric gases

Millimetre wave signals passing through the atmosphere suffers losses when they are absorbed by gaseous atmospheric constituents such as oxygen molecules and water vapor. These atmospheric gases which align with the gas molecules mechanical

resonant frequencies induce losses which increases at definite frequencies. Several peaks occur due to absorption of the radio signal by water vapor (H<sub>2</sub>O) and oxygen (O<sub>2</sub>). At these resonant frequencies, absorption results in high attenuation of the radio signal and, therefore, short propagation distance. The important absorption peaks occur at 60 and 24 GHz for current technology. The H<sub>2</sub>O and O<sub>2</sub> resonances have been studied extensively for millimeter wave propagation characteristics prediction. High incidence of absorption of signals by atmospheric gases especially at higher frequencies constitutes a major limitation (Norouzian, 2020)

### 2.7.5 Attenuation by water vapor

In addition to absorption by molecular oxygen, molecules of water vapor also interact with electromagnetic radiation in the cm and mm wave regions. The water vapor molecule, being a permanent electric dipole, produces rotational transitions of the order of 10<sup>4</sup> times stronger than that of the magnetic transitions of the oxygen molecule. So, even though the abundance of water vapor in the atmosphere is considerably less than that of oxygen, it can produce significant (and intense) level of attenuation near the resonant frequencies. Attenuation of signals by water vapour is found to depend quadratically on water vapor density, particularly at high densities, above about 12 g/m<sup>3</sup> (Karmakar *et al.*, 2010). As observed by De *et al.*, (2020), during attenuation measurement with radiometer, water vapour and rain attenuation are comparable at 5mm/hr.

### 2.7.6 Foliage losses

The propagation of waves through foliage or vegetation encounters frequency related attenuating effects which depends on the vegetation specimens shape or structure (Silva *et al.*, 2018). Foliage losses at millimeter wave frequencies are significant and as such impair signal propagation (Lv *et al.*, 2019). An empirical relationship which can predict this loss has been developed (CCIR Rpt 236-2). For foliage depth of less than 400 metres, the loss is given by

$$L = 0.2f^{0.3}R^{0.6}dB \quad (2.26)$$

where the parameter f stands for the frequency in MHz; R stands for foliage depth in meters (R < 400 meters),

This relationship applies to frequencies within the range 200-95,000 MHz range. For instance, the foliage loss at 40 GHz for a penetration of 10 meters (which is about equivalent to a large tree or two in tandem) is about 19 dB. This is clearly not a negligible value.

### **2.7.7 Attenuation by rain**

In the millimeter wave frequency region, rain heavily interrupts the wave propagation due to attenuation. This is caused by the size of the rain drop which is roughly the same size as the wavelength of radio hence scatters radio signals (Nandi *et al.*, 2019). In the temperate region, the attenuating impact of rain for small cell structure is minimal, however this is not the case in tropical region due to the predominance of rain rates that is very high. This exerts strong influence on the channel and duration of communication signals in the tropics. The incidence of broadening of pulse and distortion of symbols is caused by tropical rainfall structure. This increases the probability of occurrence of symbol errors in the system of communication of mm wave equipment (Nandi *et al.*, 2019). These rainfall effects necessitate regular monitoring with the aid of terrestrial and extra-terrestrial weather stations (Han *et al.*, 2020).

Below about 10 GHz, rain fading is not very significant (Shrestha and Choi, 2017), but, at higher frequencies, it becomes the major factor limiting the radio wave path length, particularly in areas that experience high levels of rainfall (Figure 2.6). It also limits the percentage availability of radio waves (Table 2.2), reduces the level of signal received and increases the losses of transmitted signals (Shayea, 2018). Accurate prediction of attenuation of radio signals due to rainfall effects is very important during the planning process of radio systems on the Earth's surface. (Salonen, 1997).

Some of the factors that determine radio waves attenuation with respect to millimeter frequencies are size of the raindrops, raindrops velocity, drop size distribution and time of the year. Communication signal availability is reduced by increase in rain factor (Figure 2.7).

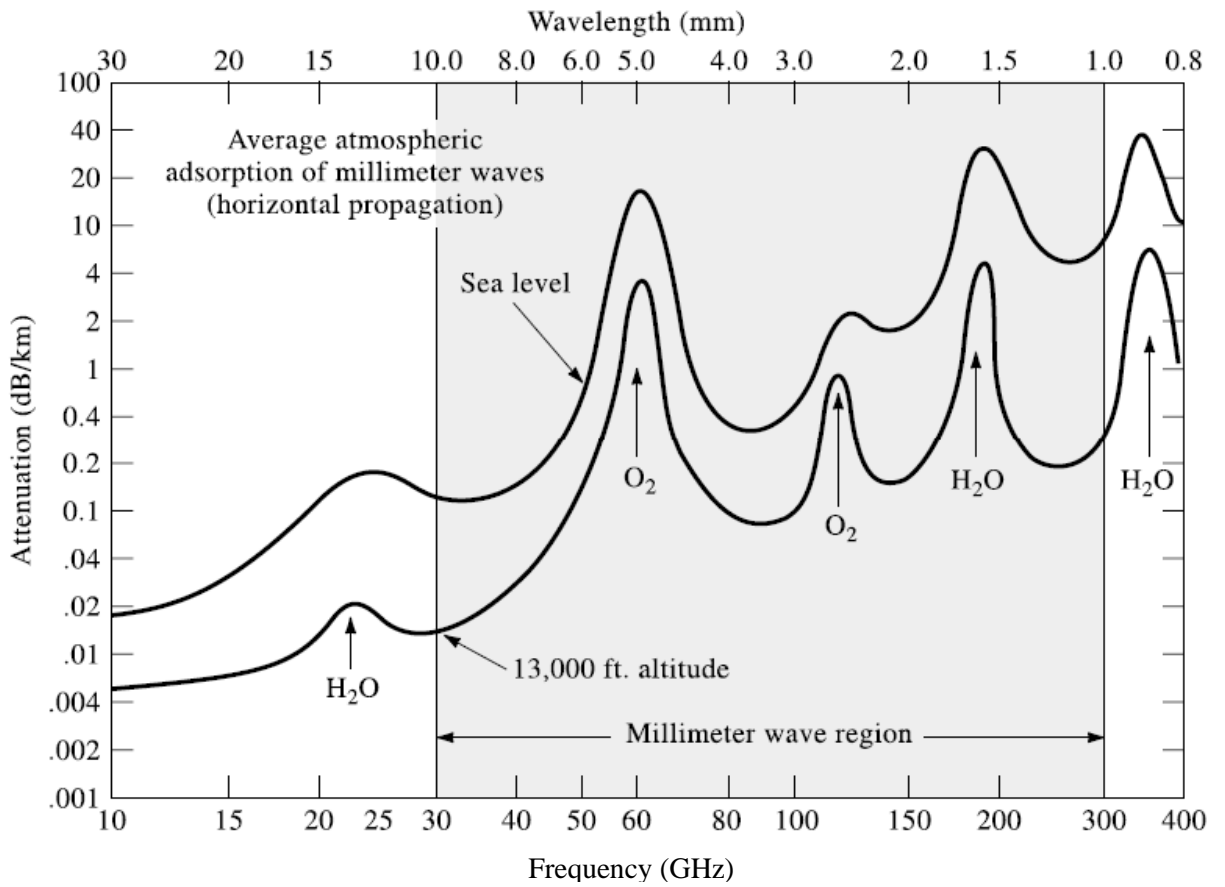


**Figure 2.6.** Attenuation of millimeter wave (Source: FCC, 1997)



**Table 2.2.** Percentage availability/outages of radio waves (FCC, 1997)

Availability (%)	Outage/Year	Months (Average)	Day (Average)
50	4380 hours	360 hours	12 hours
70	2628 hours	216 hours	7.2 hours
80	1752 hours	144 hours	4.8 hours
90	876 hours	72 hours	2.4 hours
95	438 hours	36 hours	1.2 hours
98	175 hours	14 hours	29 minutes
99	88 hours	7 hours	14.4 minutes
99.5	43.8 hours	3.6 hours	7.2 minutes
99.9	8.8 hours	43 minutes	1.44 minutes
99.99	53 minutes	4.3 minute	8.5 seconds
99.999	5.3 minutes	25 seconds	0.86 seconds
99.9999	32 seconds	2.6 seconds	0.086 seconds

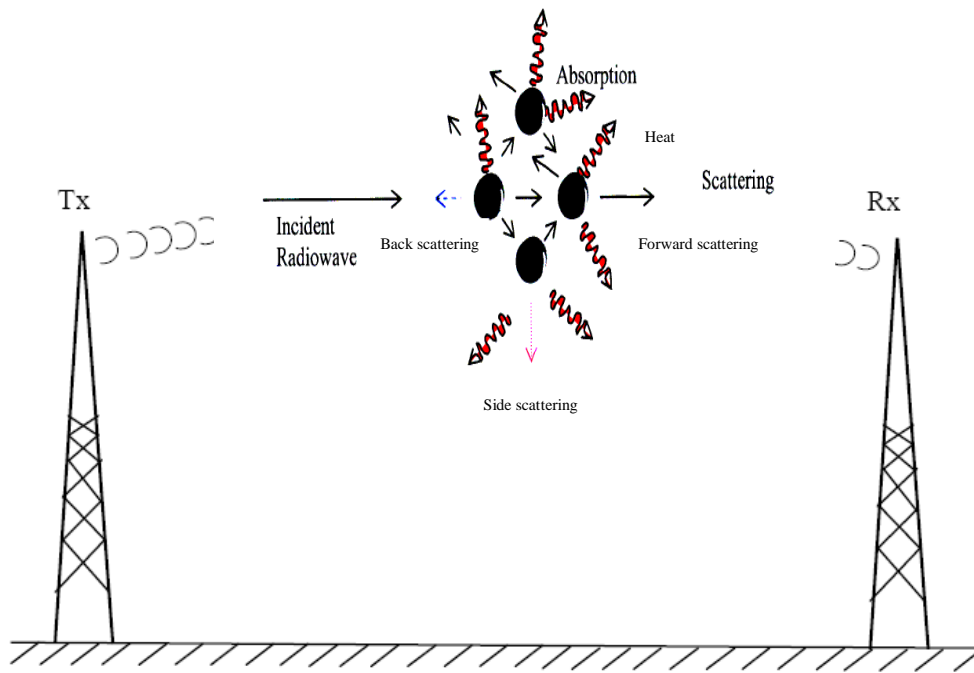


Figure 2.7. Interference of Signals by Rain Drop (source: Mulangu, 2008; Agber and Johnson, 2013).

As illustrated with Figure 2.7 above, radio signals when transmitted from point Tx, and when they encounter drops of rain, the waves are scattered in diverse directions and others are absorbed by the rain drops; which acts as poor dielectric; the radio waves loses power to the rain drops through absorption and the rain driops eventually dissipates the power through heat loss (Agber and Johnson, 2013). Considering the time varying electromagnetic field nature of radio waves, dipole moment is induced by the incident field in the raindrop, hence, the raindrop will act as antenna since its dipole shared similar time; it will therefore scatter or re-radiate the energy. This leads to a loss in the radio signal energy as it approaches the receiver ( $R_x$ ) from the transmitter ( $T_x$ ).

Beyond the limitations to millimeter wave propagations by other transmission loss factors, rain cause the major restriction to the usage and prime performance of millimeter wave band radio equipment (Owolawi et al., 2012). The attenuation by rain leads to signal outages hence compromise the link quality and availability.

## **CHAPTER THREE**

### **METHODOLOGY**

#### **3.1 Data collection**

The data used for this study was sourced from the Tropospheric Data Acquisition Network (TRODAN), Federal University of Technology (FUTA) Akure, Nigeria, the Meteorological stations of the International Institute of Tropical Agriculture (IITA), Ibadan, Oyo State and Bowen University Iwo, Osun State, Nigeria. TRODAN is a project put forward by the Nigerian Centre for Atmospheric Research (CAR). It was designed to monitor the lower atmosphere, which covers the region from the surface of the Earth to the altitude of about 11km. The project was designed to collect and provide real-time meteorological data from different locations across Nigeria for the purpose of research and development. It also serves as a tool for reliable terrestrial and satellite communication networks planning, weather prediction, agricultural usage and hydrological purposes. At the moment, the TRODAN equipment includes atmospheric monitoring facilities such as automatic weather stations, micro rain radar facilities, and Vantage Pro. The equipments used are of Campbell Scientific Electronics specification with a resolution of 5 minutes update cycle (integration time/duration of measurements). Currently there are 18 TRODAN stations spread across the country (Okeke *et al.*, 2012) the earliest of which became operational in 2007.

Tipping bucket/fast response rain gauge and data logger are the major components of TRODAN, FUTA, IITA and Bowen University automatic weather station that provided data for the present research. The rain gauges of IITA and FUTA measured rainfall at 1 minute integration time while that of TRODAN and Bowen measured it at 5 minutes interval. The values were transmitted as electronic pulses to a data logger that stores the data. A computer system equipped with the appropriate software ('Loggernet') was used for the data retrieval from the data logger. The specification of the tipping bucket rain gauge used at each TRODAN station was

TE525WS. The orifice is 20.3 cm and the resolution (rainfall per tip) is 0.254 mm. The accuracy is up to 25.4mm/hr:  $\pm 1\%$  while the operating temperature is from 0° to +50°C.) (Campbell Scientific, 2015). The specification of the equipment at FUTA and IITA is Davis 6250 electronic weather station. In Akure station, tipping bucket (0.2 mm Pertip resolution) rain gauge was used for the collection of rainfall data. The measuring range of the gauge is 2 mm/hr to 400 mm/hr, with accuracy of +1% at 1 liter per hr and 99.2% availability. System maintenance accounted for the 0.8% gauge unavailability (Obiyemi *et al.*, 2014). Bowen and IITA uses Hobo equipment and the specifications are: temperature ranged from -20°C to 40°C (-4°F to 104°F) with normal operating range of -40 to 60°C (-40 to 140°F) which extends to operating range of 0 to 2 seconds for the first data point and  $\pm 5$  seconds per week at 25°C (77°F) time accuracy, the current and direct current voltage were 0–20 mA DC and 0-2.5 VDC, 0-5 VDC, 0-10 VDC, or 0–20 VDC user configured input range (HOBO, 2018)

The six eco-climatic zones of Nigeria viz: Sudan Savanna (SS), South Guinea Savanna (SGS), Northern Guinea Savanna (NGS), Derived Savanna (DS) , Humid Forest (HF) and the Mid Altitude Savanna (MAS) were covered by the study at the fourteen locations. The duration of the study was four years on the average. The map of the stations covered by the study is shown in Figure 3.1 while Table 3.1 shows the site characteristics of the study locations. Figure 3.2 (a - c) are the setup of the TRODAN, FUTA, IITA and Bowen stations at all the locations covered.

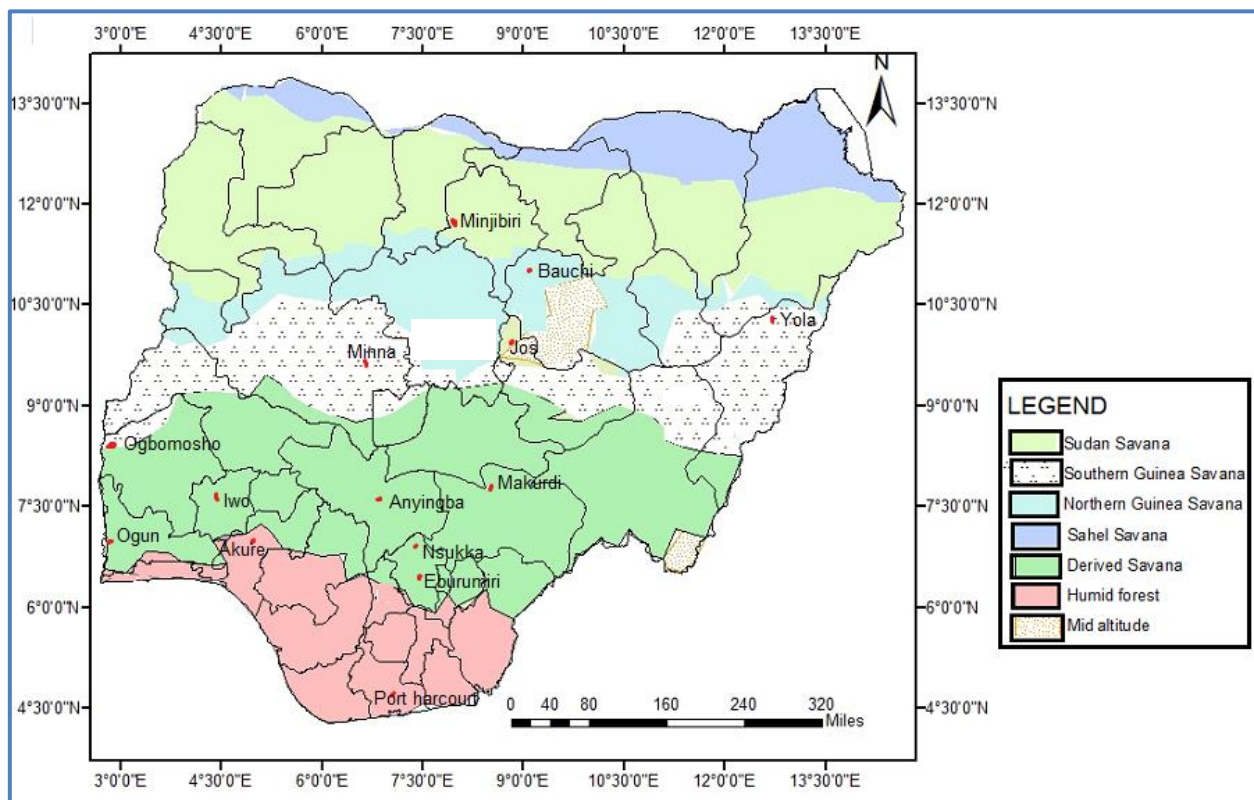


**Figure 3.1.** Map showing the stations covered by the study

**Table 3.1.** Features of the study sites

S/N	Study Area	Coordinates	Altitude (m)	Eco-climatic zones	Duration of study (Years)
1	Jos	9.93 °N, 8.89°E	1280	Mid altitude savanna	2008-2016 (9)
2	Minna	9.61 °N, 6.56 °E	223	Southern Guinea Savanna	2008-2016 (9)
3	Yola	9.23 °N, 12.46 °E	260	Southern Guinea Savanna	2010-2012 (3)
4	Nsukka	6.86 °N, 7.40 °E	259	Derived Savanna	2008-2014 (7)
5	Port Harcourt	4.75 °N, 7.00 °E	468	Humid Forest	2008-2011 (4)
6	Iwo	7.63°N, 4.19°E	224	Derived Savanna	2009 – 2013 (5)
7	Anyigba	7.63 °N, 7.29 °E	420	Derived Savanna	2010-2013 (4)
8	Eburumiri	6.61 °N, 7.35 °E	359	Derived savanna	2008-2013 (6)
9	Makurdi	7.73 °N, 8.54 °E	140	Derived savanna	2008-2011 (4)
10	Minjibiri	11.75°N, 8.66°E	477	Sudan Savanna	2007 – 2011 (4)
11	Bauchi	10.63°N, 10.08°E	600	Northern Guinea Savanna	2013 – 2015 (3)
12	Ogun	6.90°N, 3.58°E	116	Derived Savanna	2010 – 2011 (2)
13	Ogbomosho	8.11°N, 3.41°E	306	Southern Guinea Savanna,	2012 – 2013 (2)
14	Akure	6.89°N, 4.89°E	194	Humid forest	2014 – 2016 (2)

## Equipment setup

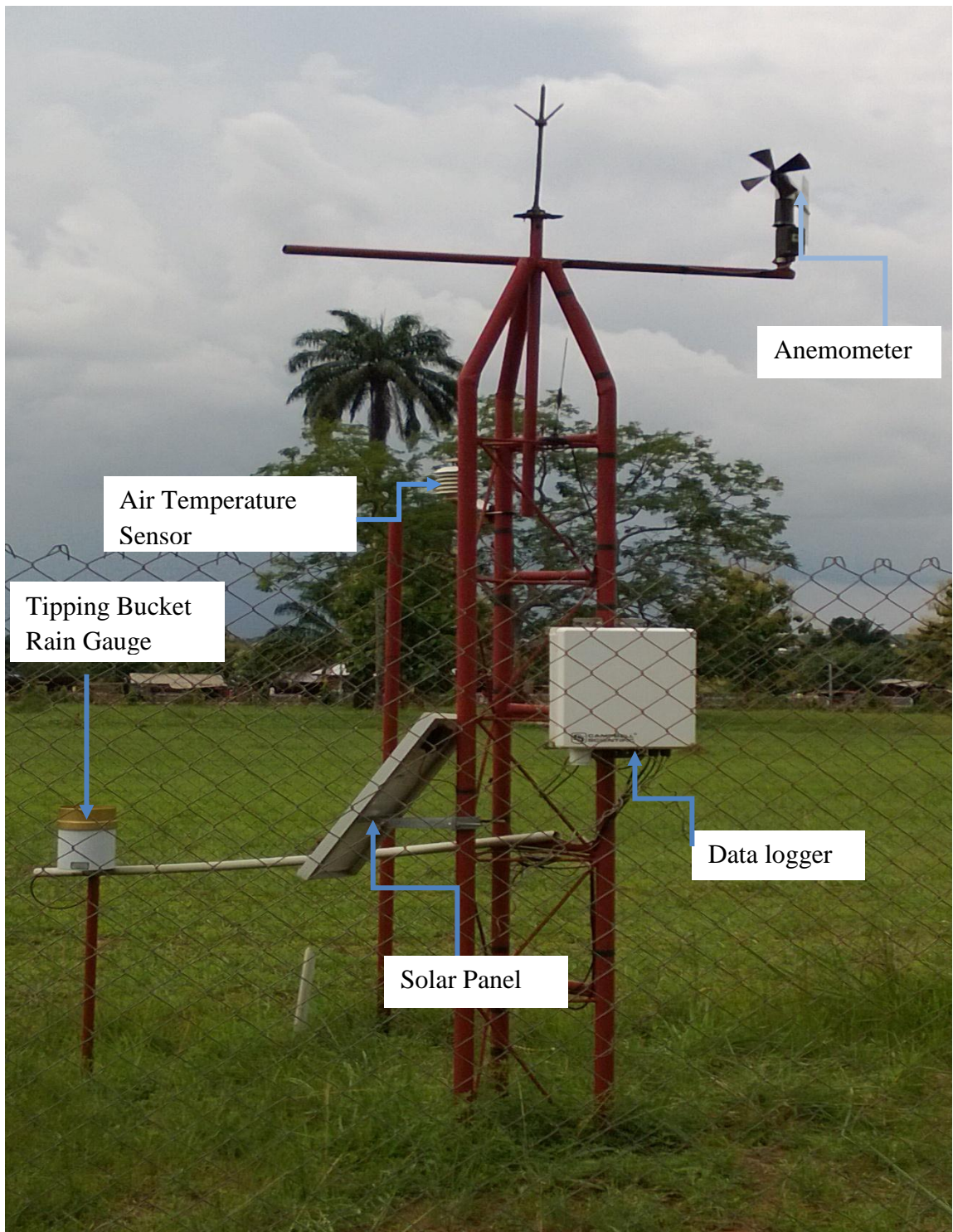


**Figure 3.2a.** A typical Setup of TRODAN Equipment (Source: TRODAN)





**Figure 3.2b.** The electronic weather station of Davis Vantage Vue with indoor console units and the outdoor ISS (Source: Obiyemi et al., 2014).



**Figure 3.2c.** HOBO rain Gauge Equipment

## 3.2 Data analysis

The lowest compromise to attenuation determination is 1-minute integration time rainfall rate in unit of millimeter per hour. To address the objectives of the research, rainfall rate conversion was effected from the measured rainfall in mm to rain rate in mm/hr. The conversion of the 5- minutes measured rainfall to 1- minute (the lowest compromise for attenuation determination) was effected by the use of Lavergnat and Gole (LG) (1998) conversion model. The 1-minute rainfall rate obtained from the conversion was used to characterize the rainfall and the attenuating effects over the eco-climatic zones of Nigeria.

### 3.2.1 Conversion from rainfall to rain rate

Rainfall attenuation is deduced from rainfall rate in millimeter per hour (mm/hr) as against values in millimeter (mm), hence for the purpose of attenuation determination, it is mandatory to convert all rainfall data into rainfall rate. The expression required for the conversion is as follows:

$$R_D = L * \frac{60}{T} (mm/hr) \quad (3.1)$$

where L is the maximum rainfall (mm) and  $R_D$  applies to the rainfall rate (mm/hr) and for time interval T (min) (Ali *et al.*, 1986; Kestwal *et al.*, 2014). The resulting rain rate ( $R_D$ ) was adopted for the attenuation determination after the conversion to 1-minute integration time.

Rainfall rate that exceeds the integration time of 1-minute under-estimates measured rain rate (Chun, 2013). The fluctuation caused by rain gauge measurement process is resolved by 1-minute accumulation. Several models have been proposed for the conversion from higher to 1-minute integration time rain rate. Among these are Flavin (1981), Moupfouma and Martins (1995), Chebil and Rahman (1999), Joo *et al.*, (2002), Semire *et al.*, (2012) and Ojo *et al.*, (2016). However, most of these models are restricted to a fixed integration time and location dependent regression coefficients, hence the need for model that is suited for arbitrary integration times and location independent. The Lavergnat and Gole (LG) model which is a semi-empirical physical stochastic model performs best over all integration time and climatic regions (Ojo *et al.*, 2016).

Lavergnat and Gole (LG) proposed a model for the conversion of rain rates of higher time integration to 1-minute integration time. The model was developed through the application of stochastic process for time interval between rain drops. The

advantage of this method is that it allows a conversion between any integration times. According to the model, the average interdrop interval  $\mu$  is given by a simple asymptotic expression:

$$\mu = \langle \tau \rangle \approx p \frac{a}{\alpha-1} + qb^\beta \lambda_0^{\beta-1} \Gamma(1 - \beta) \quad (3.2)$$

where p & q = normalization constants,  $\lambda$  = mean raindrop per unit time

$p = 1 - q$ ; a, b,  $\alpha$  &  $\beta$  = constants;  $\Gamma$  = asymptotic expression parameter

The probability that a precipitated water height  $h$  be exceeded over a given time interval  $(0,t)$  leads to a dual laplace transform of the form (LG,1998):

$$Q_c(u, s) = \frac{1-f(s)}{\mu_s^2 u} \frac{1-p(u)}{1-p(u)f(s)} \quad (3.3)$$

where

$f(s)$  = probability density function and

$$p(u) = \int_0^\infty p(h) e^{-hu} dh \int_0^\infty e^{-(u\pi D^3/6A)} p(D) d(D) \quad (3.4)$$

When focusing on higher rain rates, the asymptotic value of  $p(u)$  for  $u \rightarrow 0$  may be used in  $Q_c(u,s)$  that is

$$p(u) = 1 - (\langle v \rangle / A)u = 1 - Bu \quad (3.5)$$

This leads to

$$Q_c(u, s) \approx \frac{1-f(s)}{\mu_s^2 f(s)} \times \frac{1}{u + \frac{1-f(s)}{Bf(s)}} \quad (3.6)$$

with the following inverse Laplace transform in  $u$ :

$$Q_c(h, s) \approx \frac{1-f(s)}{\mu_s^2 f(s)} e^{-h\{[1-f(s)]/[Bf(s)]\}} \quad (3.7)$$

For integration times greater than 1 minute, the inverse transform in (3.7) will be influenced only by values of  $s$  that are greater than  $10^4$ .

Applying the scaling property of Laplace transform for rain rate measured over interval  $[0,t]$ , with  $r = h/t$

$$Q_c(r, t) = K^{\xi-1} Q_c(rk^{\xi-1}, kt) \quad (3.8)$$

where  $Q_c(r,t)$  implies the function of rain rate (r) cumulative probability that would be captured with a rain measuring gauge of integration time t. Equation (3.8) thus allows a rain rate distribution observed in all the locations of the study using an intergation time kt, to be changed into one that would have prevailed for an integration time t.

### 3.3 Rain rate prediction models

Rainfall prediction models are used to provide the one minute average rainfall rates exceedance best estimate at the mean annual percentage of the time. According to Ibiyemi (2014), four conventional models are useful in the tropics: Rice and Holmberg (1973), Ito & Hosoya (also known as Kitami model) (2002), Moupfouma and Martins (1995) and the global ITU recommendation (2017). The use of these models yields rainfall rate of a given locations and from this, the corresponding attenuation can be predicted (Mandeep, 2011). These models are briefly discussed below:

#### 3.3.1 Moupfouma model

According this model, the probability of rainfall rate exceedance

$$P(R \geq r) = 10^4 \left( \frac{R_{0.01}}{r+1} \right)^b \exp(\mu(R_{0.01} - r)) \quad (3.9)$$

The parameter P stands for 0.01% probability for a rainfall event exceedance while r represents the rainfall rate exceedance (mm/hr),  $R_{0.01}$  (mm/h) represents the 0.01% mean annual rain rate exceedance in an average year; the following expression approximates b:

$$b = \left( \frac{r-R_{0.01}}{R_{0.01}} \right) \ln \left( 1 + \frac{r}{R_{0.01}} \right) \quad (3.10)$$

From the equation (3.10), r represents the percentage of time of rain rate exceedance while  $R_{0.01}$  represents 0.01% mean annual rain rate exceedance. The parameter  $\mu$  in equation 3.9 depends on the eco-climatic features of the local climate. For tropical/subtropical regions,

$$\mu = \frac{4 \ln 10}{R_{0.01}} \exp \left( -\lambda \left[ \frac{r}{R_{0.01}} \right]^{\gamma} \right) \quad (3.11)$$

where  $\lambda = 1.066$ ,  $\gamma = 0.214$  and  $R_{0.01}$  is the 0.01% of time rainfall rate exceedance and it is obtained by using the Chebil and Rahman (1999) model. According to Chebil and Rahman (1999), the 0.01% average annual rain rate exceedance can be obtained with the expression:

$$R_{0.01} = \alpha M^\beta \quad (3.12)$$

where the regression coefficients  $\alpha$  and  $\beta$  are given as 12.2903 and 0.2973 respectively. The sum of the annual rainfall measurement is represented by M. The input of rain data at 0, 01% is the major limitation of the Moupfouma method. This shortcoming was addressed in Moupfouma and Martins (1995) method by the consideration of rainfall rate exceedance of 0.01% relationship with a range of various rain rate integration times. This is stated as follows:

$$p(1 - \min) = R(\tau)_{0.001}^\alpha \quad (3.13)$$

where

$$\alpha = 0.98(t)^{0.061} \quad (3.14)$$

and  $1 - \min < t < 1$  h

### 3.3.2 Rice and Holmberg model

The Rice and Holmberg (1973) model is a statistical model which is based upon the sum of exponential modes of rainfall rates, each with a characteristic average rate R. Descriptive analysis of this made shows that

$$\text{Rainfall} = (\text{Mode 1} + \text{Mode 2}) \text{ rain.} \quad (3.15)$$

The physical analysis of thunderstorm corresponds to Mode 1 rain while the sum of two exponential distributions which is simply all other rain corresponds to Mode 2 rain.

thus:

$$M = M_1 + M_2 \quad (3.16)$$

and

$$\beta = M_1/M_2 \quad (3.17)$$

where

M = Mean rainfall accumulation

M<sub>1</sub> = sum of thunderstorm rainfall

M<sub>2</sub> = sum of all other rain

$\beta$  = Thunderstorm ratio

Also,

$$T_1(R) = M(0.03\beta \exp(-0.03R) + 0.2(1 - \beta)[\exp(-0.258R) + 1.86 \exp(-1.63R)]) \quad (3.18)$$

where  $T_1(R)$  is the surface point rainfall exceedance in 1- minute and  
 $R=$  1-minute rain rate

The average rainfall accumulation ( $M$ ) is worked out from rainfall data whereas  $\beta$  is deduced from Rice and Holmberg (1973) map or calculated from rainfall data. The value of  $\beta$  for Nigeria from the map is 0.8.

Hence, the mean rainfall rates exceedance is:

$$p(\%) = \frac{T_1(R)}{87.66} \quad (3.19)$$

### 3.3.3: Ito & Hosoya model

The Ito – Hosoya model used data bank of rain rates of different integration time from 54 locations in 23 countries and satellite links rain attenuation of 290 sets of data covering 84 locations in 30 countries. Multiple regression analysis of the data bank was used in the development of the model. The method needs input of mean rain accretion ( $M_1$ ) and thunderstorm ratio ( $\beta$ ), and it is stated as follows:

$$R_p = a_p M^{b_p} \beta^{c_p} \quad (3.20)$$

where

$$b_p = -4.583266 \times 10^{-2} x^4 - 0.4098161 x^3 - 1.162387 x^2 - 0.826117 x + 0.911857 \quad (3.21)$$

$$c_p = 2.574688 \times 10^{-2} x^4 - 0.1549031 x^3 - 0.1747827 x^2 - 0.2846313 x + 1.255082 \times 10^{-2} \quad (3.22)$$

$$\log(a_p) = 0.1574155 x^4 + 1.348171 x^3 + 3.528175 x^2 + 1.479566 x - 2.302276$$

Hence,

$$a_p = 10^{(0.1574155 x^4 + 1.348171 x^3 + 3.528175 x^2 + 1.479566 x - 2.302276)} \quad (3.23)$$

As can be inferred from equation 3.20,  $R_p$  is the  $p\%$  of an average year 1-minute rain rate (validity between 0.001% - 1%),  $x$  is equivalent to  $\log(p)$  while  $a_p$ ,  $b_p$ , and  $c_p$  are

the coefficients needed in the forecast model (Aris et al., 2016). The sum of all other rain and thunderstorm ratio ( $\beta$ ) is as defined in equation 3.16 and 3.17.

### 3.3.4 ITU-R (837-7) model

This model deals with radio wave propagation modelling with respect to precipitation characterization. The ITU-R recommends that the prediction method for rain rate characterization:

$$R_p = Itu\_p837 - 7(p, Lat, Lon) \quad (3.24)$$

should be adopted globally to deduce the rainfall rate ( $R_p$ ) exceedance for the desired annual probability of exceedance  $p$ , for any location on the surface of the earth and for an integration time of one minute, hence the model was used to obtain the ITU-R predicted rain rate at 0.0001 to 1% exceedance for all the locations in the study. In equation 3.24,

$P$ : annual probability of exceedance (%) of the location

$Lat$ : Latitude of the location (degrees, N)

$Lon$ : Longitude of the location (degrees, E), While the output parameter is:

$R_p$ : Rainfall rate exceeded for the location probability of exceedance (mm/hr)

$itu\_p837-7$ : International telecommunication union recommendatin

### 3.3.5 Prediction models testing

As expressed by Olsen (1999) on the imperative of accurate rain rate propagation prediction, over prediction leads to costly system over-design while under prediction results in unreliable systems, hence the need for rainfall prediction model testing. The methods applicable for prediction models testing has been suggested by ITU-R P.311-17 (2017). As stated by this model, for certain percentages of time (from 0.001% to 1% of the year), for which data are available, the percentage relative error,  $E_{rel}$  (percent) of the predicted ( $A_{predicted}$ ) and the measured ( $A_{measured}$ ) rain rate values should be calculated thus:

$$E_{rel} = \frac{A_{predicted} - A_{measured}}{A_{measured}} \times 100 \quad (3.25)$$

The root mean square (RMS) was computed as follows:

$$RMS = \sqrt{(\mu_e)^2 + (\sigma_e)^2} \quad (3.26)$$

where

$$\sigma_e = \sqrt{\frac{\sum(x-\bar{x})^2}{n}}, \mu_e = \frac{1}{n} \sum_{i=1}^n |x_i - x| \quad (3.27)$$



$n$  = number of data points

$\mu_e$  =mean error

$\sigma_e$  =standard deviation

The model with the lowest RMS error is considered the best (Mandeep and Hassan, 2008; Olurotimi and Ojo, 2014,). To obtain the predicted rain rate for all the locations considered in this study, the applicable prediction model with the lowest root mean square error was used.

### 3.4 Rainfall rate characterization for worst month

The worst month in a year is that month in which the effect of any hydrometeors on radio wave propagation attains the longest duration of exceedance for a pre-selected threshold in consecutive twelve calendar months. These propagation conditions for radio waves vary on monthly basis. This presents radio communications system designer the challenge of ensuring at least 99% (ITU-R 837-7, 2017) of the systems availability and performance for the worst months of the year. As recommended by ITU-R 581-2 (1990), to ensure accurate radio-meteorological data and propagation conditions for the worst months, there is the need to specify the pre-selected threshold for any performance degradation mechanism. The procedure useful for obtaining worst month from annual rain rate statistics is given by the ITU-R 841-6 (2019) recommendation. As stated by this recommendation, the conversion factor ( $Q$ ) can be obtained from the relation:

$$P_w = QP$$

where  $1 \leq Q \leq 12$

$Q$  ( $Q_1$  and  $\beta$ ) function of  $P$  (%):

$$Q_1 = \begin{cases} 12 \text{ for } p < \left(\frac{Q_1}{12}\right)^{\frac{1}{\beta}} \% & \text{(a)} \\ Q_1 P^{-\beta} \text{ for } \left(\frac{Q_1}{12}\right)^{\frac{1}{\beta}} < P \leq 3\% & \text{(b)} \\ Q_1 3^{-\beta} \text{ for } 3\% < P \leq 30\% & \text{(c)} \\ Q_1 3^{-\beta} \frac{P}{30} \frac{\log(Q_1 3^{-\beta})}{\log(0.3)} \text{ for } 30\% < P & \text{(d)} \end{cases} \quad (3.28)$$

According to ITU-R 841-6 (2019), the calculation of P from the given value of P<sub>w</sub> is done as follows:

$$P = \frac{P_w}{Q} \quad (3.29)$$

Equation (3.29) shows the inter-dependence of the parameters P, P<sub>w</sub> and Q, hence considering the conversion factor (Q) at the exceedence percentages (P ≤ 3%) from equation (3.27b),

$$Q_1 P^{-\beta} \text{ for } \left(\frac{Q_1}{12}\right)^{\frac{1}{\beta}} < P \leq 3\% \quad (3.30)$$

Let

$$P_0 = \left(\frac{Q_1}{12}\right)^{\frac{1}{\beta}}$$

Hence

$$P_0 < P \leq 3\% \quad (3.31)$$

As stated by ITU-R 841-6 (2019),

$$Q = \frac{1}{Q_1^{(1-\beta)} P_w^{(1-\beta)}}^{-\beta} \quad (3.32)$$

Since Q (Q<sub>1</sub> and β).

For global planning purposes, (ITU-R 841-6, 2019) recommends that

Q<sub>1</sub> = 2.85 and β = 0.13 used to deduce the average worst month conversion factor

Substituting this to equation (3.32) and the output to Q in equation (3.29),

$$P = 0.30 P_w^{1.149} \quad (3.33)$$

This is the relationship between P<sub>w</sub> and P. As recommended by ITU-R 841-6 (2019), for worldwide rain rate application, the conversion factor

Q<sub>1</sub> = 2.82 and β = 0.15

should be utilized for climate regions that are characterised by frequent rain.

Substituting these values to equation (3.32) gives

$$Q = 3.384 P_w^{-0.176} \quad (3.34)$$

Substituting equation (3.34) to equation (3.29) and approximating to 2- decimal places,

$$P_a = 0.30 P_w^{1.18} \quad (3.35)$$

where  $P_a$  is equivalent to the mean annual time percentage of excess. Changing of subject and deriving  $P_w$  from equation (3.35),

$$P_w = 2.77407 P^{0.84746} \quad (3.36)$$

Equation (3.35) is for the calculation of ITU percentage annual rain rate exceedance while equation (3.36) is for the ITU average worst month rain rate exceedance.

Equation (3.34) is for the computation of Q-values.

### 3.5 Determination of rain attenuation statistics

Rain induced attenuation can be predicted using rainfall cumulative distribution measured at a point (Moupfouma, 1984). It can also be predicted by using the concept of mean rain rate over the propagation paths and the length of the effective path coverage of the radio signal. It can be deduced by using a reduction factor of a time percentage to multiply the point rainfall rate and by using a reduction coefficient to multiply the actual path length respectively (Moupfouma, 1984). On the terrestrial scale, three models are used for predicting rain attenuation (Fashuyi and Afullo, 2007). These models are the Moupfouma (1984) model, Crane Global model (1996) and ITU-R (2015). These models require rain rate ( $R_{0.01}$ ) at the 0.01% exceedance at 1-minute integration time. These models are briefly discussed below.

#### 3.5.1 ITU-R p. 530-17 (2017) Recommendations

The International Telecommunications Union (ITU) - Radio sector (R) 530-17 (2017) recommendation has given some techniques for extended period of rain induced attenuation estimation. To calculate the specific attenuation,  $\gamma_R$  (dB/km), the power law relationship of equation 3.37 should be used.

$$\gamma_R = kR^\alpha \quad (3.37)$$

$k$  and  $\alpha$  = functions of frequency (GHz) ranging from 1GHz to 1000 GHz

The values of  $k$  and  $\alpha$  were determined by ITU-R from equations 3.38 and 3.39

$$\log_{10} k = \sum_{j=1}^4 a_j \exp \left[ - \left( \frac{\log_{10} f - b_j}{c_j} \right)^2 \right] + m_k \log_{10} f + c_k \quad (3.38)$$

$$\alpha = \sum_{j=1}^5 a_j \exp \left[ - \left( \frac{\log_{10} f - b_j}{c_j} \right)^2 \right] + m_\alpha \log_{10} f + c_\alpha \quad (3.39)$$

The symbols are: frequency,  $f$ , (with units in GHz), horizontal (H) and vertical (v) polarisation,  $k_H$ ,  $\alpha_H$ ,  $k_V$  and  $\alpha_V$

Computation of that millimeter wave effective path length ( $d_{eff}$ ) was done by the use of the factor,  $r$  (distance factor) to multiply  $d$  (the actual path length). As stated by the ITU-R model, an estimate of this factor is stated as:

$$r = \frac{1}{0.477 d^{0.633} R_{0.01}^{0.073 \cdot \alpha} f^{0.123} - 10.579 (1 - \exp(-0.024 d))} \quad (3.40)$$

The value 2.5 is the ITU-R recommended maximum value for  $r$ . According to ITU-R, where the value of the denominator of equation (3.40) is less than 0.4, 2.5 should be used.

An estimate of path attenuation at 0.01% exceedance is as follows:

$$A_{0.01} = \gamma_R d_{eff} = \gamma_R dr \text{ dB} \quad (3.41)$$

The rain attenuation exceedance within the range 0.001% to 1% ( $A_p$ ) is obtainable from the equation (3.42):

$$\frac{A_p}{A_{0.01}} = C_1 p^{-(C_2 + C_3 \log_{10} p)} \quad (3.42)$$

where  $C_1$ ,  $C_2$  and  $C_3$  are the coefficient of the exceedance time percentages ( $p$ ), for 100 GHz frequency and 60 km path length. According to the ITU-R model, these prediction procedures should apply globally.

### 3.5.2 Moupfouma model (1984)

Moupfouma (1984) utilized the knowledge of 1-min. integration time recorded rainfall rate to propose an empirical model that would be useful for forecasting of line-of-sight terrestrial radio links attenuation by rain. The model states that the attenuation  $A$ (dB) by rain is given as

$$A(\text{dB}) = KR^\alpha L_{\text{eff}} \quad (3.43)$$

also, the parameters  $k$  and  $\alpha$  are the regression coefficients and they are the function of the polarisation and frequency of the radio waves. The effective path length ( $L_{\text{eff}}$ ) is given as

$$L_{\text{eff}} = rl \quad (3.44)$$

where  $l$  (km) is the actual and effective path length. The reduction coefficient,  $r$ , is given as:

$$r = \frac{1}{1+cl^m} \quad (3.45)$$

From equation (3.45), the parameters  $c$  and  $m$  depends on exceedance percentages ( $p$ ) of the rain rate, the frequency of the radio link and the length of its path respectively. The attenuation induced by rain  $A(\text{dB})$  at rainfall rate ( $R$ ) was calculated at the same time percentage. The Moupfouma (1984) model uses well known fitting procedures from experiments with radio links at 1.3 km to 58 km path length and frequency range of 7-38 GHz at tropical/subtropical and temperate locations. The expression on equation (3.46) shows the path length reduction factor,  $r$  which designates the actual length of rainfall coverage:

$$r = \frac{1}{1+0.03\left(\frac{p}{0.01}\right)^{-\beta l^m}} \quad (3.46)$$

where

$$m(f, l) = 1 + \psi(F) \log_e l \quad (3.47)$$

and

$$\psi(f) = 1.4 \times 10^{-4} F^{1.76} \quad (3.48)$$

The regression coefficient,  $\beta$  and the frequency (GHz),  $f$ , were obtained from best data fit result (Mandeep, 2009). For radio link of path length  $l \leq 50$  km and  $l \geq 50$  km and the value of the regression coefficient  $\beta$  for rain rate exceedance percentage range ( $p$ ) are as follows:

$$l \leq 50 \text{ km}$$

$$\beta = 0.45, \text{ for } 0.001 \leq P \leq 0.01$$

$$\beta = 0.6, \text{ for } 0.01 \leq P \leq 0.1$$

$$l \geq 50 \text{ km}$$

$$\beta = 0.36, \text{ for } 0.001 \leq P \leq 0.01$$

$$\beta = 0.6, \text{ for } 0.01 \leq P \leq 0.1$$

### 3.5.3 Global model by Crane

The global model by Crane was based on geophysical observations, rain structure and rain rate (Crane, 1996). Crane assumed that for point rain rates in excess of 25 mm/hr, the probability of their occurrence were independent of path length over distances greater than 10 km. This enhances a sufficient sample size at a path length of 22.5 km. According to Shebami (2017), this assumption was based upon experience with weather radar data and in agreement with observations at path lengths of 10, 15, 20 and 22.5 km and with power law approximations. This model was implemented by Crane using a piecewise representation of the path profile by exponential functions. The resulting attenuation  $A_T$  for a given rain rate (R) at distance (D) is given by Crane (1996) as:

$$A_T(R, D) = \gamma(R) \left( \frac{e^{y\delta(R)} - 1}{y} + \frac{e^{zD} - e^{z\delta(R)}}{z} e^{\alpha\beta} \right), \quad \delta(R) < D < 22.5 \quad (3.49)$$

$$A_T(R, D) = \gamma(R) \left( \frac{e^{y\delta(R)} - 1}{y} \right), \quad 0 < D < \delta(R) \quad (3.50)$$

where

$$\gamma(R) = KR^\alpha \text{ (k, } \alpha = \text{ regression coefficients)}$$

The piecewise exponential model empirical constants are as follows:

$$0.17 \ln(R) = 0.83 - B \quad (3.51)$$

$$0.03 \ln(R) = 0.026 - C \quad (\text{km}^{-1}) \quad (3.52)$$

$$0.6 \ln(R) = 3.8 - \delta(R) \quad (\text{km}^{-1}) \quad (3.53)$$

$$u = \frac{B}{\delta(R)} + C \quad (\text{km}^{-1}) \quad (3.54)$$

$$y = \alpha u \quad (\text{km}^{-1}) \quad (3.55)$$

$$z = \alpha c \quad (\text{km}^{-1}) \quad (3.56)$$

### **3.5.4 Prediction of rain attenuation at 33.4 GHz and 31.8 GHz in Nigeria**

To ensure appropriate allocation of frequencies, the International Telecommunications Union (ITU) has divided the world into three regions and Nigeria falls within region 1. Article 5 of the Radio Regulations of the ITU deals with global frequency allocations from 8.3 KHz to 300 GHz. The national frequency table of allocations is a compendium of frequency allocations to services applicable to Nigeria as well as a depiction of frequency usage in Nigeria (NCC, 2018). At present, the 5G communication network is evolving and the 31.8 to 33.4 GHz frequency bands allocated to Nigeria holds potential for its effective deployment. The features of these frequency bands are highlighted in ITU-R 1520-3 (2011) recommendation. This recommendation considers arrangements of radio frequency for fixed service systems that operates in the 31.8 GHz to 33.4 GHz frequency bands. As stated in this recommendation, sharing in radio navigation service, space research service and inter-satellite service is considered feasible at these bands; hence rain attenuation prediction is imperative for equipment design at these bands for Nigeria.

### **3.5.5 Contour mapping of rain attenuation distribution in Nigeria**

In this study, 0.01% of time rain rate exceedance was calculated for the 14 locations. To design radio equipment that will function optimally across Nigeria, the attenuation (dB) obtained from the 0.01% ( $R_{0.01}$ ) rain rate was interpolated to cover the 36 states (including the federal capital territory) of Nigeria. Using spatial interpolation techniques, the rainfall rate as well as the corresponding attenuation distribution all over Nigeria was estimated. Spatial interpolation method uses point measured data to estimate unknown values at unsampled locations (Lam *et al.*, 2015). The spatial interpolation method are of many forms which includes Nearest Neighbour (NN), Thiessen polygons, Spline, and various forms of Kriging and Inverse Distance Weighting (IDW) which are frequently used in interpolating rainfall data from rain gauge stations (Tomczak, 1998; Hutchinson, 1998; Cheng *et al.*, 2007; Mair, 2011). The IDW method has been used to interpolate rainfall data by many researchers such as Goodale *et al.* (1998) in Ireland, Dirks *et al.* (1998) in Norfolk Island and Price *et al.* (2000) in Canada). The IDW method is a simple deterministic interpolator that is exact with few decisions to make regarding model parameters. It assumes that things that are closer are more similar than those farther apart and use measured values surrounding an unmeasured location to predict its values (Lam *et al.* 2015). The

predicted values are influenced more by the measured values that are closest to them and the closest measured values are given more weight than those farther apart. The expression for an IDW is given by Azpurua and Ramos (2010) as:

$$Z_m = \sum_{i=1}^n w_n Z_n \quad (3.57)$$

where

$$w_n = \left[ \left( \frac{1}{(d_n)^\beta} \right) / \sum_{n=1}^N \left( \frac{1}{(d_n)^\beta} \right) \right] \quad (3.58)$$

$$\text{where} \quad \sum_{i=j}^n w_n = 1 \quad (3.59)$$

$$d_n = \sqrt{(x - x_n)^2 + (y - y_n)^2} \quad (3.60)$$

and

$Z_m$  = predicted value at point m,

$Z_n$  = observed value at point n,

N = sample number,

$W_n$  = weight allocated to the sample points,  $d_n$  = pythagoran distance between m and n

$\beta$  = a positive power parameter (user selected exponent or weight)

x; y and  $x_n$ ;  $y_n$  are the coordinates of the interpolating and the sample points

(Azpuruna *et al.*, 2010, Diba *et al.*, 2016) . The weights are calculated based on

Euclidean/ pythagorean distance.

The predicted attenuation values ( $Z_m$ ) and the coordinates of the locations were used to generate contour map with the aid of Contouring and 3D mapping software, Surfer 10.



## CHAPTER FOUR

### RESULTS AND DISCUSSION

#### 4.1. Rainfall Characterisation at the Study Locations

The characterization of the monthly and annual rainfall cumulative distribution is imperative for millimeter wave terrestrial wireless communication systems efficient planning and utilization (Vclav *et al.*, 2010). Detailed information on the rainfall characteristics of a particular season and month is crucial to the improvement of the Quality of Service (QoS) at any given location (Sharma *et al.*, 2010). The geography of a location is a critical factor in determining rainfall characteristics and its effects on QoS. Factors of geography such as latitude, longitude and site elevation are crucial indicators that define the rainfall characteristics of a location (Ali-Akbar *et al.*, 2015). The amount of solar radiation reaching the earth's surface is controlled by the latitude, hence the angle of arrival of the sun rays to the earth's surface. At higher latitudes, the resultant effect is temperature decrease as well as rate of evaporation. Variations in site elevation can lead to variations in temperature even for locations of the same latitude (Apaydin *et al.*, 2011). On the other hand, longitude has indirect effect on the rainfall characteristics owing to westward and eastward movement of air masses. Therefore, determination of the characteristics of rainfall of a study site is crucial for reliable prediction of rain attenuation at any location, (Owolawi *et al.*, 2008). The higher the rain rate, the more the radio signal is attenuated and the decline in the QoS. This necessitates the presentation of the results according to the locations of study on the eco-climatic zones shown in Table 4.

Table 4 shows the average annual rainfall measured at raingauge integration time of 5-minutes at the station of the eco-climatic zones; Akure and Kano are exceptions with rainfall measurement at 1-minute integration time. It can be observed from this Table that Port Harcourt recorded the highest average annual rainfall of 1684.13mm while Anyigba registered the least at 476.85mm/year.

**Table 4.1.** Characteristics of the stations used in this study

Sites	Average Annual rainfall (mm/yr)	Eco-climatic zone
Jos	812.40	Mid altitude savanna
Minna	910.08	Southern Guinea Savanna
Yola	532.30	Southern Guinea Savanna
Nsukka	1442.68	Derived Savanna
Anyigba	476.85	Derived Savanna
Eburumiri	1295.63	Derived Savanna
Makurdi	734.38	Derived Savanna
Mowe	685.9	Derived Savanna
Ogbomosho	498.5	Southern Guinea Savanna
Iwo	854.5	Derived Savanna
Bauchi	1030.6	Northern Guinea Savanna
Akure	1567.7	Humid forest
Port Harcourt	1684.13	Humid forest
Minjibiri	501.6	Sudan Savanna

#### **4.1.1 Accumulated rainfall distribution**

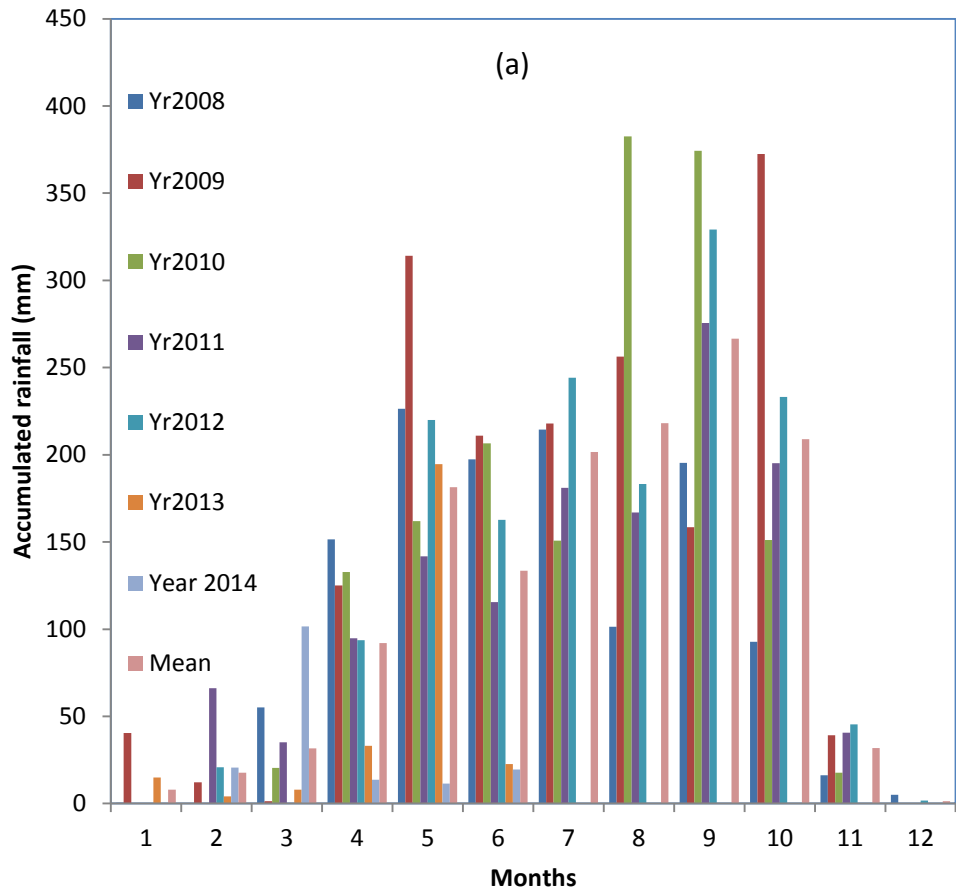
Rainfall is one of the most discontinuous atmospheric phenomena with significant spatial and temporal variability (Sulochana *et al.*, 2014), hence the need to obtain the cumulative distribution. The annual and monthly accumulated rainfall distribution for the period of study is presented in Figures 4.1 (a-f) in order of the locations on the eco-climatic zones of Nigeria (Table 4) while the comparison of the cumulative rainfall distribution is shown in figure 4.15. These results are discussed according to the the eco-climatic zones below.

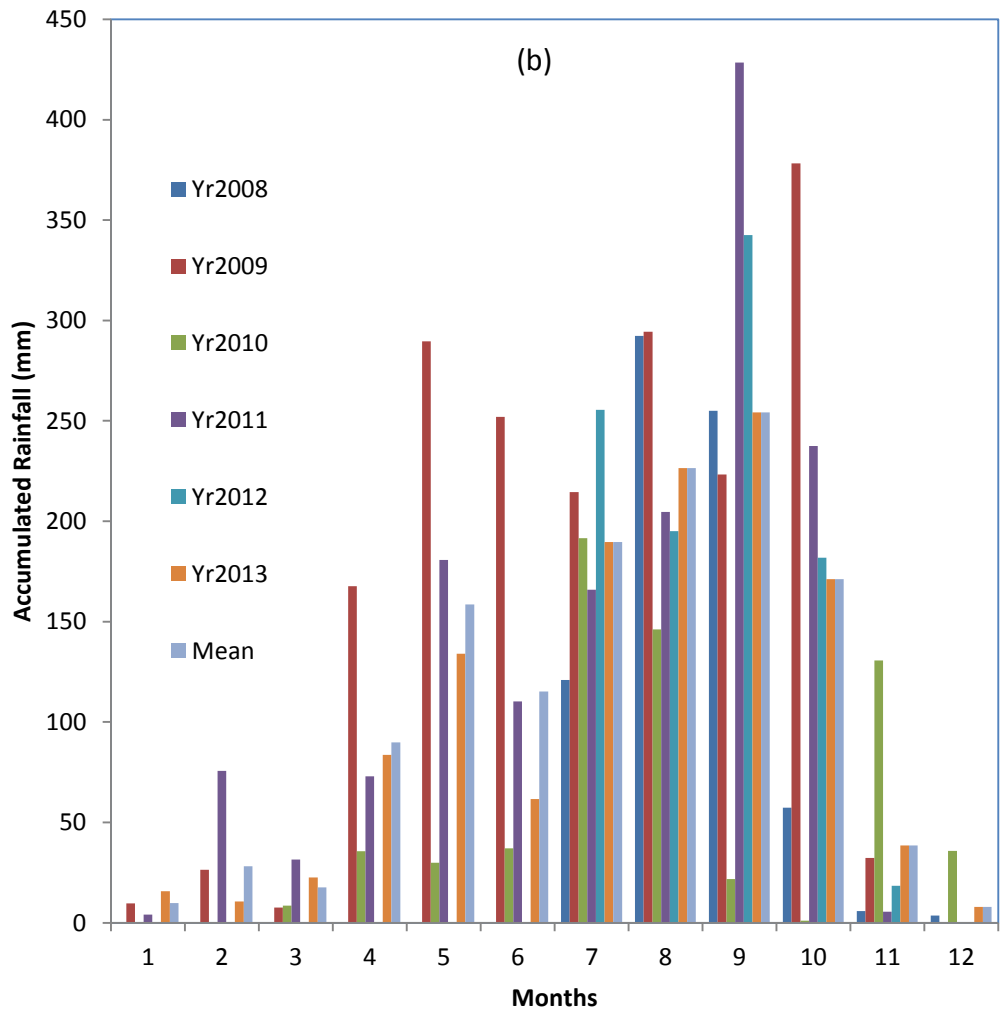
##### **4.1.1.1 Derived savanna zone**

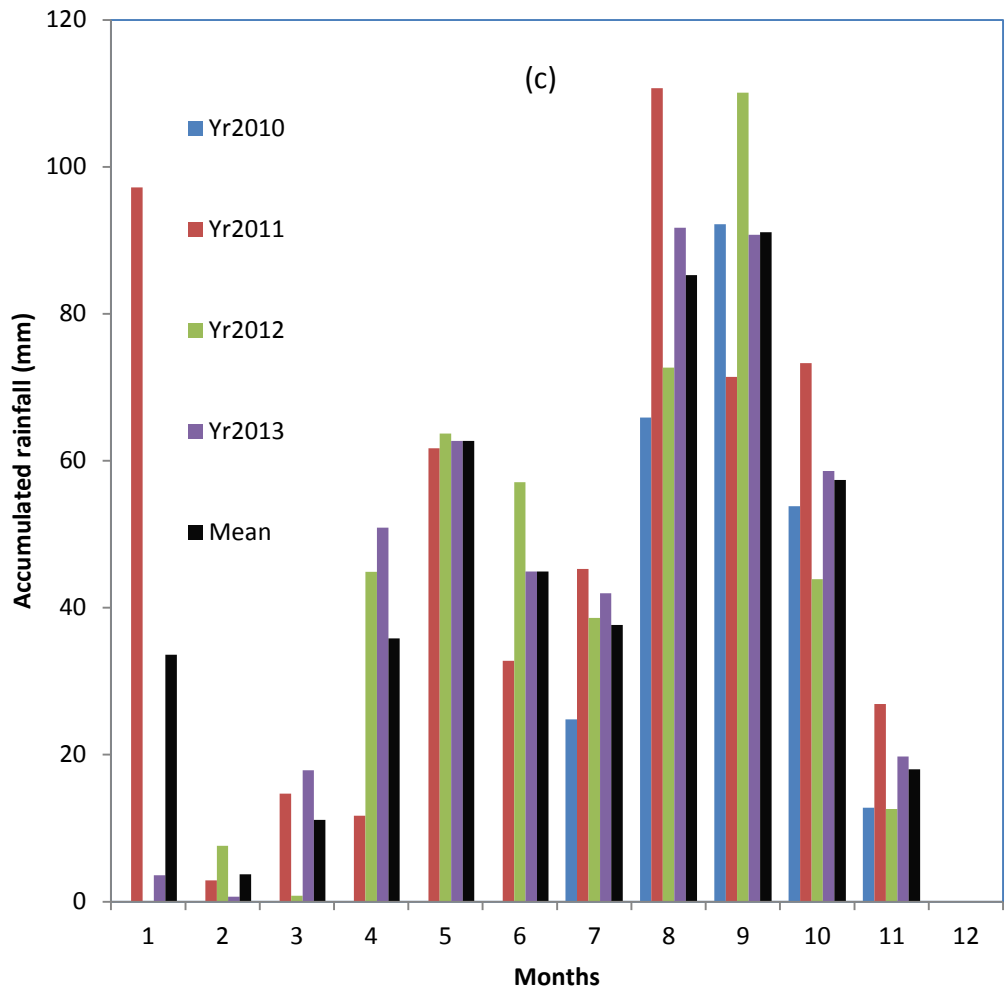
This zone is the transition zone between the Guinea Savanna and Tropical Rainforest zones. The average annual temperature and rainfall are 26.5°C and 1314 mm respectively.

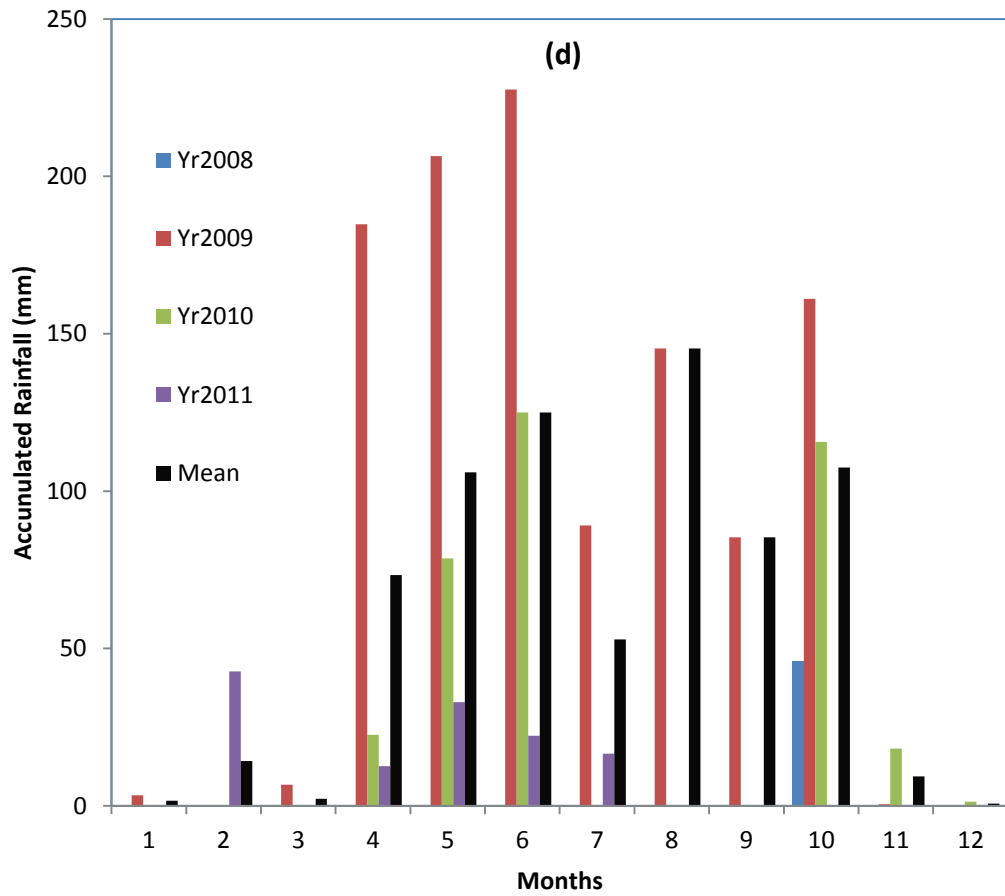
As shown in Figure 4.1 (a and b), the highest rainfall monthly accumulation of 382.60 mm was recorded in August in year 2010 in Nsukka while at Eburumiri, the highest rainfall accumulation of 428.50 mm was recorded in September, 2009. The highest mean monthly accumulated rainfall at the respective stations are 266.58 mm and 254.23 mm in September throughout the period of study. Thus, August and September is the month with the highest rainfall accumulation at these locations and is considered worst month for radio link at these locations during the period of study. Appendix 1 shows the annual accumulated rainfall situation throughout the observed period. The Year 2009 was observed as the worst year with a total rainfall accumulation of 1748.40 mm and 1895.70 mm for both Nsukka and Eburumiri respectively. This year (2009) is considered the worst calendar year of a radio link at these locations. These results agree with the works of Adeyemi *et al.*, (2014).

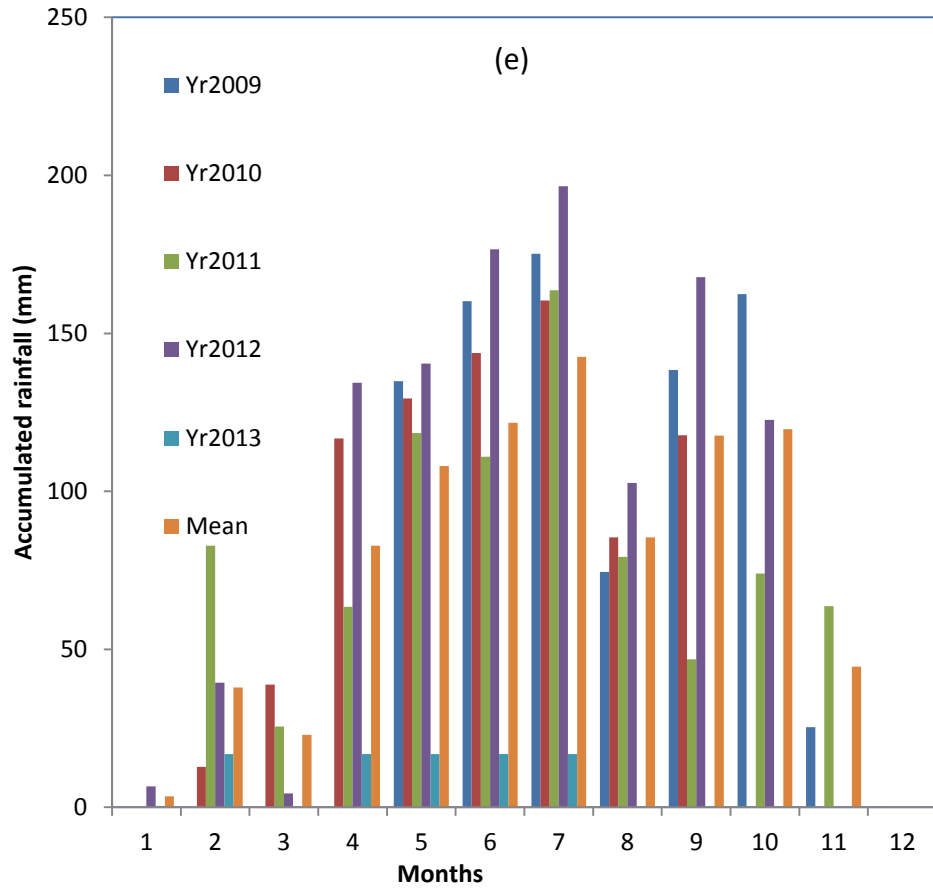
The monthly rainfall accumulation at Anyigba is presented in Figure 4.1 (c). As can be observed from the Figure, August, 2011 was the month with the worst rainfall accumulation of 110.70 mm. The month with the highest mean rainfall accumulation throughout the observed period (2010-2013) was September, hence the worst month for radio link at this location. As shown in appendix 1, 2011 was the year with the













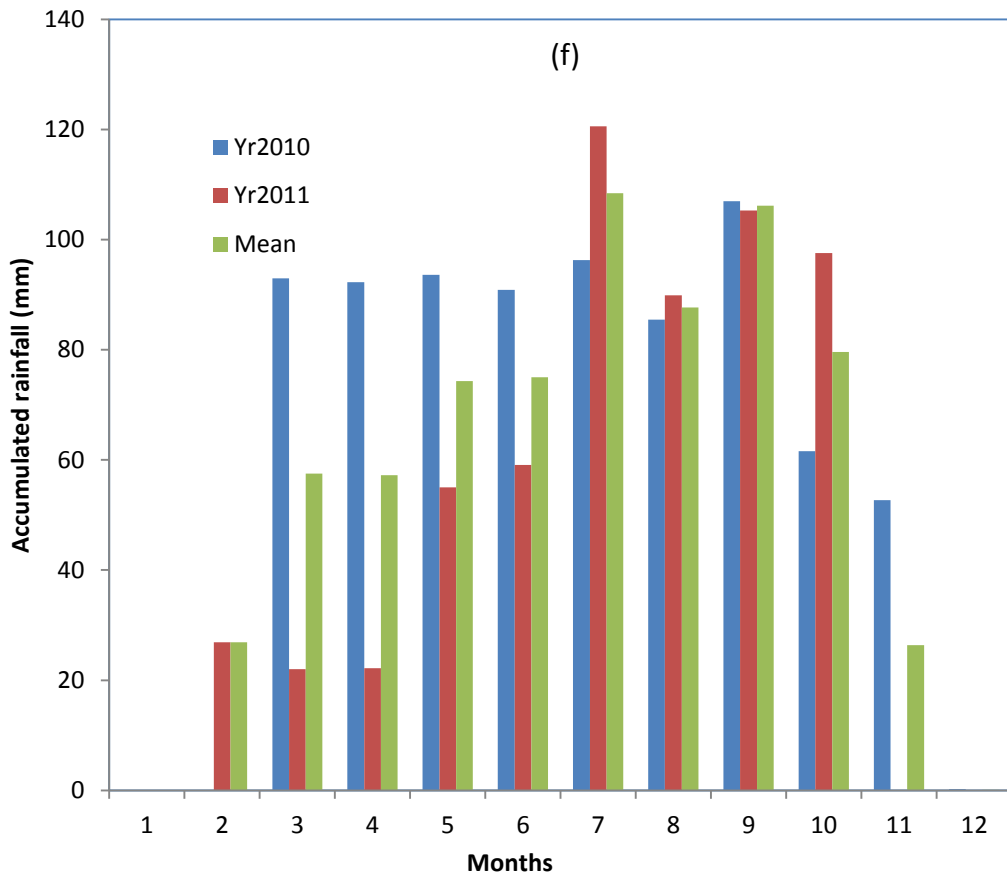


**Figure 4.1.** Cumulative monthly rainfall distribution (mm) in (a) Nsukka, (b) Eburumiri, (c) Anyigba, (d) Makurdi, (e) Iwo and (f) Mowe

the highest rainfall accumulation of 548.60 mm and hence is the worst year for radio link at Anyigba.

The situation in Makurdi for the period 2008-2011 is shown in Figures 4.1 (d). As can be seen in appendix1, June 2009 witnessed the highest rainfall accumulation of 227.60 mm, however, the month of August is characterised with the worst mean rainfall accumulation (145.30 mm) throughout the period of study hence the worst month for radio propagation at the location. The year 2009 recorded the worst rainfall accumulation of 1110.10 mm hence the worst for radio link (Appendix1). The results presented agree with the submissions of Emmanuel *et al.*, (2013).

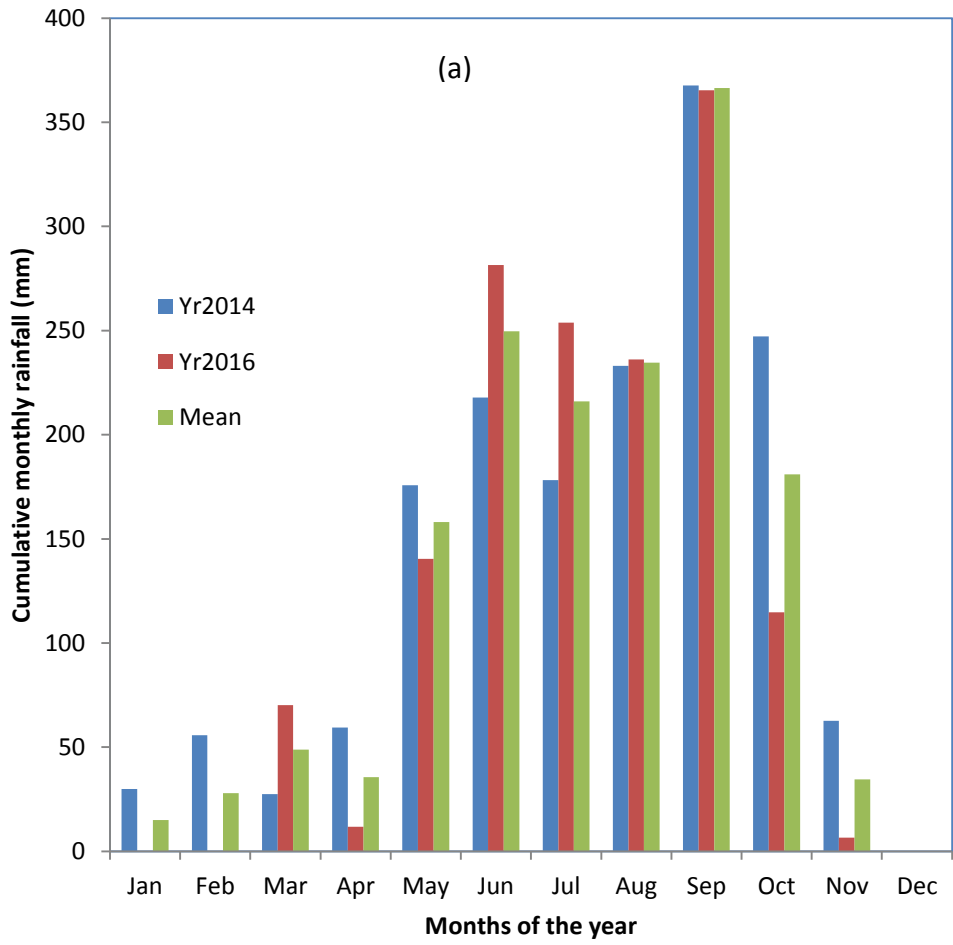
As shown in Figure (e and f), the highest monthly and mean rainfall accumulation of 196.60 mm, 142.52 mm, 120.6 mm and 108.5 mm were recorded at Iwo and Mowe in July 2012 and 2010 respectively; hence July is the worst calendar month for radio link at these location throughout the 5 and 2 years of observation. Year 2012 (Appendix1) and 2010 (Appendix1) were observed as the worst years in Iwo and Ogun with a total rainfall accumulation of 1091.40 mm and 773.1 mm respectively. These results are at variance with the findings of Adeyemi *et al.*, (2004), owing to inter-annual variations in rainfall intensities at these locations.

#### **4.1.1.2 Humid forest zone**

The humid forest zone cuts across the boundary of western Nigeria to Cameroon through the South-east. The rainfall per annum is 1300 to 1500 mm in the West and over 2000 mm in the East. This zone has high humidity that is generally over 80% and wet season that lies between 8 to 10 months. This enhances continuous presence of moisture in the air (Udoh *et al.*, 1994).

The stations covered by the study in the humid forest zone are Akure and Port Harcourt. The cumulative monthly and annual rainfall distribution are presented in Figure 4.2 (a and b) and appendix1.

In Akure (Figure 4.2a), September recorded the highest rainfall accumulation of 367.6 mm. The highest mean monthly rainfall of 366.5 mm was also recorded in the month of September. The year 2014 was the year with the highest accumulated rainfall of 1654.8 mm in Akure (Appendix1). Hence, 2014 was the worst calendar year in



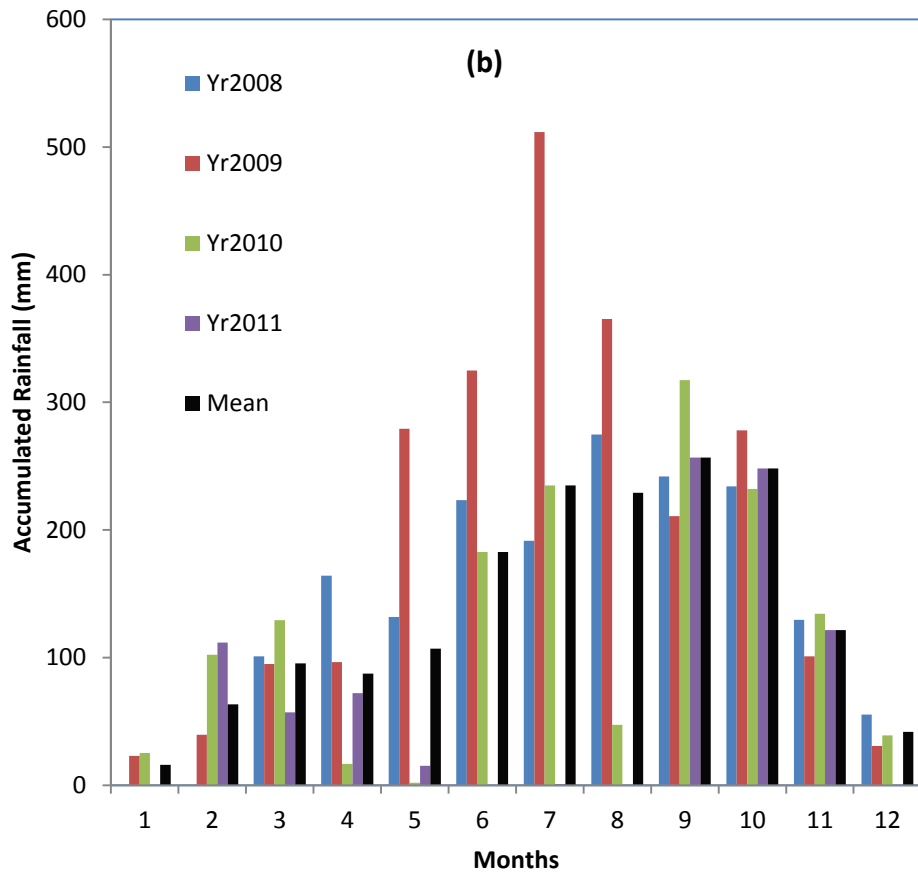


**Figure 4.2.** Cumulative monthly rainfall distribution (mm) in (a) Akure, (b) Port Harcourt

Akure eco-climatic zone. Figure 4.2b presents the accumulated rainfall amount in Port Harcourt. From the figure, the month of July, 2009 recorded the highest monthly accumulated rainfall of 511.90 mm. The highest mean monthly accumulated rainfall amount (256.68 mm) over period of study was observed in September. Hence, the month of September was the worst calendar month for radio link at the location. Appendix1 indicates the annual accumulated rainfall throughout the observed period. The year 2009 was observed as the worst year with a total rainfall accumulation of 2356.10 mm. Hence 2009 was the worst calendar year of a radio link at the Port Harcourt location.

#### **4.1.1.3 Northern guinea savanna zone**

This zone lies between latitude  $11^{\circ}\text{N}$  and  $9^{\circ}\text{N}$  and longitude  $4^{\circ}\text{E}$  and  $14^{\circ}\text{E}$ . In this zone, the rainfall distribution is unimodal with annual level of about 900 to 1200mm. The wet season lasts for about 3 to 4 months while the dry season lasts for about 4 to 5 months (Udoh *et al.*, 1994).

The station covered by the study in the Northern Guinea Savanna (NGS) was Bauchi. The accumulated rainfall amount over the period of study for Bauchi is presented in Figure 4.3 and appendix1. It can be observed from this Figure that the month of August 2013 witnessed the highest monthly accumulated rainfall of 404.12 mm and highest mean monthly rainfall of 314.9 mm also in August. The worst calendar year was 2013 (appendix1) with the annual accumulation of 1135.1 mm.

#### **4.1.1.4 Mid altitude savanna zone**

The coordinates of this zone is longitude  $9^{\circ}53'\text{E}$  and latitude  $8^{\circ}5'\text{N}$ . The range of temperature is between  $21^{\circ}\text{C}$  and  $25^{\circ}\text{C}$  while the annual rainfall lies between 1400 and 1430 mm (Udoh *et al.*, 1994).

The accumulated rainfall amount over the period of study for this zone is presented in Figure 4.4 and appendix1. It can be observed that July, 2008 was the month with the highest rainfall accumulation of 477.80 mm. Throughout the period of observation, the month of July recorded the highest mean accumulated rainfall of 223.10 mm, hence the worst calendar month for the period of study at this location. On the other hand, 2008 was the worst rainfall year; the rainfall accumulation was 1222.10 mm as shown in appendix1. This was the worst calendar year for radio wave propagation for this location.

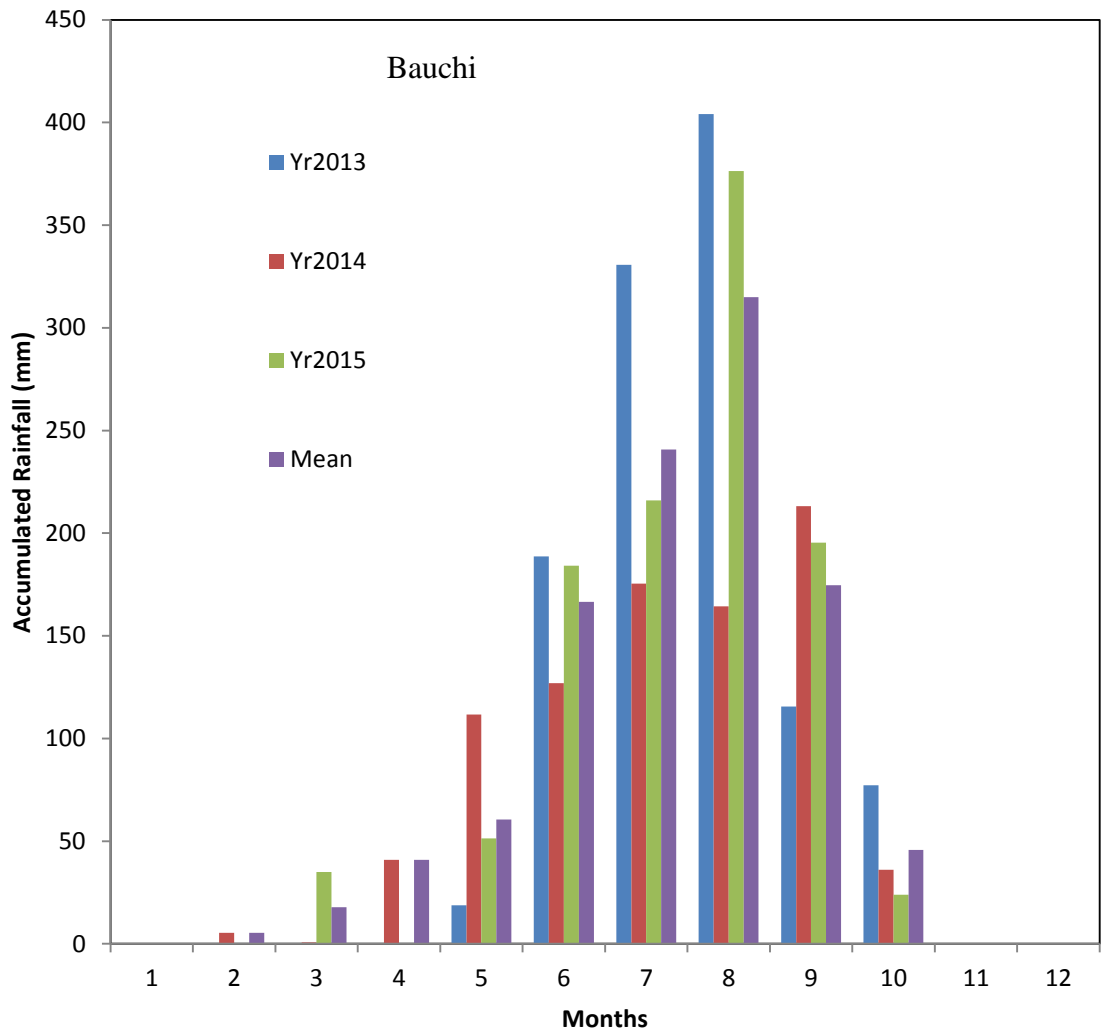


**Figure 4.3.** Cumulative monthly rainfall distribution (mm) at Bauchi

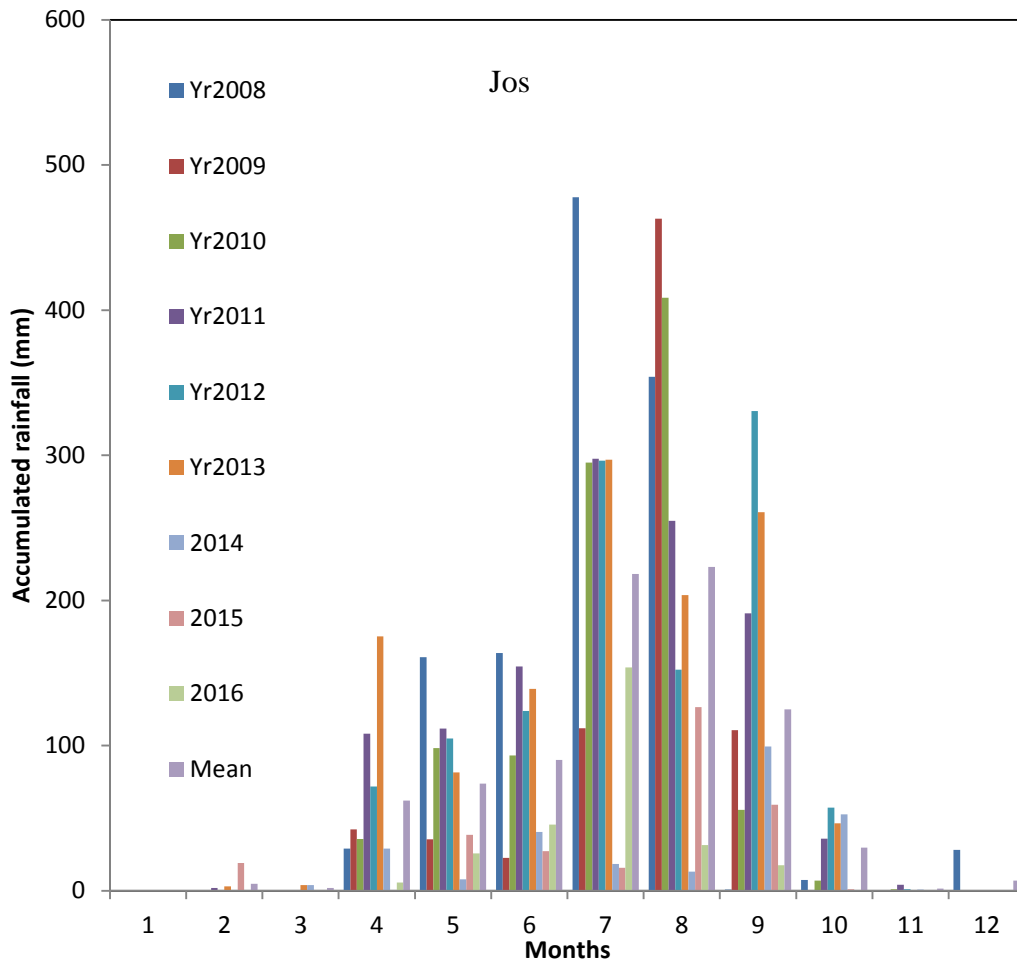


**Figure 4.4.** Cumulative monthly rainfall distribution (mm) at Jos

#### **4.1.1.5 Southern guinea savanna zone**

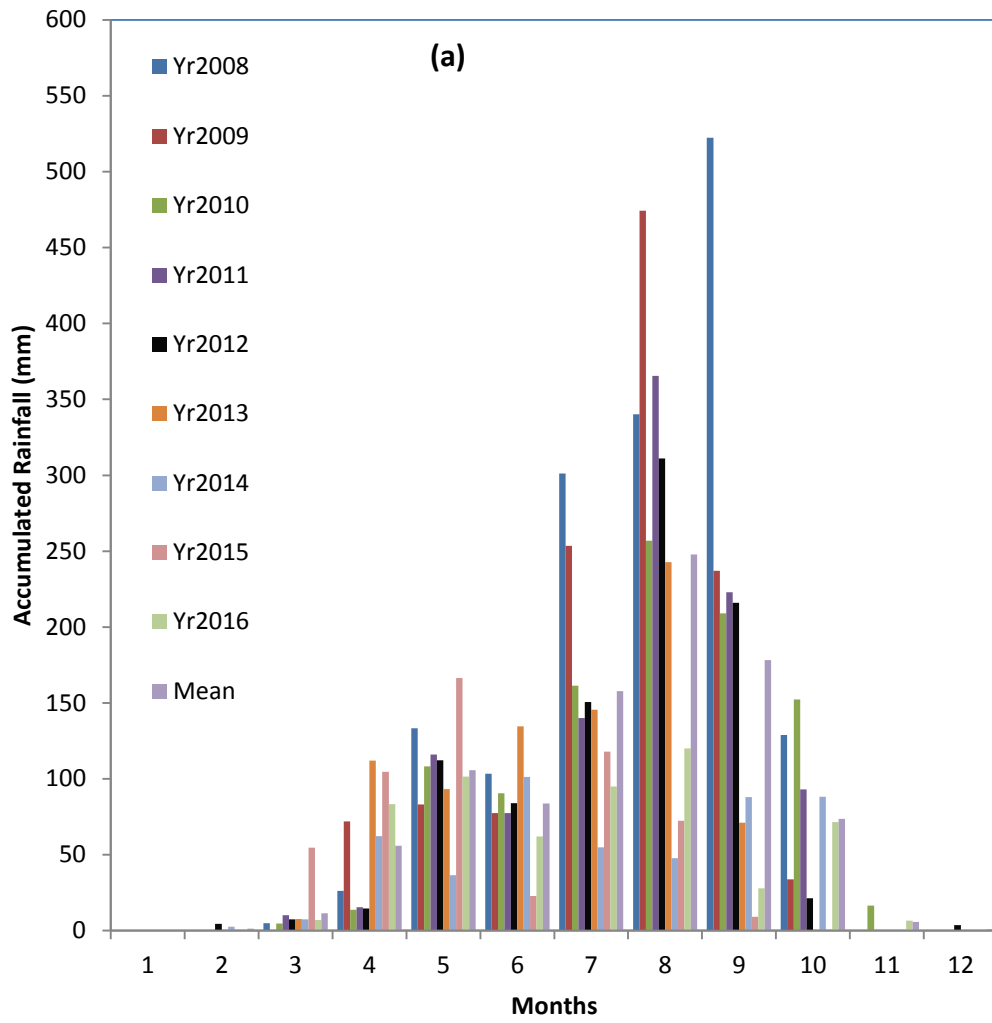
This zone is characterized by 1000 mm to 1500 mm rainfall per annum and four to six months dry season. It lies between 2°E and 12°E longitude and 9°N to 8°N latitude (Udoh et al., 1994).

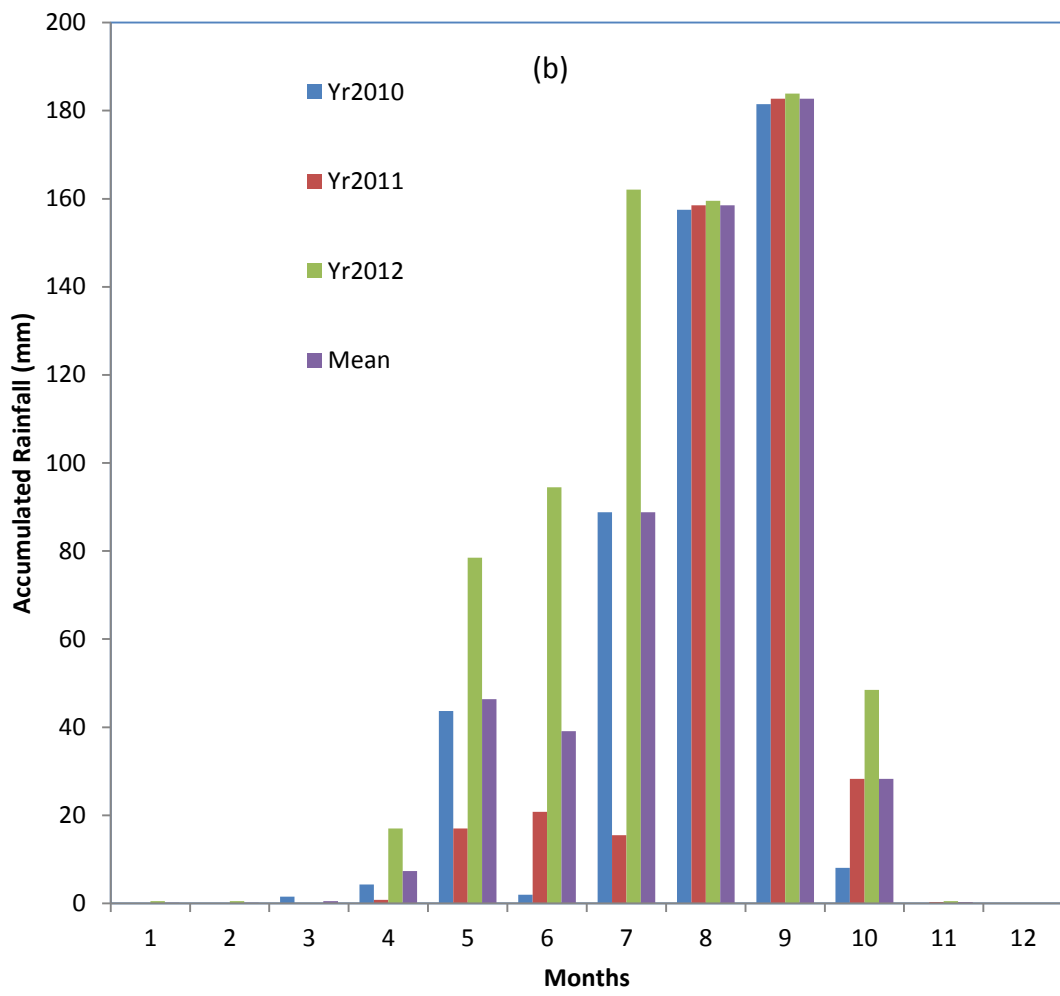
The Southern Guinea Savanna (SGS) eco-climatic zone is composed of: Minna, Yola and Ogbomosho. The rainfall cumulative distribution are presented in Figure 4.5 (a-c) and appendix 1. The rainfall accumulation for Minna is as represented by Figures 4.5a. Figure 4.5a shows that September, 2008 is the month with the worst rainfall accumulation (522.30 mm). August recorded the worst mean rainfall accumulation (247.90 mm). This is the month with the worst radio link throughout the observed period (2008-2011). The year 2008 was the year with the worst radio link throughout the observed period and the rainfall accumulation was 1560.60 mm (appendix 1).

From Figure 4.5b, September 2012 witnessed the highest monthly accumulated rainfall of 183.90 mm in Yola. The mean monthly accumulated rainfall over the observed 3 year period at this location was also highest in September (182.70 mm), hence the worst calendar month of a radio link at the location for the observed period. Appendix 1 shows that the annual accumulated rainfall throughout the observed period. Year 2012 was observed as the worst year with a total rainfall accumulation of 745.50 mm. Hence 2012 was the worst calendar year for a radio link at the location throughout the observed period.

At Ogbomosho (Figure 4.5c) September witnessed the highest rainfall accumulation (120.9 mm). The highest mean monthly rainfall was equally recorded in the same month (120 mm). Year 2013 recorded the highest annual accumulation (589.6 mm) in Ogbomosho (Appendix 1).







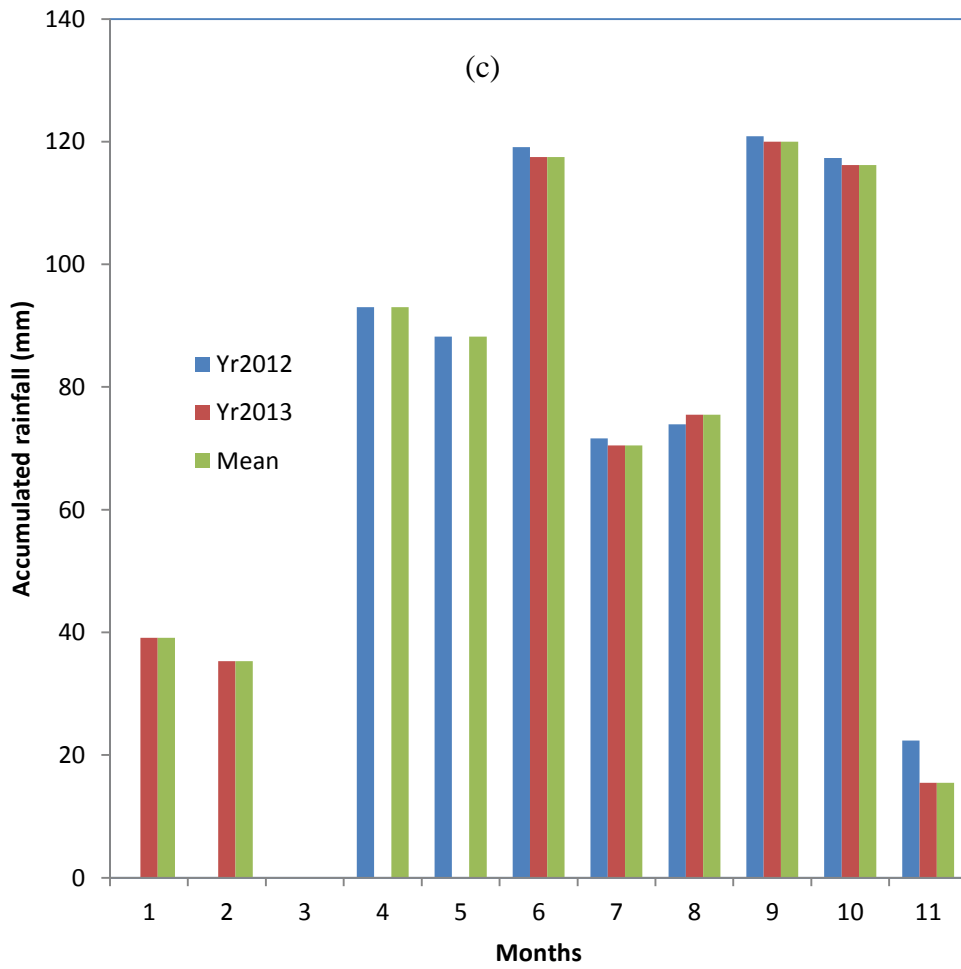


**Figure 4.5.** Cumulative monthly rainfall distribution (mm) in (a) Minna, (b) Yola, (c) Ogbomosho

#### **4.1.1.6. Sudan Savanna Zone**

The coordinate of this zone is 12°N as well as 4°E and 14°E. The relative humidity is always below 40% but sometimes rises to an average of 60% during the wet season. The rainfall per annum is less than 1000 mm and the dry season last between 6 to 8 months (Udoh *et al.*, 1994).

The station covered at this zone was Kano. The monthly distribution is presented in Figure 4.6 and appendix 1.

As can be inferred from the Figure, August 2007 witnessed the highest (260.2 mm) rainfall scenario; the highest mean monthly rainfall (195.87 mm) was recorded in July and the highest cumulative rainfall was recorded in year 2007 (608.8 mm).

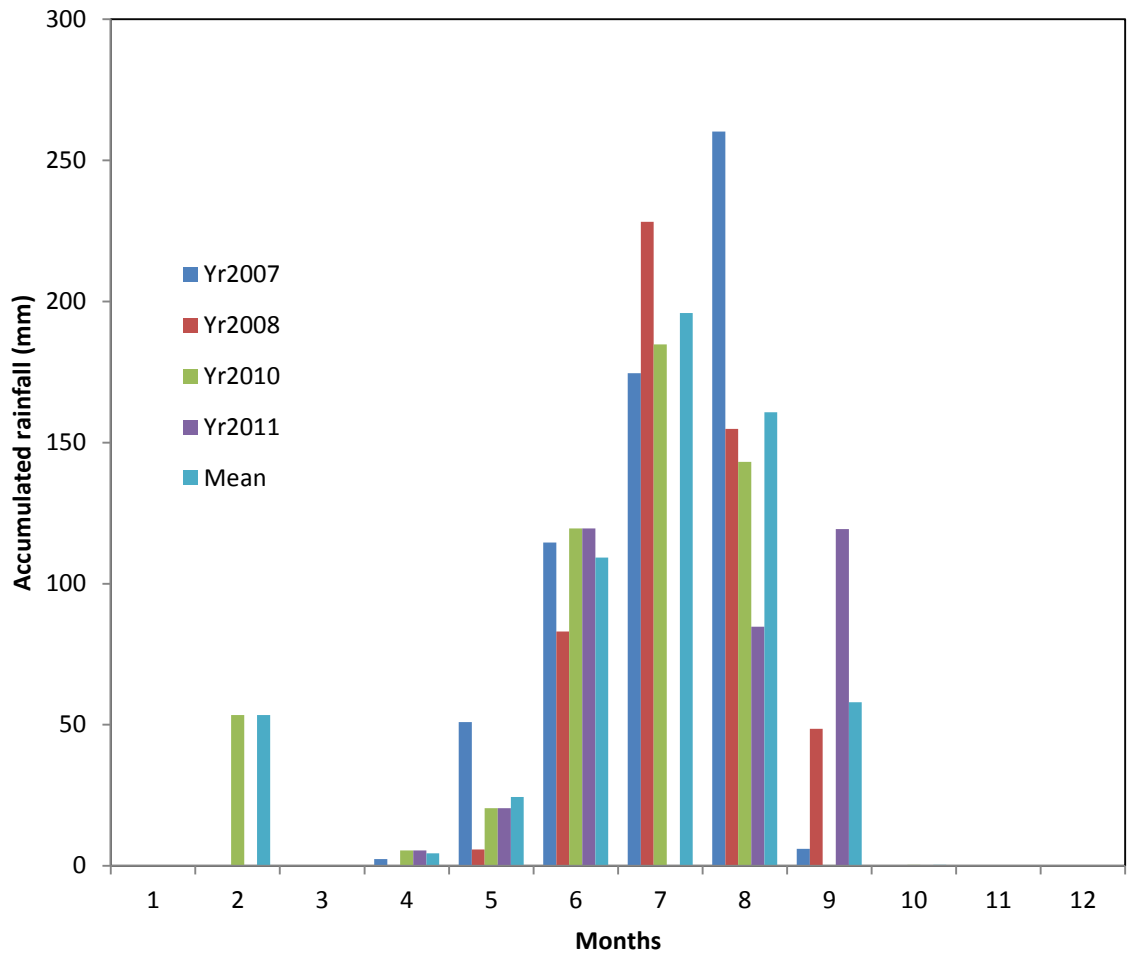


**Figure 4.6.** Cumulative monthly rainfall distribution (mm) at Kano

#### **4.1.2 Cumulative distribution function (CDF) of rain rates based on different integration times**

Rainfall rate distribution is a function of sampling interval of rain gauge. Higher rain gauge sampling interval causes the under estimation of measured rain rate (Chun, 2013). One minute accumulation corrects the defects in rain measurements by gauges and presents values that are close to the ideal (Crane, 1996). Rainfall rates CDF gives an estimate of rainfall rates as a function of raingauge sampling interval. The raingauge used for data collection at 12 out of the 14 stations used in the study were configured to capture the rainfall data at 5 minutes integration time. The LG (1998) model of equation 3.8 was used for the conversion of the 5 minutes data to 1-minute which according to Fashuyi *et al.* (2007) is the lowest integration time of rainfall data for attenuation determination.

The CDF for all the eco-climatic zones for the 12 stations with integration time of 5 minutes and two stations with in-situ rain fall rate measurements at 1-minute integration time are presented in Figure 4.7 (a-f) and appendix 2.

As can be observed from Figure 4.7 (a-f) and appendix 2, rainfall rate is underestimated at 5- minutes integration time at all percentages of exceedance in all the eco-climatic zones. Considering the adverse effects of inaccurate rainfall rate prediction on system design, Olsen (1999) stressed the imperative for accurate propagation prediction as over-prediction can lead to costly system over-design whereas, the consequence of under-prediction can be systems that under-performs.

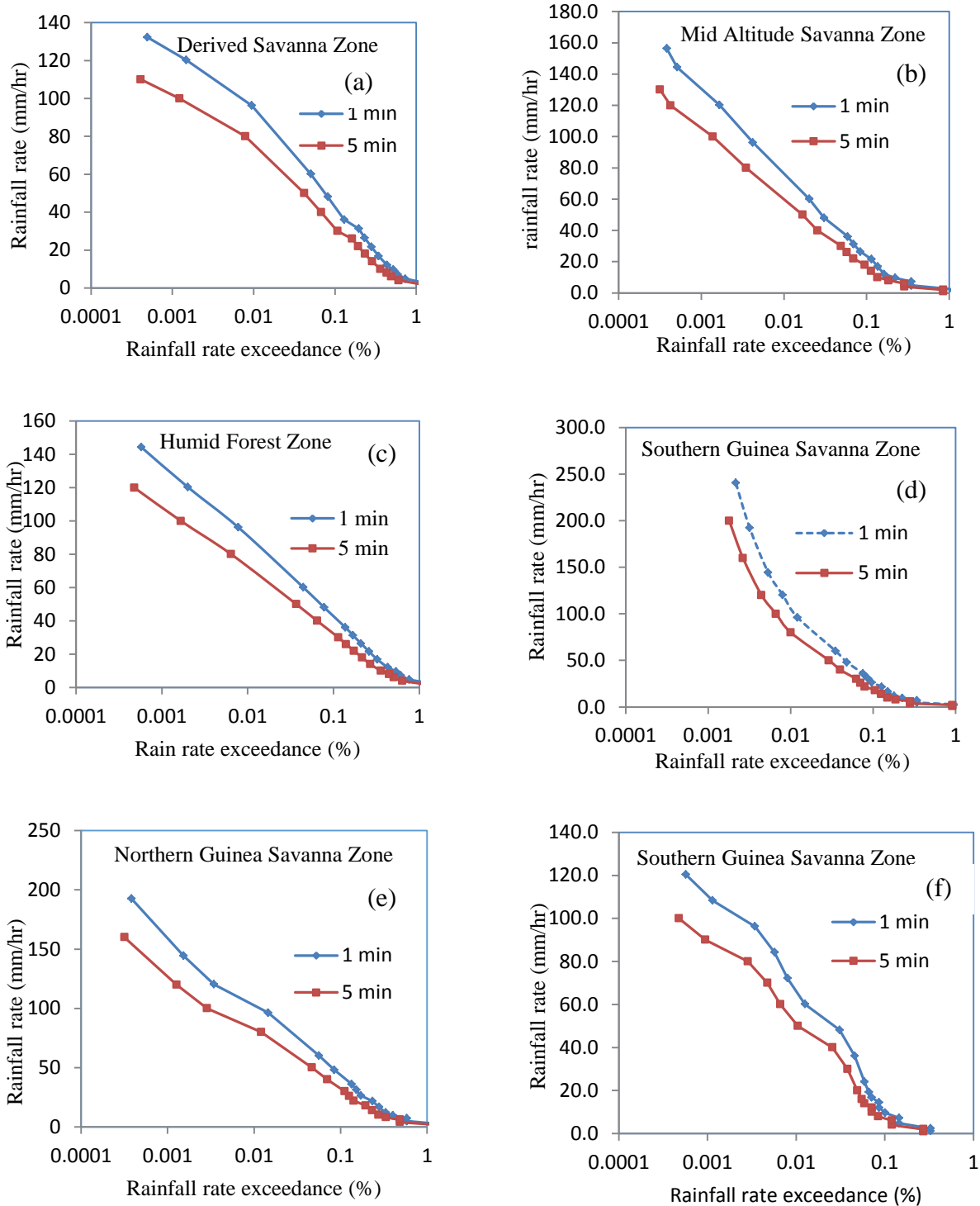


**Figure 4.7.** Cumulative distribution function of rain rates

#### **4.1.2.1 Annual rainfall rates cumulative distribution**

The percentage of time of annual rain rate exceedance was used to obtain the rainfall rates cumulative distribution. As recommended by ITU-R 837-7 (2017) on the precipitation characteristics suitable for modeling of signal propagation, consideration of the 0.01% rain rate exceedance which amounts to 99.99 % radio signal availability is the recommended standard. This is equivalent to about 53 minutes outage/year, 4.3 minutes/month and 8.5 seconds/day (Table 2.1). In this section, emphasis shall be made on this percentage of exceedance. Yearly rainfall rates percentages of exceedance are used in this section.

The variation of the yearly cumulative distribution of the averaged 1-minute integration time rainfall rate over the eco-climatic zones are shown in Figure 4.8(a - f) and appendix 3. It can be observed from Figure 4.8 (a - f) and appendix 3 that as the percentage of time decreases, the rainfall rate increases and vice versa.



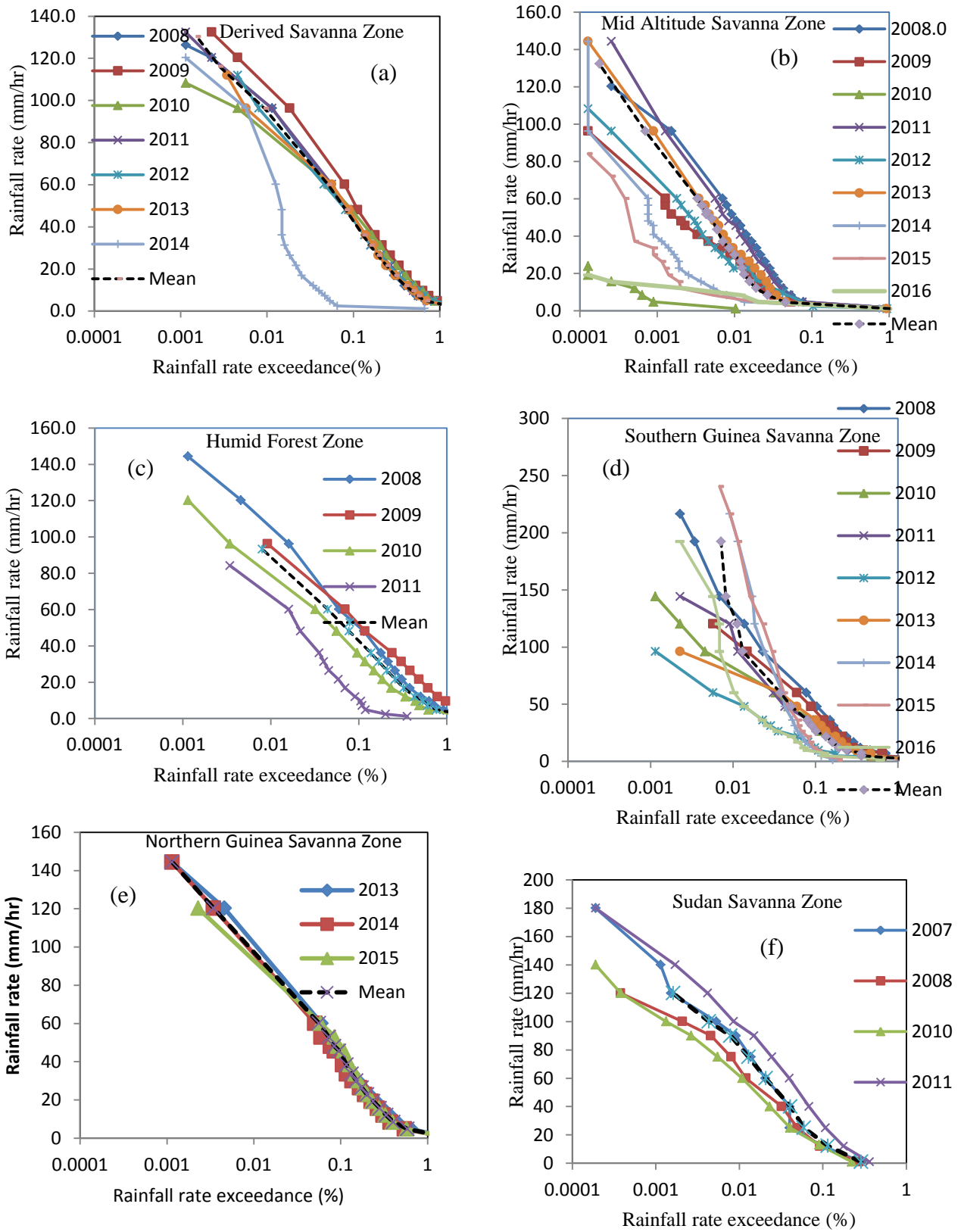


**Figure 4.8.** Annual cumulative distribution of rainfall rates

#### **4.1.2.2 Comparison with other tropical and sub-tropical locations**

To ascertain the situation in some other tropical/sub-tropical locations of the world, studies by Mandeep et al. (2008) in Indonesia, Fasuyi et al. (2007) in South-Africa, Rajar at al. (1999) in India and Sakir (2014) in Bangladesh were considered. The findings are presented in Figure 4.9.

Figure 4.9 presents a typical example of the comparison of the average cumulative distribution for the present study with the measurement from some other tropical and subtropical stations such as Malaysia, Indonesia, Bangladesh, and South Africa. The comparison shows a reasonable agreement with these other measurements. As can be observed, the rainfall rate and the percentage of time of exceedance are inversely related. Rainfall rate of about 20, 25 and 10 mm/hr were recorded in Indonesia, South Africa, India and Bangladesh respectively at 1% time while at 0.01%, 120mm/hr, 130mm/hr, 70mm/hr and 120mm/hr were the rate of rainfall at the locations respectively (Rajar *et al.*, 1999, Mandeep *et al.*, 2008, Sakir, 2014). This is in close agreement with the result of the present study; In Nigeria, the rain rate at 0.01% ranged from 43.3 mm/hr to 120.5 mm/hr while at 1% it ranged from 2.41 mm/hr to 3.5 mm/hr. The same trend was observed in other percentages of time.

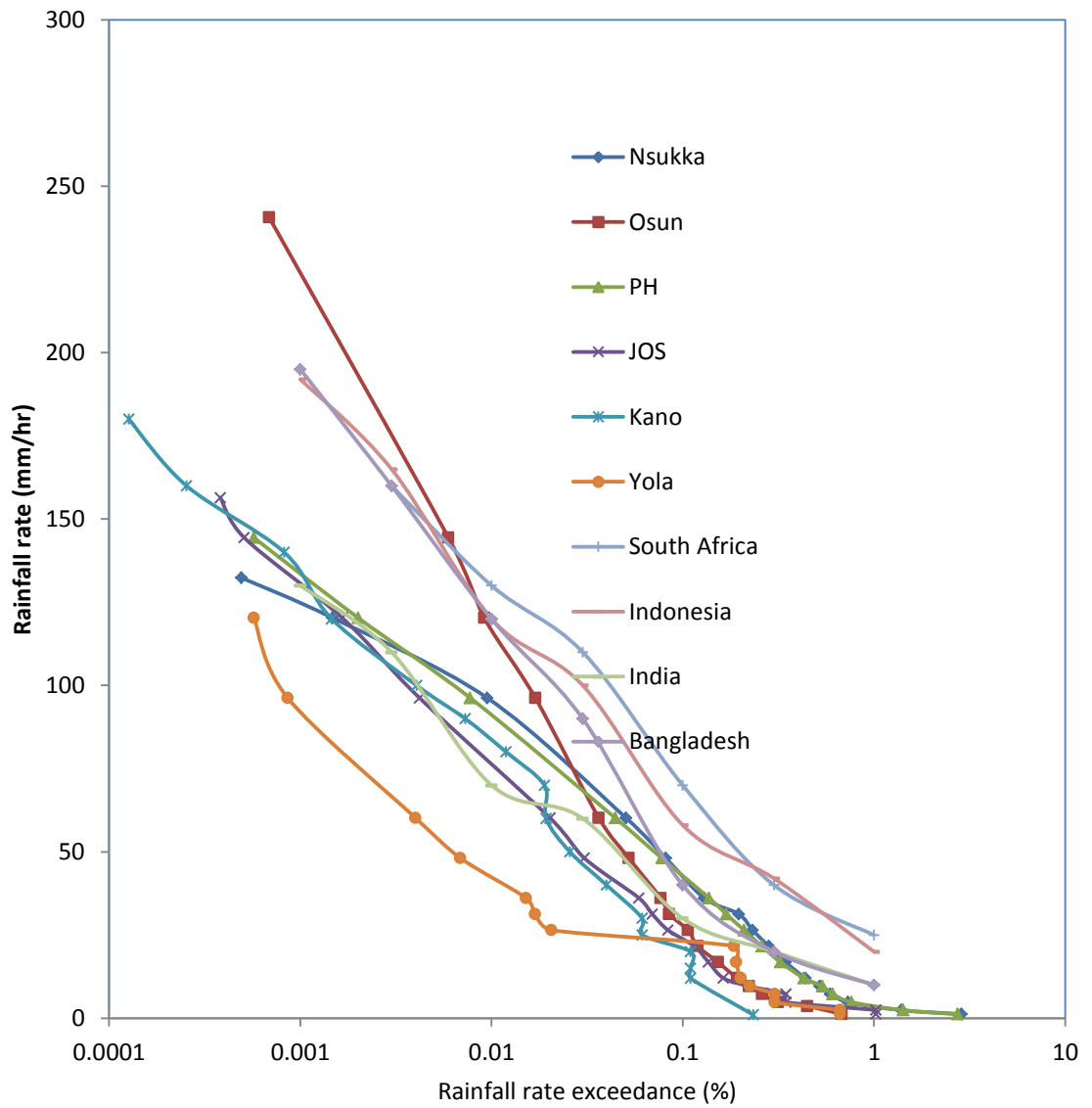


**Figure 4.9.** Comparison of cumulative distribution of rainfall rates with other tropical/sub-tropical locations.

### **4.1.3 Diurnal variation of rain**

The intensity of rain occurrence and its probability is time dependent and strongly dependent on the climatology of each location (Ojo et al., 2014). Knowledge of the highest rain rate and the corresponding time of occurrence determine millimeter wave signals fade margin at an instant of time. According to Das et al., (2013), high rain rate for shorter time duration can cause high fade since rain attenuation depends on rain rate. To ascertain this, the duration of observations in all the stations were reduced from annual to 24 hours mean. The 24 hour period were subdivided into 12 sections of two hours interval. Analysis was carried out on the quantity of rain encountered during each interval to obtain 24 hours rainfall variation at 2-hours interval. The data was further analysed to ascertain the time interval of the day that witnessed the highest and lowest rainfall duration in all the stations; hence the period of the day that signal fade would be more pervasive The results are presented in figure 4.10(a-f).

As shown in figure in figure 4.10(a-f), the time interval with the prevalent average rainfall ranged from 6-8 hours Local Time (LT) and 16-18 hours LT. The average rainfall that prevailed within the time range was 59.10mm to 433.5mm.

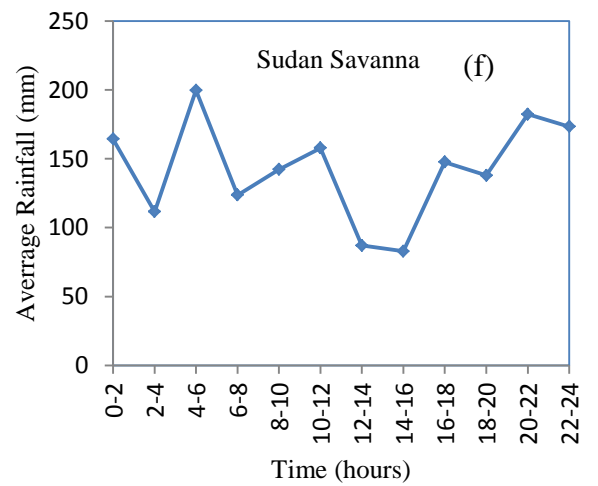
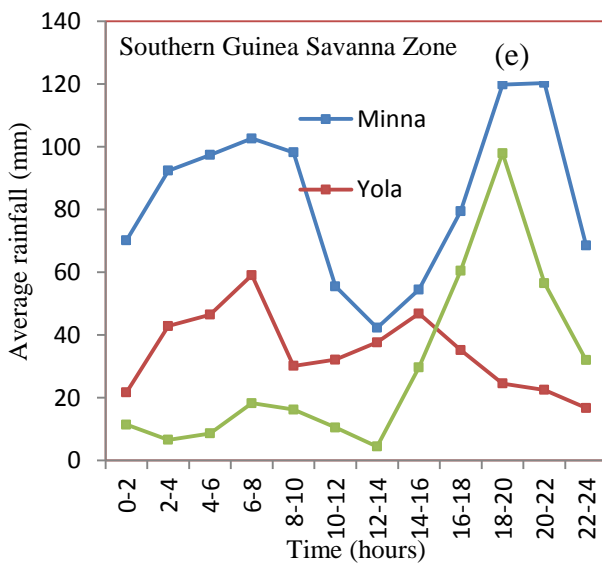
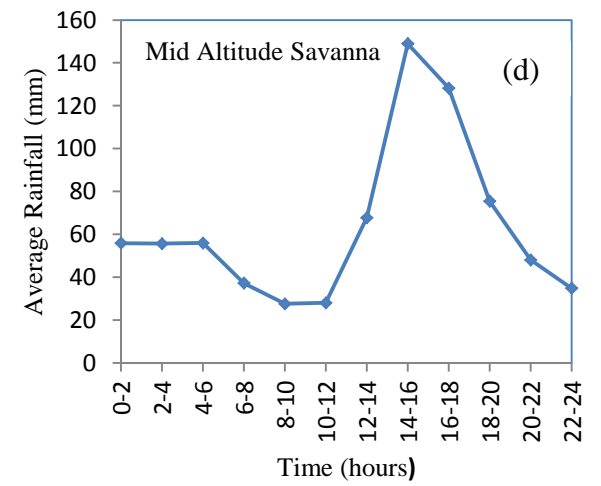
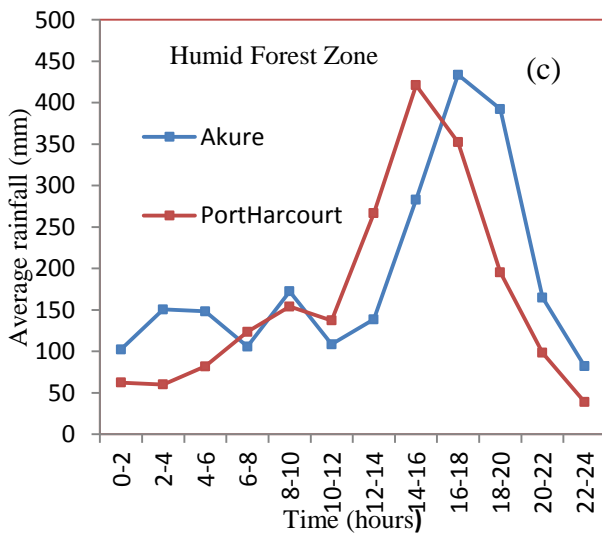
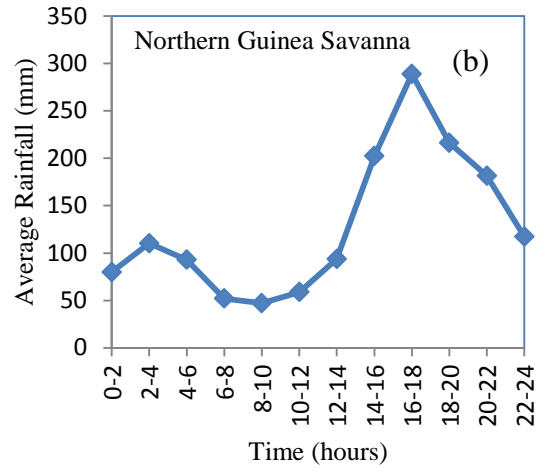
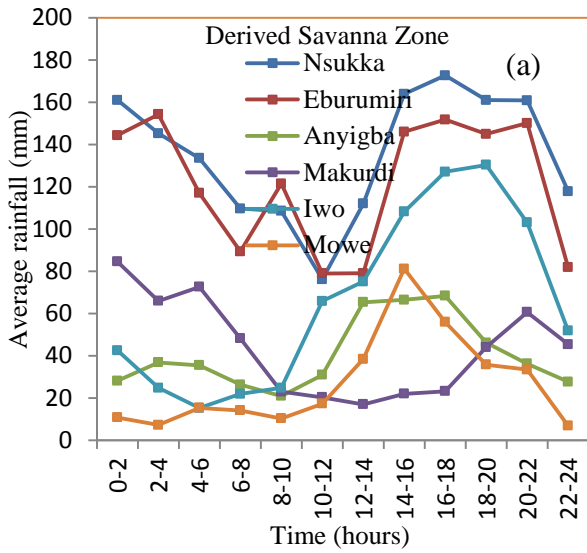


**Figure 4.10.** Diurnal variation of rainfall for each eco-climatic zone

#### 4.1.4 Time series of rainfall events

Tropical rainfall varies substantially with what obtains in temperate regions hence the empirical relationship obtained from the former does not apply to the latter (Ajayi *et al.*, 1996, Green, 2004). The dominant rainfall type in the tropics is convective with high precipitation rates that occur over short duration with limited coverage (As-syakur, 2018). Conversely, widespread rain prevails in temperate climates as the dominant rain falls are from stratiform cloud. It is characterised by rain rates that spans longer propagation paths with greater than one hour duration (Salema, 2003).

This section presents the result of highest rainfall events at the locations considered and their implication on radio wave propagation. According to Kestwal *et al.* 2014, the total atmospheric attenuation for every region increases exponentially up to a certain limit as the rain rate of the location increases.

To present the tropical rainfall structure, the time series of rain rate characterization was used (Ojo *et al.*, 2014). To characterize the rain rate, the month with the most intense rainfall rate in each location were selected in order to characterize the rainfall types in Nigeria. As reported in the work of Adimula (2003) and Joss *et al.* (1968), thunderstorm and shower rainfall events are classified as convective rain types whereas widespread and drizzle events are classified as stratiform rain types. Drizzle distribution is 5 mm/hr, widespread distribution ranges from 5 mm/hr to 10 mm/hr, showers distribution ranges from 10 mm/hr to 40 mm/hr while thunderstorm distribution constitutes rainfall intensity greater than 40 mm/hr (Obiyemi *et al.*, 2014). These values were adopted in the classification of the rainfall types that prevailed at the locations of study in Nigeria.

In the present study, the month with the most intense cumulative rainfall rate out of all the years considered in each station shall be considered the worst month (ITU-R 581-2, 1990). Two of the days with the most intense rainfall rate were selected and the rain types encountered during the period of observation were divided into convective and stratiform rain types. The time intervals of the rainfall types encountered and the corresponding rain rate were plotted to deduce the rainfall types that prevailed during the rain event. The time intervals without any rainfall recording during the event were excluded in the analysis. This section is geared towards establishing the dominant rainfall type that prevailed at each study location and the

corresponding time interval. This information will afford radio engineers information for designs for the worst hour of the day for Nigeria. Figure 4.11 (a-f) and appendix 4 presents the time series of the days of the month with the most intense rainfall rate across the six eco-climatic zones of Nigeria. The results presented in figure 4.11 (a-f) and appendix 4 revealed that convective rainfall type was the most dominant in virtually all the locations. However as opposed to the submissions of Salema (2003), the convective rainfall event is not dominant in all parts of the tropics. Deduction from the study revealed that stratiform event prevailed in an event in Yola hence the empirical relationship obtained from temperate climates could be applicable to this location.

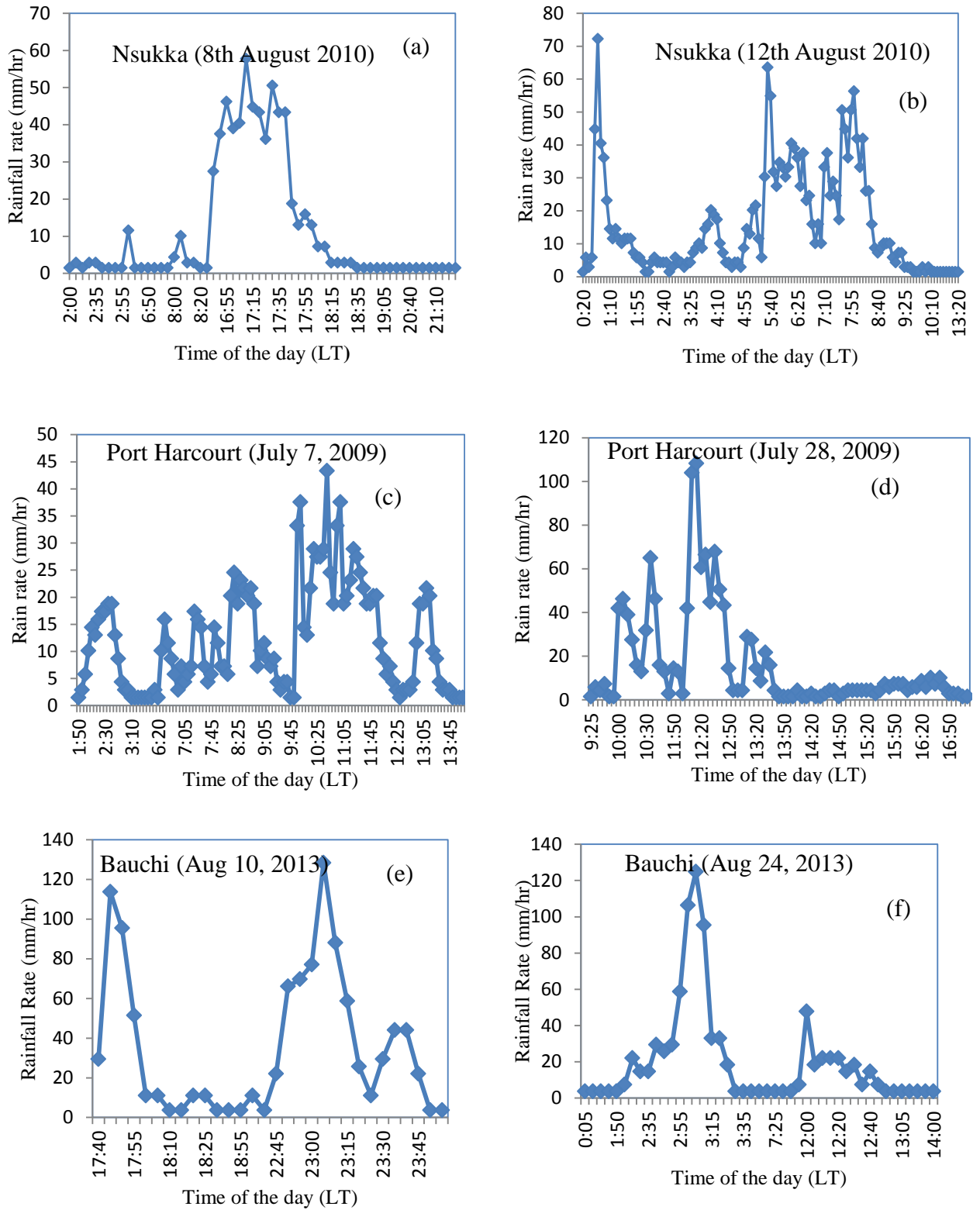


**Figure 4.11.** Time series of rainfall rates during rain events



#### **4.1.5 Dependence of annual average rainfall intensity on hour of the day**

According to Ojo *et al.* (2014), the dependence of the annual average rainfall intensity on the hour of the day is essential in determining the exact hour of the day in which the peak of the rainfall event will occur throughout the period of study at the locations. This is essential in determining the exact hour of the day when rainfall will affect direct to home communication services at the locations considered. This information will enable radio engineers to take appropriate measures to mitigate the effects. Figure 4.12 to 4.17 shows the situation over the six eco-climatic zones considered. Appendix 5 presents the scatter plots of all the rainfall events throughout the period of the day with intense rainfall. All the rainfall events in appendix 5 for each period of the day were averaged to give Figure 4.12 to 4.17.

The intensity of the rainfall event during the 24 hour of the day at the derived savanna zone can be seen in Figure 4.12. It shows that the maximum rainfall rate occurred at 15 hours LT at Eburumiri and Nsukka locations while 14 hrs and 20hrs, 12 hrs and 16 hours LT of the days were the period with the highest rainfall intensity for Anyigba, Makurdi, Iwo and Ogun respectively. These were the worst hour of rainfall events at these locations. Generally, during the period of this study, the rainfall was more intense in the active hours of the day (morning and evening). This development is bound to impact adversely on communication services both at home and offices.

The situation in the humid forest zone is shown in Figure 4.13. As can be inferred from the figure, 18 hours and 14 hours Local Time were the worst hours of rainfall events in Akure and Port Harcourt locations respectively. Considering Bauchi, the only location covered from Northern Guinea Savanna zone, Figure 4.14 presents the daily rainfall event. The result shows that 15 hours LT was the hours of maximum rainfall event in this location. Hence the 15 hours LT is the worst hour in the northern guinea savanna location.

Other locations follow the same trend although with each location having different hours with maximum and minimum rainfall intensity as presented in figure 4.15 to 4.17.

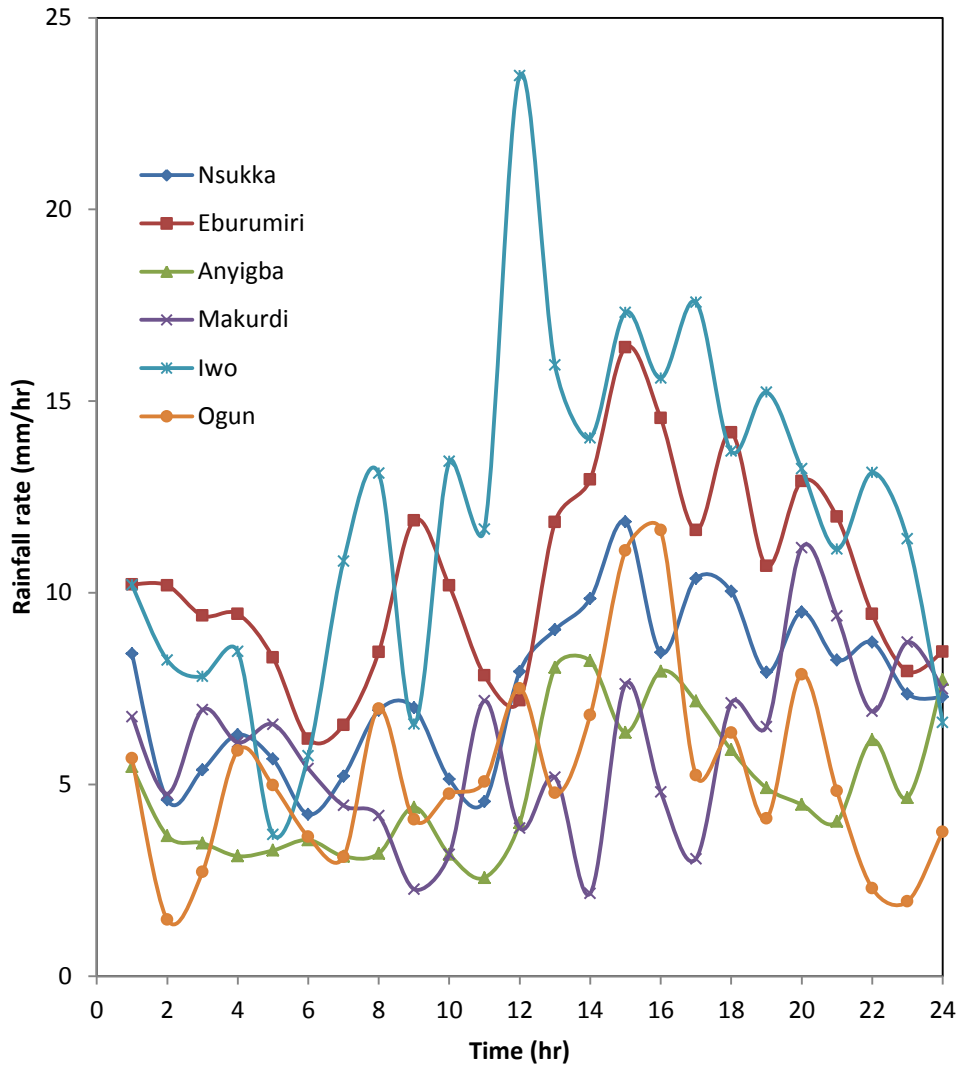


**Figure 4.12.** Diurnal variation of annual average rainfall rate events over the derived Savanna Zone

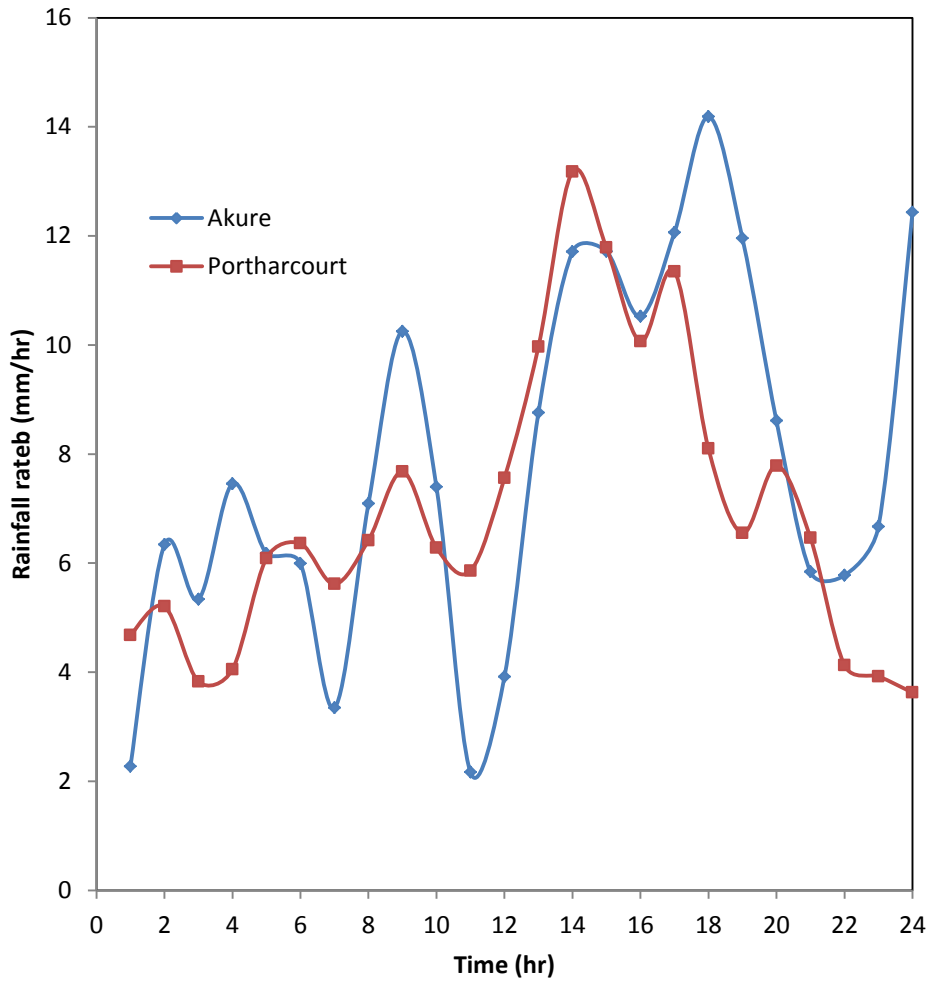


**Figure 4.13.** Diurnal variation of annual average rainfall rate events over the humid forest zone

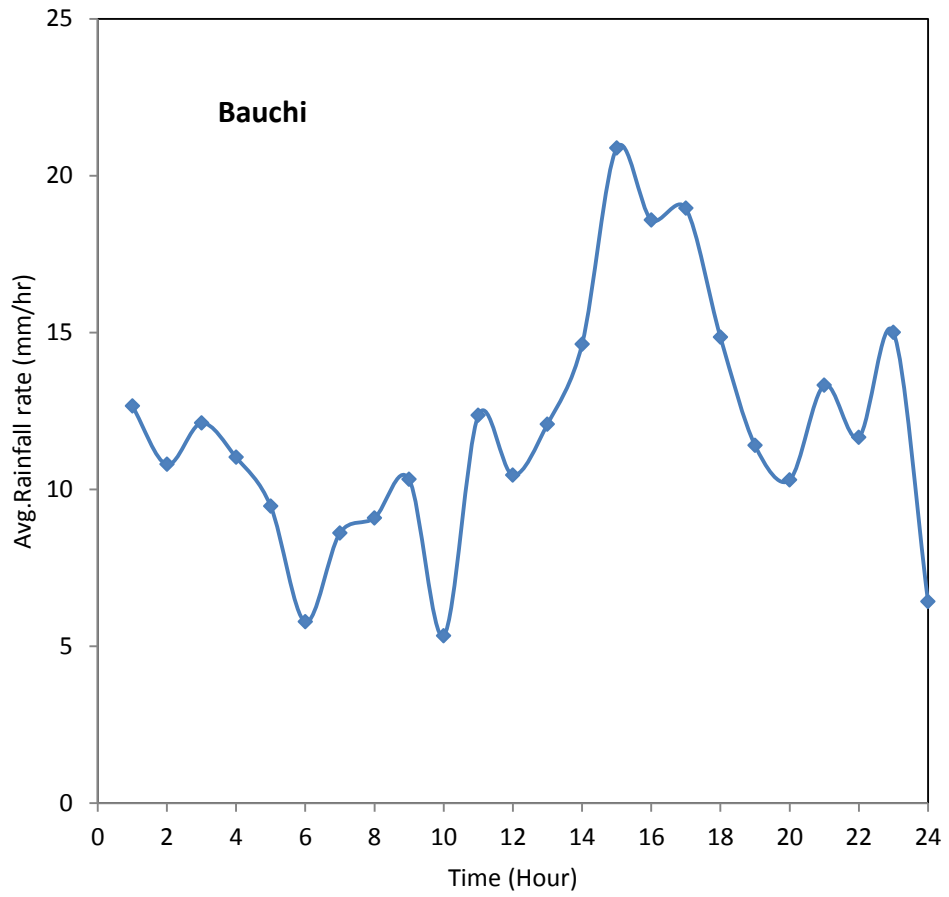


Fig. 4.14. Diurnal variation of annual average rainfall rate events over the Northern Guinea Savanna zone

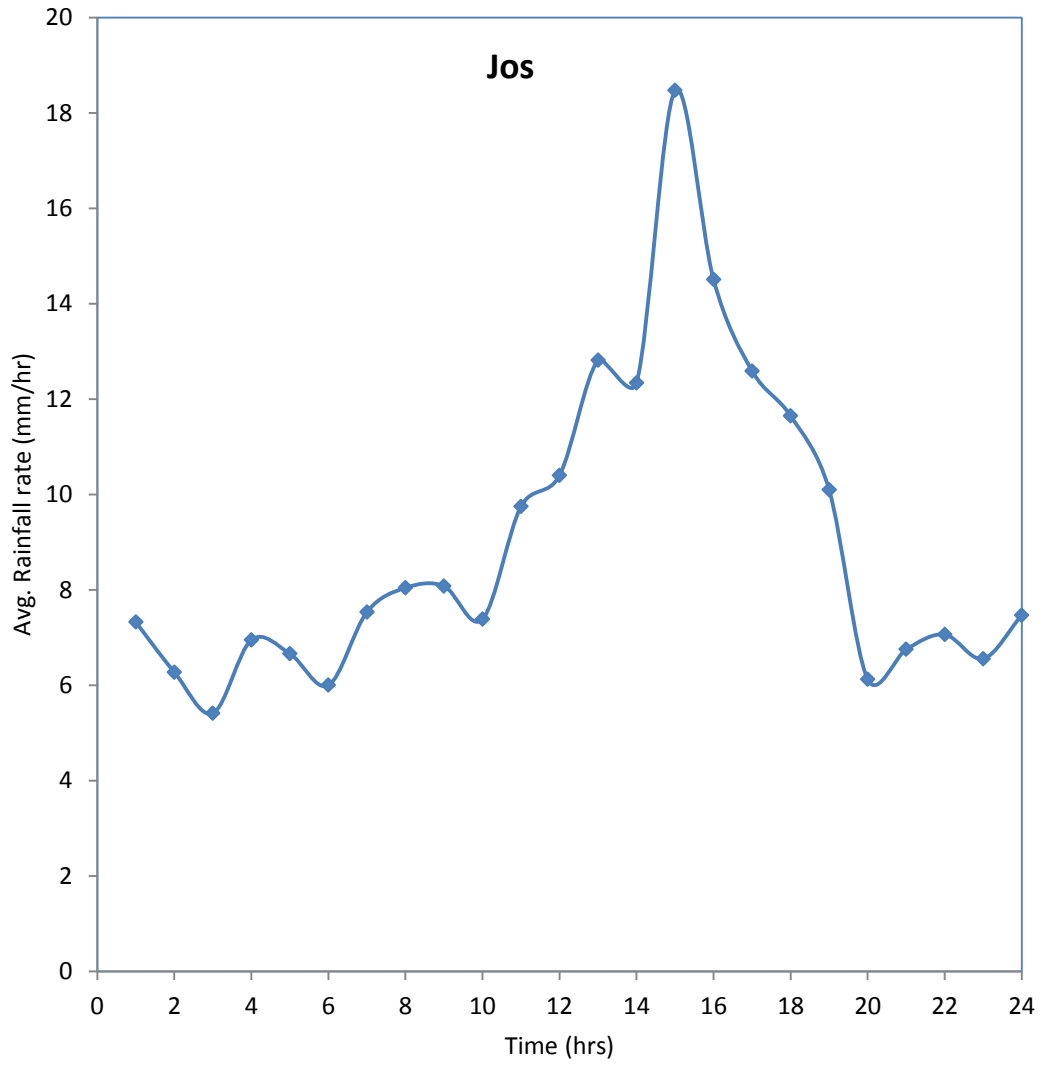


Fig. 4.15. Diurnal variation of annual average rainfall rate events over the mid altitude Savanna zone

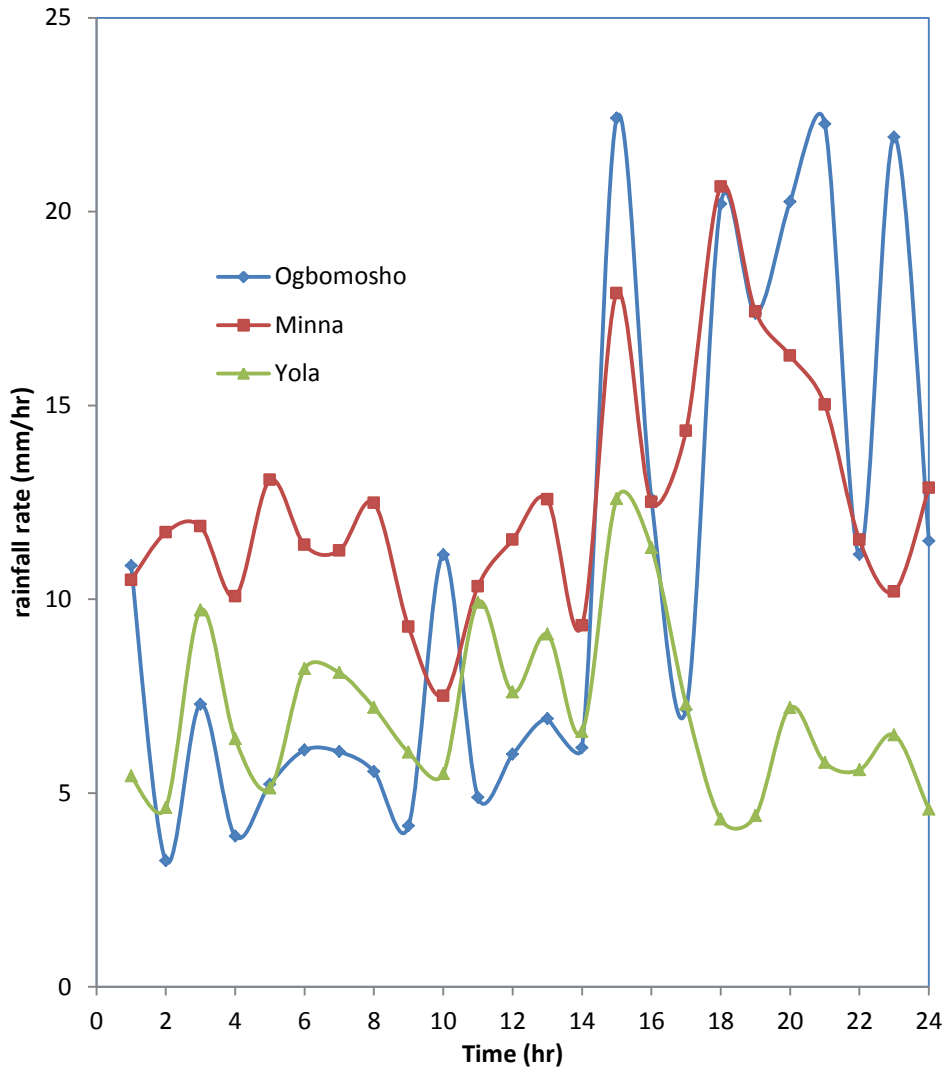


Fig. 4.16. Diurnal variation of annual average rainfall rate events over the southern Guinea Savanna Zone

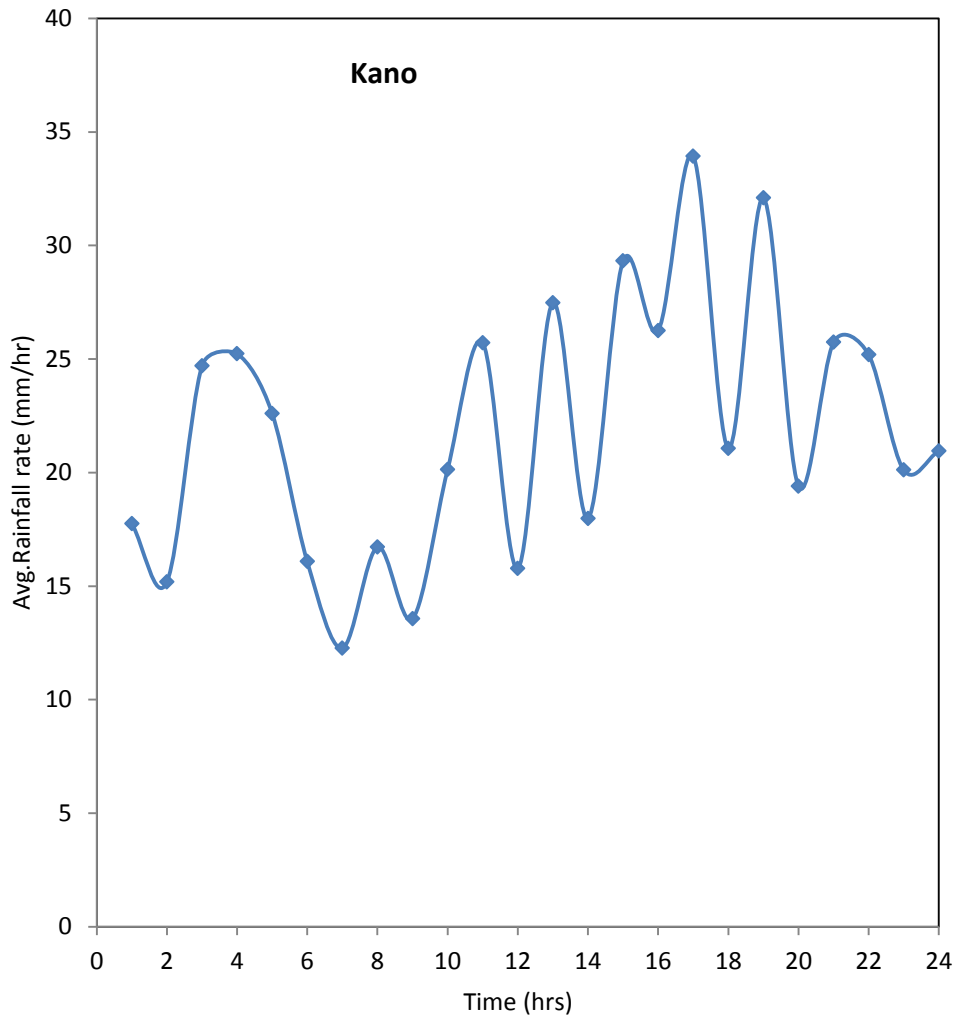


Fig. 4.17. Diurnal Variability of annual average rainfall rate events over the Sudan Savanna zone

intense in the active hours of the day (afternoon). This development is bound to impact adversely on communication services both at home and offices.

The worst hour and the corresponding rainfall rates in all the locations considered is summarized in Table 4.2. As shown from the Table, 15 hours LT was the worst hour in about 43 percent of the locations considered. Furthermore, rainfall worst hours are encountered in the afternoon at Port Harcourt, Anyigba and Iwo stations; the worst hour of rainfall in the rest of the stations considered is from late afternoon till evening. In effect, fade in the radio signal would take effect only in the afternoon hours at Port Harcourt, Anyigba and Iwo stations while in the remaining stations signal failure would prevail from afternoon till evening hours. Generally, rainfall was highest (34.0 mm/hr) at Kano location and least (8.22 mm/hr) at Anyigba.



**Table 4.2.** Summary of the worst hour and the corresponding rainfall rates in all the locations

Locations	Average Worst Hour (AWH)	Rainfall Rate (mm/hr)
Nsukka	15	11.86
Eburumiri	15	16.40
Yola	15	12.59
Anyigba	14	8.22
Akure	18	14.19
Bauchi	15	20.92
Jos	15	18.48
Kano	17	34.00
Port Harcourt	14	13.18
Makurdi	20	11.18
Minna	18	20.65
Ogbomosho	15	22.69
Ogun	16	11.56
Iwo	12	23.70

#### **4.1.6 Comparison of measured rain rate and rain rate derived from ITU-R model**

The ITU-R sector has provided guide towards obtaining the attenuating effects of rain on radio links. However, as presented in the work of Da Silva Mello *et al.* (2007) the ITU-R method does not perform well in the tropical regions, characterised by higher rainfall rates and greater raindrops diameter. This is because the ITU-R model is derived from temperate regions data collections. For reliable prediction of rain attenuation at any location, the determination of the characteristics of rainfall of the study site is crucial (Owolawi *et al.*, 2008). The comparison of ITU-R recommended rainfall rate and the measured rain rate at the locations considered is presented in this section.

As stated by Ojo *et al.*, (2016), the LG (1998) model is the best over all other models for converting different integration times, hence the converted one minute integration time using LG over all studied locations are compared with the ITU-Radio approved values. The ITU-Radio recommended percentage exceedencies are: 10% - 0.0001%. Results are presented in appendix 6 and Table 4.3 summarizes the situation at the derived savanna eco-climatic zones. From the Table, it can be observed that in the derived Savanna Zone, the rain rate is under-estimated by the ITU-R in almost all the percentages of exceedance. Eburumiri, a derived Savanna location is the only exception as ITU predicted rainfall rate tallied with the in-situ value at the 1%, 0.3% and 0.001% of exceedance. At Nsukka, only the 0.003% and 0.001% values of rain rate were over-estimated. The largest (75%) and the least (0.07%) difference between the ITU predicted value and in-situ measurement occurred in Mowe at 0.3% and Anyigba respectively. With the exception of Anyigba, the measurement at 0.0001% exceedance was not captured in all other locations at the derived Savanna zone.

To ascertain the ITU-R cumulative distribution in relation to Port Harcourt and Akure of the humid forest eco-climatic zones, Appendix6 shows the relationship between the ITU-R predicted rain rate and the estimated value while Table 4.4 presents the percentage of exceedance at different rainfall rates. As shown in Table 4.4, at virtually all measurable percentages of time, rainfall rate was over-estimated by the ITU-R in Port Harcourt and under estimated at Akure. At 0.03% of time, the ITU predicted and the derived rain rate in Akure location differed by about 92.98%.The predicted cumulative distribution by the ITU-R together with the in-situ derived values at the

**Table 4.3.** ITU percentage of exceedance at different rainfall rates CD in the derived savanna zone

ITU rain rate exceedance (%)	Nsukka			Ehurumiri			Anyigba			Makurdi			Iwo			Ogun		
	ITU-R	In-situ	Diff. (%)	ITU-R	In-situ	Diff. (%)	ITU-R	In-situ	Diff. (%)	ITU-R	In-situ	Diff. (%)	ITU-R	In-situ	Diff. (%)	ITU-R	In-situ	Diff. (%)
1	-	-	-	2.44	2.44	0.00	5.07	5.10	0.59	3.23	3.20	0.93	-	-	-	-	-	-
0.3	17	32	46.88	11.07	11.07	0.00	14.99	15.00	0.07	8.04	8.00	0.50	8.0	12.0	33.33	12.0	3.0	75.00
0.1	28	43	34.88	27.67	36.10	23.25	35.16	35.20	0.11	33.70	9.60	71.51	5.0	28.0	82.14	20.0	6.0	70.00
0.03	66	80	17.50	52.41	75.00	30.12	64.93	25.00	61.50	50.23	50.50	0.53	44.0	88.0	50.0	48.0	33.0	31.25
0.01	82	94	12.77	80.92	105.00	22.93	94.38	31.30	66.84	91.90	70.00	23.83	58.0	118.0	50.85	62.0	40.0	35.48
0.003	130	116	10.76	118.09	130.00	9.16	127.53	50.00	60.79	122.61	88.00	28.23	92.0	192.0	52.08	99.0	52.0	47.47
0.001	150	124	17.33	149.83	149.83	0.00	158.14	240.70	34.30	155.40	121.50	21.81	104.0	225.0	53.78	114.0	56.0	50.88
0.0001	-	-	-	-	-	-	162.34	-	-	-	-	-	-	-	-	-	-	-

Northern Guinea Savanna is also present in appendix 6 while Table 4.5 summarized the difference between the derived and ITU predicted rain rate values.

As established from Table 4.5, ITU under-estimated rainfall rate in all the percentages of exceedance at the Northern guinea savanna location zone. The 0.001% is the most under estimated at the location. Appendix 6 shows the aggregate rainfall rate at the mid altitude savanna zone locations while the various percentages of time rain rates is given in Table 4.6. Appendix 6 and Table 4.6 revealed that ITU-R over-estimated the rainfall rate in almost all percentages of exceedance except at 0.001% when it was under-estimated by about 22.14%. The cumulative distribution of the rain rates for the Southern Guinea Savanna as well as Sudan Savanna are shown in appendix 6 while Table 4.7 and 4.8 represented the percentage of exceedance of rainfall rate at the cumulative distribution.

The Table 4.7 shows that ITU-R over-estimated the rainfall rate in all percentages of time at the Yola location. At Ogbomosho locations, ITU-R under-estimated the rainfall rate in almost all percentages with the exception of 0.3% and 0.1% of time where it was under-estimated by about 60% and 37.5% respectively. At the location in minna, ITU-R over-predicted the rainfall rate in 50% of the measurable percentages of exceedance and under-predicted it in 50% of the percentages. The performance of ITU recommendation in Minjibiri of Sudan Savanna zone is as shown in appendix 6 and Table 4.8. The results shows that ITU-R under-predicted the rainfall rate in virtually all percentages of exceedance except at 0.3% where it under-predicted it by about 66.67%. The implication of these result is that performance of communication equipment designed with ITU-R estimates, are bound to fall below expectation in the affected locations. In summary, the departure of ITU-R rain rate estimate from in-situ measurements could lead to either costly system over-design or design of systems that are unreliable. This is in agreement with the findings of Olsen (1999).

**Table 4.4.** ITU percentage of exceedance at different rainfall rates CD in the humid forest zone

ITU rain rate exceedance (%)	<b>Akure</b>			<b>Port Harcourt</b>		
	ITU-R	In-situ	Diff (%)	ITU-R	In-situ	Diff (%)
1	3.0	18.0	83.33	8.15	-	-
0.3	12.0	48.0	75.00	25.57	16.85	34.10
0.1	20.0	66.0	70.00	47.50	45.00	5.26
0.03	8.0	114.0	92.98	83.95	66.00	21.38
0.01	62.0	130.0	52.31	109.10	95.50	12.47
0.003	99.0	158.0	37.34	145.54	118.00	18.92
0.001	114.0	164.0	30.49	173.40	135.00	22.15
0.0001	166.0	180.0	7.77	180.21	-	-

**Table 4.5.** ITU percentage of exceedance at different rainfall rates CD in the Northern Guinea Savanna zone

ITU rain rate exceedance (%)	Bauchi		
	ITU-R	In-situ	Diff. (%)
1	-	-	-
0.3	8.0	25.0	68.0
0.1	12.5	42.5	70.59
0.03	30.0	88.0	65.91
0.01	42.5	102.5	58.54
0.003	78.0	138.5	43.68
0.001	92.5	158.0	41.46
0.0001	-	-	-

**Table 4.6.** ITU percentage of exceedance at different rainfall rates CD in the mid altitude savanna location

ITU rain rate exceedance (%)	<b>Jos</b>		
	ITU-R	In-situ	Diff (%)
1	4.0	4.0	0.00
0.3	18.0	10.0	44.40
0.1	30.0	24.0	20.00
0.03	68.0	60.0	11.76
0.01	88.0	76.0	13.64
0.003	112.0	116.0	3.45
0.001	102.0	131.0	22.14
0.0001	-	-	-

**Table 4.7.** ITU percentage of exceedance at different rainfall rates CD in the Southern Guinea Savanna locations

ITU rain rate exceedance (%)	<b>Ogbomosho</b>			<b>Minna</b>			<b>Yola</b>		
	ITU	In-situ	Diff (%)	ITU	In-situ	Diff (%)	ITU	In-situ	Diff. (%)
1	-	-	-	-	-	-	-	-	-
0.3	10.0	4.0	60.00	15.0	10.0	33.33	18.0	4.0	77.78
0.1	16.0	10.0	37.50	38.0	30.0	21.05	30.0	8.0	73.33
0.03	38.5	54.0	28.70	78.0	80.0	2.50	70.0	22.0	68.57
0.01	50.0	66.0	24.24	90.0	110.0	18.18	90.0	38.0	57.78
0.003	86.0	102.0	15.69	138.0	240.0	42.50	130.0	68.0	47.69
0.001	102.0	110.0	7.27	158.0	340.0	53.53	150.0	82.0	45.33
0.0001	-	-	-	-	-	-	-	-	-



**Table 4.8.** ITU percentage of exceedance at different rainfall rates CD for Sudan savanna locations

ITU rain rate exceedance (%)	<b>Kano</b>		
	ITU	In-situ	Diff (%)
1	-	-	-
0.3	6.0	2.0	66.67
0.1	10.0	20.0	50.00
0.03	30.0	60.0	50.00
0.01	42.0	84.0	50.00
0.003	78.0	114.0	31.58
0.001	94.0	132.0	28.79
0.0001	-	-	-

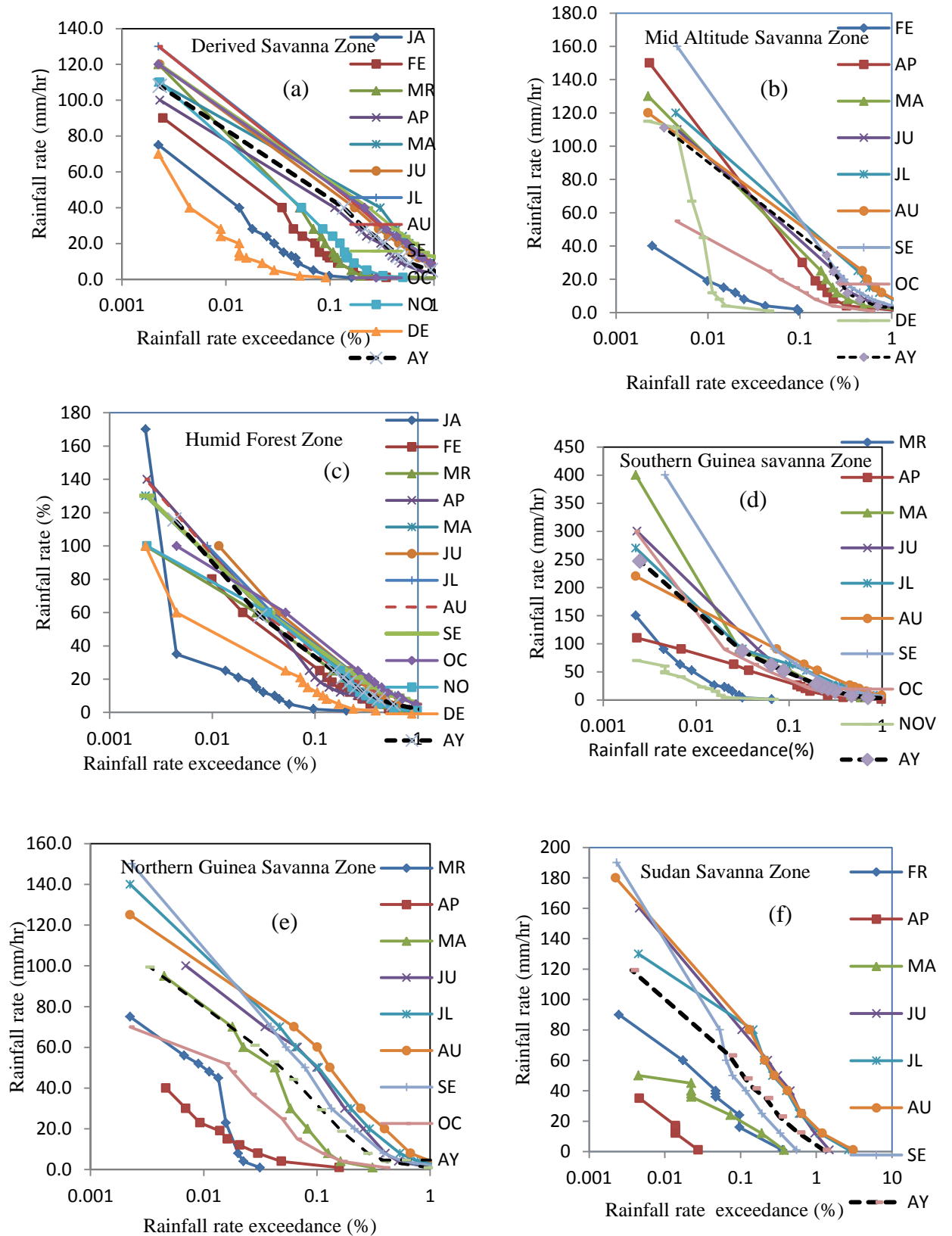
#### **4.1.7 Worst month rain rate characterization**

The conversion methods for average annual to average worst month time percentage of excess has been recommended by ITU-R 841-5 (2015). Calculation for ITU percentage annual and average worst month rain rate exceedance can be found in equations (3.35) and (3.36), respectively. These were compared with the derived values from in-situ measurements. Equation (3.34) is for the computation of conversion factor (Q) values for all the locations studied.

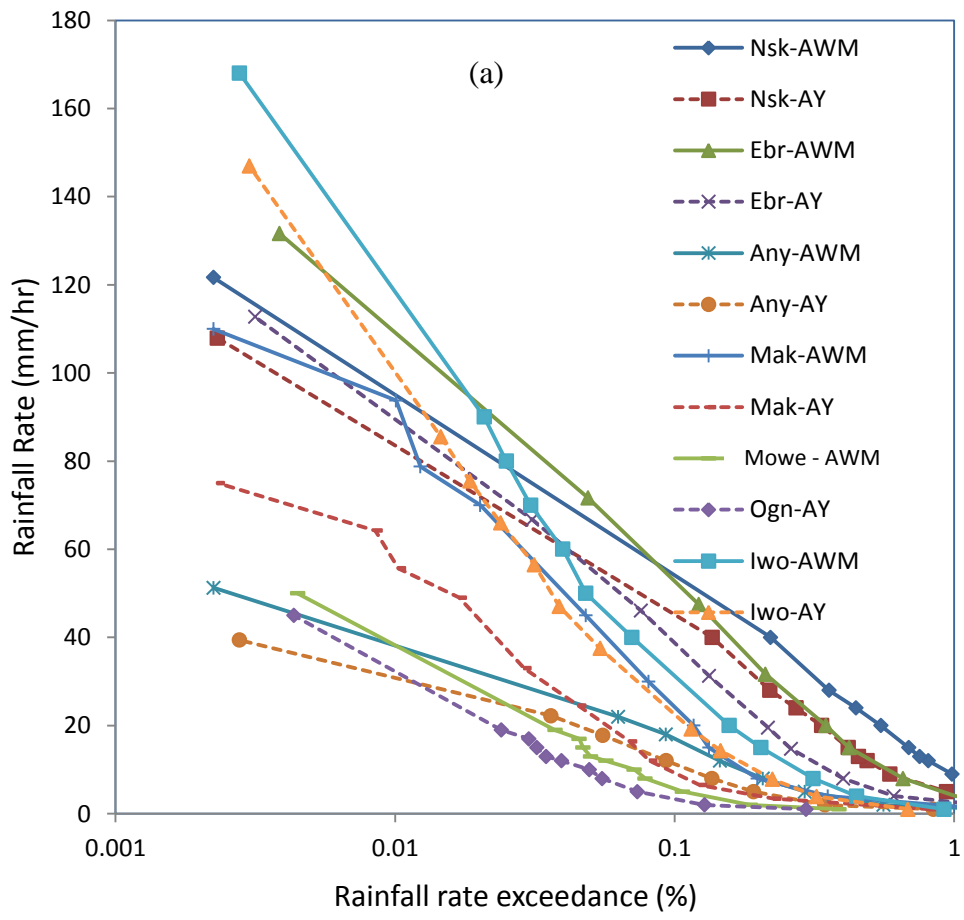
##### **4.1.7.1 Deduction of worst months**

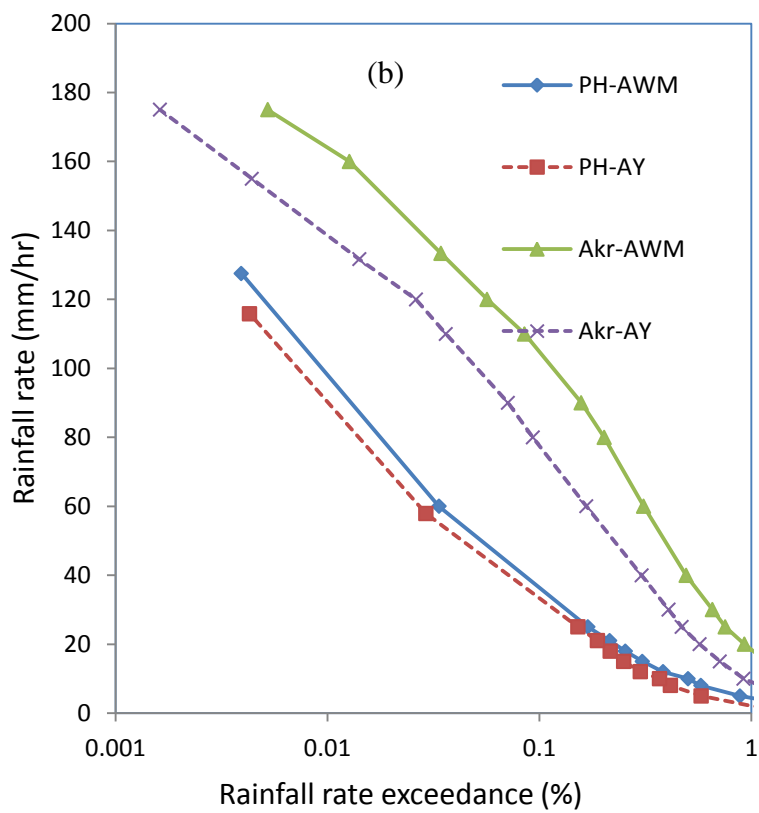
The monthly variation of rainfall rate distributions across the locations in each eco-climatic zones covered by the study are presented in figure 4.18 (a-f) and appendix 7. These are the mean monthly rain rate for the period of observations that exceeds the long term mean annual/Average Year (AY) distribution as recommended by ITU-R 841-5 (2015). The mean of the worst months for each location was computed to obtain the Average Worst Months (AWM). These values were used to derive the worst month statistics in each of the locations across the eco-climatic zones. The annual mean rain rate distributions for all the calendar months give the value for the Average Year (AY) in each of the locations. These results serve as guide to system engineers in setting their monthly objectives and designing for worst scenarios.

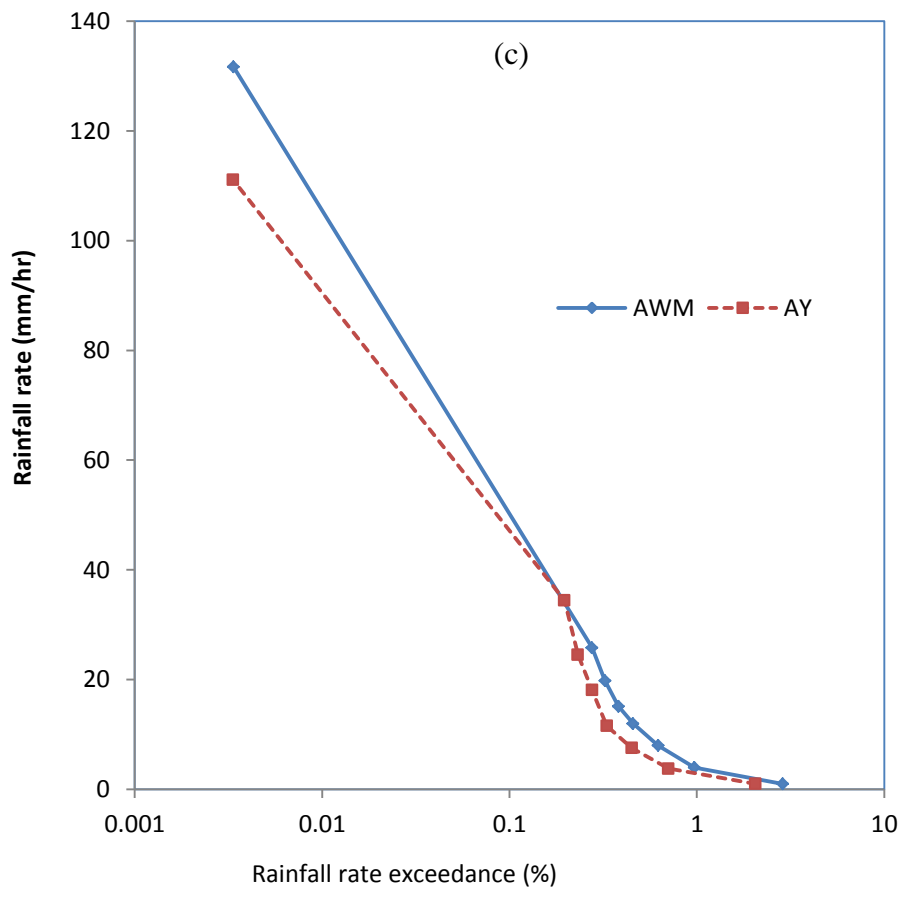
Figures 4.19 (a-f) show the relationship between the cumulative distribution of rainfall rates in average year and worst months across the eco-climatic zones. The yearly and worst month cumulative distribution for the derived savanna eco-climatic zones shows that at at 0.01% exceedance the highest rainfall rate was recorded at Iwo while Mowe recorded the least. At Iwo, rainfall rate of about 120 mm/hr was exceeded during the average worst month as against 100 mm/hr that was exceeded in the average year while in Ogun, rainfall rate of 38.5 mm/hr and 32.5 mm/hr were exceeded at the average worst month and the average year respectively. At the humid forest zones, the highest worst month rainfall rate (164 mm/hr) was exceeded on the average at Akure as against the 140 mm/hr exceedance in the average year at the location while the least average rainfall rate exceedance of 98 mm/hr and 90 mm/hr were recorded at Port Harcourt during the worst month and average year respectively.

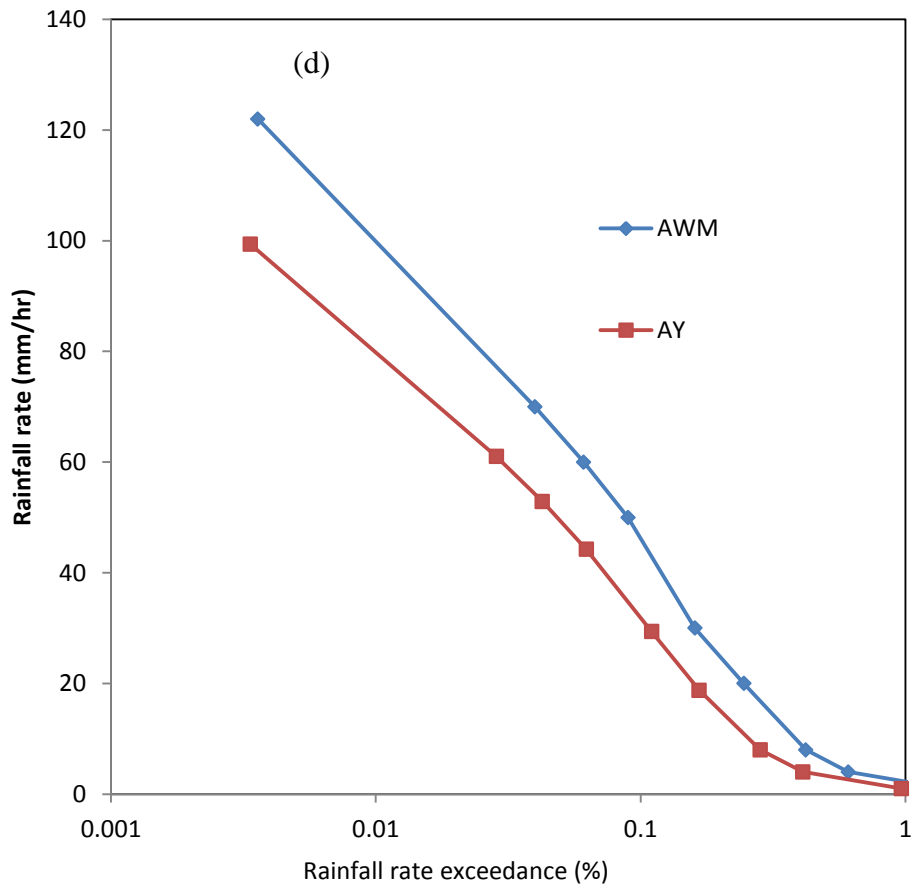


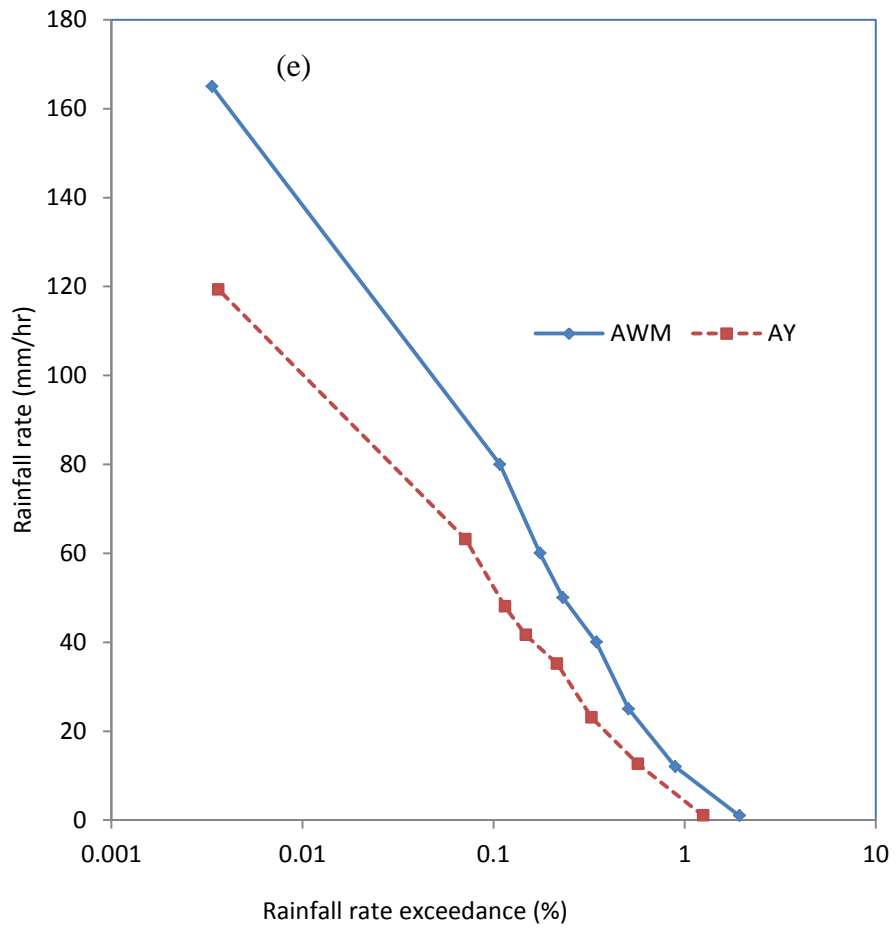
**Figure 4.18.** Monthly variation of rainfall rate distribution













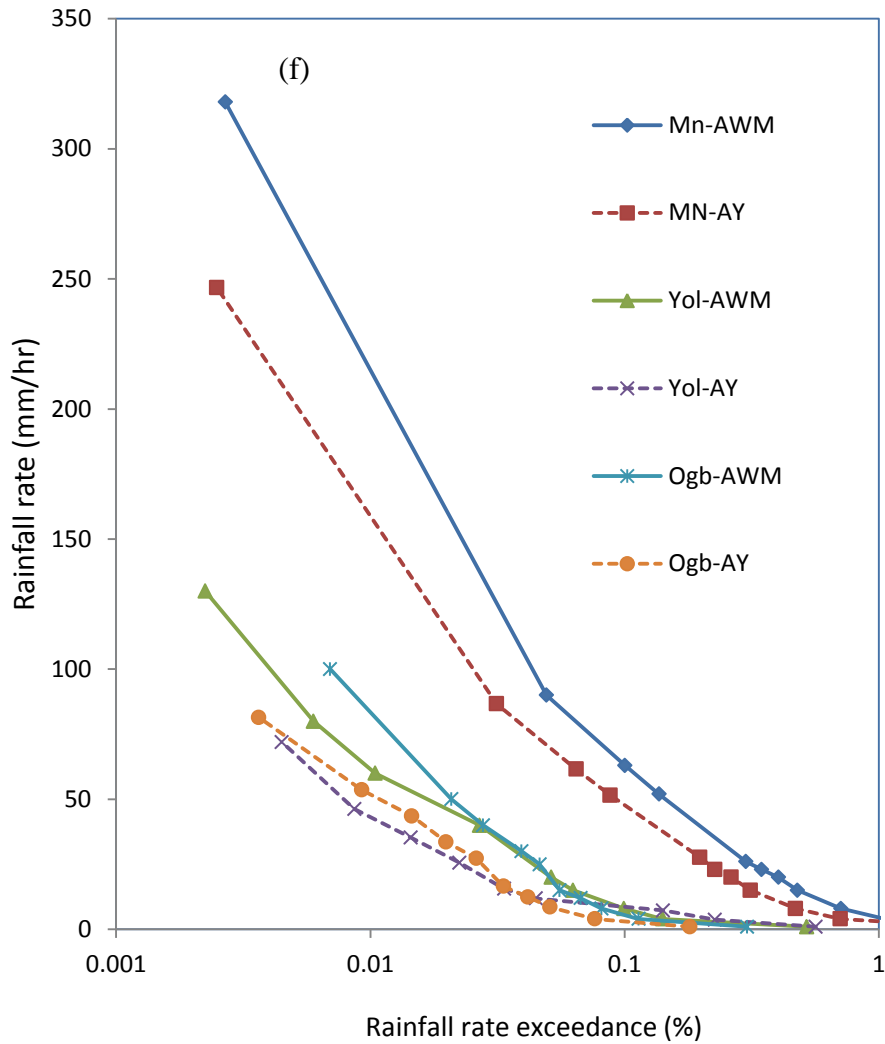


**Figure 4.19.** Cumulative distribution of rainfall rates in an average year and the worst months over (a) Derived Savanna Zone (b) Humid Forest Zone (c) Mid Altitude Savanna Zone (d) Northern Guinea Savanna Zone (e) Sudan Savanna Zone and (f) southern guinea savanna Zone

At Bauchi, the only location captured in the Northern Guinea Savanna, rainfall rate of about 98.5 mm/hr was continually exceeded on the average at the worst month as against the rain rate exceedance of 76.8 mm/hr during an average year while at Jos, the only location measured at the Mid Altitude Savanna zone, rainfall rate of about 106 mm/hr was exceeded on the average worst month as against the 90 mm/hr average year rain rate exceedance. In the southern Guinea Savanna, Minna recorded the highest average worst month rainfall rate (275 mm/hr) and average yearly rainfall rate (175 mm/hr) exceedance while Yola recorded the least, 60 mm/hr and 42 mm/hr respectively. At Kano, the only location covered in the Sudan Savanna zone, rain rate of about 140 mm/hr on the average was exceeded in the worst month as against 98 mm/hr average year exceedance. These values provide system engineers with the worst rainfall scenario for setting their monthly objectives in order to afford higher office and homes system availability. According to Cheffena (2008), fade mitigation strategies such as adaptive power control on links should be implemented in order to counteract the rainfall effects on systems.

#### **4.1.7.2 Relationship between Annual and Worst Month rainfall rate**

The relationship between mean annual rain rate and the average worst month rain rate was obtained by correlating them. The corresponding predicted mean annual rain rate by ITU-R was also correlated with the average worst month rain rate as shown in Figure 4.20 and appendix 8. The result shows a very good correlation between the mean annual and average worst rain rates with a high coefficient of determination in all the zones. The coefficient of determination ranged between 0.992 and 0.999 in the Derived Savanna zone, 0.998 and 0.999 in the humid forest zone and 0.949 and 0.998 in the Southern Guinea Savanna, In the Northern Guinea Savanna zone and Mid Altitude Savanna, the value was 0.999 while in the Sudan savanna zone the coefficient of determination was 0.998. These results varied slightly from the predicted ITU-R coefficient of determination of 1.0 in all the zones.

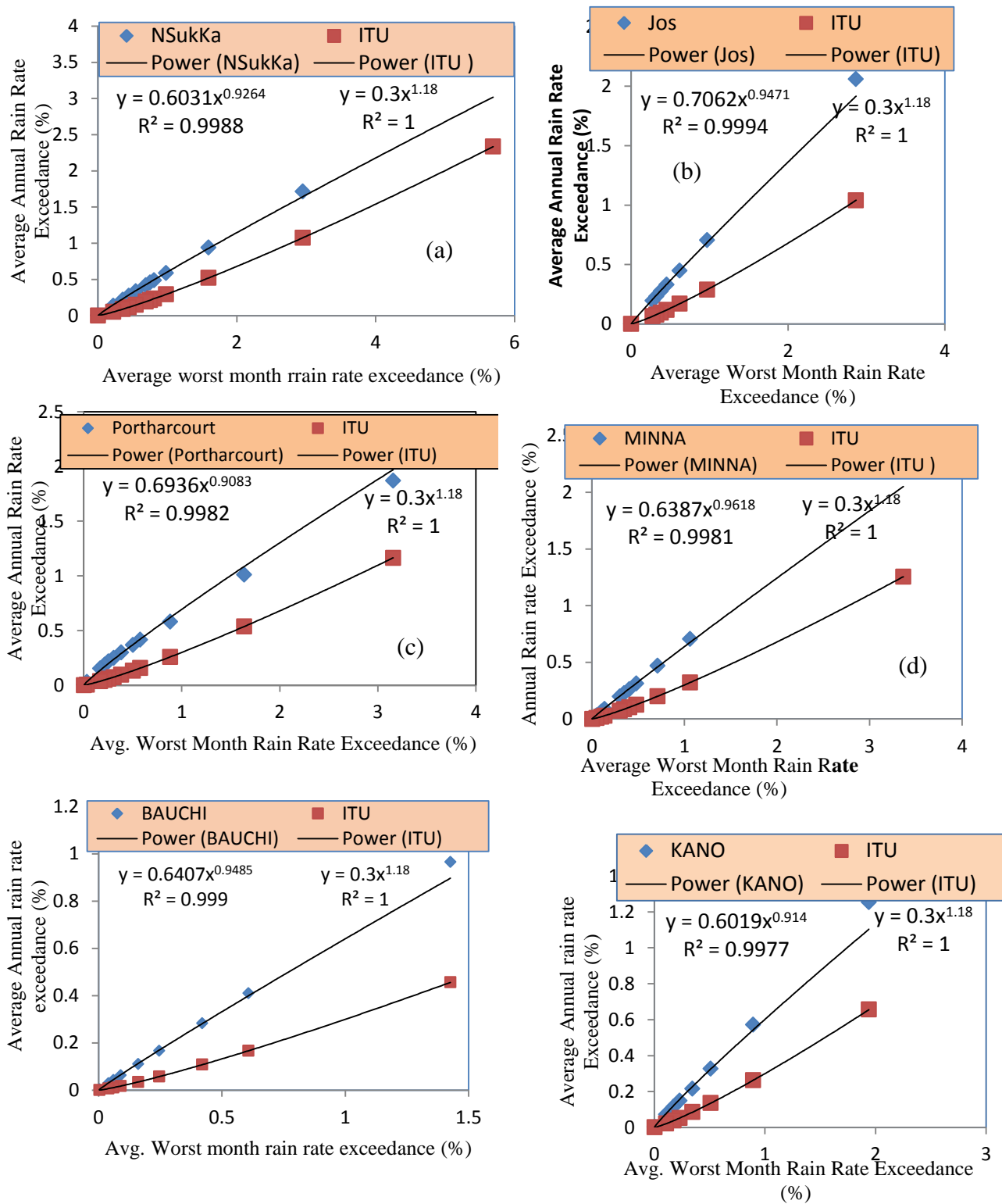


**Figure 4.20.** Relationship between average annual and worst month rainfall rate

The relationship (power law) among the mean annual and worst month rate of rain time percentage in the 14 locations across all the eco-climatic zones are obtained from the regression coefficients of the exponential functions in all the locations. The equation model is as presented in 4.1 to 4.14.

$$P_a = 0.6031P_w^{0.9264} \quad \text{- Nsukka} \quad (4.1), \quad P_a = 0.8657P_w^{0.912} \quad \text{- Yola} \quad (4.7)$$

$$P_a = 0.6000P_w^{0.9588} \quad \text{- Eburumiri} \quad (4.1), \quad P_a = 0.6407P_w^{0.9485} \quad \text{- Bauchi} \quad (4.8)$$

$$P_a = 0.6736P_w^{0.9492} \quad \text{- Iwo} \quad (4.2), \quad P_a = 0.7062P_w^{0.9471} \quad \text{- Jos} \quad (4.9)$$

$$P_a = 0.6121P_w^{0.9464} \quad \text{- Ogun} \quad (4.3), \quad P_a = 0.6387P_w^{0.9618} \quad \text{- Minna} \quad (4.10)$$

$$P_a = 0.7206P_w^{1.081} \quad \text{- Ogbomosho} \quad (4.4), \quad P_a = 0.5459P_w^{0.8939} \quad \text{- Anyigba} \quad (4.11)$$

$$P_a = 0.5798P_w^{1.1054} \quad \text{- Akure} \quad (4.5), \quad P_a = 0.5347P_w^{0.9074} \quad \text{- Makurdi} \quad (4.12)$$

$$P_a = 0.6936P_w^{0.9083} \quad \text{- Port Harcourt} \quad (4.6), \quad P_a = 0.6019P_w^{0.914} \quad \text{- Kano} \quad (4.14)$$

where  $P_a$  denotes the mean annual percentage and  $P_w$ , the mean worst month percentage

The ITU-R 841-5 (2016) universal recommended model for the conversion from mean annual rainfall rate percentage to mean worst month rain rate percentage for tropical, sub-tropical and temperate climate with frequent rain is

$$P_a = 0.3P_w^{1.18} \quad (4.15)$$

As can be observed, the ITU-R recommended model (equation 4.14) differs remarkably from the measured data derivations shown in equations 4.0 to 4.14, hence the need to adopt the derived model by designers in obtaining the the mean annual and worst month rain rate exceedance percentages at each location in order to enhance system performance.

#### 4.1.7.3 Evaluation of conversion factor parameters $\beta$ and $Q_1$

The ITU-R 841-5 (2016) recommend that the conversion factor,  $Q$  which consists of two parameters  $Q_1$ ,  $\beta$  should be used for the computation of the mean annual worst month from mean annual time rain rate percentage exceedance. The

ITU-R recommends that for global rain rate application,  $Q_1=2.83$  and  $\beta=0.15$  should be used for tropical, sub-tropical and temperate climate regions with frequent rain. These values were compared with deductions from measured rainfall data in order to enhance reliable system design for Nigeria. Figure 4.21 to 4.34 present the average year exceedance against Q-value in order to obtain the parameters at the locations covered by the study.

These values deviated greatly from the one proposed by ITU-R which are approximately  $\beta = 0.15$  and  $Q_1 = 2.83$  for global application (ITU-R 841-5, 2015). These deviations are in agreement with previous observations by Marzuki et al., (2016) and Yagaseena (2000) in the tropical regions. Considering the deviations of the  $\beta$  and  $Q_1$  values proposed by ITU-R for global application from the values derived from data at the locations of study, the  $\beta$  and  $Q_1$  values from local data is recommended to be used for systems design in order to enhance system performance; this deduction is in agreement with Durodola et al., (2017).

The worst month model parameters a and b (equations 4.1 to 4.14) as well as  $\beta$  and  $Q_1$  for locations in Nigeria as compared with values from other tropical countries and ITU are summarised in Table 4.9. As can be seen from the Table, ITU values falls short of that obtained from measured data from all the tropical locations. Hence, system carried out done with ITU recommended worst months statistics is bound to malfunction in the tropics.

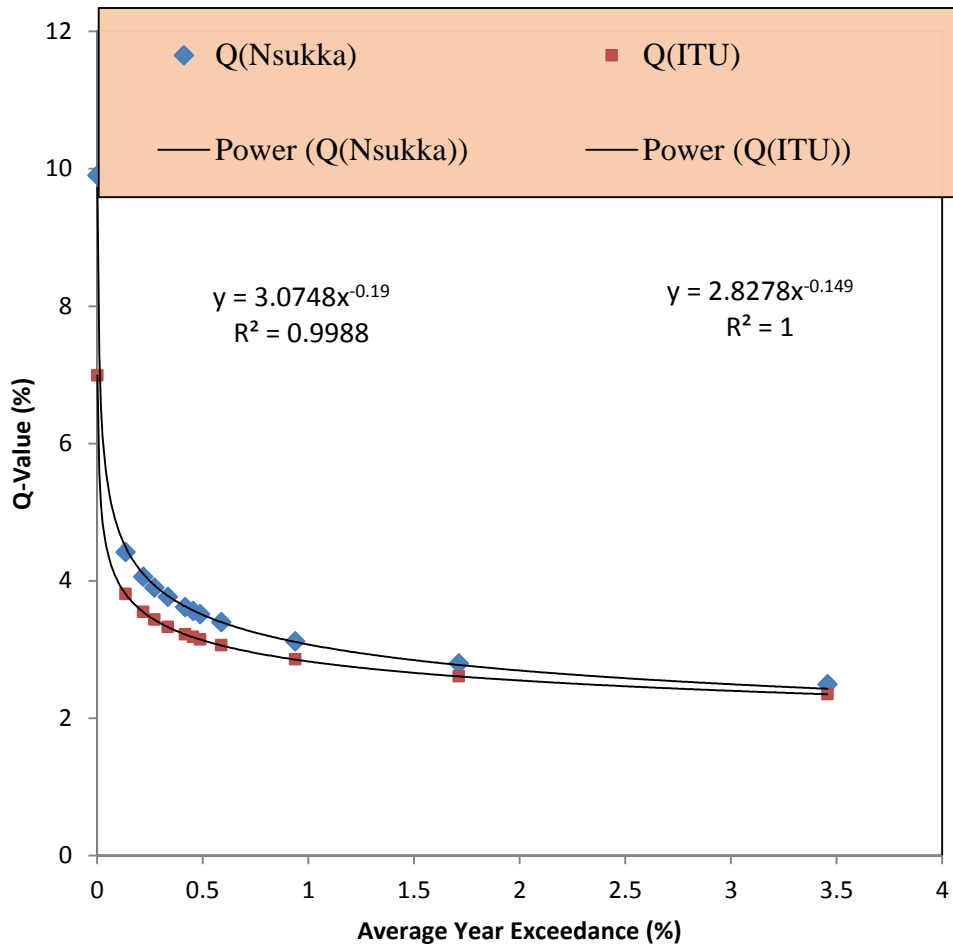


**Figure 4.21.** Determination of conversion factors  $\beta$  and  $Q_1$  for Nsukka (Derived Savanna Zone)

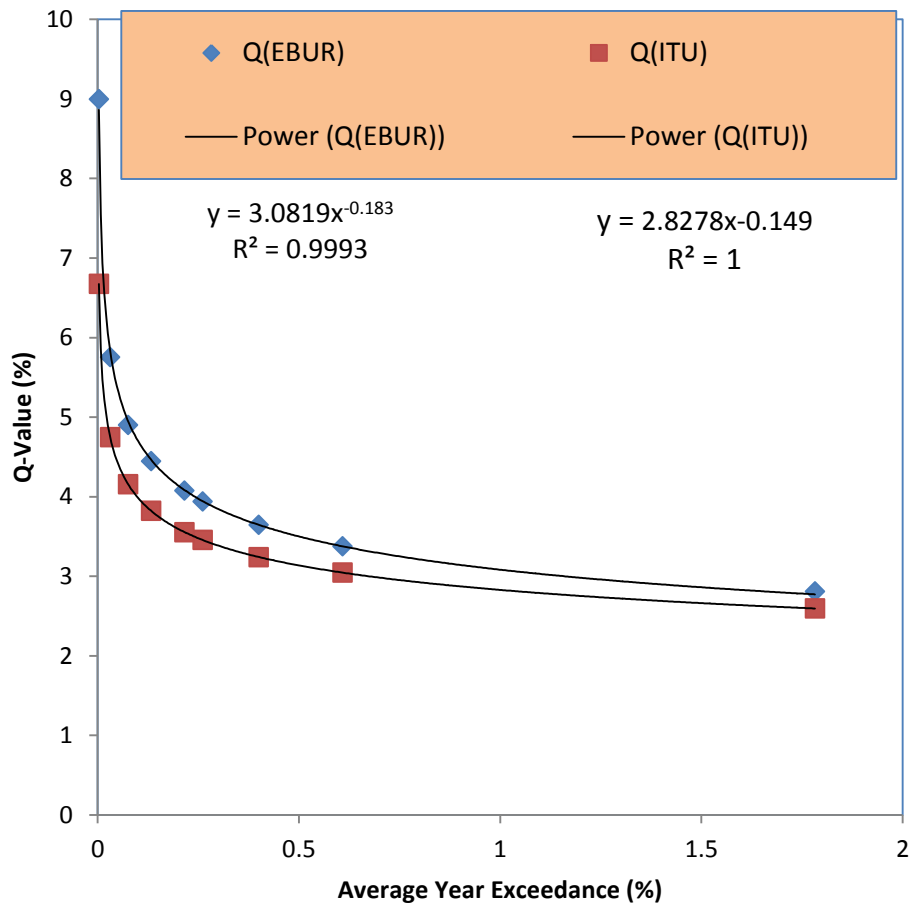


**Figure 4.22.** Determination of conversion factors  $\beta$  and  $Q_1$  for Eburumiri (Derived Savanna Zone)

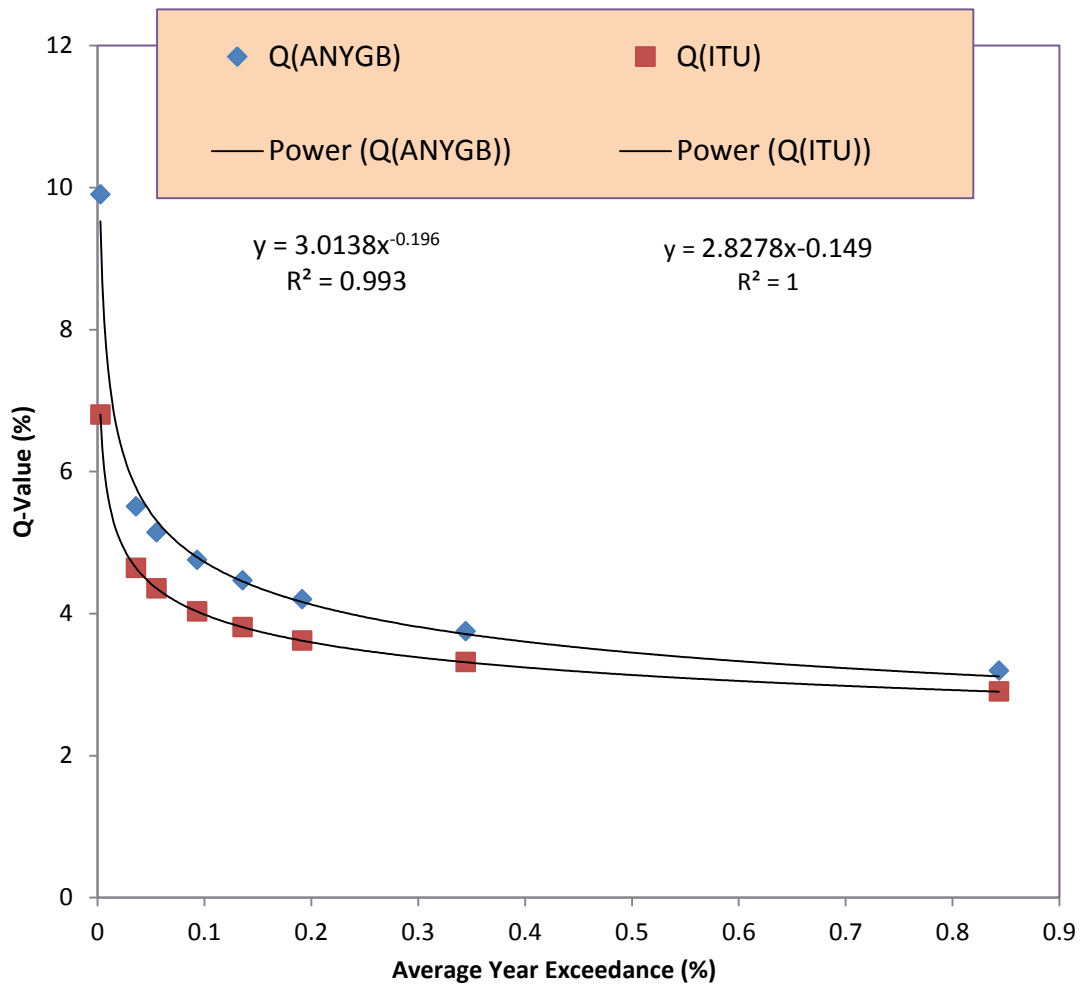


**Figure 4.23.** Determination of conversion factors  $\beta$  and  $Q_1$  for Anyigba (Derived Savanna Zone)



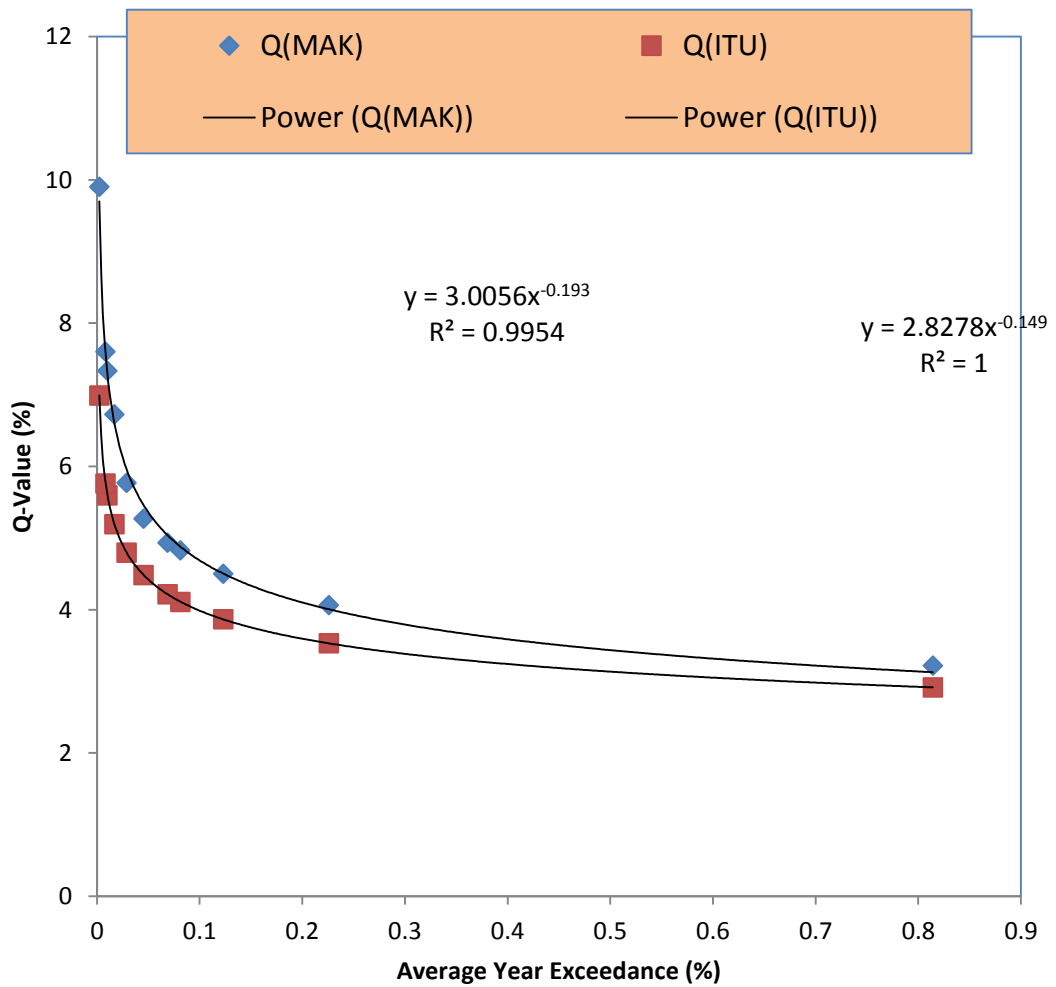


**Figure 4.24.** Determination of conversion factors  $\beta$  and  $Q_1$  for Anyigba (Derived Savanna Zone)

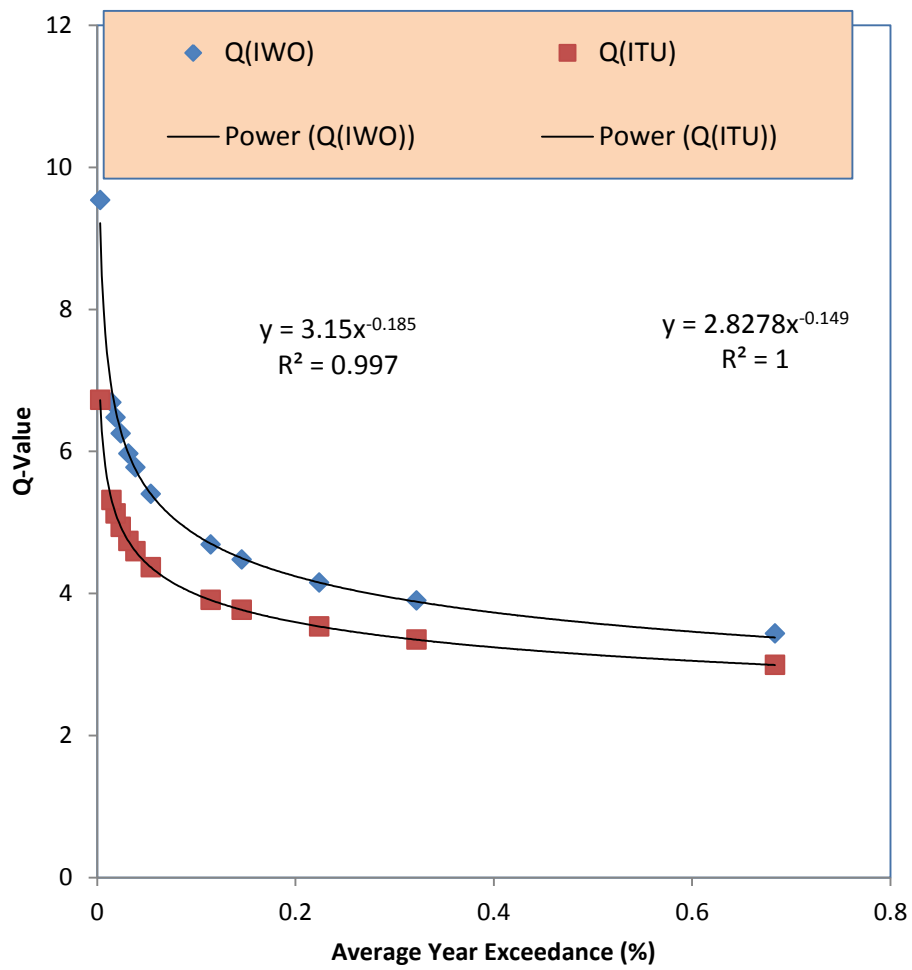


**Figure 4.25.** Determination of conversion factors  $\beta$  and  $Q_1$  for Iwo (Derived Savanna Zone)

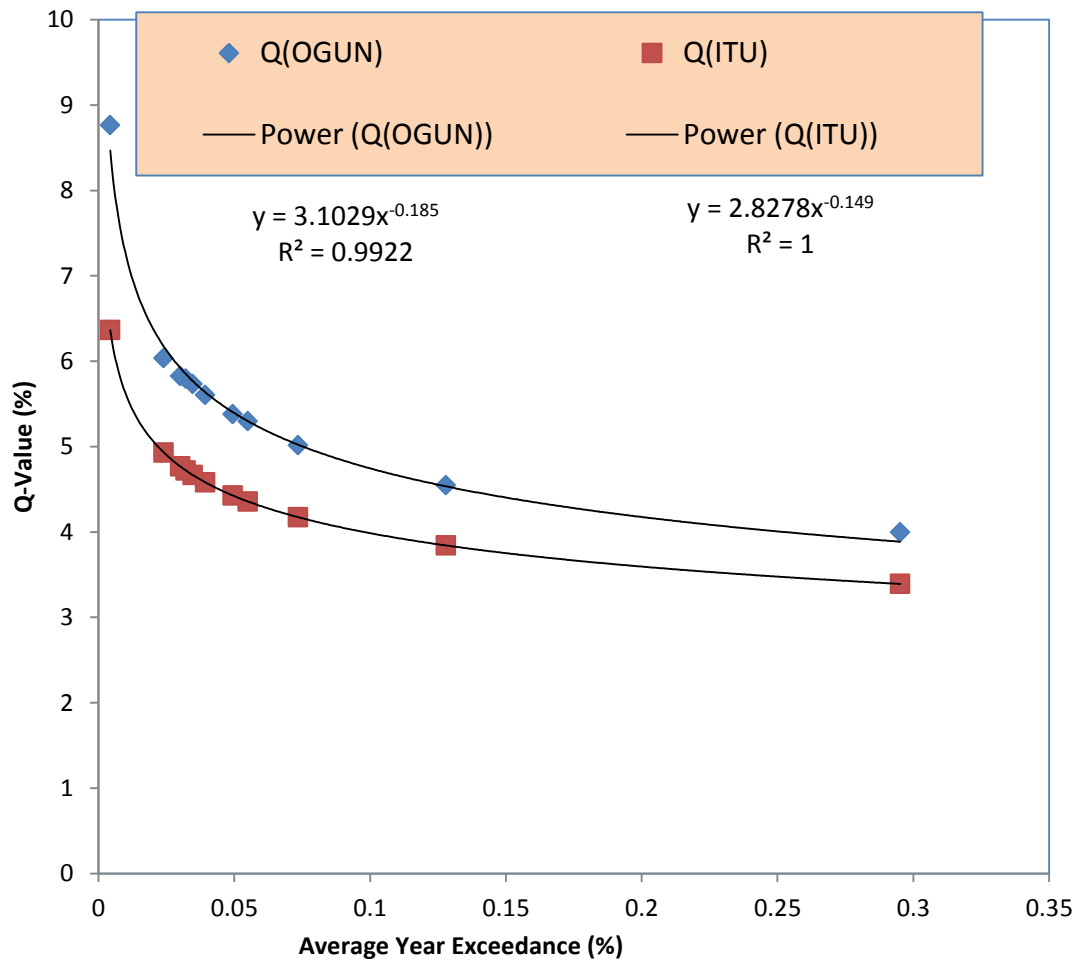


**Figure 4.26.** Determination of conversion factors  $\beta$  and  $Q_1$  for Ogun (Derived Savanna Zone)

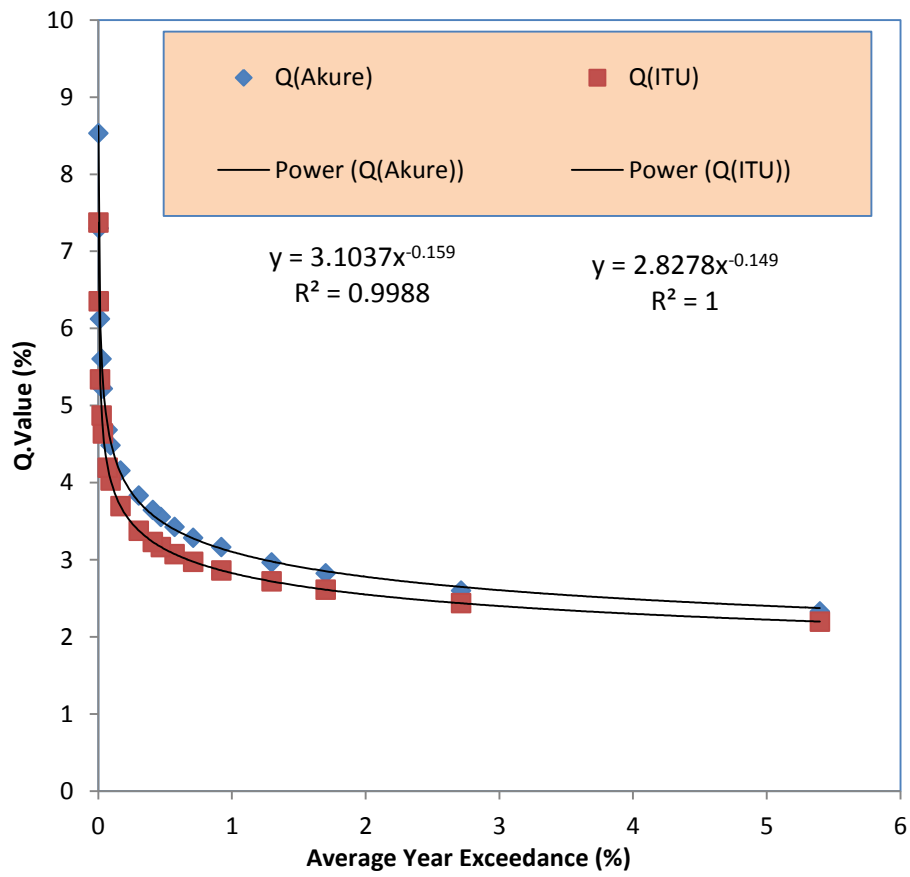


**Figure 4.27.** Determination of conversion factors  $\beta$  and  $Q_1$  for Akure (Humid Forest Zone)

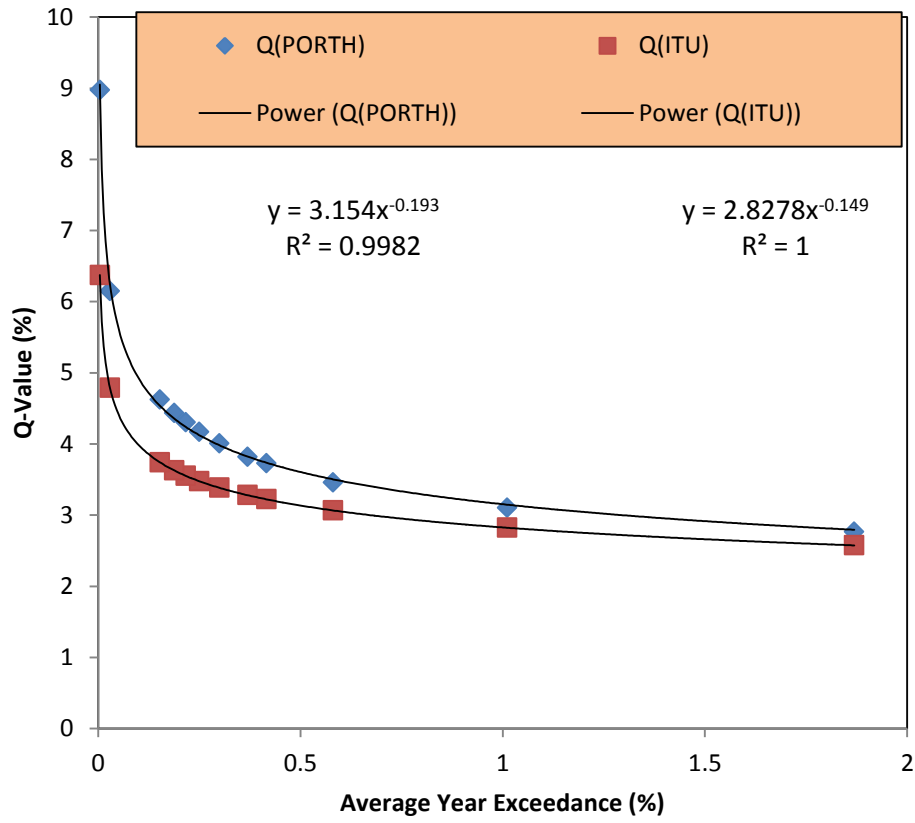


**Figure 4.28.** Determination of conversion factors  $\beta$  and  $Q_1$  for Port Harcourt (Humid Forest Zone)

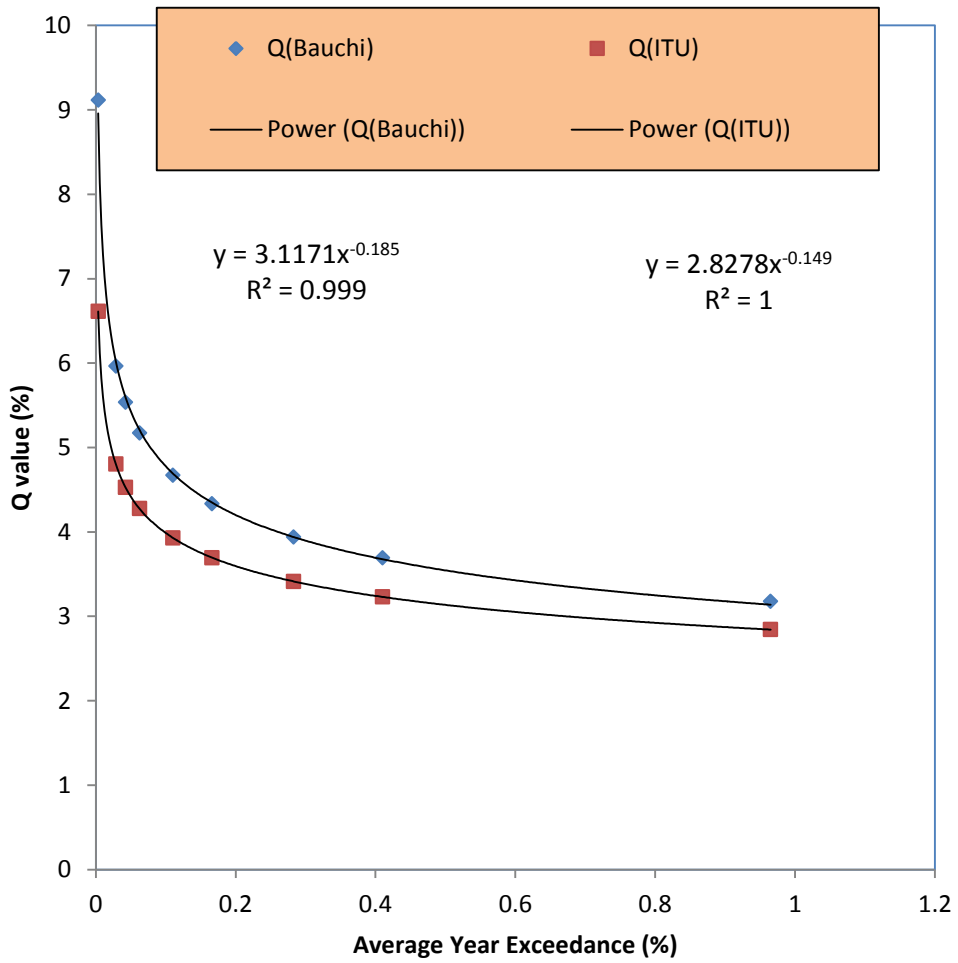


**Figure 4.29.** Determination of conversion factors  $\beta$  and  $Q_1$  for Bauchi (Northern Guinea Savanna Zone)

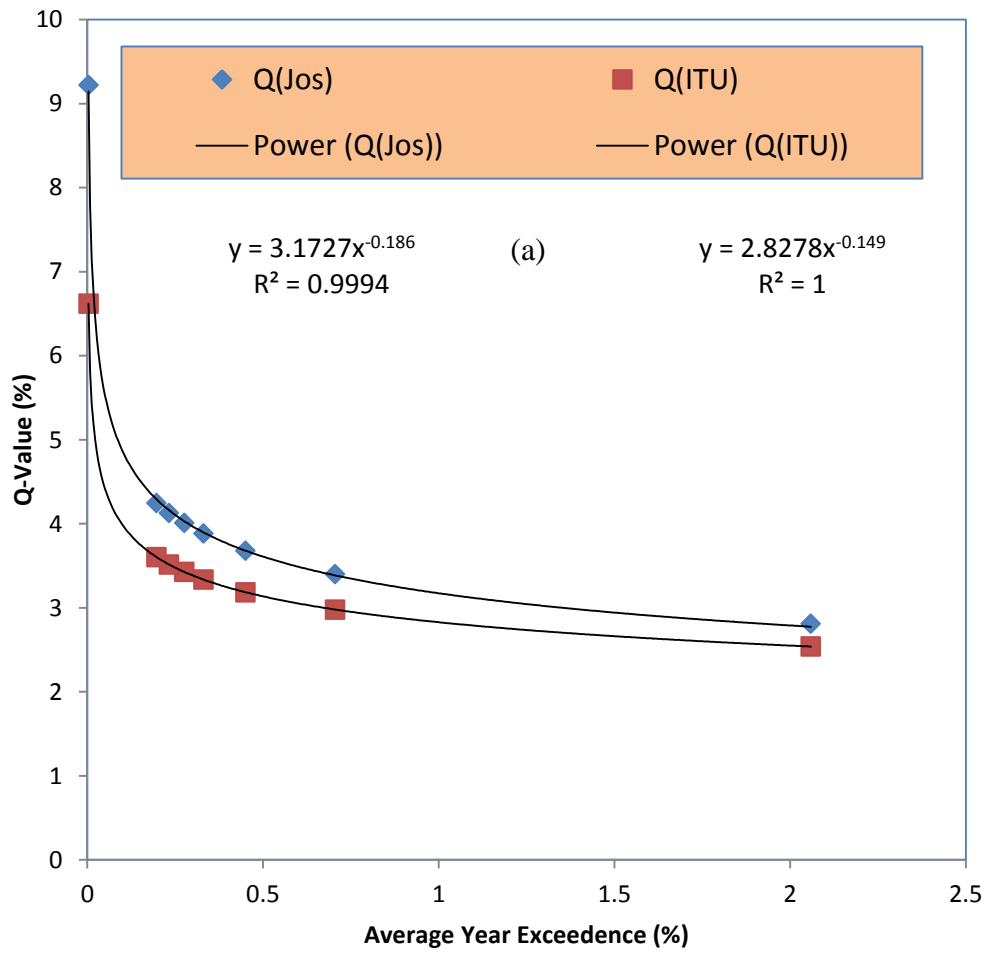


**Figure 4.30.** Determination of conversion factors  $\beta$  and  $Q_1$  for Jos (Mid Altitude Savanna Zone)

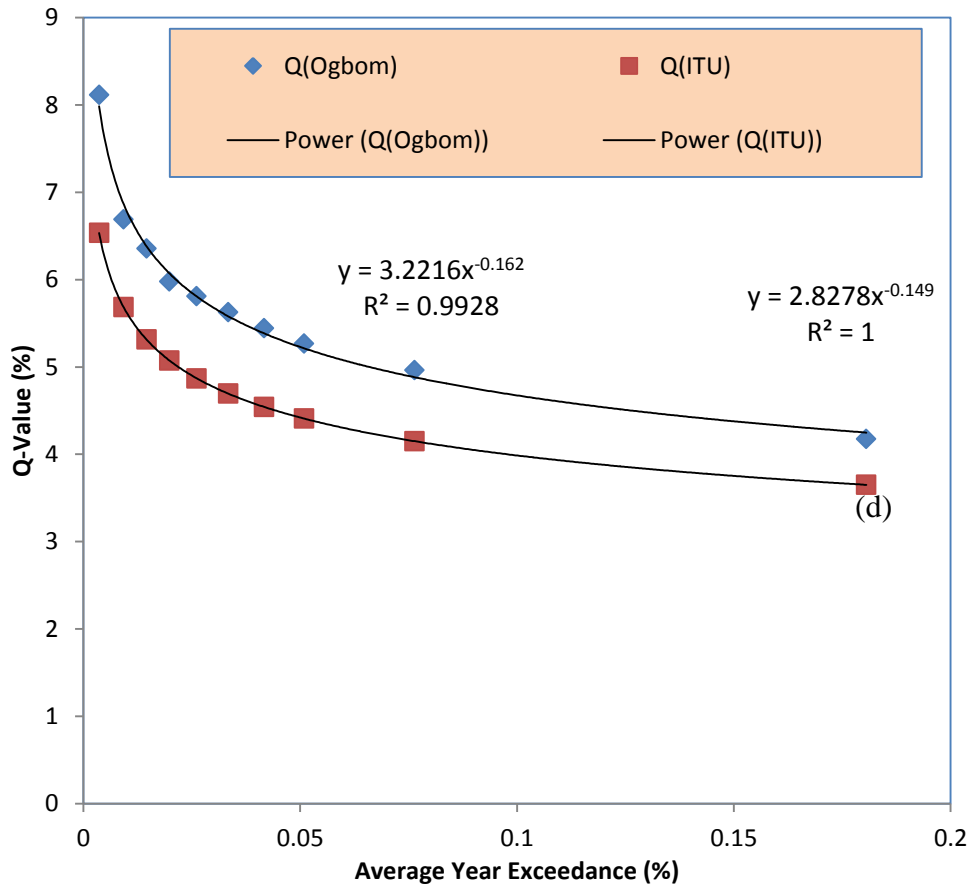


**Figure 4.31.** Determination of conversion factors  $\beta$  and  $Q_1$  for Ogbomosho (Southern Guinea Savanna Zone)



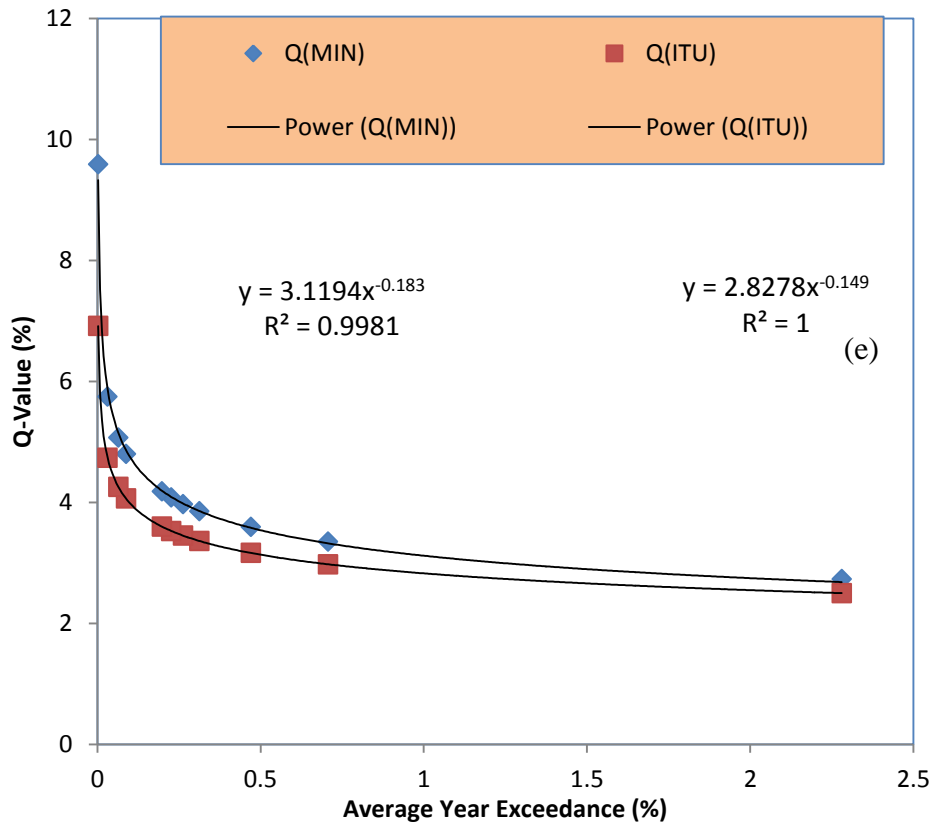


**Figure 4.32.** Determination of conversion factors  $\beta$  and  $Q_1$  for Minna (Southern Guinea Savanna Zone)

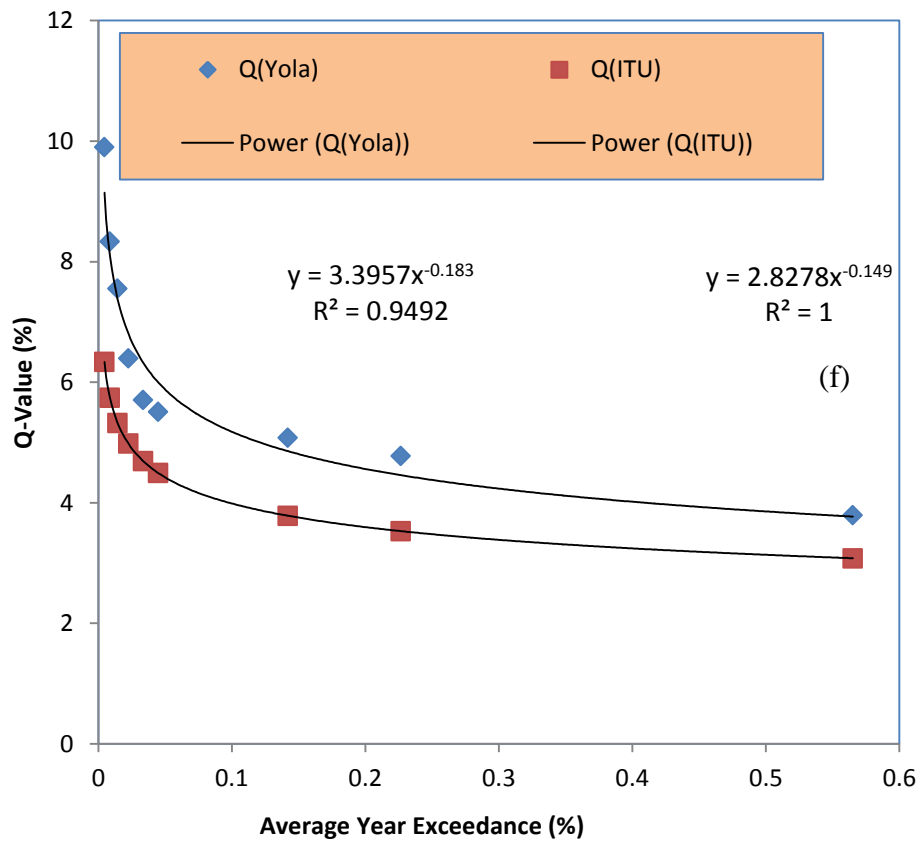


**Figure 4.33.** Determination of conversion factors  $\beta$  and  $Q_1$  for Yola (Southern Guinea Savanna Zone)

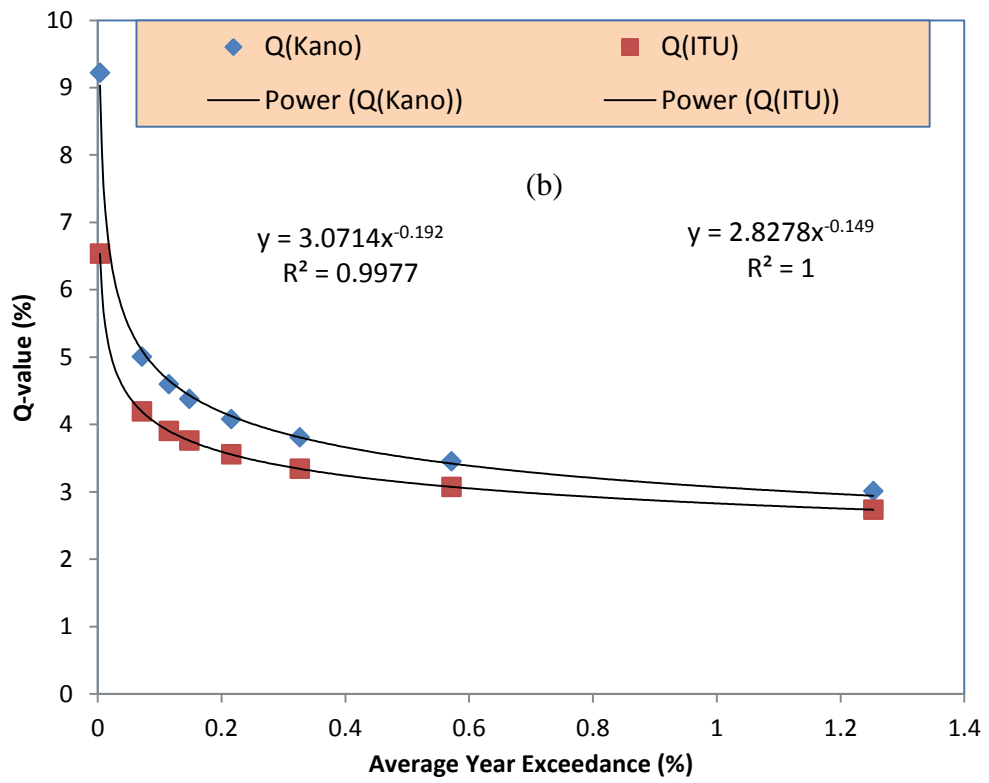


**Figure 4.34.** Determination of conversion factors  $\beta$  and  $Q_1$  for the Kano (Sudan Savanna Zones)

**Table 4.9.** Model Parameters for worst months in Nigeria, other tropical countries and ITU

<b>Locations</b>	<b>Q<sub>1</sub></b>	<b>β</b>	<b>a</b>	<b>b</b>
Jos	3.173	-0.186	0.706	0.947
Eburumiri	3.082	-0.183	0.600	0.959
Bauchi	3.117	-0.185	0.641	0.949
Nsukka	3.075	-0.190	0.603	0.926
Makurdi	3.006	-0.193	0.535	0.907
Minna	3.119	-0.183	0.638	0.962
Ogbomosho	3.222	-0.162	0.721	1.081
Ogun	3.103	-0.185	0.612	0.946
Bowen (Iwo)	3.150	-0.185	0.674	0.949
Port Harcourt	3.154	-0.193	0.694	0.908
Yola	3.396	-0.183	0.866	0.912
Kano	3.071	-0.192	0.602	0.914
Akure	3.104	-0.159	0.580	1.105
Anyigba	3.014	-0.196	0.546	0.894
USM, Malaysia (Yagasena, 2000)	1.398	0.293	-	-
USM, Malaysia (Yagasena, 2000)	1.220	0.298	-	-
Indonesia (Yagasena, 2000)	1.700	0.220	-	-
Kototabang (Marzuki et al., 2016)	1.390	0.240	-	-
ITU	2.828	-0.149	0.300	1.180

#### 4.1.8 Modelling of Rainfall Rate Cumulative Distribution

The power law relationship by Ajayi et al., (1996):

$$R_{\tau} = a \cdot R_T^b \quad (4.16)$$

was used to obtain rain rate  $R_{\tau}$  from available rain rate  $R_T$  where  $a$  and  $b$  are regression coefficient. The limitation of equation (4.15) is that it is location dependent (Semire et al., 2012) hence the need to obtain the values of the regression coefficient at each of the locations of study. To obtain the values for the regression coefficient, the logarithmic form of equation (4.16) was adopted to obtain equation (4.17).

$$\ln R_{\tau} = \ln a + b \ln R_T \quad (4.17)$$

The logarithmic relationship (equation 4.16) by Semire et al., (2012) were used to obtain the regression coefficients  $a$  and  $b$  for one minute integration time modeling for all the locations used in the study. The plots of the power law relationship between the rainfall rates across all the stations considered is shown in Figure 4.35 and appendix 10 while Table 4.10 is the regression and correlation coefficients for the power law relationships. The substitution of the regression coefficient parameters of equation (4.15) yielded the model equations (4.18 to 4.29) for all the locations considered in this study.

From Table 4.10, it can be observed that the correlation coefficients ( $R^2$ ) are positive and highly significant in all the locations considered. It is highest in Yola and least in Minna. These regression coefficients and the location specific power laws, corroborates the findings of Semire at al., (2012) that different conversion factors are required for different locations even within the same climatic region for the conversion of rainfall data of a given integration time to another as against unified time integration regression coefficients suggested by the ITU-R.

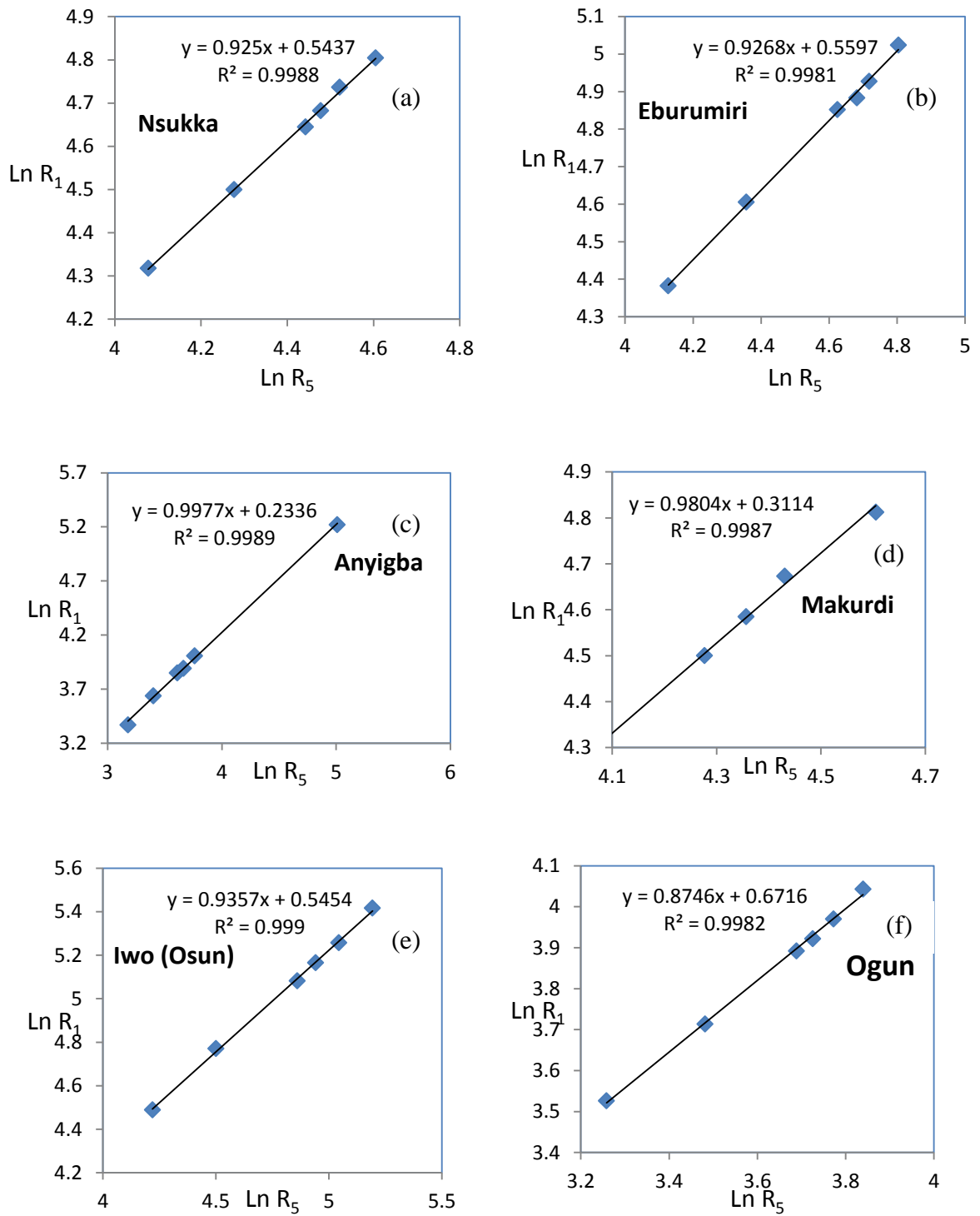


**Figure 4.35.** Power law relationship between rainfall rates

**Table 4.10.** The conversion factors parameters

Location	$\zeta$	a	b	$R^2$
Nsukka	1	1.72237	0.9250	0.9988
Eburumiri	1	1.75015	0.9268	0.9981
Ogun	1	1.95737	0.8746	0.9982
Ogbomosho	1	1.64050	0.9358	0.9947
Iwo	1	1.72530	0.9357	0.9990
PortHarcourt	1	1.50622	0.9579	0.9973
Yola	1	1.78105	0.9167	0.9993
Bauchi	1	1.23343	1.0021	0.9967
Jos	1	2.94350	0.8075	0.9861
Minna	1	3.02920	0.8181	0.9057
Makurdi	1	1.36534	0.9804	0.9987
Anyigba	1	1.26314	0.9977	0.9989

The model equations for rain rate cumulative distribution for all the locations considered are:

$$R_1 = 1.72237R_5^{0.9250} \quad \text{-Nsukka} \quad (4.18) \quad R_1 = 1.23343R_5^{1.0021} \quad \text{- Bauchi} \quad (4.24)$$

$$R_1 = 1.75015R_5^{0.9268} \quad \text{- Eburumiri} \quad (4.19), \quad R_1 = 2.94350R_5^{0.8075} \quad \text{- Jos} \quad (4.25)$$

$$R_1 = 1.72530R_5^{0.9357} \quad \text{- Iwo} \quad (4.20), \quad R_1 = 3.02920R_5^{0.8181} \quad \text{- Minna} \quad (4.26)$$

$$R_1 = 1.95737R_5^{0.8746} \quad \text{- Ogun} \quad (4.21), \quad R_1 = 1.36534R_5^{0.9804} \quad \text{- Makurdi} \quad (4.27)$$

$$R_1 = 1.64050R_5^{0.9358} \quad \text{- Ogbomosho} \quad (4.22), \quad R_1 = 1.26314R_5^{0.9977} \quad \text{- Anyigba} \quad (4.28)$$

$$R_1 = 1.50622R_5^{0.9579} \quad \text{- Port Harcourt} \quad (4.23), \quad R_1 = 1.78105R_5^{0.9167} \quad \text{- Yola} \quad (4.29)$$

#### 4.1.9 Rainfall rate prediction modeling and model validation

In the works of Mandeep (2011), prediction models provide the best rainfall estimate for attenuation predictions. The existing models prediction that applies to the tropics are Moupfouma and Martins (MM) (1995) model, ITUR (2009a, b) model, Kitami Institute of Technology (Ito and Hosoya (IH), 1999) simplified model and Rice and Holmberg (RH) (1973) model. The comparison of rain rate values derived from the prediction models with the in-situ data obtained at 1-minute integration time from Kano and Akure locations would afford the appropriate prediction model for Nigeria. Figures 4.36 and 4.37 present typical plot of the rain rate prediction models for prediction models comparison, while the predicted values at Akure and Kano is shown in appendix 12`1.

From Figure 4.36 and 4.37, it can be seen that Rice and Holmberg rainfall rate prediction model is the closest to the measured value in both Akure and Kano while Moupfouma and Martins prediction model is furthest from the measured value, hence for the prediction of rainfall rate in Nigeria, the Rice and Holmberg model is the most ideal as shown by the Root Mean Square Error (RMSE) value derived from equation 3.25 and presented in Table 4.11.



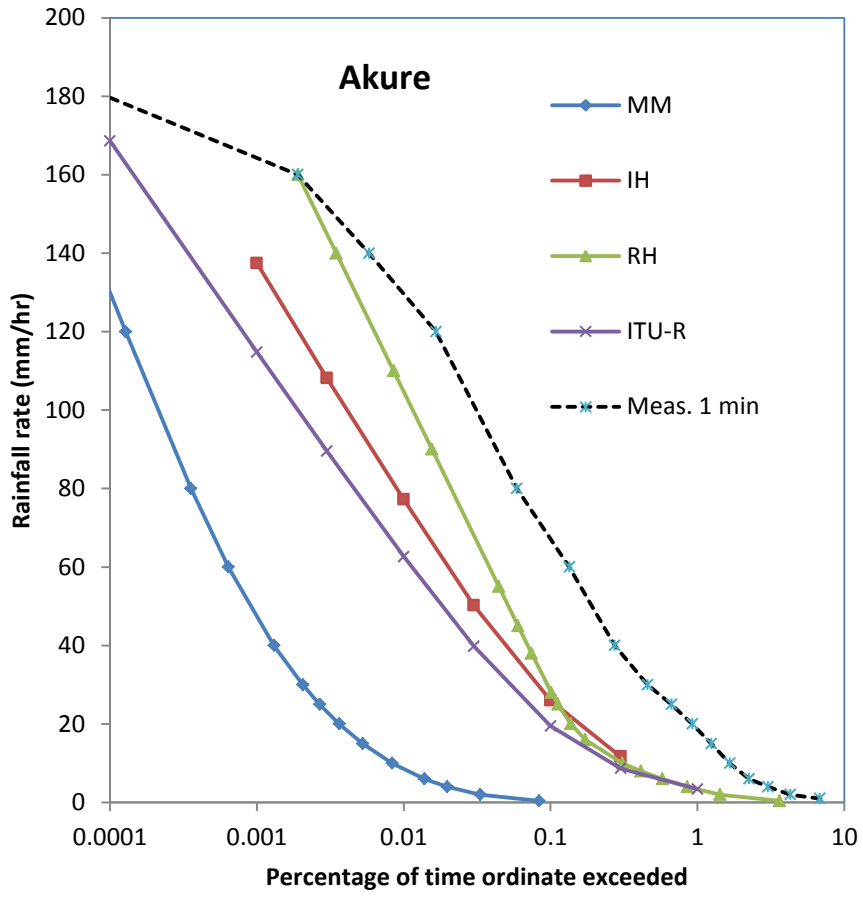


**Figure 4.36.** 1- minute rainfall rate prediction models comparison for Akure

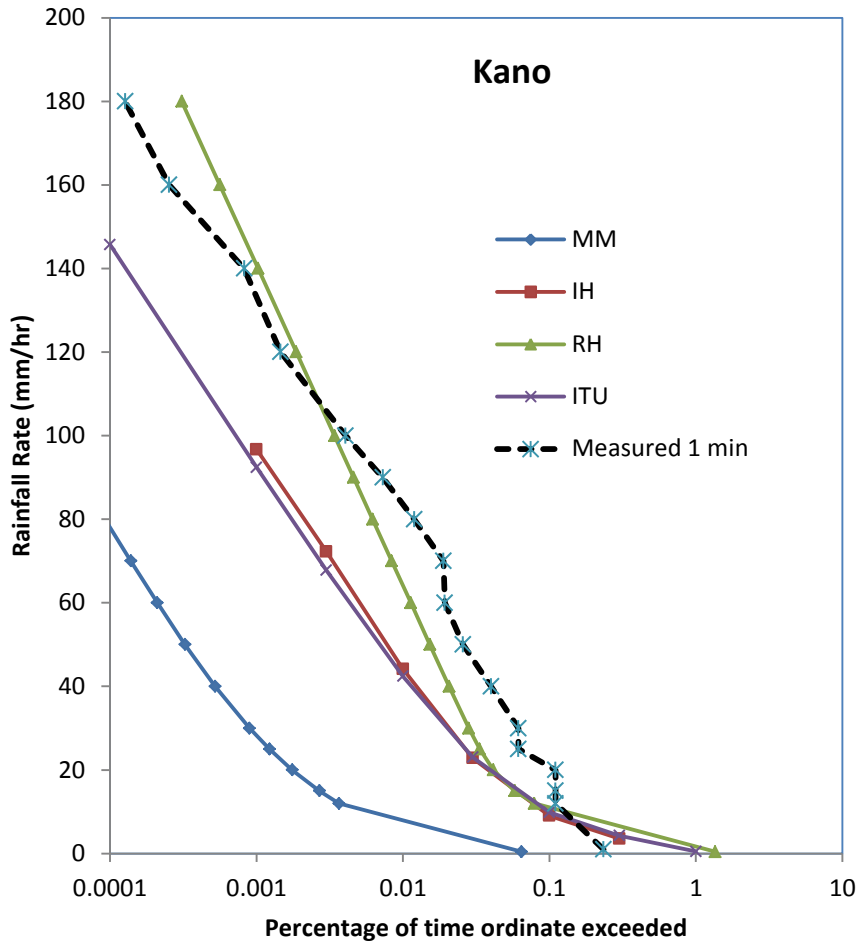


**Figure 4.37.** 1- minute rainfall rate prediction models comparison for Kano

#### 4.1.10 Validation of the Models

The ITU-R p. 311-17 (2017) has put up suggestions on the method that should be used for validating prediction models (Mandeep, 2011); these are the percentage relative error and the root mean square error (RMSE) connecting the observed values with what was obtained through prediction. The results are presented in Table 4.11.

Analysis of the prediction models revealed that the Rice and Holmberg prediction model gave the least root mean square error value of 0.1114 in Kano and 0.2922 in Akure. This finding agrees with the submission of Obiyemi *et al.* (2014). Furthermore, the Moupfouma and Martins model gave the highest value (0.8899 in Kano and 0.9070 in Akure). However, Rice and Holmberg prediction model is suitable for monthly rainfall accumulation observed over a period of three decades (Ojo *et al.*, 2008). The model equally overestimated rain rates in the high availability range (0.01%) and underestimated it in the lower availability range (0.1% to 1%) (Ojo *et al.*, 2008). On the other hand, the use of the kitami prediction model is limited by the thunderstorm ratios which are not readily available in local weather agencies (Ojo *et al.*, 2008). The ITU-R prediction model is preferred because it has global application (ITU-R 837-7, 2017) and the parameters for rainfall rate prediction (coordinates of the location, percentage of exceedance) are readily obtainable with Matlab rain rate statistics.

**Table 4.11.** Prediction models validation

---

Models	Average Relative Error		Root Mean Square Error	
	Akure	Kano	Akure	Kano
Rice & Holmberg	-0.2615	0.0643	<b>0.2922</b>	<b>0.1114</b>
Ito amd Hosoya (Kitami)	-0.3756	-0.4375	0.3866	0.4487
Moupfouma & Martins	-0.9045	-0.8893	0.9070	0.8899
ITU-R	-0.4939	-0.4558	0.5010	0.4642

---

## 4.2 Statistics of rain attenuation

Rainfall induced attenuation is one of the main impediments confronting the transmission of millimeter waves in the tropics. It leads to the scattering, diffraction and absorption of radio waves and the resultant effect is the drop in the signal strength (Shayea *et al.*, 2018).

Rainfall is a natural occurrence and varies from time to time, year to year and location to location. In the planning of LOS radio systems for terrestrial paths, accuracy is needed in the prediction of how rain would attenuate the signals (Segal, 1986). Three established models are utilized for the terrestrial paths rain attenuation prediction, these are: ITU-R, Crane Global and the Moupfouma methods (Fashuyi and Afullo, 2007). The  $R_{0.01}$  is defined as 0.01% rain rate exceedance in a location at 1-minute integration time. This percentage of rain rate exceedance was used for attenuation determination.

### 4.2.1 Computation of specific attenuation

Specific attenuation  $\gamma$ , also referred to as attenuation per unit distance is essential for rain attenuation computation for terrestrial as well as earth-space paths (Olsen et al., 1978). The relationship between  $\gamma$  and rainrate (R) is given as:

$$\gamma = kR^\alpha \quad (4.30)$$

Equation (4.29) is an empirical procedure and is known as rain specific attenuation power law (Zhang and Moayeri, 1999) where the parameter R stands for the rainfall rate in unit of millimeter per hour,  $k$  and the parameter  $\alpha$  are known as power law parameters and this depends on the distribution of rain drop sizes, temperature of the rain, millimeter wave polarisation and frequency. The values of  $k$  and  $\alpha$  were obtained for 30 to 300GHz frequency range. The specific attenuation  $\gamma_R$  (dB/km) for the fourteen stations across the eco-climatic zones used for the study were computed based on the recommendation by ITU-R 838-3 (2005). Using the actual local rain data from these locations, the 0.01% (99.99%) rain rate exceedance ( $R_{0.01}$ ) was determined for all the years and the mean of the duration was obtained. Table 4.12 shows the statistics of rainfall rate cumulative distribution at 0.01% exceedance.

**Table 4.12. Rain rate statistics at 0.01% exceedance**

<b>Locations</b>	<b>2007</b> (mm per hr)	<b>2008</b> (mm per hr)	<b>2009</b> (mm per hr)	<b>2010</b> (mm per hr)	<b>2011</b> (mm per hr)	<b>2012</b> (mm per hr)	<b>2013</b> (mm per hr)	<b>2014</b> (mm per hr)	<b>2015</b> (mm per hr)	<b>2016</b> (mm per hr)	<b>Average</b>	<b>ITUR</b>
Jos		50.00	28.00	2.00	47.00	24.00	30.00	7.00	7.00	10.00	22.78	87.10
Minna		130.00	108.50	82.50	118.50	52.50	78.50	208.50	208.50	62.50	116.67	91.60
Nsukka		99.00	107.00	85.00	98.50	92.00	87.50	70.00			91.29	81.90
Eburumiri		86.00	122.00	90.00	126.50	62.00	56.00				90.42	80.90
Iwo			70.00	35.00	90.00	110.00	8.00				62.60	57.10
Port Har		106.00	98.00	77.50	67.50						87.25	109.10
Makurdi		22.00	100.00	58.00	24.00						51.00	91.90
Anyigba				32.00	45.00	38.00	19.00				33.50	94.40
Kano	88.00	67.00		97.50	62.00						78.63	42.40
Yola				22.00	4.00	73.50					33.17	90.60
Bauchi							102.00	96.00	92.00		96.67	42.80
Ogun				35.00	45.00						40.00	62.20
Ogbomos ho						82.00	52.00				67.00	51.80
Akure								118.00		124.00	121.00	62.70

The specific attenuation ( $\gamma_R$ ) was calculated for both for the horizontal and vertical polarisation. The specific attenuation is known to increase with frequency up to around 100 GHz and decreases at higher frequencies (Das and Maitra, 2010; Sakir, 2014). However, Diba *et al.* (2016) reported that specific attenuation can remain stable for frequency of 150 GHz and reduces afterwards. The specific attenuation derived from local data and rain rate predicted values by the ITU-R over all the eco-climatic zones of Nigeria covered in this study at horizontal and vertical polarisation is shown in Figure 4.38 to 4.49. From these figures, it can be observed that  $\gamma_R$  increases rapidly for frequencies of 50 GHz, followed by a slow rise from 50 to 100 GHz in all the locations. The frequencies become fairly stable up to 150 GHz and then gradually decrease afterwards. As observed, there is a slight difference between the specific attenuation at the horizontal polarisation and the vertical polarisation. This finding agrees with the work of Okamura *et al.* (1961) and Shayea *et al.* (2018). The differences in the attenuation by horizontal polarisation and vertical polarisation has been ascribed to the distortion in rain drops (Okamura and Oguchi, 2010). As stated by Magono (1954) the drops were not spherical but asymmetrical about the horizontal plane, generally with flattened base for large drops.

Considering the average rain rate over the periods of observation, specific attenuation for the horizontal polarisation decreases at Ogbomosho, Ogun, Iwo, Yola and Jos locations after 150 GHz frequency of propagation while at all other locations, the specific attenuation decreases after 120 GHz propagation frequency. This is attributed by Das *et al.* (2010) to variation in rain drop sizes distribution at higher rain rates.

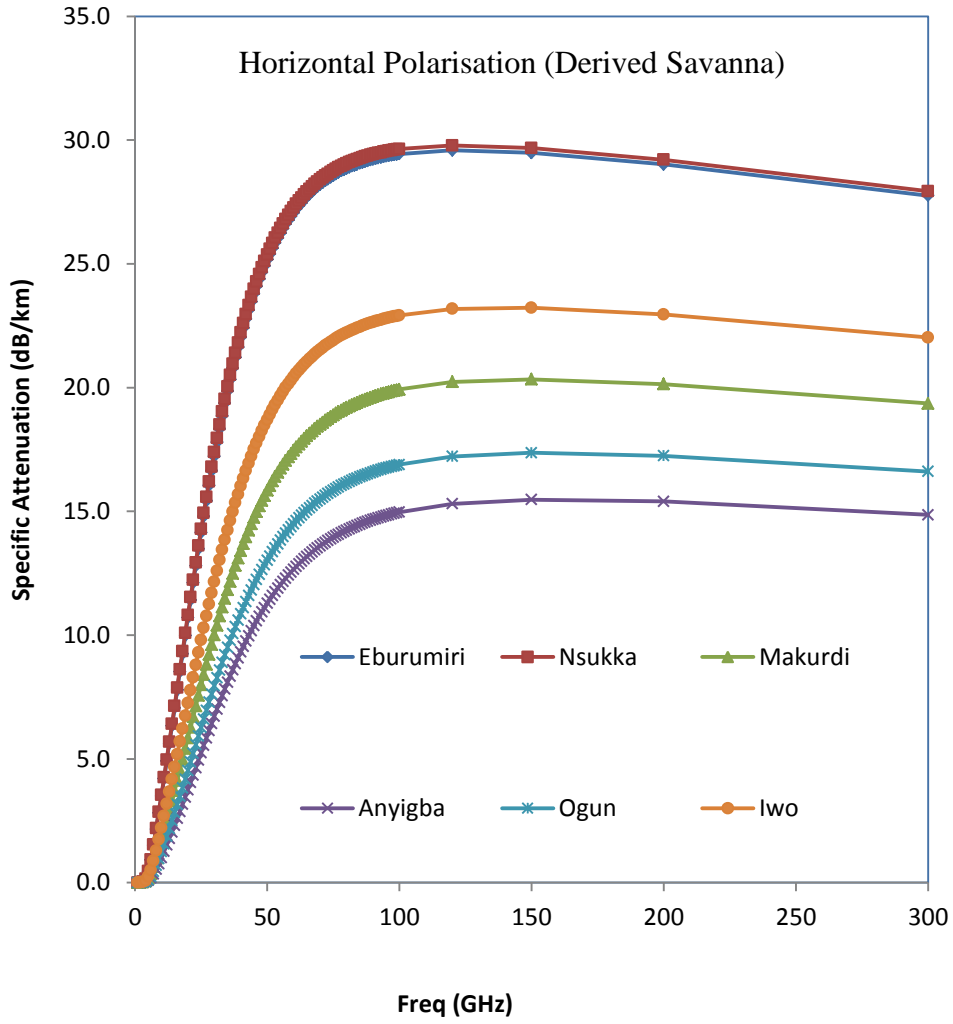


**Fig. 4.38.** Specific rain attenuation versus frequency for horizontal polarisation over the derived savanna zone



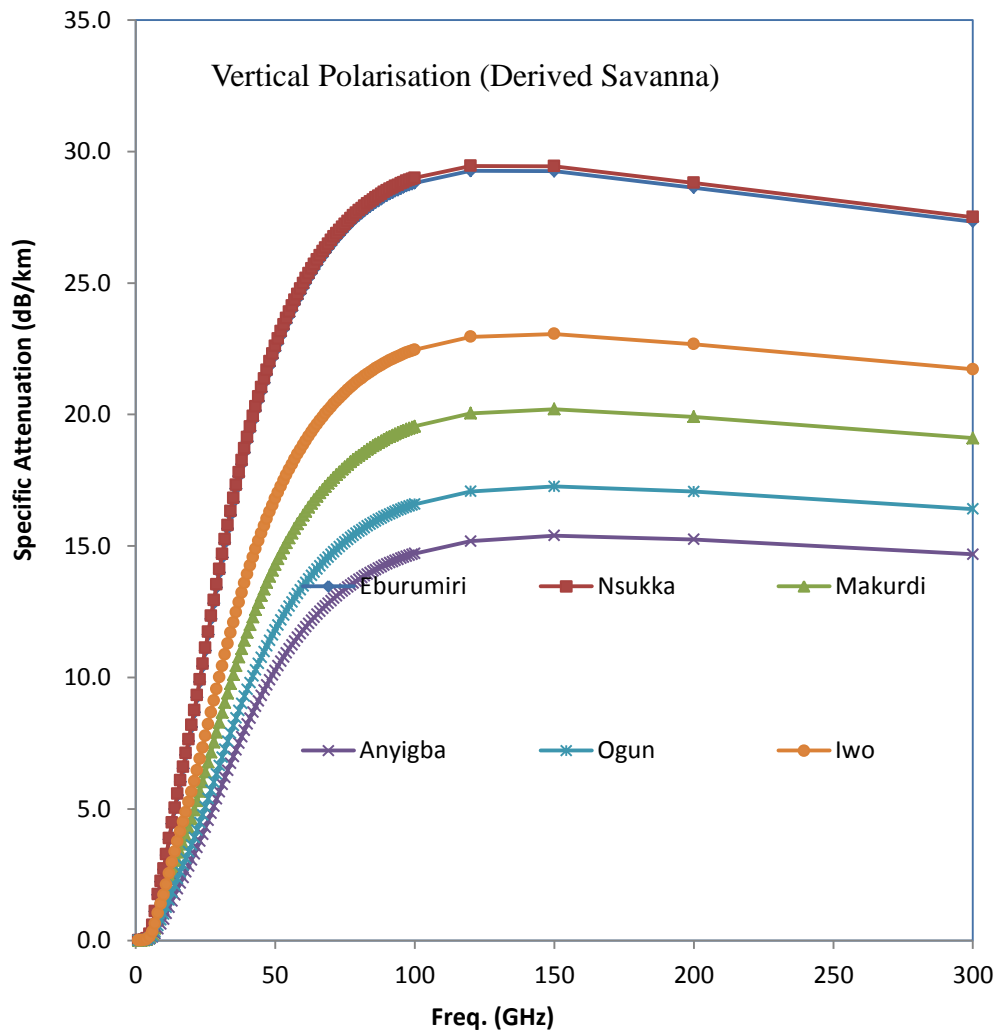


**Fig. 4.39.** Specific rain attenuation versus frequency for vertical polarisation over the derived savanna zone

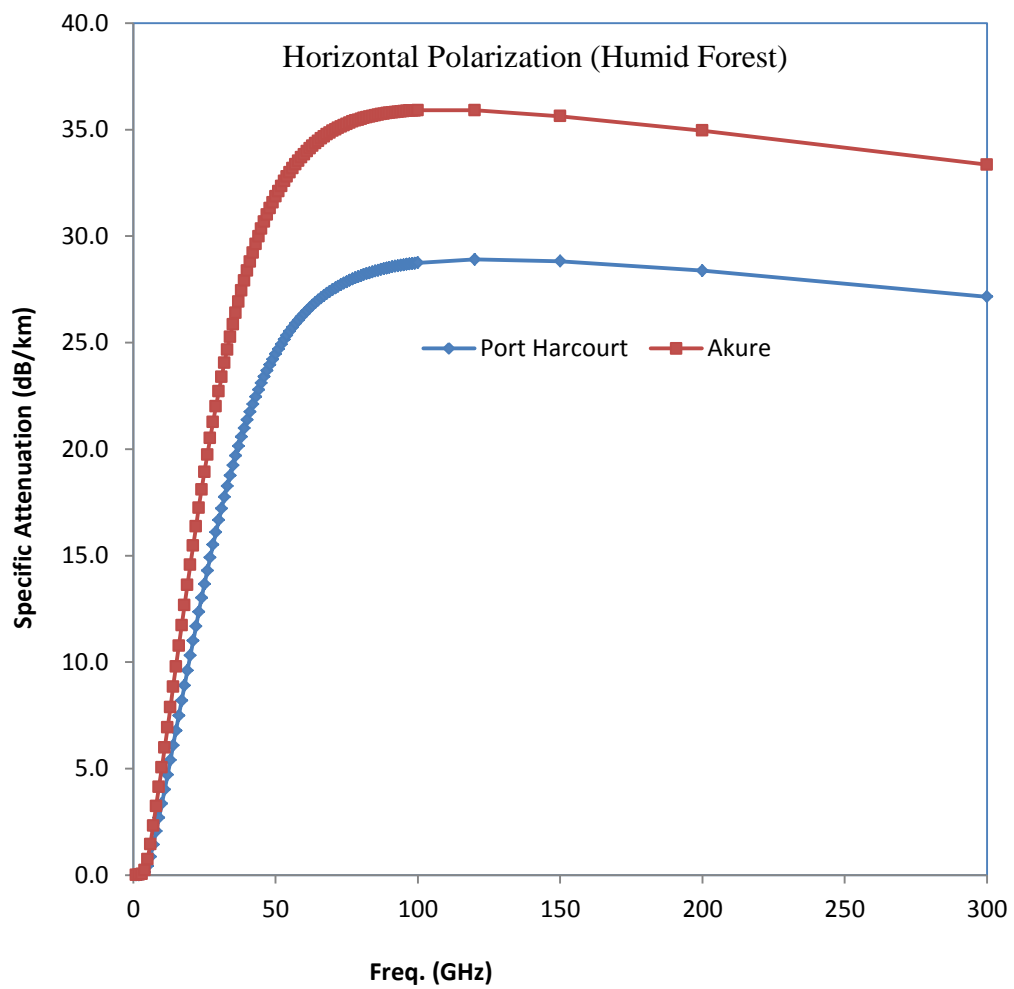


**Fig. 4.40.** Specific rain attenuation versus frequency for horizontal polarisation over the humid forest zone

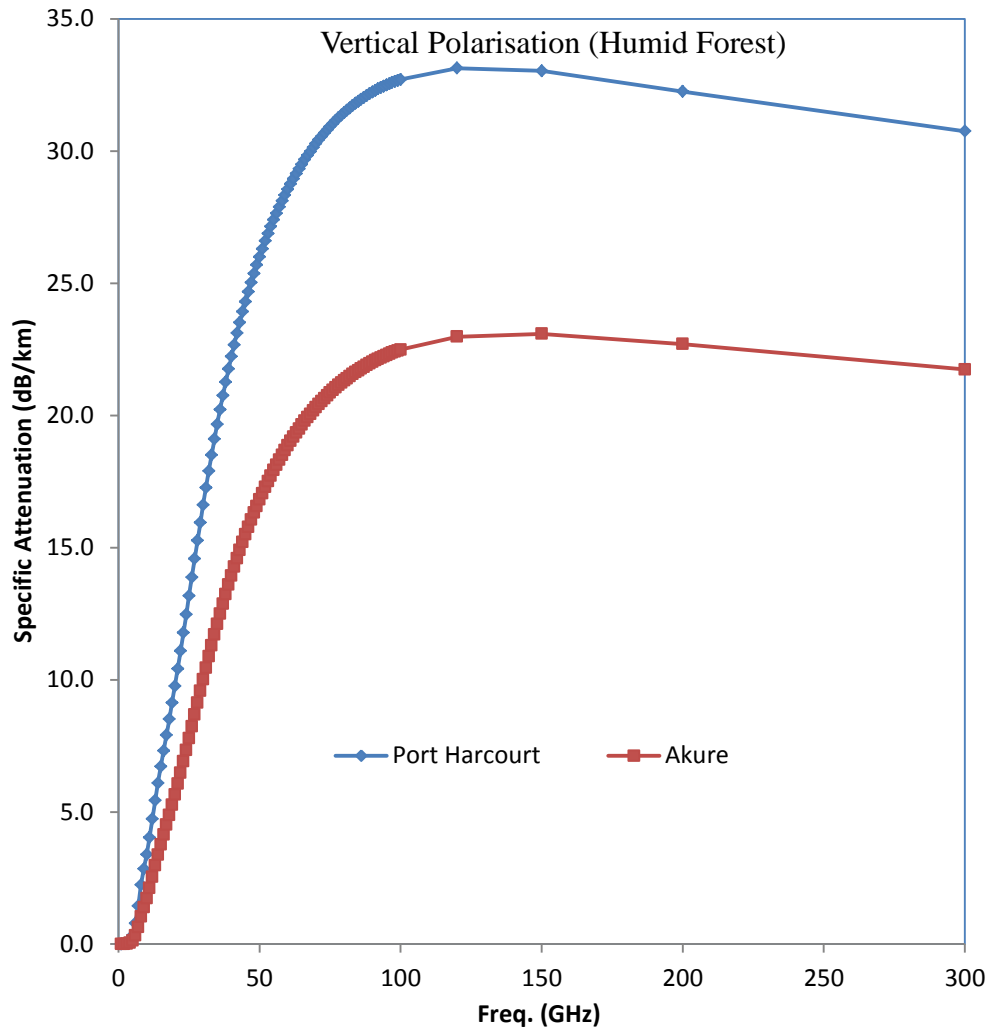


**Fig. 4.41.** Specific rain attenuation versus frequency for vertical polarisation over the humid forest zone

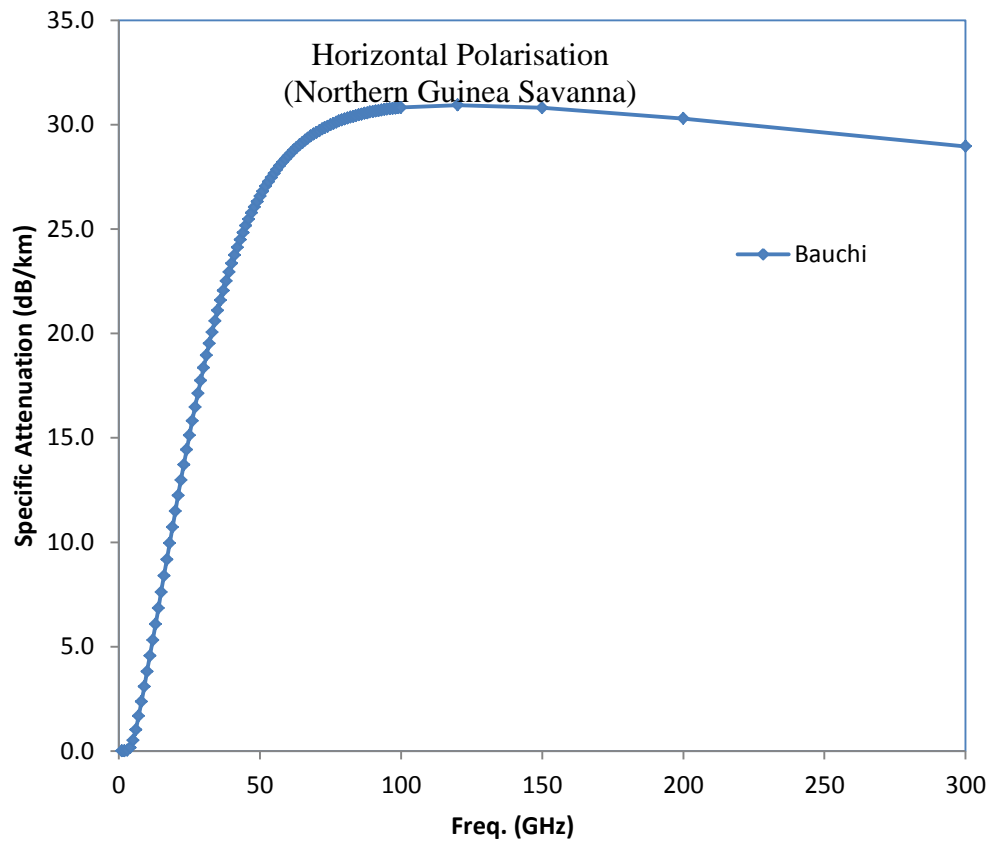


**Fig. 4.42.** Specific rain attenuation versus frequency for horizontal polarisation over the northern guinea savanna zone

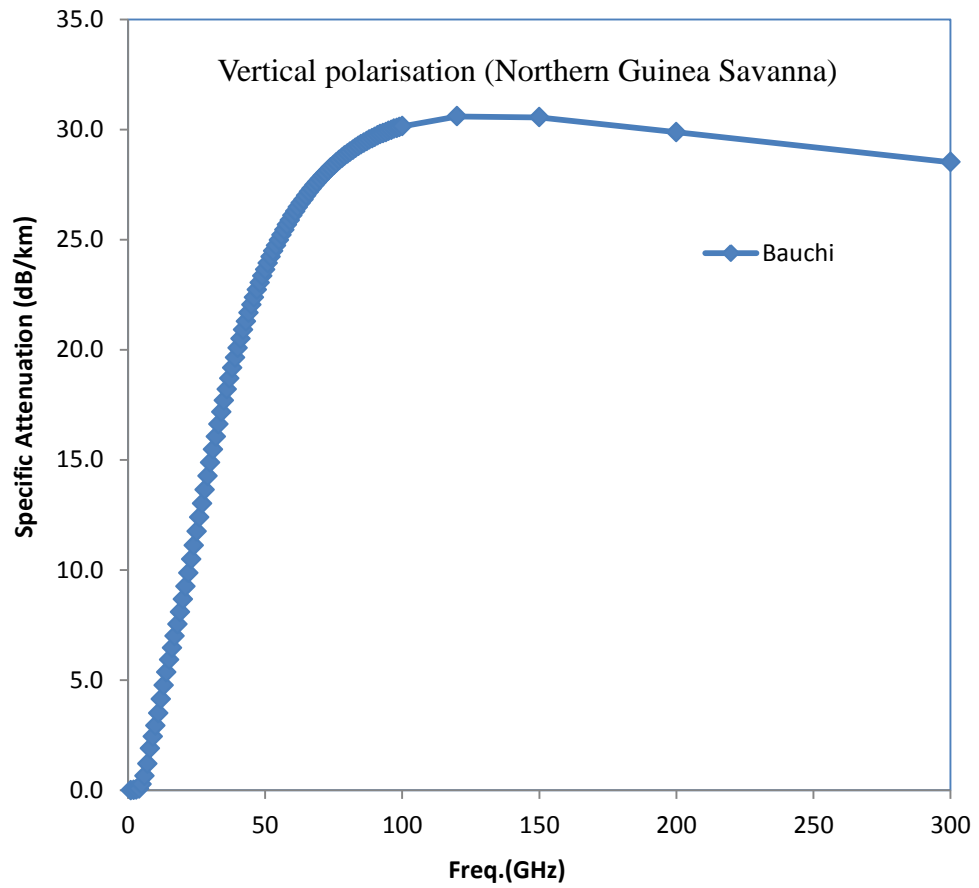


**Fig. 4.43.** Specific rain attenuation versus frequency for vertical polarisation over the northern guinea savanna zone

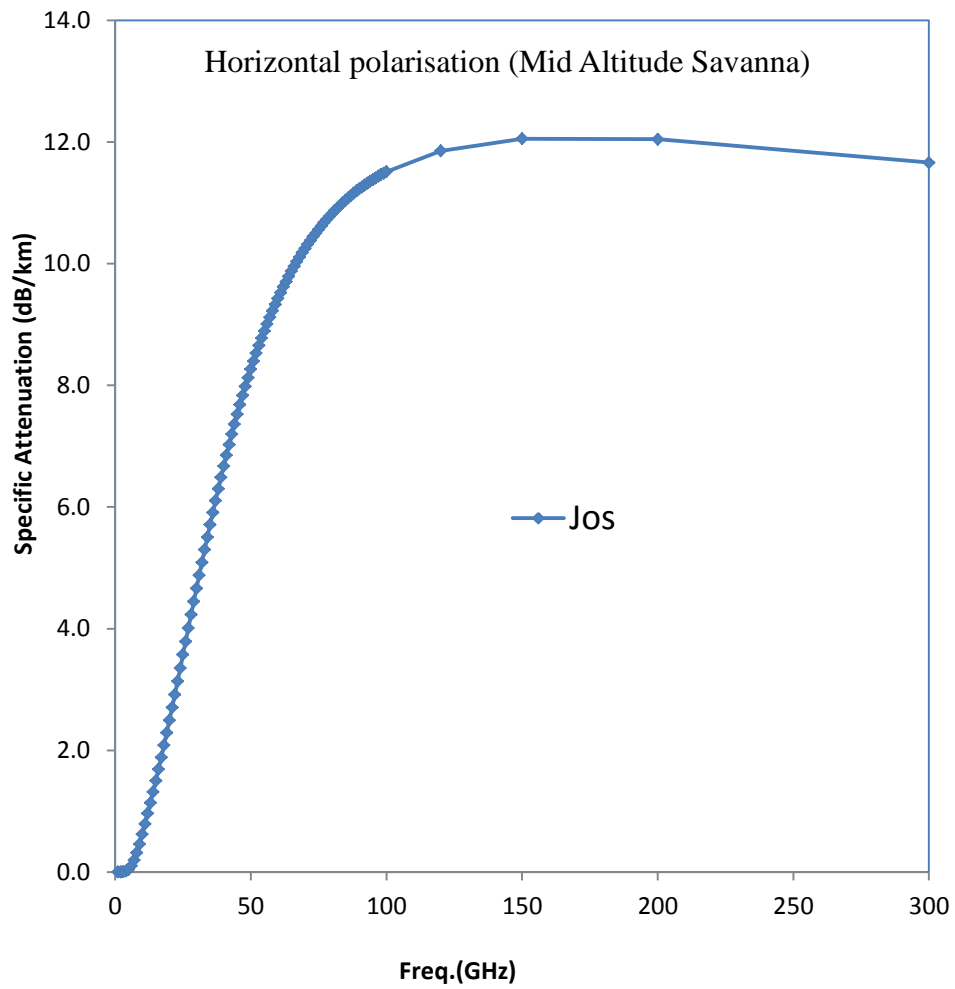


**Fig. 4.44.** Specific rain attenuation versus frequency for horizontal polarisation over the mid altitude savanna zone

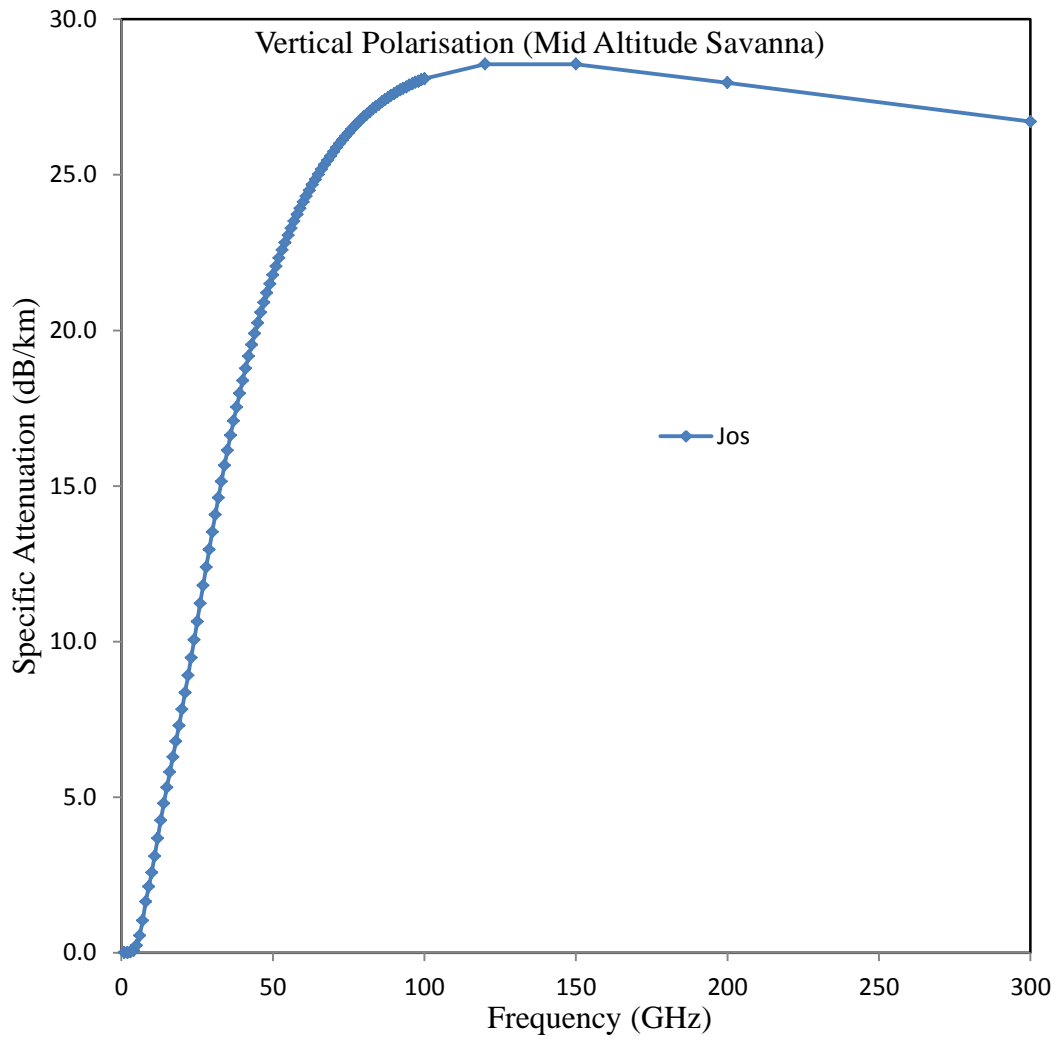


**Figure 4.45.** Specific rain attenuation versus frequency for vertical polarisation over the mid altitude savanna zone

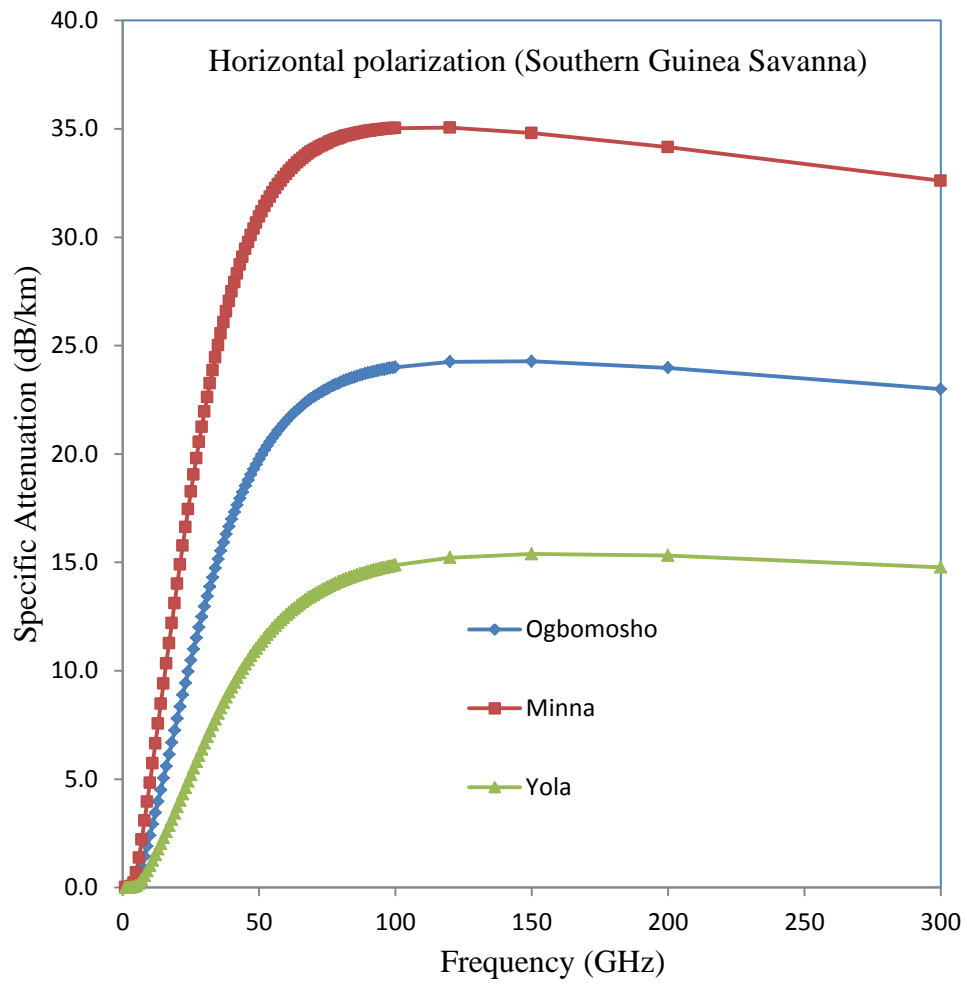


**Figure 4.46.** Specific rain attenuation versus frequency for horizontal polarisation over the southern guinea savanna zone



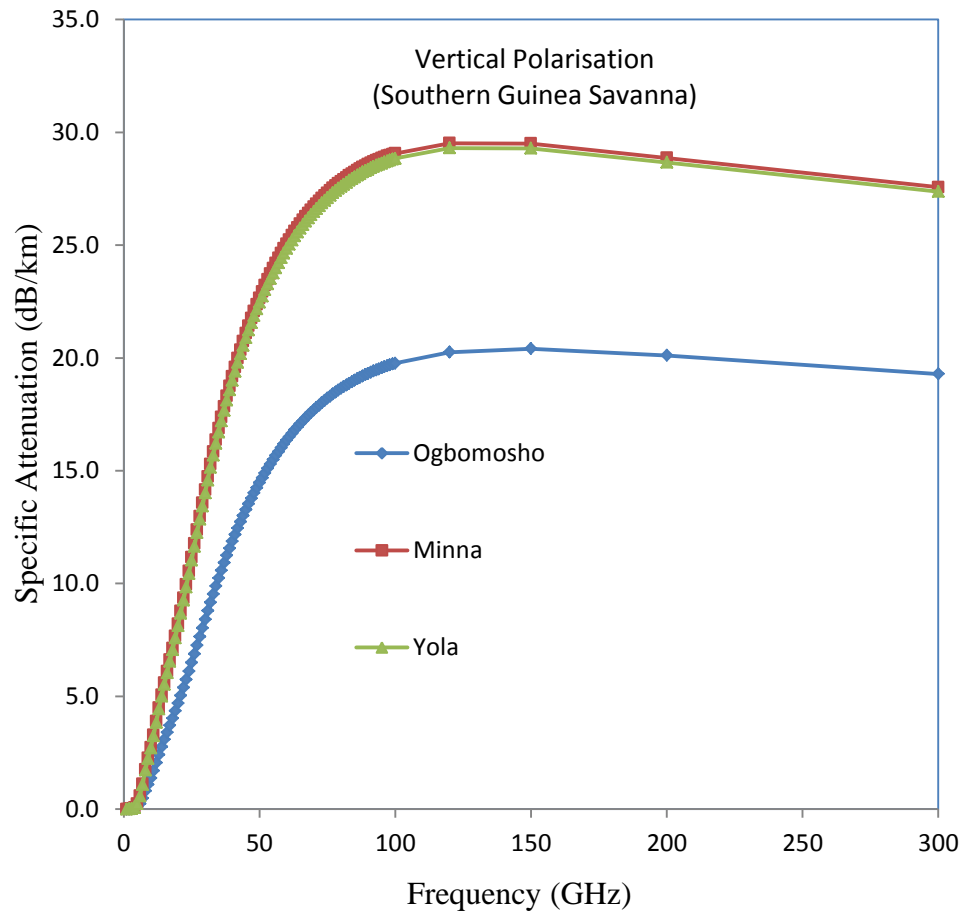


**Figure 4.47.** Specific rain attenuation versus frequency for vertical polarisation over the southern guinea savanna zone

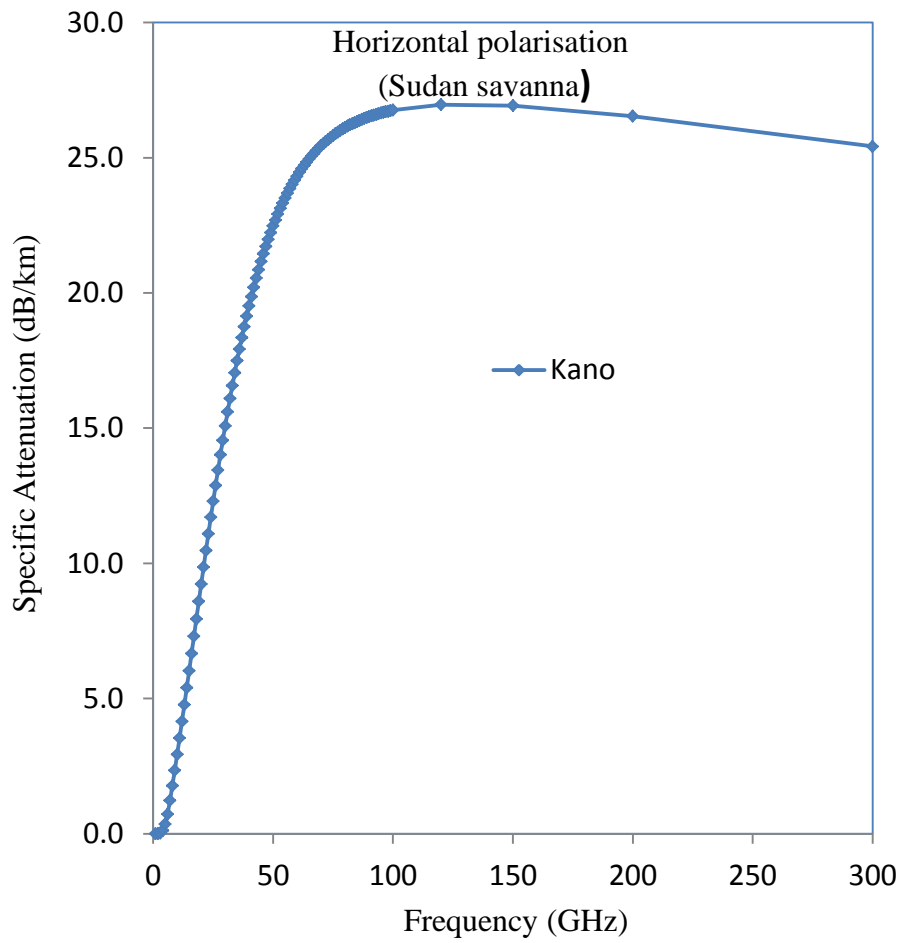


**Figure 4.48.** Specific rain attenuation versus frequency for horizontal polarisation over the Sudan savanna zone

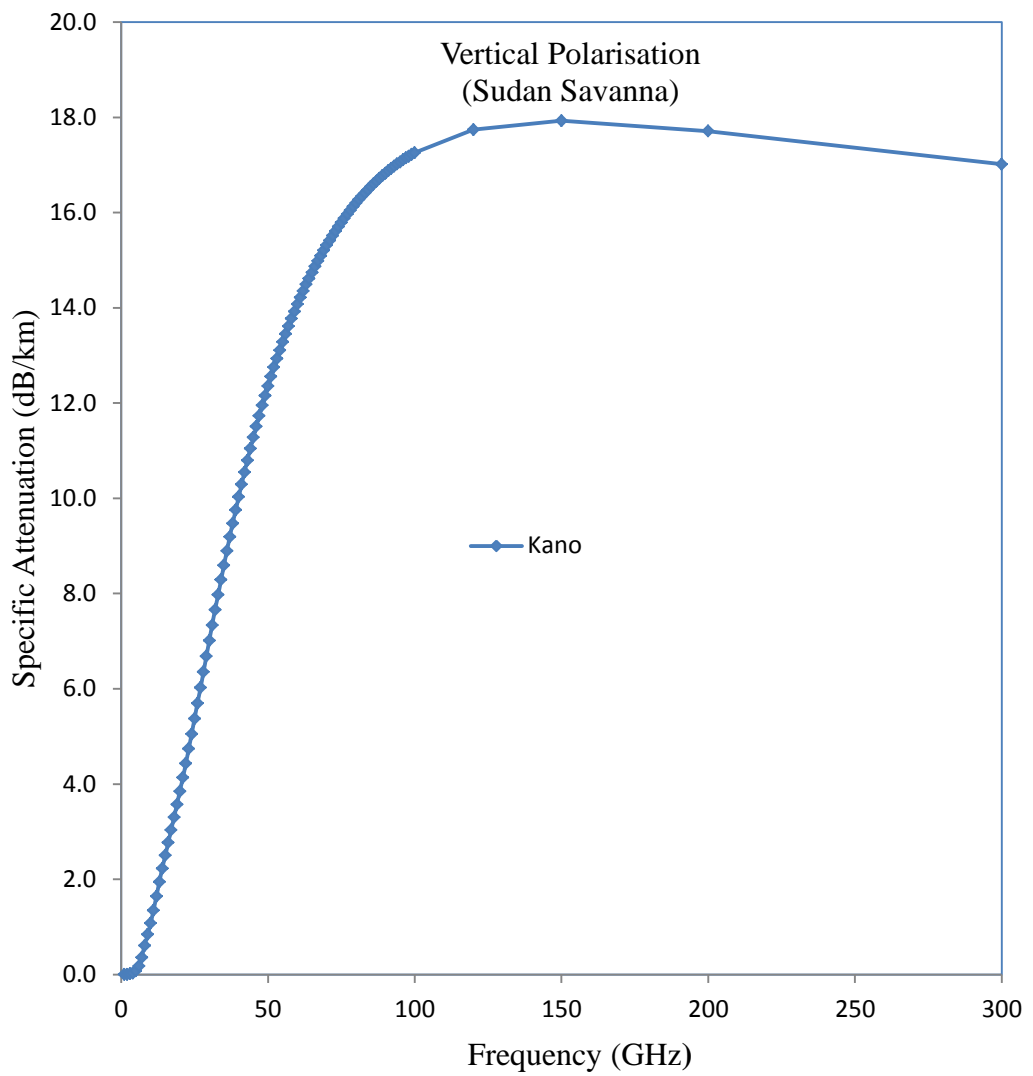


**Figure 4.49.** Specific rain attenuation versus frequency for vertical polarisation over the sudan savanna zone

The specific rain attenuation for the fourteen locations was computed at the maximum frequencies of either 120 GHz or 150 GHz which are specific attenuation threshold at each location. Figure 4.50 and appendix 10 shows the plot of specific rain attenuation at vertical and horizontal polarisation at 0.01% exceedance rainfall rate across all the eco-climatic zone locations (Table 4.12).

Table 4.13 is the summary of the specific attenuation at the horizontal and vertical polarisation for the average rainfall throughout the period of study at each location and the predicted value by the ITU-R.

From Table 4.13, it can be observed that the specific attenuation produced by horizontal (Horiz.) polarisation was slightly higher than that derived for vertical (vert.) polarisation. Also, the specific attenuation estimate by the ITU-R differs remarkably from that derived from measurement. In the Derived Savanna eco-climatic zone, the maximum specific attenuation predicted by ITU-R was 30.56 dB/km which differed from attenuation of 29.78 dB/km derived from measured rainfall by 0.78 dB/km. On the other hand, at the Humid Forest eco-climatic zone, the maximum predicted value of specific attenuation by ITU-R was 33.52 dB/km and it differed from the attenuation of 35.91 dB/km derived from measured rainfall by about 2.30 dB/km. The threshold frequency of propagation for the predicted and measured values at this zone was 120 GHz. At the Northern Guinea Savanna eco-climatic zone, the maximum predicted specific attenuation by ITU-R was 18.14 dB/km and it differed from the derived value of 30.94 dB/km by 12.80 dB/km. Other zones follow the same trend, however with variation in the differences in specific attenuation due to rain. These imply that to ensure stable signal in Nigeria, ITU-R measurement should be replaced with specific attenuation derived from the measured local data.

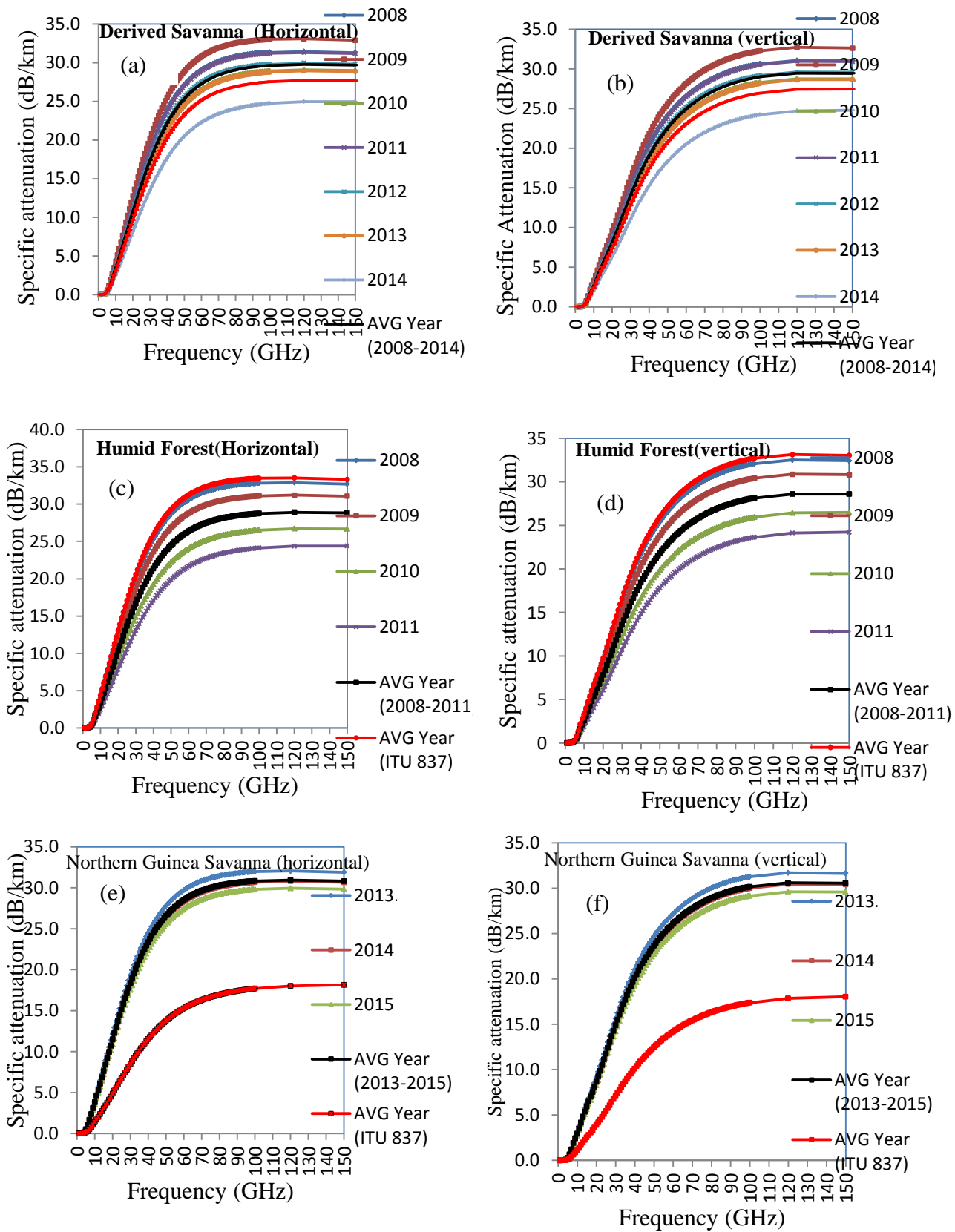


**Figure 4.50.** Specific rain attenuation at vertical and horizontal polarisation at 0.01% exceedance rainfall rate

**Table 4.13:** Specific attenuation values at 120 GHz and 150 GHz

Location	Freq (GHz)	ITU-R		Estimate	
		Horiz. (dBkm <sup>-1</sup> )	Vert. (dBkm <sup>-1</sup> )	Horiz. (dBkm <sup>-1</sup> )	Vert. (dBkm <sup>-1</sup> )
Nsukka	120	27.70	27.41	29.78	29.46
	150	27.66	27.44	29.68	29.44
Eburumiri	120	29.48	27.19	29.59	29.26
	150	27.44	27.22	29.49	29.25
Iwo (Osun)	120	22.95	21.81	21.81	21.06
	150	23.06	21.88	23.23	21.73
Ogbomosho	120	24.25	24.01	20.44	20.25
	150	24.27	24.10	20.54	20.41
Mowe	120	17.21	17.07	23.08	22.86
	150	17.36	17.26	23.13	22.97
Akure	120	23.20	22.98	35.91	35.48
	150	23.25	23.09	35.63	35.32
Port Harcourt	120	33.52	33.14	29.91	28.60
	150	33.32	33.03	28.83	28.60
Yola	120	29.63	29.31	15.21	15.09
	150	29.53	29.29	15.38	15.31
Bauchi	120	18.01	17.85	30.94	30.60
	150	18.14	18.04	30.81	30.55
Jos	120	28.86	28.55	11.85	11.77
	150	28.78	28.56	12.05	12.00
Minna	120	29.85	29.52	35.05	34.64
	150	29.74	29.50	34.81	34.50
Makurdi	120	29.91	29.58	20.23	20.05
	150	29.80	29.56	20.33	20.20
Anyigha	120	30.56	20.00	15.30	15.18
	150	30.43	30.18	15.47	15.40
Kano	120	17.90	17.74	26.96	26.68
	150	18.03	17.93	26.93	26.72

#### **4.2.2 Estimating Path Attenuation Using Different Existing Models for Terrestrial Paths**

The specific attenuation based on the average rain rate statistics may be inadequate for attenuation determination along a radio link path (Crane, 1996). This, according to Hall et al., (1996), is due to the variations in the rainfall distributions over communications paths. In a bid to quantify the path attenuation by rainfall of communication signals, some authors adopted the use of reduction factor to multiply the measured rain rate at a given point for a given percentage of time while other authors assumed constant rainfall intensity over the signal path hence multiplied the length of the actual path by a reduction coefficient (Moupfouma, 1984).

As can be seen from Figure 4.51 and appendix 11, ITU-R model, in comparison with the other recommended path attenuation models, gave the lowest attenuation value over the path length in all the zones. This finding agrees with the deduction of Fashuyi and Afullo (2007) from his work in South Africa on modeling and prediction of attenuation by rain on terrestrial paths line of sight links. As reported by by Kestwal *et al.* (2014), attenuation induced by rain adversely affects the performance of line of sight communication equipment. Furthermore, Olsen (1999) stressed on the imperative of accurate. Hence, the ITU-R model is preferred over other models for terrestrial paths attenuation determination over the study sites at threshold frequencies of 120 GHz and 150 GHz.

Considering the estimation of the lowest attenuation by ITU-R at 150 GHz threshold and 20 km path length, in comparison with Moupfouma and Crane Global model (Figure 4.51 and appendix 14), the ITU-R model (equation 3.41) was adopted in the estimate of the path attenuation in all the locations considered in this study.

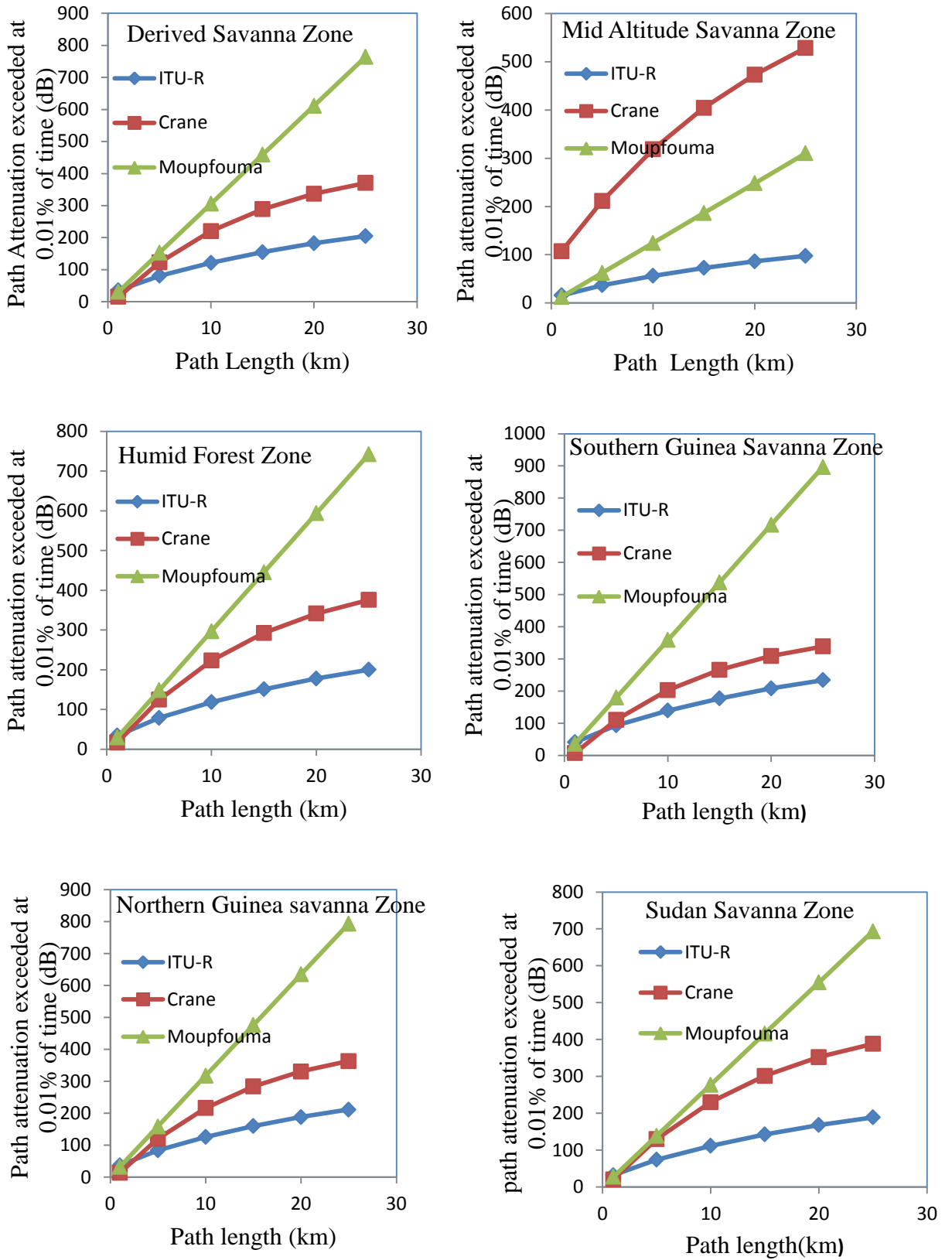


Figure 4.51. Path attenuation at 0.01% rain rate exceedance



The path attenuation across all the eco-climatic zones was plotted at their frequency threshold of 120 GHz and 150 GHz respectively and the maximum recommended path length of 60km by ITU-R (ITU-R 530-17, 2017). The plots of the path attenuation are shown in Figure 4.55 to 4.68. At the recommended maximum path length of 20 km for millimeter radio equipment deployment (Shebani *et al*, 2017), the path attenuation was obtained.

As shown in Figures 4.52a to 4.65a, the maximum frequency for clear signals transmission at Nsukka, Eburumiri, Akure, Port Harcourt, Bauchi, Minna and Kano is 40 GHz. At higher frequency beyond 40 GHz, the transmitted signal suffers from overlap, for transmission at millimetric waveband at these locations, the frequency limits are 30 and 40 GHz. These frequencies are equivalent to the upper limit of Ka frequency band and lower limit of V- frequency band (COST Action 280, 2001). The path attenuation exceeded at 20 km path length at 0.01% in these locations at 30 GHz are 135.00 dB, 85.00 dB, 167.50 dB, 130.00 dB, 140.00 dB, 165.00 dB and 120.00 dB respectively while at 40 GHz, the path attenuation is 170.00 dB, 167.50 dB, 205.00 dB, 165.00 dB, 175.00 dB, 200.00 dB and 155.00 dB at these respective locations. The same trend applies at 30 to 45 GHz clear signal band frequency threshold at other locations. However, Iwo, Makurdi and Kano experiences clear signal at 150 GHz band at 150 dB, 135 dB and 155 dB respectively but this band suffers overlap at Ogun, Anyigba, Yola and Minna locations.

Considering the path attenuation at ITU-R predicted rain rate, Figure 4.52b to 4.65b revealed that at 20 km path length, clear signal occurred in Eburumiri, Port Harcourt, Jos, Minna and Anyigba at 30 to 40 GHz band, also at Bauchi and Kano, clear signal occurred at 30 to 45 GHz band. At Iwo, Ogbomosho, Akure and Ogun, clear signal occurred at 30 to 150 GHz band. However, at Nsukka, Yola and Makurdi, clear signal occurred at 30 GHz band only, while 45 GHz band overlapped with the 150 GHz with path attenuation of 170 dB, 180 dB and 185 dB respectively.

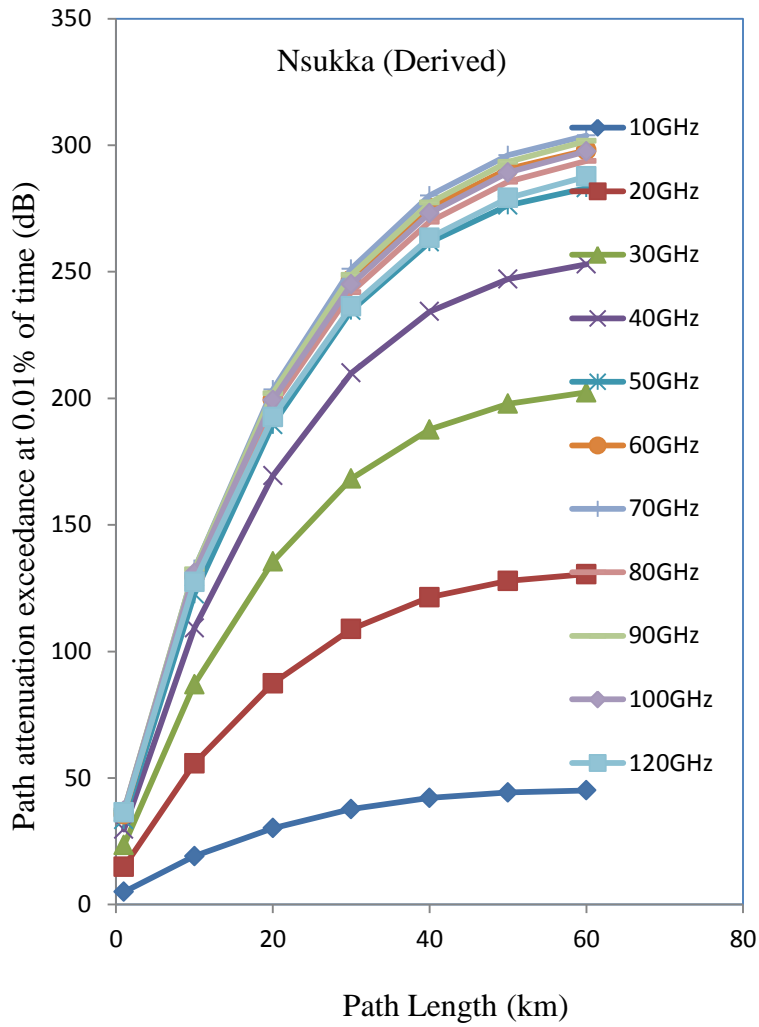


**Figure 4.52a.** Path attenuation at 0.01% measured rain rate exceedance at Nsukka

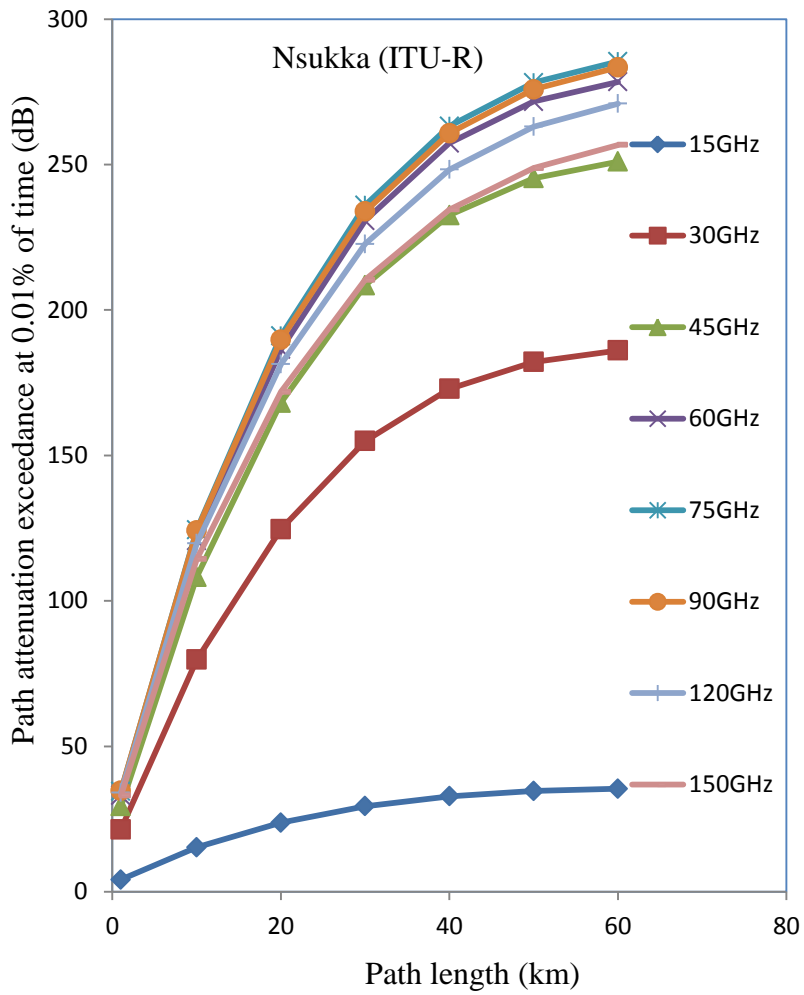


**Figure 4.52b.** Path attenuation at 0.01% ITU-R rain rate prediction at Nsukka

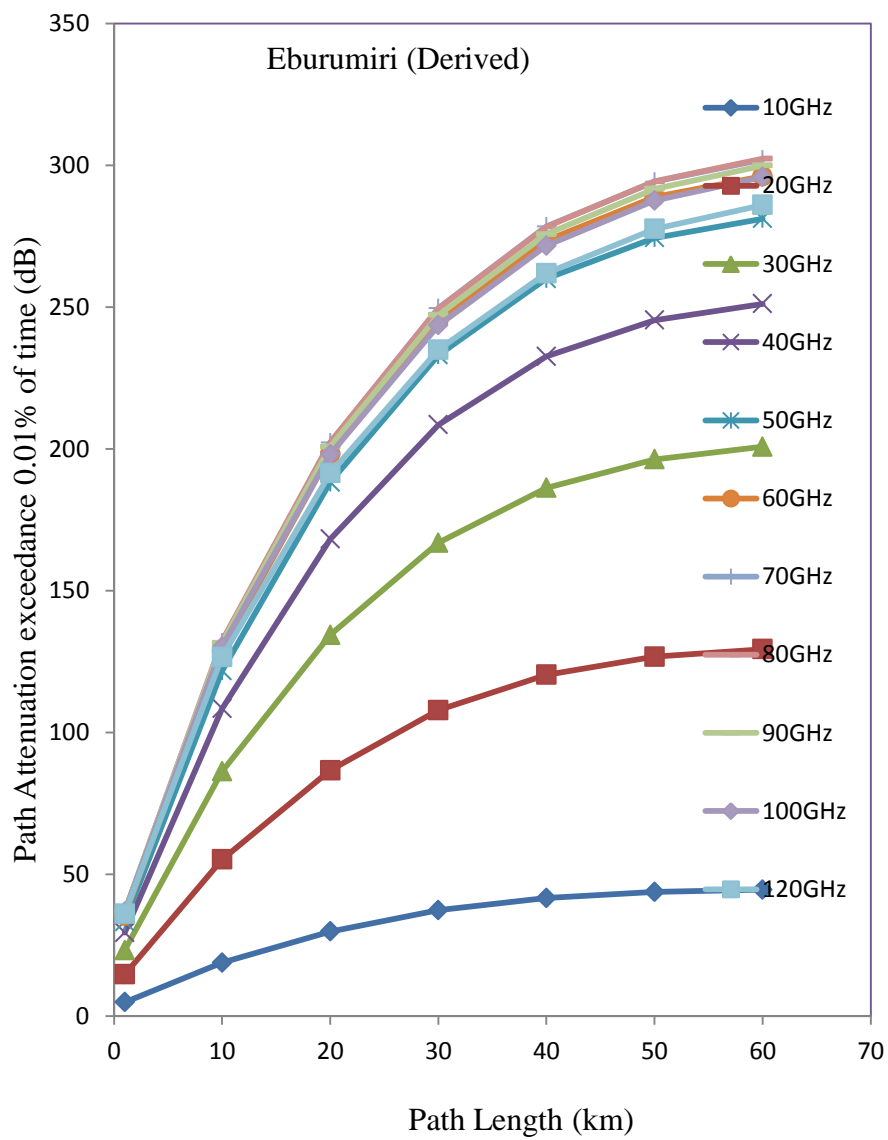


Figure 4.53a. Path attenuation at 0.01% measured rain rate exceedance at Eburumiri

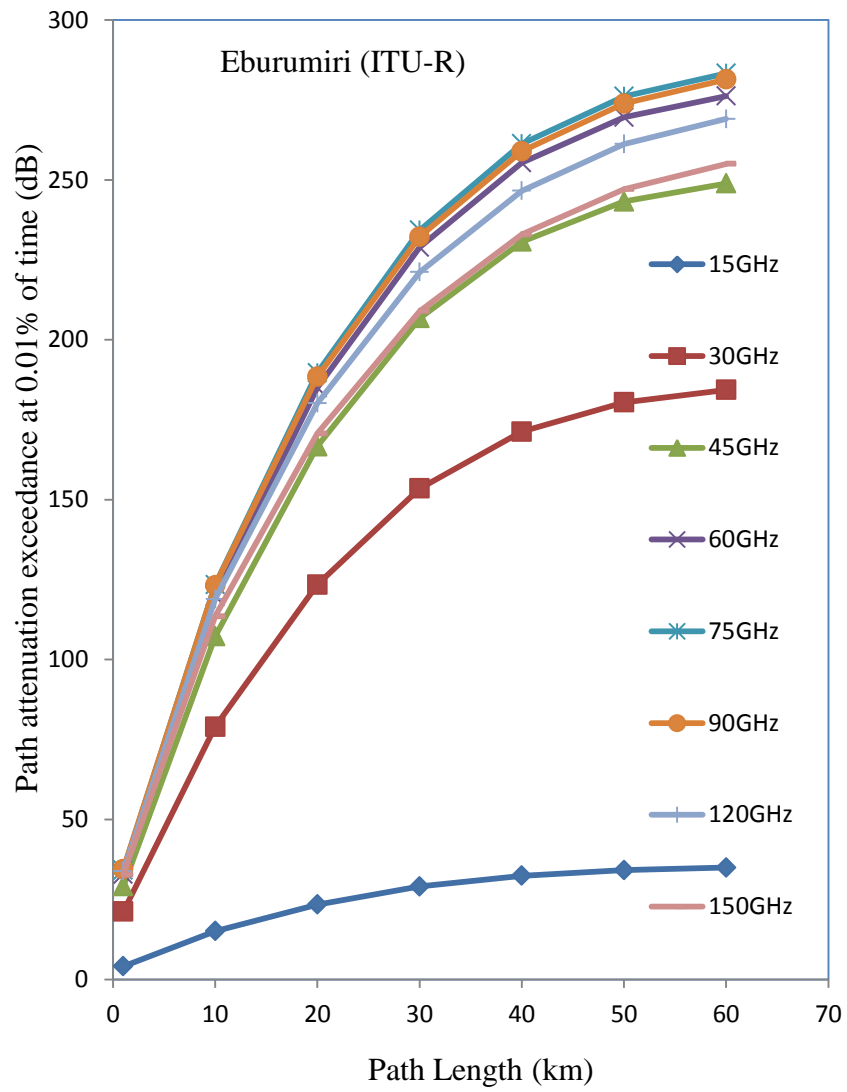
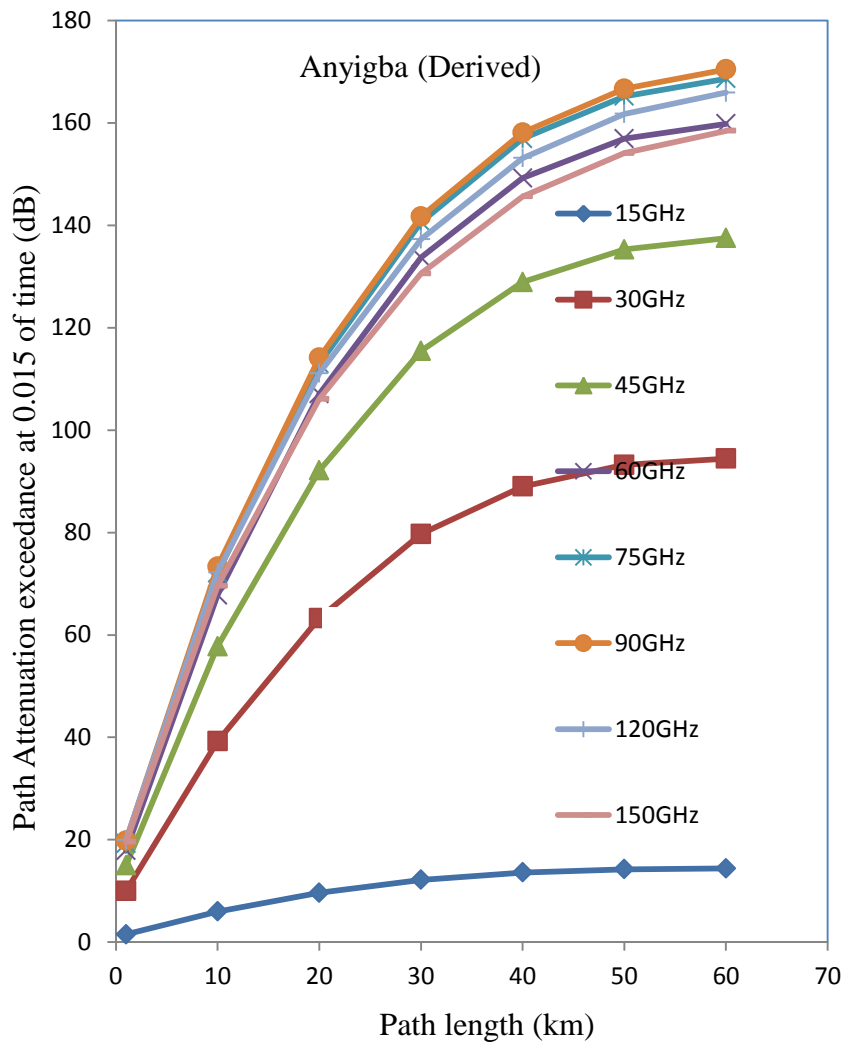


Figure 4.53b. Path attenuation at 0.01% ITU R rain rate prediction at Eburumiri



**Figure 4.54a.** Path attenuation at 0.01% measured rain rate exceedance at Anyiba

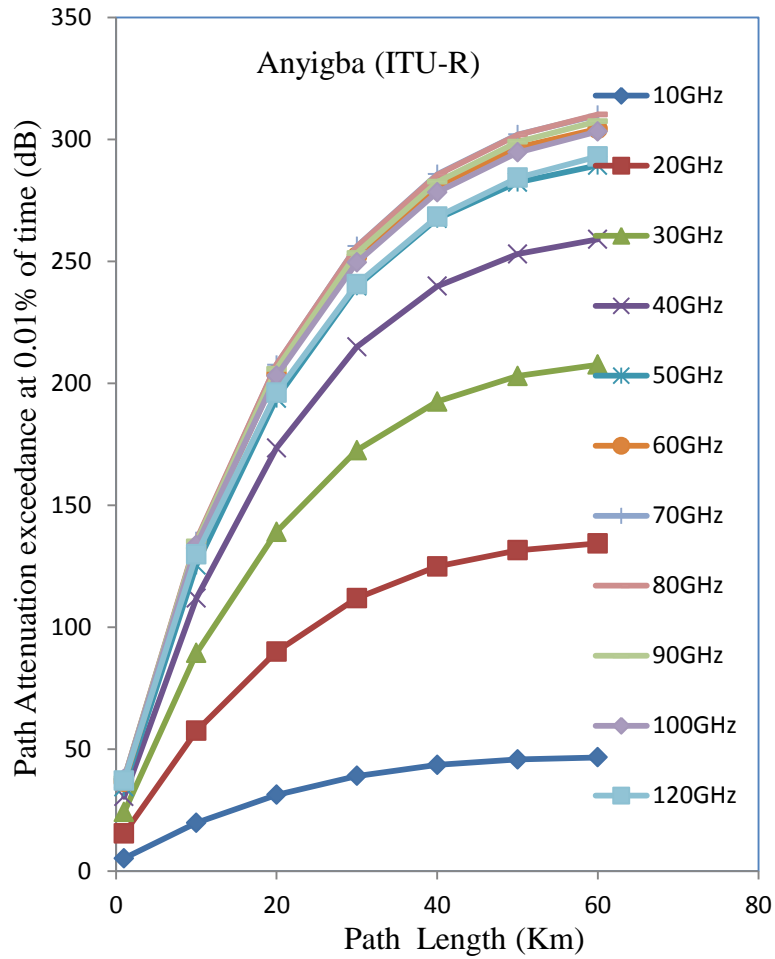


Figure 4.54b. Path attenuation at 0.01% ITU R rain rate prediction at Anyigba

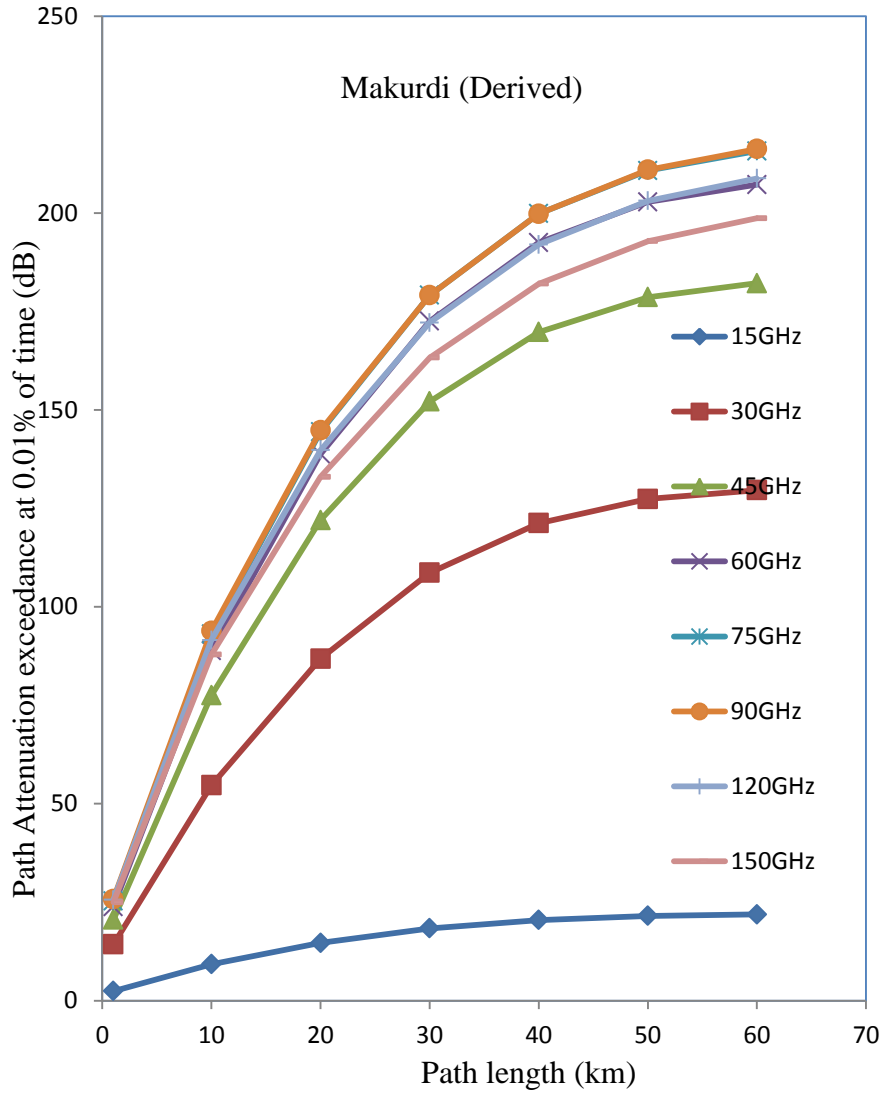
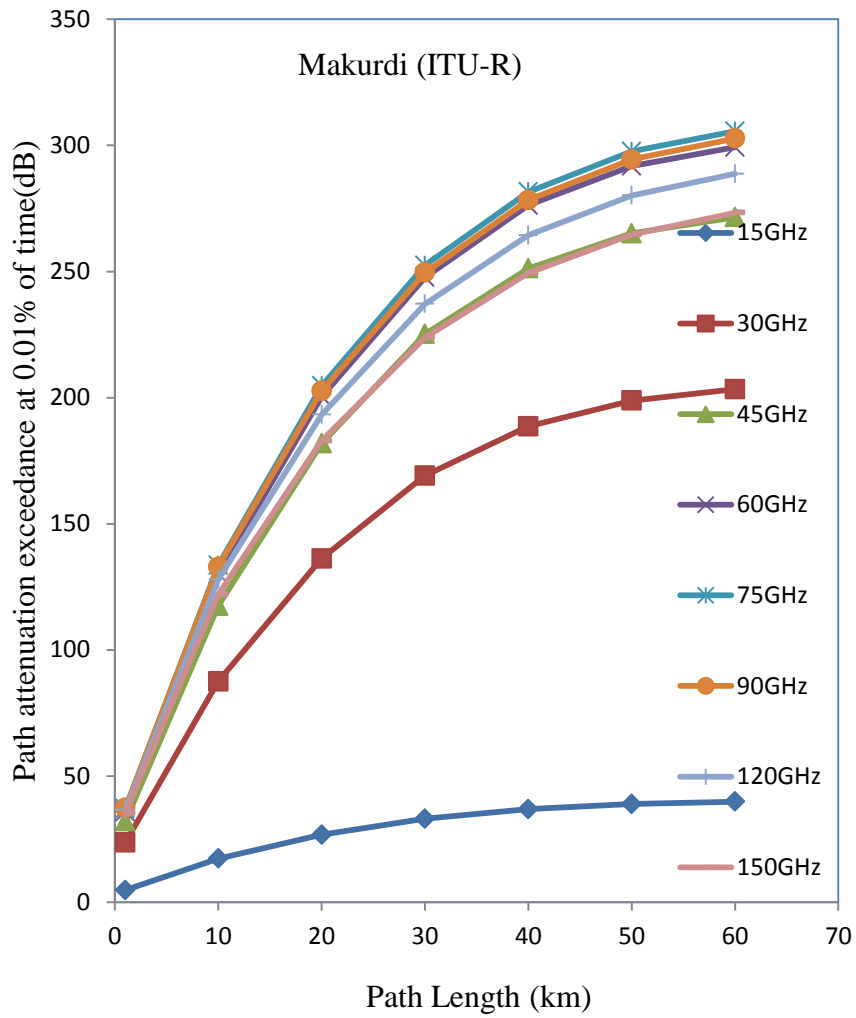
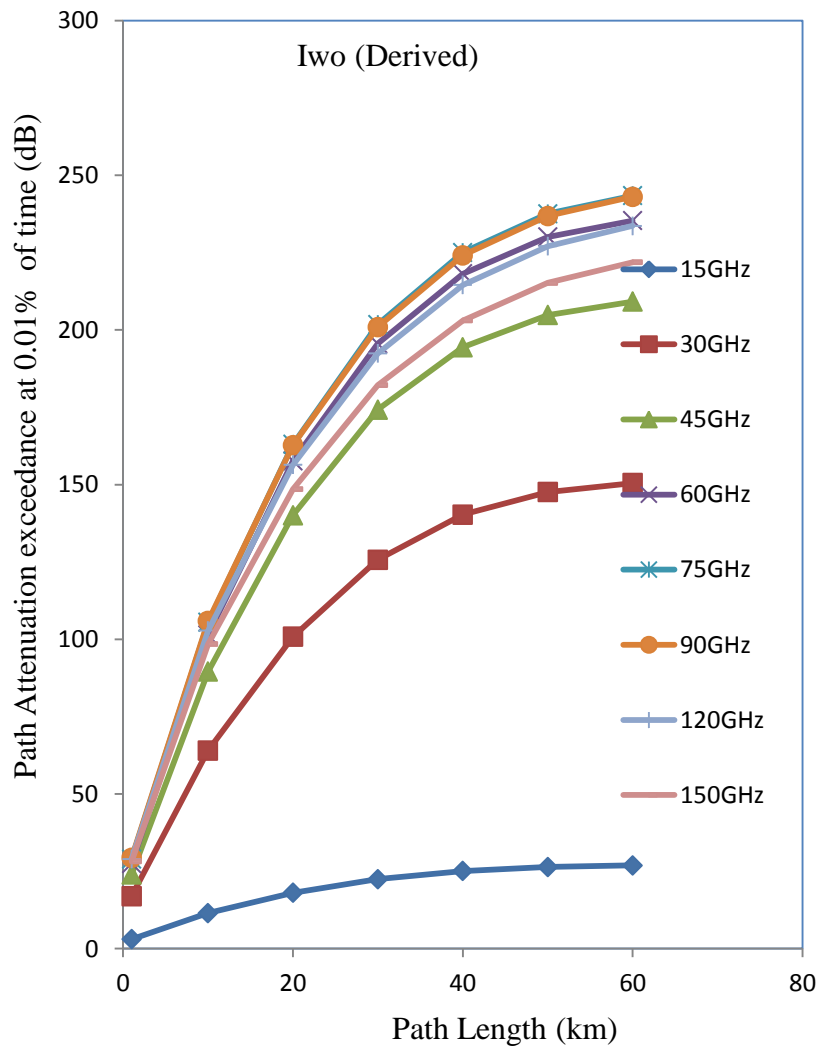


Figure 4.55a. Path attenuation at 0.01% measured rain rate exceedance at Makurdi





**Figure 4.55b.** Path attenuation at 0.01% ITU R rain rate prediction at Makurdi



**Figure 4.56a.** Path attenuation at 0.01% measured rain rate exceedance at Iwo

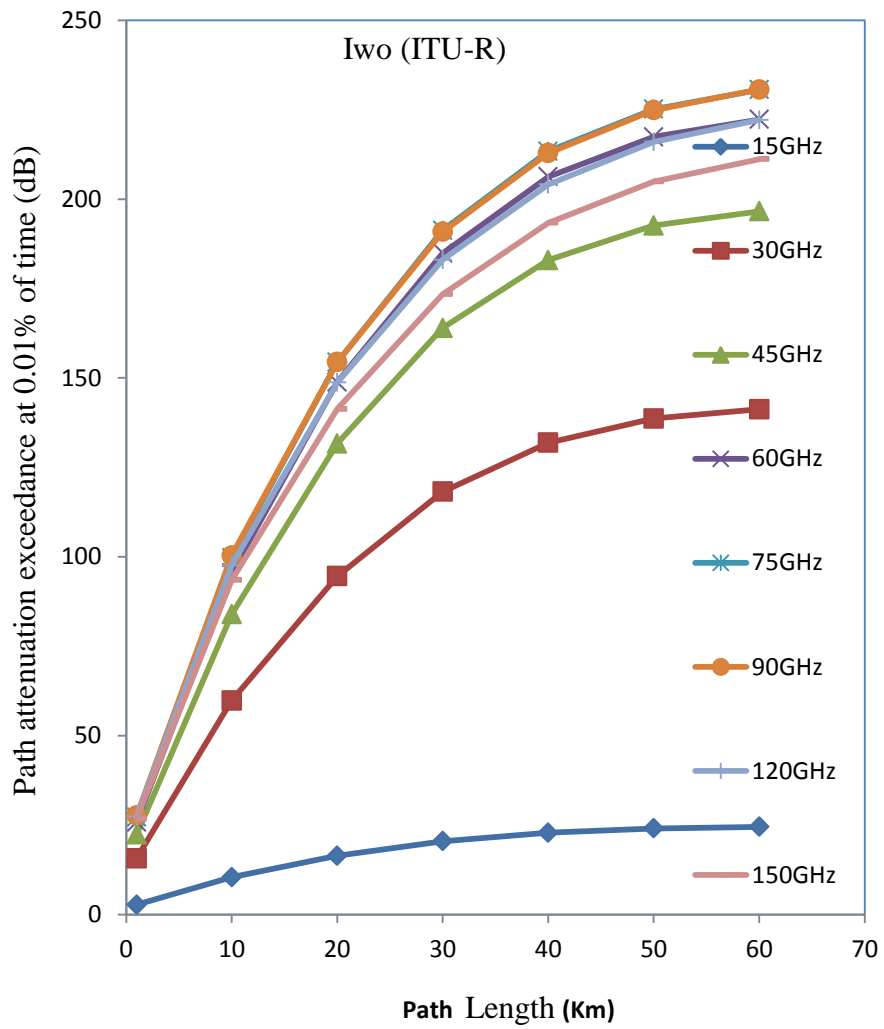
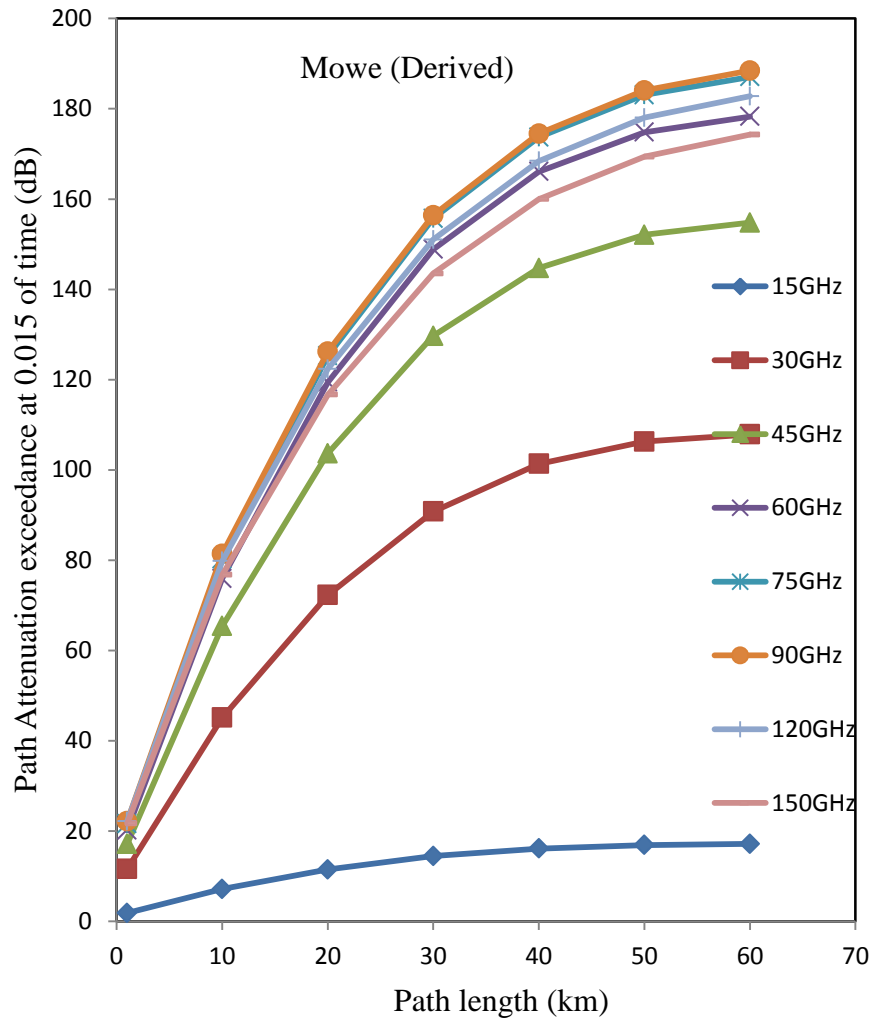


Figure 4.56b. Path attenuation at 0.01% ITU R rain rate prediction at Iwo



**Figure 4.57a.** Path attenuation at 0.01% measured rain rate exceedance at Ogun

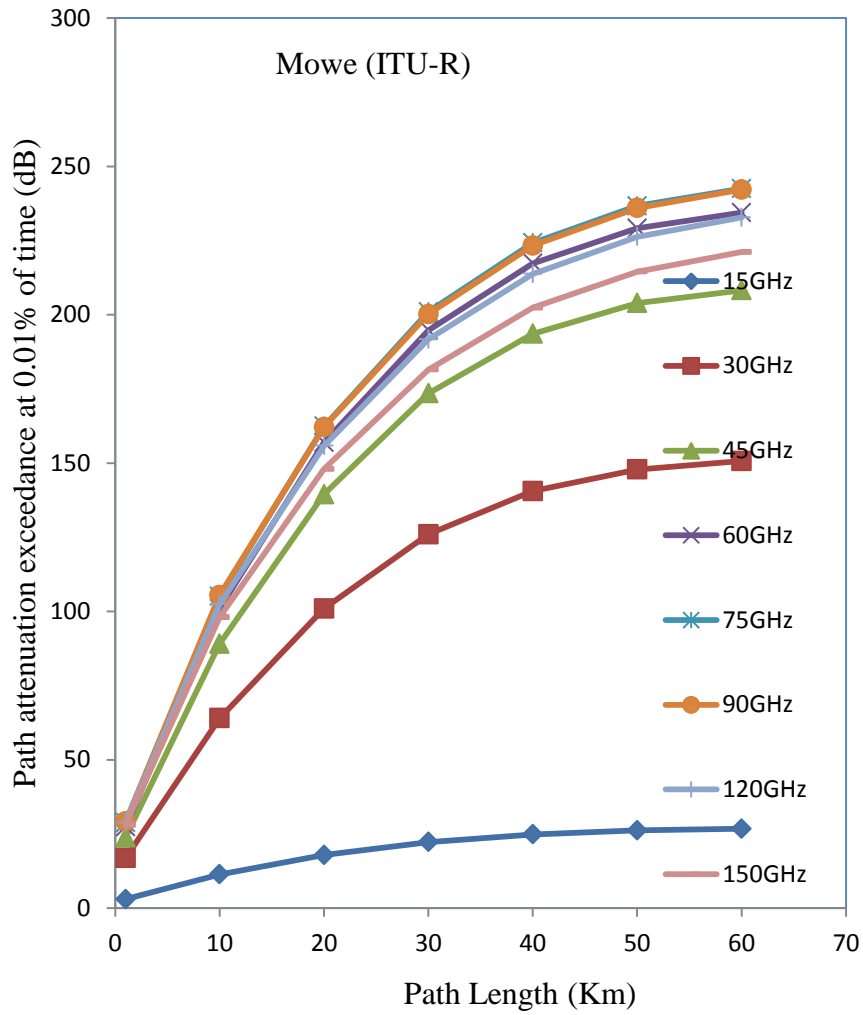


Figure 4.57b. Path attenuation at 0.01% ITU R rain rate prediction at Ogun

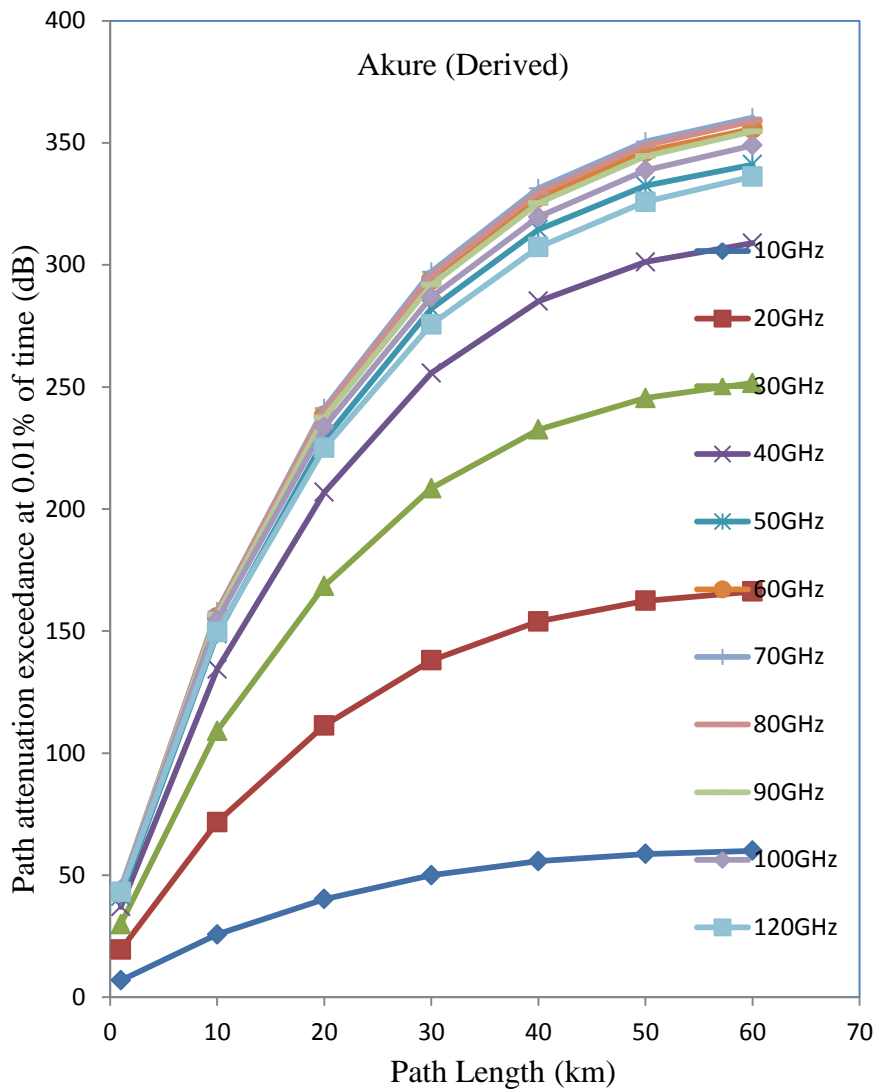


Figure 4.58a. Path attenuation at 0.01% measured rain rate exceedance at Akure

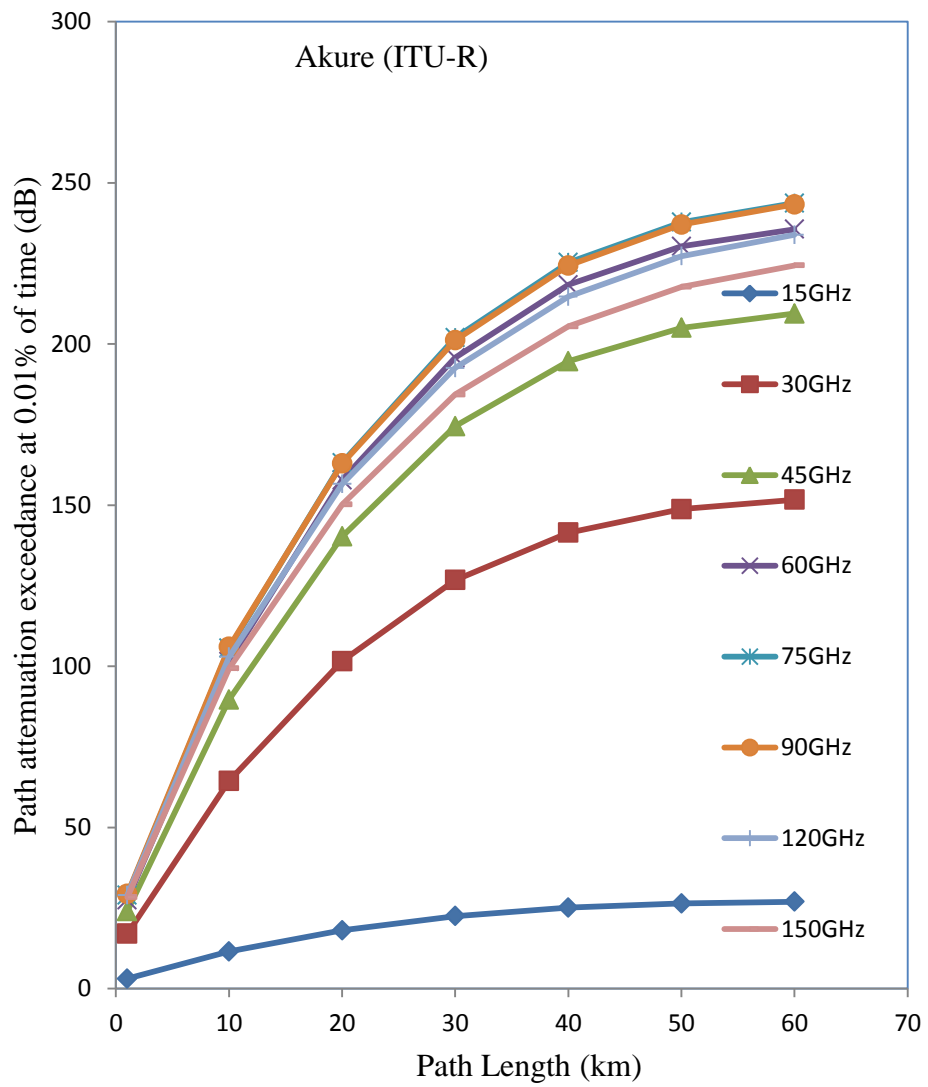
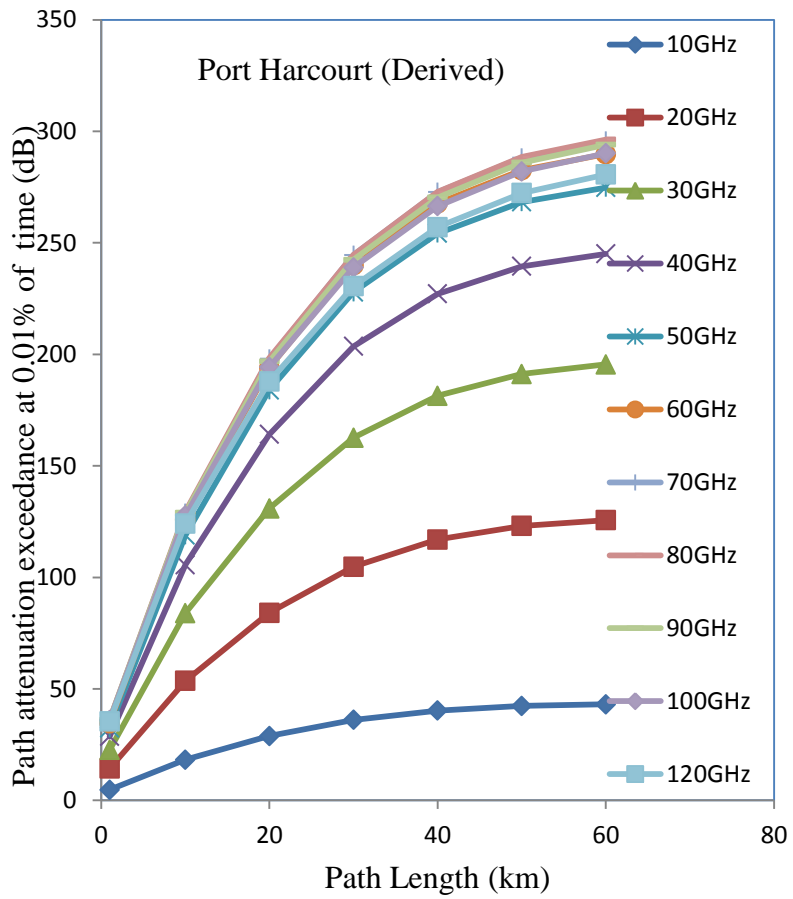
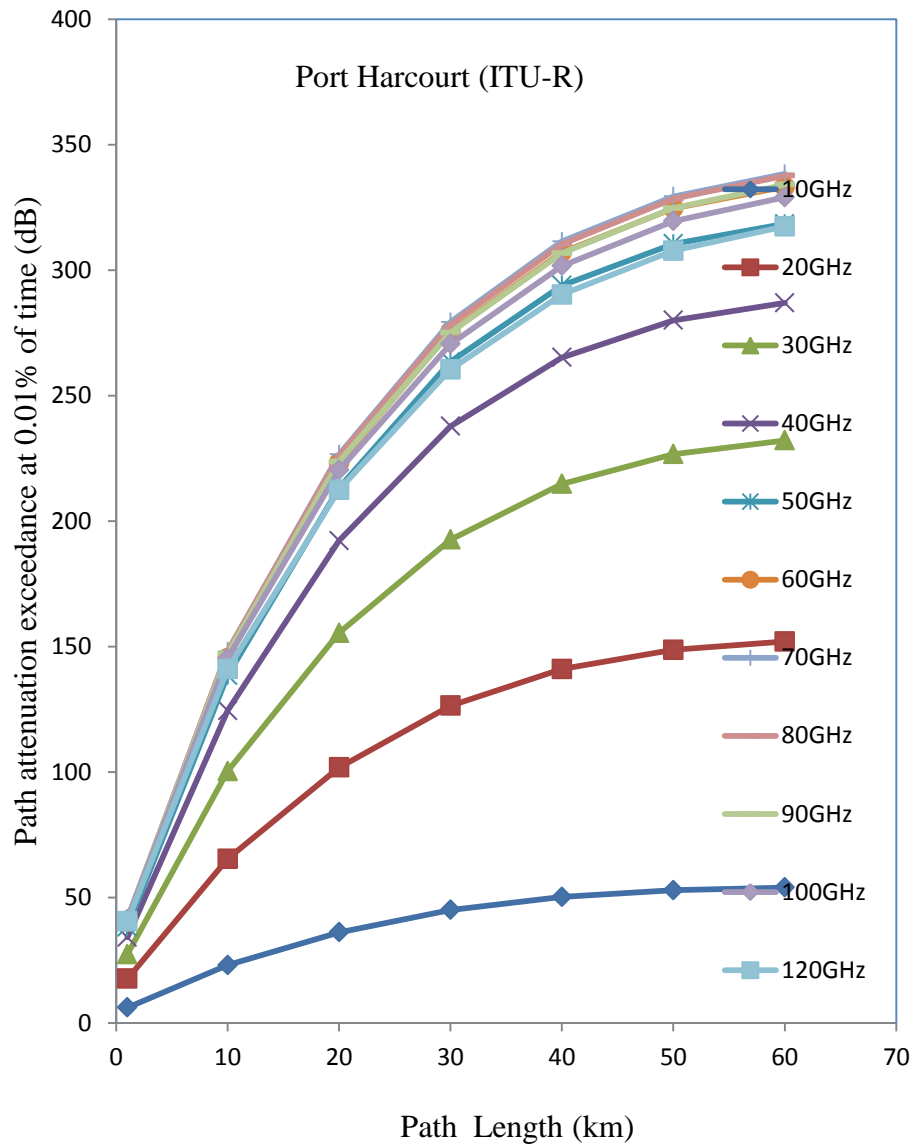


Figure 4.58b. Path attenuation at 0.01% ITU R rain rate prediction at Akure



**Figure 4.59a.** Path attenuation at 0.01% measured rain rate exceedance at Port Harcourt





**Figure 4.59b.** Path attenuation at 0.01% ITU R rain rate prediction at Port Harcourt

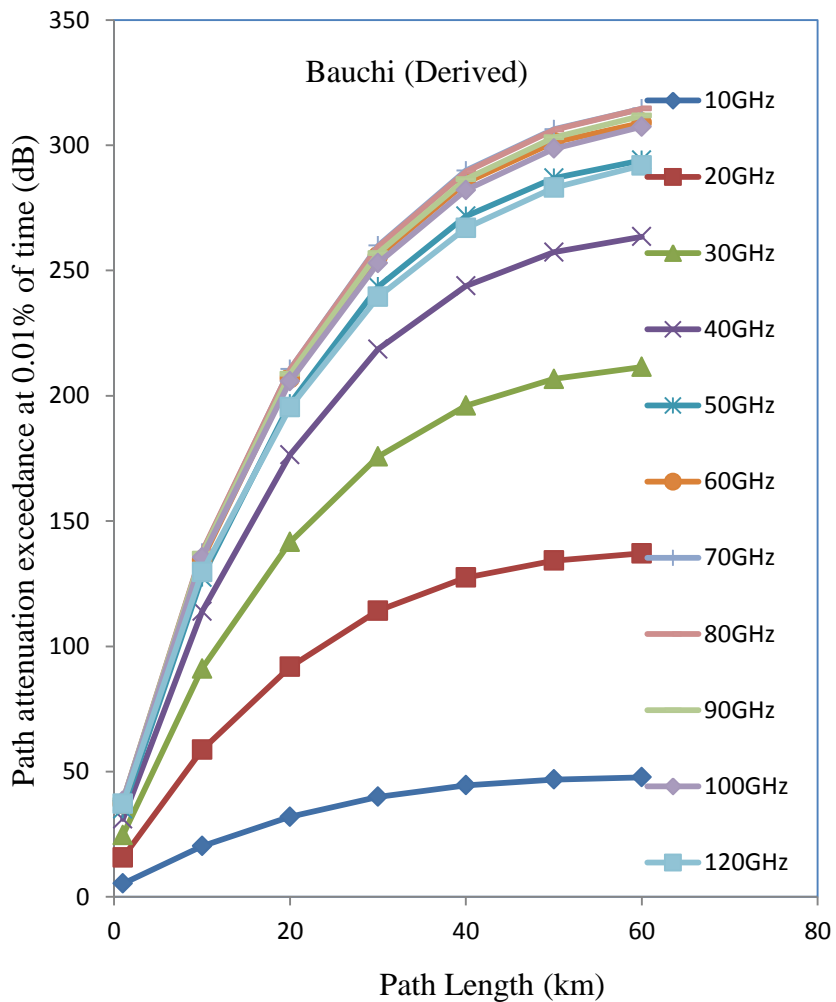
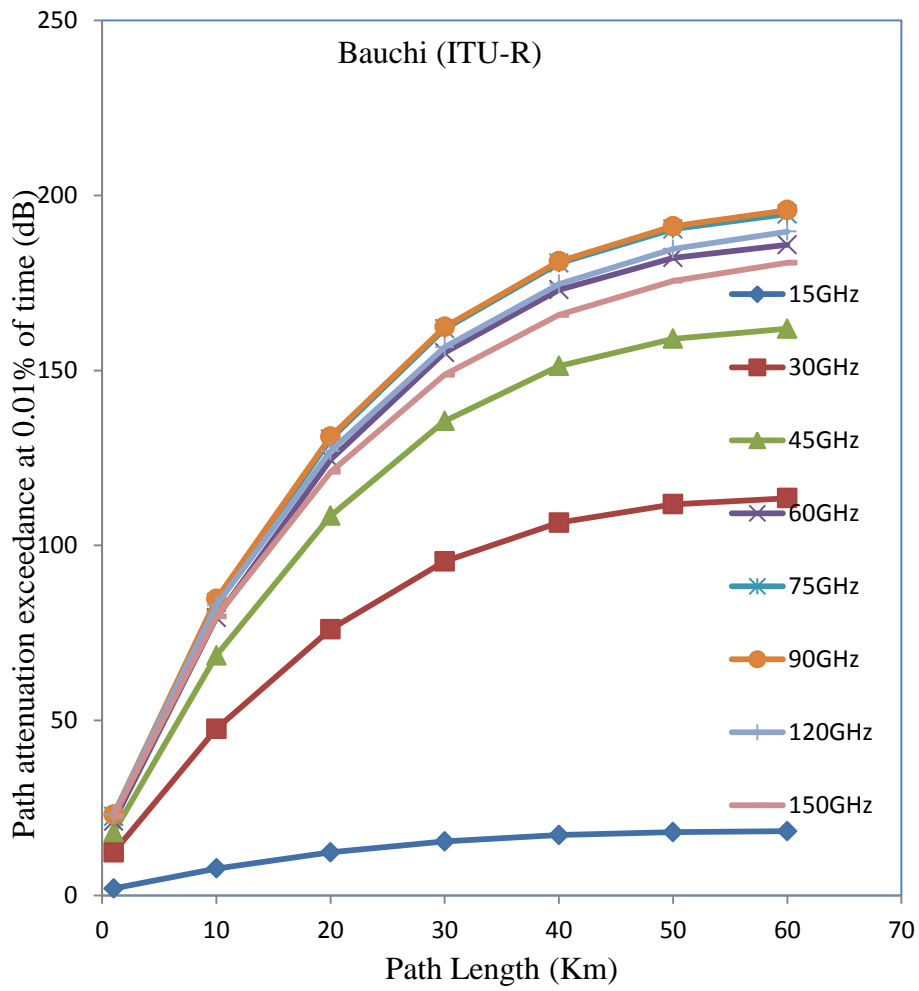


Figure 4.60a. Path attenuation at 0.01% measured rain rate exceedance at Bauchi



**Figure 4.60b.** Path attenuation at 0.01% ITU R rain rate prediction at Bauchi

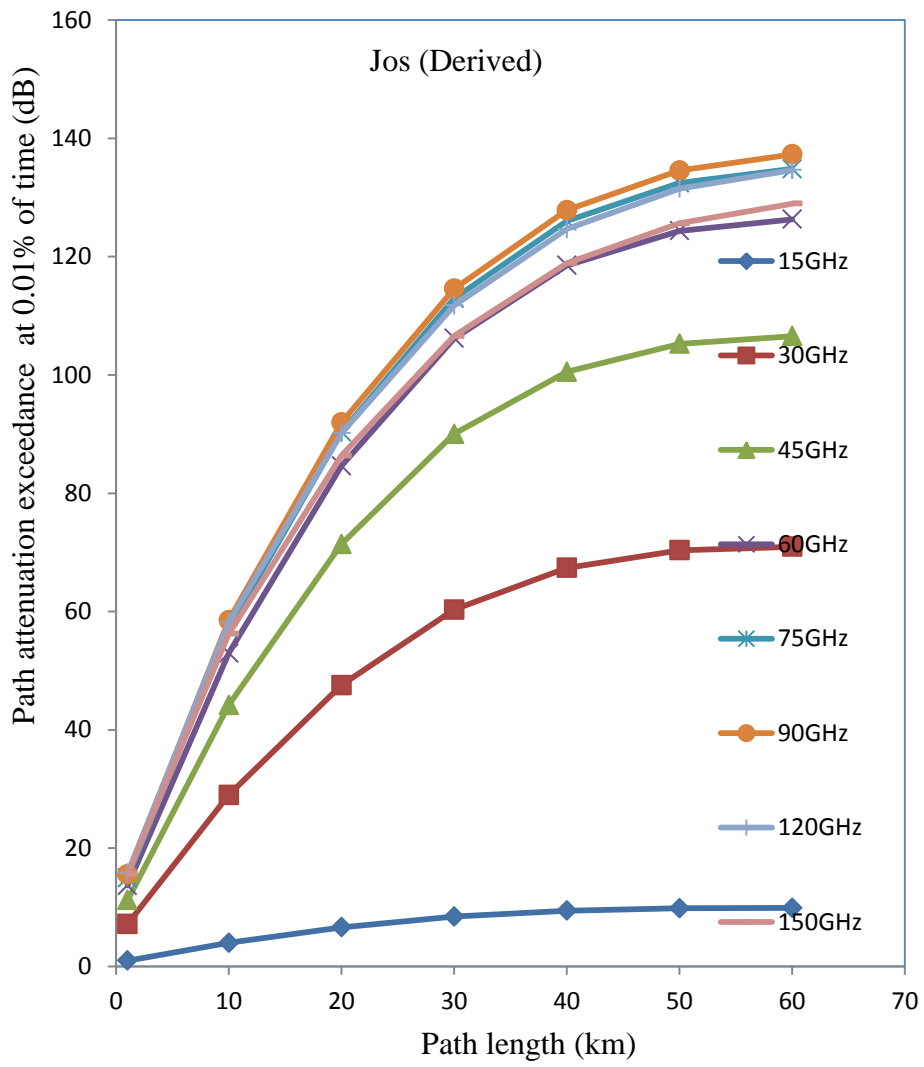


Figure 4.61a. Path attenuation at 0.01% measured rain rate exceedance at Jos

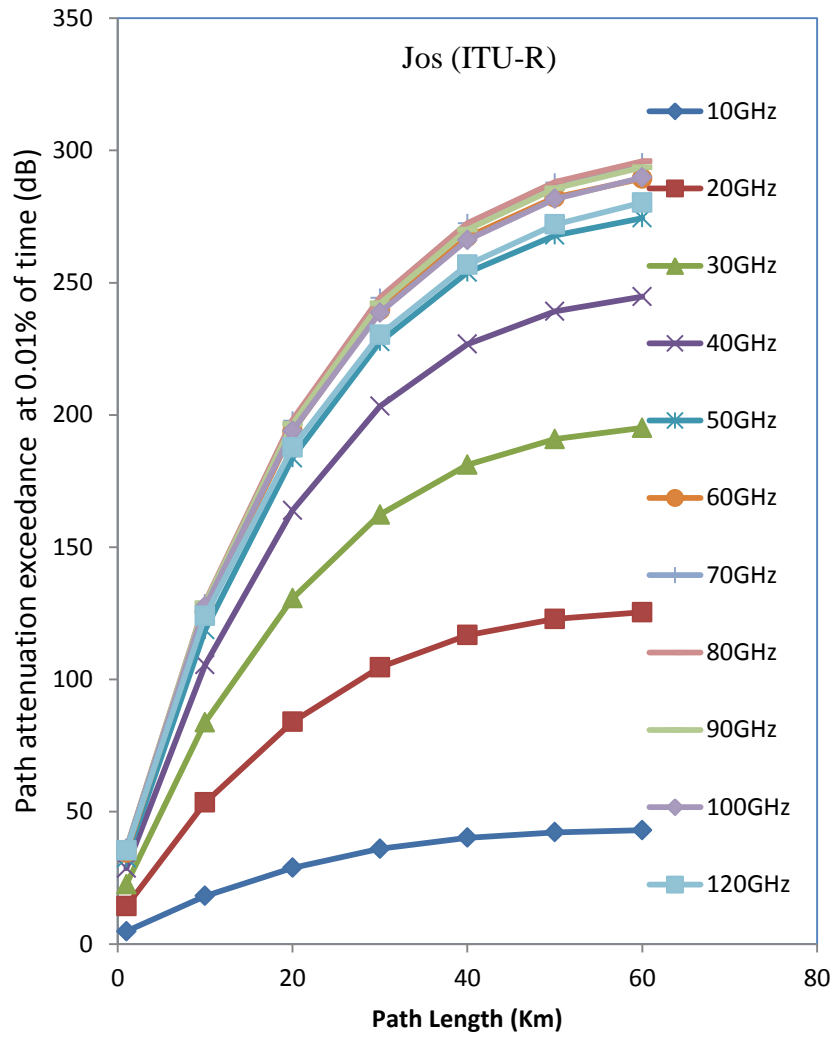
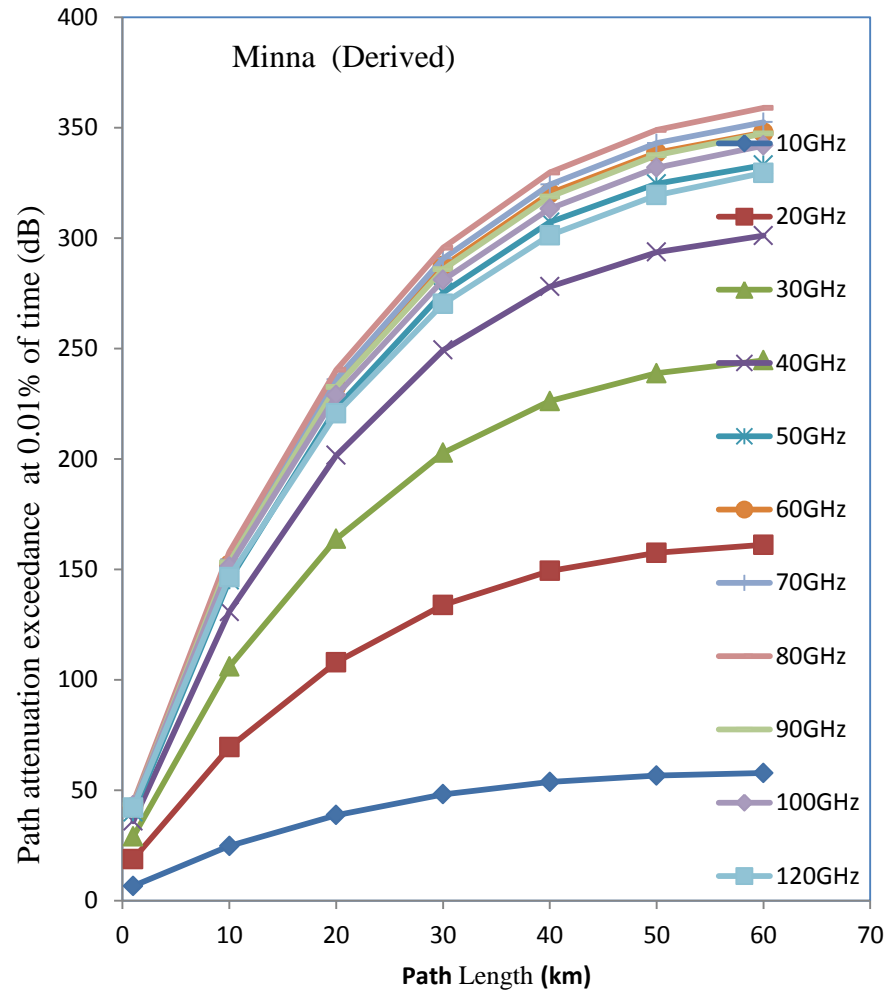
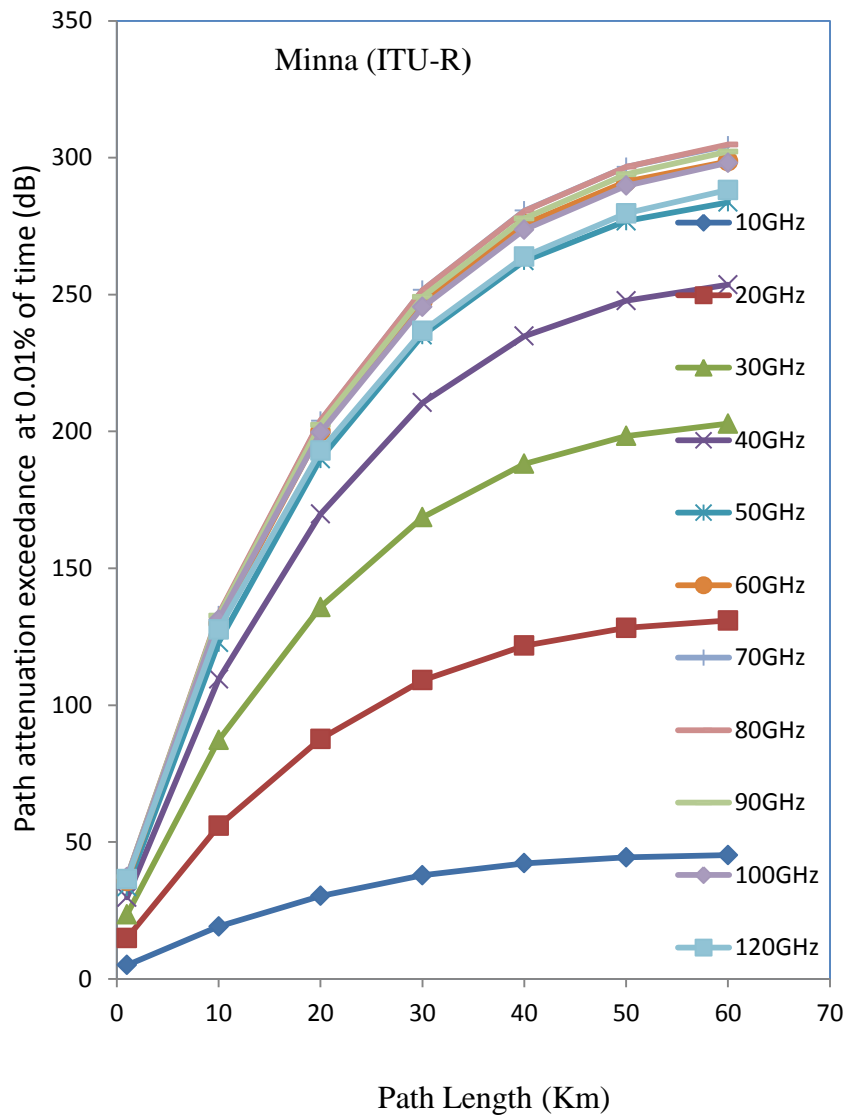


Figure 4.61b. Path attenuation at 0.01% ITU R rain rate prediction at Jos



**Figure 4.62a.** Path attenuation at 0.01% measured rain rate exceedance at Minna



**Figure 4.62b.** Path attenuation at 0.01% ITU R rain rate prediction at Minna

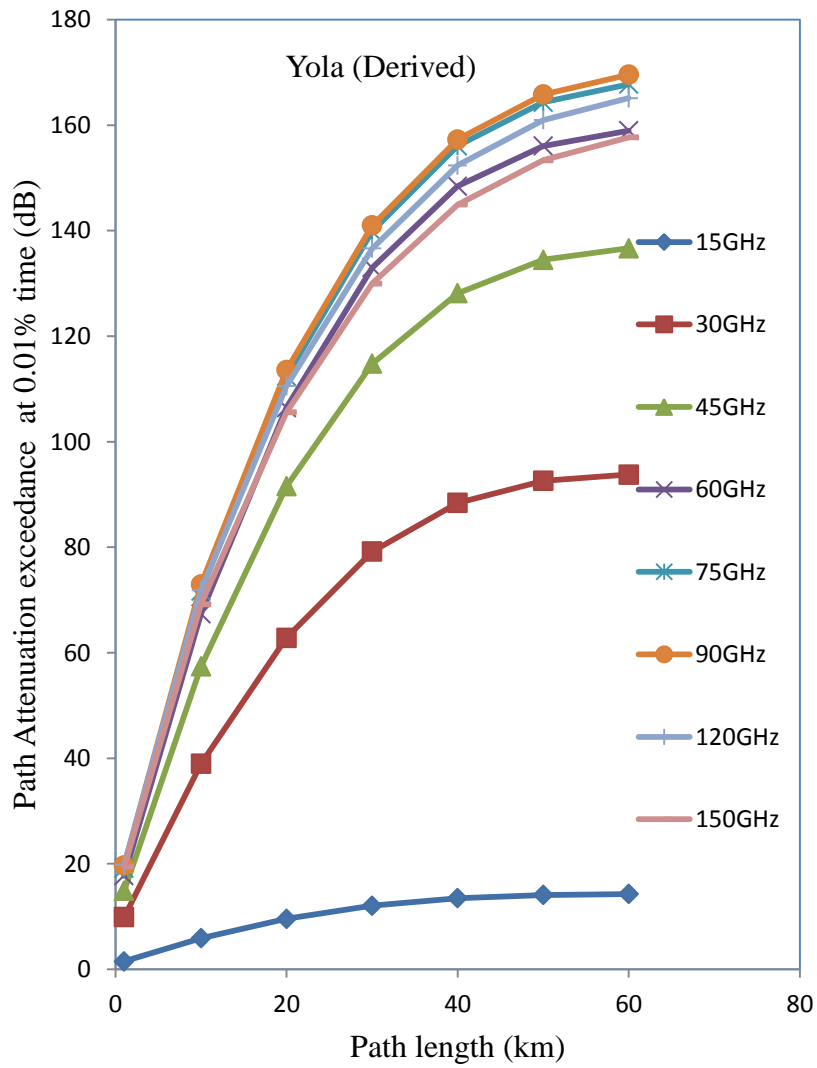
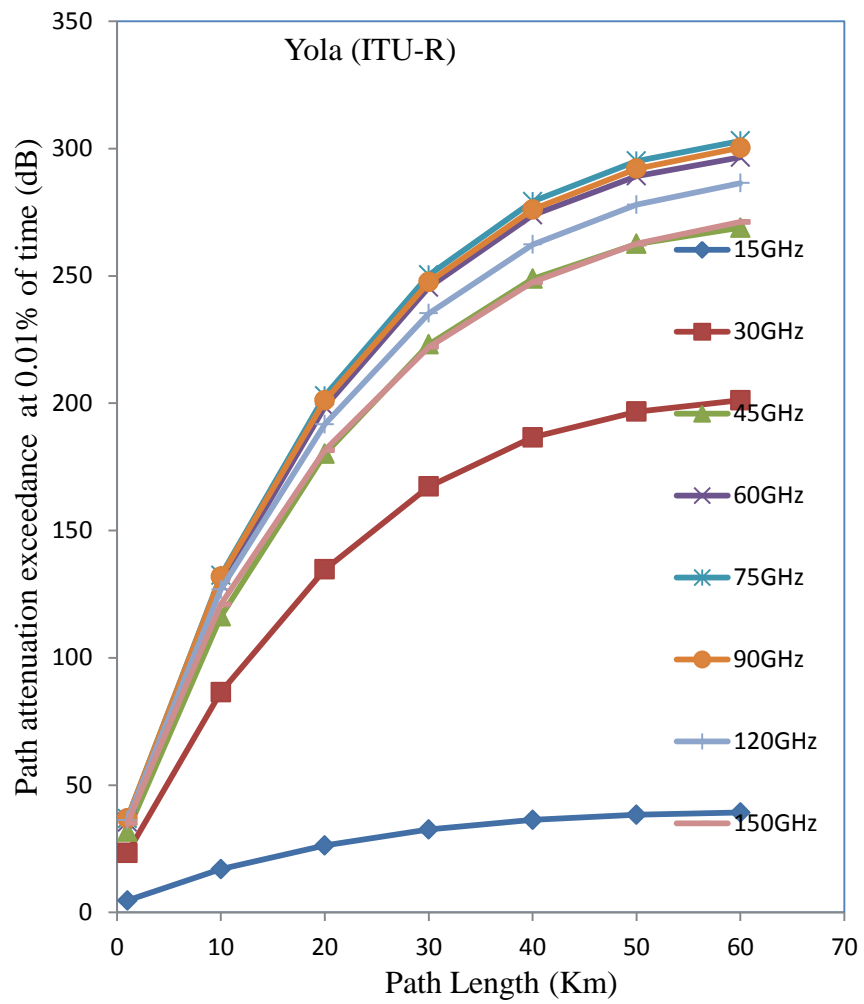


Figure 4.63a. Path attenuation at 0.01% measured rain rate exceedance at Yola





**Figure 4.63b.** Path attenuation at 0.01% ITU R rain rate prediction at Yola

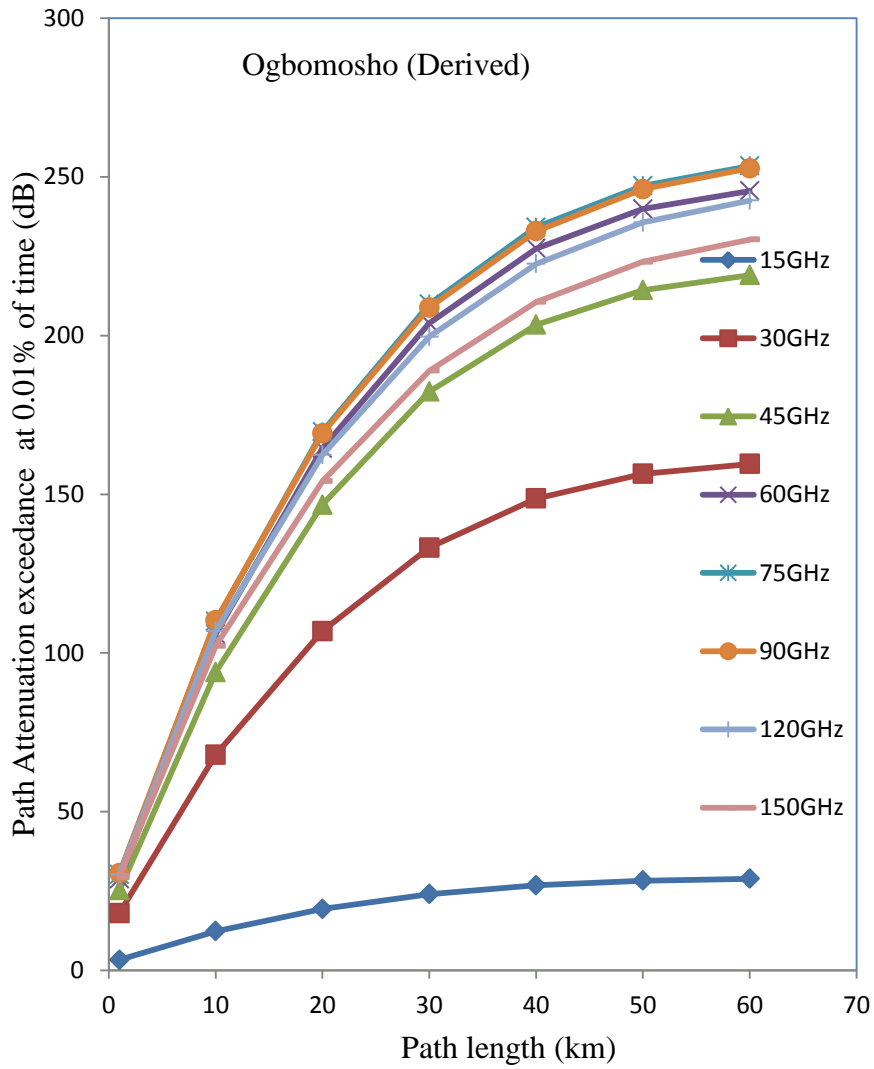


Figure 4.64a. Path attenuation at 0.01% measured rain rate exceedance at Ogbomosho

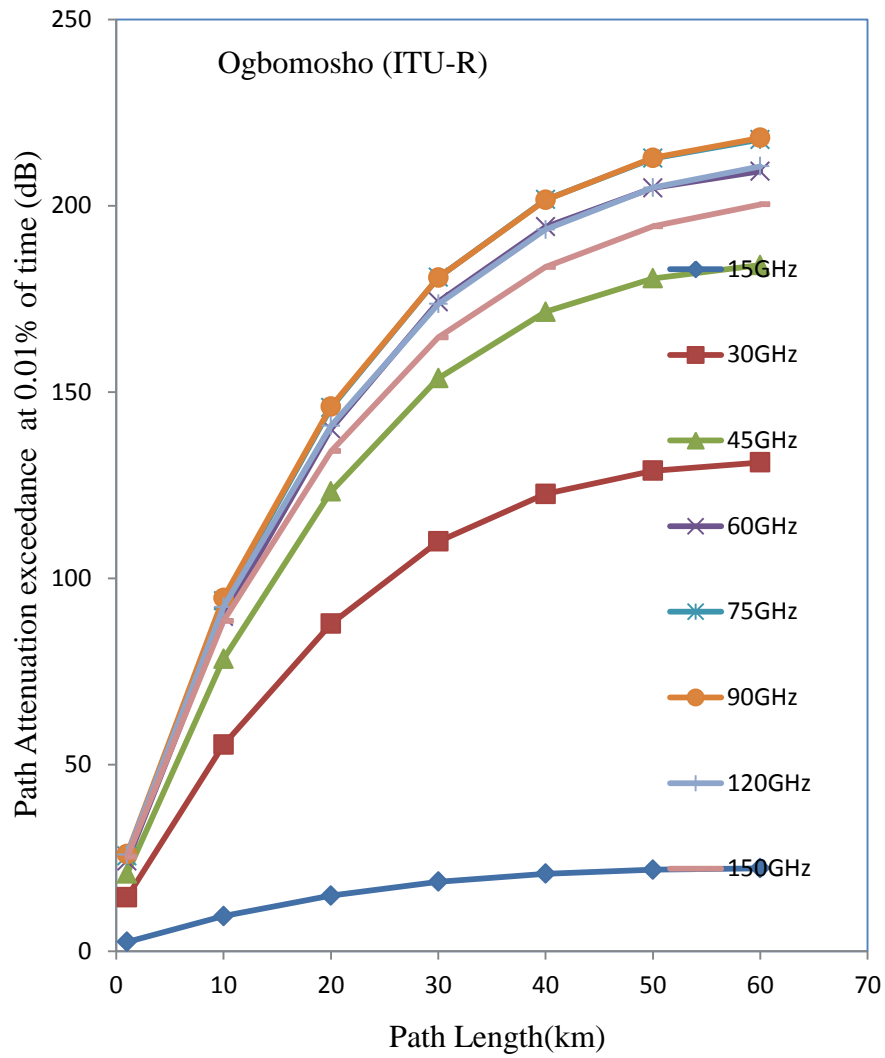
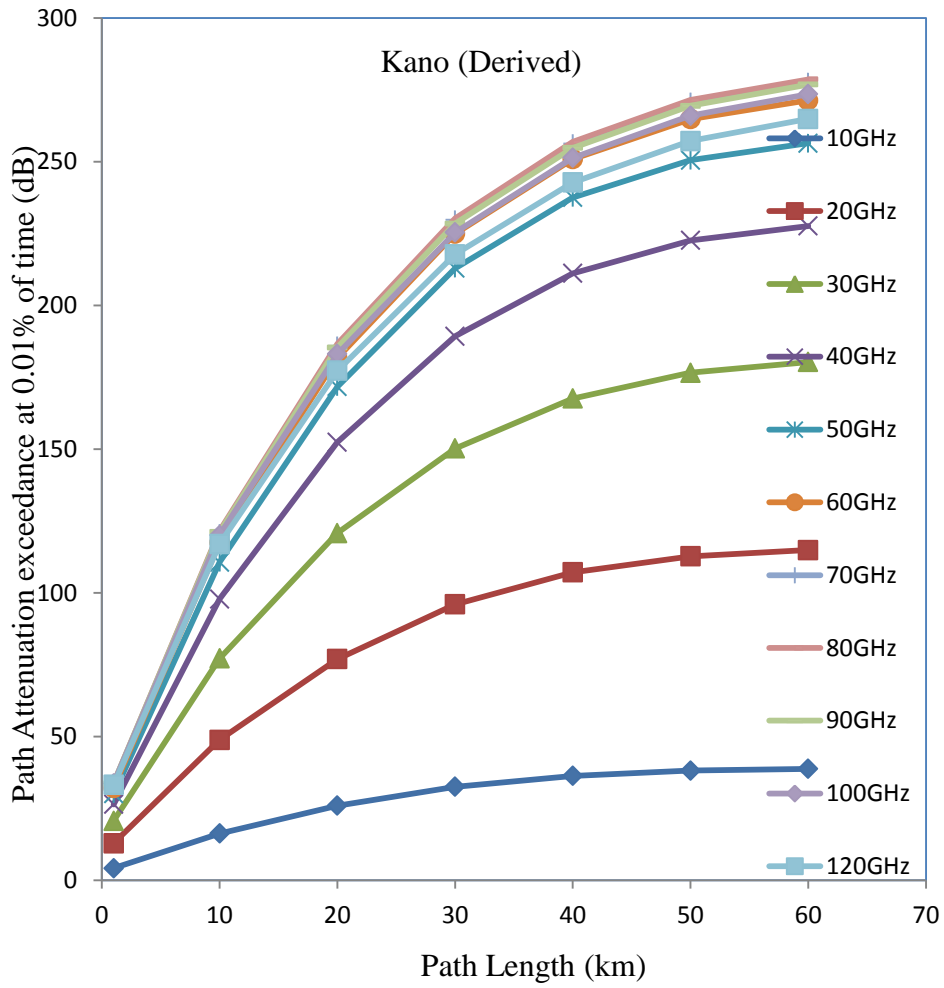
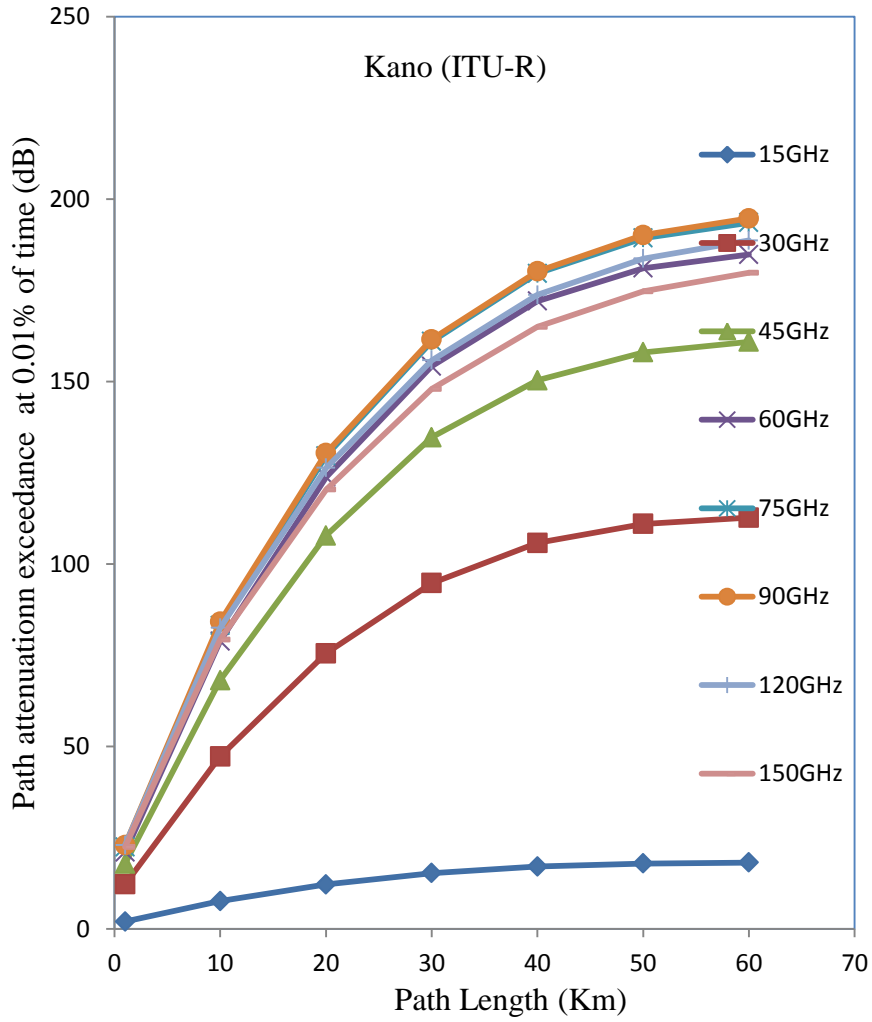


Figure 4.64b. Path attenuation at 0.01% ITU R rain rate prediction at Ogbomosho



**Figure 4.65a.** Path attenuation at 0.01% measured rain rate exceedance at Kano



**Figure 4.65b.** Path attenuation at 0.01% ITU R rain rate prediction at Ogbomosho

### **4.2.3 Path Attenuations at the 40 GHz and 45 GHz frequency bands**

At the 30-300 GHz millimeter wave bands, the frequency threshold of the specific attenuation for the horizontal and vertical polarisation at 0.01% of rain rate for the 14 locations considered ranged from 120 GHz to 150 GHz. At these frequency thresholds, the highest frequency band without overlaps at 20km path length were 40 GHz and 45 GHz respectively. These are the frequency threshold for millimetric communication equipment design for these locations in Nigeria. The path attenuation derived for the 14 locations at the 40 GHz and 45 GHz frequency bands is shown in Figures 4.66 to 4.69 and Table 4.14. As seen in Table 4.14, the predicted path attenuation by the ITU differs remarkably from the value derived from the measured rain rate (Table 4.12) from the locations especially at the 40 GHz and 45 GHz frequency bands. The path attenuation across all the eco-climatic zones at 40 GHz ranged from 64.65 dB to 206.85 dB while at 45 GHz, it ranged from 71.40 dB to 219.45 dB. The ITU predicted range of path attenuation at 40 GHz and 45 GHz were 99.01 dB to 192.18 dB and 107.79 dB to 204.43 dB respectively.

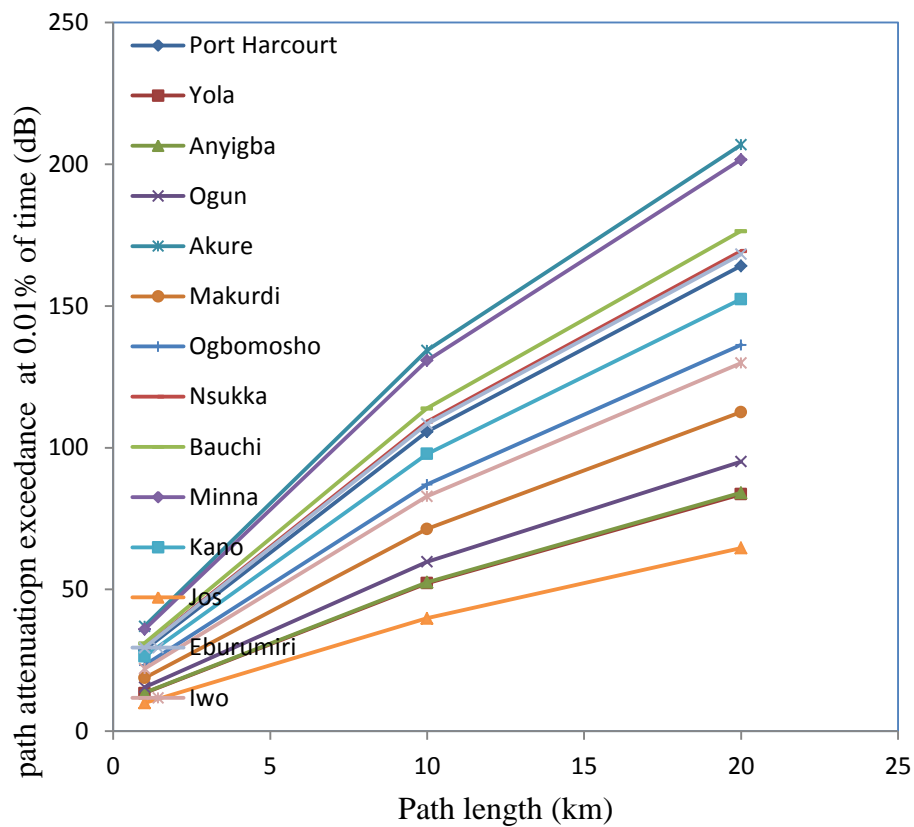


**Figure 4.66.** Derived path attenuation for 40 GHz frequency bands at 0.01%

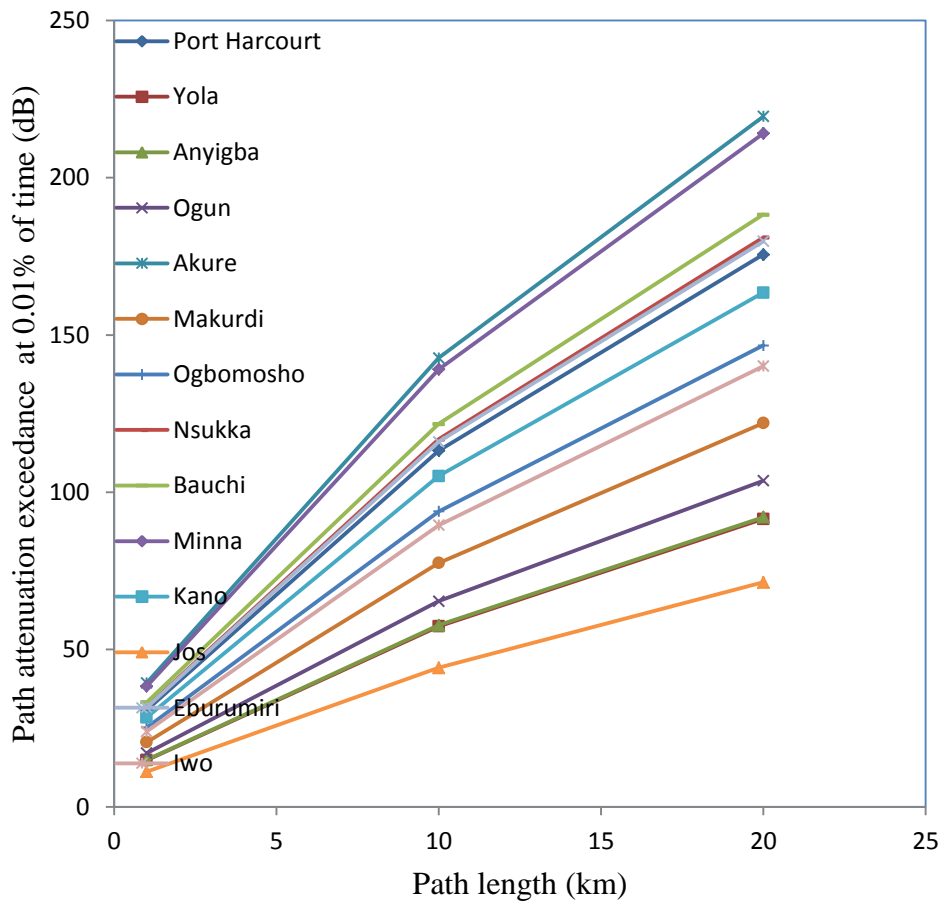


**Figure 4.67.** Derived path attenuation for 45 GHz frequency bands at 0.01%



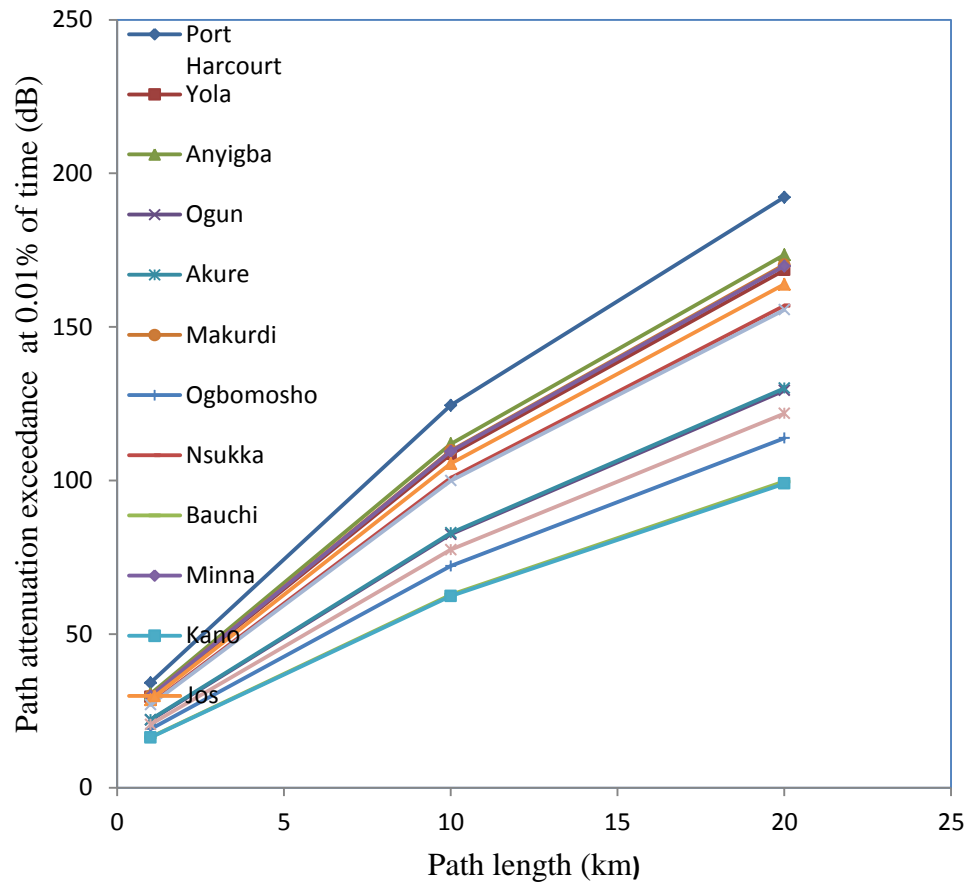


**Figure 4.68.** ITU predicted path attenuation for 40 GHz frequency bands at 0.01%

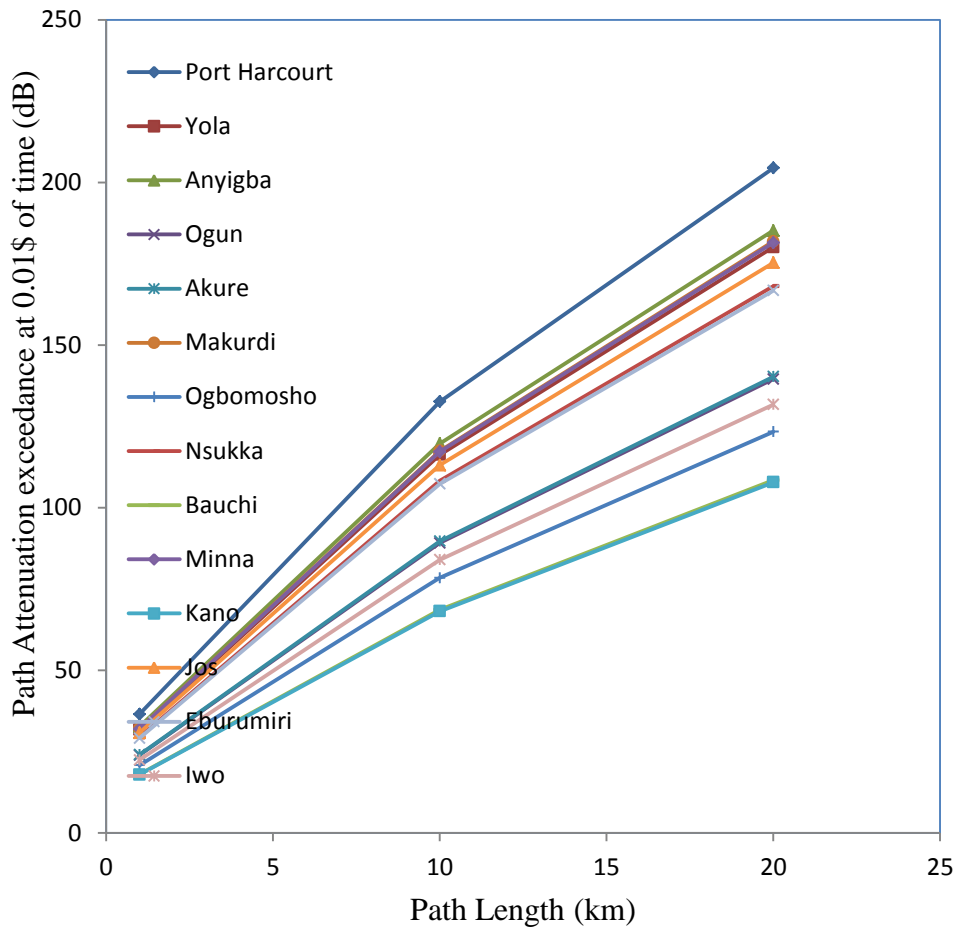


**Figure 4.69.** ITU predicted path attenuation for 45 GHz frequency bands at 0.01%

**Table 4.14. Estimated path attenuation for 40 GHz and 45 GHz frequency bands at 0.01%**

Locations	Path Attenuation at 40 GHz band (dB)		Path attenuation at 45 GHz band (dB)	
	At In-Situ rain rate estimate	ITU-Predicted	At In-Situ rain rate estimate	ITU-Predicted
Akure	206.85	130.05	219.45	140.25
Anyigba	84.14	173.46	92.11	185.18
Bauchi	176.44	99.66	188.25	108.47
Eburumiri	168.23	155.55	179.80	166.71
Iwo	129.91	121.81	140.10	131.67
Jos	64.65	163.87	71.40	175.30
Kano	152.43	99.01	163.47	107.79
Makurdi	112.58	170.20	122.02	181.83
Minna	201.59	169.81	214.08	181.42
Nsukka	169.41	156.91	181.02	168.11
Ogbomos	136.24	113.8	146.69	123.30
Mowe	95.10	129.32	103.67	139.50
Port Harcourt	164.14	192.18	175.57	204.43
Yola	83.62	168.49	91.56	180.07

#### **4.2.4 Contour Mapping of Rainfall Attenuation Distribution at 40 GHz and 45 GHz Frequency Bands in Nigeria**

Spatial inhomogeneity is present in rain (Hall et al., 1996); this makes it inadequate to depend only on 0.01% exceedance mean rain rate statistics (Crane, 1996) for attenuation estimation, hence the need to consider other time percentages (0.001% to 1%) path attenuation with an integration time of 1-minute for a radio link. Tables 4.15 and 4.16 give the path attenuation generated with equation (3.41) and (3.42) for different values of percentage of time (0.001% to 1%) using measured rainfall rate exceeded at 40 GHz and 45 GHz frequency bands respectively. It can be observed from these Tables that the path attenuation of radio link signals decreases as the percentage of time of exceedance increases. This implies that radio links availability reduces as the percentage of time of rainfall exceedance decreases. To mitigate this rainfall induced signal fade, Das and Maitra (2015) proposed the implementation of coding of signal power and data rate adaptation control in radio communication equipment designs.

Inverse Distance Weighting (IDW) interpolation is frequently used in interpolating rainfall data from rain gauge stations (Tomczak, 1998; Hutchinson, 1998; Goodale *et al.*, 1998; Dirks *et al.*, 1998; Price *et al.*, 2000; Cheng *et al.*, 2007; Azpurua and Ramos, 2010; Mair and Fares, 2011; Lam *et al.*, 2015). It uses measured values surrounding an unmeasured location to predict its values (Lam *et al.*, 2015). It was applied to the 14 locations in order to capture the path attenuation for un-sampled locations across the 36 states of Nigeria including the Federal Capital Territory (FCT). The procedure is stated in equations (3.57) to (3.61). Interpolation of data was done with Microsoft excel and MATLAB software while Surfer 10.0 was used to plot the contours. The path attenuation across Nigerian at 40 GHz and 45 GHz at 0.001% to 1% rain rate exceedance using the inverse distance weighting interpolation are shown in Tables 4.17 and 4.18. These Tables were used to generate contour maps of path attenuation shown in Figure 4.70 to 4.77 at 0.001% to 1% rain rate exceedance at 40 and 45 GHz for Nigeria. These contour maps of path attenuation can be used by radio propagation engineers for designs especially at 0.01% exceedance for Nigeria. From Table 4.17 and 4.18 it can as well be inferred that the path attenuation decreases with increase in percentage of rain rate exceedance.

**Table 4.15.** Path attenuation for different values of system availability at 40 GHz

Location	Path Attenuation (dB) at 0.001- 1% exceedance			
	0.001%	0.01%	0.1%	1%
Nsukka	320.36	169.41	63.76	17.18
Port Harcourt	310.38	164.14	61.77	16.64
Eburumiri	318.12	168.23	63.31	17.06
Iwo	245.65	129.91	48.89	13.17
Mowe	179.83	95.10	35.79	9.64
Ogbomosho	257.63	136.24	51.27	13.81
Akure	391.14	206.85	77.85	20.97
Minna	381.21	201.59	75.87	20.44
Kano	288.23	152.43	57.36	15.45
Yola	158.12	83.62	31.47	8.48
Jos	122.26	64.65	24.33	6.56
Bauchi	333.64	176.44	66.40	17.89
Makurdi	212.88	112.58	42.37	11.41
Anyigba	159.10	84.14	31.66	8.53

**Table 4.16.** Path attenuation for different values of system availability at 45 GHz

Location	PathAttenuation (dB) at 0.001- 1% exceedance			
	0.001%	0.01%	0.1%	1%
Nsukka	340.10	181.02	68.07	18.19
Port Harcourt	329.88	175.57	66.02	17.64
Eburumiri	337.81	179.80	67.61	18.07
Iwo	263.23	140.10	52.69	14.08
Mowe	194.78	103.67	38.99	10.42
Ogbomosho	275.61	146.69	55.16	14.74
Akure	412.31	219.45	82.52	22.05
Minna	402.22	214.08	80.50	21.51
Kano	307.14	163.47	61.47	16.43
Yola	172.02	91.56	34.43	9.20
Jos	134.15	71.40	26.85	7.18
Bauchi	353.70	188.25	70.79	18.91
Makurdi	229.25	122.02	45.88	12.26
Anyigba	173.05	92.11	34.64	9.26

**Table 4.17.** Path attenuation at 0.001% to 1% rain rate exceedance for 40 GHz frequency band using Inverse Distance Weighing Interpolation

S/N	States	Coordinates		Path Attenuation (dB)				Eco-climatic. Zone
		Longitude (°N)	Latitude (°E)	0.001%	0.01%	0.1%	1%	
1	Sokoto	5.22	12.93	316.35	167.30	62.96	16.96	Sudan Savanna
2	Gusau	6.23	12.18	301.63	159.51	60.03	16.17	Sudan Savanna
3	Katsina	7.61	12.51	281.40	148.82	56.00	15.09	Sudan Savanna
4	Maiduguri	13.17	12.20	320.74	169.62	63.83	17.20	Sudan Savanna
5	Dutse	9.72	12.44	306.53	162.11	61.00	16.43	Sudan Savanna
6	Damaturu	11.70	12.18	319.22	168.81	63.53	17.12	Sudan Savanna
7	Kano	8.66	11.75	288.23	152.43	57.36	15.45	Sudan Savanna
8	Birnin-Kebbi	4.06	11.67	343.58	181.69	68.38	18.42	Sudan Savanna
9	Kaduna	8.13	10.15	239.07	126.43	47.58	12.82	Northern Guinea Savanna
10	Gombe	11.16	10.24	323.69	171.18	64.42	17.36	Northern Guinea Savanna
11	Abuja	7.36	9.07	206.32	109.11	41.06	11.06	Northern Guinea Savanna
12	Bauchi	10.08	10.63	333.64	176.44	66.40	17.89	Northern Guinea Savanna
13	Ilorin	4.56	8.98	229.54	121.39	45.68	12.31	Derived Savanna
14	Jalingo	10.26	8.00	217.17	114.85	43.22	11.64	Derived Savanna
15	Lafia	8.30	8.57	178.39	94.34	35.50	9.57	Derived Savanna
16	Ado Ekiti	5.31	7.66	267.92	141.69	53.32	14.36	Derived Savanna
17	Awka	7.00	6.27	319.03	168.71	63.49	17.11	Derived Savanna
18	Abakaliki	7.95	6.17	296.29	156.68	58.97	15.89	Derived Savanna
19	Nsukka	7.40	6.86	320.36	169.41	63.76	17.18	Derived Savanna
20	Eburumiri	7.35	6.61	318.12	168.23	63.31	17.06	Derived Savanna
21	Iwo	7.63	4.19	245.65	129.91	48.89	13.17	Derived Savanna
22	Mowe	3.58	6.90	179.83	95.10	35.79	9.64	Derived Savanna
23	Makurdi	8.83	7.35	212.88	112.58	42.37	11.41	Derived Savanna
24	Anyigba	6.57	7.90	159.10	84.14	31.66	8.53	Derived Savanna
25	Ikeja	3.62	6.60	219.88	116.28	43.76	11.79	Humid Forest
26	Benin City	5.89	6.54	286.79	151.67	57.08	15.38	Humid Forest
27	Asaba	5.89	5.53	300.71	159.03	59.85	16.12	Humid Forest
28	Yenagoa	5.89	4.86	304.53	161.05	60.61	16.33	Humid Forest
29	Calabar	8.66	6.16	266.14	140.74	52.97	14.27	Humid Forest
30	Owerri	7.00	5.60	308.53	163.15	61.40	16.54	Humid Forest
31	Uyo	7.87	4.93	290.01	153.37	57.72	15.55	Humid Forest
32	Umuahia	7.52	5.43	299.98	158.64	59.70	16.09	Humid Forest
33	Portharcourt	6.92	4.85	310.38	164.14	61.77	16.64	Humid Forest
34	Akure	7.26	5.21	391.14	206.85	77.85	20.97	Humid Forest
35	Ogbomosho	3.41	8.11	257.63	136.24	51.27	13.81	Southern Guinea Savanna
36	Minna	5.39	10.21	381.21	201.59	75.87	20.44	Southern Guinea Savanna
37	Yola	12.43	9.32	158.12	83.62	31.47	8.48	Southern Guinea Savanna
38	Jos	9.36	9.24	122.26	64.65	24.33	6.56	Mid Altitude Savanna

**Table 4.18.** Path attenuation at 0.001% to 1% rain rate exceedance for 45 GHz frequency band using Inverse Distance Weighing Interpolation

S/N	States	Coordinates		Path Attenuation (dB)				Eco-Climatic Zone
		Longitude (°N)	Latitude (°E)	0.001%	0.01%	0.1%	1%	
1	Sokoto	5.22	12.93	335.56	178.60	67.16	17.95	Sudan Savanna
2	Gusau	6.23	12.18	320.43	170.54	64.13	17.14	Sudan Savanna
3	Katsina	7.61	12.51	299.88	159.61	60.02	16.04	Sudan Savanna
4	Maiduguri	13.17	12.20	340.48	181.21	68.14	18.21	Sudan Savanna
5	Dutse	9.72	12.44	325.91	173.46	65.23	17.43	Sudan Savanna
6	Damaturu	11.70	12.18	338.91	180.38	67.83	18.12	Sudan Savanna
7	Kano	8.66	11.75	307.14	163.47	61.47	16.43	Sudan Savanna
8	Birnin-Kebbi	4.06	11.67	363.54	193.49	72.76	19.44	Sudan Savanna
9	Kaduna	8.13	10.15	255.68	136.08	51.17	13.68	Northern Guinea Savanna
10	Gombe	11.16	10.24	343.50	182.82	68.75	18.37	Northern Guinea Savanna
11	Abuja	7.36	9.07	221.65	117.97	44.36	11.86	Northern Guinea Savanna
12	Bauchi	10.08	10.63	353.70	188.25	70.79	18.91	Northern Guinea Savanna
13	Ilorin	4.56	8.98	246.40	131.15	49.32	13.18	Derived Savanna
14	Jalingo	10.26	8.00	233.10	124.07	46.65	12.47	Derived Savanna
15	Lafia	8.30	8.57	192.90	102.67	38.61	10.32	Derived Savanna
16	Ado Ekiti	5.31	7.66	285.70	152.06	57.18	15.28	Derived Savanna
17	Awka	7.00	6.27	338.74	180.30	67.80	18.12	Derived Savanna
18	Abakaliki	7.95	6.17	315.28	167.81	63.10	16.86	Derived Savanna
19	Nsukka	7.40	6.86	340.10	181.02	68.07	18.19	Derived Savanna
20	Eburumiri	7.35	6.61	337.81	179.80	67.61	18.07	Derived Savanna
21	Iwo	7.63	4.19	263.23	140.10	52.69	14.08	Derived Savanna
22	Mowe	3.58	6.90	194.78	103.67	38.99	10.42	Derived Savanna
23	Makurdi	8.83	7.35	229.25	122.02	45.88	12.26	Derived Savanna
24	Anyigba	6.57	7.90	173.05	92.11	34.64	9.26	Derived Savanna
25	Ikeja	3.62	6.60	236.01	125.61	47.24	12.62	Humid Forest
26	Benin City	5.89	6.54	304.86	162.26	61.02	16.31	Humid Forest
27	Asaba	5.89	5.53	319.49	170.05	63.94	17.09	Humid Forest
28	Yenagoa	5.89	4.86	323.59	172.23	64.76	17.31	Humid Forest
29	Calabar	8.66	6.16	284.18	151.26	56.88	15.20	Humid Forest
30	Owerri	7.00	5.60	327.90	174.53	65.63	17.54	Humid Forest
31	Uyo	7.87	4.93	308.81	164.37	61.81	16.52	Humid Forest
32	Umuahia	7.52	5.43	319.09	169.84	63.86	17.07	Humid Forest
33	Portharcourt	6.92	4.85	329.88	175.57	66.02	17.64	Humid Forest
34	Akure	7.26	5.21	412.31	219.45	82.52	22.05	Humid Forest
35	Ogbomosho	3.41	8.11	275.61	146.69	55.16	14.74	Southern Guinea Savanna
36	Minna	5.39	10.21	402.22	214.08	80.50	21.51	Southern Guinea Savanna
37	Yola	12.43	9.32	172.02	91.56	34.43	9.20	Southern Guinea Savanna
38	Jos	9.36	9.24	134.15	71.40	26.85	7.18	Mid Altitude Savanna



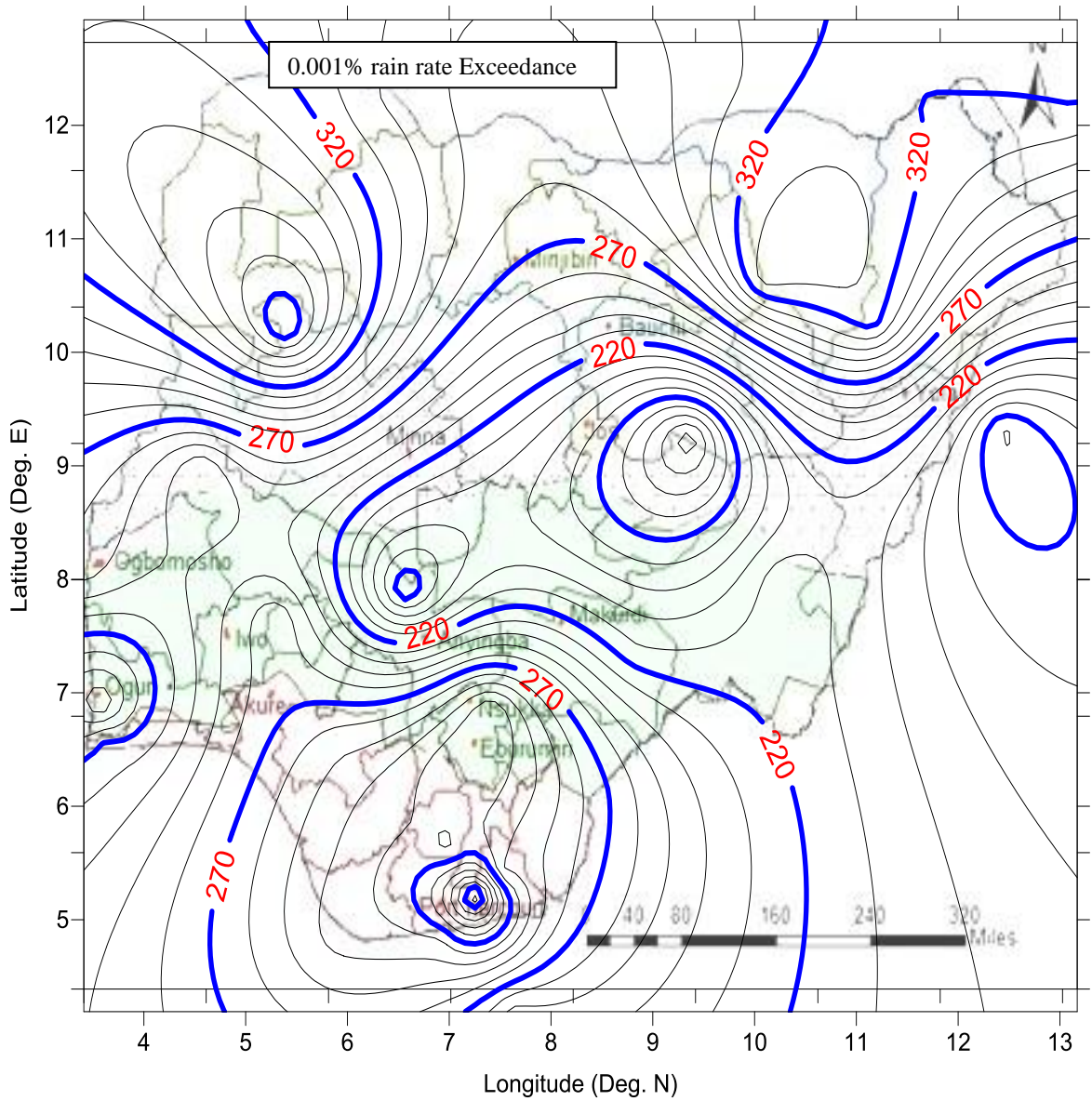


**Figure 4.70.** Contour Mapping of Path Attenuation at 0.001% rain rate Exceedance for 40GHz Frequency band in Nigeria

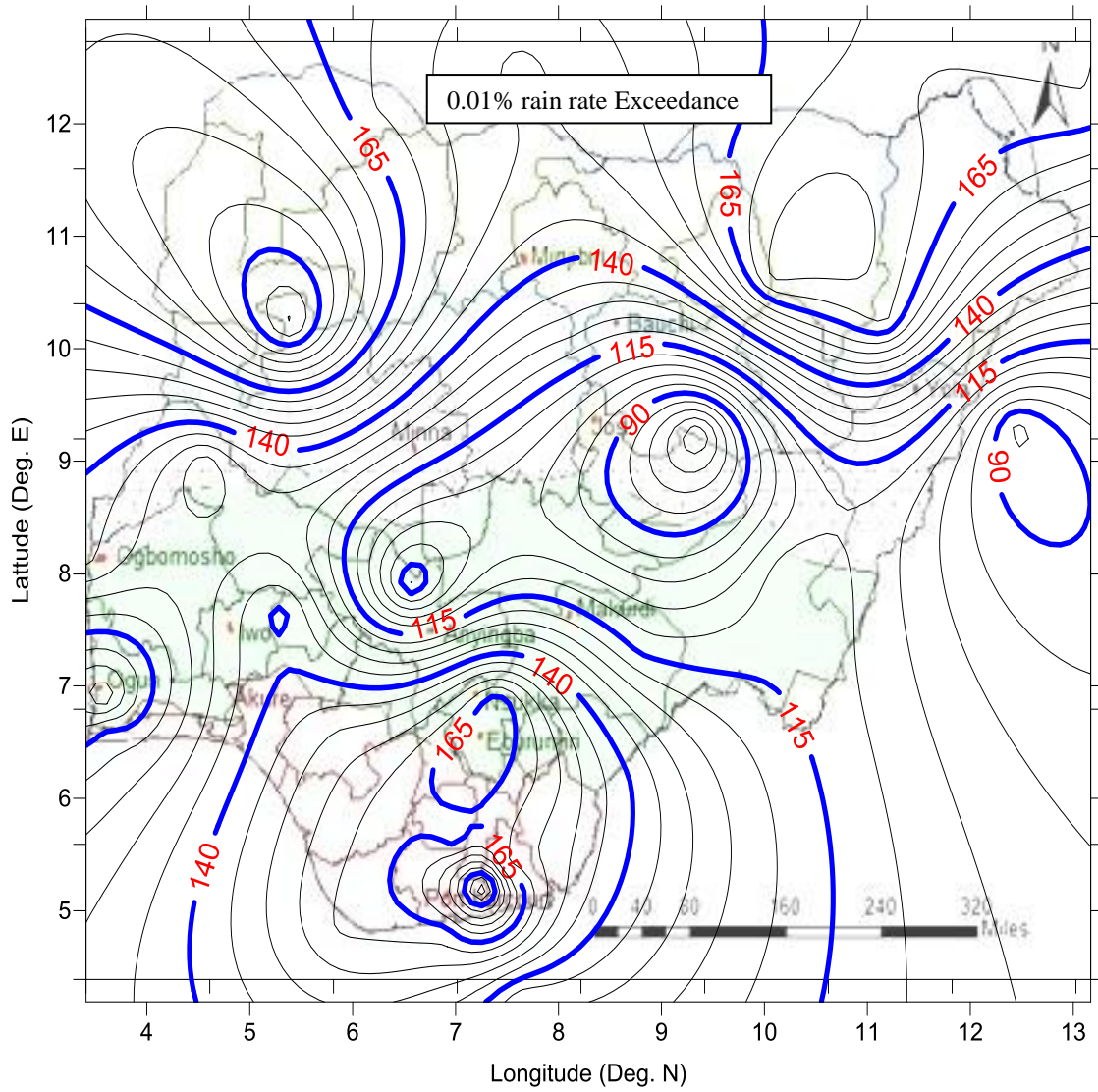


**Figure 4.71.** Contour Mapping of Path Attenuation at 0.01% rain rate Exceedance for 40GHz Frequency band in Nigeria

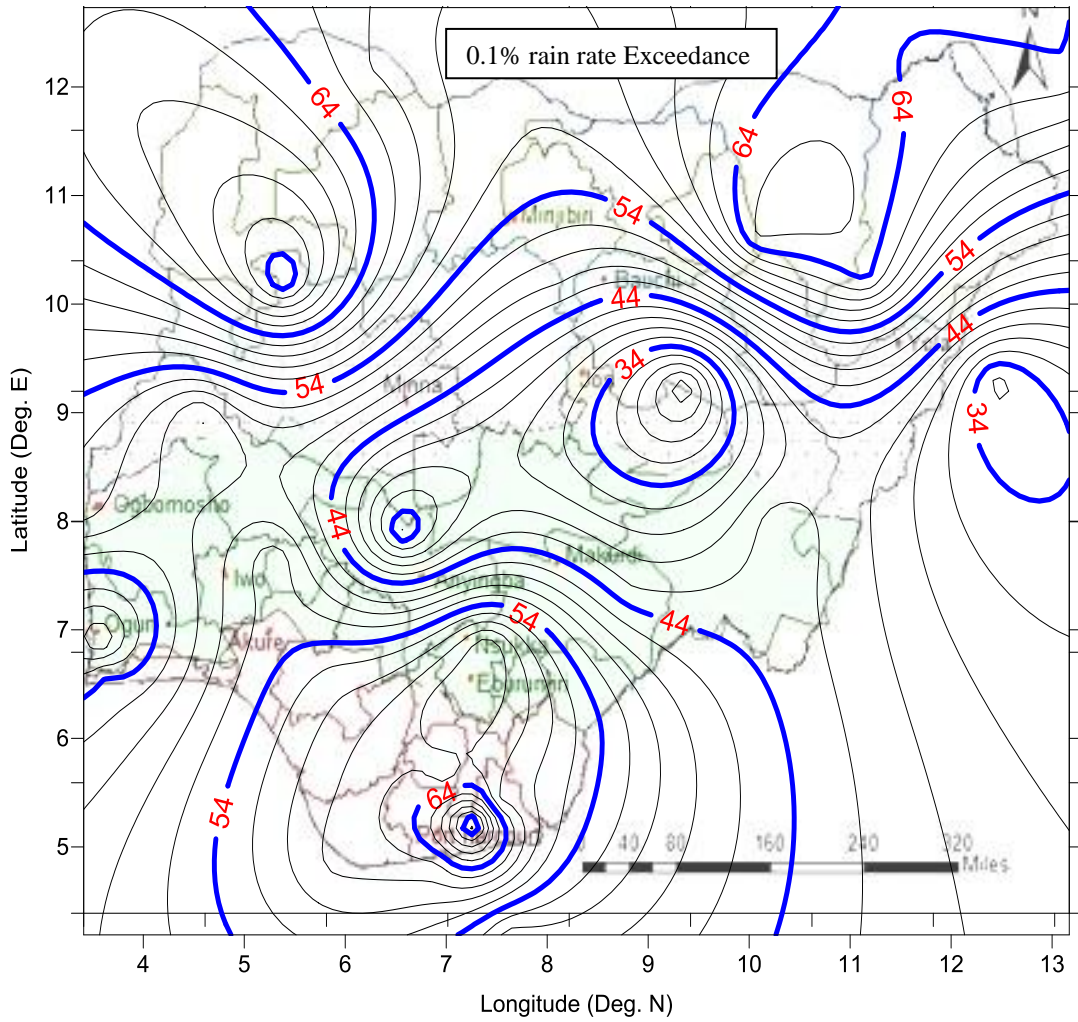


**Figure 4.72.** Contour Mapping of Path Attenuation at 0.1% rain rate Exceedance for 40GHz Frequency band in Nigeria

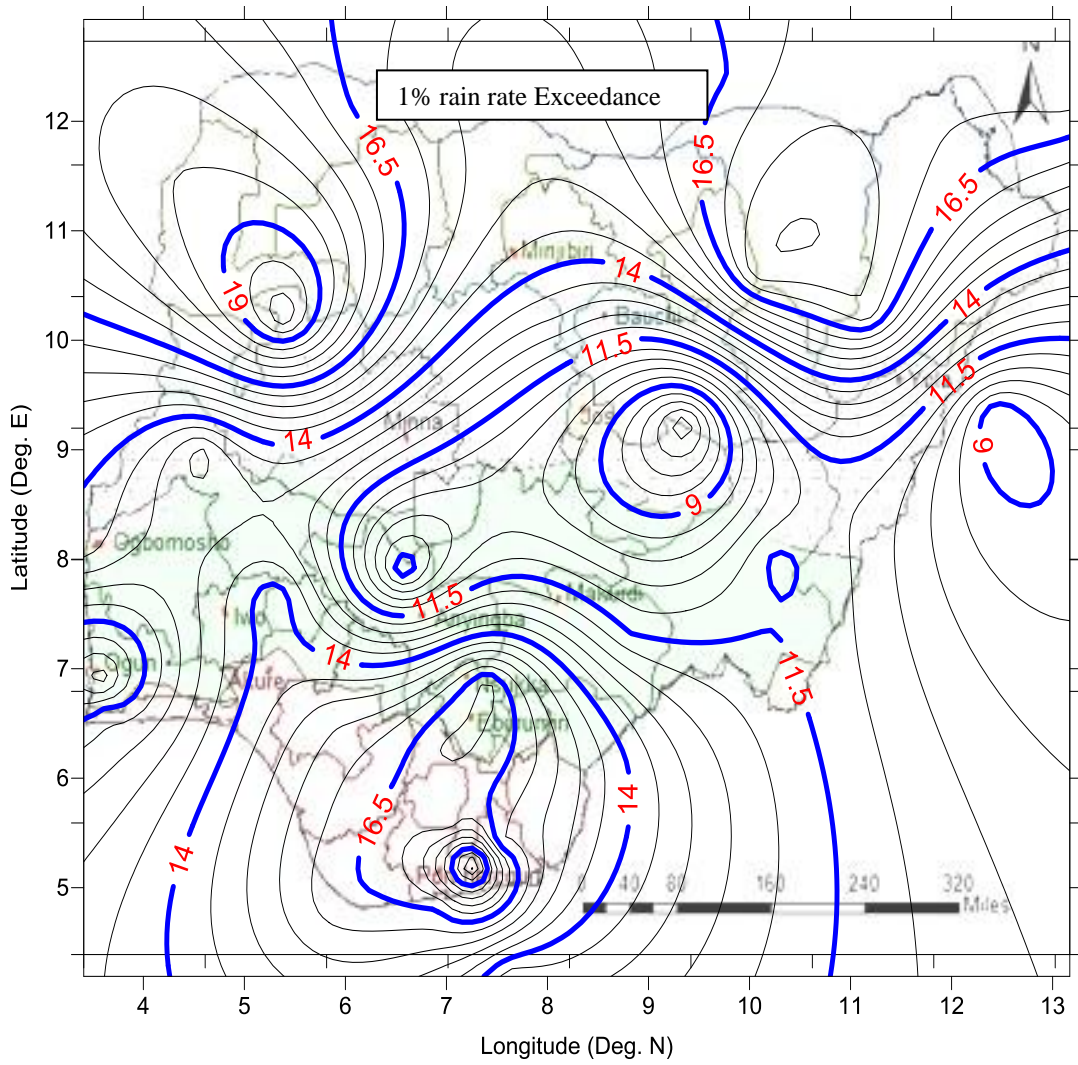


**Figure 4.73.** Contour Mapping of Path Attenuation at 1% rain rate Exceedance for 40GHz Frequency band in Nigeria

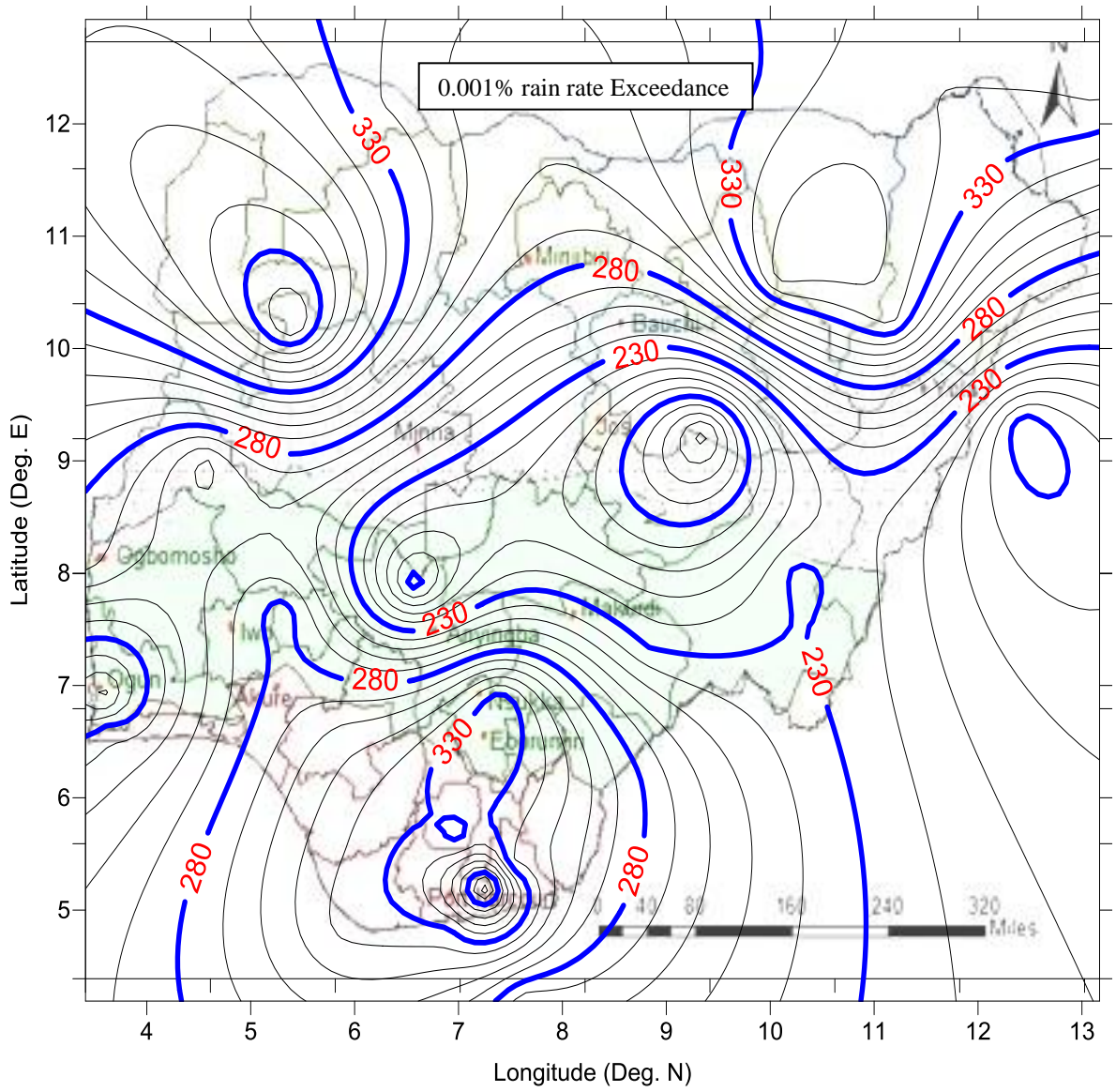


**Figure 4.74.** Contour Mapping of Path Attenuation at 0.001% rain rate Exceedance for 45GHz Frequency band in Nigeria

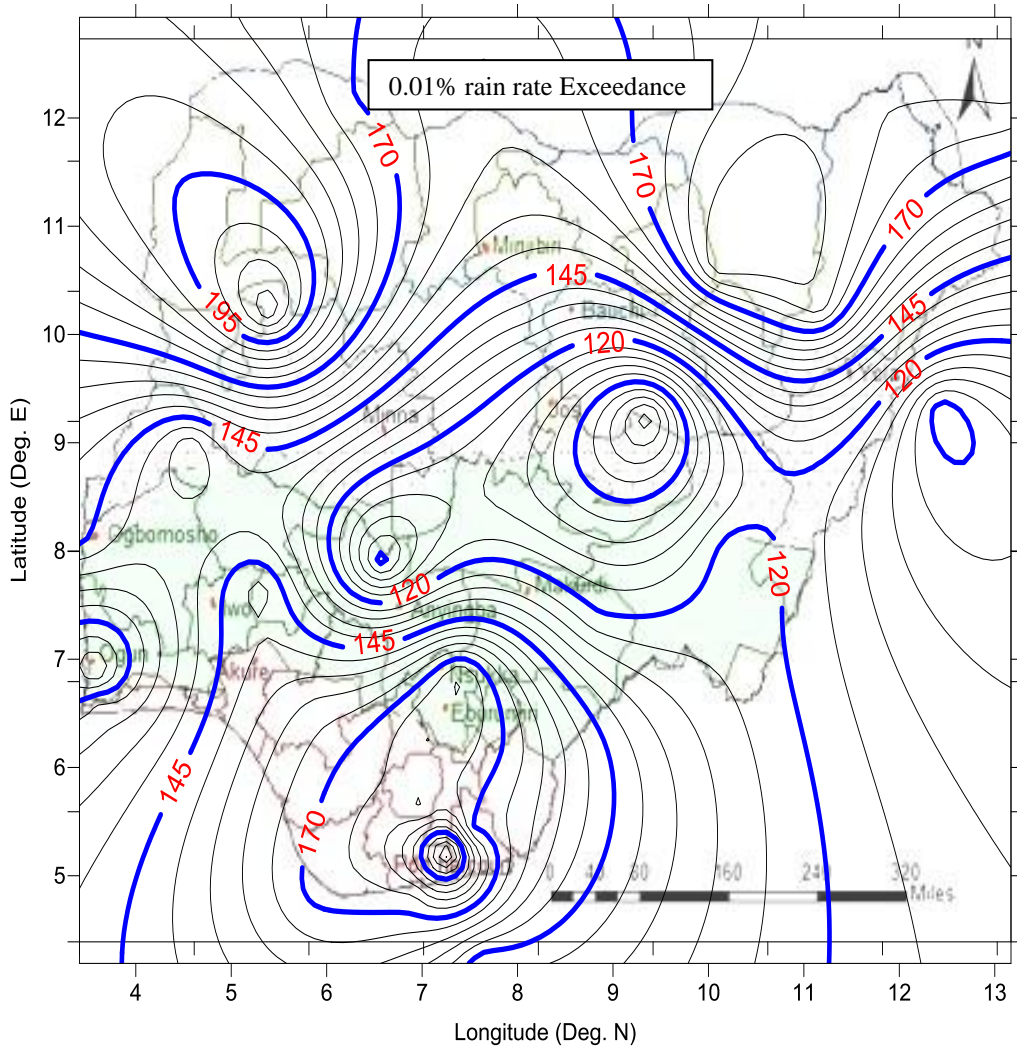


**Figure 4.75.** Contour Mapping of Path Attenuation at 0.01% rain rate Exceedance for 45GHz Frequency band in Nigeria

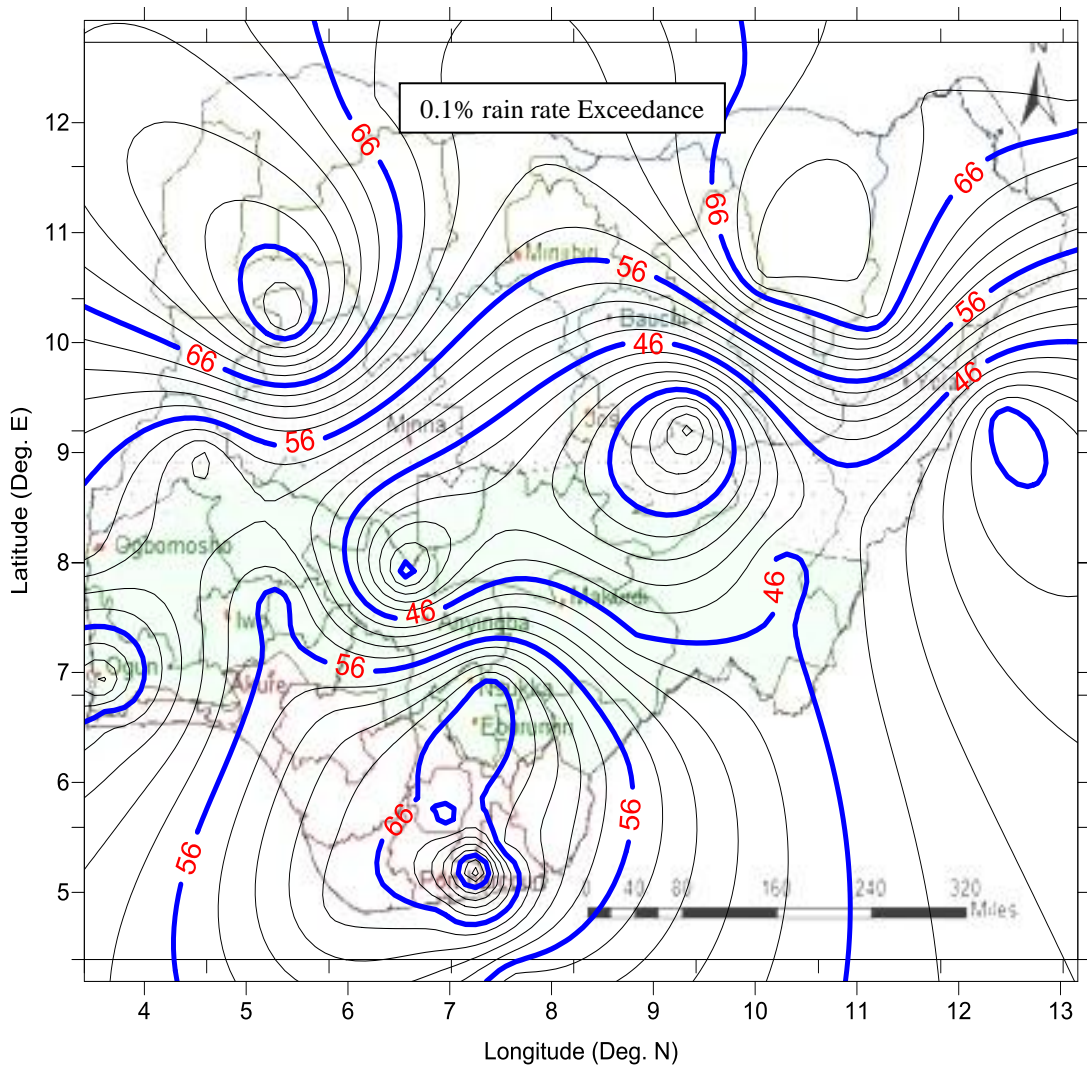


**Figure 4.76.** Contour Mapping of Path Attenuation at 0.1% rain rate Exceedance for 45GHz Frequency band in Nigeria

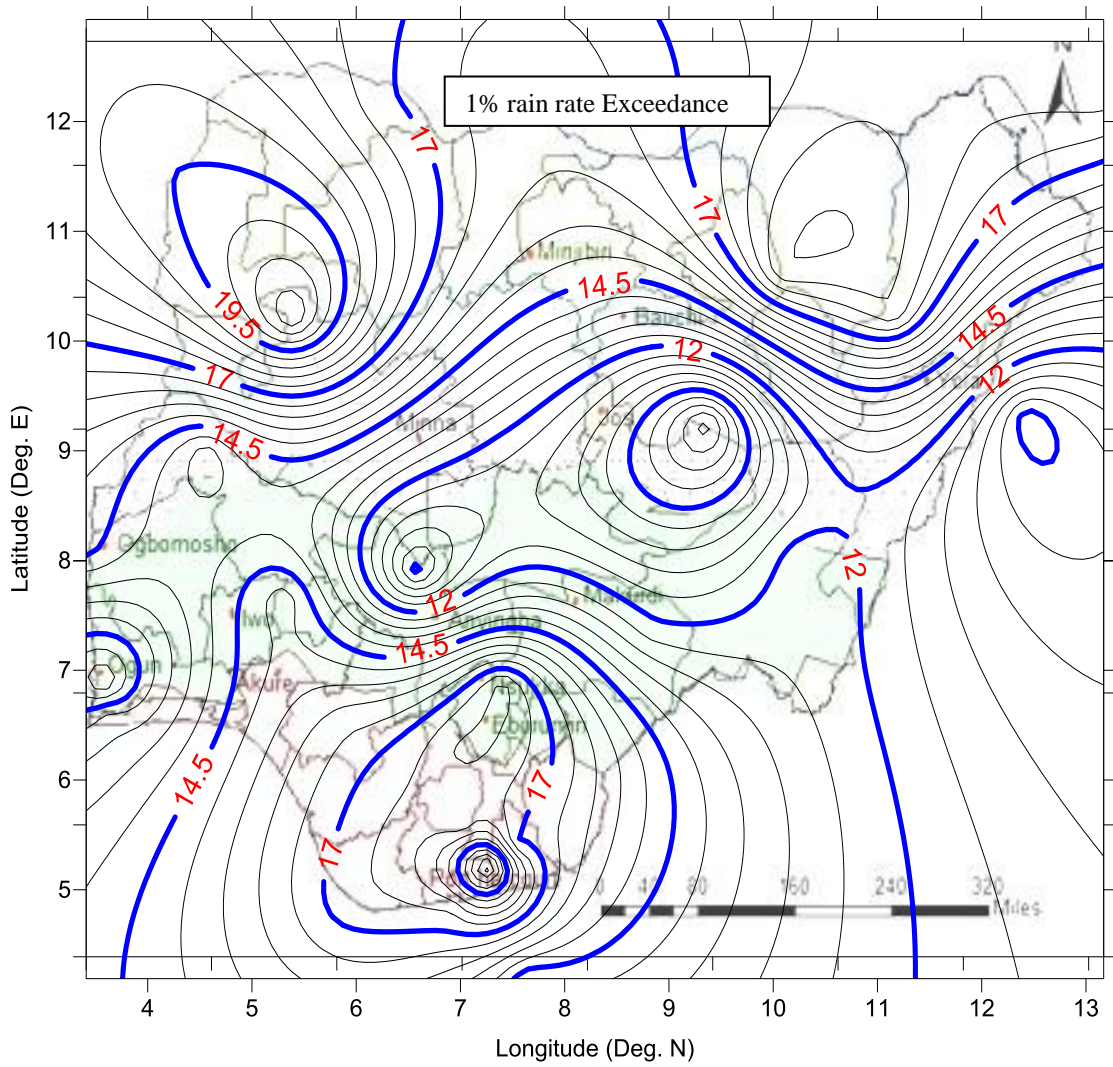


**Figure 4.77.** Contour Mapping of Path Attenuation at 1% rain rate Exceedance for 45GHz Frequency band in Nigeria



Across Nigeria, path attenuation ranges from 391.14 dB to 122.26 dB, 206.85 dB to 64.65 dB, 77.85 dB to 24.33dB and 20.97 dB to 6.56 dB at 0.001% to 1% exceedance respectively at 40GHz frequency band while at 45GHz band, it ranges from 412.31 dB to 134.15 dB, 219.45 dB to 71.40 dB, 82.52 dB to 26.85 dB and 22.05 dB to 7.18 dB at 0.001% to 1% respectively. However, in the 0.001% to 1% exceedance, path attenuation at the 40 and 45 GHz frequency band was highest in the humid forest eco-climatic zone and least in the mid altitude zone. As recommended by Ojo *et al.* (2008), the peculiarity of these zones should be factored in to radio frequency modifications through the use of larger antenna and larger amplifiers in order to enhance service availability of communication equipment.

Furthermore, as seen from the contour maps of, rain rate path attenuation of radio waves varies throughout the eco-climatic zones and even within the zones. This is a function of rainfall variation even within locations that fall within the same rain zone. This finding which was also asserted by Olubunmi (2010) debunks ITU-R 837-7 (2017) and Crane (1996) classification of the globe into climate rain zones. It corroborated Owolawi *et al.*, (2008) assertion that rainfall is location dependent.

#### **4.2.5. Path Attenuations on the 31.8 GHz to 33.4 GHz NCC frequency bands**

As stated by Perlman (1995), Shebani *et al.* (2017) the maximum path length for effective millimeter wave propagation is 20 km. Considering the frequencies of clear signals band in the millimeter wave band which ranges from 30 GHz to 40 GHz and 45 GHz (Figure 4.52a to 4.65a) in all the locations considered, emphasis was laid on the 31.8 GHz to 33.4 GHz frequencies which falls within the clear signal bands. These frequencies have been assigned by ITU to the Nigerian Communications Commission (NCC) but are currently not in use (appendix 13). Some of the features of the 31.8 GHz to 33.4 GHz frequency bands are: Radio Navigation Services (RN), Fixed Services (FS), Radio Astronomy (RA), Earth Exploration Satellite Service (EESS), Space Research (SR) and Inter Satellite Service (ISS) Hence, we seek to ascertain the possible effects of rain in hampering the exploitation of the 31.8 GHz to 33.4 GHz features by determining the attenuation values of these frequency bands. The attenuation of radio signals at millimeter path length of 20 km over the 0.001 to 1% exceedance are presented in Figure 4.78 to 4.83 for 31.8 GHz while Figure 4.84 to 4.89 are the path attenuation at 33.4 GHz for all the respective stations covered. As

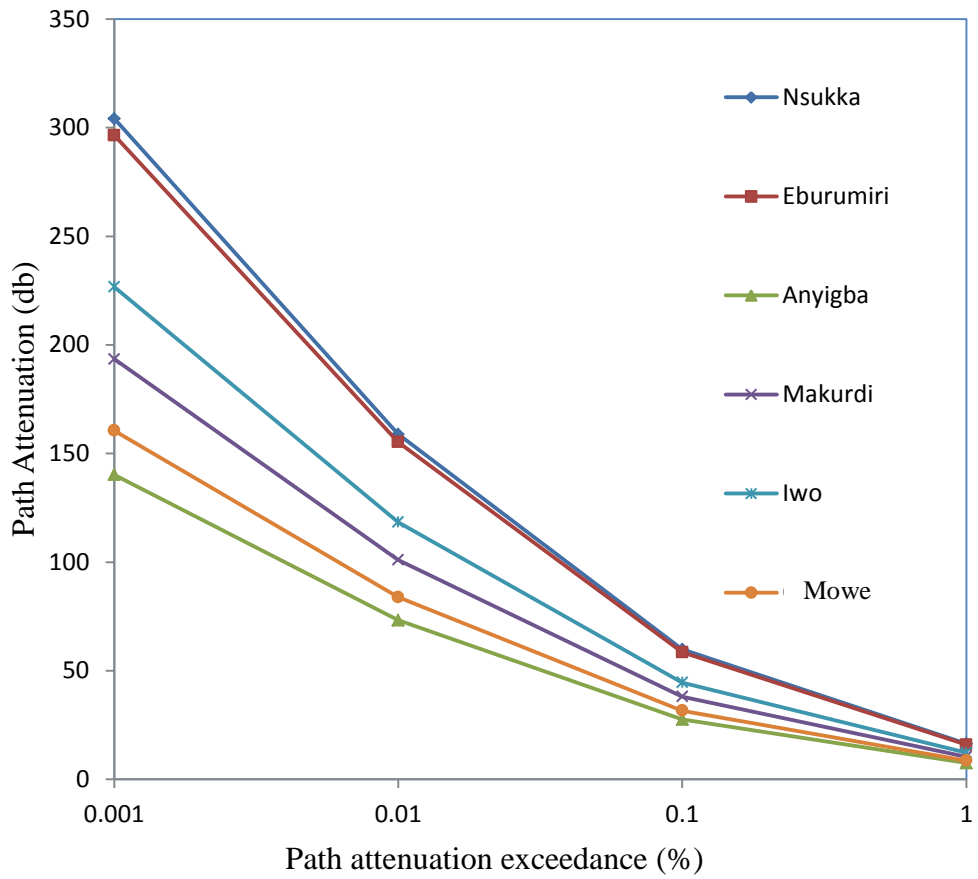


**Figure 4.78.** Path attenuation for horizontal polarisation at 31.8 GHz and 20 km path length in Derived Savanna zone

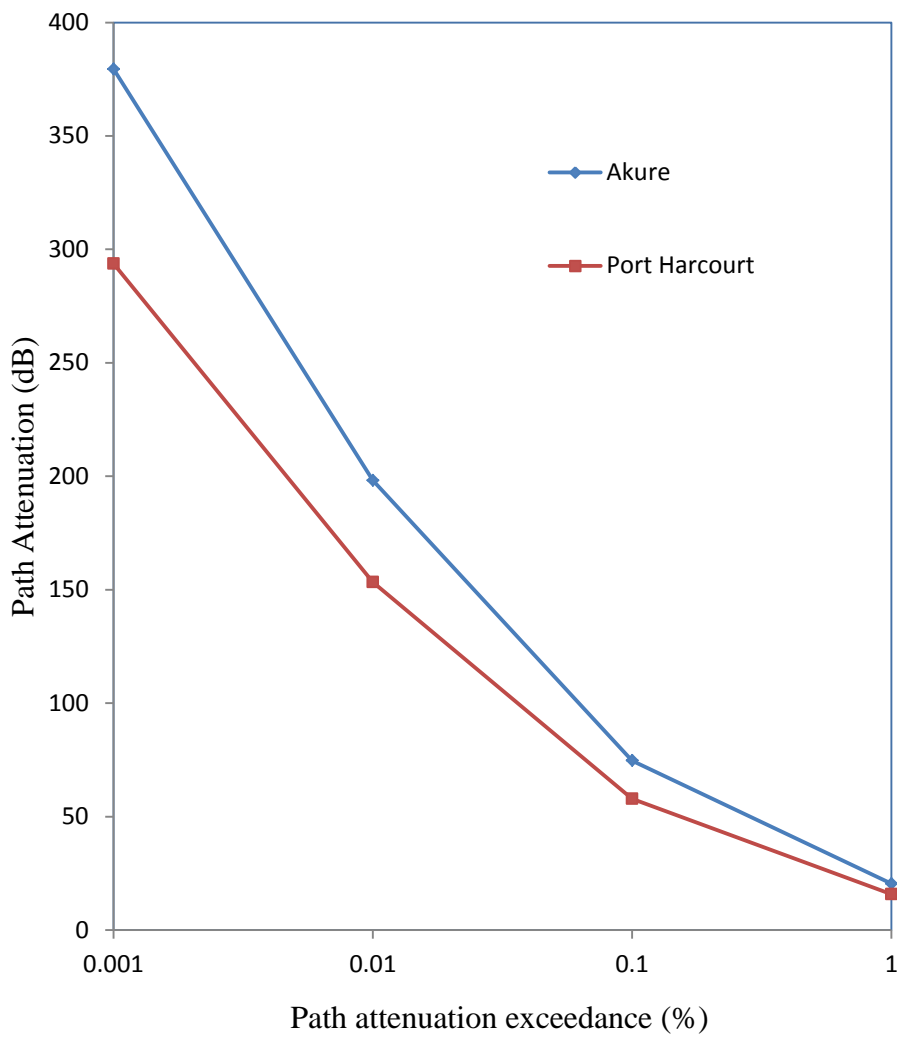


**Figure 4.79.** Path attenuation at horizontal polarisation at 31.8 GHz and 20 km path length in Humid Forest zone

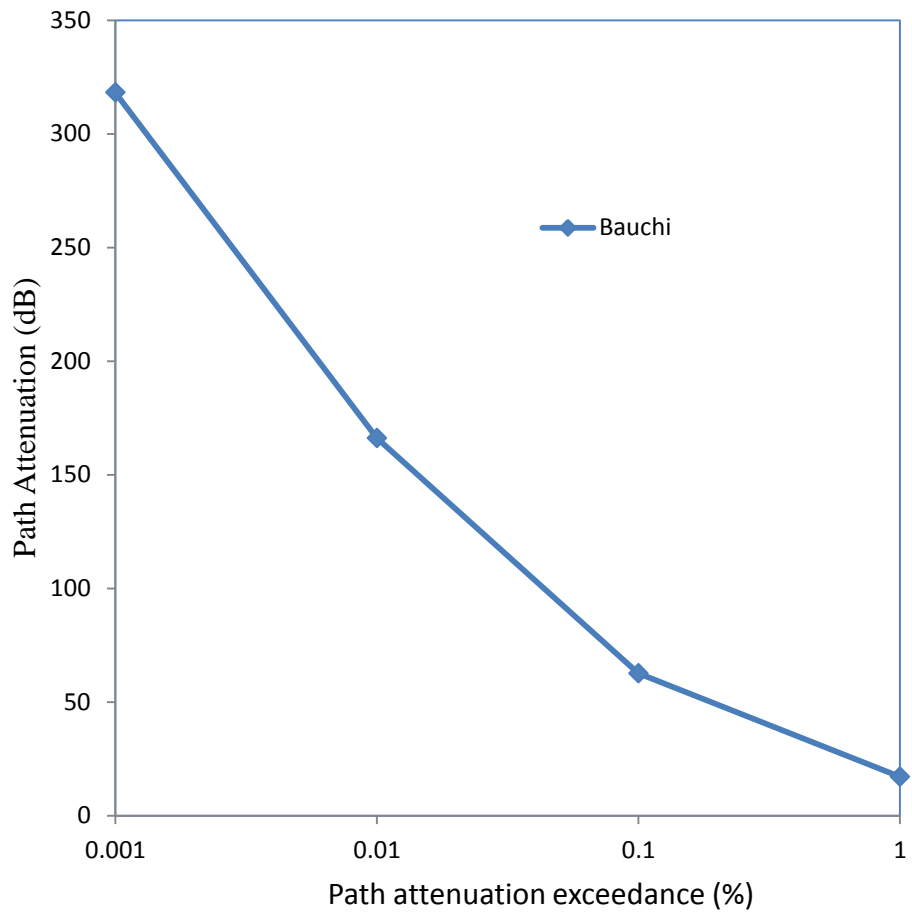


**Figure 4.80.** Path attenuation at horizontal polarisation at 31.8 GHz and 20 km path length in Northern Guinea Savanna zone

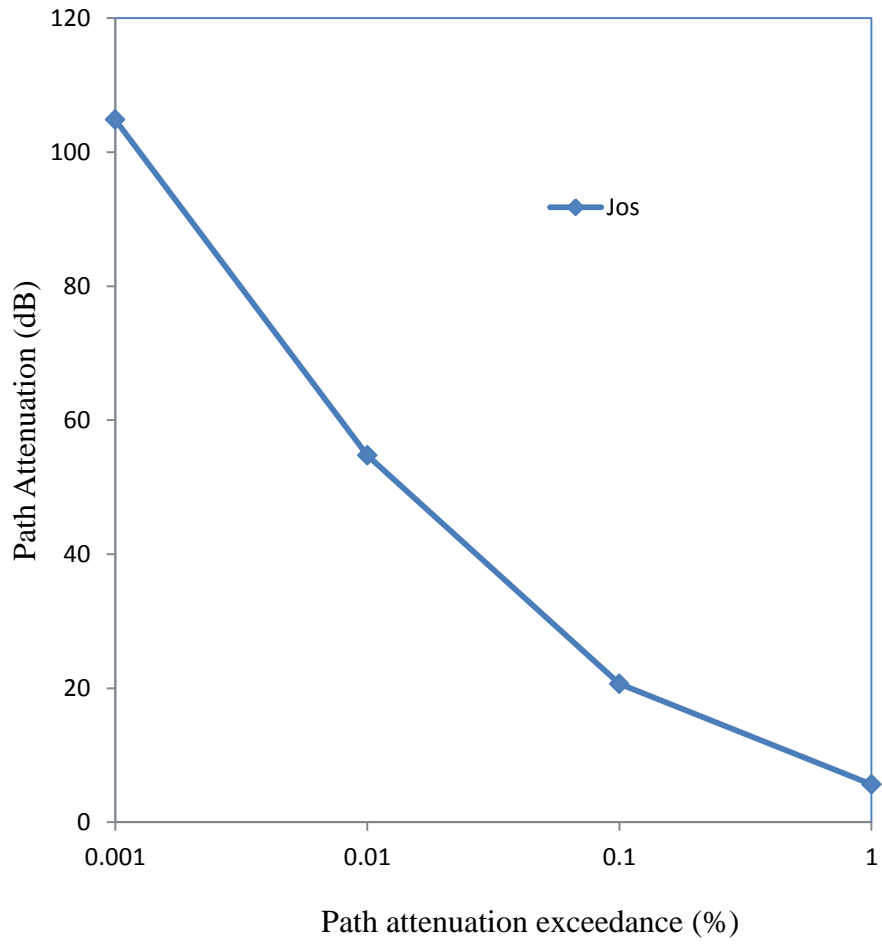


**Figure 4.81.** Path attenuation at horizontal polarisation at 31.8 GHz and 20 km path length in the mid altitude savanna zone

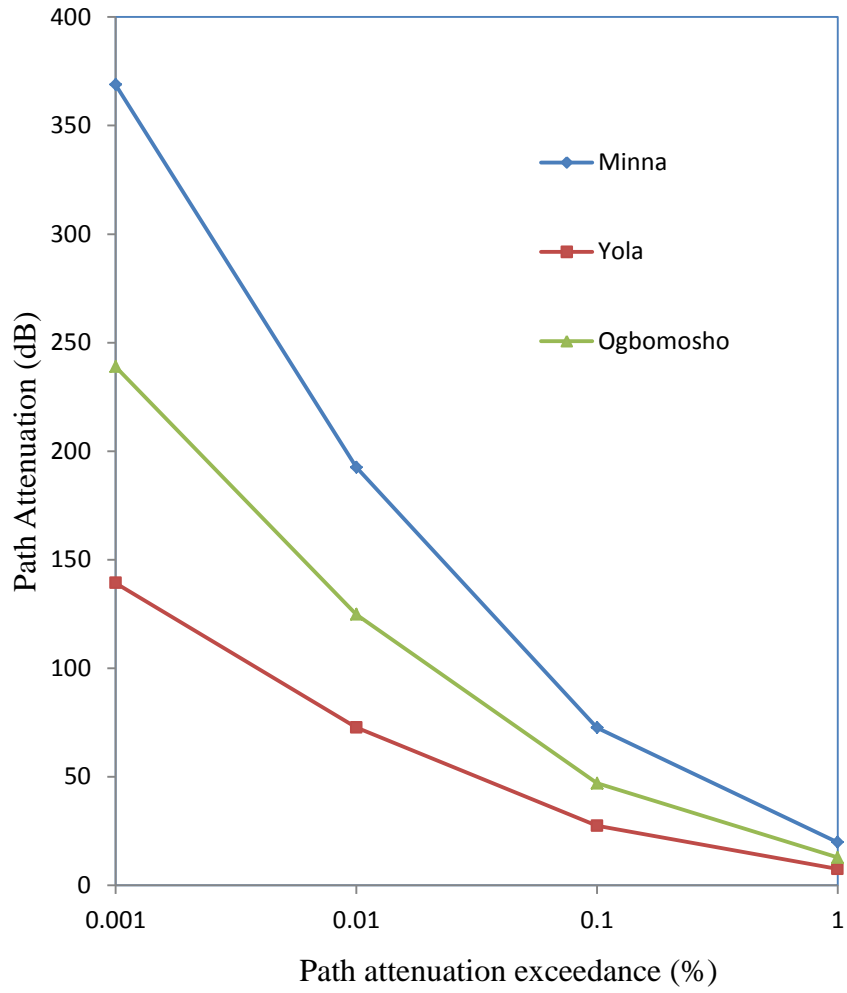


**Figure 4.82.** Path attenuation at horizontal polarisation at 31.8 GHz and 20 km path length in the Southern Guinea Savanna zone

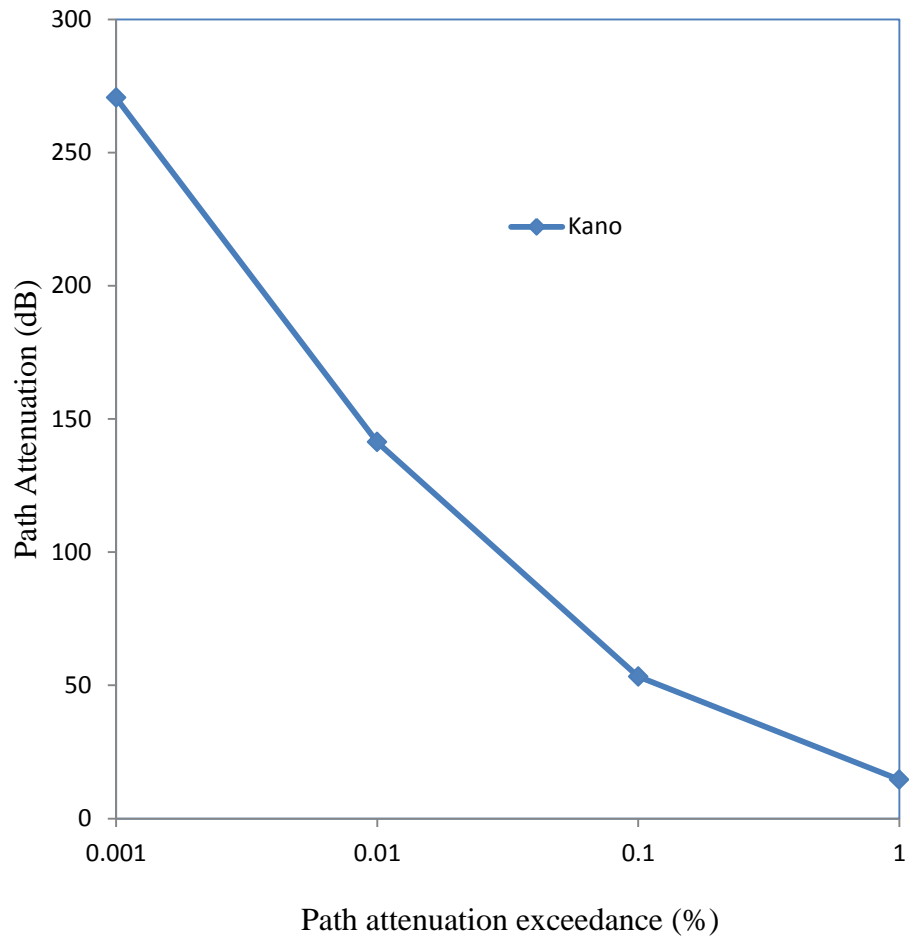


**Figure 4.83.** Path attenuation at horizontal polarisation at 31.8 GHz and 20 km path length in the Sudan Savanna zone

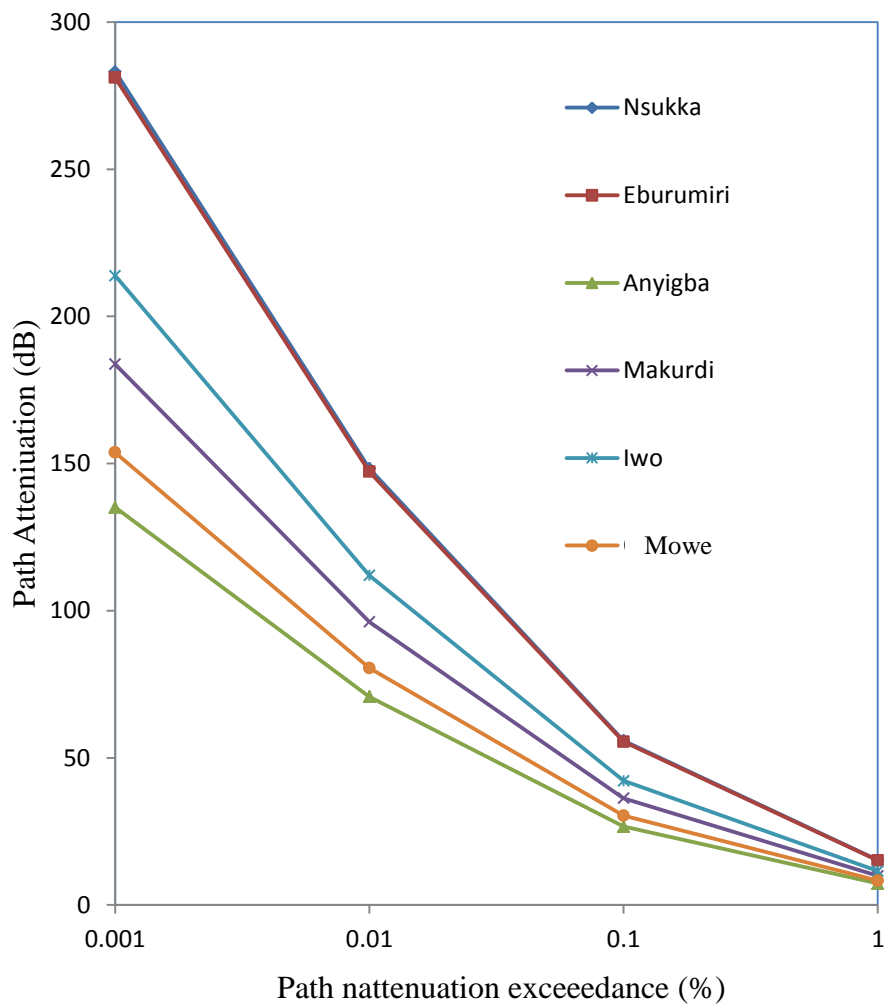


**Figure 4.84.** Path attenuation at horizontal polarisation at 33.4 GHz and 20 km path length in the Humid Forest zone



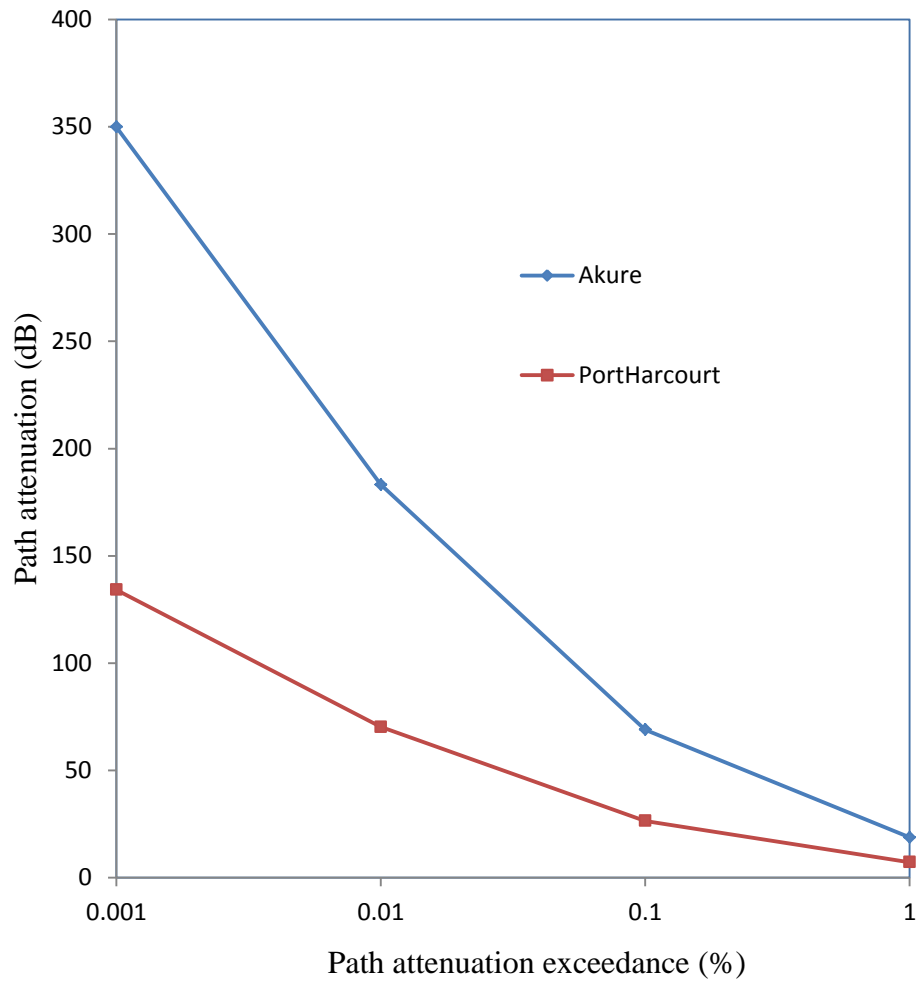


**Figure 4.85.** Path attenuation at horizontal polarisation at 33.4 GHz and 20 km path length in humid forest zone

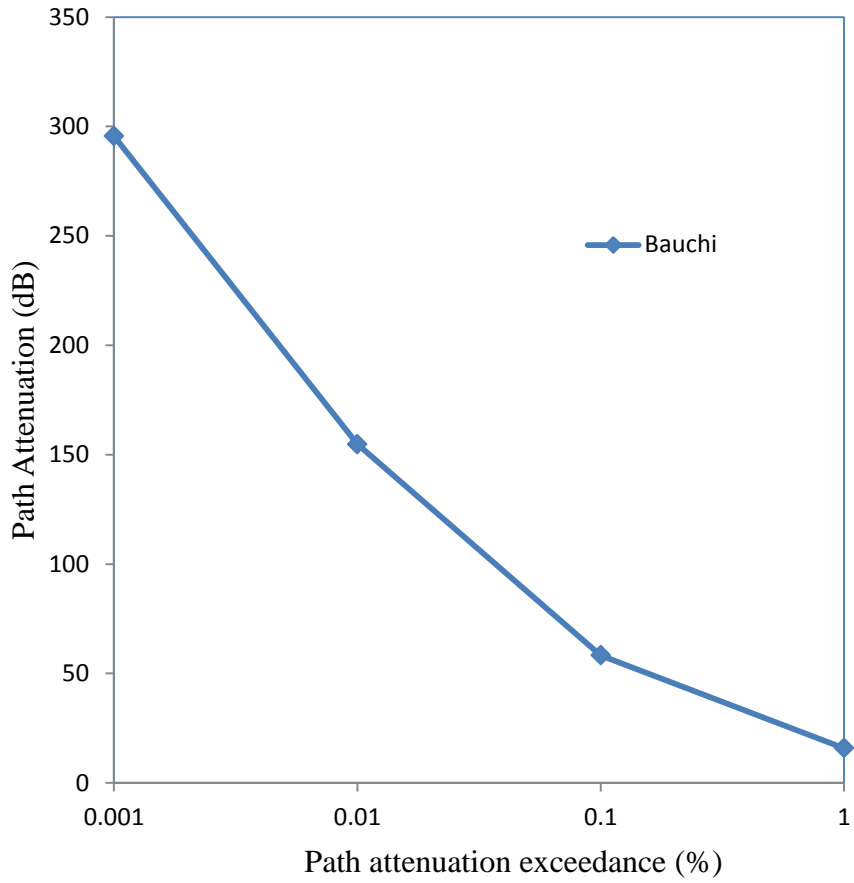


**Figure 4.86.** Path attenuation at horizontal polarisation at 33.4 GHz and 20 km path length in northern guinea savana

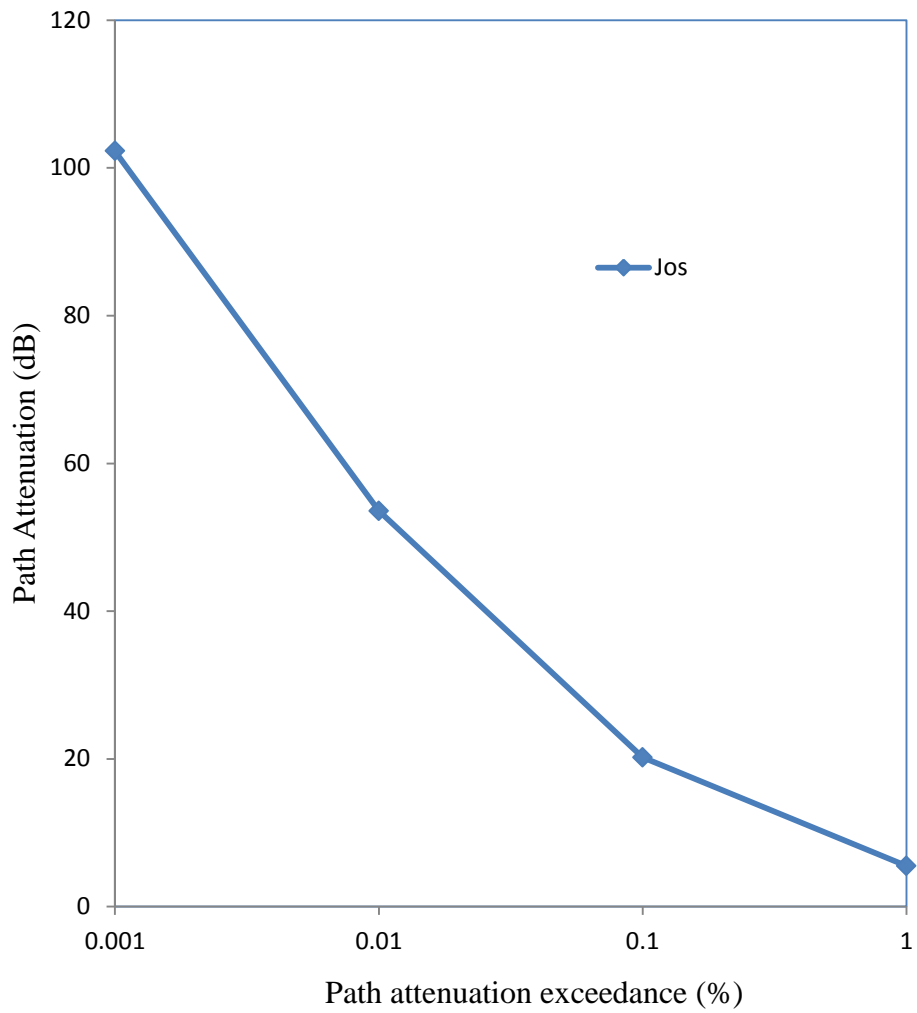


**Figure 4.87.** Path attenuation at horizontal polarisation at 33.4 GHz and 20 km path length in the mid altitude savanna zone

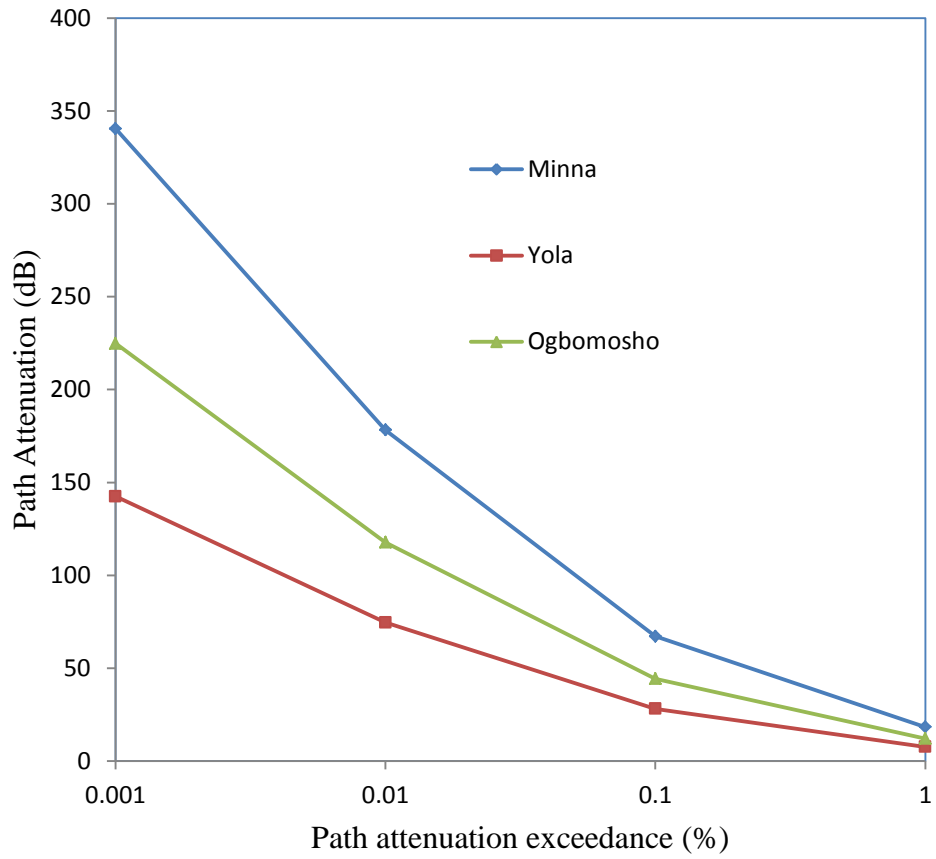


**Figure 4.88.** Path attenuation at horizontal polarisation at 33.4 GHz and 20 km path length in the Southern Guinea Savanna zone

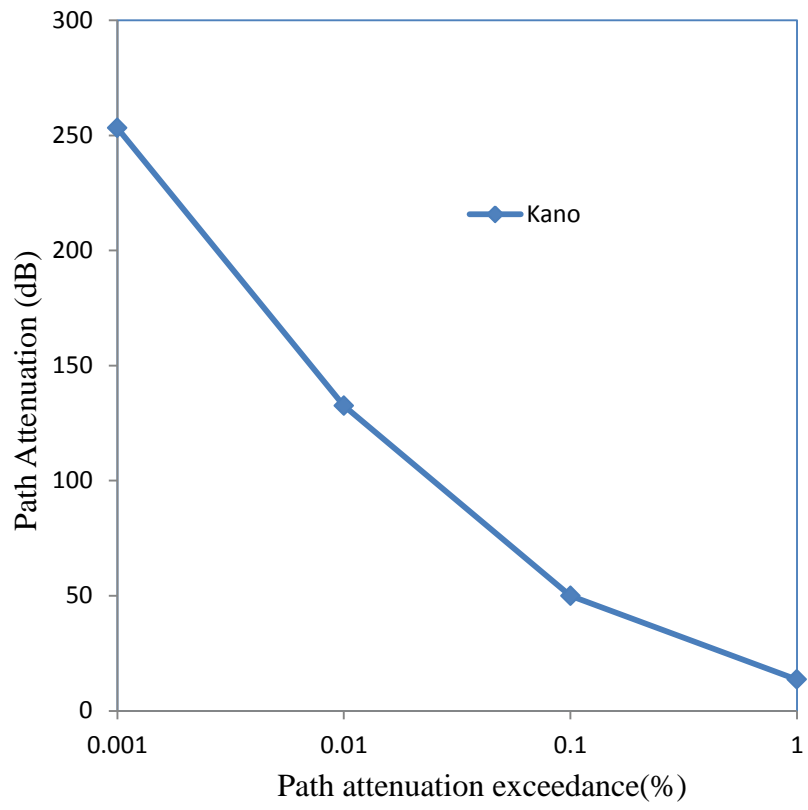


**Figure 4.89.** Path attenuation at horizontal polarisation at 33.4 GHz and 20 km path length in the Sudan Savanna zone

As observed from these Figures, attenuation due to rain increases with decrease in exceeded percentage of time, hence the higher the rainfall event, the lesser the millimeter wave availability. Table 4.19 and 4.20 lists the rain attenuation for different values of percentage of time exceeded at 31.8 GHz and 33.4 GHz respectively.

**Table 4.19. Path attenuation for different values of system availability at 31.8 GHz**

Location	Rain Attenuation (dB) at 0.001- 1% of exceedance			
	0.001%	0.01%	0.1%	1%
Nsukka	304.16	158.84	59.87	16.38
Port Harcourt	293.68	153.37	57.81	15.82
Eburumiri	296.45	155.23	58.49	15.95
Osun	226.67	118.37	44.62	12.21
Mowe	160.53	83.83	31.60	8.65
Ogbomosho	238.94	124.78	47.03	12.87
Akure	379.46	198.16	74.69	20.44
Minna	368.80	192.59	72.59	19.87
Kano	270.56	141.29	53.26	14.57
Yola	139.26	72.72	27.41	7.50
Jos	104.84	54.75	20.64	5.65
Bauchi	318.16	166.15	62.63	17.14
Makurdi	193.46	101.03	38.08	10.42
Anyigba	140.22	73.23	27.60	7.55

**Table 4.20. Path attenuation for different values of system availability at 33.4 GHz**

Location	Rain Attenuation (dB) at 0.001- 1% of exceedance			
	0.001%	0.01%	0.1%	1%
Nsukka	283.18	148.28	69.03	15.24
Port Harcourt	134.19	70.26	26.48	7.22
Eburumiri	281.09	147.19	55.46	15.13
Osun	213.79	111.95	42.18	11.50
Mowe	153.72	80.49	30.33	8.27
Ogbomosho	224.84	117.73	44.36	12.10
Akure	349.87	183.20	69.03	18.83
Minna	340.46	178.28	67.18	18.32
Kano	253.21	132.59	49.76	13.63
Yola	142.44	74.59	28.10	7.67
Jos	102.28	53.56	20.18	5.50
Bauchi	295.64	154.80	58.33	15.91
Makurdi	183.74	96.21	36.25	9.89
Anyigba	135.07	70.72	26.65	7.27



As can be observed from Table 4.18 to 4.19, Akure from the humid forest eco-climatic zone has the highest rainfall attenuation of 379.46dB/km to 20.44dB/km in all the 0.001% to 1% exceedance percentages while the attenuation in Jos, mid altitude savanna was the least at the range of 104.84dB/km to 5.65dB/km. On the other hand, Minna has the highest attenuation of 368.80 dB/km to 19.87 dB/km from the Southern Guinea Savanna. Generally, the path attenuation in Akure was highest throughout the country but lowest in Jos. It can also be inferred from the results of all the stations that maximum attenuation at 33.4 GHz frequency of propagation at 20 km path length is less than what is obtained at 31.8 GHz frequency of signals propagation. In effect, planning for attenuation of signals at 31.8 GHz frequency is sufficient for system designs that will afford benefits of the whole 31.8 to 33.4 GHz frequency bands in Nigeria.

#### **4.2.6. Contour mapping of rainfall attenuation distribution at 31.8 GHz and 33.4 GHz frequency bands**

In this research, the path attenuation exceeded from 0.001% to 1% of time at 31.8 GHz and 33.4 GHz was computed using the ITU-R 530-17 (2017) model for terrestrial paths. Table 30 to 31 is the path attenuations at 31.8 GHz and 33.4 GHz frequencies at 20 km path length. The Inverse Distance Weighting (IDW) spatial interpolation was used to compute the values for all the states in Nigeria including the Federal Capital territory (FCT); The IDW computations for 31.8 GHz and 33.4 GHz for 0.001% to 1% of exceedance was carried out with the observed values in Tables 4.18 and 4.19 while Tables 4.21 and 4.22 gives the path attenuation computed with the IDW interpolation. The contour maps for each of the percentages of exceedance are shown in Figures 4.90 to 4.97.

Considering the rain region as categorized in the work of Adeniyi (2014) which is based on rainfall variation across the eco-climatic zone of Nigeria, the contour map of Figure 4.90 to 4.97 shows the variation of path attenuation across and even within the same rain zones of the country. Hence, to enhance system availability, maximum path attenuation for each zone should be factored into equipment designs to forestall any possible signal failure especially during intense rainfall.

**Table 4.21.** Path Attenuation at 0.001% to 1% rain rate exceedance for 31.8 GHz frequency band using Inverse Distance Weighing Interpolation

S/N	States	Coordinates		Path Attenuation (dB)				Eco-climatic Zone
		Longitude (°N)	Latitude (°E)	0.001%	0.01%	0.1%	1%	
1	Sokoto	5.22	12.93	301.25	157.32	59.30	16.23	Sudan Savanna
2	Gusau	6.23	12.18	285.91	149.31	56.28	15.40	Sudan Savanna
3	Katsina	7.61	12.51	264.17	137.95	52.00	14.23	Sudan Savanna
4	Maiduguri	13.17	12.20	304.64	159.09	59.97	16.41	Sudan Savanna
5	Dutse	9.72	12.44	289.75	151.31	57.04	15.61	Sudan Savanna
6	Damaturu	11.70	12.18	303.04	158.25	59.65	16.32	Sudan Savanna
7	Kano	8.66	11.75	270.56	141.29	53.26	14.57	Sudan Savanna
8	Birnin-Kebbi	4.06	11.67	329.61	172.12	64.88	17.76	Sudan Savanna
9	Kaduna	8.13	10.15	222.12	115.99	43.73	11.96	Northern Guinea Savanna
10	Gombe	11.16	10.24	307.73	160.71	60.58	16.58	Northern Guinea Savanna
11	Abuja	7.36	9.07	189.14	98.77	37.23	10.19	Northern Guinea Savanna
12	Bauchi	10.08	10.63	318.16	166.15	62.63	17.14	Northern Guinea Savanna
13	Ilorin	4.56	8.98	210.69	110.03	41.47	11.35	Derived Savanna
14	Jalingo	10.26	8.00	199.55	104.21	39.28	10.75	Derived Savanna
15	Lafia	8.30	8.57	160.19	83.65	31.53	8.63	Derived Savanna
16	Ado Ekiti	5.31	7.66	251.11	131.13	49.43	13.53	Derived Savanna
17	Awka	7.00	6.27	299.58	156.70	59.05	16.12	Derived Savanna
18	Abakaliki	7.95	6.17	277.07	144.87	54.60	14.91	Derived Savanna
19	Nsukka	7.40	6.86	304.16	158.84	59.87	16.38	Derived Savanna
20	Eburumiri	7.35	6.61	296.45	155.23	58.49	15.95	Derived Savanna
21	Iwo	7.63	4.19	226.67	118.37	44.62	12.21	Derived Savanna
22	Mowe	3.58	6.90	160.53	83.83	31.60	8.65	Derived Savanna
23	Makurdi	8.83	7.35	193.46	101.03	38.08	10.42	Derived Savanna
24	Anyigba	6.57	7.90	140.22	73.23	27.60	7.55	Derived Savanna
25	Ikeja	3.62	6.60	202.03	105.50	39.77	10.88	Humid Forest
26	Benin City	5.89	6.54	271.44	141.75	53.43	14.62	Humid Forest
27	Asaba	5.89	5.53	283.59	148.20	55.86	15.27	Humid Forest
28	Yenagoa	5.89	4.86	287.58	150.24	56.63	15.49	Humid Forest
29	Calabar	8.66	6.16	246.84	129.02	48.62	13.29	Humid Forest
30	Owerri	7.00	5.60	289.20	151.24	57.00	15.57	Humid Forest
31	Uyo	7.87	4.93	270.77	141.57	53.35	14.58	Humid Forest
32	Umuahia	7.52	5.43	280.76	146.81	55.33	15.11	Humid Forest
33	Portharcourt	6.92	4.85	293.68	153.37	57.81	15.82	Humid Forest
34	Akure	7.26	5.21	379.46	198.16	74.69	20.44	Humid Forest
35	Ogbomosho	3.41	8.11	238.94	124.78	47.03	12.87	Southern Guinea Savanna
36	Minna	5.39	10.21	368.80	192.59	72.59	19.87	Southern Guinea Savanna
37	Yola	12.43	9.32	139.26	72.72	27.41	7.50	Southern Guinea Savanna
38	Jos	9.36	9.24	104.84	54.75	20.64	5.65	Mid Altitude Savanna

**Table 4.22.** Path Attenuation at 0.001% to 1% rain rate Exceedance for 33.4 GHz Frequency band Using Inverse Distance Weighing Interpolation

	States	Coordinates		Path Attenuation (dB)				Eco-climatic Zone
		Longitude (°N)	Latitude (°E)	0.001 %	0.01%	0.1%	1%	
1	Sokoto	5.22	12.93	280.09	146.66	55.20	15.07	Sudan Savanna
2	Gusau	6.23	12.18	266.38	139.49	52.48	14.34	Sudan Savanna
3	Katsina	7.61	12.51	247.21	129.45	48.63	13.31	Sudan Savanna
4	Maiduguri	13.17	12.20	283.59	148.49	55.90	15.26	Sudan Savanna
5	Dutse	9.72	12.44	270.31	141.54	53.21	14.55	Sudan Savanna
6	Damaturu	11.70	12.18	282.16	147.75	55.61	15.19	Sudan Savanna
7	Kano	8.66	11.75	253.21	132.59	49.76	13.63	Sudan Savanna
8	Birnin-Kebbi	4.06	11.67	305.43	159.94	60.23	16.44	Sudan Savanna
9	Kaduna	8.13	10.15	208.83	109.35	41.13	11.24	Northern Guinea Savanna
10	Gombe	11.16	10.24	286.35	149.94	56.45	15.41	Northern Guinea Savanna
11	Abuja	7.36	9.07	178.99	93.73	35.30	9.63	Northern Guinea Savanna
12	Bauchi	10.08	10.63	295.64	154.80	58.33	15.91	Northern Guinea Savanna
13	Ilorin	4.56	8.98	199.19	104.30	39.30	10.72	Derived Savanna
14	Jalingo	10.26	8.00	189.87	99.42	37.45	10.22	Derived Savanna
15	Lafia	8.30	8.57	153.29	80.27	30.24	8.25	Derived Savanna
16	Ado Ekiti	5.31	7.66	235.15	123.13	46.39	12.65	Derived Savanna
17	Awka	7.00	6.27	282.33	147.63	60.97	15.17	Derived Savanna
18	Abakaliki	7.95	6.17	261.04	136.62	56.20	14.04	Derived Savanna
19	Nsukka	7.40	6.86	283.18	148.28	69.03	15.24	Derived Savanna
20	Eburumiri	7.35	6.61	281.09	147.19	55.46	15.13	Derived Savanna
21	Iwo	7.63	4.19	213.79	111.95	42.18	11.50	Derived Savanna
22	Mowe	3.58	6.90	153.72	80.49	30.33	8.27	Derived Savanna
23	Makurdi	8.83	7.35	183.74	96.21	36.25	9.89	Derived Savanna
24	Anyigba	6.57	7.90	135.07	70.72	26.65	7.27	Derived Savanna
25	Ikeja	3.62	6.60	190.90	99.96	37.67	10.27	Humid Forest
26	Benin City	5.89	6.54	253.06	132.50	49.93	13.62	Humid Forest
27	Asaba	5.89	5.53	265.70	139.04	54.70	14.29	Humid Forest
28	Yenagoa	5.89	4.86	213.76	111.87	43.55	11.50	Humid Forest
29	Calabar	8.66	6.16	233.10	122.01	48.99	12.54	Humid Forest
30	Owerri	7.00	5.60	272.48	142.54	58.81	14.65	Humid Forest
31	Uyo	7.87	4.93	255.23	133.58	54.68	13.73	Humid Forest
32	Umuahia	7.52	5.43	264.47	138.41	57.06	14.23	Humid Forest
33	Portharcourt	6.92	4.85	134.19	70.26	26.48	7.22	Humid Forest
34	Akure	7.26	5.21	349.87	183.20	69.03	18.83	Humid Forest
35	Ogbomosho	3.41	8.11	224.84	117.73	44.36	12.10	Southern Guinea Savanna
36	Minna	5.39	10.21	340.46	178.28	67.18	18.32	Southern Guinea Savanna
37	Yola	12.43	9.32	142.44	74.59	28.10	7.67	Southern Guinea Savanna
38	Jos	9.36	9.24	102.28	53.56	20.18	5.50	Mid Altitude Savanna

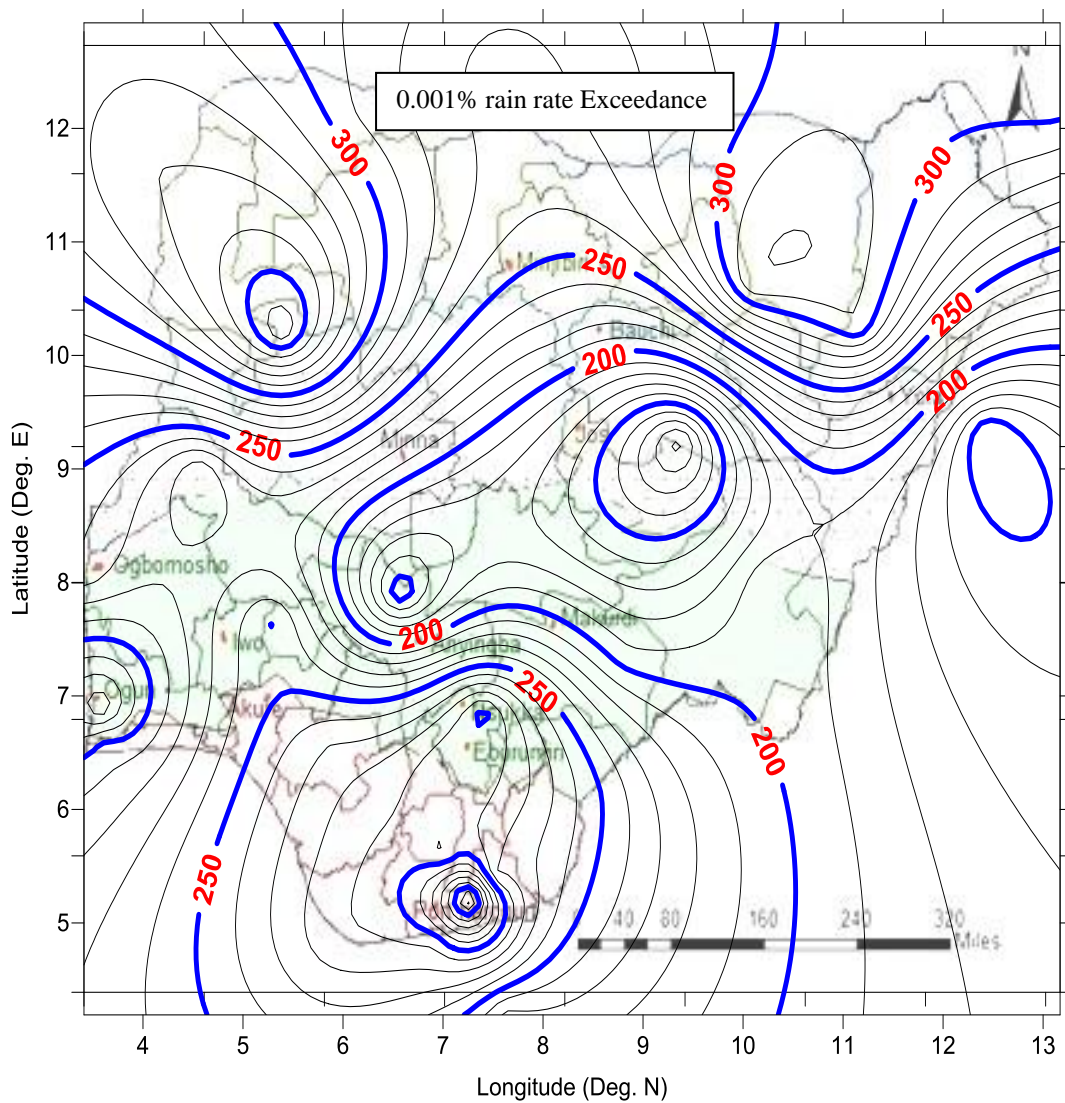


**Figure 4.90.** Contour Mapping of Path Attenuation at 0.001% rain rate exceedance for 31.8 GHz Frequency band in Nigeria

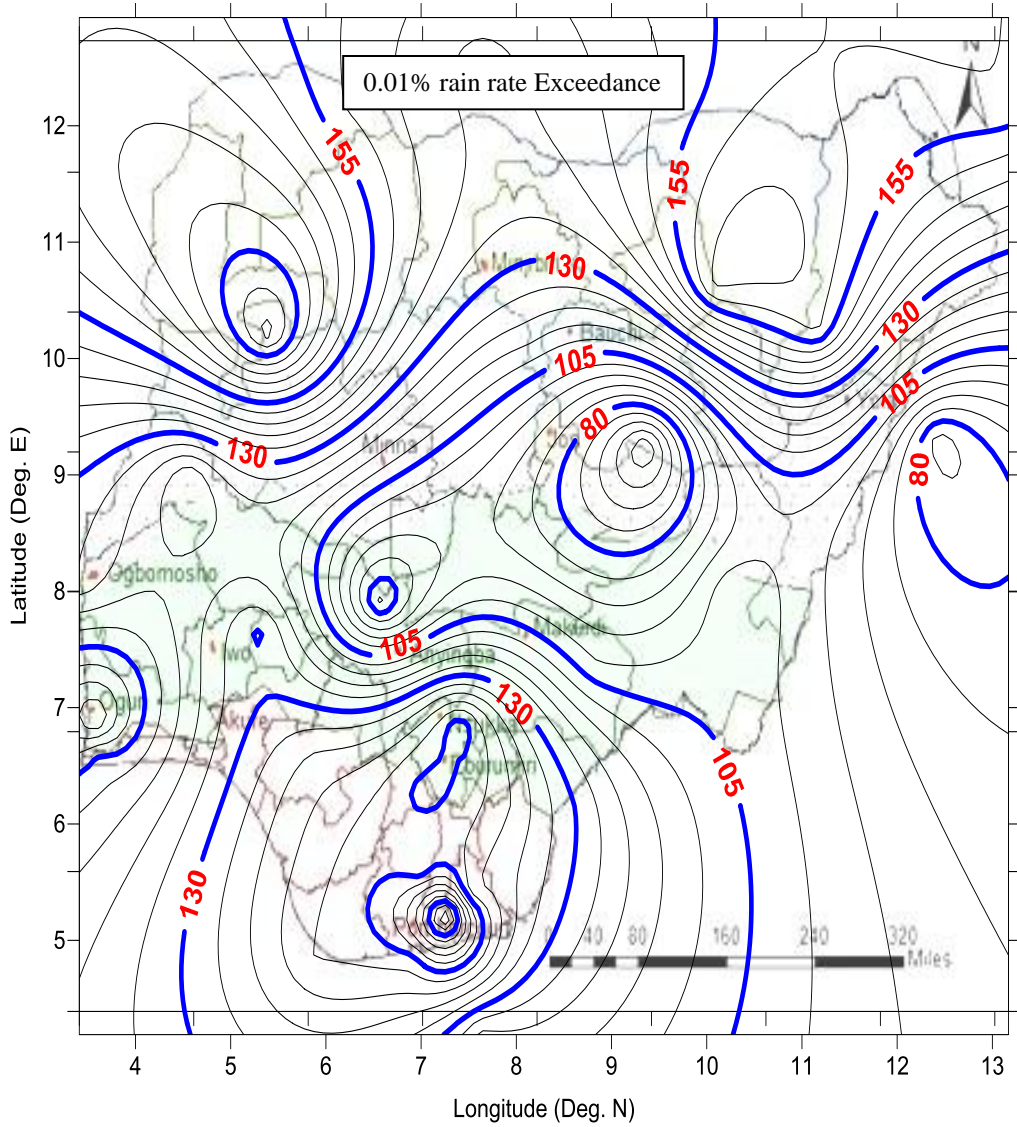


**Figure 4.91.** Contour Mapping of Path Attenuation at 0.01% rain rate exceedance for 31.8 GHz Frequency band in Nigeria



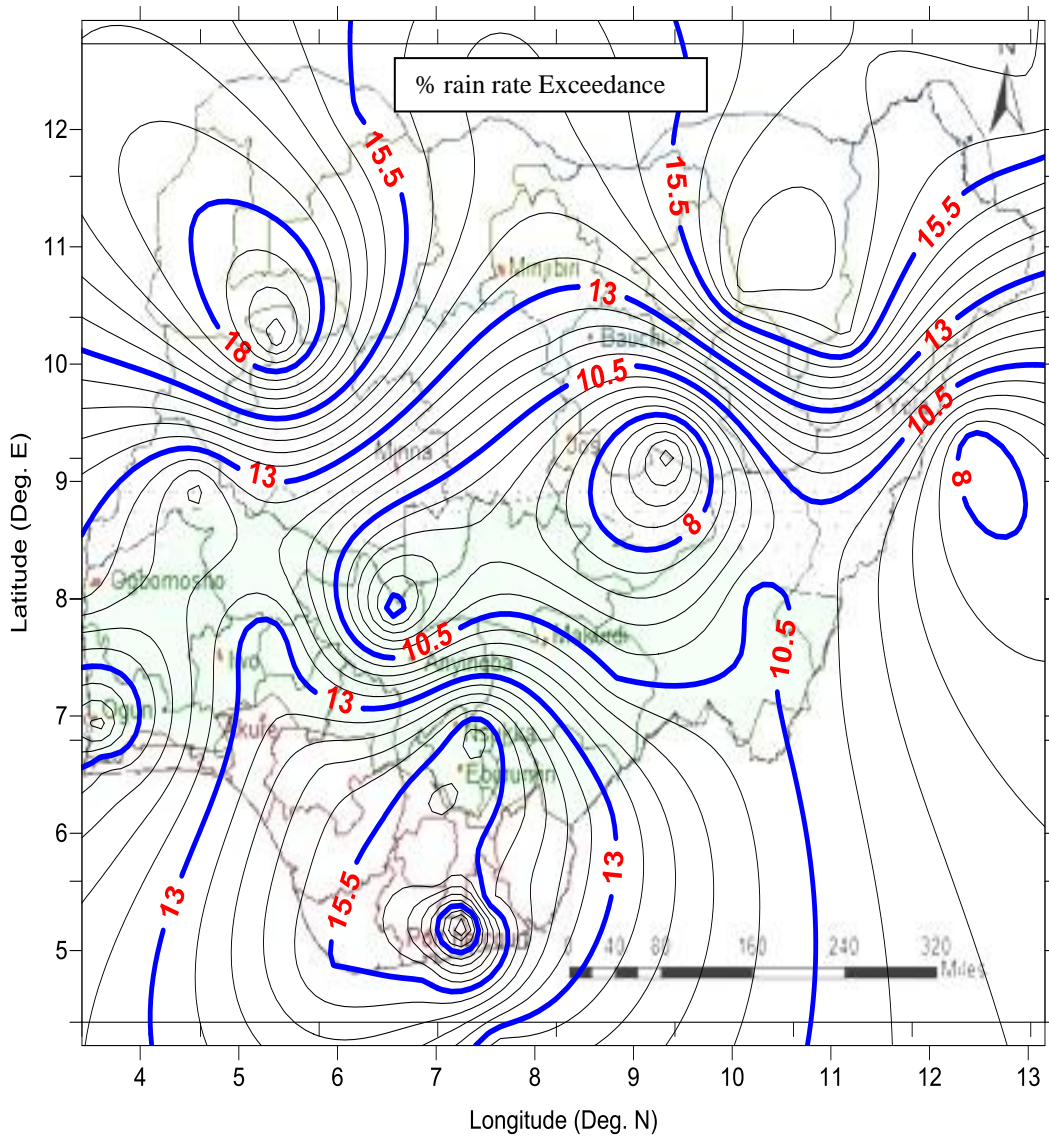
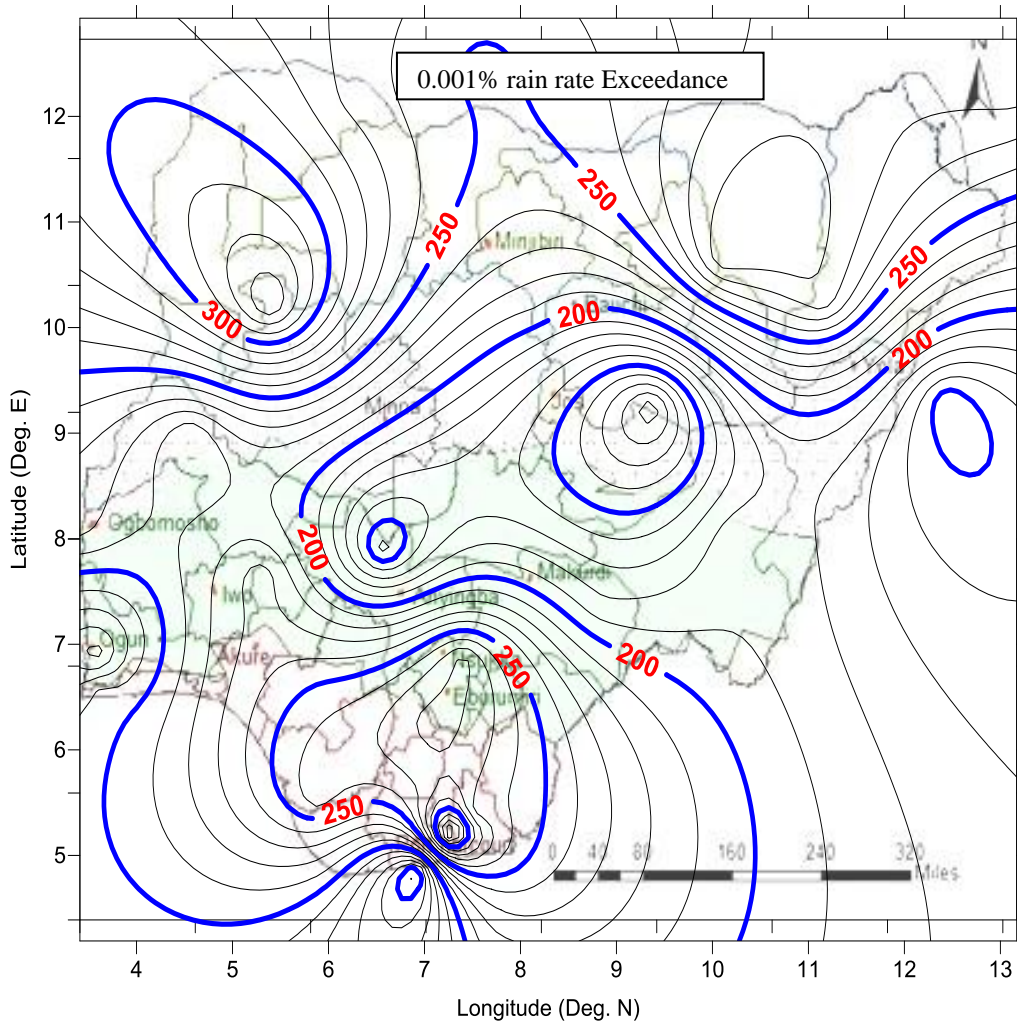
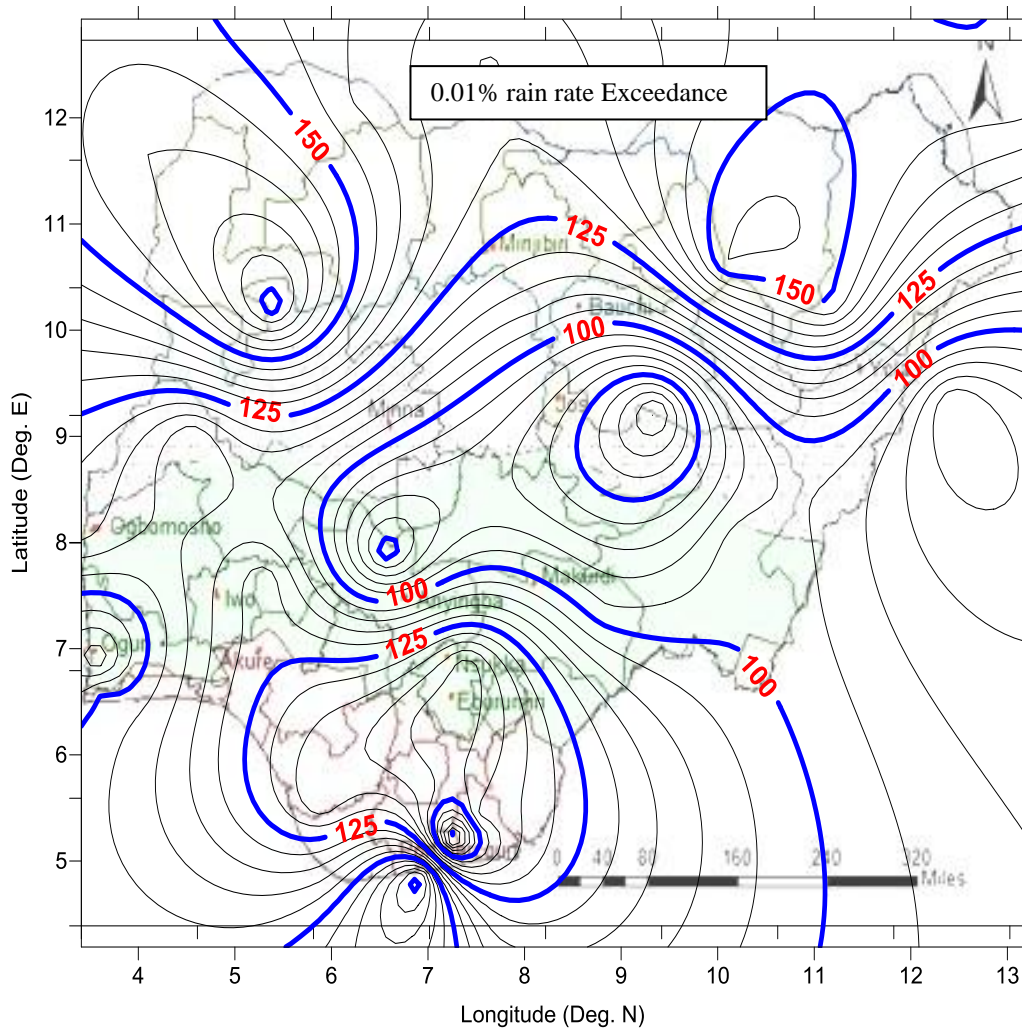


Figure 4.93. Contour Mapping of Path Attenuation at 1% rain rate exceedance for 31.8 GHz Frequency band in Nigeria



**Figure 4.94.** Contour Mapping of Path Attenuation at 0.001% rain rate exceedance for 33.4 GHz Frequency band in Nigeria





**Figure 4.95.** Contour Mapping of Path Attenuation at 0.01% rain rate exceedance for 33.4 GHz Frequency band in Nigeria

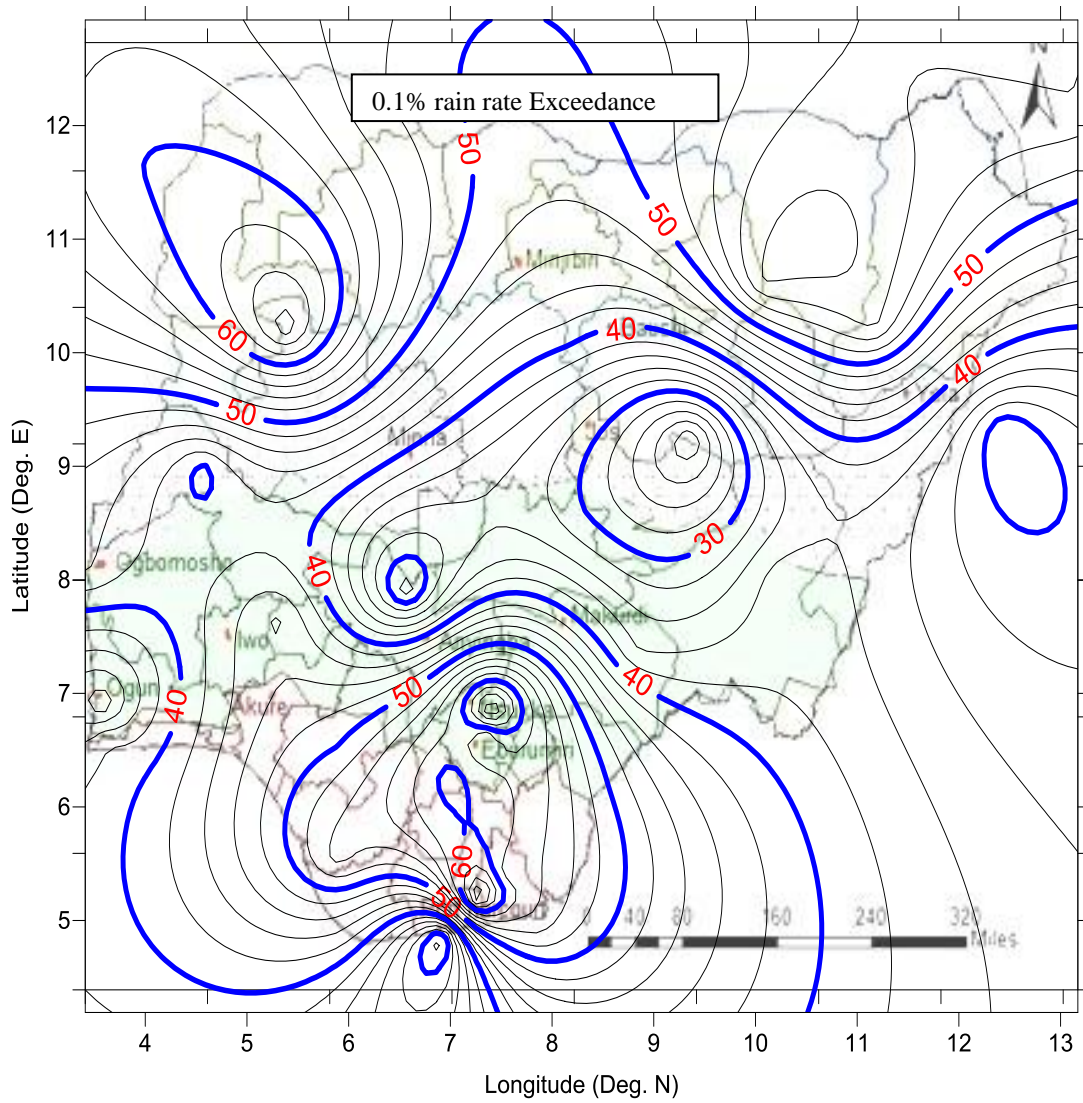


**Figure 4.96.** Contour Mapping of Path Attenuation at 0.1% rain rate exceedance for 33.4 GHz Frequency band in Nigeria

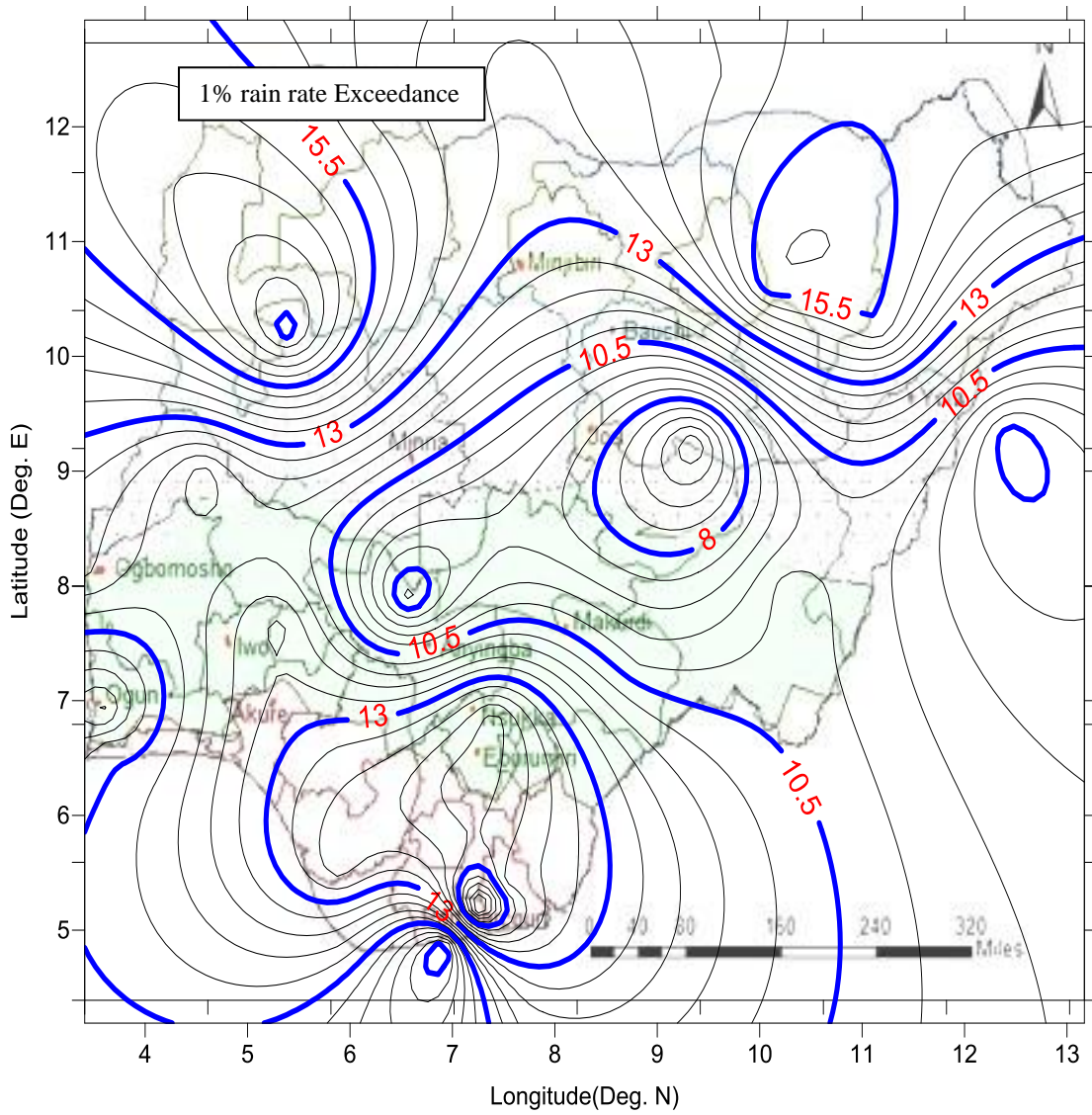


**Figure 4.97.** Contour Mapping of Path Attenuation at 1% rain rate exceedance for 33.4 GHz Frequency band in Nigeria

## **CHAPTER FIVE**

### **CONCLUSION AND RECOMMENDATIONS**

#### **5.1 Conclusion**

This research estimated and modelled rain induced attenuation at millimeter wave frequency bands on terrestrial paths over selected locations that cuts across the eco-climatic zones of Nigeria. The main rain characteristics studied were rain rate cumulative distribution, worst-month and worst hours distribution. The Lavergnat and Gole model was used to obtain the 1- minute equivalence of the 5 minutes integration time data from 12 out of the 14 locations considered; the remaining stations which were of 1 –minute integration time (in-situ) were used for rain rate model validations. The derived 1-minute rain rate was used to obtained rain induced attenuation at different percentages of occurrence.

It was observed that the rain rate cumulative distribution of worst month was higher compared with all months at the same probability of exceedence. Also, the months of rainfall peak and the cessation have changed in Nigeria, hence altering the worst months for radio propagation equipment planning and designs. This may not be unconnected with the prevalence of climate change. On the other hand, since communication services takes place on 24 – hour basis, hourly variations of rainfall intensity were deduced; the results obtained revealed that 15 hours LT was the worst hour in about 43 percent of the locations considered and the corresponding rain rate ranged from 11.86 to 22.69b mm/hr.

Additionally, power law regression coefficients for rain rate integration time conversions as well as mean annual and worst month time percentage of excess were determined. The results show good correlation between the parameters with a high coefficient of determination. It equally varied slightly from the predicted ITU-R coefficient of determination in all the zones.

Furthermore, the comparison with existing rain conversion models revealed the non-universality of their applications as the regression coefficients obtained through

the study varied from one location to another. Hence different conversion factors are required for different locations even within the same climate region for the conversion of rainfall data of a given integration time to another as against unified time integration regression coefficients suggested by the ITU-R. Therefore, a suitable model was deduced for each location under study.

The specific attenuation was computed for both horizontal and vertical polarisation. The result obtained implied that there is a slight difference between the specific attenuation at the horizontal and the vertical polarisation. This difference has been attributed to the distortion in rain drops which are not spherical but asymmetrical about the horizontal plane with flattened base for large drops. The frequency threshold for specific attenuation was 120 and 150 GHz across the locations. Also, the path attenuation determination at the frequency threshold revealed that 40 and 45 GHz are the clear signal band frequencies over the locations and even the nation at large.

## **5.2 Recommendations**

It is hereby recommended that in view of the anthropogenic changes in the atmosphere which has triggered global warming, periodic measurement of point rainfall rates in every eco-climatic location be effected. This will provide radio propagation engineers with data for equipment designs that are suitable for the Nigerian climate so as to forestall failures. On the other hand, apart from the use of average worst years and average worst month rainfall rates data for communication equipments designs, the average worst hours data should be incorporated as communication service is a 24-hours affair. Additionally, there is a compelling need for the modification of ITU-R rain rate prediction model as it applies to the locations considered by the incorporation of the truth values obtained at the ground stations in Nigeria. Furthermore, fade counter-measure techniques such as Radio Frequency (RF) modifications, adaptive control of signal power coding and data rate should be effectively implemented to mitigate signal attenuating effects of rainfall in Nigeria.

## **5.3 Suggestions for further research**

To fully address the propagation characteristics that will afford communication system designs suitable for the tropics, these are suggested for further research:

- Deductions of the worst hour rainfall rates from higher rainfall integration times and the use of the statistics to deduce attenuation characteristics at the affected locations;
- Considering the reduction in attenuation as the frequency of propagation increases, it is suggested that studies be conducted to ascertain the maximum frequencies before the reduction throughout all the millimetric frequency bands.
- The 31.8 GHz and 33.4 GHz frequency bands assigned to Nigeria (NCC) by the International Telecommunications Union (ITU) and the utilization covers both the terrestrial and earth space path. Further research is suggested by applying the suitable ITU recommendations for the earth space path.

## REFERENCES

- Abayomi, I.O.Y., George T, Nor H.H.K. 2019. Rain Attenuation models at Ka band for selected stations in the south western region of Nigeria. Indonesian Journal of Electrical Engineering and Informatics (IJEI), Vol. 7, No. 1, p. 144-151.
- Adeniyi, M.O. 2014. Variability of Daily Precipitation Over Nigeria. Meteorology and Atmospheric Physics, 126:161–176. DOI 10.1007/s00703-014-0340-6.
- Adeyemi, B. and Aro T.O. 2004. Variation in surface water vapour density over four Nigeria Stations. Nig. J. Pure Appl. Phys. 3:46-55.
- Adimula, I.A. 2003. Characteristics of Rain Induced Attenuation and Phase Shift at Ilorin, Nigeria. Zuma Journal of Pure and Applied Science Vol. 5(2), p. 193-196.
- Adimula, I.A, and Oyeleke O. 2005. Rain Rate Model for Tropical Stations for Radio Propagation Application. NIJOSTER, Vol. 1 No. 1, P. 70-77.
- Agber, J. U. and Johnson M.A. 2013. A High Performance Model for Rainfall Effect on Radio Signals. Journal of Information Engineering and Applications ([www.iiste.org](http://www.iiste.org)) Vol.3 (7): 25-35.
- Ajayi, G.O, Feng, S., Radicella, S.M. and Reddy B.M. (Ed). 1996. A hand book on radiopropagation related to satellite communication in tropical and subtropical countries, ICTP, Trieste, Italy, pp. 2-14.
- Ahmed , M., Azmi, A., Rahman,A., Al-Mqdashi F.Y. and Abdulmajid. (2020). Millimeter Wave Propagation Measurements and Characteristics for 5G System. Applied Sciences. DOI: 10.335. 10.3390/app10010335.
- Ali, A.A., Alhadier, M.A., and Shatila, M.A. 1986. Rain map for radiowave propagation design in Soudi Arabia, Int. J. of Infrared and Millimeter wave , vol, 7, no. 11, pp. 1777-1793.
- Ali-Akbar S., Somayeh M., Hossein A., MASOODIYAN A. and MARYANAJI Z. 2015. Geographical Factors Affecting the Precipitation Regime in Iran., Aerul și Apa: Componente ale Mediului, p.172-178 DOI.: 10.17378/AWC2015\_23.
- Aloaba, O.A. and Ajayi G.O. 2000. VHF Radio wave propagation Measurements in Nigeria. Proceedings of ISAP, Fukuoka, Japan.
- Al-Saman, A., Mohamed, M., Cheffena, M., and Moldsvor, A. 2021. Wideband channel characterization for 6G networks in industrial environments. *Sensor*. 21:2-18. <https://doi.org/10.3390/s21062015>.

- Al-Samman, A.M., Azmi, M.H., Al-Gumaei, Y.A., Al-Hadhrami, T., Abd. Rahman, T., Fazea, Y. and Al-Mqdashi, A. 2020. Millimeter wave propagation measurements and characteristics for 5G system. *Applied Sciences*. 10(1):335. <https://doi.org/10.3390/app10010335>.
- Al-Saman, A., Cheffena, M., Mohamed, M., Marwan Hadri Azmi, M.A., and Yun Ai, Y. 2020. Statistical analysis of rain at millimeter waves in tropical area. *IEEE Access*. 8: 51044-51061. DOI: 10.1109/ACCESS.2020.2979683.
- Alsarhan, Y. 2015. Terrestrial millimeter line of sight link design at 45GHz. MSc. Thesis. Communication Systems Engineering, University of Portsmouth  
DOI:10.13140/RG.2.1.4707.8001.
- American Meteorological Society (AMS) Glossary. 2000.  
Retrieved October 2013, from [http://hydroviz.cilat.org/hydro/rain\\_gauges.pdf](http://hydroviz.cilat.org/hydro/rain_gauges.pdf)
- As-Syakur Abd.Rahman. 2018. TRMM PR observed spatial patterns of the convective-stratiform rainfall over Indonesia and their response to ENSO, IOP conference series: earth and Environment science 165 (2018) 012009.  
Doi:10.1088/1755-1315/165/1/012009.
- Azpurua, M. and Ramos K. D. 2010. A comparison of spatial interpolation methods forestimation of average electromagnetic field magnitude. *Progress in Electromagnetics Research M*, vol. 14, 135-145.  
Doi:10.2528/PIERM10083103.
- Barry, G. and Chorly J.R. 1987. *Atmosphere, Weather and Climate*, 5th Edition, Chapman andHall Inc, New York, Chapter 2.
- Best, C.A. 19650a. The size distribution of rain drops. *Quarterly Journal on Research Meteorology Society* 76, 302-311.
- Bhartia, p., Bahl, I.J. 1984. *Millimeter Wave Engineering and Applications*, John Wiley & Sons, New York, Chapter 3 & 4.
- Blair, T. A. 1957. *Weather Element*, Prentice-Hall, Inc. Eaglewood Cliffs, New Jersey. pp.7-30, Chapters one and two.
- Bryant, G.H., Adimula I.A. and Riva C. 1998. Rain cell diameter and heights. A new model of attenuation presented in URSI Comm F, Aveiro, Portugese.
- Burgueno, A. M., M. Puigcever, and E. Vilar. 1988. Influence of rain gauge integration time on the rain rate statistics used in microwave communication, *Ann. Telecomm.*, Vol. 43 (9-10): 522-527.
- Campbell Scientific .2015. Retrieved October 2015, from [www.campbellsci.com](http://www.campbellsci.com).



- CCIR .1982b. Line of sight radio relay systems Propagation data requirement. Rep. 338-4, Recommendations and Reports of the CCIR, Vol. 5, Int. Telecomm Union, Geneva, 279-314.
- CCIR .1982c. Propagation data required for Space Communication Systems. Rep. 564-2, Recommendations and Reports of the CCIR, (Vol,V), Int. Telecomm Union, Geneva, 331- 373.
- Chalmers, J.A. 1967. Atmospheric electricity, Clarendon press, Oxford.
- Chebil, J. and Rahman T. A. 1999. Development of 1-minute rain rate contour maps for microwave application in Malaysia Peninsula, *Electronic Letters*, Vol. 35, 1712-1774.
- Cheng, S.J., Hsieh, H.H. and WangY.M. 2007. Geostatistical interpolation of space-time rainfall on Tamshui River Basin, Taiwan, *Hydrological Processes*, vol.21 (23): 3136–3145, 2007.
- Chittimoju, G. and Yalavarthi, U.D. 2021. A comprehensive review on millimeter waves applications and antennas. *Journal of physics: conference series*. 1804 (2021) 012205. doi:10.1088/1742-6596/1804/1/012205.
- Crane, R.K. (1996): *Electromagnetic Wave Propagation through Rain*, John Wiley, New Yk, 1996, Chapter 1, 2, 3, 4.
- Das D. and Maitra A. 2015. Rain attenuation prediction during Rain evens in different climatic regions. *Journal of Atmospheric and Solar-Terrestrial Physics*, 128: 1-7.
- Da Silva Mello, L.A.R., M.S. Pontes, R.M. De Souza, P. Garcia .2007. Prediction of rain attenuation in terrestrial links using full rainfall rate distribution. *Electronic Letters* 43(25), 1442–1443.
- Das S., Maitra A. and Shukla. S. 2013. Diurnal variation of slant path Ka-band rain attenuation at four tropical locations in India, *Indian Journal of Radio Science*, Vol. 42: 34-41.
- Das S and Maitra A. 2010. Rain attenuation modelling in the 10-100GHz frequency using drop size distributions for different climate zones in tropical India. *Progress in Electromagnetic Research B*, vol. 25(25): 211-224. DOI: 10.2528/PIERB10072707.

- De Maagt, P.J.I., Touw S.I.E., Dijk, J., Brussaard, G., Allnutt J.E. 1993. Results of 11.2 GHz propagation experiments in Indonesia. *Electronics letters*; 29(22):1988-1990.
- De, A., and Maitra, A. 2020. Radiometric measurements of atmospheric attenuation over a tropical location. *Radio science*, 55, e2020RS007093.  
<https://doi.org/10.1029/2020RS007093>
- Diba, F.D., Afullo, T. and Alonge, A. 2016. Rainfall rate and attenuation performance analysis at microwave and millimeter bands for designing line of sight radio links in Ethiopia. *SAIEE African Research Journal*. 107. 17-29. 10.23919/SAIEE.2016.8532241.
- Doble, J. 1996. Introduction to radio propagations for fixed and mobile communications, MA: Arctech House, Boston, 1996.
- Dirks, K. N., J. E. Hay, C.D. Stow, and D. Harris. 1998. High resolution studies of rainfall on Norfolk Island part II: Interpolation of rainfall data, *Journal of Hydrology* 208, 187-193.
- Durodola, O.M., Ojo J.S. and Ajewole M.O. 2017. Characterization of Worst month Statistics for Satellite-Earth Links Performance in Tropical Regions. *Physical science International journal* 13(3): 1-9.
- Emmanuel, I., Adeyemi, B. and Adedayo, K. D. 2013. Regional variation of columnar refractivity with meteorological variables from climate monitoring satellite application facility (CM SAF) data over Nigeria. *International Journal of Physical Sciences*, Vol. 8(17), pp. 825-834.
- Ettinger, A., Golovachev, Y., Shoshanim, O., Pinhasi, G., and Pinhasi, Y. 2020. Experimental Study of Fog and Suspended Water Effects on the 5G Millimeter Wave Communication Channel. *Electronics*. 9. 10.3390/electronics9050720.
- Ette, A.I.I. and Ladiran, E.O. 1980. Characteristics of rain electricity in Nigeria II – Experimental and theoretical relations. *Pageoph* volume 118 (1980), Birkhauser verlag, Basel. 765- 773.
- Fashuyi, M.O. and Afullo T.J. 2007. Rain attenuation prediction and modelling for line of sight links on terrestrial paths in South Africa. *Radion Science*, vol. 42, doi:10.1029/2007RS003618.

- Fashuyi, M.O., Owolawi, P.A. and Afullo T.J. 2007. Rainfall rate modelling for LOS radio systems in South Africa. South African Institute of Electrical Engineering, vol. 97 (1), p. 74-81.
- Federal Communications Commission (FCC). 1997. Millimeter Wave Propagation: Spectrum Management Implications. Bulletin Number 70.
- Flavin, R.K. 1981. Rain attenuation considerations for satellite paths. *Report No. 7505*, Telecom Australia Research Laboratories.
- Goodale, C. L., J. D. Aber, and S.V. Ollinger. 1998. Mapping monthly precipitation, temperature, and solar radiation for Ireland with polynomial regression and a digital elevation model, *Climate Research* 10, 35 – 49.
- Green, H. E. 2004. Propagation impairment on Ka-band SATCOM links in tropical and equatorial regions, *IEEE Antennas Propag. Mag.*, 46 ( 2), 31– 44.
- Habib, E., Lee G., Kim D. ,and Ciach Grzegorz J. 2010. Ground-Based Direct Measurement. Geophysical Monograph Series 191 Copyright 2010 by the American Geophysical Union. 10.1029/2010GM000953
- Halit, A., Alper S. A. and Fazli, O. 2011. Evaluation of topographical and geographical effectson some climatic parameters in the Central Anatolia Regionof Turkey. *International Journal of Climatology* 31: 1264 – 1279 (2011), DOI: 10.1002/joc.2154
- Hall, M.P.M., Barclay, L.W. and Hewitt, M.T. 1996. *Propagation of Radiowaves*, IEEE, London United kingdom, Chapter 1 and Chapter 4.
- Han, C., Huo, J., Gao, Q., Su, G., and Wang, H. 2020. Rainfall Monitoring Based on Next Generation Millimeter-Wave Backhaul Technologies in a Dense Urban Environment. doi:10.3390/rs12061045. Retrieved January 29, 2020, from <https://www.mdpi.com/journal/remotesensing>.
- Hassan, M., Adel A. and Mohammed, A. .1985. Rain Measurements for MM Wave Propagation: A Review. *Journal of. Engineering, Science, King Saud University* Vol. 11 (2), 179-200.
- He, S. and Huang, Y. (2019). An Introduction on Millimeter Wave Communications. In Wiley 5G Ref (eds R. Tafazolli, C.-L. Wang and P. Chatzimisios). <https://doi.org/10.1002/9781119471509.w5GRef080>
- Hogg, D.D. and Chu, T.S. 1975. The role of rainfall satellite communications, *Proc IEEE (USA)*, 63, 1308.

- Hossain, S. 2014. Rain Attenuation Prediction for Terrestrial Microwave Link in Bangladesh. *Journal of Electrical and Electronics Engineering*, Volume 7, Number 1, May 2014.
- Hutchinson, M.F.1998. Interpolation of rainfall data with thin plate smoothing splines—part I: two dimensional smoothing of data with short range correlation. *Journal of Geographic Information and Decision Analysis*, vol. 2, pp. 139–151, 1998.
- Ibe, O. and Nymphas, E.F. 2010. Temperature variations and their effects on rainfall in Nigeria. *Global Warming, Green Energy and Technology*. Published by Springer Science + Business Media. <http://www.springerlink.com/content/rx58w57487544021/.di>
- Ippolito, Jr. L.J. 1986. “*Radio wave propagation in satellite communication*”. Third Ed., Van Nostrand Reinhold Company, New York.
- Isikwue, B. C., Ikoyo, A. H and Utah, E.U. 2013. Analysis Of Rainfall Rates And Attenuations For Line – Of –Sight Ehf / Shf Radio Communication Links Over Makurdi, Nigeria. *Research Journal of Earth and Planetary Sciences* Vol. 3(2) pp. 60 – 74.
- Ito, C. and Hosoya, Y. 2006. Proposal of a global conversion method for different integration timerain rates by using M distribution and regional climatic parameters, *Electronics and Communications in Japan*, Part 1, Volume 89 (4).
- ITU-R 841-6. 2019. *Conversion of annual statistics to worst month statistics*, International Telecommunication Union, Geneva, Switzerland. Retrieved March 20, 2020 from <https://www.itu.int/rec/R-REC-P.841/en>.
- ITU-R 838-3. 2005. *Specific attenuation model for rain for use in prediction methods*, International Telecommunication Union, Geneva, Switzerland. Retrieved September 5, 2016 from [https://www.itu.int/dms\\_pubrec/itu-r/rec/p/R-REC-P.838-3-200503-I!!PDF-E.pdf](https://www.itu.int/dms_pubrec/itu-r/rec/p/R-REC-P.838-3-200503-I!!PDF-E.pdf).
- ITU-R 530-17. 2017. Prediction methods and Propagation data required for the design of terrestrial line of sight systems. International Telecommunication Union, Geneva, Switzerland. Retrieved March 15, 2019 from <https://www.itu.int/rec/R-REC-P.530-17-201712-I/en>.
- ITU-R 837-7. 2017. Characteristics of Precipitation for Propagation Modelling, *International Telecommunication Union*,

- Geneva, Switzerland. Retrieved May 10, 2018 from [https://www.itu.int/dms\\_pubrec/itu-r/rec/p/R-REC-P.837-7-201706-I!!PDF-E.pdf](https://www.itu.int/dms_pubrec/itu-r/rec/p/R-REC-P.837-7-201706-I!!PDF-E.pdf)
- ITU-R 581-2. 1990. The concept of worst month, *International Telecommunication Union*, Geneva, Switzerland. Retrieved June 5, 2017 from [https://www.itu.int/dms\\_pubrec/itu-r/rec/p/R-REC-P.581-2-199006-I!!PDF-E.pdf](https://www.itu.int/dms_pubrec/itu-r/rec/p/R-REC-P.581-2-199006-I!!PDF-E.pdf).
- ITU-R 311-17. 2017. Acquisition, presentation and analysis of data in studies of radiowave propagation. International Telecommunication Union, Geneva, Switzerland. Retrieved May 3, 2021 from [https://www.itu.int/dms\\_pubrec/itu-r/rec/p/R-REC-P.311-17-201712-I!!PDF-E.pdf](https://www.itu.int/dms_pubrec/itu-r/rec/p/R-REC-P.311-17-201712-I!!PDF-E.pdf).
- ITU-R 1520-3. 2011. Radio frequency arrangements for systems in the fixed service operating in the band 31.8-33.4GHz . International Telecommunication Union, Geneva, Switzerland. Retrieved May 3, 2021 from <https://www.itu.int/rec/R-REC-F.1520-3-201104-I/en>.
- Ivanovs, G. and D. Serdega .2006. Rain Intensity Influence on Microwave Line Payback Terms, *Electronic and Electrical Engineering*, ISSN 1392-1215, Nr.6(70).
- Joo, H. L., S. K. Yang, H. K. Jong, and S. C. Yong .2002. Empirical conversion process of rain rate distribution for various integration times," *Proc. URSI Commission F Wave Propagation and Remote Sensing*, 1450-1454, Maastricht.
- Joss J., Thams J.C. and Waldvogel A. 1968.The variation of raindrop size distribution at Lorano, Switzerland. *Proc. Int. Conf. On cloud Physics*, Toronto, Canada, pp.369-3.
- Juneja, S., Pratap, R. and Rajnish Sharma, R. 2021. Semiconductor technologies for 5G implementation at millimeter wave frequencies – Design challenges and current state of work, *Engineering Science and Technology, an International Journal* 24. 205-217. <https://doi.org/10.1016/j.jestch.2020.06.012>.
- Karipidis, K., Mate, R., Urban, D. 2021. 5G mobile networks and health—a state-of-the-science review of the research into low-level RF fields above 6 GHz. *J Expo Sci Environ Epidemiol* (2021). <https://doi.org/10.1038/s41370-021-00297-6>
- Karmakar, P.K., Sengupta, L. Maiti, M. and Angelis, C. F. 2010. Some of the atmospheric influences on microwave propagation through atmosphere.

American Journal of Scientific and Industrial Research, vol. 1 (2): 350-358.  
DOI: [10.5251/ajsir.2010.1.2.350.358](https://doi.org/10.5251/ajsir.2010.1.2.350.358)

- Kestwal, C.K., Joshi, S. and Garia, L.S. 2014. Prediction of rain attenuation and impact of rain in wave propagation at microwave frequency for tropical region (Uttarakhand, India), *International Journal of Microwave Science and Technology*, Volume 2014, article 958498, 6 pages.
- Lam, K.C. Bryant R.G and Wainright J. 2015. Application of spatial interpolation method for estimation of the spatial variability of rainfall in semi-arid new front Mexico, USA. *Mediterranean Journal of social Sciences*, Vol. 6 (4), S3.
- Lam, H.Y., Luini L., Din J., Alhilali M.J., Jong S.L. and Cuervo F. 2017. Impact of Rain Attenuation on 5G millimeter wave communication systems in equatorial Malaysia investigated through disdrometer data. *IEEE: 2017 11th European Conference on Antennas and Propagation (EUCAP)*. DOI: 10.23010/EUCAP.2017.7928616.
- Lavergnat, J. and Gole, P. 1998. A stochastic raindrop time distribution model. *American Meteorological society*, p.805-818.
- Lee, Y.H. and Winkler, S. 2011. Effects of rain attenuation on satellite video transmission, *Conference proc. IEEE 73rd Vehicular Technology conference: VTC 2011*, DOI: 10.1109/VETECS.2011.5956732
- Liebe, H.J., Takeshi, M., George, A. H. 1989. Millimeter wave attenuation and delay rates due to fog/cloud conditions, *IEEE: transactions on antennas and propagation*, 37(12).
- Lin, D.P. and Chen, H.Y. 2001. Volume integral equation solution of extinction cross section by raindrops in the range 0.6 – 100GHz, *IEEE: transactions on antennas and propagation (USA)*, 49: 494.
- Lin, D. P. and H. Y. Chen 2002. An empirical formula for the prediction of rain attenuation in frequency range 0.6–100 GHz, *IEEE: transactions on antennas and propagation*, 50(4): 545–551.
- Lutgens, F. K. and Tarbuck, E. J. *The Atmosphere 8<sup>th</sup> Edition*:  
Retrieved October, 2013, from  
[http://www.ux1.eiu.edu/~cfjps/1400/atmos\\_origin.html](http://www.ux1.eiu.edu/~cfjps/1400/atmos_origin.html)
- Lv, Y., Yin, X. , Zhang, C. and Wang, H. 2019. Measurement-based characterization of 39 GHz millimeter-wave dual-polarized channel under foliage loss

impact. *IEEE Access*. 7: 151558-151568. Doi:  
10.1109/ACCESS.2019.2945042.

- Magono, C. 1954. On the shape of water drops falling in stagnant air. *J. Meteorol.* 11,77–79.
- Mair, A. and Fares, A. 2011. Comparison of rainfall interpolation methods in a mountainous region of a tropical island. *Journal of Hydrologic Engineering*, vol.16,no.4,pp.371–383,2011.
- Mandeep, J.S. and J.E. Allnutt .2007. Rain attenuation predictions at ku-band in South East Asia countries, *Progress in Electromagnetic Research*, 76, pp. 65-74.
- Mandeep, J.S., Syed S.H., Kenji T. and Mitsuyoshi L. 2006. Rainfall rate conversions in South East Asia Countries., *International J. Infrared Milli. Waves*, vol. 27, p. 1655-1666.
- Mandeep, J.S. 2011. Comparison of rain rate models for equatorial climate in South East Asia. *GEOFIZIKA* vol. 28.p. 265 – 274.
- Mandeep, J.S. and Hassan S.I.S. 2008. Performance existing rain rate models in equatorial region. *Journal of geophysical research*. Vol. 113, D11113, doi: 10.1029/2007JD009737.
- Mandeep, J.S. 2009. Rain attenuation statistics over a terrestrial link at 32.6 GHz at Malaysia. *IET Microwave Antennas Propagation*., pp. 1086–1093, Vol. 3, Iss. 7.
- Mätzler, C. 2002b. Drop-size distributions and Mie computations for rain, *IAP Research Report No. 2002-16*, Uni. Bern, Switzerland, November.
- Medeiros, Filho, F. C., R. S. Cole, and A. D. Sarma.1986. Millimeter-wave rain induced attenuation: Theory and Experiment, *IEE Proc. Part H, Microwave Antennas Propagation*, 133(4): 308 –314.
- Medhurst, R. G. 1965. Rainfall attenuation of centimeter waves: Comparison of theory and measurements, *IEEE Trans. on Antennas Propag*, 13(4), 550–564.
- Melloda Silva, L. A. R.,Pontes, M. S. and. de Souza, R. S. L.2007. New method for prediction of rain attenuation in terrestrial links using concept of effective rainfall rate, *In Proc. Microwave Opt. Conf.*, pp. 899 – 901, Brazil.
- Migliora, C.G.S., Pontes, M.S. and Silva Mello, L.A.R.1990. Rain rate and attenuation measurements in Brazil. ;*RSI Commission F. Open Symposium on Regional*

- Factors in Predicting Radiowave Attenuation due to Rain*, Rio de Janeiro, Brazil, ; 8-13.
- Moron, V. and Robertson, A.W. 2020. Tropical rainfall subseasonal-to-seasonal predictability types. *npj Climate and Atmospheric Science* **3**, 4.  
<https://doi.org/10.1038/s41612-020-0107-3>.
- Moupfouma, F. 1985. Model of rainfall-rate distribution for radio system design," *IEEE Proceedings*, Vol. 132, Pt. H, No. 1, p.39– 43.
- Moupfouma, F. and L. Martin.1995. Modelling of the rainfall rate cumulative distribution for the design of satellite and terrestrial communication systems," *Int. J. of Satellite Comm.*, Vol. 13, No. 2, 105–115.
- Moupfouma, F. 1987. Rainfall-rate distribution for radio system design," *IEE Proceedings*, Vol. 134, Pt. H, No. 6, 527-537.
- Moupfouma, F. 1984. Improvement of a Rain Attenuation prediction Method for Terrestrial Microwave Links. *IEEE Transactions on Antennas and Propagation*, Vol. AP-32, No. 12, December, pp. 1368-1372
- Mulangu, C.T. 2008. Rain Attenuation Modelling for Southern Africa . M.Sc. Thesis. School of Electrical, Electronic and Computer Engineering, University of Kwazulu-Natal, South Africa.
- Nakamura, K., Iwasawa, N., Kawasaki, K., Yoshida, S. and Masaharu Takahashi, M. 2020. The attenuation characteristics of millimeter-wave by snow accretion. *IEICE Communications Express*, Vol.9, No.12, p.674–678.
- Nandi, D. and Maitra, A. 2019. Effects of Rain on millimeter wave communication for tropical region, URSI AP-RASC 2019. New Delhi, India, Retrieved October, 2013, from  
[ursi.org/proceedings/procAP19/papers2019/ManuscriptDaliaAPRASC2019.pdf](http://ursi.org/proceedings/procAP19/papers2019/ManuscriptDaliaAPRASC2019.pdf)
- NCC .2018. Retrieved April, 2018, from  
[www.ncc.gov.ng/technology/spectrum/frequency-allocation](http://www.ncc.gov.ng/technology/spectrum/frequency-allocation)
- Nespor, V., and B. Sevruk.1999. Estimation of wind-induced error of rainfall gauge measurements using a numerical simulation, *J. Atmos. Oceanic Technol.*, 16, 450–464.



- Norouzian, F., Marchetti, E., Gashinova M., Hoare, E., Constantinou, E., Gardner, P. 2020. Rain Attenuation at Millimeter Wave and Low-THz Frequencies. *IEEE Transactions on Antennas and Propagation*, vol. 68, no. 1, p. 421-431, Jan. 2020, doi: 10.1109/TAP.2019.2938735.
- Obiyemi, O.O., Ojo, J.S. and Ibiyemi, T.S. 2014. Performance analysis of rain rate models for microwave propagation designs over tropical climate. *Progress in Electromagnetic Research M*. vol. 39:115-122.
- Oguchi, T. 1973. Attenuation and phase rotation of radio waves due to Rain: Calculation at 19.3 and 34.8 GHz, *Radio Sci. J.*, 8(1), 31 – 38.
- Ojo, J. S., Ajewole, M. O. and Sarkar, S. K. 2008. Rain rate and attenuation prediction for satellite communication in *Ku* and *Ka* bands over Nigeria. *Progress in Electromagnetic Research B*, vol. 5: 207-223.
- Ojo, J. S. and Olurotimi, E. O. 2014. Tropical Rainfall Structure Characterization over Two Stations in Southwestern Nigeria for Radiowave Propagation Purposes. *Journal of Emerging Trends in Engineering and Applied Sciences (JETEAS)* 5(2): 116-122.
- Ojo, J. S and Falodun, S. E. 2012. NECOP Propagation Experiment: Rain-rate Distributions Observations and Prediction Model Comparisons. *Internal Journal of Antennas and Propagation*, Vol.2012, Pages 4, Article ID 913596.
- Ojo, J.S, Adenugba, A.K. and Adediji, A.T. 2016. Dynamical Model for Deriving 1-Min Rain Rate from Various Integration Times in a Tropical Region. *Journal of Telecommunications System & Management*, Volume 5 • Issue 1 • 1000127.
- Okeke, P.N., Opara, F.E, Onuh, J. Y., Ikwelegwu, J.O., Omaliko, K.C., Okere B.I., Obasuyi, G.D., Ayatunji, B.G. and Omawa, E. 2012. Brief Profile, Centre for Basic Space Science (CBSS) Nsukka, National Space Research and Development Agency (NASRDA), Abuja, Nigeria.
- Okamura, S., Funakawa, K., Uda, H., Kato, J. and Oguchi, T. 1961, Effect of polarisation on the attenuation by rain at millimeter-wave length. *J. Radio Res. Labs. (Japan)* 8,73–80.
- Okamura S. and Oguchi T. 2010. Electromagnetic wave propagation in rain and polarisation effects. *Proceedings of the Japan Academy. Series B, Physical and Biological Sciences*. P. 539-562. Doi: 10.2183/pjab.86.539.

- Oladiran .1976. Studies on rain electricity in a tropical region.PhD thesis, Department of physics, University of Ibadan.
- Olsen, R. L. 1999. Radioclimatological modeling of propagation effects in clear-air and precipitation conditions: Recent advances and future directions, *in Proceedings of Radio Africa '99 Conference*, pp. 92 – 106, Gaborone, Botswana.
- Olsen, R. L., D. V. Rogers, and D. B. Hodge .1978. The aRb relation in the calculation of rain attenuation, *IEEE Trans. Antennas Propag.*, 26(2), 547 – 556.
- Olurotimi, E.O. and Ojo J.S. 2014. Testing rainfall rate models for rain attenuation prediction purposes in tropical climate. 10.1109/URSIGASS.2014.6929688
- Oluwadare, E. J., Tomiwa, A. C. and Ajewole, M. O. 2012. Investigation of Radiowav Propagation Impairment at Super High Frequency due to Rain in Akure. *American International Journal of Contemporary Research Vol. 2 No.10*.
- Omotosho, TV. and Oluwafemi, CO .2009. Impairment of radio wave signal by rainfall on fixed satellite service on earth–space path at 37 stations in Nigeria. *J. Atmos. Solar-Terrestrial Phys.*, 71: 830-840.
- Owolawi P. A., Afullo T. J. and Malinga S. J. 2008. Rainfall Rate Characteristics for the Design of Terrestrial Retrieve October 24, 2015, from <http://satnac.org.za/proceedings/2008/papers/access/Owolawi%20No%2035.pdf>
- Owolawi, P. A., Afullo T. J. and Malinga S. J. 2009. Effect of Rainfall on Millimeter Wavelength Radio in Gough and Marion Islands. *Progress In Electromagnetics Research Symposium, Beijing, China*, p. 91-98.
- Owolawi, P. A., Malinga, S.J. and Afullo T. J. 2012. Estimation of Terrestrial Rain attenuation at microwave and millimeter wave signals in South Africa using the ITU-R model. *Progress in Electromagnetics Research Symposium*, p. 952-962.
- Panter, P. 1972. *Communication Systems Design: Line-of-sight and Troposcatter Systems*, McGraw-Hill Inc., New York. Perlman B.S. (1995), "Millimeter-Wave Technology," A Tutorial given at the FCC, Sept. 6.
- Prassana, A. 2008. Understanding Millimeter Wave and Wireless Communication. Loea Corporation, San Diego.

- Pratt, T., Bostian, C.W., and Alnutt, J.E. 2003. *Satellite Communication*. Third Ed., Wiley: New York.
- Price, D. T., D. W. Mckenney, I. A. Nalder, M. F. Hutchinson, and J. L. Kesteven.2000. A comparison of two statistical methods for spatial interpolation of Canadian monthly mean climate data, *Agricultural and Forest Meteorology* 101, 81 – 94.
- Qamar, F., Hindia, M.N., Rahman, T.A., , Hassan, R., Dimyati, K., and Quang Ngoc Nguyen, Q.N. 2021. Propagation characterization and analysis for 5G mmWave through field experiments. *Computers, materials and continua*. 68:2249-2264. DOI:10.32604/cmc.2021.017198
- RafiqulMD, I.Yusuf, A. and Tharek A R. .2012. An Improved ITU-R Rain Attenuation Prediction Model Over Terrestrial Microwave Links In Tropical Region. *EURASIP Journal on Wireless Communications and Networking* 2012, 2012:189.<http://jwcn.eurasipjournals.com/content/2012/1/189>.
- Rajar S. and Singh M.P. 1999. Statistics of one-minute rain rate distributions in India.*Indian journal of radio and space physics*, vol. 28, p. 66-69.
- Ramakrishna K., Punyaseshudu, D. 2014. Estimation of rain induced Specific attenuation. *International Journal of Scientific Engineering and Technology*. Volume No.3 Issue No.2, pp : 144 – 146.
- Rao, P.R. 2010. Role of mm waves in Terrestrial and satellite communications. *International Journal of systems and technologies*, vol. 3, No. 1, p.25-34.
- Rappaport, T.S. 2019. *Wireless Communication and Applications above 100GHz: Opportunities and Challenges for 6G and above*. NYU Wireless for Federal Communications Commission Retrieved June, 2019, from [.https://docs.fcc.gov/public/attachments/DOC- 356643A1.pdf](https://docs.fcc.gov/public/attachments/DOC-356643A1.pdf)
- Rappaport, T.S., Xing, Y., MacCartney, G.R., Molisch, A.F., Mellios E. and Zhang, J. 2017.Overview of Millimeter wave communications for fifth-generation (5G) wireless networks-with a focus on propagation models. *IEEE Transactions on Antennas and Propagation*, special issue on 5G . Retrieved June, 2019, from <https://arxiv.org/pdf/1708.02557.pdf>
- Report on International Symposium on Rainfall Rate and Radio Wave (ISRR'07)Propagation

- Rice, P. and N. Holmberg. 1973. Cumulative time statistics of surface-point rainfall rate," *IEEE Transactions on Communications*, 1772-1774, COM-2.
- Salonen, E. T. and J. P. V. Poyares-Baptista .1997. A new global rainfall rate model," *Proceedings of the 10th International Conf.on Ant. and Propag. (Pub N 14-176-436)*, 182–185.
- Sarkar, S.K .1998. Some studies on attenuation and atmospheric water vapour measurement in India. *Int. J. Remote Sensing* 19 (3), 473–480.
- Sakir, H. 2014. Rain attenuation prediction for terrestrial microwave link in Bangladesh. *Journal of Electrical and electronics Engineering*, vol. 7, No.1. p. 63-68.
- Segal, B. 1986 .The influence of rain gauge integration time on measured rainfall-intensity distribution functions," *J. of Atmospheric and Oceanic Tech.*, Vol. 3, 662-671.
- Semire, F.A and Raji T.I. 2011.Characteristics of Measured Rainfall Rate at Ogbomoso, Nigeria for Microwave Applications.*Journal of Telecommunications and Information Technology*.P.85-89.
- Semire,F.A., Mokhtara R.M., Omotosho T.V., Ismaila W., Mohamada N., and MandeepdJ.S. 2012. Analysis of Cumulative Distribution Function of 2-year Rainfall Measurements in Ogbomoso, Nigeria.*International Journal of Applied Science and Engineering* 2012. 10, 3: 171-179.
- Sevruk, B., and W. R. Hamon .1984. International comparison of national precipitation gauges with a reference pit gauge, *Instruments and Observing Methods Rep. 17*, World Meteorological Organization, Geneva, Switzerland.
- Sevruk, B., and M. Lapin (Eds.) .1993. Precipitation measurement and quality control, *Proceedings of the International Symposium on Precipitation and Evaporation*, vol. 1, Slovak Hydrometeorological Institute, Bratislava.
- Shafi, M. ., Zhang, J., Tataria, H., Molisch, A.F., Sun, S., Rappaport, T.S., Tufvesson, F. 2018. Microwave vs. Millimeter-Wave Propagation Channels: Key Differences and Impact on 5G Cellular Systems," in *IEEE Communications Magazine*, vol. 56, no. 12, pp. 14-20. doi: 10.1109/MCOM.2018.1800255.
- Sharma, A. and Jain P. 2010. Effects of Rain on Radion Propagation in GSM. *International Journal of Advanced Engineering & Applications*, p. 83-85.

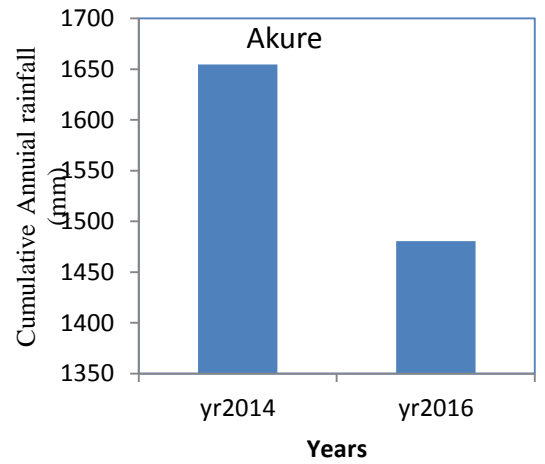
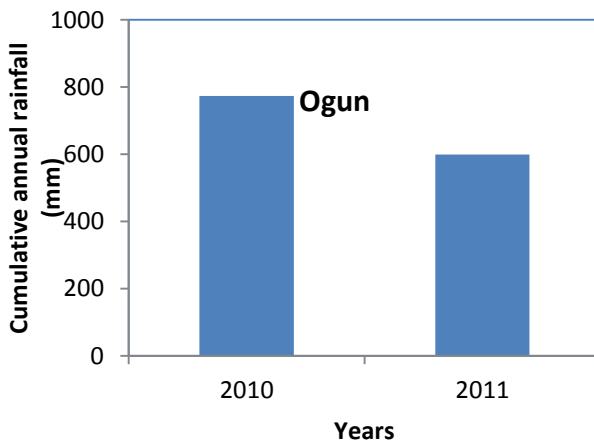
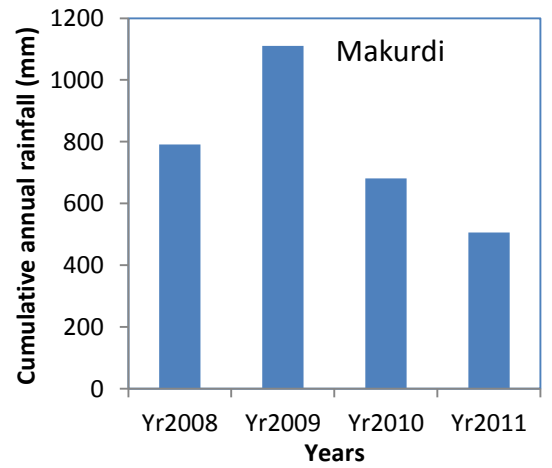
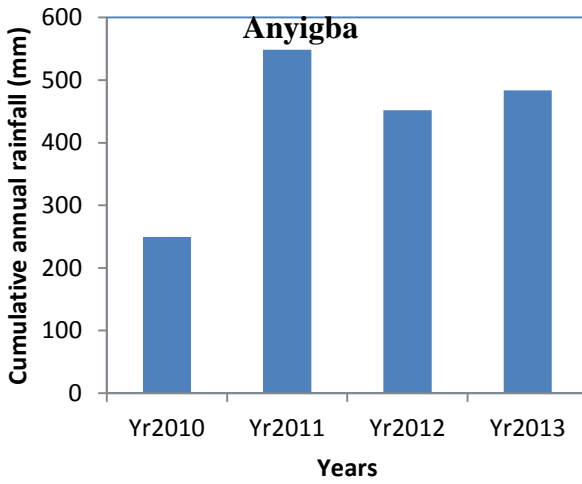
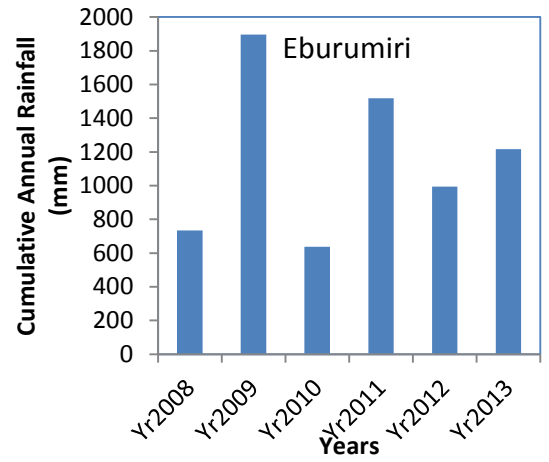
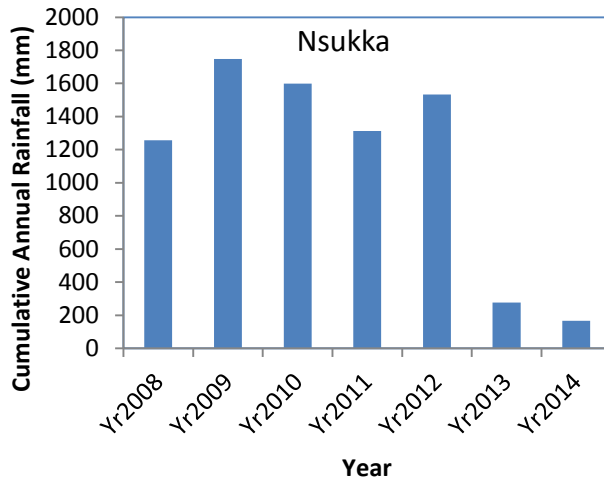
- Shayea, Ibraheem , Abd, Rahman, T., Hadri A. and Islam Md Rafiqul .2018. Real Measurement Study for Rain Rate and Rain Attenuation Conducted Over 26GHz Microwave 5G Link System in Malaysia. IEEE Access Vol.6, 2018. P. 19044 - 19064 doi 10.1109/ACCESS.2018.2810855
- Shayea I.,Tharekm A. R., Marwan, H.A. and Arsany A. 2018. Rain attenuation of millimetre wave above 10 GHz for terrestrial links in tropical regions. *Wiley Online Librara*, vol. 29, Issue 8.<https://doi.org/10.1002/ett.3450>.
- Shebani, N. M., kaeib, A. F., and Zerek A. R. 2017. Estimation of rain attenuation based on ITU-R model for terrestrial link in Libya. Retrieved April, 2018, from [www.researchgate.net/publications](http://www.researchgate.net/publications).
- Shrestha, S. and Choi D. 2017..Rain Attenuation Statistics over millimetre wave bands in South Korea.*Journal of atmosphere and solar terrestrial physics* 152, p. 1-10. <http://dx.doi.org/10.1016/j.jastp.2016.11.004>.
- Shrestha, S. and Choi, D. 2019.Rain Attenuation Studyat Ku-Band over Earth-space path in South Korea.*Hindawi Advances in Astronomy*, vol.2019, Article ID, 9538061, 12 pages<https://doi.org/10.1155/2019/9538061>.
- Siddique, U., Ahmad, L., and Raja, G. 2011. Microwave attenuation and prediction of rain outage for wireless networks in Pakistan's tropical region," *International Journal of Microwave Science and Technology*, vol. 2011,Article ID 714927, 6 pages.
- Silva, J. C., Siqueira, G. L. and Castellanos, P. V. G. 2018. Propagation Model for Path Loss Through Vegetated Environments at 700 – 800 MHz Band. *Journal of Microwaves, Optoelectronics and Electromagnetic Applications*, 17(1), p. 179-187. <https://doi.org/10.1590/2179-10742018v17i11183>.
- Simpson, G.C.1949. Atmospheric electricity during disturbed weather, *Geophys. Mem.*, London, 84, 1-51.
- Singh, H., Prasad, R. and Bonev, B. 2018. The Studies of millimetre waves at 60GHz in outdoor environment for IMT Applications: A state of art. *Wireless Personal Communications*, vol. 100, issue 2, p. 463-474.
- Skolnik, M.I. 1970 .Millimetre and sub millimetre wave applications *of the symposium on Submillimeter waves, Polytechnic Press of Poly. Institute of Brooklyn*, New York, pp9-25*Proceedings*
- Sulochana, Y., Chandrika, P. and Rao S.V.B .2014.Rain rate and rain attenuation

- statistics for different homogenous regions in India. *Indian Journal of Radio and space physics*, vol. 43, p. 303-314.
- Tattelman, P. and Scharr, K.G. 1993. A model for estimating one-minute rainfall rates. *Journal of climate and applied meteorology*.22 (13) 1575- 1579.
- Tomczak, M.1998. Spatial interpolation and its uncertainty using automated anisotropic Inverse Distance Weighting (IDW)— cross validation/Jackknife approach. *JournalofGeographic Information and Decision Analysis*,vol.2,no.2,pp.18–30,1998.
- Udoh, J., Ikotun, T., Cardwell, K. 1994. Storage systems for maize (*Zea mays* L.) in Nigeria from five agro-ecological zones. *Proceedings of the 6<sup>th</sup> International working conference on stored-product protection Canberra, Australia*, p. 960-965.
- Uwaechia, Anthony & Mahyuddin, Nor. 2020. A Comprehensive Survey on Millimeter Wave Communications for Fifth-Generation Wireless Networks: Feasibility and Challenges. *IEEE Access*. 8. 62367 - 62414. 10.1109/ACCESS.2020.2984204.
- Uzunoglu, N. K., B. G Evans, and A. R. Holt .1977.Scattering of electromagnetic radiation by precipitation particles and propagation characteristics of terrestrial and space communication systems, *IEE Proc*, 124(5), 417 – 424.
- Van de Hulst H.C. 1957. Light scattering by small particles, *New York: Wiley*.
- Wagner, A. 2009. Literature Study on the Correction of Precipitation Measurements, 29, 1–32.
- Watson, P. A., V. Sathiaselan, and B. Potter. 1981. “Development of a climatic map Weible, G.E. and Dressel, H.O. (1967).Propagation studies in millimeter wave link systems, *Proceedings of the IEEE*, 55, No.4, 497-512.
- Yang, X., Xie, X.,Liu, D.L., Ji F. and Wang L. 2015.Spatial Interpolation of Daily Rainfall Data for Local Climate Impact Assessment over Greater Sydney Region. Hindawi Publishing Corporation. Volume 2015, Article ID 563629 12 pages.
- Yussuff, A. I.O. and Nor H. H. K. 2012. Rain Attenuation Modelling and Mitigation in The Tropics: Brief Review. *International Journal of Electrical and Computer Engineering (IJECE)* Vol.2, No.6, December 2012, pp. 748-757. *Journal homepage: <http://iaesjournal.com/online/index.php/IJECE>*

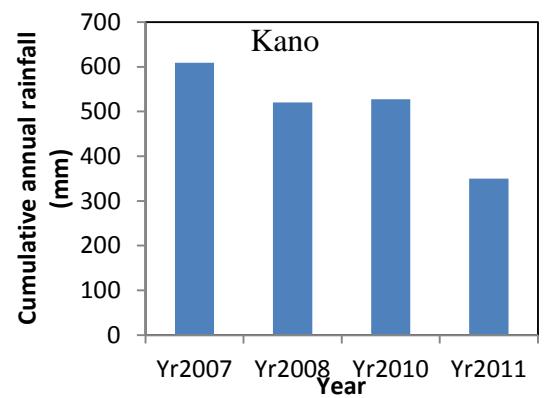
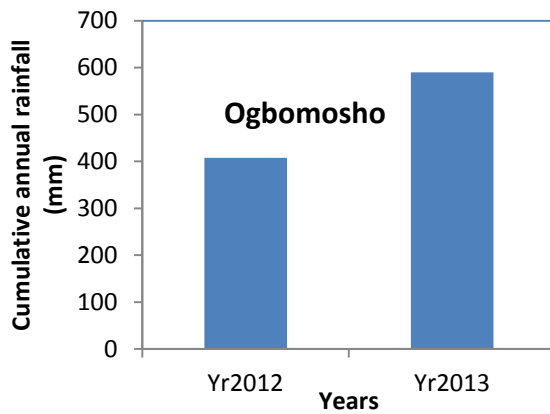
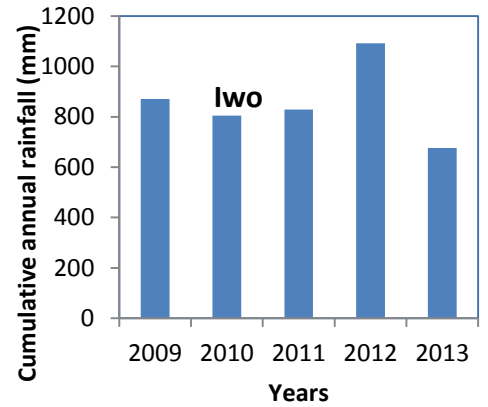
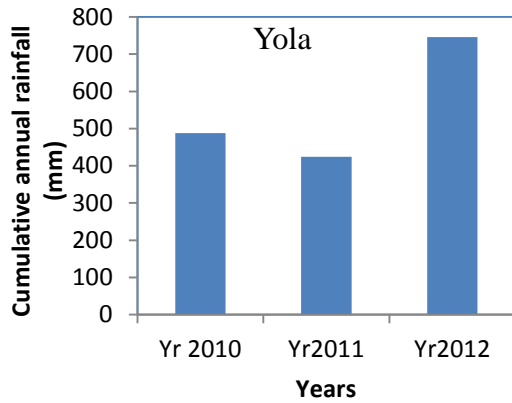
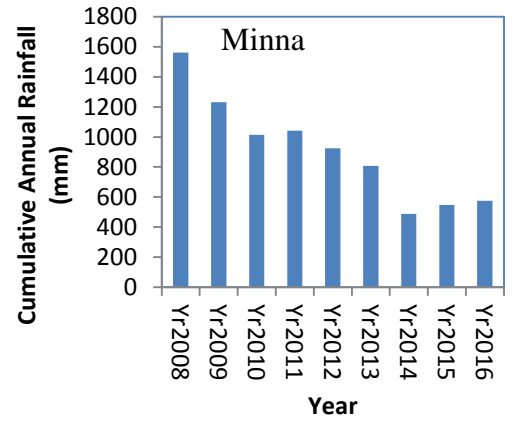
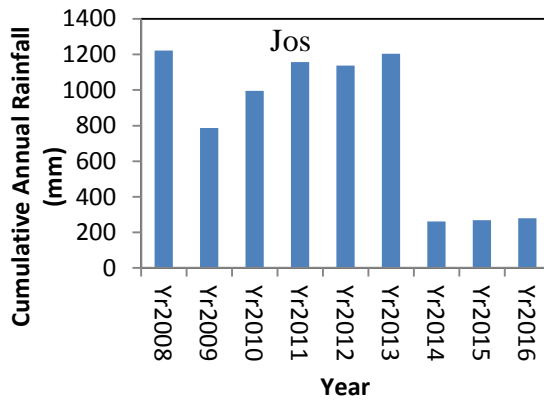
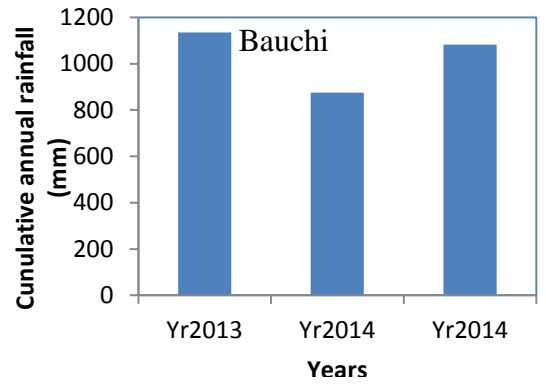
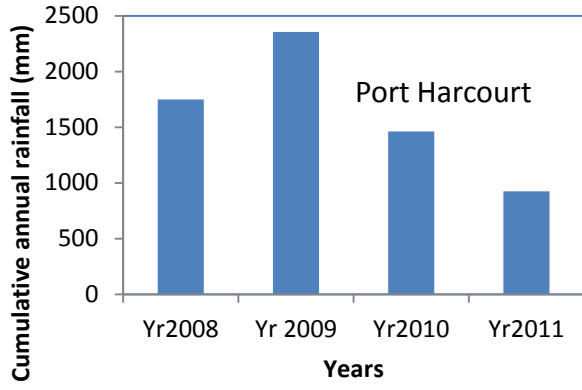
- Yussuff, A.I.O. and Nor H. H. K. 2014. Rain Attenuation Prediction Model for Lagos at Millimeter Wave Bands. *Journal of Atmospheric and Oceanic Technology* Vol.31, pp. 639- 646. DOI:10.1175/JTECH-D-13-00024-1
- Zhang, W. and N. Moayeri .1999. Power-Law Parameters of Rain Specific Attenuation, Rep. IEEE, 802.16 WG, 1 – 8.

## APPENDICES

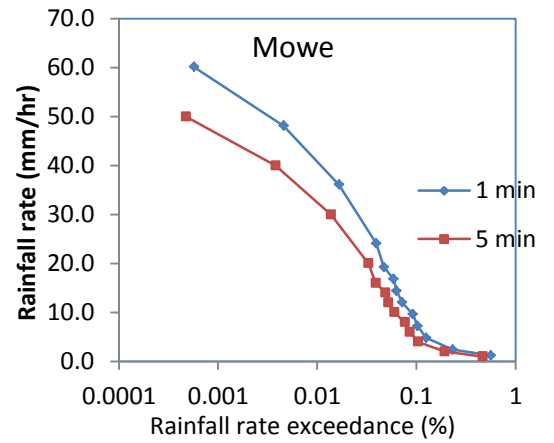
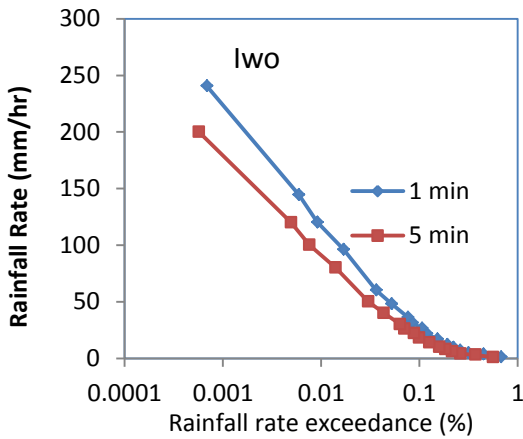
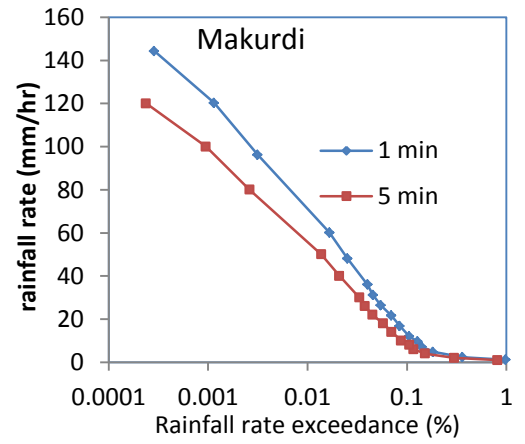
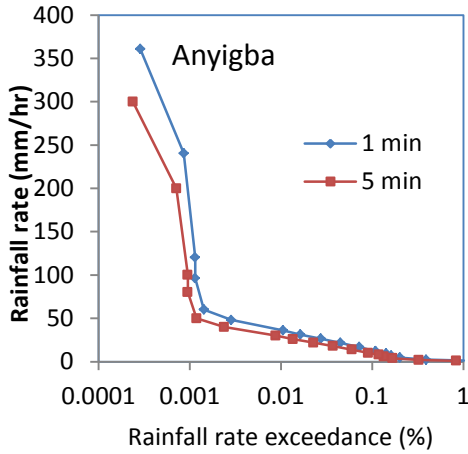
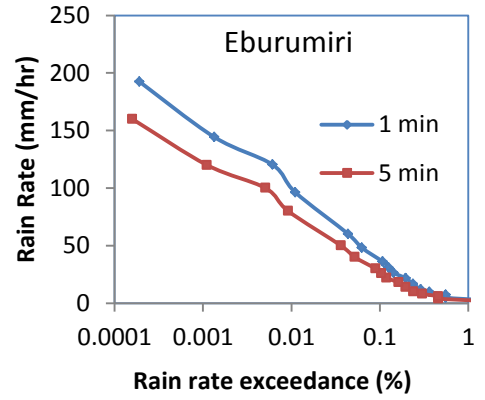
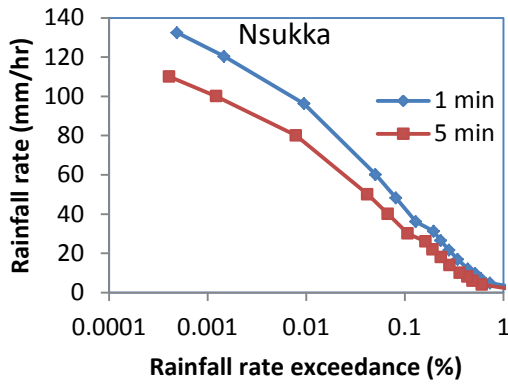
### APPENDIX 1: Annual Accumulated Rainfall at the Sites

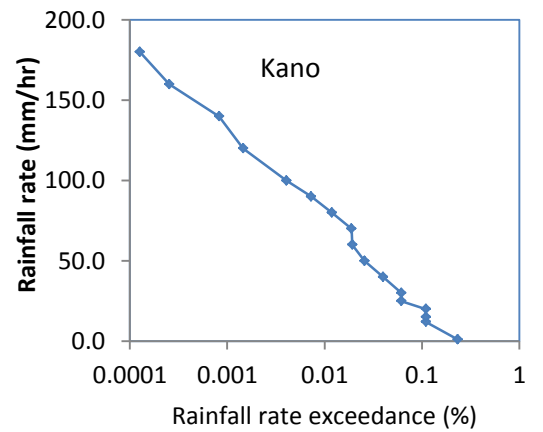
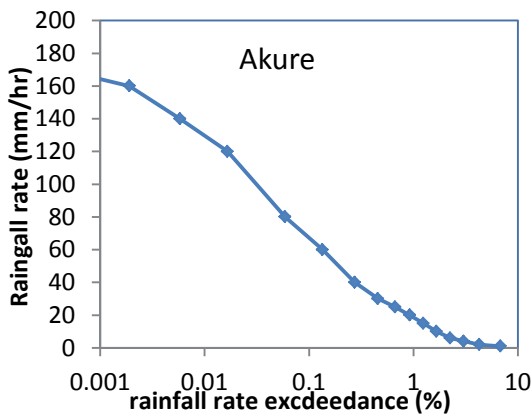
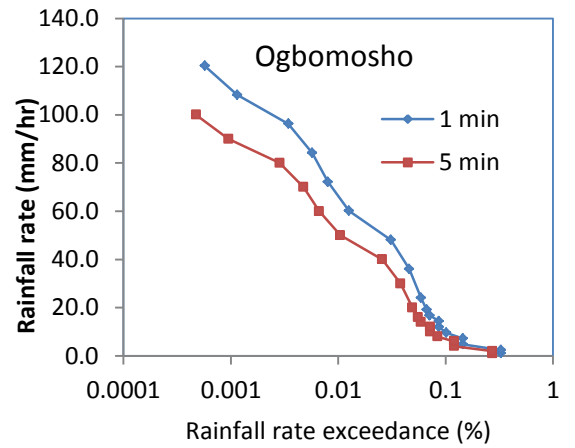
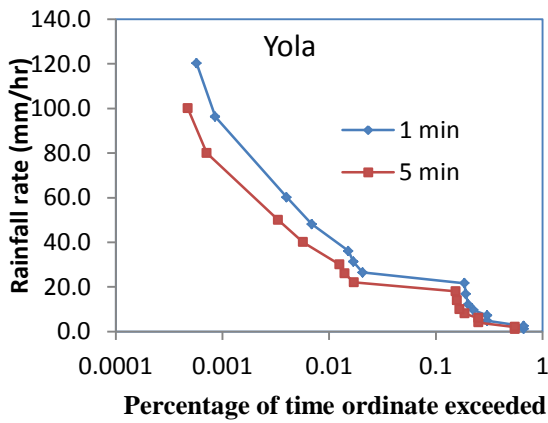
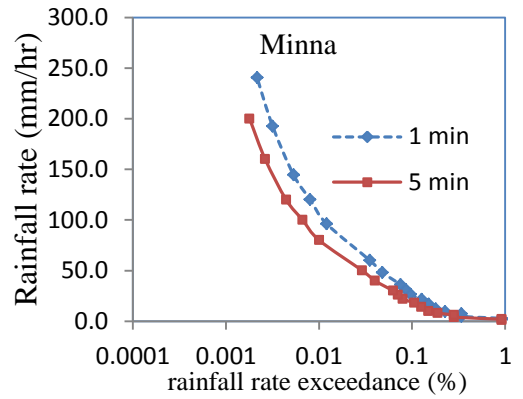
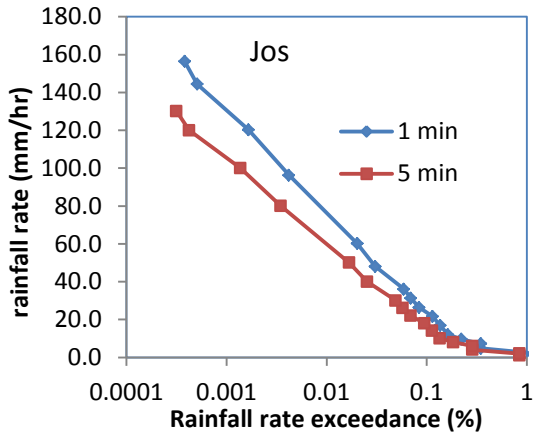
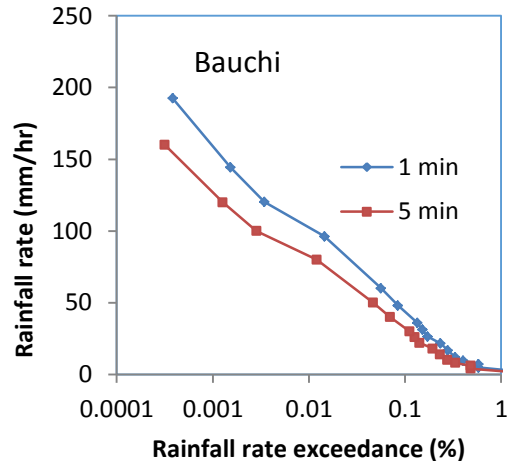
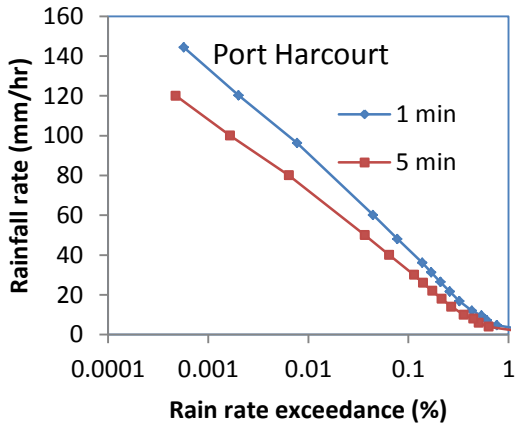




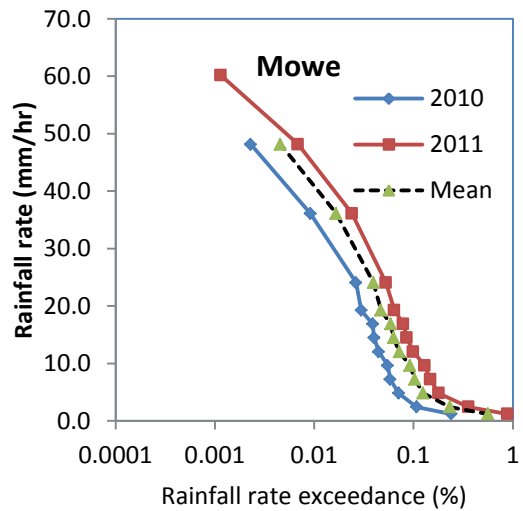
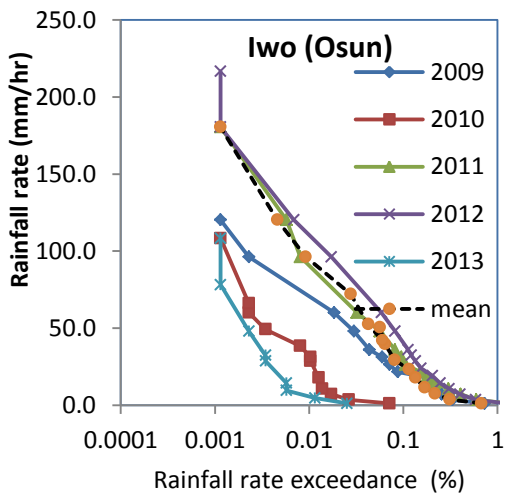
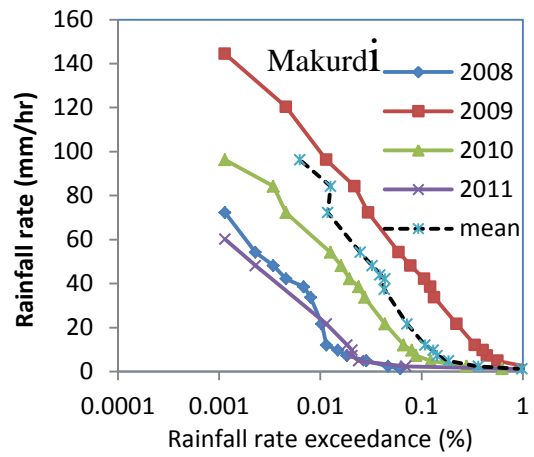
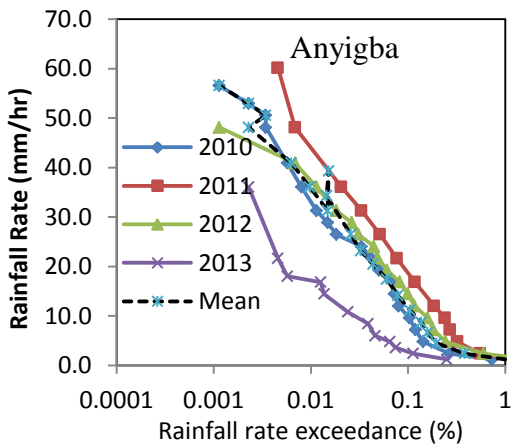
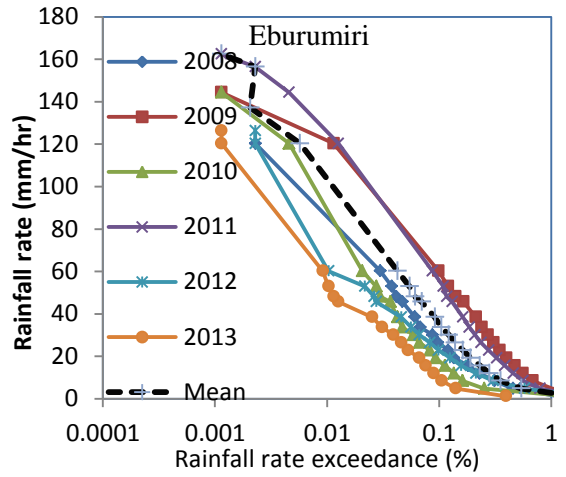
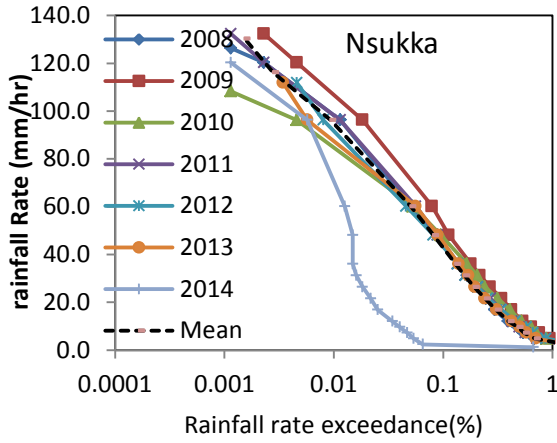


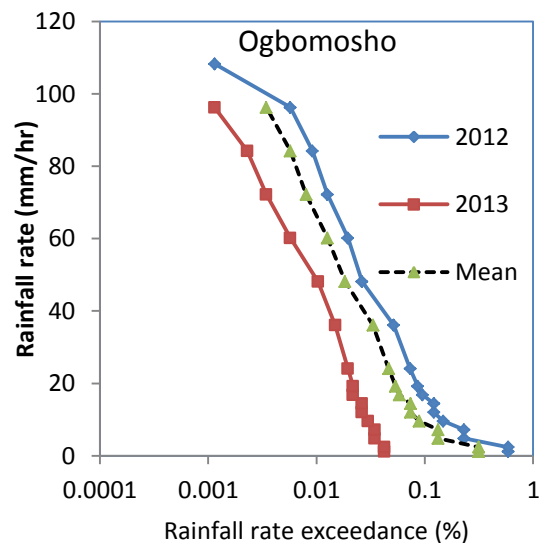
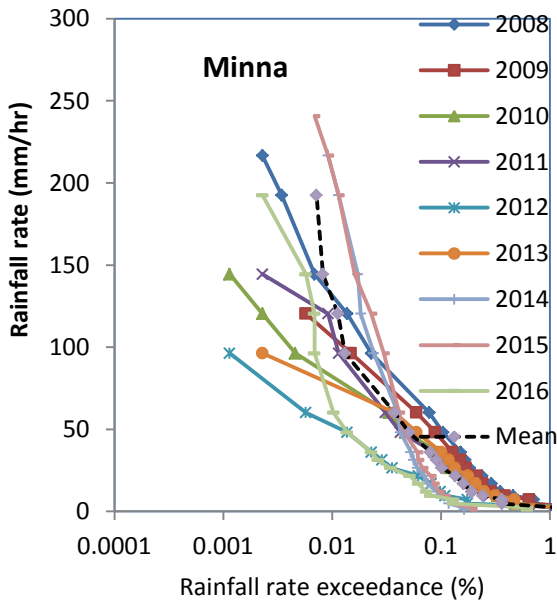
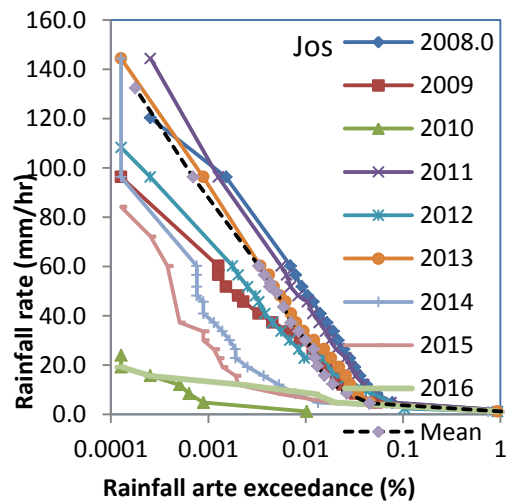
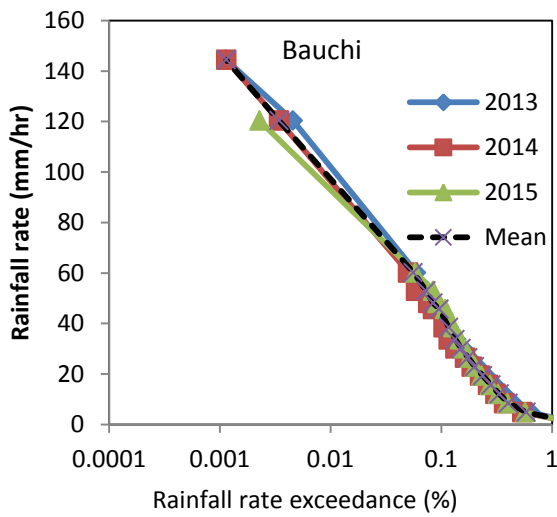
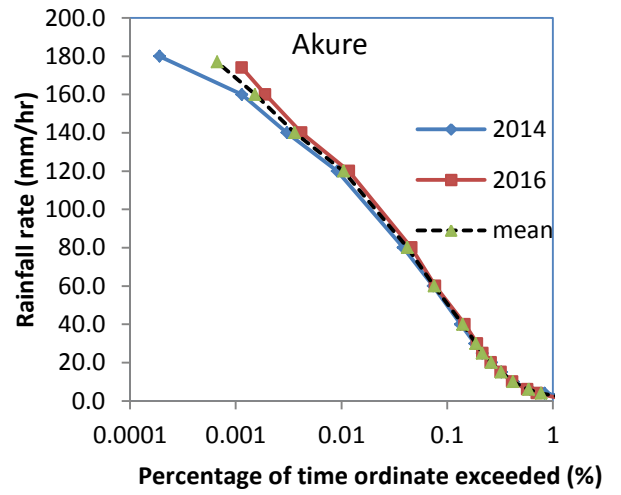
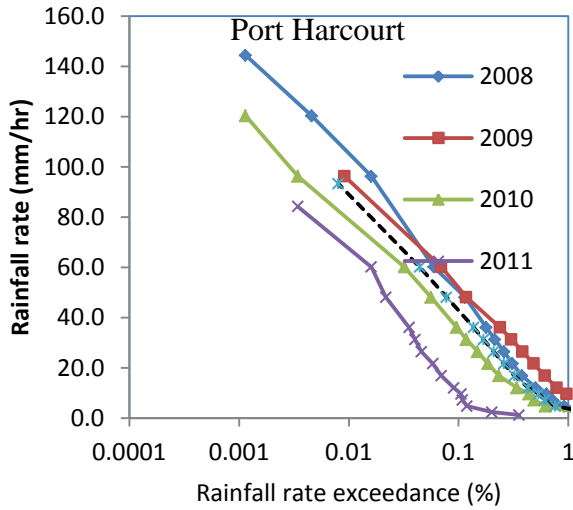
**APPENDIX 2: Cumulative distribution function (CDF) of rain rates based on different integration times**

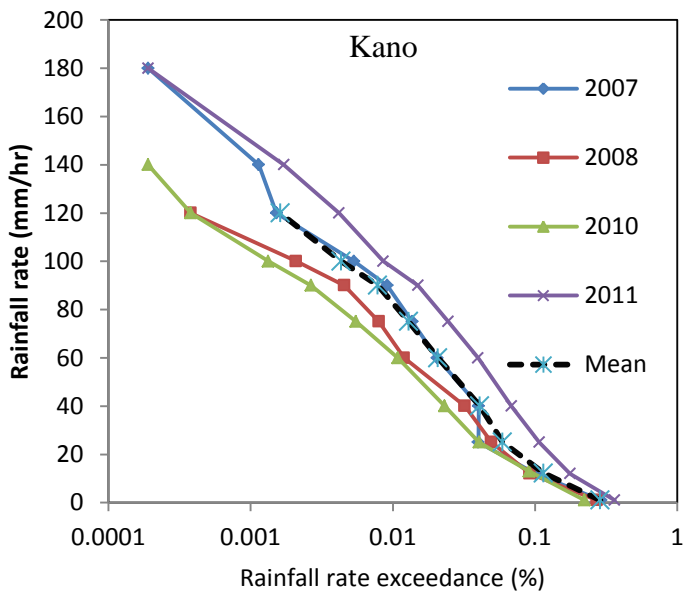
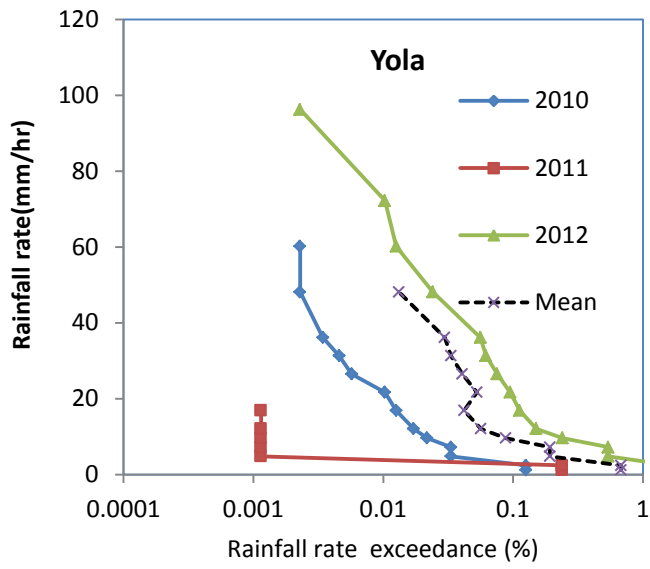




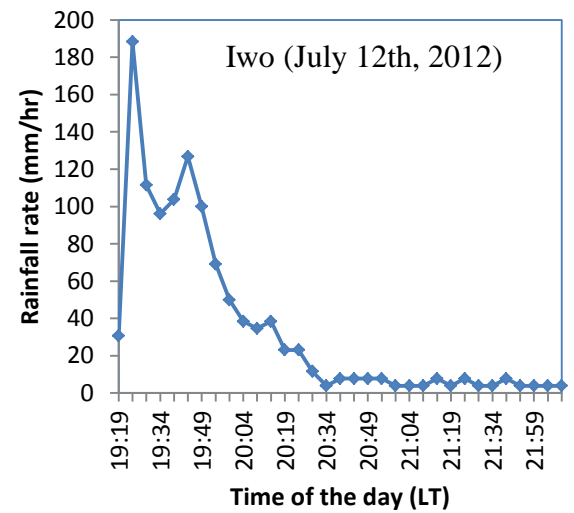
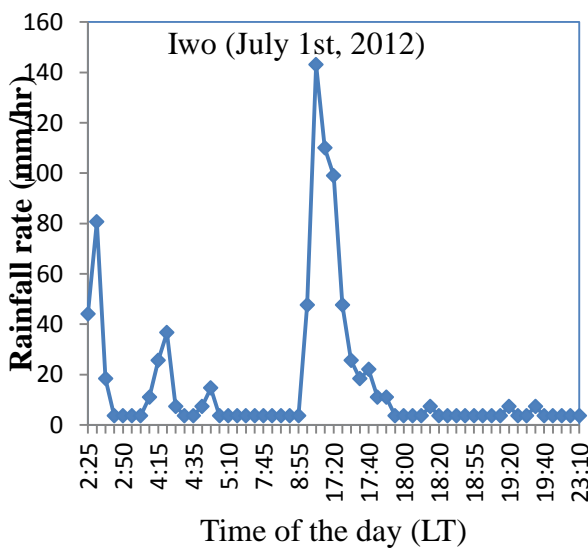
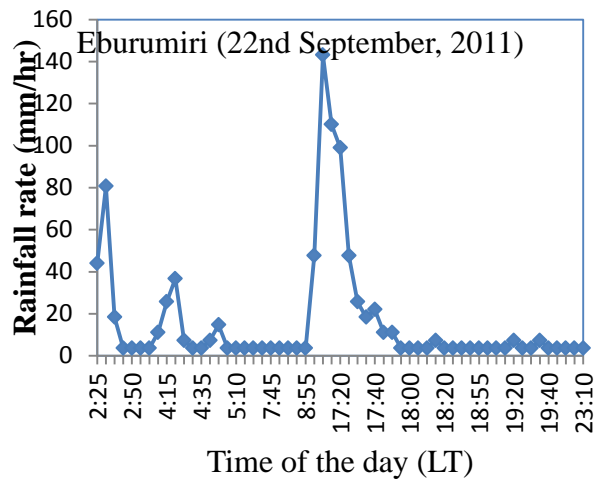
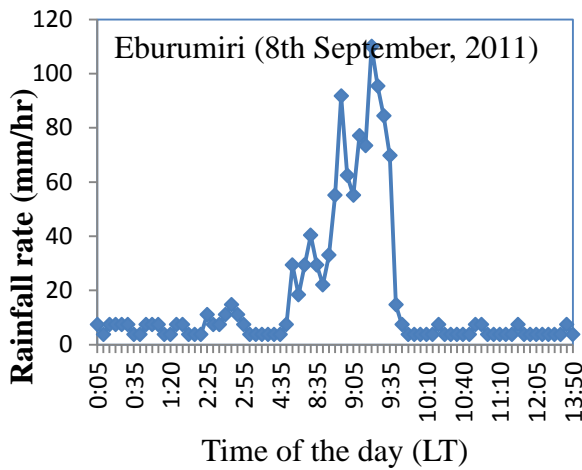
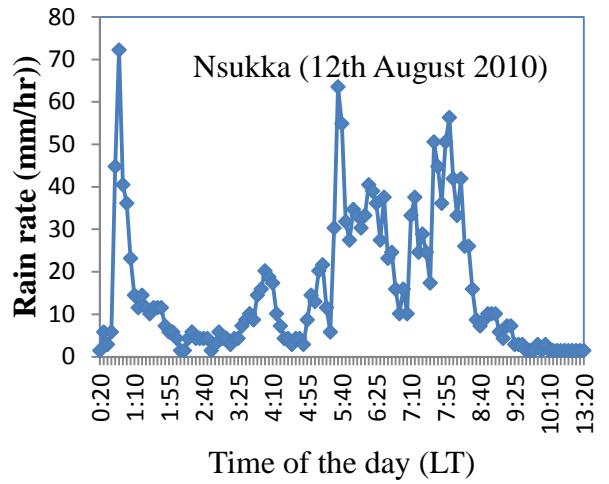
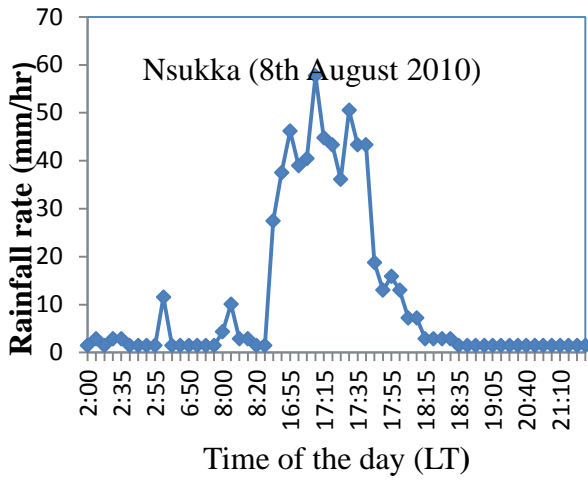
**Appendix 3: Annual cumulative distribution rainfall rates over study locations**

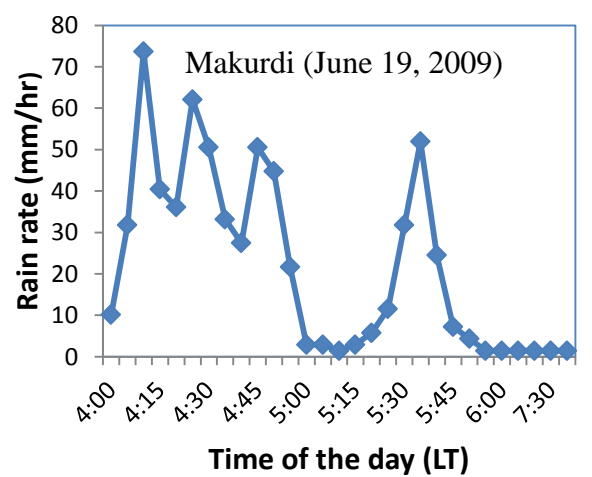
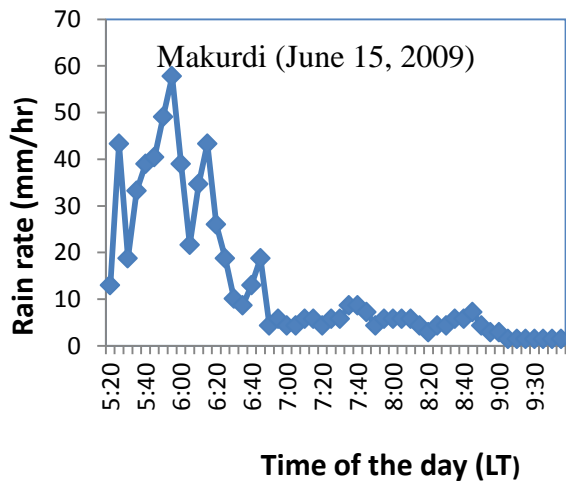
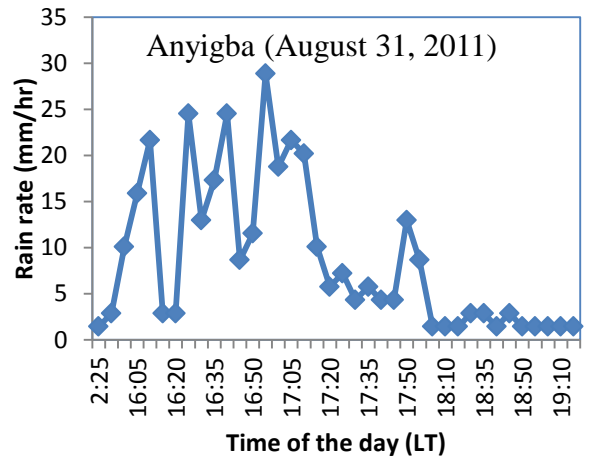
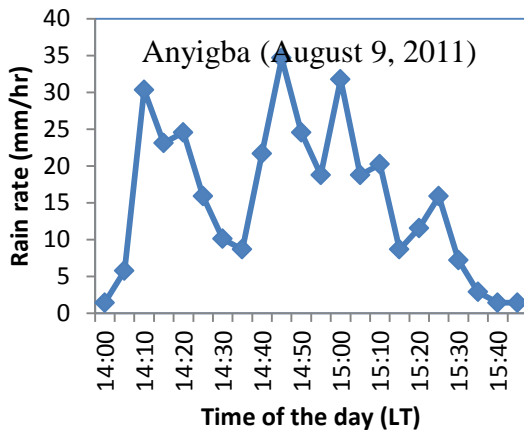
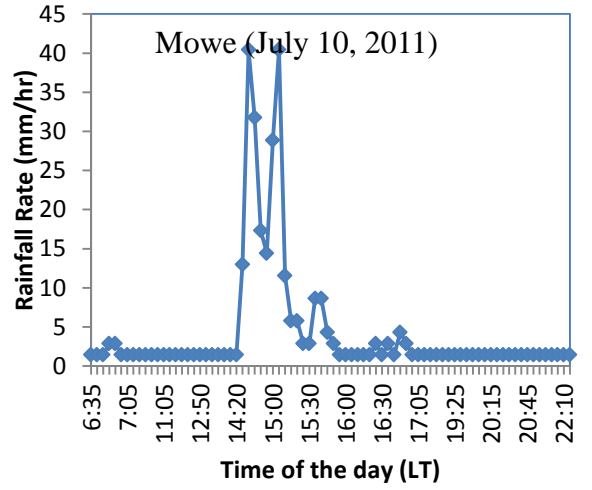
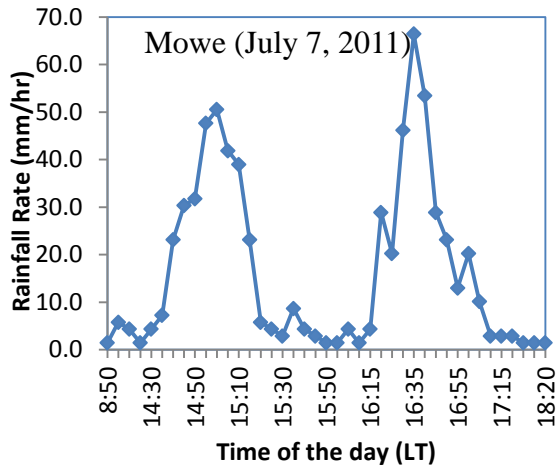




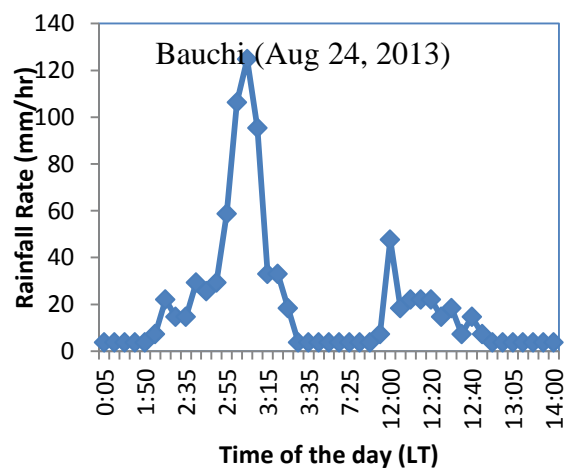
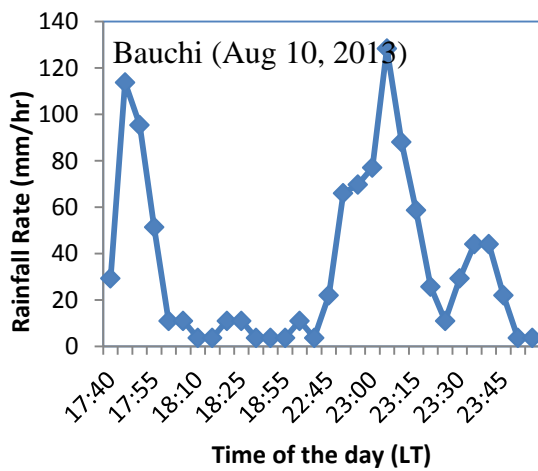
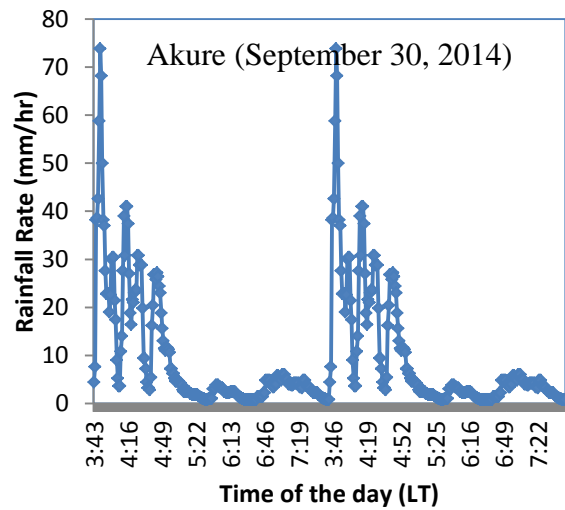
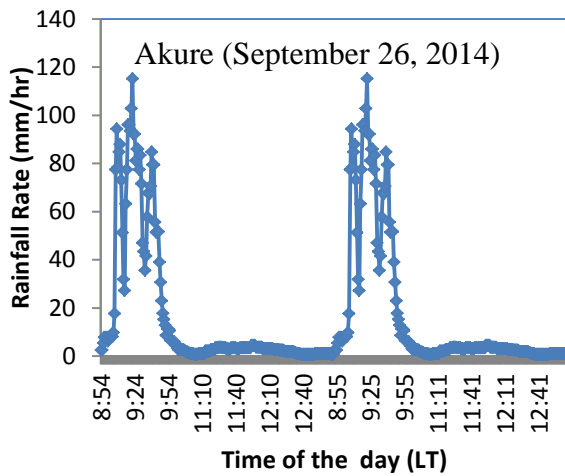
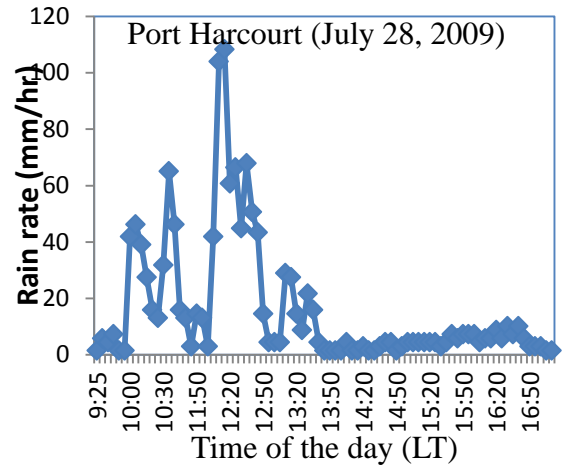
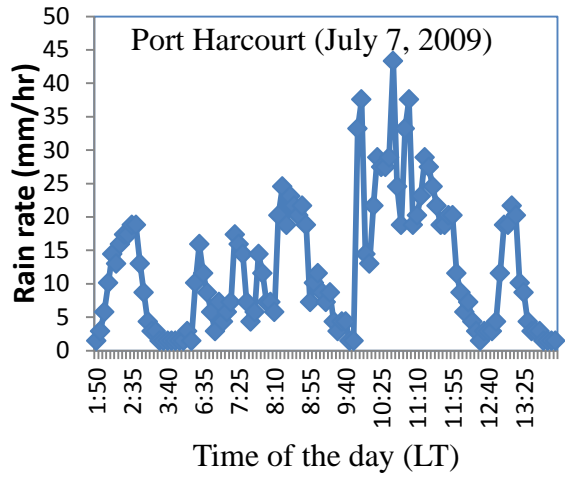


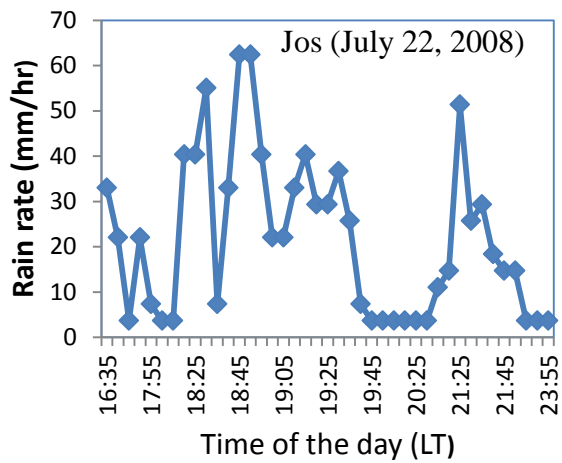
**Appendix 4: Time Series of rainfall rate during rain events**

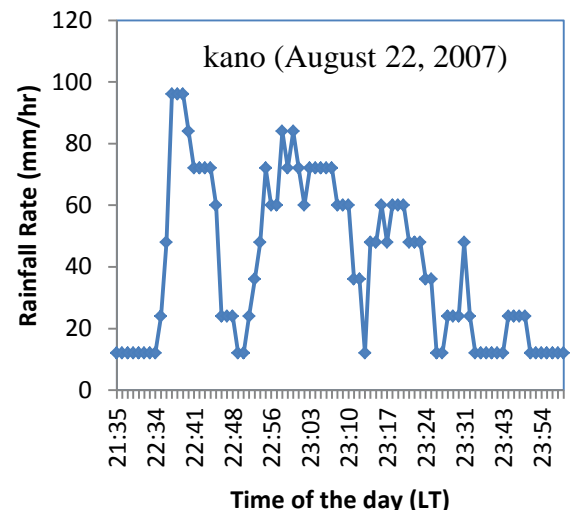
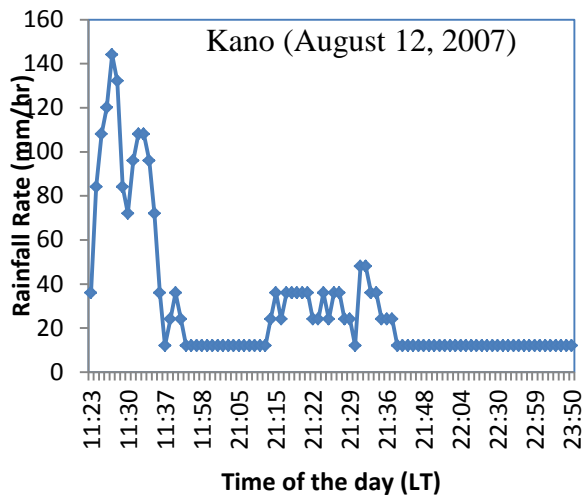
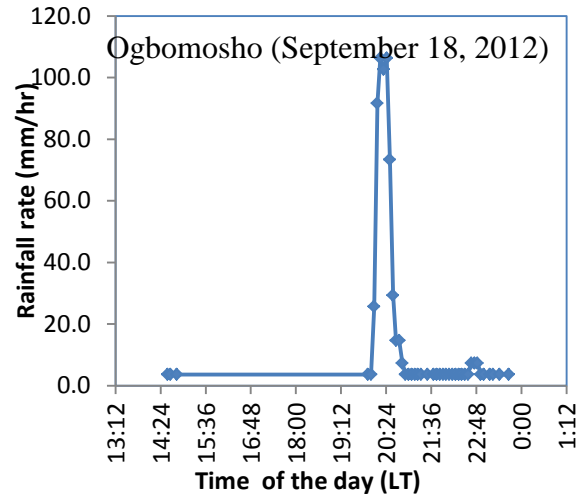
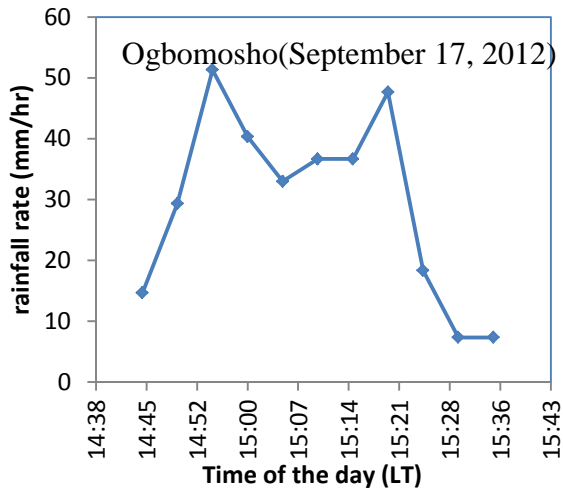




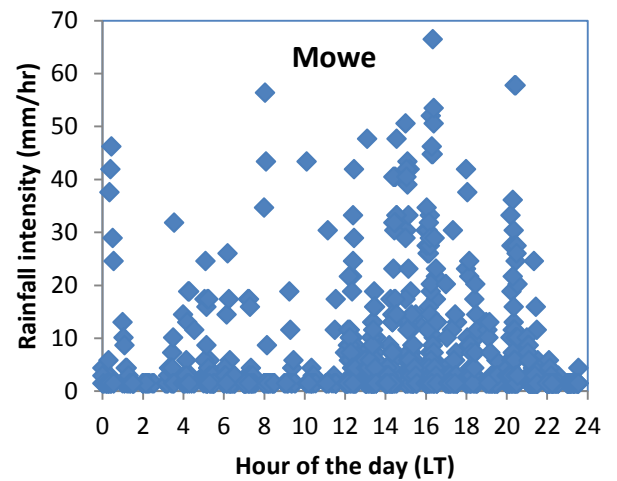
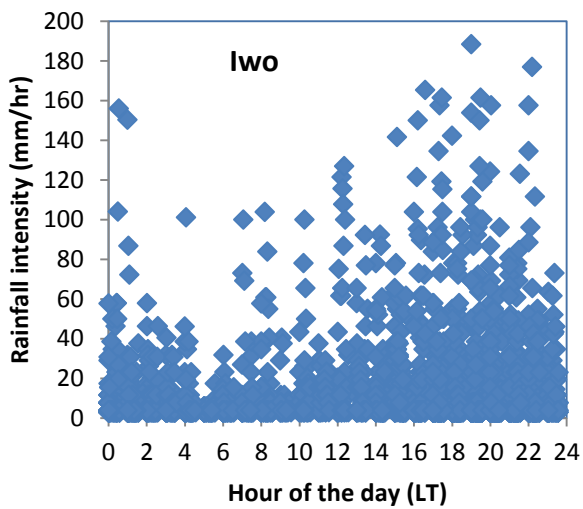
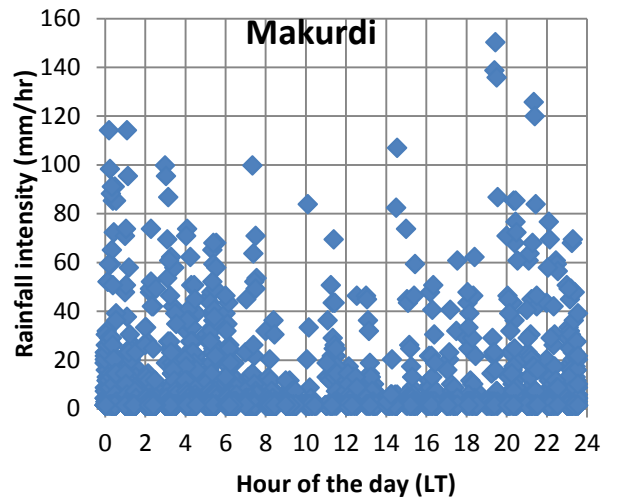
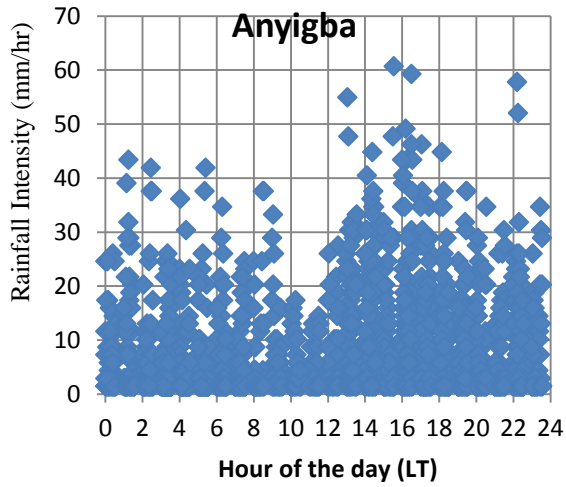
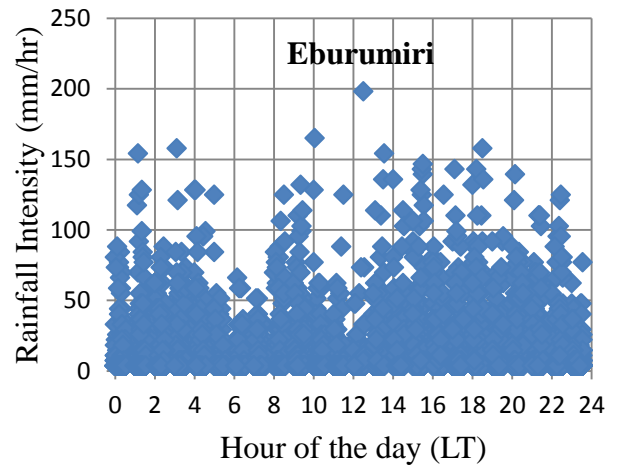
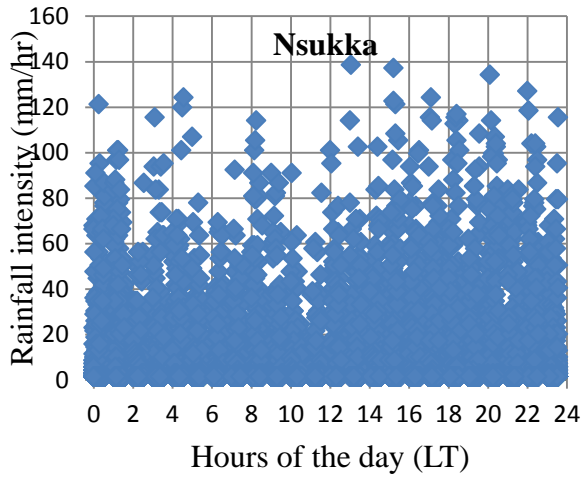


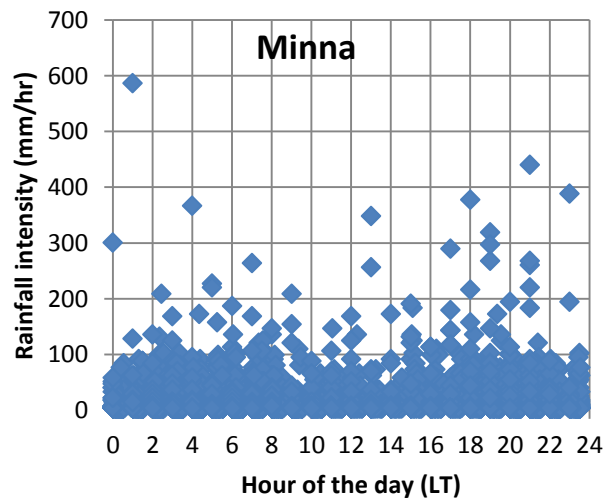
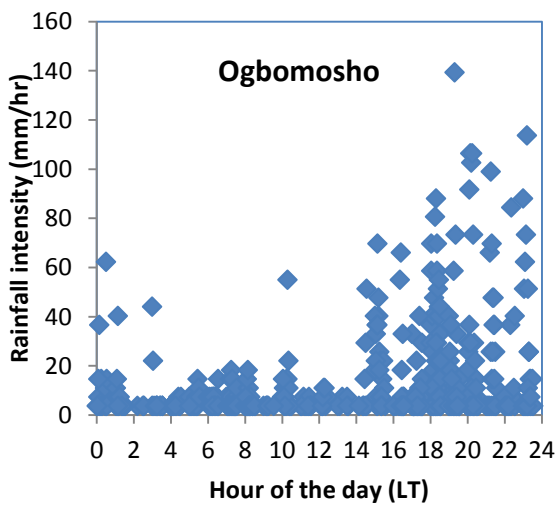
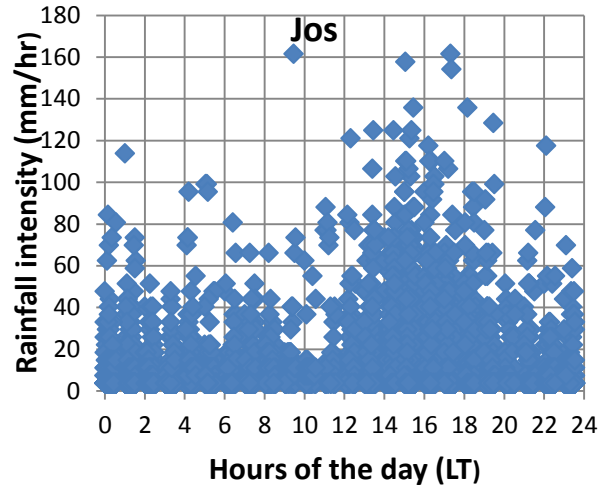
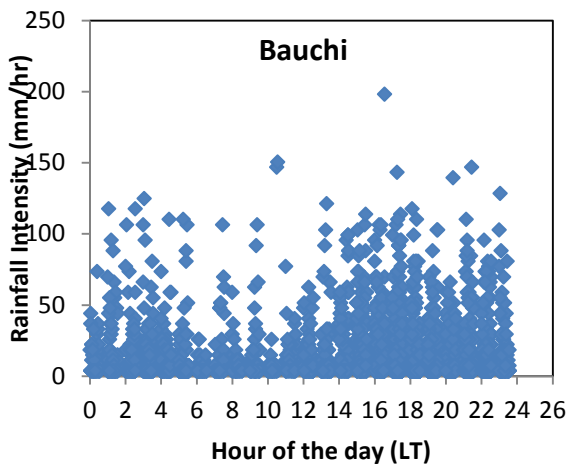
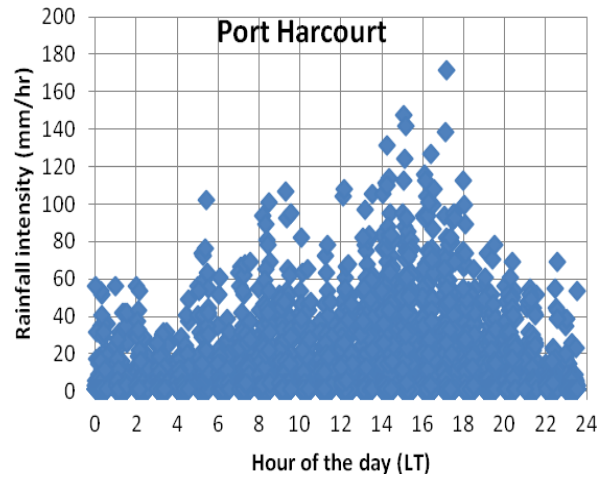
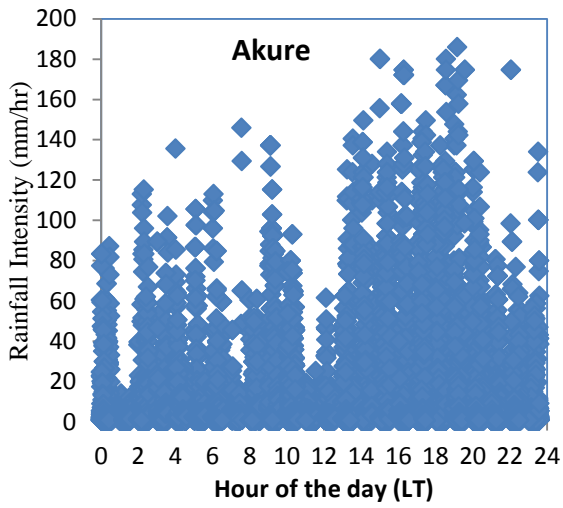


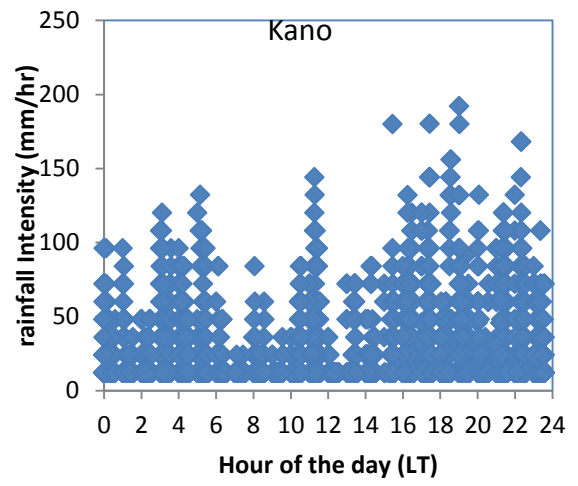
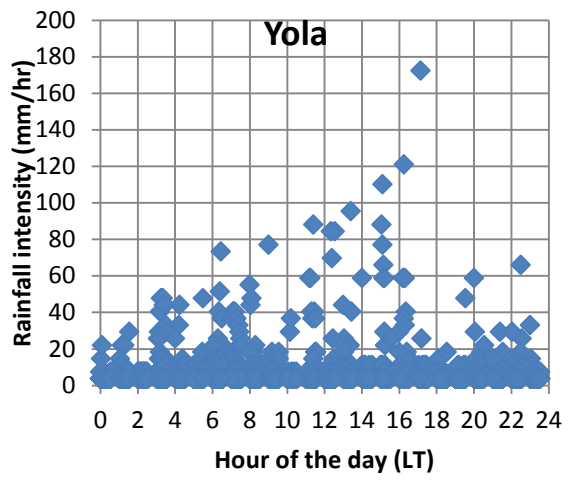




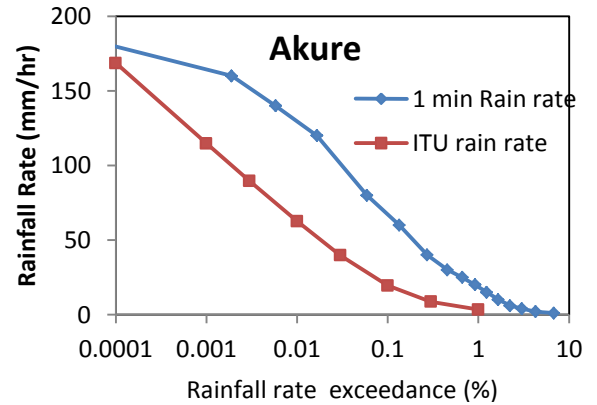
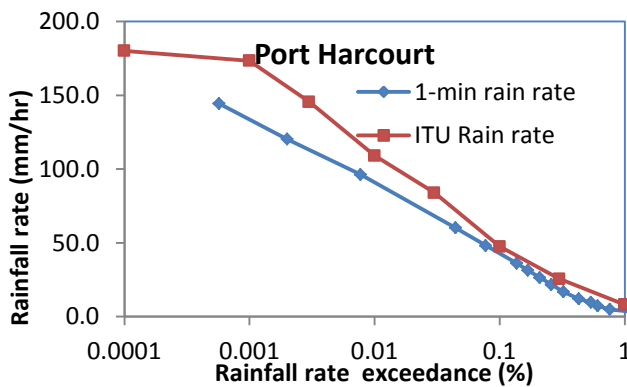
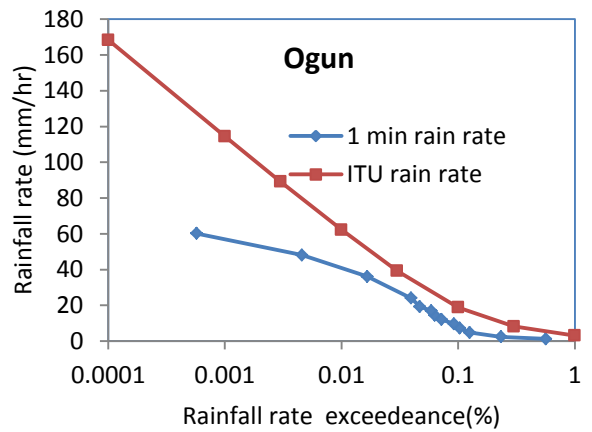
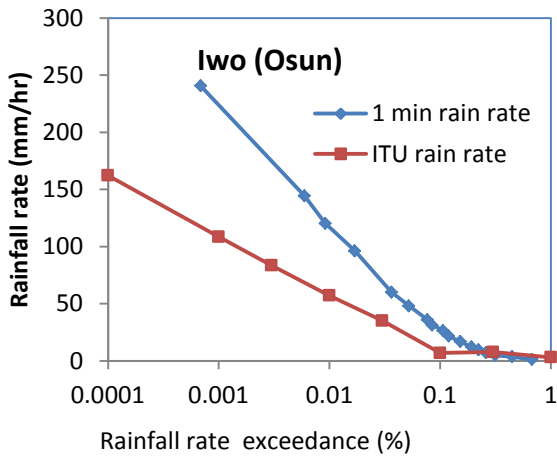
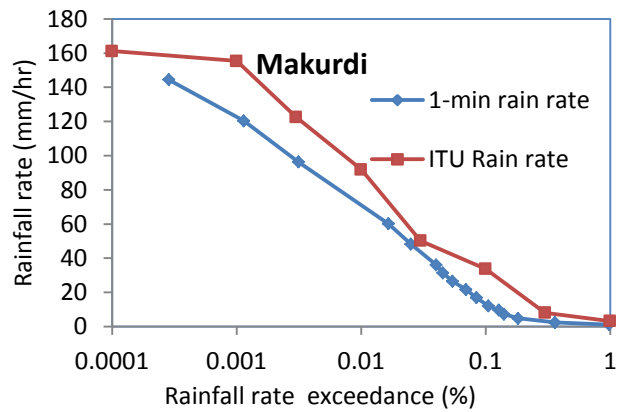
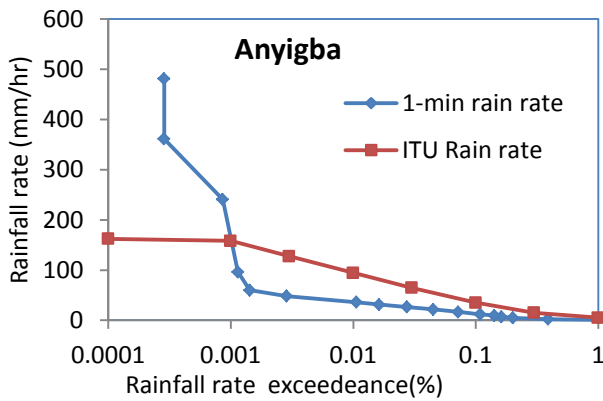
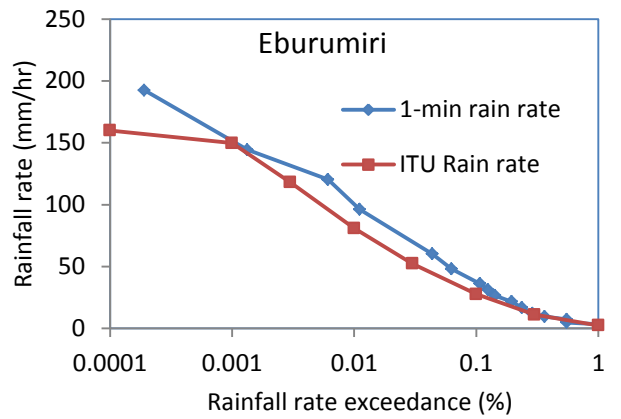
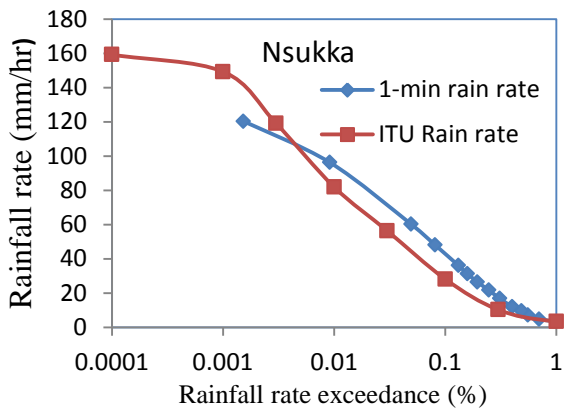
## Appendix 5: Scatter Plots of rainfall Events

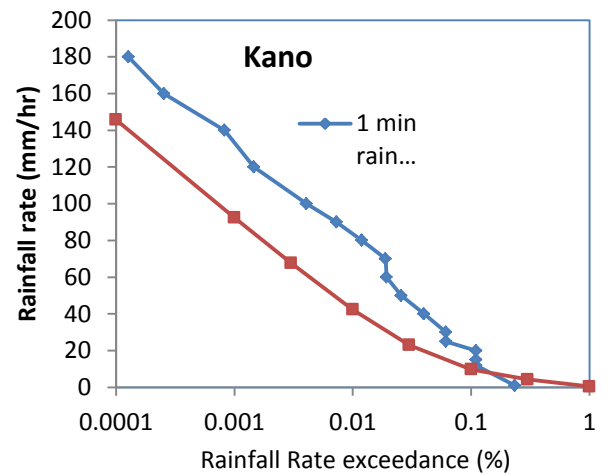
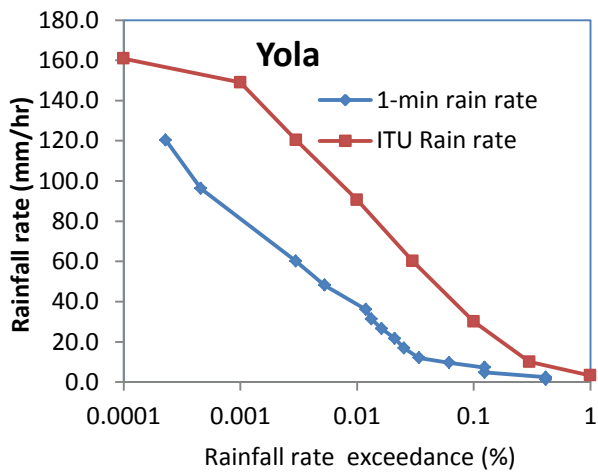
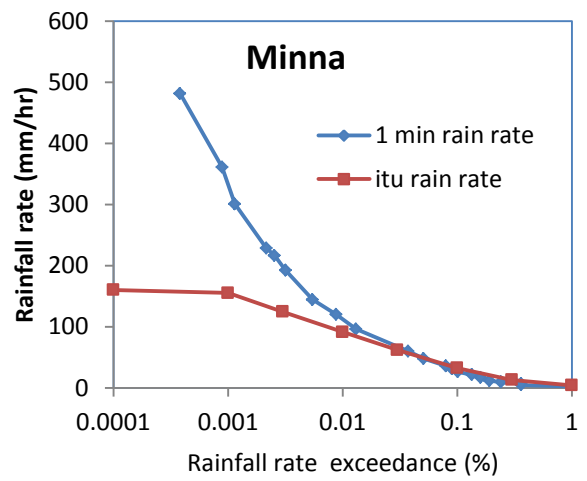
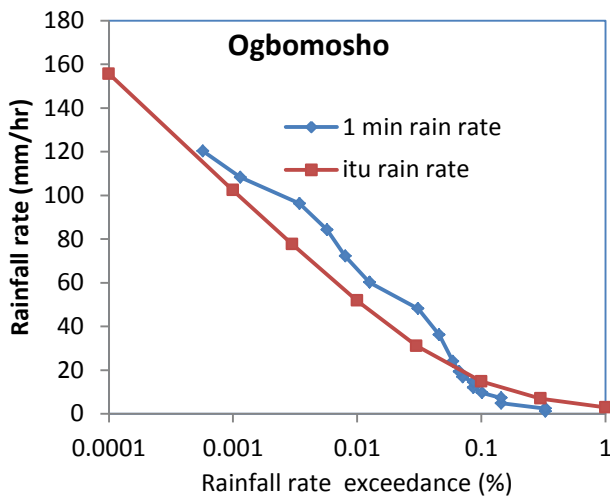
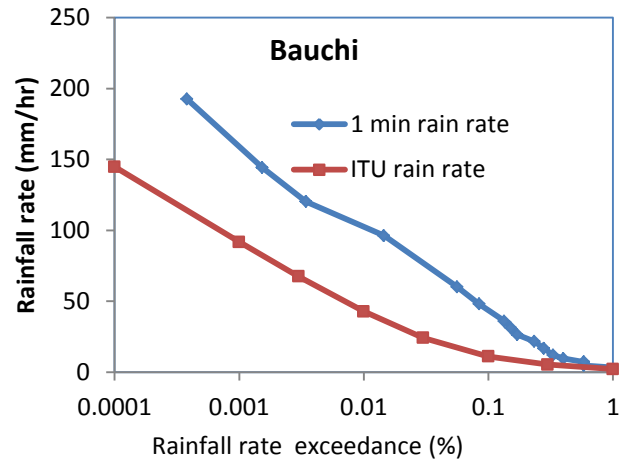
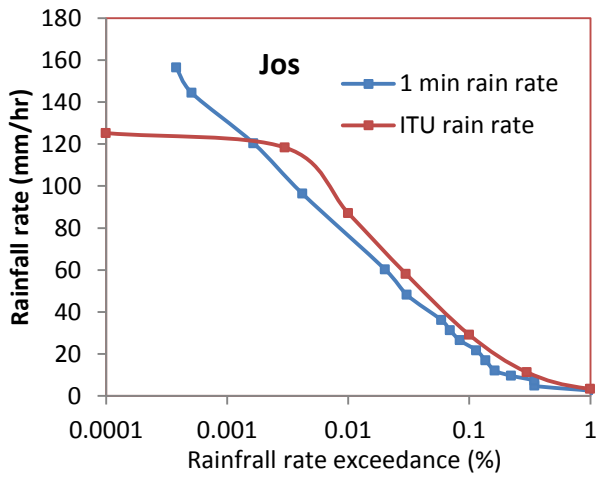






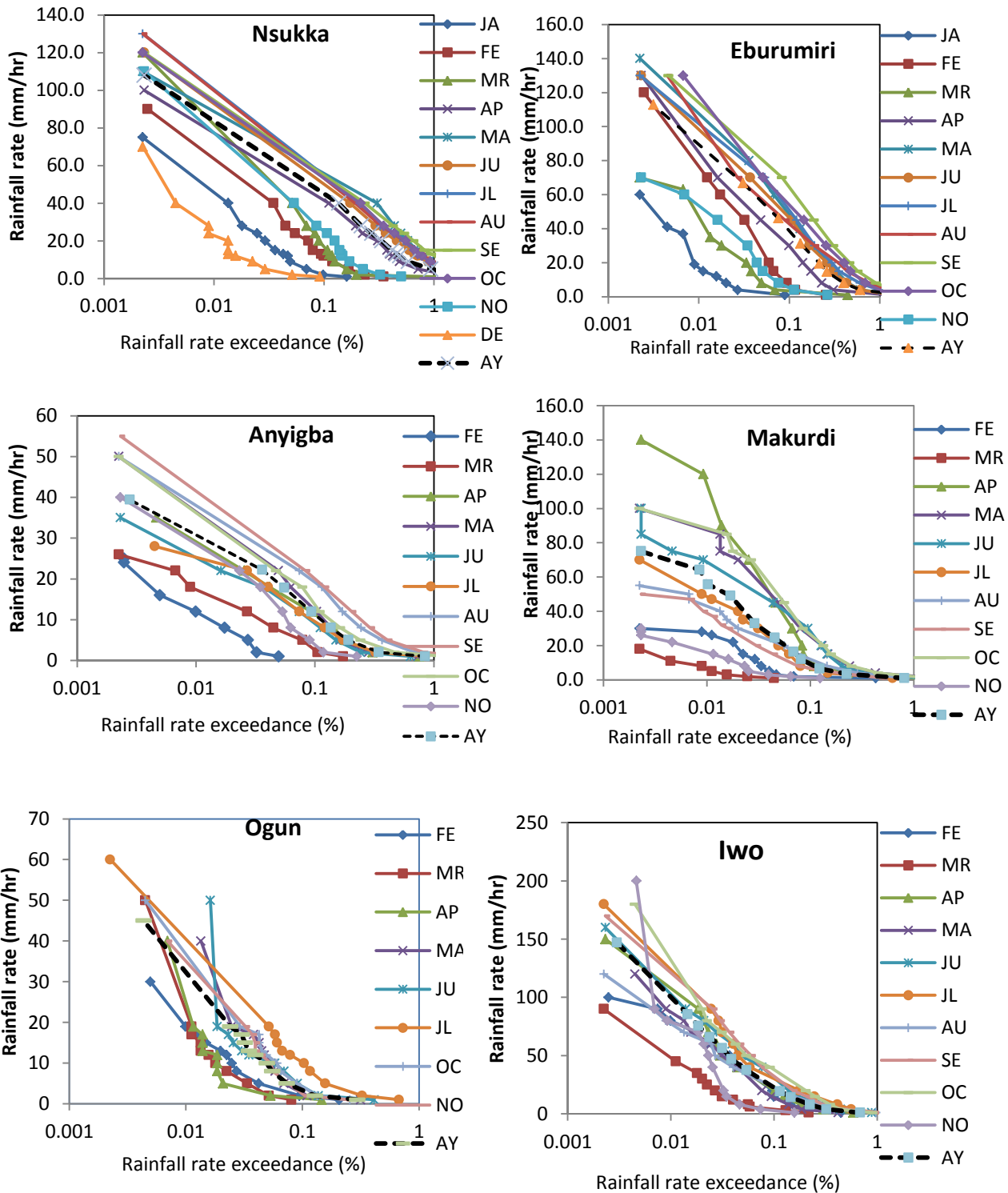
### Appendix 6: Cumulative rainfall rates Vs ITU-R estimate

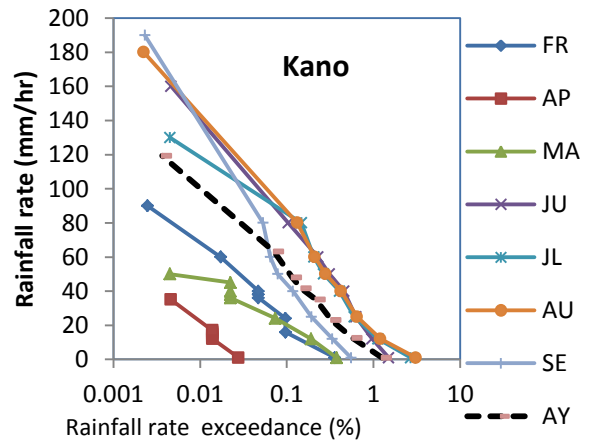
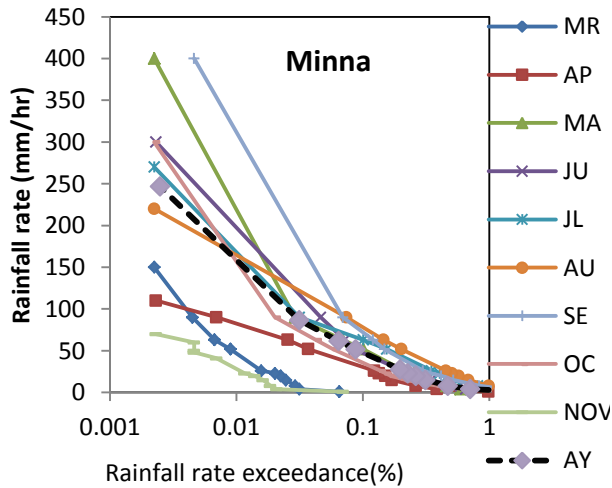
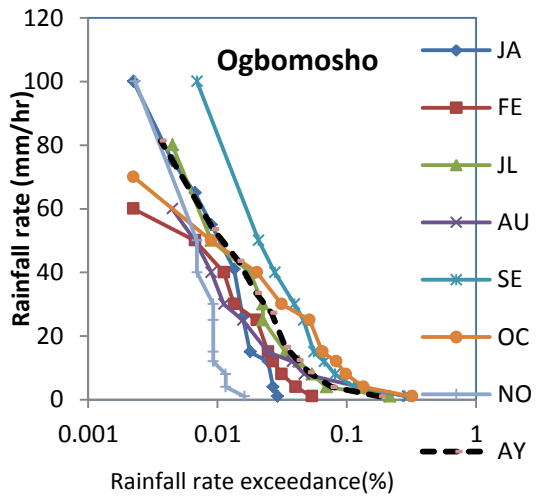
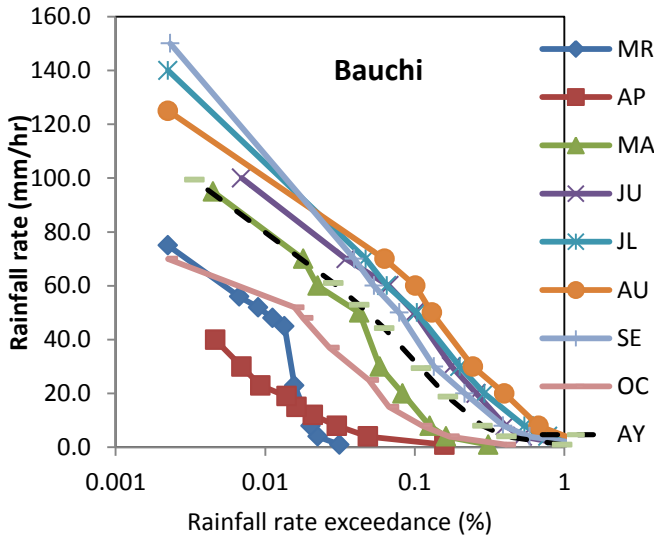
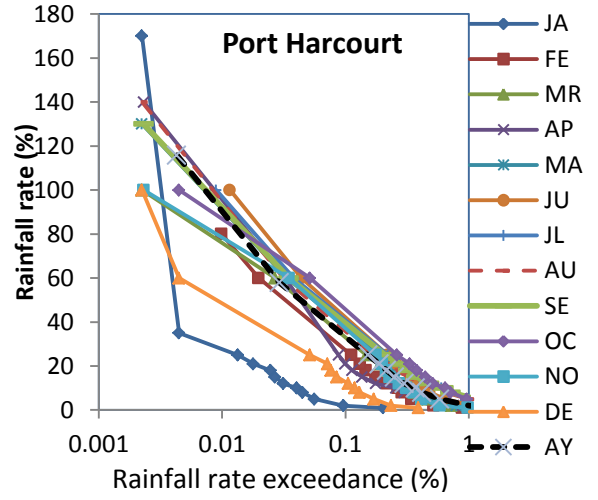
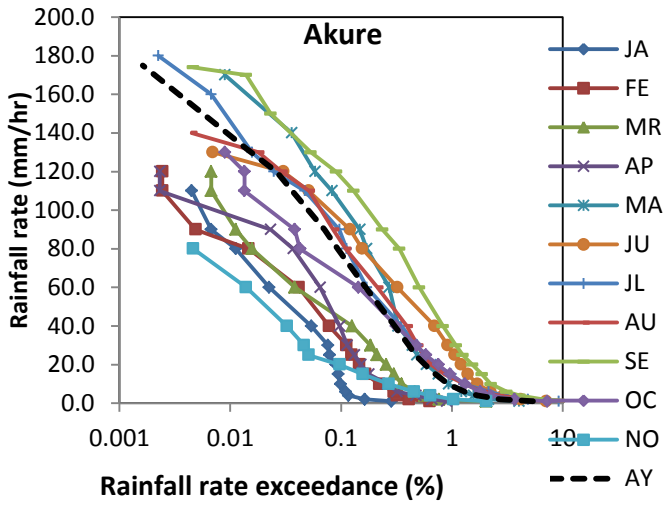


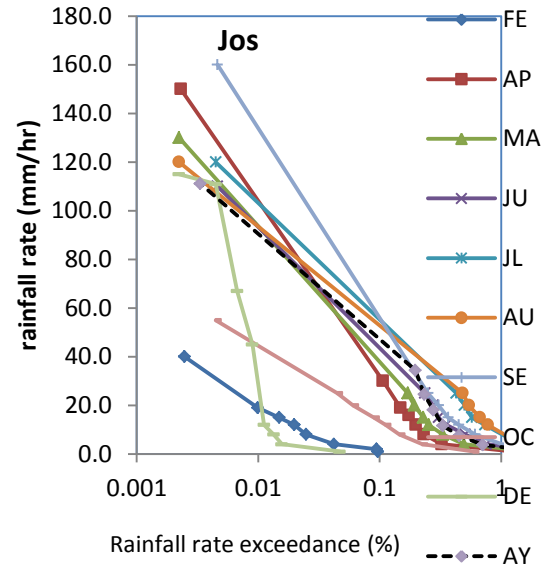
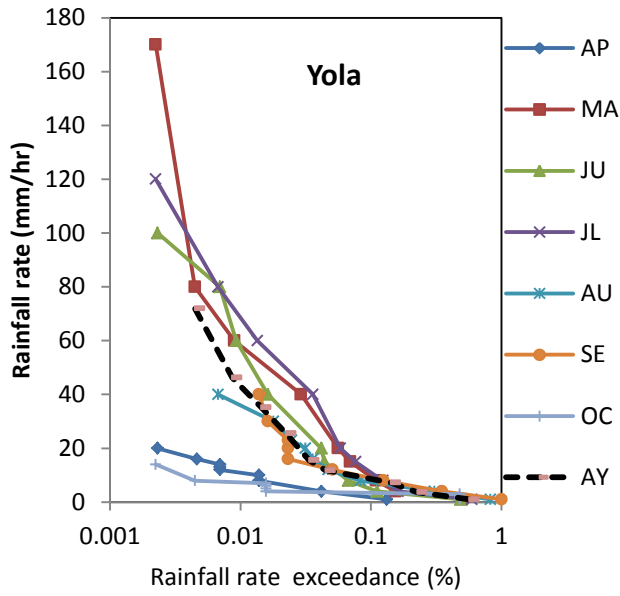




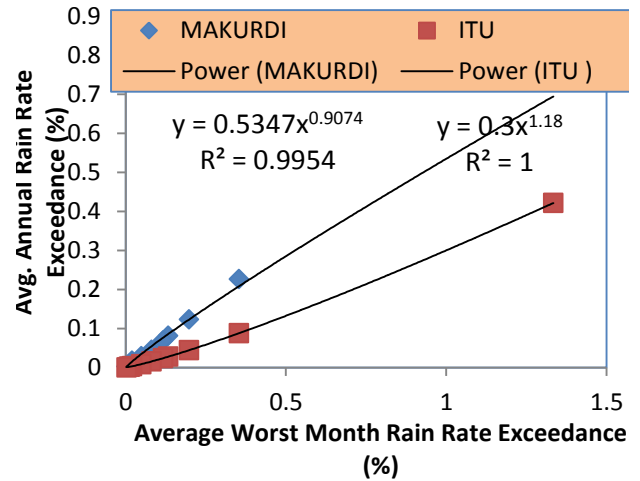
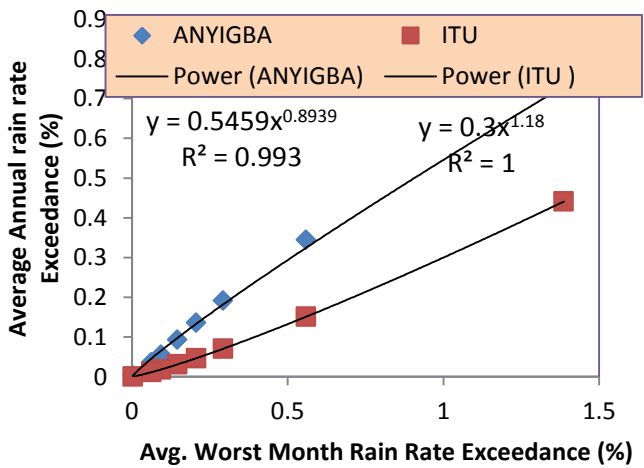
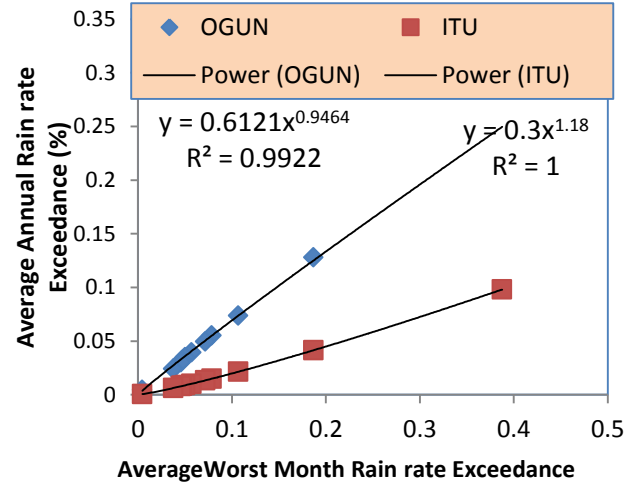
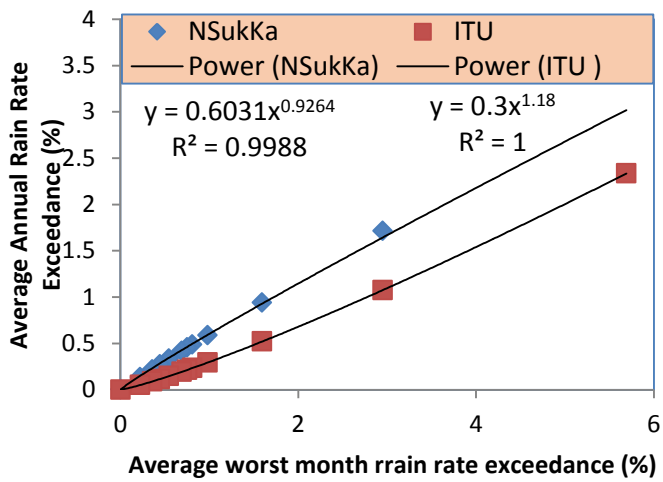
## Appendix 7: Deduction of worst months

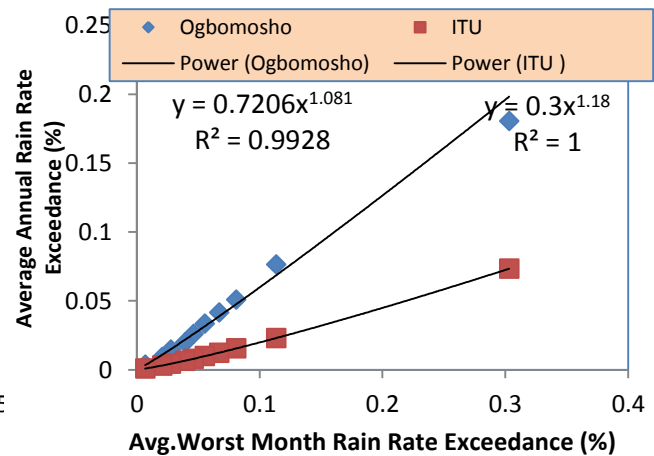
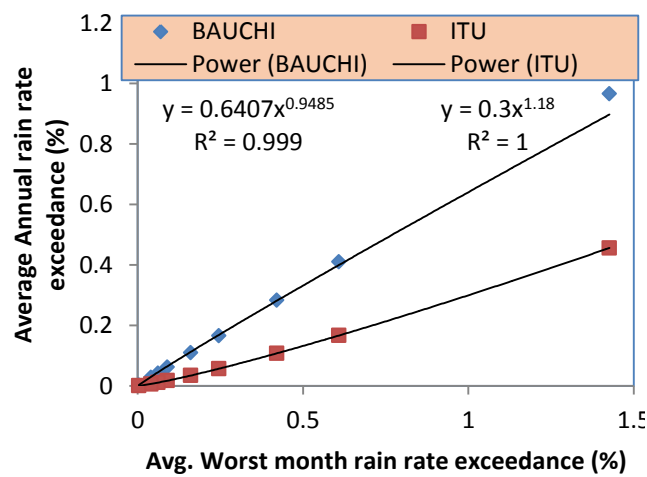
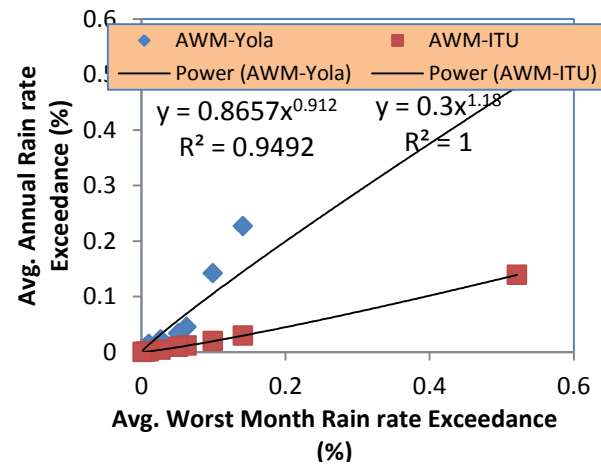
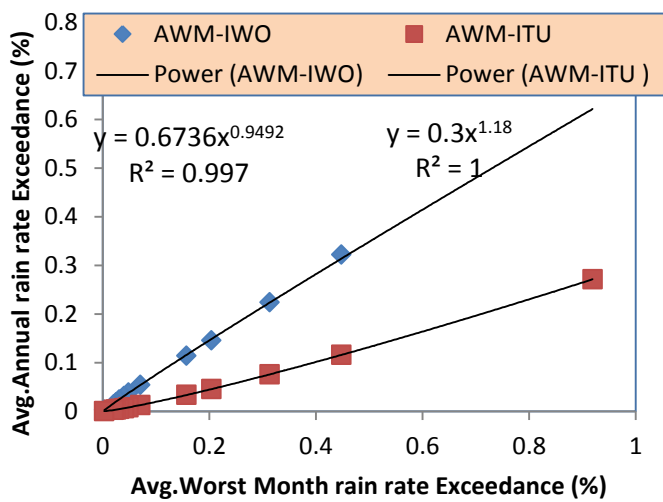
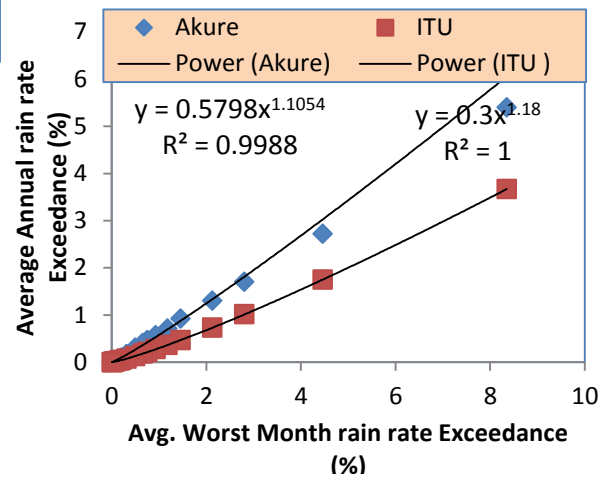
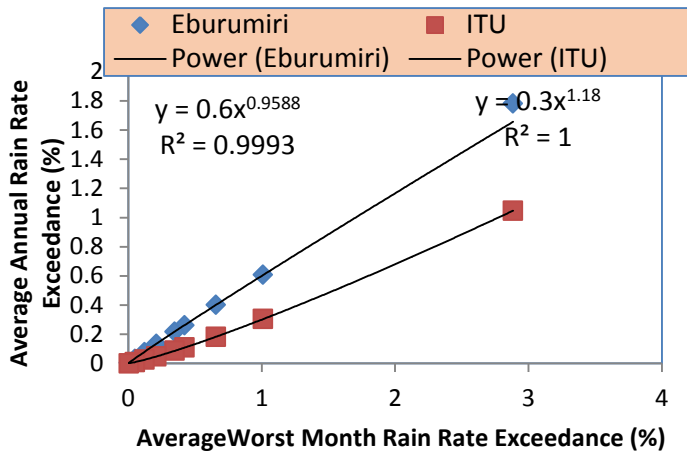


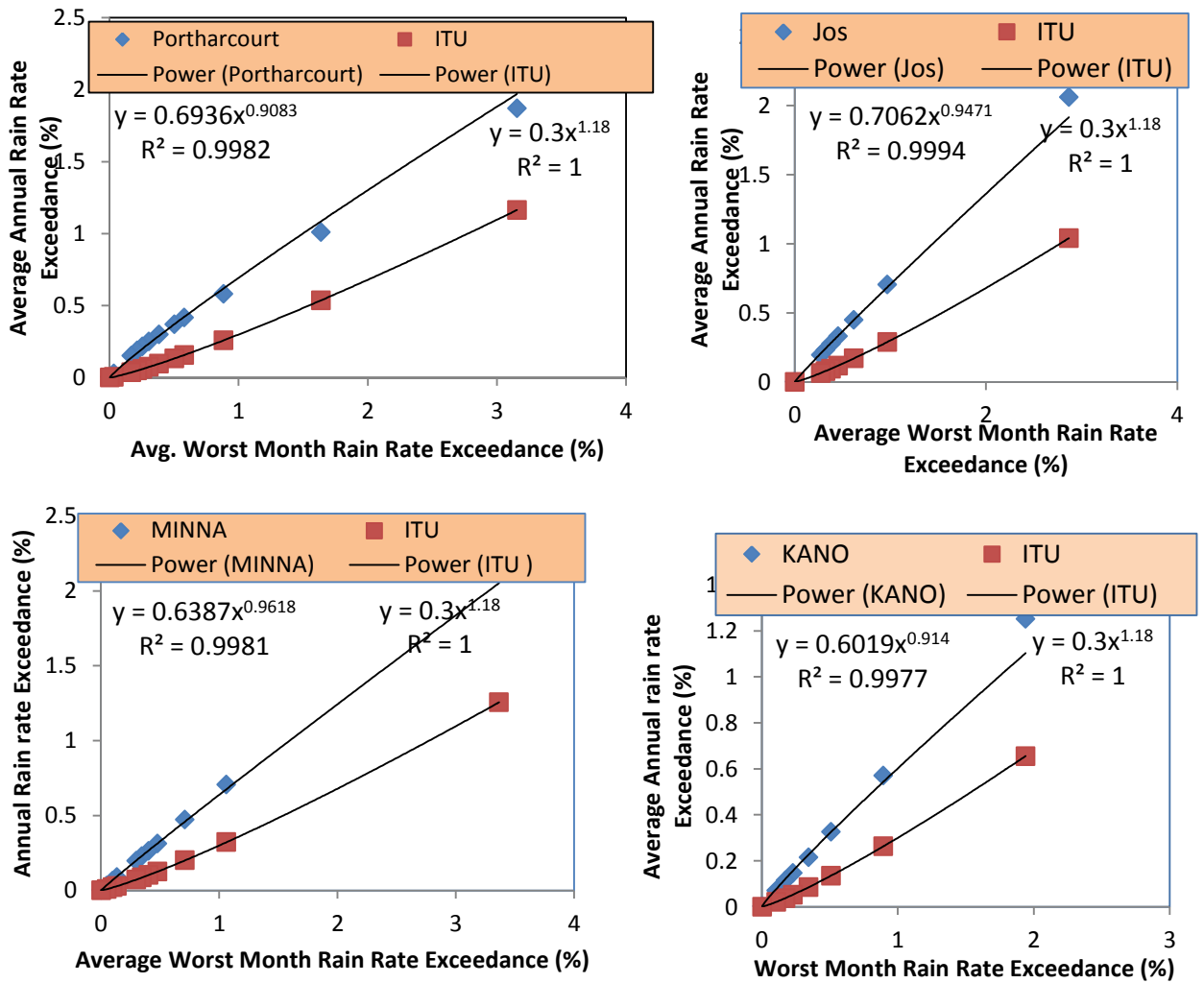




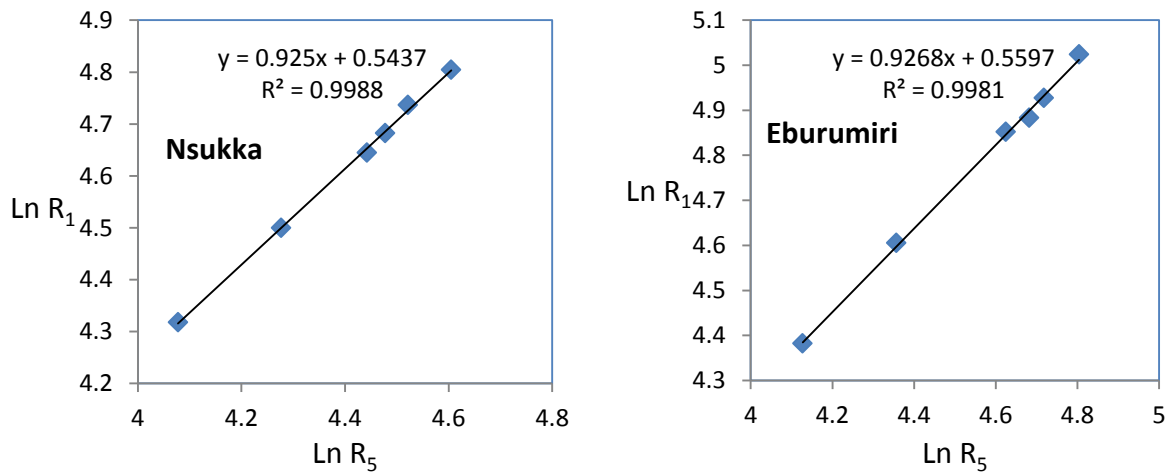
**Appendix 8. Relationship between Annual and Worst Month Rainfall Rate**

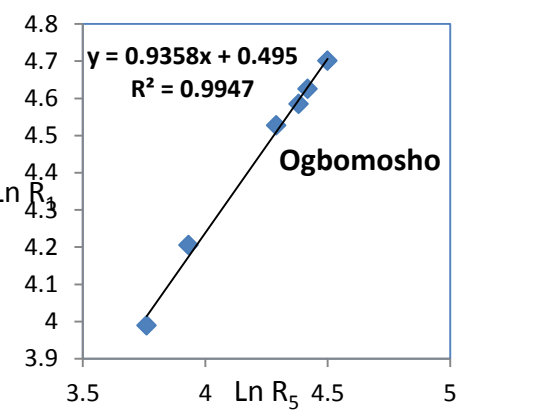
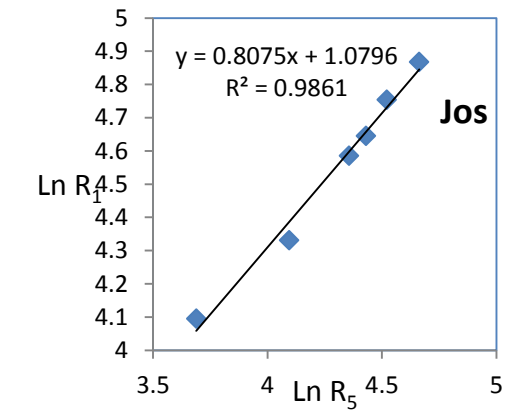
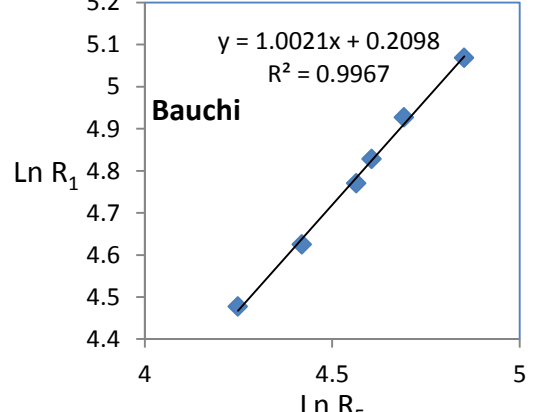
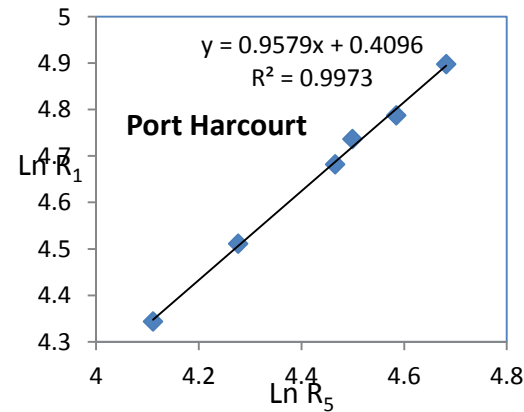
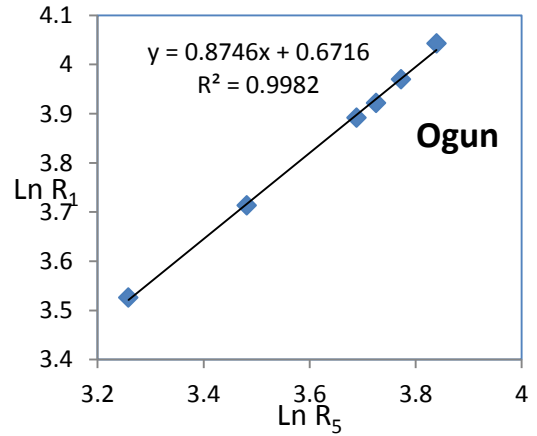
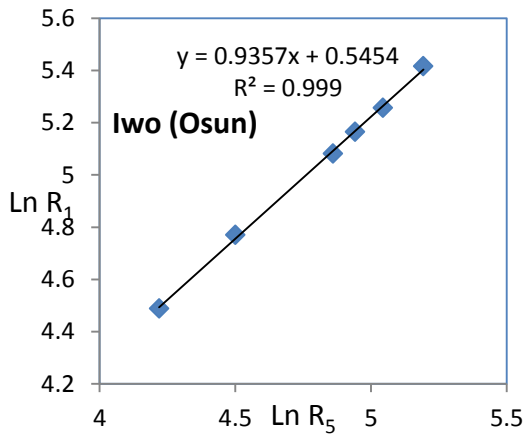
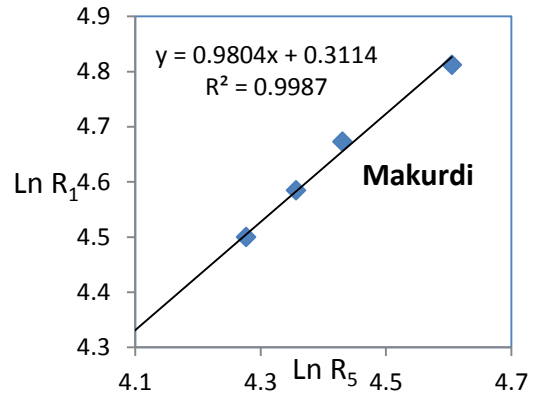
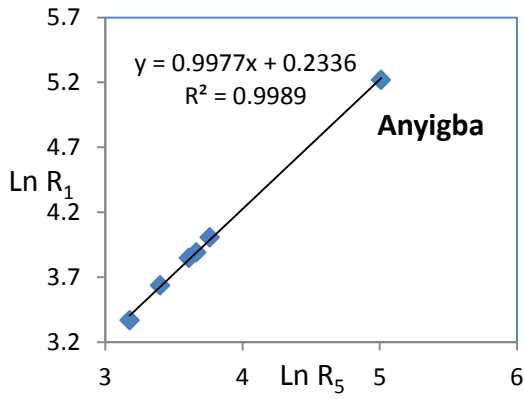


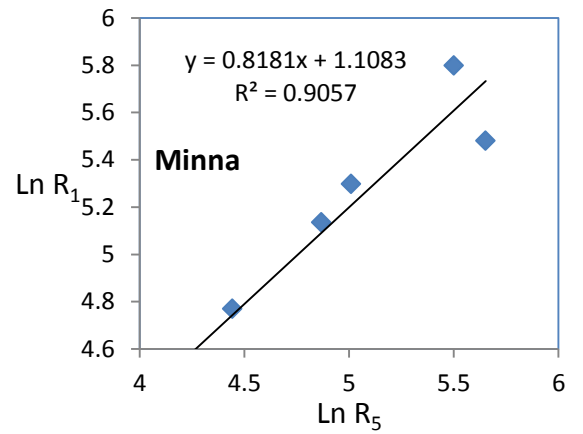
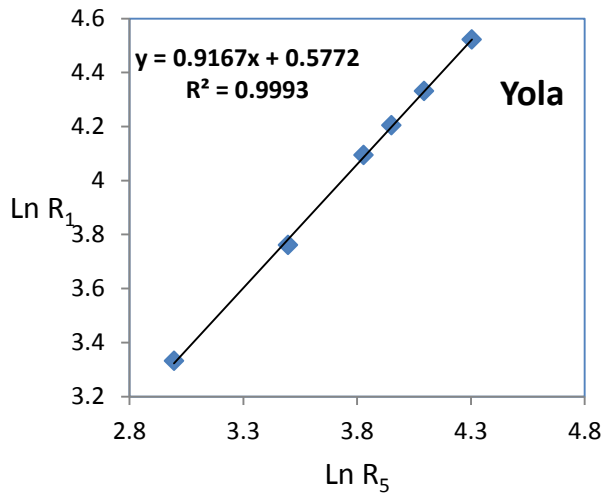




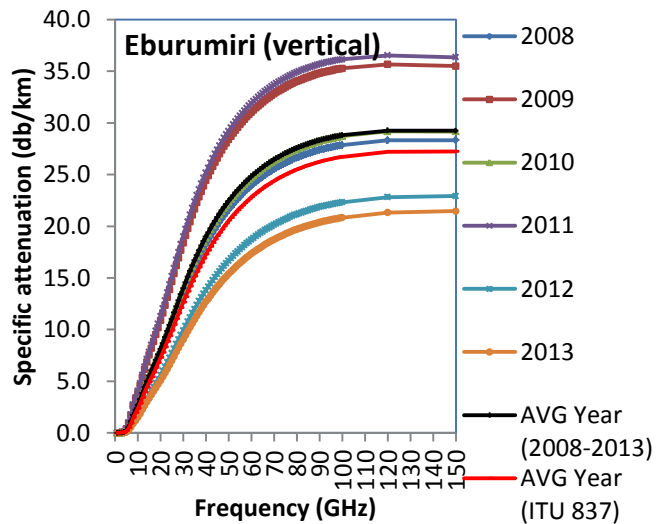
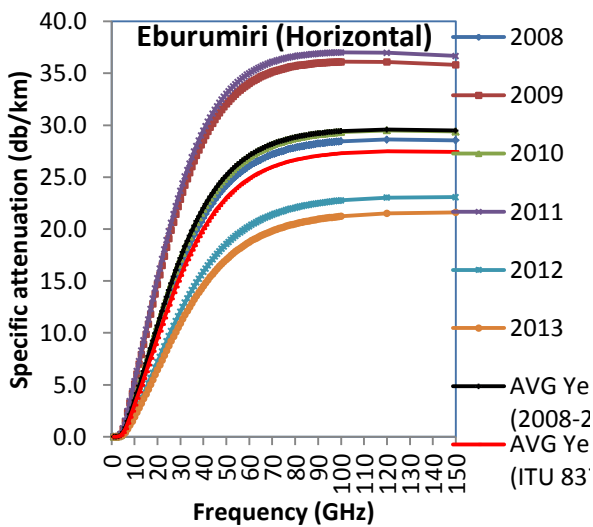
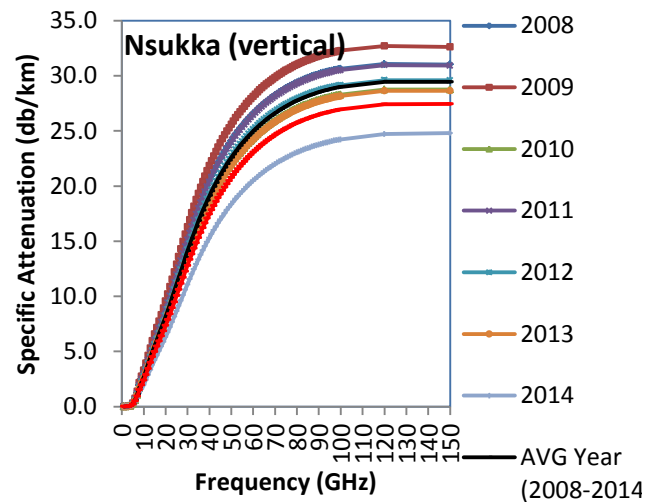
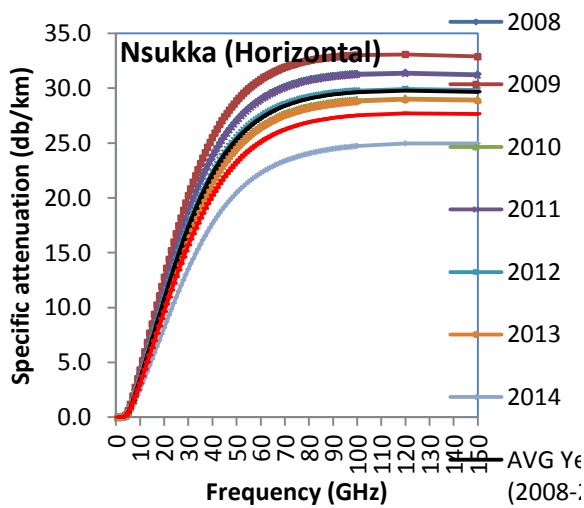
**Appendix 9: Power law relationship between rainfall rates across all the stations**

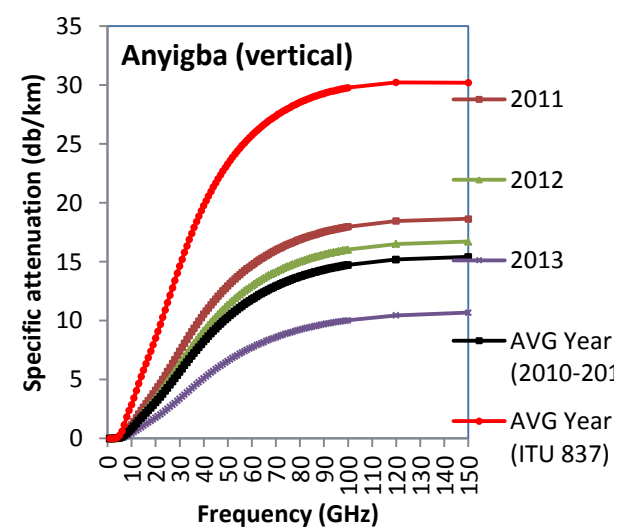
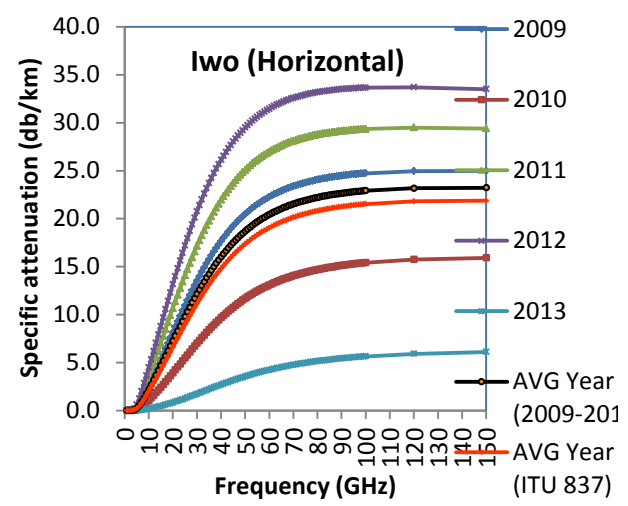
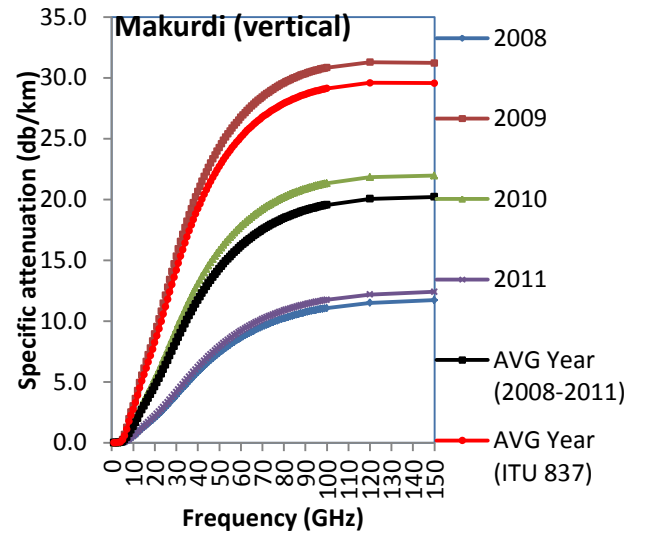
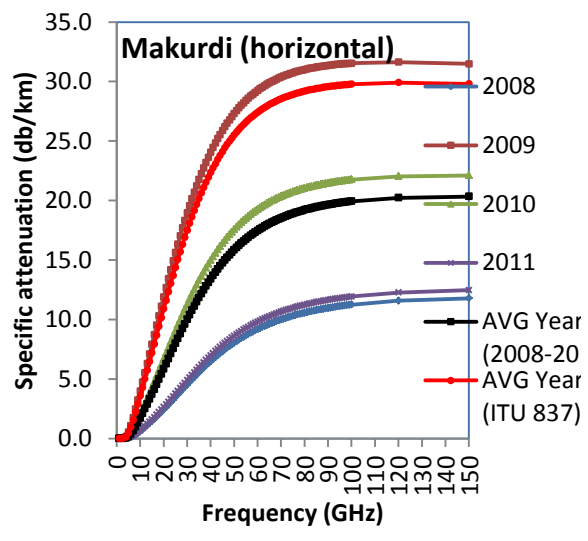
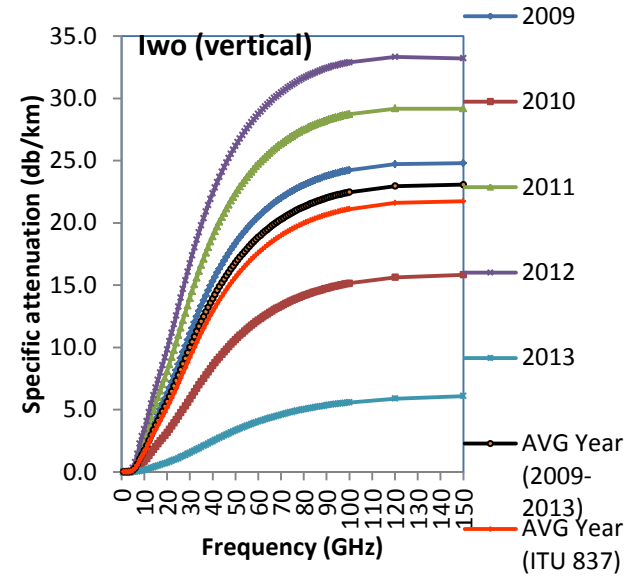
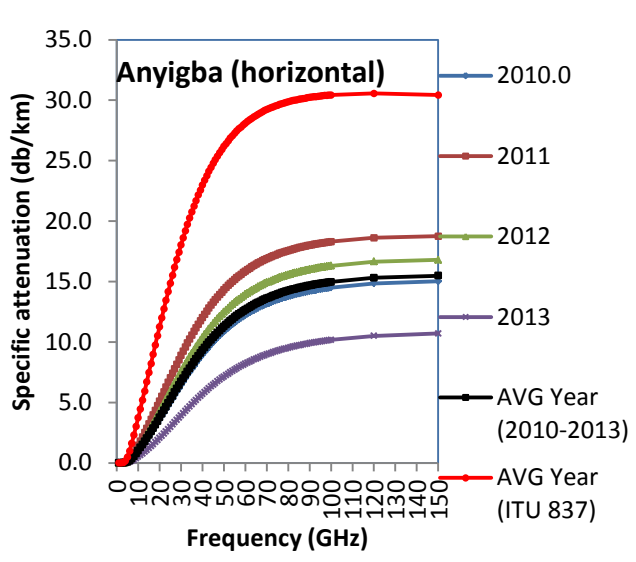




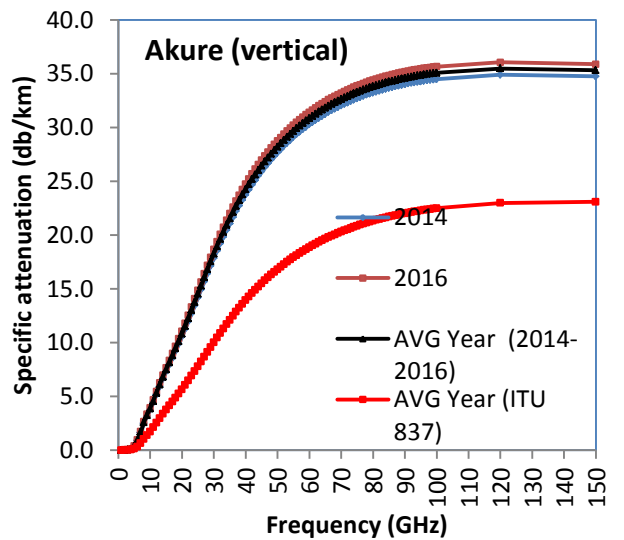
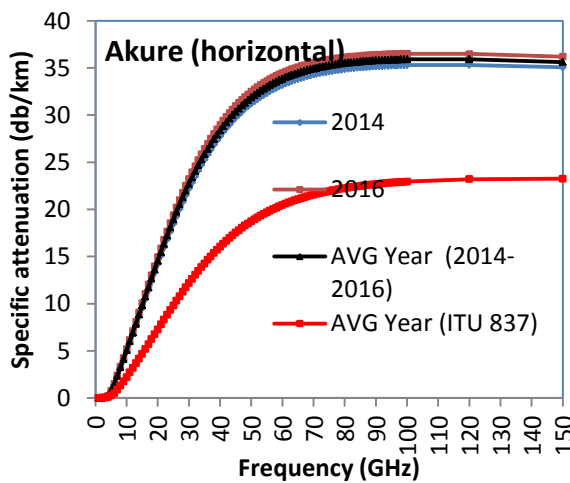
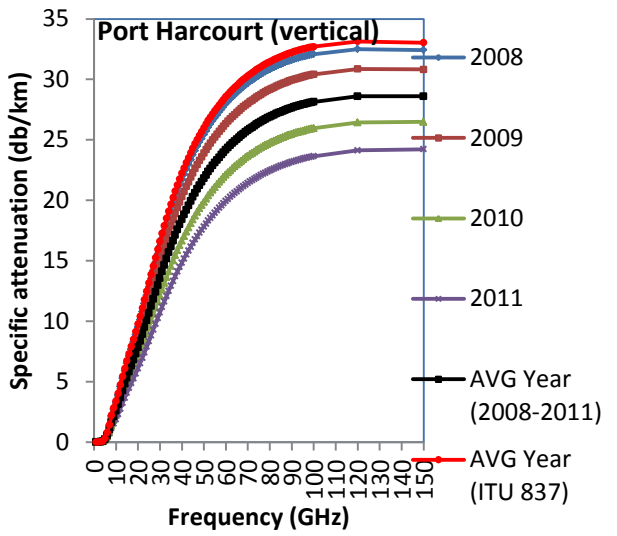
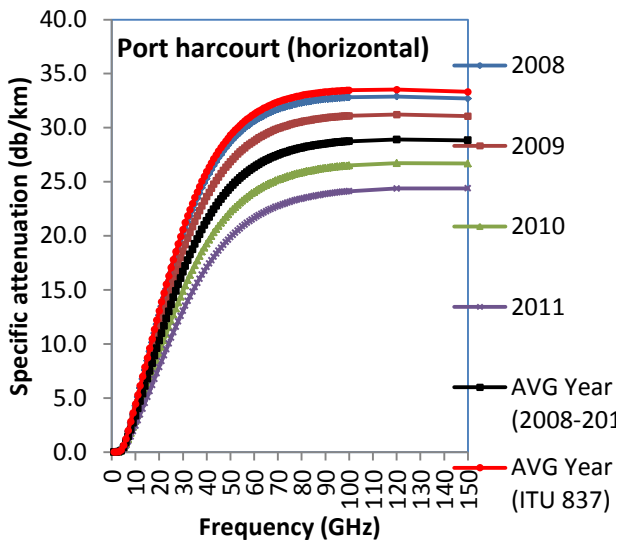
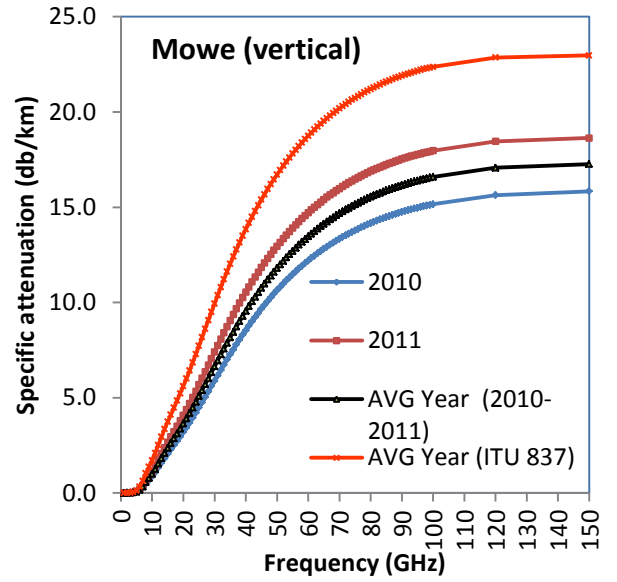
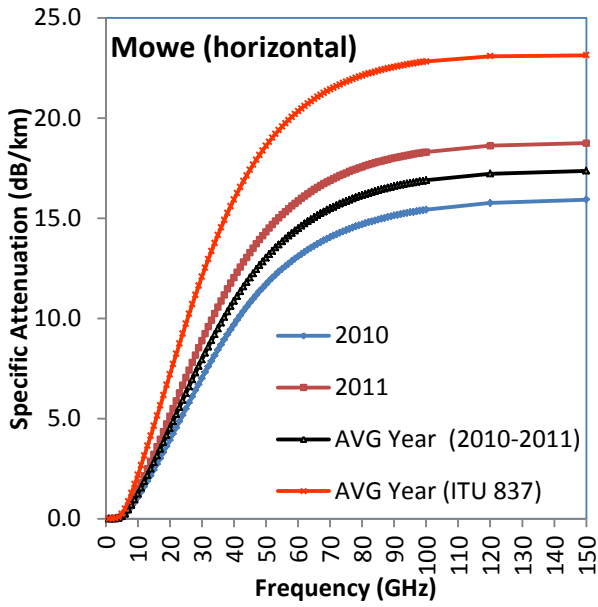


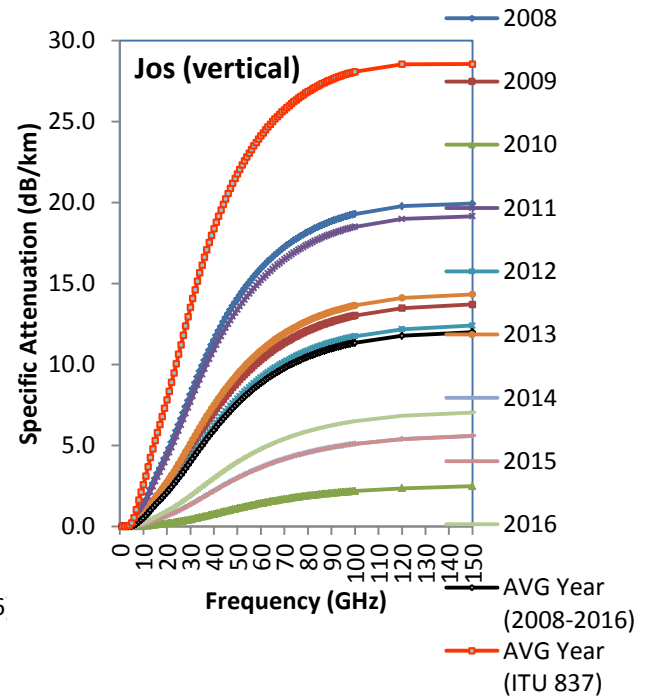
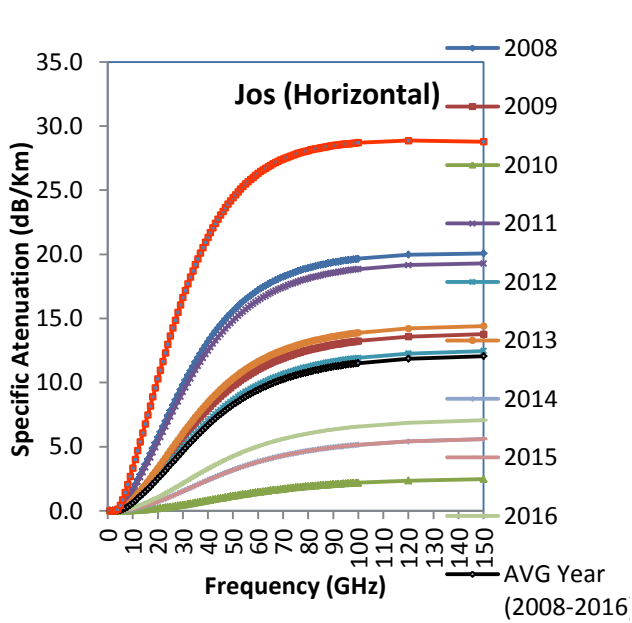
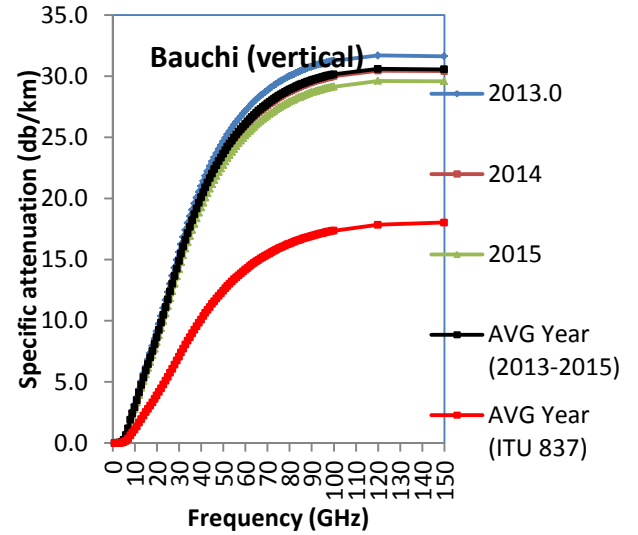
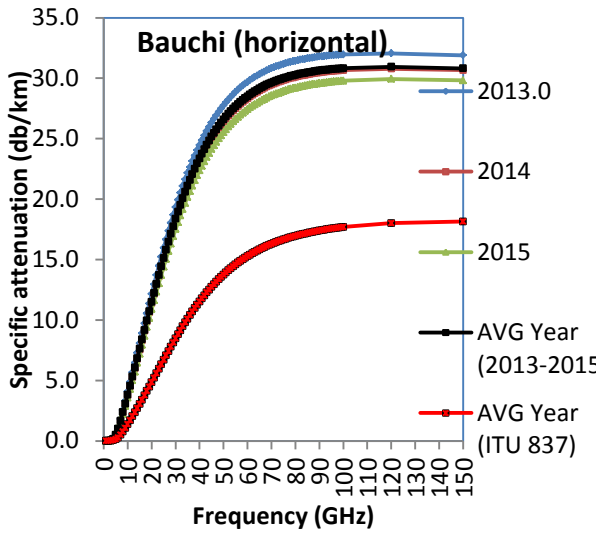
**Appendix 10: Specific attenuation due to rain at 0.01% of time**

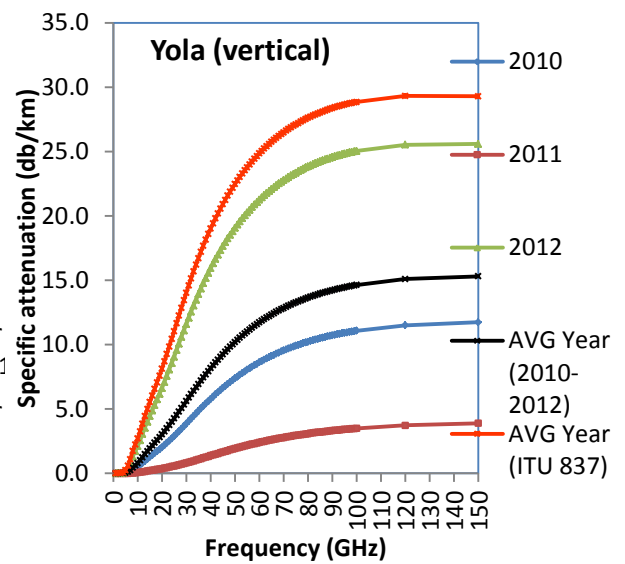
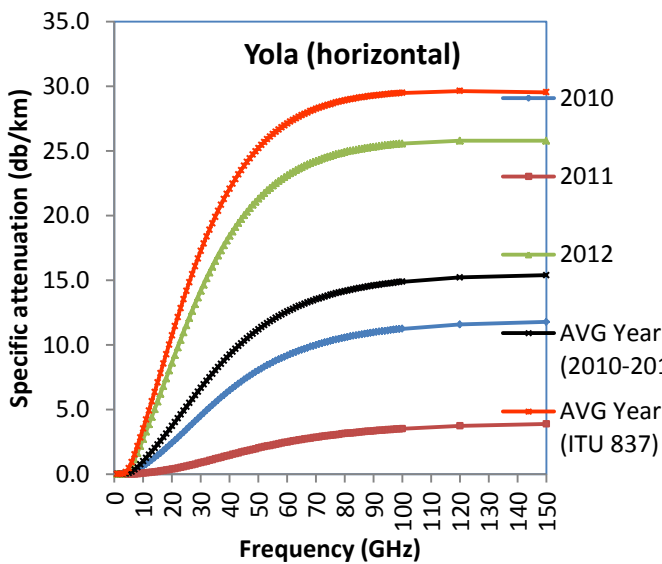
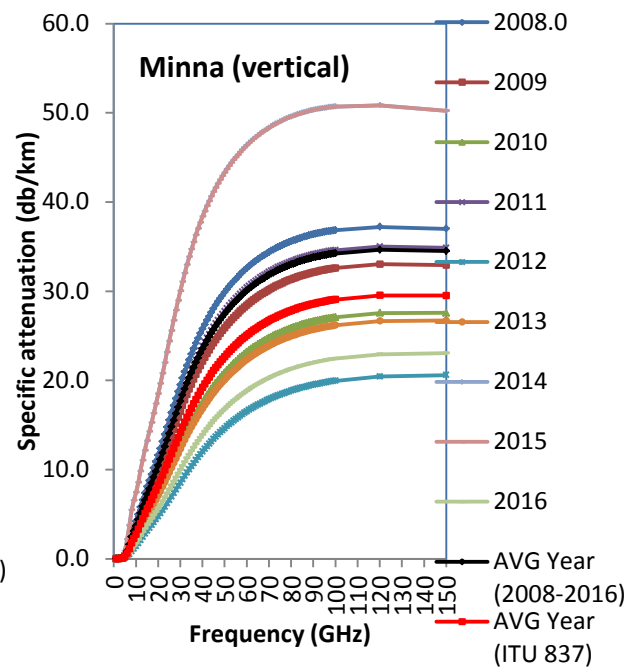
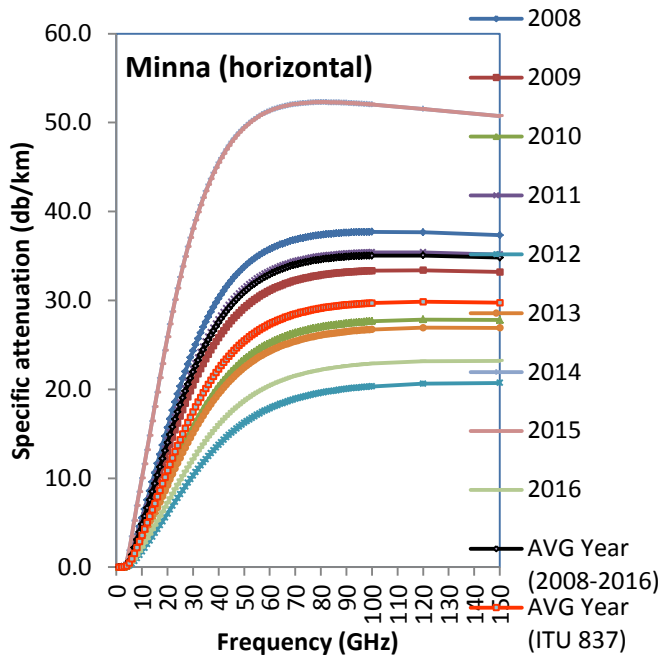


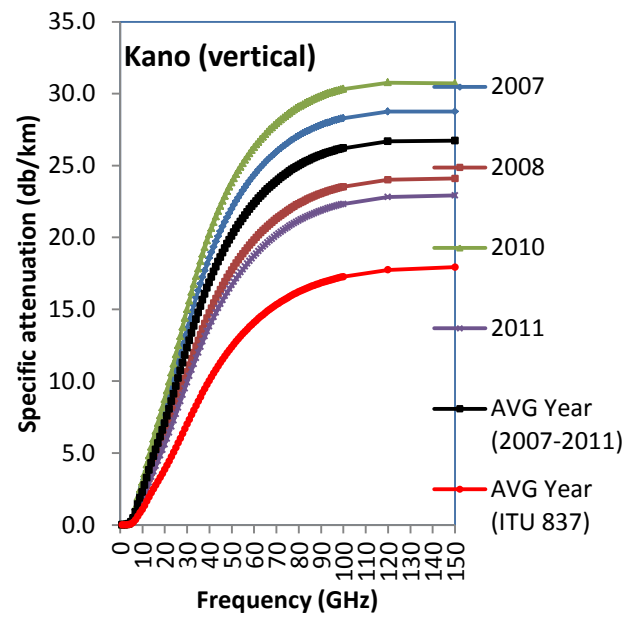
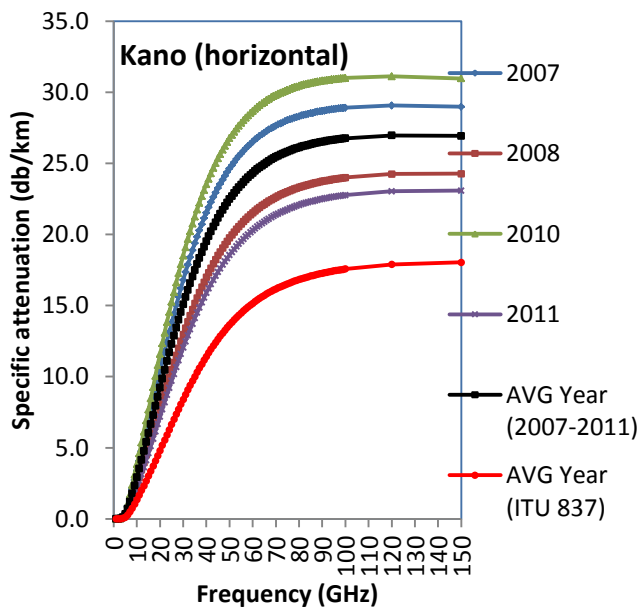
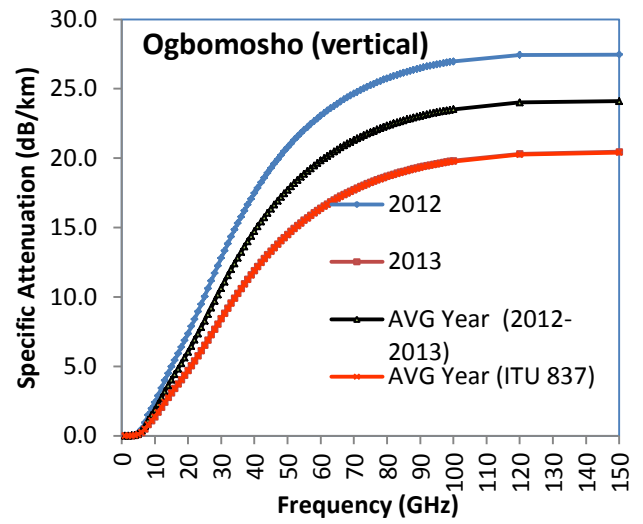
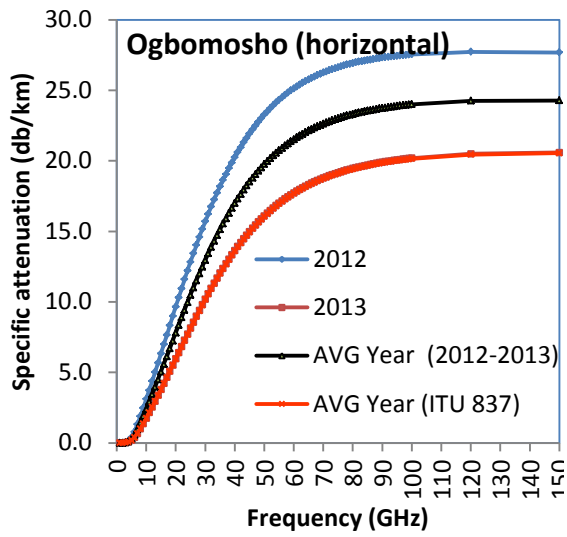




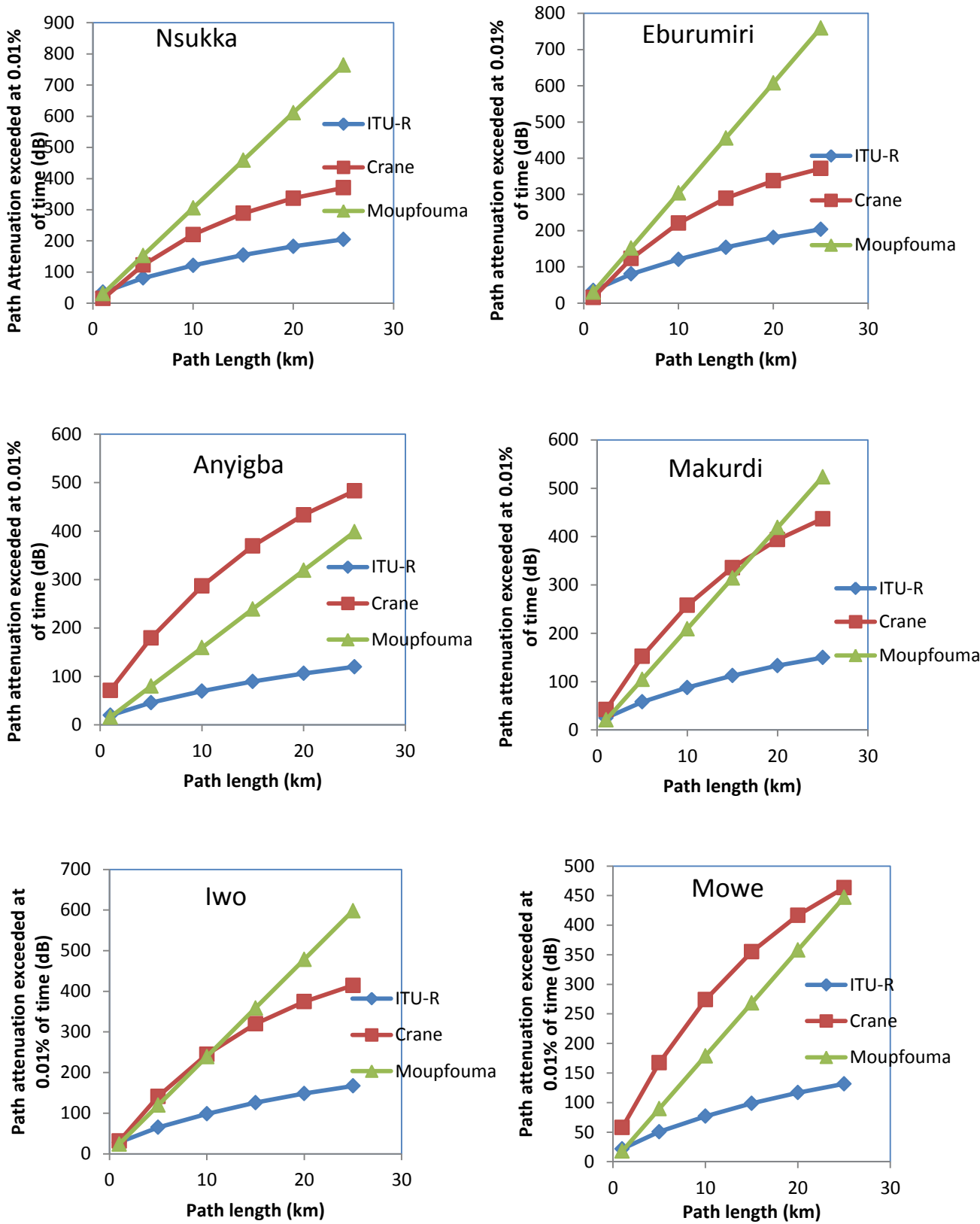


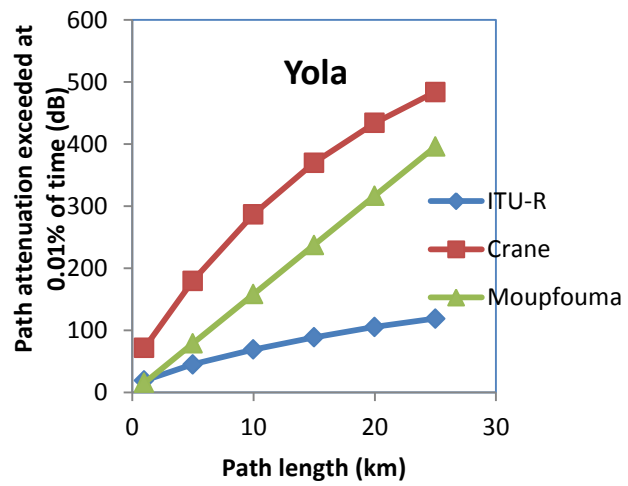
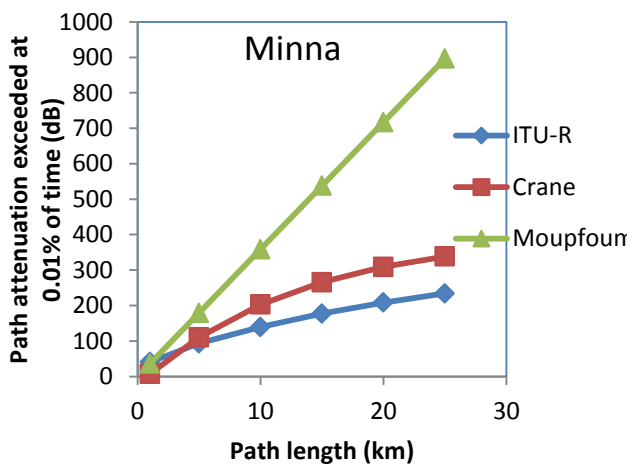
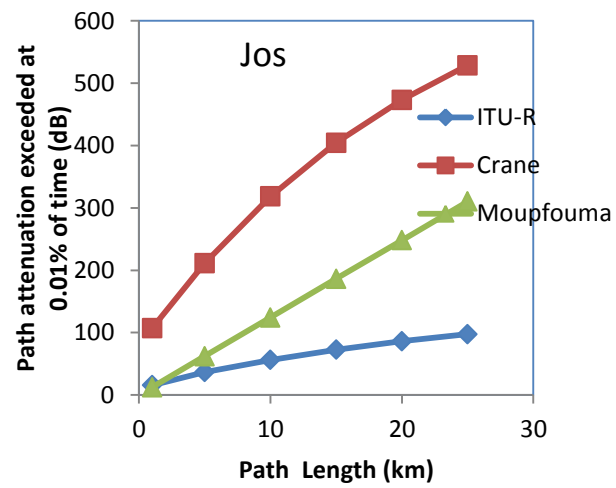
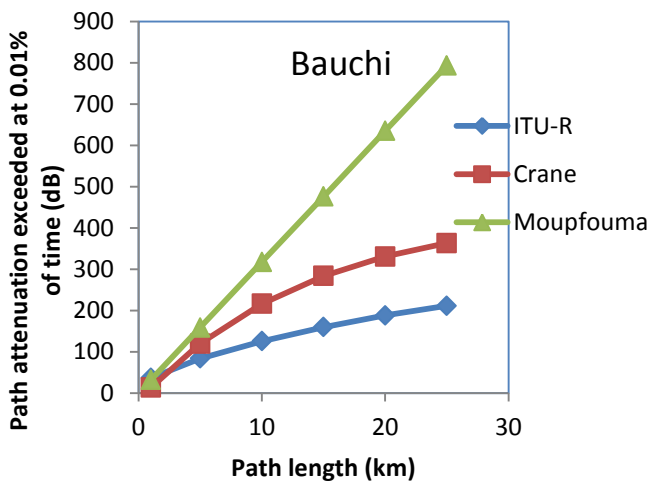
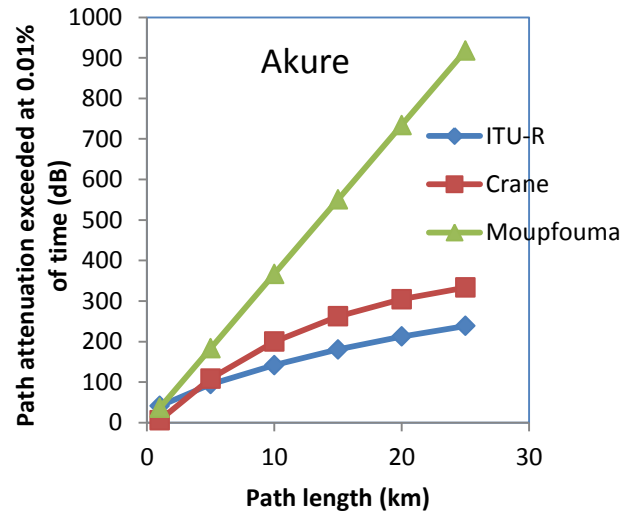
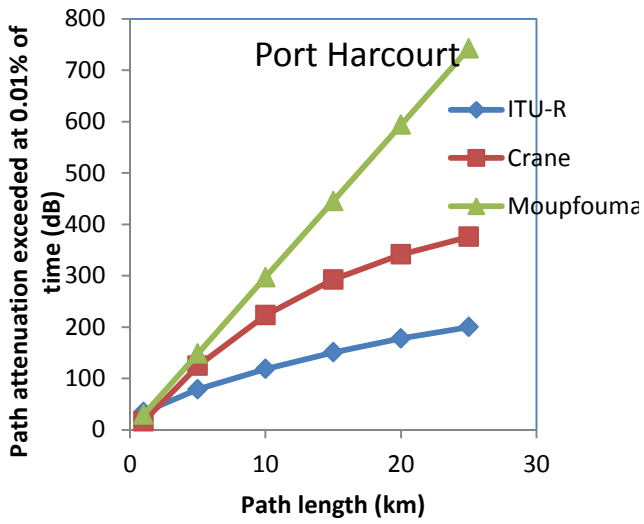


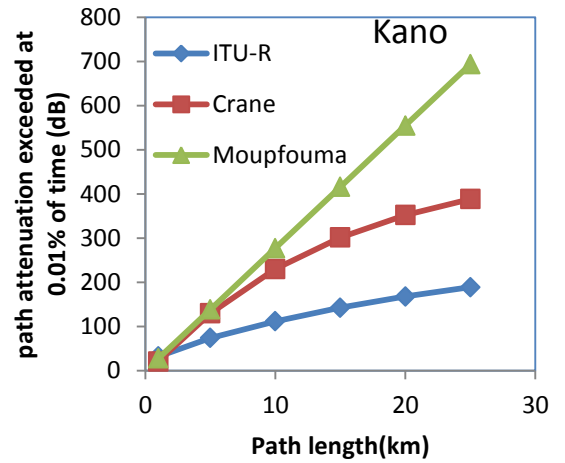
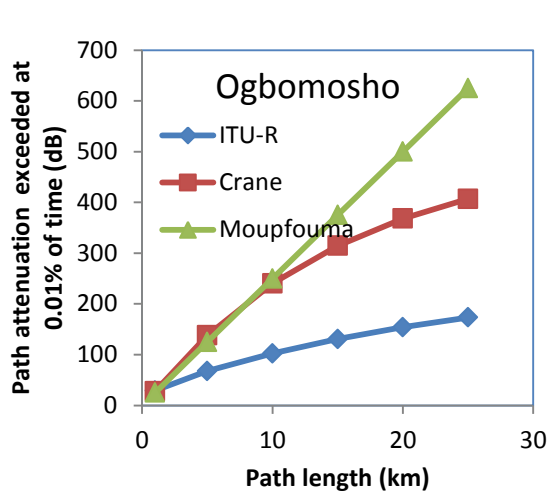




## Appendix 11: Prediction models path attenuation exceedance at 0.01%







**APPENDIX 12: Rain Rate Prediction Models**

**Akure**

(a) Rice and Holmberg

Rain Rate (R)	Average Annual Rfall Depth (M)	Thunderstorm Rfall(M1)	Total Annual Rfall (M2)	Thunderstorm Ratio ( $\beta$ )	T1(R)	T1(R)/87.66	T1/M
0.4	1467.9	1352	2935.8	0.460522	316.3689	3.609045	0.107762
2	1467.9	1352	2935.8	0.460522	124.9453	1.425339	0.042559
4	1467.9	1352	2935.8	0.460522	74.85066	0.853875	0.025496
6	1467.9	1352	2935.8	0.460522	50.63908	0.577676	0.017249
8	1467.9	1352	2935.8	0.460522	36.05903	0.411351	0.012283
10	1467.9	1352	2935.8	0.460522	27.0249	0.308292	0.009205
16	1467.9	1352	2935.8	0.460522	15.10123	0.172271	0.005144
20	1467.9	1352	2935.8	0.460522	12.03927	0.137341	0.004101
25	1467.9	1352	2935.8	0.460522	9.829917	0.112137	0.003348
28	1467.9	1352	2935.8	0.460522	8.87053	0.101192	0.003022
38	1467.9	1352	2935.8	0.460522	6.494677	0.074089	0.002212
45	1467.9	1352	2935.8	0.460522	5.25883	0.059991	0.001791
55	1467.9	1352	2935.8	0.460522	3.894881	0.044432	0.001327
90	1467.9	1352	2935.8	0.460522	1.362928	0.015548	0.000464
110	1467.9	1352	2935.8	0.460522	0.747991	0.008533	0.000255
140	1467.9	1352	2935.8	0.460522	0.30411	0.003469	0.000104
160	1467.9	1352	2935.8	0.460522	0.166899	0.001904	5.68E-05

(b) Moupfouma

	Moupfouma Model												
r	lambda ( $\lambda$ )	gamma( $\gamma$ )	M(mm)	$\alpha$	$\beta$	R0.01	b	r/R0.01	u	r+1	R0.01-r	R0.01/(r+1)	p(%)
0.4	1.066	0.214	1567.7	12.2903	0.2973	130	-0.00306	0.003077	0.052006	1.4	129.6	92.85714	0.083393
2	1.066	0.214	1567.7	12.2903	0.2973	130	-0.01503	0.015385	0.045798	3	128	43.33333	0.033211
4	1.066	0.214	1567.7	12.2903	0.2973	130	-0.02937	0.030769	0.042712	5	126	26	0.019755
6	1.066	0.214	1567.7	12.2903	0.2973	130	-0.04304	0.046154	0.040797	7	124	18.57143	0.01388
10	1.066	0.214	1567.7	12.2903	0.2973	130	-0.06841	0.076923	0.038277	11	120	11.81818	0.008345
15	1.066	0.214	1567.7	12.2903	0.2973	130	-0.0966	0.115385	0.036199	16	115	8.125	0.005248
20	1.066	0.214	1567.7	12.2903	0.2973	130	-0.12109	0.153846	0.034688	21	110	6.190476	0.003641
25	1.066	0.214	1567.7	12.2903	0.2973	130	-0.14207	0.192308	0.033497	26	105	5	0.00268
30	1.066	0.214	1567.7	12.2903	0.2973	130	-0.15972	0.230769	0.032514	31	100	4.193548	0.002054
40	1.066	0.214	1567.7	12.2903	0.2973	130	-0.18572	0.307692	0.030945	41	90	3.170732	0.001307
60	1.066	0.214	1567.7	12.2903	0.2973	130	-0.20434	0.461538	0.028706	61	70	2.131148	0.000639
80	1.066	0.214	1567.7	12.2903	0.2973	130	-0.18445	0.615385	0.027106	81	50	1.604938	0.000355
120	1.066	0.214	1567.7	12.2903	0.2973	130	-0.0503	0.923077	0.024845	121	10	1.07438	0.000128
140	1.066	0.214	1567.7	12.2903	0.2973	130	0.056222	1.076923	0.023987	141	-10	0.921986	7.83E-05
160	1.066	0.214	1567.7	12.2903	0.2973	130	0.185157	1.230769	0.023246	161	-30	0.807453	4.79E-05
180	1.066	0.214	1567.7	12.2903	0.2973	130	0.334245	1.384615	0.022594	181	-50	0.718232	2.89E-05



(c) Ito & Hosoya

p(%)	log(p)	M	M1	m2	$\beta$	log(ap)	ap	bp	Cp	Rp
0.001	-3.000	1467.9	1352	2935.8	0.460522	1.36264	23.04833	0.281314	0.342603	137.4374
0.003	-2.523	1467.9	1352	2935.8	0.460522	1.150013	14.1258	0.321545	0.398743	108.1365
0.01	-2.000	1467.9	1352	2935.8	0.460522	0.584572	3.84213	0.459749	0.45367	77.21207
0.03	-1.523	1467.9	1352	2935.8	0.460522	-0.28763	0.51567	0.674987	0.442764	50.20542
0.1	-1.000	1467.9	1352	2935.8	0.460522	-1.44442	0.03594	0.93957	0.342809	26.02982
0.3	-0.523	1467.9	1352	2935.8	0.460522	-2.29212	0.005104	1.081167	0.188988	11.69417

(d) ITU-R

% time										
	<i>PH</i>	<i>Abuja</i>	<i>Minna</i>	<i>Jos</i>	<i>Yola</i>	<i>Nsukka</i>	<i>Lagos</i>	<i>Anyingba</i>	<i>Eburumi</i>	<i>Makurdi</i>
10	0.6849	0.66219	0.060211	0.030211	0.051211	0.0234	1.234	0.1246	0.0234	0.0221
1	8.1501	1.9859	4.3502	3.3502	3.2402	3.4423	3.5423	5.0667	2.4423	3.2323

0.3	25.565	7.0402	13.281	11.281	10.008	10.27	11.27	14.991	11.07	8.0402
0.1	47.5	21.097	32.6	29.1	30.12	28.172	29.373	35.163	27.672	33.7
0.03	83.949	48.666	62.133	58.12	60.135	56.414	58.558	64.926	52.414	50.234
0.01	109.1	77.757	91.557	87.1	90.558	81.923	87.936	94.379	80.923	91.9
0.003	145.54	110.85	124.71	118.34	120.31	119.09	121.09	127.53	118.09	122.61
0.001	173.4	141.46	155.33	100.5	149.01	149.3	151.72	158.14	149.83	155.4
0.0001	180.21	151.31	160.23	125.23	160.9	159.23	162.34	162.34	159.98	161.23

%	Bauchi	Ibadan	Lapai	Ogbomo	Ogun	Osun	Kano	Akure	Anyigba
10									
1	2.145	3.1406	2.9711	2.9283	3.0878	3.1081	0.4825	3.4159	3.0372
0.3	5.3112	8.0031	6.8034	6.9905	8.1544	7.6788	4.2977	8.6903	7.0441
0.1	11.1513	18.0081	13.8413	14.798	18.849	6.8406	9.8205	19.508	14.5482
0.03	24.1431	37.5063	28.5596	31.0641	39.2532	35.1819	23.0465	39.7997	30.1293
0.01	42.8151	60.0407	48.1875	51.8163	62.2375	57.1186	42.4226	62.6542	50.3663
0.003	67.5594	86.7741	73.3159	77.6058	89.2127	83.5358	67.7681	89.5346	75.843
0.001	91.854	111.9542	97.7265	102.3382	114.5126	108.563	92.4004	114.7787	100.4183
0.0001	144.7863	165.7253	150.7129	155.6532	168.4126	162.1743	145.7108	168.6101	153.5675

## Kano

### Rice & Holmberg

Rain Rate (R)	Average Annual Rfall Depth (M)	Thunderstorm Rfall(M1)	Total Annual Rfall (M2)	Thunderstorm Ratio ( $\beta$ )	T1(R)	T1(R)/87.66	T1/M
0.4	501.5675	799.57	2006.27	0.398536	118.8127	1.355381	0.059221
12	501.5675	799.57	2006.27	0.398536	6.912746	0.078859	0.003446
15	501.5675	799.57	2006.27	0.398536	5.082202	0.057976	0.002533
20	501.5675	799.57	2006.27	0.398536	3.637525	0.041496	0.001813
25	501.5675	799.57	2006.27	0.398536	2.928037	0.033402	0.001459
30	501.5675	799.57	2006.27	0.398536	2.464357	0.028113	0.001228
40	501.5675	799.57	2006.27	0.398536	1.808183	0.020627	0.000901
50	501.5675	799.57	2006.27	0.398536	1.338212	0.015266	0.000667
60	501.5675	799.57	2006.27	0.398536	0.991272	0.011308	0.000494
70	501.5675	799.57	2006.27	0.398536	0.734344	0.008377	0.000366
80	501.5675	799.57	2006.27	0.398536	0.544015	0.006206	0.000271
90	501.5675	799.57	2006.27	0.398536	0.403016	0.004597	0.000201
100	501.5675	799.57	2006.27	0.398536	0.298562	0.003406	0.000149
120	501.5675	799.57	2006.27	0.398536	0.163854	0.001869	8.17E-05
140	501.5675	799.57	2006.27	0.398536	0.089925	0.001026	4.48E-05
160	501.5675	799.57	2006.27	0.398536	0.049352	0.000563	2.46E-05
180	501.5675	799.57	2006.27	0.398536	0.027085	0.000309	1.35E-05

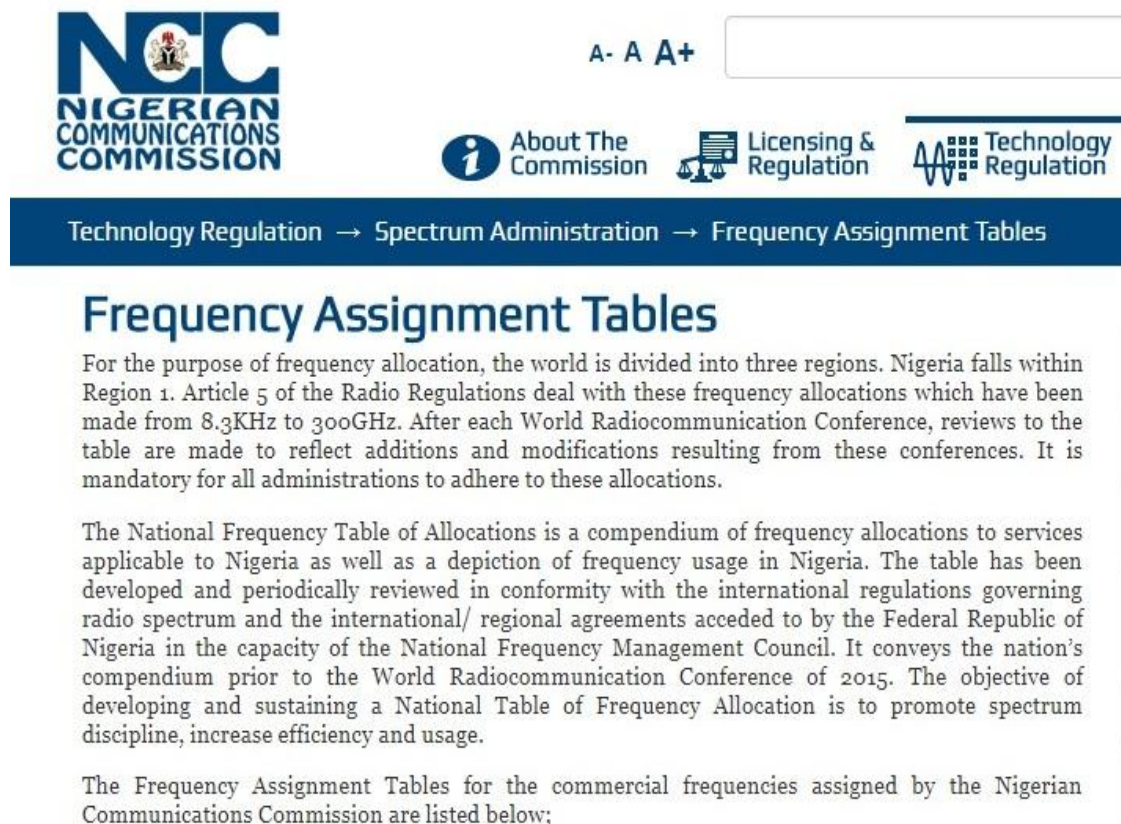
(a) Moupfouma

	Moupfouma Model												
r	lambda ( $\lambda$ )	gamma( $\gamma$ )	M(mm)	$\alpha$	$\beta$	R0.01	b	r/R0.01	u	r+1	R0.01-r	R0.01/(r+1)	p(%)
0.4	1.066	0.214	501.5675	12.2903	0.2973	78.04955	-0.00509	0.005125	0.083587	1.4	77.64955	55.74968	0.064551
12	1.066	0.214	501.5675	12.2903	0.2973	78.04955	-0.12103	0.153748	0.057782	13	66.04955	6.003812	0.003658
15	1.066	0.214	501.5675	12.2903	0.2973	78.04955	-0.142	0.192186	0.055799	16	63.04955	4.878097	0.002692
20	1.066	0.214	501.5675	12.2903	0.2973	78.04955	-0.16967	0.256247	0.053207	21	58.04955	3.716645	0.001756
25	1.066	0.214	501.5675	12.2903	0.2973	78.04955	-0.18886	0.320309	0.051174	26	53.04955	3.001906	0.001227
30	1.066	0.214	501.5675	12.2903	0.2973	78.04955	-0.20023	0.384371	0.049501	31	48.04955	2.517727	0.000897
40	1.066	0.214	501.5675	12.2903	0.2973	78.04955	-0.20171	0.512495	0.046844	41	38.04955	1.903648	0.000522
50	1.066	0.214	501.5675	12.2903	0.2973	78.04955	-0.17792	0.640619	0.044774	51	28.04955	1.530383	0.000326
60	1.066	0.214	501.5675	12.2903	0.2973	78.04955	-0.13188	0.768742	0.043081	61	18.04955	1.279501	0.000211
70	1.066	0.214	501.5675	12.2903	0.2973	78.04955	-0.06603	0.896866	0.041649	71	8.04955	1.099289	0.000139
80	1.066	0.214	501.5675	12.2903	0.2973	78.04955	0.017632	1.02499	0.040411	81	-1.95045	0.963575	9.24E-05
90	1.066	0.214	501.5675	12.2903	0.2973	78.04955	0.117425	1.153114	0.03932	91	-11.9504	0.857687	6.14E-05
100	1.066	0.214	501.5675	12.2903	0.2973	78.04955	0.231942	1.281237	0.038347	101	-21.9504	0.772768	4.06E-05
120	1.066	0.214	501.5675	12.2903	0.2973	78.04955	0.500492	1.537485	0.03667	121	-41.9504	0.645038	1.72E-05
140	1.066	0.214	501.5675	12.2903	0.2973	78.04955	0.815463	1.793732	0.03526	141	-61.9504	0.553543	6.95E-06
160	1.066	0.214	501.5675	12.2903	0.2973	78.04955	1.170869	2.04998	0.034047	161	-81.9504	0.48478	2.63E-06
180	1.066	0.214	501.5675	12.2903	0.2973	78.04955	1.561997	2.306227	0.032984	181	-101.95	0.431213	9.31E-07

Ito & Hosoya

$\rho(\%)$	$\log(\rho)$	M	M1	m2	$\beta$	$\log(ap)$	ap	bp	Cp	Rp
0.001	-3.000	501.5675	799.57	2006.27	0.398536	1.36264	23.04833	0.281314	0.342603	96.69402
0.003	-2.523	501.5675	799.57	2006.27	0.398536	1.150013	14.1258	0.321545	0.398743	72.27365
0.01	-2.000	501.5675	799.57	2006.27	0.398536	0.584572	3.84213	0.459749	0.45367	44.13575
0.03	-1.523	501.5675	799.57	2006.27	0.398536	-0.28763	0.51567	0.674987	0.442764	22.81186
0.1	-1.000	501.5675	799.57	2006.27	0.398536	-1.44442	0.03594	0.93957	0.342809	9.031582
0.3	-0.523	501.5675	799.57	2006.27	0.398536	-2.29212	0.005104	1.081167	0.188988	3.563555

## Appendix 13: Frequency allocation Tables by ITU to the Nigerian Communications Commission and the usage



The screenshot shows the Nigerian Communications Commission (NCC) website. At the top left is the NCC logo. To its right is a search bar with the text "A- A A+" and an empty input field. Below the logo are three navigation icons: "About The Commission" (info icon), "Licensing & Regulation" (scales icon), and "Technology Regulation" (wave icon). A dark blue navigation bar contains the breadcrumb "Technology Regulation → Spectrum Administration → Frequency Assignment Tables". The main heading is "Frequency Assignment Tables". The text below explains that the world is divided into three regions for frequency allocation, with Nigeria in Region 1. It mentions that Article 5 of the Radio Regulations deals with these allocations, which range from 8.3KHz to 300GHz. It states that the table is updated after World Radiocommunication Conferences and is mandatory for all administrations. The text further describes the National Frequency Table of Allocations as a compendium of frequency allocations to services applicable to Nigeria, developed and reviewed in conformity with international regulations. It notes that the table has been developed and periodically reviewed in conformity with international regulations governing radio spectrum and regional agreements. The objective of developing and sustaining a National Table of Frequency Allocation is to promote spectrum discipline, increase efficiency and usage. Finally, it states that the Frequency Assignment Tables for commercial frequencies assigned by the NCC are listed below.

SEGMENT 6: 30 GHz – 300 GHz				
FREQUENCY BANDS (GHz)	ITU REGION 1 ALLOCATIONS	NIGERIA ALLOCATIONS	NIGERIAN UTILIZATION	REMARKS
31.50 - 31.80	EARTH EXPLORATION-SATELLITE (passive) RADIO ASTRONOMY SPACE RESEARCH (passive) Fixed Mobile except aeronautical mobile 5.149 5.546	EARTH EXPLORATION-SATELLITE (passive) RADIO ASTRONOMY SPACE RESEARCH (passive) Fixed Mobile except aeronautical mobile 5.149		
31.80 - 32	FIXED 5.547A RADIONAVIGATION SPACE RESEARCH (deep space)(s-E) 5.547 5.547B 5.548	FIXED 5.547A RADIONAVIGATION SPACE RESEARCH (deep space)(s-E) 5.547 5.548		
32 - 32.30	FIXED 5.547A RADIONAVIGATION SPACE RESEARCH (deep space)(s-E) 5.547 5.547C 5.548	FIXED 5.547A RADIONAVIGATION SPACE RESEARCH (deep space)(s-E) 5.547 5.548		
32.30 - 33	FIXED 5.547A INTER-SATELLITE RADIONAVIGATION 5.547 5.547D 5.548	FIXED 5.547A INTER-SATELLITE RADIONAVIGATION 5.547 5.548		

SEGMENT 6: 30 GHz – 300 GHz				
FREQUENCY BANDS (GHz)	ITU REGION 1 ALLOCATIONS	NIGERIA ALLOCATIONS	NIGERIAN UTILIZATION	REMARKS
33 - 33.40	FIXED 5.547A RADIONAVIGATION 5.547 5.547E	FIXED 5.547A RADIONAVIGATION 5.547		
33.40 - 34.20	RADIOLOCATION 5.549	FIXED MOBILE RADIOLOCATION 5.549		
34.20 - 34.70	RADIOLOCATION SPACE RESEARCH (deep space)(E-s) 5.549	FIXED MOBILE RADIOLOCATION SPACE RESEARCH (deep space)(E-s) 5.549		
34.70 - 35.20	RADIOLOCATION Space research 5.550 5.549	FIXED MOBILE RADIOLOCATION Space Research 5.549		

Frequency band	Affected Service	In band
31,8 – 33,4 GHz	RN - Radar	31,8 – 33,4 GHz
	EESS (passive)	31,3 – 31,8 GHz
	RA	31,3 – 31,8 GHz
	SRS (passive)	31,3 – 31,8 GHz
	FS	31,8 – 33,4 GHz
	ISS	32,3 – 33,0 GHz



### Appendix 14: Computations of Path Attenuation at 150GHz Frequency Threshold

#### NSUKKA

ITU-R Model											Deff	Deff	A0.01	
F(GHz)	KH	$\alpha$ H	R0.01	YR (H)	(B2/10)^0.8	Co	C3	C2	C1	r (H)	d(km)	V(d*r)	H(d*r)	(H)
150	1.5823	0.6494	91.3000	29.6769	8.727161	0.496349	0.09065	0.699372	0.091832	1.185712	1	1.187132	1.185712	35.18825
150	1.5823	0.6494	91.3000	29.6769	8.727161	0.496349	0.09065	0.699372	0.091832	0.545084	5	2.72958	2.725421	80.88206
150	1.5823	0.6494	91.3000	29.6769	8.727161	0.496349	0.09065	0.699372	0.091832	0.409344	10	4.100716	4.09344	121.4806
150	1.5823	0.6494	91.3000	29.6769	8.727161	0.496349	0.09065	0.699372	0.091832	0.347558	15	5.223547	5.213374	154.7168
150	1.5823	0.6494	91.3000	29.6769	8.727161	0.496349	0.09065	0.699372	0.091832	0.307115	20	6.155003	6.142296	182.2843
150	1.5823	0.6494	91.3000	29.6769	8.727161	0.496349	0.09065	0.699372	0.091832	0.276113	25	6.917601	6.902813	204.8541

#### Moupfouma Model

											Leff	A0.01
F(GHz)	KH	$\alpha$ H	R0.01	YR (H)	M	B	p	r (H)	L(km)	(r*I)	(H)	
150	1.5823	0.6494	91.3000	29.6769	1	0.6	0.01	1.03	1	1.03	30.56721	
150	1.5823	0.6494	91.3000	29.6769	2.523081	0.6	0.01	1.03	5	5.15	152.836	
150	1.5823	0.6494	91.3000	29.6769	3.179036	0.6	0.01	1.03	10	10.3	305.6721	
150	1.5823	0.6494	91.3000	29.6769	3.562745	0.6	0.01	1.03	15	15.45	458.5081	
150	1.5823	0.6494	91.3000	29.6769	3.834991	0.6	0.01	1.03	20	20.6	611.3442	
150	1.5823	0.6494	91.3000	29.6769	4.046161	0.6	0.01	1.03	25	25.75	764.1802	

#### Crane Global Model

F(GHz)	KH	$\alpha$ H	R0.01	YR (H)	d(km)	$\delta$ (R)	C	B	U	y	Z	AT
150	1.5823	0.6494	91.3000	29.6769	1	1.09151	-0.10942	0.062594	-0.05208	-0.03382	-0.07106	15.07986

150	1.5823	0.6494	91.3000	29.6769	5	1.09151	-0.10942	0.062594	-0.05208	-0.03382	-0.07106	122.4902
150	1.5823	0.6494	91.3000	29.6769	10	1.09151	-0.10942	0.062594	-0.05208	-0.03382	-0.07106	220.192
150	1.5823	0.6494	91.3000	29.6769	15	1.09151	-0.10942	0.062594	-0.05208	-0.03382	-0.07106	288.6772
150	1.5823	0.6494	91.3000	29.6769	20	1.09151	-0.10942	0.062594	-0.05208	-0.03382	-0.07106	336.6827
150	1.5823	0.6494	91.3000	29.6769	25	1.09151	-0.10942	0.062594	-0.05208	-0.03382	-0.07106	370.3328

### Eburumiri

#### ITU-R Model

F(GHz)	KH	$\alpha H$	R0.01	YR (H)	$(B2/10)^{0.8}$	Co	C3	C2	C1	r (H)	d(km)	Deff V(d*r)	Deff H(d*r)	A0.01 (H)
150	1.5823	0.6494	90.4000	29.4866	8.727161	0.496349	0.09065	0.699372	0.091832	1.186434	1	1.187853	1.186434	34.98391
150	1.5823	0.6494	90.4000	29.4866	8.727161	0.496349	0.09065	0.699372	0.091832	0.545507	5	2.731691	2.727537	80.42577
150	1.5823	0.6494	90.4000	29.4866	8.727161	0.496349	0.09065	0.699372	0.091832	0.409714	10	4.104411	4.097141	120.8107
150	1.5823	0.6494	90.4000	29.4866	8.727161	0.496349	0.09065	0.699372	0.091832	0.347903	15	5.228714	5.218548	153.8772
150	1.5823	0.6494	90.4000	29.4866	8.727161	0.496349	0.09065	0.699372	0.091832	0.307438	20	6.161459	6.148759	181.306
150	1.5823	0.6494	90.4000	29.4866	8.727161	0.496349	0.09065	0.699372	0.091832	0.276413	25	6.925114	6.910333	203.7622

#### Moupfouma Model

F(GHz)	KH	$\alpha H$	R0.01	YR (H)	M	B	p	r (H)	L(km)	Leff (r*I)	A0.01 (H)
150	1.5823	0.6494	90.4000	29.4866	1	0.6	0.01	1.03	1	1.03	30.37119
150	1.5823	0.6494	90.4000	29.4866	2.523081	0.6	0.01	1.03	5	5.15	151.856

150	1.5823	0.6494	90.4000	29.4866	3.179036	0.6	0.01	1.03	10	10.3	303.7119
150	1.5823	0.6494	90.4000	29.4866	3.562745	0.6	0.01	1.03	15	15.45	455.5679
150	1.5823	0.6494	90.4000	29.4866	3.834991	0.6	0.01	1.03	20	20.6	607.4238
150	1.5823	0.6494	90.4000	29.4866	4.046161	0.6	0.01	1.03	25	25.75	759.2798

Crane Global Model

F(GHz)	KH	$\alpha$ H	R0.01	YR (H)	d(km)	$\delta$ (R)	C	B	U	y	Z	AT
150	1.5823	0.6494	90.4000	29.4866	1	1.097453	-0.10913	0.064278	-0.05056	-0.03283	-0.07087	15.44303
150	1.5823	0.6494	90.4000	29.4866	5	1.097453	-0.10913	0.064278	-0.05056	-0.03283	-0.07087	122.9706
150	1.5823	0.6494	90.4000	29.4866	10	1.097453	-0.10913	0.064278	-0.05056	-0.03283	-0.07087	220.863
150	1.5823	0.6494	90.4000	29.4866	15	1.097453	-0.10913	0.064278	-0.05056	-0.03283	-0.07087	289.5481
150	1.5823	0.6494	90.4000	29.4866	20	1.097453	-0.10913	0.064278	-0.05056	-0.03283	-0.07087	337.7402
150	1.5823	0.6494	90.4000	29.4866	25	1.097453	-0.10913	0.064278	-0.05056	-0.03283	-0.07087	371.5536

**Anyigba**

ITU-R Model

ITU-R Model											Deff	Deff	A0.01	
F(GHz)	KH	$\alpha$ H	R0.01	YR (H)	$(B2/10)^{0.8}$	Co	C3	C2	C1	r (H)	d(km)	V(d*r)	H(d*r)	(H)
150	1.5823	0.6494	33.5000	15.4758	8.727161	0.496349	0.09065	0.699372	0.091832	1.261698	1	1.262891	1.261698	19.52578
150	1.5823	0.6494	33.5000	15.4758	8.727161	0.496349	0.09065	0.699372	0.091832	0.590356	5	2.955398	2.95178	45.68113
150	1.5823	0.6494	33.5000	15.4758	8.727161	0.496349	0.09065	0.699372	0.091832	0.449487	10	4.501373	4.494866	69.56163
150	1.5823	0.6494	33.5000	15.4758	8.727161	0.496349	0.09065	0.699372	0.091832	0.385326	15	5.789166	5.779893	89.44843

150	1.5823	0.6494	33.5000	15.4758	8.727161	0.496349	0.09065	0.699372	0.091832	0.342727	20	6.866282	6.854546	106.0795
150	1.5823	0.6494	33.5000	15.4758	8.727161	0.496349	0.09065	0.699372	0.091832	0.309402	25	7.748819	7.735048	119.706

Moupfouma Model

F(GHz)	KH	$\alpha$ H	R0.01	YR (H)	M	B	p	r (H)	L(km)	Leff (r*I)	A0.01 (H)	
150	1.5823	0.6494	33.5000	15.4758		1	0.6	0.01	1.03	1	1.03	15.94007
150	1.5823	0.6494	33.5000	15.4758	2.523081		0.6	0.01	1.03	5	5.15	79.70034
150	1.5823	0.6494	33.5000	15.4758	3.179036		0.6	0.01	1.03	10	10.3	159.4007
150	1.5823	0.6494	33.5000	15.4758	3.562745		0.6	0.01	1.03	15	15.45	239.101
150	1.5823	0.6494	33.5000	15.4758	3.834991		0.6	0.01	1.03	20	20.6	318.8013
150	1.5823	0.6494	33.5000	15.4758	4.046161		0.6	0.01	1.03	25	25.75	398.5017

Crane Global Model

F(GHz)	KH	$\alpha$ H	R0.01	YR (H)	d(km)	$\delta$ (R)	C	B	U	y	Z	AT
150	1.5823	0.6494	33.5000	15.4758	1	1.693073	-0.07935	0.233037	0.058295	0.037857	-0.05153	71.1241
150	1.5823	0.6494	33.5000	15.4758	5	1.693073	-0.07935	0.233037	0.058295	0.037857	-0.05153	179.2024
150	1.5823	0.6494	33.5000	15.4758	10	1.693073	-0.07935	0.233037	0.058295	0.037857	-0.05153	286.4479
150	1.5823	0.6494	33.5000	15.4758	15	1.693073	-0.07935	0.233037	0.058295	0.037857	-0.05153	369.3353
150	1.5823	0.6494	33.5000	15.4758	20	1.693073	-0.07935	0.233037	0.058295	0.037857	-0.05153	433.3969
150	1.5823	0.6494	33.5000	15.4758	25	1.693073	-0.07935	0.233037	0.058295	0.037857	-0.05153	482.9086

### Makurdi

#### ITU-R Model

F(GHz)	KH	$\alpha H$	R0.01	YR (H)	$(B2/10)^{0.8}$	Co	C3	C2	C1	r (H)	d(km)	Deff V(d*r)	Deff H(d*r)	A0.01 (H)
150	1.5823	0.6494	51.0000	20.3322	8.727161	0.496349	0.09065	0.699372	0.091832	1.229134	1	1.230427	1.229134	24.99103
150	1.5823	0.6494	51.0000	20.3322	8.727161	0.496349	0.09065	0.699372	0.091832	0.570759	5	2.857656	2.853793	58.02396
150	1.5823	0.6494	51.0000	20.3322	8.727161	0.496349	0.09065	0.699372	0.091832	0.431974	10	4.326603	4.319738	87.82989
150	1.5823	0.6494	51.0000	20.3322	8.727161	0.496349	0.09065	0.699372	0.091832	0.36876	15	5.541103	5.531402	112.4657
150	1.5823	0.6494	51.0000	20.3322	8.727161	0.496349	0.09065	0.699372	0.091832	0.327049	20	6.553191	6.540983	132.9927
150	1.5823	0.6494	51.0000	20.3322	8.727161	0.496349	0.09065	0.699372	0.091832	0.294713	25	7.38209	7.367817	149.8041

#### Moupfouma Model

F(GHz)	KH	$\alpha H$	R0.01	YR (H)	M	B	p	r (H)	L(km)	Leff (r*l)	A0.01 (H)
150	1.5823	0.6494	51.0000	20.3322	1	0.6	0.01	1.03	1	1.03	20.94219
150	1.5823	0.6494	51.0000	20.3322	2.523081	0.6	0.01	1.03	5	5.15	104.711
150	1.5823	0.6494	51.0000	20.3322	3.179036	0.6	0.01	1.03	10	10.3	209.4219
150	1.5823	0.6494	51.0000	20.3322	3.562745	0.6	0.01	1.03	15	15.45	314.1329
150	1.5823	0.6494	51.0000	20.3322	3.834991	0.6	0.01	1.03	20	20.6	418.8438
150	1.5823	0.6494	51.0000	20.3322	4.046161	0.6	0.01	1.03	25	25.75	523.5548

Crane Global Model

F(GHz)	KH	$\alpha$ H	R0.01	YR (H)	d(km)	$\delta$ (R)	C	B	U	y	Z	AT
150	1.5823	0.6494	51.0000	20.3322	1	1.440905	-0.09195	0.16159	0.02019	0.013111	-0.05972	42.37667
150	1.5823	0.6494	51.0000	20.3322	5	1.440905	-0.09195	0.16159	0.02019	0.013111	-0.05972	152.4778
150	1.5823	0.6494	51.0000	20.3322	10	1.440905	-0.09195	0.16159	0.02019	0.013111	-0.05972	257.8143
150	1.5823	0.6494	51.0000	20.3322	15	1.440905	-0.09195	0.16159	0.02019	0.013111	-0.05972	335.9605
150	1.5823	0.6494	51.0000	20.3322	20	1.440905	-0.09195	0.16159	0.02019	0.013111	-0.05972	393.9351
150	1.5823	0.6494	51.0000	20.3322	25	1.440905	-0.09195	0.16159	0.02019	0.013111	-0.05972	436.9449

Iwo

ITU-R Model												Deff	Deff	A0.01
F(GHz)	KH	$\alpha$ H	R0.01	YR (H)	$(B2/10)^{0.8}$	Co	C3	C2	C1	r (H)	d(km)	V(d*r)	H(d*r)	(H)
150	1.5823	0.6494	62.6000	23.2265	8.727161	0.496349	0.09065	0.699372	0.091832	1.213632	1	1.214972	1.213632	28.18846
150	1.5823	0.6494	62.6000	23.2265	8.727161	0.496349	0.09065	0.699372	0.091832	0.561533	5	2.81164	2.807667	65.21235
150	1.5823	0.6494	62.6000	23.2265	8.727161	0.496349	0.09065	0.699372	0.091832	0.423802	10	4.24504	4.23802	98.43447
150	1.5823	0.6494	62.6000	23.2265	8.727161	0.496349	0.09065	0.699372	0.091832	0.361077	15	5.426045	5.416162	125.7986
150	1.5823	0.6494	62.6000	23.2265	8.727161	0.496349	0.09065	0.699372	0.091832	0.319809	20	6.40858	6.396177	148.561
150	1.5823	0.6494	62.6000	23.2265	8.727161	0.496349	0.09065	0.699372	0.091832	0.287947	25	7.213152	7.198677	167.2002

Moupfouma Model

												Leff	A0.01
F(GHz)	KH	$\alpha$ H	R0.01	YR (H)	M	B	p	r (H)	L(km)	(r*I)	(H)		
150	1.5823	0.6494	62.6000	23.2265		1	0.6	0.01	1.03	1	1.03	23.92332	

150	1.5823	0.6494	62.6000	23.2265	2.523081	0.6	0.01	1.03	5	5.15	119.6166
150	1.5823	0.6494	62.6000	23.2265	3.179036	0.6	0.01	1.03	10	10.3	239.2332
150	1.5823	0.6494	62.6000	23.2265	3.562745	0.6	0.01	1.03	15	15.45	358.8498
150	1.5823	0.6494	62.6000	23.2265	3.834991	0.6	0.01	1.03	20	20.6	478.4664
150	1.5823	0.6494	62.6000	23.2265	4.046161	0.6	0.01	1.03	25	25.75	598.083

Crane Global Model

F(GHz)	KH	$\alpha$ H	R0.01	YR (H)	d(km)	$\delta$ (R)	C	B	U	y	Z	AT
150	1.5823	0.6494	62.6000	23.2265	1	1.317941	-0.0981	0.12675	-0.00193	-0.00125	-0.06371	31.31375
150	1.5823	0.6494	62.6000	23.2265	5	1.317941	-0.0981	0.12675	-0.00193	-0.00125	-0.06371	141.3407
150	1.5823	0.6494	62.6000	23.2265	10	1.317941	-0.0981	0.12675	-0.00193	-0.00125	-0.06371	244.7508
150	1.5823	0.6494	62.6000	23.2265	15	1.317941	-0.0981	0.12675	-0.00193	-0.00125	-0.06371	319.9516
150	1.5823	0.6494	62.6000	23.2265	20	1.317941	-0.0981	0.12675	-0.00193	-0.00125	-0.06371	374.6384
150	1.5823	0.6494	62.6000	23.2265	25	1.317941	-0.0981	0.12675	-0.00193	-0.00125	-0.06371	414.4072

Ogun

ITU-R Model

F(GHz)	KH	$\alpha$ H	R0.01	YR (H)	$(B2/10)^{0.8}$	Co	C3	C2	C1	r (H)	d(km)	Deff V(d*r)	Deff H(d*r)	A0.01 (H)
150	1.5823	0.6494	40.0000	17.3647	8.727161	0.496349	0.09065	0.699372	0.091832	1.247829	1	1.249065	1.247829	21.66815
150	1.5823	0.6494	40.0000	17.3647	8.727161	0.496349	0.09065	0.699372	0.091832	0.581973	5	2.91359	2.909865	50.52886
150	1.5823	0.6494	40.0000	17.3647	8.727161	0.496349	0.09065	0.699372	0.091832	0.44197	10	4.426362	4.419698	76.7466
150	1.5823	0.6494	40.0000	17.3647	8.727161	0.496349	0.09065	0.699372	0.091832	0.378199	15	5.682443	5.672979	98.50943

150	1.5823	0.6494	40.0000	17.3647	8.727161	0.496349	0.09065	0.699372	0.091832	0.335971	20	6.731362	6.719414	116.6804
150	1.5823	0.6494	40.0000	17.3647	8.727161	0.496349	0.09065	0.699372	0.091832	0.303065	25	7.590621	7.576624	131.5656

Moupfouma Model

F(GHz)	KH	$\alpha$ H	R0.01	YR (H)	M	B	p	r (H)	L(km)	Leff (r*I)	A0.01 (H)	
150	1.5823	0.6494	40.0000	17.3647		1	0.6	0.01	1.03	1	1.03	17.88561
150	1.5823	0.6494	40.0000	17.3647	2.523081		0.6	0.01	1.03	5	5.15	89.42806
150	1.5823	0.6494	40.0000	17.3647	3.179036		0.6	0.01	1.03	10	10.3	178.8561
150	1.5823	0.6494	40.0000	17.3647	3.562745		0.6	0.01	1.03	15	15.45	268.2842
150	1.5823	0.6494	40.0000	17.3647	3.834991		0.6	0.01	1.03	20	20.6	357.7122
150	1.5823	0.6494	40.0000	17.3647	4.046161		0.6	0.01	1.03	25	25.75	447.1403

Crane Global Model

F(GHz)	KH	$\alpha$ H	R0.01	YR (H)	d(km)	$\delta$ (R)	C	B	U	y	Z	AT
150	1.5823	0.6494	40.0000	17.3647	1	1.586672	-0.08467	0.20289	0.043205	0.028058	-0.05498	57.88776
150	1.5823	0.6494	40.0000	17.3647	5	1.586672	-0.08467	0.20289	0.043205	0.028058	-0.05498	167.1267
150	1.5823	0.6494	40.0000	17.3647	10	1.586672	-0.08467	0.20289	0.043205	0.028058	-0.05498	273.8663
150	1.5823	0.6494	40.0000	17.3647	15	1.586672	-0.08467	0.20289	0.043205	0.028058	-0.05498	354.95
150	1.5823	0.6494	40.0000	17.3647	20	1.586672	-0.08467	0.20289	0.043205	0.028058	-0.05498	416.5443
150	1.5823	0.6494	40.0000	17.3647	25	1.586672	-0.08467	0.20289	0.043205	0.028058	-0.05498	463.3337



**Port Harcourt**

ITU-R Model											Deff	Deff	A0.01	
F(GHz)	KH	$\alpha$ H	R0.01	YR (H)	$(B2/10)^{0.8}$	Co	C3	C2	C1	r (H)	d(km)	V(d*r)	H(d*r)	(H)
150	1.5823	0.6494	87.3000	28.8259	8.727161	0.496349	0.09065	0.699372	0.091832	1.188985	1	1.190396	1.188985	34.2736
150	1.5823	0.6494	87.3000	28.8259	8.727161	0.496349	0.09065	0.699372	0.091832	0.547001	5	2.739145	2.735007	78.83916
150	1.5823	0.6494	87.3000	28.8259	8.727161	0.496349	0.09065	0.699372	0.091832	0.411022	10	4.117465	4.110217	118.4809
150	1.5823	0.6494	87.3000	28.8259	8.727161	0.496349	0.09065	0.699372	0.091832	0.349122	15	5.246975	5.236835	150.9567
150	1.5823	0.6494	87.3000	28.8259	8.727161	0.496349	0.09065	0.699372	0.091832	0.30858	20	6.184281	6.171607	177.9024
150	1.5823	0.6494	87.3000	28.8259	8.727161	0.496349	0.09065	0.699372	0.091832	0.277477	25	6.951681	6.936926	199.9634

Moupfouma Model

											Leff	A0.01
F(GHz)	KH	$\alpha$ H	R0.01	YR (H)	M	B	p	r (H)	L(km)	(r*I)	(H)	
150	1.5823	0.6494	87.3000	28.8259	1	0.6	0.01	1.03	1	1.03	29.69072	
150	1.5823	0.6494	87.3000	28.8259	2.523081	0.6	0.01	1.03	5	5.15	148.4536	
150	1.5823	0.6494	87.3000	28.8259	3.179036	0.6	0.01	1.03	10	10.3	296.9072	
150	1.5823	0.6494	87.3000	28.8259	3.562745	0.6	0.01	1.03	15	15.45	445.3608	
150	1.5823	0.6494	87.3000	28.8259	3.834991	0.6	0.01	1.03	20	20.6	593.8144	
150	1.5823	0.6494	87.3000	28.8259	4.046161	0.6	0.01	1.03	25	25.75	742.268	

Crane Global Model

F(GHz)	KH	$\alpha$ H	R0.01	YR (H)	d(km)	$\delta$ (R)	C	B	U	y	Z	AT
150	1.5823	0.6494	87.3000	28.8259	1	1.11839	-0.10808	0.07021	-0.0453	-0.02942	-0.07019	16.74823
150	1.5823	0.6494	87.3000	28.8259	5	1.11839	-0.10808	0.07021	-0.0453	-0.02942	-0.07019	124.6658
150	1.5823	0.6494	87.3000	28.8259	10	1.11839	-0.10808	0.07021	-0.0453	-0.02942	-0.07019	223.2107
150	1.5823	0.6494	87.3000	28.8259	15	1.11839	-0.10808	0.07021	-0.0453	-0.02942	-0.07019	292.5891
150	1.5823	0.6494	87.3000	28.8259	20	1.11839	-0.10808	0.07021	-0.0453	-0.02942	-0.07019	341.4334
150	1.5823	0.6494	87.3000	28.8259	25	1.11839	-0.10808	0.07021	-0.0453	-0.02942	-0.07019	375.8211

**Akure**

ITU-R Model

ITU-R Model											Deff	Deff	A0.01	
F(GHz)	KH	$\alpha$ H	R0.01	YR (H)	$(B2/10)^{0.8}$	Co	C3	C2	C1	r (H)	d(km)	V(d*r)	H(d*r)	(H)
150	1.5823	0.6494	121.0000	35.6328	8.727161	0.496349	0.09065	0.699372	0.091832	1.165388	1	1.166866	1.165388	41.52602
150	1.5823	0.6494	121.0000	35.6328	8.727161	0.496349	0.09065	0.699372	0.091832	0.533243	5	2.670502	2.666217	95.0047
150	1.5823	0.6494	121.0000	35.6328	8.727161	0.496349	0.09065	0.699372	0.091832	0.399025	10	3.997695	3.99025	142.1837
150	1.5823	0.6494	121.0000	35.6328	8.727161	0.496349	0.09065	0.699372	0.091832	0.337966	15	5.07985	5.069493	180.6401
150	1.5823	0.6494	121.0000	35.6328	8.727161	0.496349	0.09065	0.699372	0.091832	0.298144	20	5.975777	5.962882	212.474
150	1.5823	0.6494	121.0000	35.6328	8.727161	0.496349	0.09065	0.699372	0.091832	0.26777	25	6.709228	6.694252	238.5348

### Moupfouma Model

F(GHz)	KH	$\alpha H$	R0.01	YR (H)	M	B	p	r (H)	L(km)	Leff (r*l)	A0.01 (H)	
150	1.5823	0.6494	121.0000	35.6328		1	0.6	0.01	1.03	1	1.03	36.70176
150	1.5823	0.6494	121.0000	35.6328	2.523081		0.6	0.01	1.03	5	5.15	183.5088
150	1.5823	0.6494	121.0000	35.6328	3.179036		0.6	0.01	1.03	10	10.3	367.0176
150	1.5823	0.6494	121.0000	35.6328	3.562745		0.6	0.01	1.03	15	15.45	550.5264
150	1.5823	0.6494	121.0000	35.6328	3.834991		0.6	0.01	1.03	20	20.6	734.0352
150	1.5823	0.6494	121.0000	35.6328	4.046161		0.6	0.01	1.03	25	25.75	917.544

### Crane Global Model

F(GHz)	KH	$\alpha H$	R0.01	YR (H)	d(km)	$\delta(R)$	C	B	U	y	Z	AT
150	1.5823	0.6494	121.0000	35.6328	1	0.922526	-0.11787	0.014716	-0.10192	-0.06619	-0.07655	6.080526
150	1.5823	0.6494	121.0000	35.6328	5	0.922526	-0.11787	0.014716	-0.10192	-0.06619	-0.07655	108.8371
150	1.5823	0.6494	121.0000	35.6328	10	0.922526	-0.11787	0.014716	-0.10192	-0.06619	-0.07655	200.0538
150	1.5823	0.6494	121.0000	35.6328	15	0.922526	-0.11787	0.014716	-0.10192	-0.06619	-0.07655	262.2629
150	1.5823	0.6494	121.0000	35.6328	20	0.922526	-0.11787	0.014716	-0.10192	-0.06619	-0.07655	304.6891
150	1.5823	0.6494	121.0000	35.6328	25	0.922526	-0.11787	0.014716	-0.10192	-0.06619	-0.07655	333.6234

### Bauchi

ITU-R Model											Deff	Deff	A0.01	
F(GHz)	KH	$\alpha$ H	R0.01	YR (H)	$(B2/10)^{0.8}$	Co	C3	C2	C1	r (H)	d(km)	V(d*r)	H(d*r)	(H)
150	1.5823	0.6494	96.7000	30.8053	8.727161	0.496349	0.09065	0.699372	0.091832	1.18153	1	1.182962	1.18153	36.39733
150	1.5823	0.6494	96.7000	30.8053	8.727161	0.496349	0.09065	0.699372	0.091832	0.542639	5	2.71738	2.713194	83.58063
150	1.5823	0.6494	96.7000	30.8053	8.727161	0.496349	0.09065	0.699372	0.091832	0.407207	10	4.079381	4.072068	125.4411
150	1.5823	0.6494	96.7000	30.8053	8.727161	0.496349	0.09065	0.699372	0.091832	0.345568	15	5.19373	5.183517	159.6796
150	1.5823	0.6494	96.7000	30.8053	8.727161	0.496349	0.09065	0.699372	0.091832	0.305251	20	6.117765	6.105017	188.0666
150	1.5823	0.6494	96.7000	30.8053	8.727161	0.496349	0.09065	0.699372	0.091832	0.274378	25	6.874271	6.859442	211.3068

### Moupfouma Model

F(GHz)	KH	$\alpha$ H	R0.01	YR (H)	M	B	p	r (H)	L(km)	Leff	A0.01
										(r*I)	(H)
150	1.5823	0.6494	96.7000	30.8053	1	0.6	0.01	1.03	1	1.03	31.72941
150	1.5823	0.6494	96.7000	30.8053	2.523081	0.6	0.01	1.03	5	5.15	158.6471
150	1.5823	0.6494	96.7000	30.8053	3.179036	0.6	0.01	1.03	10	10.3	317.2941
150	1.5823	0.6494	96.7000	30.8053	3.562745	0.6	0.01	1.03	15	15.45	475.9412
150	1.5823	0.6494	96.7000	30.8053	3.834991	0.6	0.01	1.03	20	20.6	634.5882
150	1.5823	0.6494	96.7000	30.8053	4.046161	0.6	0.01	1.03	25	25.75	793.2353

### Crane Global Model

F(GHz)	KH	$\alpha$ H	R0.01	YR (H)	d(km)	$\delta$ (R)	C	B	U	y	Z	AT
150	1.5823	0.6494	96.7000	30.8053	1	1.057032	-0.11115	0.052826	-0.06117	-0.03973	-0.07218	13.03692

150	1.5823	0.6494	96.7000	30.8053	5	1.057032	-0.11115	0.052826	-0.06117	-0.03973	-0.07218	119.7089
150	1.5823	0.6494	96.7000	30.8053	10	1.057032	-0.11115	0.052826	-0.06117	-0.03973	-0.07218	216.2573
150	1.5823	0.6494	96.7000	30.8053	15	1.057032	-0.11115	0.052826	-0.06117	-0.03973	-0.07218	283.5562
150	1.5823	0.6494	96.7000	30.8053	20	1.057032	-0.11115	0.052826	-0.06117	-0.03973	-0.07218	330.467
150	1.5823	0.6494	96.7000	30.8053	25	1.057032	-0.11115	0.052826	-0.06117	-0.03973	-0.07218	363.166

**Jos**

ITU-R Model											Deff	Deff	A0.01	
F(GHz)	KH	$\alpha$ H	R0.01	YR (H)	$(B2/10)^{0.8}$	Co	C3	C2	C1	r (H)	d(km)	V(d*r)	H(d*r)	(H)
150	1.5823	0.6494	22.8000	12.0540	8.727161	0.496349	0.09065	0.699372	0.091832	1.292455	1	1.293549	1.292455	15.57927
150	1.5823	0.6494	22.8000	12.0540	8.727161	0.496349	0.09065	0.699372	0.091832	0.609143	5	3.049081	3.045714	36.71308
150	1.5823	0.6494	22.8000	12.0540	8.727161	0.496349	0.09065	0.699372	0.091832	0.466474	10	4.670863	4.664736	56.2288
150	1.5823	0.6494	22.8000	12.0540	8.727161	0.496349	0.09065	0.699372	0.091832	0.401529	15	6.031734	6.022931	72.6005
150	1.5823	0.6494	22.8000	12.0540	8.727161	0.496349	0.09065	0.699372	0.091832	0.358149	20	7.174188	7.162984	86.34271
150	1.5823	0.6494	22.8000	12.0540	8.727161	0.496349	0.09065	0.699372	0.091832	0.323903	25	8.110774	8.097581	97.60836

**Moupfouma Model**

											Leff	A0.01
F(GHz)	KH	$\alpha$ H	R0.01	YR (H)	M	B	P	r (H)	L(km)	(r*I)	(H)	
150	1.5823	0.6494	22.8000	12.0540	1	0.6	0.01	1.03	1	1.03	12.41564	
150	1.5823	0.6494	22.8000	12.0540	2.523081	0.6	0.01	1.03	5	5.15	62.07818	

150	1.5823	0.6494	22.8000	12.0540	3.179036	0.6	0.01	1.03	10	10.3	124.1564
150	1.5823	0.6494	22.8000	12.0540	3.562745	0.6	0.01	1.03	15	15.45	186.2345
150	1.5823	0.6494	22.8000	12.0540	3.834991	0.6	0.01	1.03	20	20.6	248.3127
150	1.5823	0.6494	22.8000	12.0540	4.046161	0.6	0.01	1.03	25	25.75	310.3909

Crane Global Model

F(GHz)	KH	$\alpha H$	R0.01	YR (H)	d(km)	$\delta(R)$	C	B	U	y	Z	AT
150	1.5823	0.6494	22.8000	12.0540	1	1.923944	-0.0678	0.298451	0.087322	0.056707	-0.04403	106.9698
150	1.5823	0.6494	22.8000	12.0540	5	1.923944	-0.0678	0.298451	0.087322	0.056707	-0.04403	211.3592
150	1.5823	0.6494	22.8000	12.0540	10	1.923944	-0.0678	0.298451	0.087322	0.056707	-0.04403	318.4694
150	1.5823	0.6494	22.8000	12.0540	15	1.923944	-0.0678	0.298451	0.087322	0.056707	-0.04403	404.4139
150	1.5823	0.6494	22.8000	12.0540	20	1.923944	-0.0678	0.298451	0.087322	0.056707	-0.04403	473.3753
150	1.5823	0.6494	22.8000	12.0540	25	1.923944	-0.0678	0.298451	0.087322	0.056707	-0.04403	528.7094

**Minna**

ITU-R Model

F(GHz)	KH	$\alpha H$	R0.01	YR (H)	$(B2/10)^{0.8}$	Co	C3	C2	C1	r (H)	d(km)	Deff	Deff	A0.01
												V(d*r)	H(d*r)	(H)
150	1.5823	0.6494	116.7000	34.8052	8.727161	0.496349	0.09065	0.699372	0.091832	1.167975	1	1.169446	1.167975	40.65166
150	1.5823	0.6494	116.7000	34.8052	8.727161	0.496349	0.09065	0.699372	0.091832	0.534744	5	2.677992	2.673722	93.05955
150	1.5823	0.6494	116.7000	34.8052	8.727161	0.496349	0.09065	0.699372	0.091832	0.400329	10	4.010715	4.003291	139.3355
150	1.5823	0.6494	116.7000	34.8052	8.727161	0.496349	0.09065	0.699372	0.091832	0.339176	15	5.097972	5.087637	177.0764

150	1.5823	0.6494	116.7000	34.8052	8.727161	0.496349	0.09065	0.699372	0.091832	0.299274	20	5.998347	5.985475	208.3259
150	1.5823	0.6494	116.7000	34.8052	8.727161	0.496349	0.09065	0.699372	0.091832	0.26882	25	6.735445	6.720492	233.9083

Moupfouma Model

F(GHz)	KH	$\alpha$ H	R0.01	YR (H)	M	B	p	r (H)	L(km)	Leff (r*l)	A0.01 (H)	
150	1.5823	0.6494	116.7000	34.8052		1	0.6	0.01	1.03	1	1.03	35.8494
150	1.5823	0.6494	116.7000	34.8052	2.523081		0.6	0.01	1.03	5	5.15	179.247
150	1.5823	0.6494	116.7000	34.8052	3.179036		0.6	0.01	1.03	10	10.3	358.494
150	1.5823	0.6494	116.7000	34.8052	3.562745		0.6	0.01	1.03	15	15.45	537.741
150	1.5823	0.6494	116.7000	34.8052	3.834991		0.6	0.01	1.03	20	20.6	716.988
150	1.5823	0.6494	116.7000	34.8052	4.046161		0.6	0.01	1.03	25	25.75	896.2349

Crane Global Model

F(GHz)	KH	$\alpha$ H	R0.01	YR (H)	d(km)	$\delta$ (R)	C	B	U	y	Z	AT
150	1.5823	0.6494	116.7000	34.8052	1	0.944236	-0.11679	0.020867	-0.09469	-0.06149	-0.07584	7.096071
150	1.5823	0.6494	116.7000	34.8052	5	0.944236	-0.11679	0.020867	-0.09469	-0.06149	-0.07584	110.604
150	1.5823	0.6494	116.7000	34.8052	10	0.944236	-0.11679	0.020867	-0.09469	-0.06149	-0.07584	202.7759
150	1.5823	0.6494	116.7000	34.8052	15	0.944236	-0.11679	0.020867	-0.09469	-0.06149	-0.07584	265.8584
150	1.5823	0.6494	116.7000	34.8052	20	0.944236	-0.11679	0.020867	-0.09469	-0.06149	-0.07584	309.0322
150	1.5823	0.6494	116.7000	34.8052	25	0.944236	-0.11679	0.020867	-0.09469	-0.06149	-0.07584	338.5803

## Yola

ITU-R Model											Deff	Deff	A0.01	
F(GHz)	KH	$\alpha H$	R0.01	YR (H)	$(B2/10)^{0.8}$	Co	C3	C2	C1	r (H)	d(km)	V(d*r)	H(d*r)	(H)
150	1.5823	0.6494	33.2000	15.3857	8.727161	0.496349	0.09065	0.699372	0.091832	1.262407	1	1.263597	1.262407	19.42295
150	1.5823	0.6494	33.2000	15.3857	8.727161	0.496349	0.09065	0.699372	0.091832	0.590786	5	2.957541	2.953929	45.44812
150	1.5823	0.6494	33.2000	15.3857	8.727161	0.496349	0.09065	0.699372	0.091832	0.449873	10	4.505229	4.498731	69.2159
150	1.5823	0.6494	33.2000	15.3857	8.727161	0.496349	0.09065	0.699372	0.091832	0.385693	15	5.794662	5.7854	89.01214
150	1.5823	0.6494	33.2000	15.3857	8.727161	0.496349	0.09065	0.699372	0.091832	0.343076	20	6.87324	6.861515	105.5689
150	1.5823	0.6494	33.2000	15.3857	8.727161	0.496349	0.09065	0.699372	0.091832	0.309729	25	7.756984	7.743225	119.1346

## Moupfouma Model

											Leff	A0.01
F(GHz)	KH	$\alpha H$	R0.01	YR (H)	M	B	p	r (H)	L(km)	(r*I)	(H)	
150	1.5823	0.6494	33.2000	15.3857	1	0.6	0.01	1.03	1	1.03	15.84722	
150	1.5823	0.6494	33.2000	15.3857	2.523081	0.6	0.01	1.03	5	5.15	79.23611	
150	1.5823	0.6494	33.2000	15.3857	3.179036	0.6	0.01	1.03	10	10.3	158.4722	
150	1.5823	0.6494	33.2000	15.3857	3.562745	0.6	0.01	1.03	15	15.45	237.7083	
150	1.5823	0.6494	33.2000	15.3857	3.834991	0.6	0.01	1.03	20	20.6	316.9444	
150	1.5823	0.6494	33.2000	15.3857	4.046161	0.6	0.01	1.03	25	25.75	396.1805	

## Crane Global Model

F(GHz)	KH	$\alpha H$	R0.01	YR (H)	d(km)	$\delta(R)$	C	B	U	y	Z	AT
150	1.5823	0.6494	33.2000	15.3857	1	1.69847	-0.07908	0.234567	0.059028	0.038333	-0.05135	71.84403



150	1.5823	0.6494	33.2000	15.3857	5	1.69847	-0.07908	0.234567	0.059028	0.038333	-0.05135	179.8532
150	1.5823	0.6494	33.2000	15.3857	10	1.69847	-0.07908	0.234567	0.059028	0.038333	-0.05135	287.1139
150	1.5823	0.6494	33.2000	15.3857	15	1.69847	-0.07908	0.234567	0.059028	0.038333	-0.05135	370.0857
150	1.5823	0.6494	33.2000	15.3857	20	1.69847	-0.07908	0.234567	0.059028	0.038333	-0.05135	434.2687
150	1.5823	0.6494	33.2000	15.3857	25	1.69847	-0.07908	0.234567	0.059028	0.038333	-0.05135	483.9177

### Ogbomosho

#### ITU-R Model

F(GHz)	KH	$\alpha H$	R0.01	YR (H)	$(B2/10)^{0.8}$	Co	C3	C2	C1	r (H)	d(km)	Deff V(d*r)	Deff H(d*r)	A0.01 (H)
150	1.5823	0.6494	67.0000	24.2740	8.727161	0.496349	0.09065	0.699372	0.091832	1.208547	1	1.209902	1.208547	29.33631
150	1.5823	0.6494	67.0000	24.2740	8.727161	0.496349	0.09065	0.699372	0.091832	0.558522	5	2.796617	2.792609	67.78787
150	1.5823	0.6494	67.0000	24.2740	8.727161	0.496349	0.09065	0.699372	0.091832	0.421144	10	4.218511	4.211442	102.2287
150	1.5823	0.6494	67.0000	24.2740	8.727161	0.496349	0.09065	0.699372	0.091832	0.358585	15	5.388718	5.378779	130.5646
150	1.5823	0.6494	67.0000	24.2740	8.727161	0.496349	0.09065	0.699372	0.091832	0.317464	20	6.361748	6.349286	154.1227
150	1.5823	0.6494	67.0000	24.2740	8.727161	0.496349	0.09065	0.699372	0.091832	0.285759	25	7.158503	7.143966	173.4128

#### Moupfouma Model

F(GHz)	KH	$\alpha H$	R0.01	YR (H)	M	B	p	r (H)	L(km)	Leff (r*I)	A0.01 (H)
150	1.5823	0.6494	67.0000	24.2740	1	0.6	0.01	1.03	1	1.03	25.00225
50	1.5823	0.6494	67.0000	24.2740	2.523081	0.6	0.01	1.03	5	5.15	125.0112

150	1.5823	0.6494	67.0000	24.2740	3.179036	0.6	0.01	1.03	10	10.3	250.0225
150	1.5823	0.6494	67.0000	24.2740	3.562745	0.6	0.01	1.03	15	15.45	375.0337
150	1.5823	0.6494	67.0000	24.2740	3.834991	0.6	0.01	1.03	20	20.6	500.0449
150	1.5823	0.6494	67.0000	24.2740	4.046161	0.6	0.01	1.03	25	25.75	625.0562

Crane Global Model

F(GHz)	KH	$\alpha H$	R0.01	YR (H)	d(km)	$\delta(R)$	C	B	U	y	Z	AT
150	1.5823	0.6494	67.0000	24.2740	1	1.277184	-0.10014	0.115202	-0.00994	-0.00646	-0.06503	28.01344
150	1.5823	0.6494	67.0000	24.2740	5	1.277184	-0.10014	0.115202	-0.00994	-0.00646	-0.06503	137.8261
150	1.5823	0.6494	67.0000	24.2740	10	1.277184	-0.10014	0.115202	-0.00994	-0.00646	-0.06503	240.4285
150	1.5823	0.6494	67.0000	24.2740	15	1.277184	-0.10014	0.115202	-0.00994	-0.00646	-0.06503	314.5499
150	1.5823	0.6494	67.0000	24.2740	20	1.277184	-0.10014	0.115202	-0.00994	-0.00646	-0.06503	368.0962
150	1.5823	0.6494	67.0000	24.2740	25	1.277184	-0.10014	0.115202	-0.00994	-0.00646	-0.06503	406.7788

**Kano**

ITU-R Model

F(GHz)	KH	$\alpha H$	R0.01	YR (H)	$(B2/10)^{0.8}$	Co	C3	C2	C1	r (H)	d(km)	Deff V(d*r)	Deff H(d*r)	A0.01 (H)
150	1.5823	0.6494	78.6000	26.9263	8.727161	0.496349	0.09065	0.699372	0.091832	1.196697	1	1.198086	1.196697	32.2226
150	1.5823	0.6494	78.6000	26.9263	8.727161	0.496349	0.09065	0.699372	0.091832	0.551531	5	2.761742	2.757655	74.25337
150	1.5823	0.6494	78.6000	26.9263	8.727161	0.496349	0.09065	0.699372	0.091832	0.414993	10	4.157111	4.149932	111.7422
150	1.5823	0.6494	78.6000	26.9263	8.727161	0.496349	0.09065	0.699372	0.091832	0.35283	15	5.302508	5.292444	142.5058

150	1.5823	0.6494	78.6000	26.9263	8.727161	0.496349	0.09065	0.699372	0.091832	0.312057	20	6.253741	6.241147	168.0508
150	1.5823	0.6494	78.6000	26.9263	8.727161	0.496349	0.09065	0.699372	0.091832	0.280716	25	7.032579	7.017906	188.9661

Moupfouma Model

F(GHz)	KH	$\alpha$ H	R0.01	YR (H)	M	B	p	r (H)	L(km)	Leff (r*I)	A0.01 (H)	
150	1.5823	0.6494	78.6000	26.9263		1	0.6	0.01	1.03	1	1.03	27.73406
150	1.5823	0.6494	78.6000	26.9263	2.523081		0.6	0.01	1.03	5	5.15	138.6703
150	1.5823	0.6494	78.6000	26.9263	3.179036		0.6	0.01	1.03	10	10.3	277.3406
150	1.5823	0.6494	78.6000	26.9263	3.562745		0.6	0.01	1.03	15	15.45	416.0109
150	1.5823	0.6494	78.6000	26.9263	3.834991		0.6	0.01	1.03	20	20.6	554.6812
150	1.5823	0.6494	78.6000	26.9263	4.046161		0.6	0.01	1.03	25	25.75	693.3515

Crane Global Model

F(GHz)	KH	$\alpha$ H	R0.01	YR (H)	d(km)	$\delta$ (R)	C	B	U	y	Z	AT
150	1.5823	0.6494	78.6000	26.9263	1	1.181377	-0.10493	0.088057	-0.03039	-0.01974	-0.06814	20.92292
150	1.5823	0.6494	78.6000	26.9263	5	1.181377	-0.10493	0.088057	-0.03039	-0.01974	-0.06814	129.8079
150	1.5823	0.6494	78.6000	26.9263	10	1.181377	-0.10493	0.088057	-0.03039	-0.01974	-0.06814	230.1449
150	1.5823	0.6494	78.6000	26.9263	15	1.181377	-0.10493	0.088057	-0.03039	-0.01974	-0.06814	301.5109
150	1.5823	0.6494	78.6000	26.9263	20	1.181377	-0.10493	0.088057	-0.03039	-0.01974	-0.06814	352.2711
150	1.5823	0.6494	78.6000	26.9263	25	1.181377	-0.10493	0.088057	-0.03039	-0.01974	-0.06814	388.3749